



TECHNISCHE UNIVERSITÄT MÜNCHEN  
FAKULTÄT CHEMIE  
LEHRSTUHL FÜR ORGANISCHE CHEMIE II

**INSIGHTS INTO PHOTOCROSSLINKER-ASSOCIATED OFF-TARGET  
PROTEIN BINDING**

and

**DISCOVERY OF A SMALL MOLECULE ANTIBIOTIC ACTIVE AGAINST  
MULTIDRUG-RESISTANT GRAM-POSITIVE PATHOGENS**

Philipp Kleiner

Vollständiger Abdruck der von der Fakultät für Chemie der Technischen Universität München  
zur Erlangung des akademischen Grades eines

Doktors der Naturwissenschaften (Dr. rer. nat.)

genehmigten Dissertation.

Vorsitzender: Prof. Dr. Michael Groll  
Prüfer der Dissertation: 1. Prof. Dr. Stephan A. Sieber  
2. Prof. Dr. Tobias A. M. Gulder

Die Dissertation wurde am 18.01.2018 bei der bei der Technischen Universität München  
eingereicht und durch die Fakultät für Chemie am 20.02.2018 angenommen.





TECHNISCHE UNIVERSITÄT MÜNCHEN  
FAKULTÄT CHEMIE  
LEHRSTUHL FÜR ORGANISCHE CHEMIE II

**INSIGHTS INTO PHOTOCROSSLINKER-ASSOCIATED OFF-TARGET  
PROTEIN BINDING**

**and**

**DISCOVERY OF A SMALL MOLECULE ANTIBIOTIC ACTIVE AGAINST  
MULTIDRUG-RESISTANT GRAM-POSITIVE PATHOGENS**

Philipp Kleiner

Vollständiger Abdruck der von der Fakultät für Chemie der Technischen Universität München  
zur Erlangung des akademischen Grades eines

Doktors der Naturwissenschaften (Dr. rer. nat.)

genehmigten Dissertation.

Vorsitzender: Prof. Dr. Michael Groll  
Prüfer der Dissertation: 1. Prof. Dr. Stephan A. Sieber  
2. Prof. Dr. Tobias A. M. Gulder

Die Dissertation wurde am 18.01.2018 bei der bei der Technischen Universität München  
eingereicht und durch die Fakultät für Chemie am 20.02.2018 angenommen.



Meiner Familie gewidmet.



## TABLE OF CONTENTS

|  |            |
|--|------------|
| <b>TABLE OF CONTENTS</b> .....   | <b>I</b>   |
| <b>INTRODUCTORY REMARKS</b> .....  | <b>VII</b> |
| <b>SUMMARY</b> .....   | <b>IX</b>  |
| <b>ZUSAMMENFASSUNG</b> .....   | <b>XI</b>  |
| <b>1. INTRODUCTION</b> .....   | <b>1</b>   |
| 1.1.    ANTIMICROBIAL RESISTANCE – A SEVERE GLOBAL HEALTH CHALLENGE                            | 1          |
| 1.1.1.    History of Antibiotics .....   | 2          |
| 1.1.2.    Modes of Action and Resistance Mechanisms .....                                      | 4          |
| 1.1.3.    Methicillin- and Vancomycin-Resistant <i>Staphylococcus Aureus</i> .....             | 7          |
| 1.2.    PHENOTYPIC AND TARGET-BASED SCREENING APPROACHES .....                                 | 8          |
| 1.3.    ACTIVITY- AND AFFINITY-BASED PROTEIN PROFILING .....                                   | 9          |
| <b>2. INSIGHTS INTO PHOTOCROSSLINKER-ASSOCIATED OFF-TARGET PROTEIN</b>                         |            |
| <b>BINDING</b> .....   | <b>17</b>  |
| 2.1.    NON-SPECIFIC CROSSLINKING EVENTS IN PHOTOAFFINITY LABELLING                            | 18         |
| 2.2.    RESULTS AND DISCUSSION .....   | 20         |
| 2.2.1.    Design and Synthesis of Minimal Photoprobes .....                                    | 20         |
| 2.2.2.    Evaluation of Photocrosslinker-Associated Background Labelling by Gel-Based          |            |
| Affinity-Based Protein Profiling .....   | 21         |
| 2.2.3.    Analysis of Photocrosslinker-Specific Protein Labelling Profiles via SILAC-Based     |            |
| Quantitative Proteomics .....  | 23         |
| 2.2.3.1.    Photocrosslinker-Specific Protein Labelling Profiles .....                         | 23         |
| 2.2.3.2.    Diazirine-Specific Protein Labelling Profiles .....                                | 25         |
| 2.2.4.    Evaluation of Critical Experimental Parameters on Diazirine-Associated               |            |
| Background Labelling by Label-Free Quantitative Proteomics .....                               | 30         |
| 2.2.4.1.    Label-Free Diazirine-Specific Protein Labelling Profiles .....                     | 30         |
| 2.2.4.2.    Impact of Experimental Parameters on the Target Identification of Kinase Inhibitor |            |
| SP600125 .....   | 31         |
| 2.2.5.    Proof-of-Principle Study: Target Elucidation of Reversible Protein Kinase A          |            |
| Inhibitor H8 via Affinity-Based Protein Profiling .....  | 35         |
| 2.3.    CONCLUSION AND OUTLOOK .....   | 39         |
| <b>3. DISCOVERY OF A SMALL MOLECULE ANTIBIOTIC ACTIVE AGAINST</b>                              |            |
| <b>MULTIDRUG-RESISTANT GRAM-POSITIVE PATHOGENS</b> .....                                       | <b>41</b>  |
| 3.1.    REPURPOSING NON-ANTIMICROBIAL DRUGS AS ANTIBIOTICS .....                               | 42         |
| 3.2.    RESULTS AND DISCUSSION .....   | 44         |
| 3.2.1.    Antibacterial Screen of Kinase Inhibitors .....                                      | 44         |
| 3.2.2.    Target Deconvolution via Affinity-Based Protein Profiling .....                      | 45         |

---

|   |           |
|---|-----------|
| 3.2.2.1. Photoprobe Design and Synthesis.....   | 46        |
| 3.2.2.2. Gel-Based Affinity-Based Protein Profiling.....  | 47        |
| 3.2.2.3. Gel-Free Preparative Affinity-Based Protein Profiling.....   | 48        |
| 3.2.3. Target Validation.....   | 51        |
| 3.2.3.1. Narrowing Down the List of Putative Target Proteins.....   | 51        |
| 3.2.3.2. Type I Signal Peptidase, a Putative Bacterial Target of Sorafenib.....   | 53        |
| 3.2.3.3. Validation of Type I Signal Peptidase as a Putative Target of Sorafenib.....   | 54        |
| 3.2.4. Medicinal Chemistry – The Relationship Between Structure and Antibacterial as well as SpsB-Activating Properties.....                        | 59        |
| 3.2.4.1. Structure-Activity Relationship of Hit Compound Sorafenib.....   | 59        |
| 3.2.4.2. Structure-Activity Relationship of PK150.....  | 65        |
| 3.2.4.3. Correlation Between Bacterial Killing and Compound-Induced SpsB Stimulation.....   | 66        |
| 3.2.4.4. Antibacterial Characteristics of PK150.....  | 67        |
| 3.2.4.5. Verification of PK150.....   | 71        |
| 3.2.4.6. Molecular Basis of Compound-Induced SpsB Stimulation.....  | 73        |
| 3.2.5. Insights into the Effects of SpsB Stimulation.....   | 75        |
| 3.2.5.1. Secretome and Surfome Analysis.....  | 75        |
| 3.2.5.2. Electron Microscopy.....   | 79        |
| 3.2.6. Pharmacological Profile of PK150.....  | 81        |
| 3.2.6.1. In Vitro Toxicological Profile of PK150.....   | 81        |
| 3.2.6.2. In Vivo Pharmacokinetic Profile of PK150.....  | 84        |
| 3.2.6.3. In Vivo Pharmacodynamic Profile of PK150.....  | 85        |
| 3.3. CONCLUSION AND OUTLOOK.....  | 87        |
| <b>4. EXPERIMENTAL SECTION.....</b>   | <b>91</b> |
| 4.1. ORGANIC SYNTHESIS.....   | 91        |
| 4.1.1. General Methods and Materials.....   | 91        |
| 4.1.2. Synthetic Procedures for Chapter 2: Insights into Photocrosslinker-Associated Off-Target Protein Binding.....                                | 92        |
| 4.1.2.1. Procedures for the Synthesis of Building Blocks.....   | 92        |
| 4.1.2.2. Synthesis of Minimal Photoprobes.....  | 93        |
| 4.1.2.3. Synthesis of Kinase Inhibitor Photoprobes.....   | 97        |
| 4.1.3. Synthetic Procedures for Chapter 3: Discovery of a Small Molecule Antibiotic Active Against Multidrug-Resistant Gram-Positive Pathogens..... | 98        |
| 4.1.3.1. Synthesis of Sorafenib-Based Photoprobe SFNp.....  | 98        |
| 4.1.3.2. Synthesis of Minimal Photocrosslinker Probes and Corresponding Control Compounds.....  | 100       |

---

|  |     |
|--|-----|
| 4.1.3.3. Synthesis of a Sorafenib-Based Compound Library .....   | 101 |
| 4.1.3.3.1. General Procedure for the Synthesis of Urea and Thiourea Containing<br>Compounds .....  | 102 |
| 4.1.3.3.2. Synthesis of Derivatives Bearing Structural Variations of the Central Urea Motif<br>.....   | 118 |
| 4.1.3.3.3. Synthesis of Further Derivatives Not Highlighted in Chapter 3 .....   | 121 |
| 4.1.3.3.4. Synthesis of Compound Library Building Blocks .....   | 129 |
| 4.2. BIOCHEMISTRY .....  | 133 |
| 4.2.1. General Methods and Materials .....   | 133 |
| 4.2.1.1. Cell Culture .....  | 133 |
| 4.2.1.2. Bacterial Strains and Culture Media .....   | 133 |
| 4.2.2. Proteomics – Chapter 2: Insights into Photocrosslinker-Associated Off-Target<br>Protein Binding .....                                 | 135 |
| 4.2.2.1. Analytical In Situ Affinity-Based Protein Profiling .....   | 135 |
| 4.2.2.2. Preparative In Situ Affinity-Based Protein Profiling with Quantification via SILAC<br>.....   | 136 |
| 4.2.2.3. Preparative In Situ Affinity-Based Protein Profiling with Label-Free Quantification<br>.....  | 137 |
| 4.2.2.4. Mass Spectrometry Setup and Settings .....  | 138 |
| 4.2.2.4.1. Mass Spectrometry Setup and Settings for SILAC-Based Quantification .....   | 138 |
| 4.2.2.4.2. Mass Spectrometry Setup and Settings for Label-Free Quantification .....  | 139 |
| 4.2.2.5. Bioinformatics .....  | 139 |
| 4.2.2.5.1. Analysis of SILAC-Based Experiments .....   | 139 |
| 4.2.2.5.2. Analysis of Label-Free Experiments .....  | 141 |
| 4.2.3. Proteomics – Chapter 3: Discovery of a Small Molecule Antibiotic Active Against<br>Multidrug-Resistant Gram-Positive Pathogens .....  | 141 |
| 4.2.3.1. Target Deconvolution via Affinity-Based Protein Profiling .....   | 141 |
| 4.2.3.1.1. General Experiment Procedure for Affinity-Based Protein Profiling .....   | 141 |
| 4.2.3.1.2. Gel-Based Analytical In Situ Affinity-Based Protein Profiling .....   | 142 |
| 4.2.3.1.3. Gel-Free Preparative In Situ Affinity-Based Protein Profiling with Quantification<br>via Dimethyl Labelling .....                 | 143 |
| 4.2.3.1.4. Mass Spectrometry Setup and Settings .....  | 143 |
| 4.2.3.1.5. Bioinformatics – Analysis of Affinity-Based Protein Profiling Experiments Based<br>on Quantification via Dimethyl Labelling ..... | 144 |
| 4.2.3.2. Surfome and Secretome Analysis .....  | 145 |
| 4.2.3.2.1. Experimental Procedure for the Preparation of Secretome Samples .....   | 145 |
| 4.2.3.2.2. Experimental Procedure for the Preparation of Surfome Samples .....   | 146 |

|   |            |
|---|------------|
| 4.2.3.2.3. Mass Spectrometry Setup and Settings .....   | 147        |
| 4.2.3.2.4. Bioinformatics – Analysis of Secretome and Surfome Data .....  | 147        |
| 4.2.3.3. Kinase Selectivity Profiling via the Kinobead Technology .....   | 148        |
| 4.2.3.3.1. Experimental Procedure of the Preparation of Kinobead Samples .....  | 148        |
| 4.2.3.3.2. Mass Spectrometry Setup and Settings .....   | 149        |
| 4.2.3.3.3. Bioinformatics – Analysis of Kinobeads Selectivity Profiling Data .....  | 149        |
| 4.2.4. Biochemical Procedures and Microbiology – Chapter 3: Discovery of a Small<br>Molecule Antibiotic Active Against Multidrug-Resistant Gram-Positive Pathogens<br>..... | 150        |
| 4.2.4.1. Minimum Inhibitory Concentration Assay .....   | 150        |
| 4.2.4.2. Cloning, Expression and Purification of Full-Length SpsB.....  | 151        |
| 4.2.4.3. Preparation of Membrane Fractions from the <i>Escherichia Coli</i> SpsB Expression<br>Strain and <i>Staphylococcus Aureus</i> NCTC 8325.....                       | 153        |
| 4.2.4.4. FRET-Based In Vitro Peptidase Activity Assay .....   | 153        |
| 4.2.4.5. Cell Permeability Assay .....  | 154        |
| 4.2.4.6. Bacterial Killing Kinetics.....  | 154        |
| 4.2.4.7. Persister Cell Assay.....  | 155        |
| 4.2.4.8. Biofilm Eradication and Inhibition Assay.....  | 156        |
| 4.2.4.9. Resistance Development Assay .....   | 157        |
| 4.2.4.10. Zymography.....   | 157        |
| 4.2.4.11. ClpP Peptidase Assay .....  | 159        |
| 4.2.4.12. Cytotoxicity Assay.....   | 159        |
| 4.2.4.13. Hemolysis Assay .....   | 159        |
| 4.2.4.14. In Vitro Stability in Murine Blood Plasma.....  | 160        |
| 4.2.5. In Vivo Animal Studies – Chapter 3: Discovery of a Small Molecule Antibiotic<br>Active Against Multidrug-Resistant Gram-Positive Pathogens .....                     | 161        |
| 4.2.5.1. General Information .....  | 161        |
| 4.2.5.2. Pharmacokinetic Study .....  | 161        |
| 4.2.5.3. Pharmacodynamic Efficacy Study Using a Neutropenic Thigh Infection Model   | 162        |
| 4.2.5.4. Efficacy Experiment Mimicking a <i>Staphylococcus Aureus</i> Bloodstream Infection<br>.....  | 163        |
| 4.2.6. Further Experimental Procedures – Chapter 3: Discovery of a Small Molecule<br>Antibiotic Active Against Multidrug-Resistant Gram-Positive Pathogens .....            | 163        |
| 4.2.6.1. Colloidal Aggregation Determination by Dynamic Light Scattering .....  | 163        |
| 4.2.6.2. Molecular Docking and Dynamic Simulations .....  | 164        |
| 4.2.6.3. Electron Microscopy .....  | 165        |
| <b>5. BILIOGRAPHY .....</b>   | <b>167</b> |

---

|  |            |
|--|------------|
| <b>6. LIST OF ABBREVIATIONS, ACRONYMS AND SYMBOLS .....</b>  | <b>189</b> |
| <b>7. APPENDICES.....</b>  | <b>193</b> |
| 7.1. Kinase Inhibitor Library .....  | 193        |
| 7.2. Antibacterial Profile of Sorafenib and PK150 .....  | 199        |
| 7.3. Resistance Profile of Clinical Isolates .....   | 200        |
| 7.4. Library of Sorafenib and PK150 Analogs .....  | 202        |
| 7.5. Selected <sup>1</sup> H and <sup>13</sup> C NMR Spectra – Chapter 2: Insights into Photocrosslinker-<br>Associated Off-Target Protein Binding .....                               | 207        |
| 7.6. Selected <sup>1</sup> H and <sup>13</sup> C NMR Spectra – Chapter 3: Discovery of a Small Molecule<br>Antibiotic Active Against Multidrug-Resistant Gram-Positive Pathogens ..... | 216        |
| <b>8. CURRICULUM VITAE .....</b>   | <b>288</b> |



## INTRODUCTORY REMARKS

The present doctoral dissertation was accomplished between May 2013 and January 2018 under the supervision of Prof. Dr. Stephan A. Sieber, Chair of Organic Chemistry II, Technische Universität München.

PARTS OF THIS THESIS ARE BASED ON THE FOLLOWING PUBLICATIONS AND MANUSCRIPT SUBMITTED FOR PUBLICATION:

### CHAPTER 2.

**P. Kleiner\***, W. Heydenreuter\*, M. Stahl\*, V. S. Korotkov, S. A. Sieber. A Whole Proteome Inventory of Background Photocrosslinker Binding. *Angew. Chem. Int. Ed.* **2017**, *56*, 1396. \*These authors contributed equally to this work.

W. Heydenreuter. Target identification of natural products by activity based protein profiling and a whole proteome inventory of background photocrosslinker binding. Dissertation, Technische Universität München, **2016**.

### CHAPTER 3.

E. Kunold\*, **P. Kleiner\***, K. Rox, M. C. Jennings, I. M. Ugur, M. Reinecke, B. Küster, I. Antes, M. Rohde, W. M. Wuest, E. Medina, S. A. Sieber. Repurposing human kinase inhibitors to create an antibiotic active against drug-resistant *Staphylococcus aureus*. Manuscript submitted for publication. \*These authors contributed equally to this work.

**P. Kleiner**, S. A. Sieber, E. Kunold. Urea motif containing compounds and derivatives thereof as antibacterial drugs. International Patent Application PCT/EP2017/063014, **2017**.

All compounds mentioned in this manuscript are numbered consecutively with Arabic numerals in the format **X.Y** with **X** being the number of the chapter and **Y** representing the order of appearance. Photoreactive probes of bioactive compounds are named after the respective parental compound and highlighted by the postposition **p**. In Chapter 2, minimal photoprobes are numbered in the **XX-Y** format with **XX** indicating the photoreactive functionality (BP = benzophenone, AA = aryl azide and DA = diazirine) and **Y** representing the order of appearance.



## SUMMARY

Phenotypic screening approaches of diverse chemical space either of natural or synthetic origin have contributed in large measure to the identification of bioactive scaffolds. While the identification of potential bioactive skeletons lays the foundation in phenotype-driven drug development, the elucidation of the mode of action is vital for rational hit compound optimization. Affinity-based protein profiling (AfBPP) has matured to a powerful proteomic platform for direct target deconvolution. AfBPP utilizes close analogs of the molecule of interest modified with a photoreactive crosslinking moiety as well as a traceable reporter group to zoom in on proteins that directly engage with these photoprobes.

However, AfBPP experiments are often hampered by strong background protein labelling that is related to ligand-independent photocrosslinker-associated off-target binding. Although this non-specific background labelling is recognized as a major obstacle for the interpretation and reliability of AfBPP results, little is known about the nature and identity of these promiscuous protein hits. To access the specificity of three commonly applied photocrosslinking functionalities – benzophenone, aryl azide and diazirine – in photoaffinity labelling experiments their protein profiles were elucidated. First, gel-free quantitative proteomics identified characteristic off-targets for each photoreactive functionality and underscored the beneficial properties of diazirines. Second, in-depth analysis of the widely applied diazirine photocrosslinking moiety, which was incorporated into minimal photoprobes of differing steric demand and hydrophobicity, resulted in a comprehensive list of diazirine-specific off-target hits. Third, systematic evaluation of critical experimental parameters utilizing a diazirine-based photoprobe of c-Jun N-terminal kinase inhibitor **SP600125** showed that AfBPP experiments can benefit from low photoprobe concentrations and long irradiation times. Finally, a proof-of-principal study collaborating a diazirine-based photoprobe of protein kinase A inhibitor **H8** illustrated the significance of this off-target list for the interpretation of proteomic results. Data interpretation would have been challenging without the awareness and knowledge of promiscuous proteins that are presumably not addressed by the molecule of interest but rather specific for the photocrosslinking functionality applied. Here, the putative protein target of **H8** protruded from the bulk of background binders only after consideration of diazirine-specific background binders.

To deal with the successive waves of resistant bacterial pathogens novel antibiotics are urgently needed. While natural products provide an essential source for novel antibiotic scaffolds, synthetic chemical efforts are still in play. Besides these two standard approaches in antibiotic drug discovery there is a growing recognition of drug repurposing efforts.

Based on the concept of repurposing existing drugs to identify new antibiotic applications outside their original scope, a library of eukaryotic kinase inhibitors was mined for

activity against *Staphylococcus aureus*. This phenotypic screening approach revealed sorafenib, an approved anticancer drug, to effectively kill *S. aureus*, including multidrug-resistant clinical isolates. In-depth structure-activity relationship studies established structural key features within the sorafenib scaffold as hallmarks for antibacterial activity and resulted in an analog – **PK150** – with a minimal inhibitory concentration of 300 nM against various multidrug-resistant *S. aureus* strains. In addition to improved antistaphylococcal properties, **PK150** showed activity against several Gram-positive pathogens including mycobacteria and vancomycin-resistant enterococci. In situ resistance acquisition in *S. aureus* was not observed. Rapid bactericidal killing mediated by **PK150** treatment was accompanied by effective eradication of challenging persisters and established biofilms. In vivo evaluation of the pharmacokinetic and –dynamic profile of **PK150** showed good oral bioavailability and efficacy in MRSA-infected mice, although dose-limiting toxicity was observed.

In parallel, chemical proteomic studies with a sorafenib photoaffinity probe revealed binding to several potential target proteins, foremost type I signal peptidase (SpsB), a membrane-anchored serine protease essential for protein secretion. Biochemical analysis showed a sorafenib- and **PK150**-induced stimulation of SpsB activity that was generally in line with the established phenotypic structure-activity relationship of the core scaffold. Compound-induced SpsB stimulation resulted in increased secretion levels of extracellular proteins, thereby dysregulating the strictly balanced secretory machinery. While it is difficult to trace down the mode of action to a single target pathway and observed antibiotic effects likely result from a multi-target profile, it is conceivable that dysregulation of the secretory machinery in *S. aureus* by **PK150** contributes to bacterial killing.

## ZUSAMMENFASSUNG

Phänotyp-basierte Screenings Naturstoff-basierter und/oder synthetisch-generierter Substanzbibliotheken haben in großem Umfang zur Entdeckung bioaktiver chemischer Strukturen beigetragen. Während die Identifizierung einer bioaktiven Struktur die Basis für eine Phänotyp-basierte Entwicklung von Arzneimitteln darstellt, ist die Aufklärung des Wirkungsmechanismus grundlegend für eine rationale Optimierung der ursprünglich identifizierten bioaktiven Struktur. In diesem Zusammenhang ist die proteomische Methodologie des Affinity-Based Protein Profiling (AfBPP) zu einer leistungsstarken und zuverlässigen Möglichkeit gereift, potentielle Proteintargets der entsprechenden bioaktiven Struktur zu identifizieren. Hierbei kommen Derivate der jeweiligen Struktur zum Einsatz, welche mittels einer photoreaktiven Einheit und einer rückverfolgbaren Markierung zu einer sogenannten Photosonde modifiziert wurden und somit die Identifizierung von direkt mit der bioaktiven Struktur interagierenden Proteinen ermöglichen.

Allerdings wird die proteomische Analyse von AfBPP-basierten Experimenten häufig durch einen starken Proteinhintergrund, dessen Interaktion mit der Photosonde nicht auf die eigentliche bioaktive Struktur zurückzuführen ist, sondern unspezifisch durch die photoreaktive Einheit erfolgt, erschwert. Obgleich dieser unspezifische Proteinhintergrund als Problem für die Interpretation und Zuverlässigkeit von AfBPP-basierten Ergebnissen weithin erkannt ist, ist wenig über die Identität und Art dieser Hintergrundproteine bekannt. Im Rahmen dieser Arbeit wurde daher die Spezifität von drei weitverbreiteten photoreaktiven Einheiten – Benzophenon, Arylazid und Diazirin – untersucht und ihre jeweiligen charakteristischen proteomischen Anreicherungsprofile mittels Gel-unabhängiger, quantitativer Proteomik aufgezeigt. Anhand der Ergebnisse konnten die vorteilhaften Eigenschaften von Diazirinen unterstrichen werden. Weiterführende Experimente mit Diazirin-basierten Minimal-Photosonden unterschiedlicher Sterik und Hydrophobizität resultierten in einer umfassenden Auflistung von Diazirin-spezifischen Hintergrundproteinen. Des Weiteren ergab eine systematische Analyse kritischer experimenteller Parameter anhand einer Diazirin-basierten Photosonde von **SP600125**, einem Inhibitor der c-Jun-N-terminalen Kinase, dass die Ergebnisse von AfBPP-basierten Experimenten durch geringe Photosonden-Konzentrationen sowie längere Bestrahlungszeiten profitieren können. Die Bedeutung dieser Ergebnisse für die Interpretation von AfBPP-basierten Daten wurde abschließend anhand einer Diazirin-basierten Photosonde des Proteinkinase A Inhibitors **H8** veranschaulicht. Ohne die Kenntnis des Diazirin-spezifischen Proteinhintergrunds, der nicht auf eine Interaktion mit der **H8**-Grundstruktur zurückzuführen ist, wäre eine Datenanalyse nicht möglich gewesen. Das bekannte und validierte Proteintarget von **H8** trat erst nach Berücksichtigung der Diazirin-spezifischen Off-Targets aus der Vielzahl markierter Proteine hervor.

Im Kampf gegen multiresistente bakterielle Krankheitserreger wird die Entwicklung neuer Antibiotika immer dringlicher. Während Naturstoffe weiterhin eine wichtige Quelle für neue antibiotisch wirksame Strukturen darstellen, sind chemisch-synthetische Anstrengungen nach wie vor unerlässlich. Neben diesen beiden traditionellen Methoden der Antibiotika-Entwicklung, gerät die Neupositionierung von ursprünglich für andere Indikationen eingesetzte bioaktive Strukturen als Antibiotika verstärkt in den Fokus.

Basierend auf diesem Konzept wurde eine Bibliothek an eukaryotischen Kinaseinhibitoren auf eine Aktivität gegen *Staphylococcus aureus* Bakterien getestet. Dieser Phänotyp-basierte Ansatz identifizierte Sorafenib, ein zugelassenes Krebsmedikament, als antibiotisch wirksam gegen *S. aureus* Bakterien sowie gegen mehrere multiresistente klinische Isolate. Untersuchungen zur Struktur-Wirkungsbeziehung etablierten charakteristische Struktur motive der Sorafenib-Grundstruktur als essentiell für die antibiotische Aktivität und führten zu einem optimierten Derivat – **PK150** – mit einer minimalen Hemm-Konzentration von 300 nM gegenüber multiresistenten *S. aureus* Bakterienstämmen. Darüber hinaus zeigte **PK150** antibiotische Wirksamkeit gegenüber weiteren grampositiven Krankheitserregern, wie zum Beispiel Mykobakterien und Vancomycin-resistenten Enterokokken. Eine Resistenz von *S. aureus* Bakterien gegenüber **PK150** konnte in situ nicht erzeugt werden. **PK150** zeigte eine bakterizide Wirkweise und war in der Lage schwierige Persistierbakterien zu töten sowie bestehende Biofilme aufzulösen. Eine in vivo Beurteilung des pharmakokinetischen und –dynamischen Profils zeigte eine gute orale Bioverfügbarkeit sowie eine effektive Wirksamkeit von **PK150** in Tiermodellen mit *S. aureus* infizierten Mäusen, wengleich eine Dosis-limitierende Toxizität beobachtet wurde.

Parallel hierzu erfolgte die Identifizierung von potentiellen Proteintargets mit Hilfe einer Sorafenib-basierten Photosonde. Diese AfBPP-basierten Experimente in *S. aureus* Bakterien zeigten eine mögliche Bindung von Sorafenib zu mehreren Proteinen, insbesondere zur Type I Signalpeptidase (SpsB), einer membrangebundenen Serinprotease, welche essentiell in der Proteinsekretion ist, auf. In weiterführenden biochemischen Untersuchungen konnte eine Stimulierung der proteolytischen Aktivität von SpsB durch Sorafenib und **PK150** gezeigt werden. Diese Stimulierung war weitestgehend im Einklang mit den Ergebnissen der phänotypisch etablierten Struktur-Wirkungsbeziehung und resultierte in situ in einem deutlichen Anstieg in der Sekretion von SpsB-abhängigen extrazellulären Proteinen. Dies ist beachtlich, da hierdurch die normalerweise präzise regulierte bakterielle Proteinsekretion dysreguliert wird. Wengleich es schwierig ist, den genauen Wirkungsmechanismus auf einen einzelnen Targetpathway zurückzuführen und die beobachteten antibiotischen Effekte auf ein Multitarget-Profil schließen lassen, ist es denkbar, dass eine Dysregulierung der bakteriellen Sekretionsmaschinerie zur antibiotischen Aktivität von **PK150** beiträgt.

## 1. INTRODUCTION

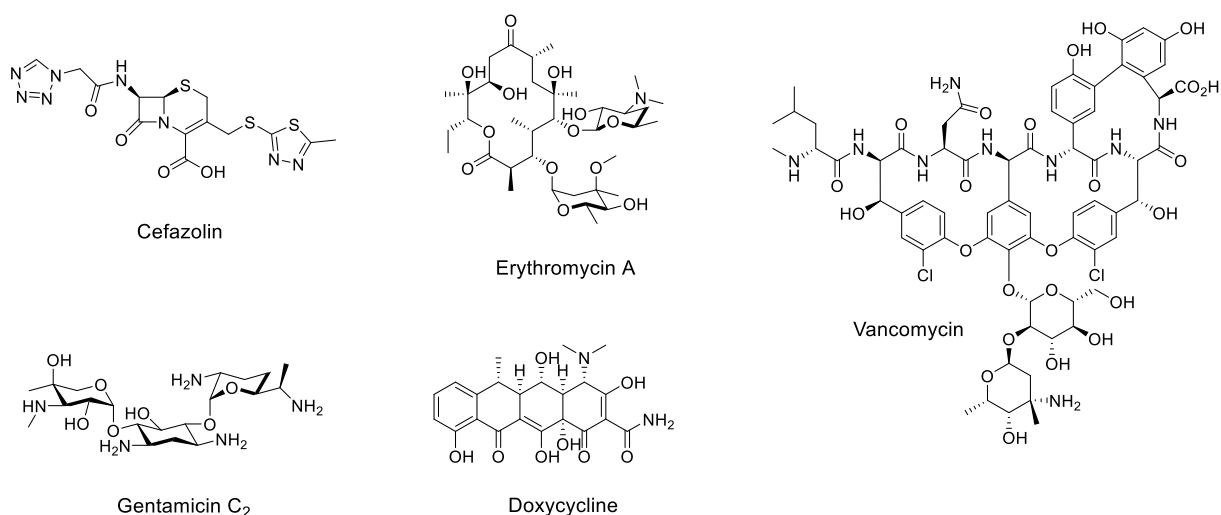
### 1.1. ANTIMICROBIAL RESISTANCE – A SEVERE GLOBAL HEALTH CHALLENGE

Antibiotics laid the foundations for unprecedented medical and social developments over the past decades and are more than ever vital to all facets of modern medicine. Globally, they have saved countless lives and have enabled significant advances in modern medicine – major surgery, organ transplantation, treatment of premature babies, cancer chemotherapy, and treatment of chronic diseases would not have been possible without the availability of effective treatment for bacterial infections.<sup>1</sup> However, the rapid emergence of antibiotic-resistant pathogens combined with an increased aggressiveness thereof has endangered these achievements and has resulted in a dramatic rise of severe and often fatal bacterial infections. A conservatively estimated 25,000 people die annually from antibiotic-resistant bacteria in Europe,<sup>2</sup> and more than two million people are infected with antibiotic-resistant bacteria in the United States annually with at least 23,000 die as a direct result.<sup>3</sup> As resistances are evolving fast and are spreading rapidly existing clinical relevant antibiotics continue to lose their effectiveness and there have been reports about pathogenic strains resistant to all currently available antibiotics.<sup>3-5</sup> The continuing antibiotic resistance crisis is understood to be correlated to a liberal and widespread use of antibiotics as a result of inappropriate and extensive medication as well as arbitrary use in farming and livestock. In addition, a significant drop in antibiotic research activities by the pharmaceutical industry in recent years has aggravated the situation. As a consequence the invigoration of this old foe threatens to return the treatment of bacterial infections to what the World Health Organization (WHO) has called a “post-antibiotic era”.<sup>6</sup> In this clinicians may no longer have access to reliable treatment options for infected patients and therefore, common bacterial infections may once again be life-threatening.<sup>6</sup> In this light it is highly alarming that there has been resistance reported against all antibacterial drugs that the WHO has recommend to keep in reverse as the last treatment option in situations where all other antimicrobials have failed.<sup>7</sup> These include aztreonam<sup>8</sup>, fosfomycin<sup>9</sup>, tigecycline<sup>10</sup>, daptomycin<sup>11</sup>, polymyxins (e.g. colistin<sup>12-13</sup>), oxazolidinones (e.g. linezolid<sup>14</sup>) and 4<sup>th</sup> and 5<sup>th</sup> generation cephalosporins (e.g. cefepime<sup>15</sup> and ceftaroline<sup>14</sup>, respectively).

To fight the successive waves of resistant bacteria, new chemical scaffolds either from natural or synthetic origin that address novel, resistance-free pathways are urgently needed. This combined with a deeper understanding of resistance mechanisms, methodological innovation as well as alternative approaches display key elements in response to the continuing bacterial threat.

### 1.1.1. History of Antibiotics

Historically, the beginning of the modern “golden antibiotic era” is often associated with the name of Sir Alexander Fleming. Here, it should be noted that there is evidence for effective treatment of microbial infections with antibiotic substances in ancient Egypt, Greece, China and other places of the world.<sup>16</sup> Following Alexander Fleming’s breakthrough discovery of penicillin in 1928<sup>17</sup> and its introduction into clinical use in the 1940s, the “golden era” of antibiotic discovery peaked in the 1950s, discovering lifesaving drug classes with many of them of natural origin. Among these were the cephalosporins (e.g. cefazolin), the macrolides (e.g. erythromycin A), the glycopeptides (e.g. vancomycin), the tetracyclines (e.g. doxycycline) and the aminoglycosides (e.g. gentamicin; Figure 1.1).<sup>18</sup> These discoveries revolutionized medical practice and offered successful treatment to previously untreatable and often fatal diseases associated with bacterial infections.



#### Antibiotics derived from natural products

#### Antibiotics of synthetic origin

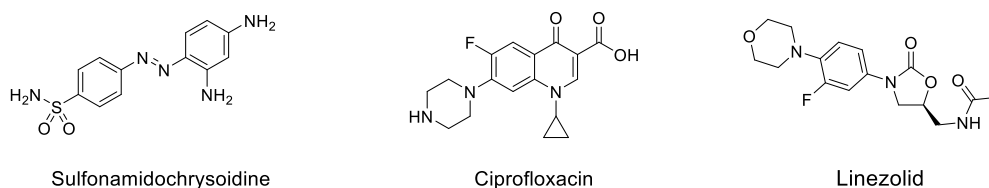


**Figure 1.1.** Antibiotics of natural and pure synthetic origin, respectively.

Compared to natural products relatively few antibiotic scaffolds are purely synthetic in origin (Figure 1.1). Aromatic sulfa scaffolds originated from the dye industry in the 1930s represent one example. These sulfonamide drugs, such as sulfonamidochrysoidine (prontosil)<sup>19</sup>, a prodrug that is metabolized to sulfanilamide, were the first broad-spectrum antibacterial agents in clinical use, even before the clinical introduction of penicillin during World War II.<sup>16</sup> Other examples of synthetically derived antibiotic scaffolds successful in clinical use are given by

quinolones (e.g. ciprofloxacin) that were first introduced into clinical practice during the 1960s, and the oxazolidinone linezolid, approved by the FDA in 2000.<sup>20</sup>

Following the “golden era”, synthetic tailoring of existing antibiotic scaffolds has characterized the subsequent era of medicinal chemistry and has resulted in successive generations of penicillins, cephalosporins, quinolones, macrolides and tetracyclines.<sup>20</sup>

Despite extensive research and development efforts, most antibiotics approved for clinical use are still derived from a limited number of structural classes that were discovered by the mid-1980s. This is highly alarming as resistance to one antibiotic often leads to resistance to multiple antibiotics within the same class (Chapter 1.1.2). In this light it is concerning to notice that the discovery rate of new clinically relevant antibiotic classes has dramatically slowed down from the 1980s onwards (Figure 1.2 A) prompting the WHO to underscore the urgency for novel antimicrobial agents against certain bacterial pathogens<sup>21</sup> (Figure 1.2 B). Of the 30 new antibiotics that have been approved in the period of 2000 to end-2015, only five are defined as members of a novel class: The synthetic oxazolidinone linezolid (approved in 2000), the natural occurring lipopeptide daptomycin (approved in 2003), retapamulin as a member of the terpenoid pleuromutilins (approved in 2007), the macrocyclic natural product fidaxomicin (approved in 2011) and the synthetic diarylquinoline bedaquiline (approved in 2012).<sup>22</sup> Strikingly, all these antibiotics possess Gram-positive activities only.

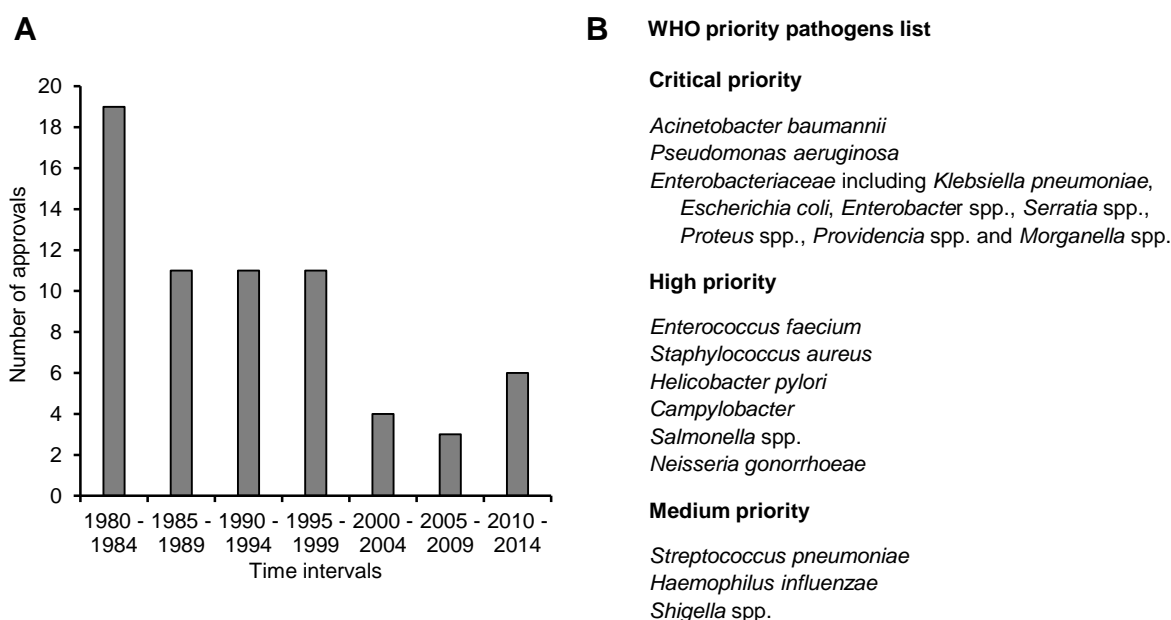


**Figure 1.2.** (A) Number of antibacterial drugs approved by the FDA per 5-year period. This figure is adapted from a report by Ventola.<sup>23</sup> (B) WHO list of bacteria that pose the greatest threat to human health categorized according to the urgency for new antibiotics.<sup>21</sup>

As few early stage candidates diminish the prospects of future approvals, the innovation gap is further widening.<sup>22, 24</sup> This trend is partly related to the fact that several major drug companies

have scaled back or abandoned their antibiotic research as they are faced with poor discovery prospects, increasingly stringent regulatory criteria for the approval of new drugs and diminishing returns on investment.<sup>25</sup> How threatening the current situation is can be highlighted by the reintroduction of polymyxins, an old class of cationic, cyclic polypeptide antibiotics (namely polymyxin B and polymyxin E (colistin)) to clinical practice in recent years.<sup>12-13</sup> These natural product antibiotics were originally abandoned due to toxicity issues (common and serious nephrotoxicity and neurotoxicity) in the early 1980s.<sup>12-13</sup>

### **1.1.2. Modes of Action and Resistance Mechanisms**

#### **Antibiotic targets**

Historically, the treatment of bacterial infections by antibiotics has been a target-poor therapeutic area. Given the enormous number of molecules with antibiotic properties it is surprising that the main classes of antibacterial drugs address only a limited set of target pathways (Figure 1.3; Table 1.1): These include (a) the peptidoglycan/cell wall biosynthesis that is targeted by  $\beta$ -lactam antibiotics, such as penicillins and cephalosporins, or glycopeptides, e.g. vancomycin;<sup>26</sup> (b) the disruption of membrane integrity by antibiotics like daptomycin;<sup>27</sup> (c) the DNA/RNA replication and repair with most antibiotics targeting the DNA gyrase (e.g. quinolones) and RNA polymerase (e.g. rifamycins);<sup>27-28</sup> (d) protein biosynthetic pathways with most antibiotic drugs targeting the ribosome, the protein-synthesizing factories of the cell, such as linezolid or tetracycline antibiotics;<sup>29</sup> (e) and the folate coenzyme biosynthesis that is blocked by sulfonamides, for example.<sup>30</sup>

#### **Resistance mechanisms**

The narrow scope of target pathways exploited by antibiotics makes it easy for bacteria to escape antibiotic therapy by resistance acquisition. Examples thereof are known since the first days of antibiotic treatment. Already in 1946, Sir Alexander Fleming noted that “there is probably no chemotherapeutic drug to which in suitable circumstances the bacteria cannot react by in some way acquiring ‘fastness’ [resistance].”<sup>31</sup> While Fleming himself characterized several staphylococcal isolates that were insensitive to penicillin, first resistant clinical isolates were observed shortly after penicillin’s clinical introduction in the 1940s.<sup>32-33</sup> Although the emergence of resistance has been reported for most antibiotics shortly after their widespread clinical use (Table 1.1), vancomycin is often regarded as an exception: Here, first resistant strains of enterococci were reported in Europe by 1986 and in the United States by 1987, roughly 30 years after its introduction to clinical practice.<sup>34-35</sup> This delayed emergence of resistance, however, has to be seen in the context that a dramatic increase in vancomycin’s clinical use only occurred from the early 1980s onwards.<sup>36</sup>

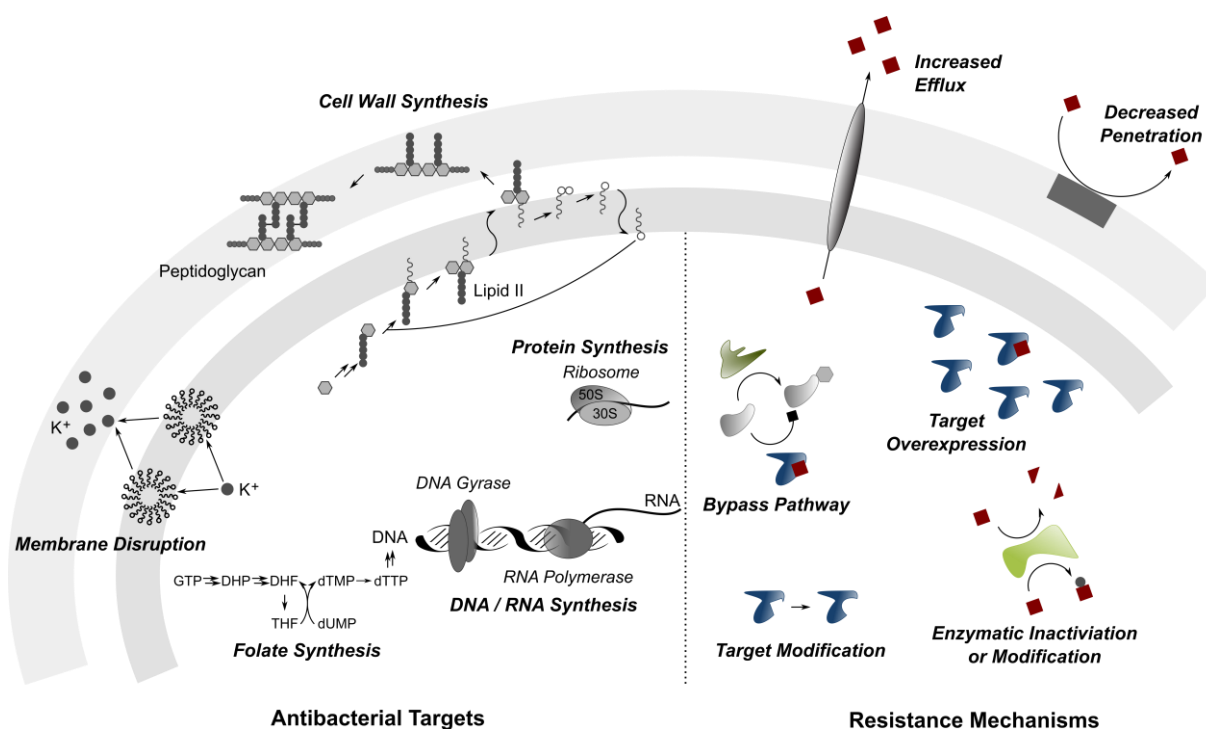


**Figure 1.3.** Antibacterial target pathways and how bacteria evade antibacterial treatment. This figure was modified from previous reports by Walsh et al.<sup>20</sup> and Lewis<sup>37</sup>.

**Table 1.1.** Evolution of resistance to antibiotics in clinical use. This table was modified from previous reports by Palumbi<sup>38</sup>, Walsh et al.<sup>20</sup> and Lewis<sup>37</sup>.

| <i>Antibiotic drug</i>    | <i>Year of clinical introduction/approval</i> | <i>Year of resistance observed (clinic)</i> | <i>Molecular target</i>               |
|---------------------------|---|---|---------------------------------------|
| Sulfonamides              | 1930s   | 1940s <sup>38</sup>                         | Dihydropteroate synthase              |
| Penicillin <sup>a</sup>   | 1940s   | 1946 <sup>32</sup>                          | Cell wall biosynthesis                |
| Streptomycin <sup>a</sup> | 1947  | 1960s <sup>39-40</sup>                      | 30S ribosomal subunit                 |
| Chloramphenicol           | 1949  | 1959 <sup>38</sup>                          | 50S ribosomal subunit                 |
| Tetracycline              | 1950s   | 1953 <sup>41</sup>                          | 30S ribosomal subunit                 |
| Erythromycin              | 1952  | 1968 <sup>42</sup>                          | 50S ribosomal subunit                 |
| Vancomycin                | 1958  | 1986 <sup>34</sup>                          | Cell wall biosynthesis                |
| Methicillin               | 1960  | 1961 <sup>43</sup>                          | Cell wall biosynthesis                |
| Ampicillin                | 1961  | 1962 <sup>44</sup>                          | Cell wall biosynthesis                |
| Cephalosporins            | 1960s   | late 1960s <sup>38</sup>                    | Cell wall biosynthesis                |
| Nalidixic acid            | 1964  | 1966 <sup>45</sup>                          | DNA gyrase / topoisomerase IV         |
| Fluoroquinolones          | 1980s   | 1980s <sup>20, 46</sup>                     | DNA gyrase / topoisomerase IV         |
| Linezolid                 | 2000  | 2001 <sup>47-48</sup>                       | 50S ribosomal subunit                 |
| Daptomycin                | 2003  | 2004 <sup>11</sup>                          | Cell membrane (depolarization)        |
| Retapamulin <sup>b</sup>  | 2007  | 2007 <sup>49-50</sup>                       | 50S ribosomal subunit                 |
| Fidaxomicin               | 2011  | 2011 <sup>51</sup>                          | RNA polymerase                        |
| Bedaquiline <sup>c</sup>  | 2012  | 2014 <sup>52</sup>                          | F <sub>1</sub> F <sub>0</sub> -ATPase |

<sup>a</sup> Limited use prior to widespread clinical usage stated here; <sup>b</sup> approved for topical use only; <sup>c</sup> approved only for use in combination therapy for treatment of multi-resistant tuberculosis.

Resistance to certain antibiotics can be an intrinsic feature of bacteria as a result of structural or functional characteristics.<sup>53</sup> In particular, Gram-negative bacteria possess intrinsic resistances to many classes of antibacterial compounds that are often related to the permeability barrier presented by the outer membrane and/or the action of efflux pumps. In addition to intrinsic resistance, bacteria are endowed by nature with the ability to acquire or develop resistances. Over millennia, they have elaborated several general mechanisms in order to survive antibacterial exposure (Figure 1.3):<sup>5, 53-54</sup> These include the reduction of effective antibiotic concentrations within the cell (a) by altered cell wall/membrane permeability – e.g. mechanisms affecting the barrier properties of the outer membrane lipid bilayer or the expression and/or function of porin channels, such as downregulation or replacement by more selective channels;<sup>55</sup> or (b) by enhanced efflux pump expression – e.g. active efflux mediates resistance to tetracyclines, chloramphenicol and fluoroquinolones;<sup>55-56</sup> (c) the inactivation of antibiotic agents by enzymatic mechanisms – e.g. diverse  $\beta$ -lactamases hydrolyze penicillins and cephalosporins, and modifying enzymes, like acetyltransferases, phosphotransferases and nucleotidyltransferases, inactivate aminoglycosides, such as streptomycin and gentamicin;<sup>57</sup> and (d) the modification of the antibiotic target by genetic mutation or post-translational modification to lower their susceptibility to antibiotics – e.g. resistance to linezolid is based on alterations of its 23S rRNA ribosomal subunit target.<sup>58</sup>

While a single resistance mechanism generally results in protection against a certain antibacterial compound or members within the same class, bacteria can accumulate multiple resistance genes, each encoding for a single resistance mechanism, resulting in multidrug resistance collectively.

### **Resistance is mobile**

Drug resistance is mobile as all bacteria are endowed by nature with the ability to exchange genetic information (horizontal gene transfer, HGT). The acquisition of foreign, mobile genetic elements, such as plasmids, transposons, integrons and bacteriophages, is accomplished through the processes of transformation (via incorporation of free DNA segments into the chromosome), conjugation (via plasmids and conjugative transposons) or transduction (via infection by bacteriophages).<sup>5</sup> Hereby, genetic transfer occurs not only among bacteria within the same species or genus but also among taxonomically different groups, including transfer between Gram-positive and -negative bacteria.<sup>59</sup>

Many antibiotics in clinical use today are originated from antibiotic-producing microorganisms that have exposed species in their local environment to these antimicrobial molecules. The need for self-protection of the antimicrobial producer species as well as the resulting constant selection pressure for the others are probably the source of many antibiotic resistance genes that contribute in large measure to the resistome.<sup>53, 60-61</sup> Furthermore, the

resistome is not limited to genetic information encoding resistance to purely naturally occurring antimicrobials as for example, the spread of resistance to quinolone antibiotics through plasmid-mediated transfer has been reported.<sup>62</sup> A direct link between resistance found in human pathogens and this environmental reservoir of resistance genes has been shown recently.<sup>63</sup> An accumulation of these genes in foodborne and farm-soil bacteria<sup>61, 64-66</sup> as well as bacteria found in antibiotic-producing factory effluents and waste water treatment plants<sup>61, 67-68</sup> stresses the downside of today's widespread use of antibiotics and demonstrates how this constant antibiotic pressure impacts the prevalence, diversity, mobility and spread of resistance encoding genes. In this context, a contribution of the human microbiome to this resistance reservoir has been discussed.<sup>69</sup> In particular, gastrointestinal organisms, which are continuously exposed to antimicrobials either by antibiotic treatment or by ingestion of food, are suspected to accumulate resistance genes.<sup>69</sup>

### **1.1.3. Methicillin- and Vancomycin-Resistant *Staphylococcus Aureus***

Gram-positive *S. aureus* is frequently colonizing the anterior nares of the human nose, the human respiratory tract, and skin where it acts as a commensal bacterium. However, it also acts as an opportunistic human pathogen causing infections that range from minor skin and wound infections to severe, life-threatening pneumonia, endocarditis, osteomyelitis and sepsis infections.<sup>70</sup> Consequently, *S. aureus* is considered as one of the highest of all bacterial threats emphasized by its categorization to the multi-resistant ESKAPE organisms (*Enterococcus faecium*, *Staphylococcus aureus*, *Klebsiella pneumoniae*, *Acinetobacter baumannii*, *Pseudomonas aeruginosa* and *Enterobacter* species).<sup>71</sup>

### **Antibiotic treatment of MRSA- and VRSA-associated infections**

Historically, penicillin and methicillin provided effective treatment for staphylococcal infections since their clinical introduction in the 1940s and 1960s, respectively. However, since the emergence of strains resistant to these antibiotics (late 1940s<sup>32</sup> and 1961<sup>43</sup>, respectively; Chapter 1.1.2, Table 1.1), in particular MRSA has spread and is found in virtually all hospitals worldwide. Today, MRSA displays one of the most common causes of healthcare-associated infections with 80,461 invasive bacterial infections resulting in 11,285 death in the United States in 2011.<sup>3</sup> While MRSA infections had mostly been confined to at-risk patients in health care settings, community-associated infections caused by MRSA (CA-MRSA) first emerged in the mid-1990s indicating the ability of MRSA to cause severe infections in otherwise healthy humans.<sup>72-73</sup> Until recently, most severe MRSA infections were treated effectively with vancomycin. However, first clinical strains with reduced susceptibility were isolated in 1996<sup>74</sup> and resistance to vancomycin (VRSA) was reported in a clinical setting in 2002<sup>75</sup>. Fortunately, these VRSA-associated infections are still rare cases with 13 reported VRSA infections in the

United States between 2002 and 2013, for example.<sup>3</sup> As there are only few treatment options available for severe MRSA- and VRSA-associated infections, which are often also characterized by resistance to multiple other antibiotics including quinolones, cephalosporins and macrolides,<sup>76</sup> MRSA and VRSA pose a serious if not urgent global health threat, emphasized by the WHO that currently ranked the need for novel antistaphylococcal drugs as high priority (Chapter 1.1.1, Figure 1.2 B).<sup>21</sup>

### **Biofilm formation and persister cells**

Adding to the challenge of multidrug-resistant *S. aureus* is a phenomenon termed persistence and biofilm formation. The ability of *S. aureus* to attach to implanted medical devices (e.g. central venous or urinary catheters, prosthetic heart valves, pace makers and orthopedic devices) and host tissue combined with the establishment of mature biofilms, is often a crucial factor in the persistence of chronic infections, such as osteomyelitis and endocarditis.<sup>77</sup> In these biofilms, bacteria encase themselves in a polymer-based matrix that consists of host factors, secreted and lysis-derived proteins, polysaccharides (mainly, polysaccharide intercellular adhesin (PIA), also known as polymeric *N*-acetyl-glucosamine (PNAG)) and extracellular DNA (eDNA).<sup>77</sup> This results in decreased susceptibility to immune defense mechanisms (e.g. macrophages or neutrophils)<sup>78</sup> and antibiotic treatment<sup>79</sup>, making biofilm-associated infections difficult to eradicate. In the case of affected medical implants, removal thereof often represents the only treatment option.<sup>80</sup> Biofilms are largely composed of a specific subpopulation of persister cells that are responsible for high levels of biofilm tolerance to antibiotics.<sup>81</sup> These persister cells form by differentiation from regularly growing bacteria by a stochastic process and in addition, in response to environmental factors, such as antibiotic stress.<sup>82-83</sup> Persister cells are dormant and show a reversible and substantial reduction in growth rates and metabolism resulting in the protection of cellular processes from antibiotic action.<sup>82-83</sup> While persister cells are not limited to biofilms, biofilms contain 100 to 1,000-fold more persisters than other planktonic cultures.<sup>82, 84</sup> Resuscitation, a process not fully understood to-date, enables persisters to reinitiate growth and repopulate biofilms after termination of antibiotic treatment and is seen as a main cause for the persistent and relapsing course of many bacterial infections.<sup>82</sup> Interestingly, the phenomenon of persistence is known since the first days of modern antibiotic treatment and was first described by Bigger in 1944, who observed cells in a “dormant, non-dividing phase” that were not affected by penicillin treatment.<sup>85</sup>

## **1.2. PHENOTYPIC AND TARGET-BASED SCREENING APPROACHES**

The end of the “golden era of antibiotic medicinal chemistry” (Chapter 1.1.1.) was combined with an encouraging prospect for future antibiotic discovery projects based on advances in the sequencing of the bacterial genome. Genomic approaches identified numerous essential

conserved bacterial proteins as starting points for target-based screening approaches as well as rational drug design.<sup>24</sup> However, these genomic-derived, target-based approaches largely failed to identify novel antibiotics.<sup>24</sup> In this light, phenotypic drug discovery (PDD) approaches experienced a recent revival. For example, the reemergence of natural product-based phenotypic screening efforts combined with advances in the cultivation of previously unculturable bacteria resulted in the discovery of new antibiotics of natural origin, such as teixobactin<sup>86</sup> or lugdunin<sup>87</sup>.

While classical target-based strategies rely on a deep knowledge of a specific, disease-related target and its role in an often complex and incompletely understood biological system or cellular signaling pathway, phenotypic-based approaches benefit from the ability to interrogate all possible target pathways in an unbiased physiological environment.<sup>88</sup> In addition, several potential target mechanisms can be addressed simultaneously.<sup>88</sup> Thereby, one of the major limitations of target-based approaches is avoided: The misconception of drug selectivity – the simplified “one drug, one target” paradigm – as many bioactive compounds are found to interact with multiple targets that contribute to the biological phenotype.<sup>89</sup> Moreover, the prospect of discovering first-in-class drugs is relatively high compared to target-based approaches as a strong contribution of phenotypic screenings to the discovery thereof has been shown recently.<sup>90</sup> Nevertheless, these phenotypic approaches depict considerable challenges including hit validation as well as target deconvolution and validation.<sup>88</sup> In particular the latter is essential for rational hit compound optimization as structure-activity relationship (SAR) studies based on a phenotypic readout only are complex and challenging as new derivatives may alter their specificity profile or even act by a different target mechanism – changes that might not reflect in a phenotypic readout.<sup>88</sup> Therefore, deconvolution of potential molecular targets of a phenotypic hit is essential for further medicinal chemistry optimization and rapid and reliable methods for target identification are fundamental.

### **1.3. ACTIVITY- AND AFFINITY-BASED PROTEIN PROFILING**

Various technologies from different areas have been developed to unravel molecular targets and target mechanisms of bioactive compounds identified by phenotypic screening approaches. In particular, genomic and proteomic-based platforms for target deconvolution have been widely applied and advanced in recent years.<sup>91-94</sup>

In general, chemical proteomics enable to effectively identify interactions between small molecules and their protein binding partners. These approaches are based on the direct application of bioactive molecules to reduce the enormous complexity of a whole proteome and thereby enable to zoom in on proteins that directly interact with these molecules. Classical affinity chromatography-based profiling approaches (also often referred to as compound-centric chemical proteomics) are accomplished by the modification of the bioactive molecule

with an affinity tag (e.g. biotin) or by direct immobilization thereof on a solid support (e.g. sepharose or agarose).<sup>92, 95</sup> Incubation of the resulting affinity probe with cell extracts leads to a reduction in complexity through direct and specific probe-protein interaction. Subsequent SDS-PAGE analysis or mass spectrometry measurement enables the identification of interacting proteins after elution from the solid support and proteolytic digestion.

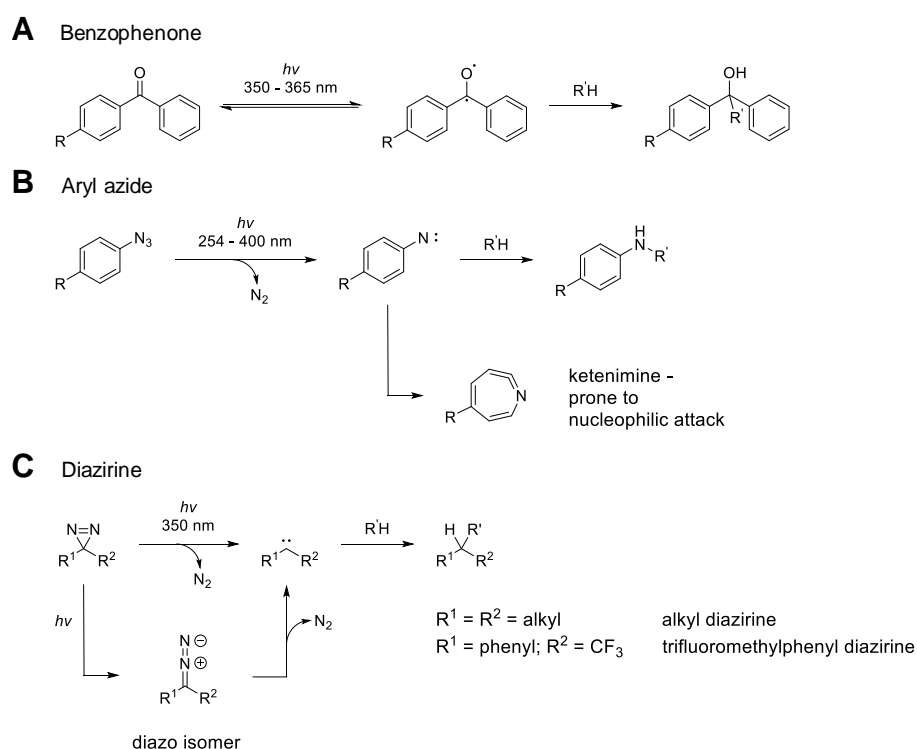
As an alternative to immobilized affinity chromatography-based profiling approaches that are restricted to the interrogation of cell lysates and are often limited by affinity issues due to the relatively weak and reversible nature of the probe-protein interaction,<sup>92, 95</sup> reactive probes can be employed. These reactive probes covalently attach to the active site of the target protein and are employed in a technology named Activity-Based Protein Profiling (ABPP), which is based on the work of Powers et al.<sup>96-97</sup> and was further improved and established by Cravatt et al.<sup>98-100</sup> and Bogyo et al.<sup>101-102</sup>. Combined with advances in separation and analytical strategies, in particular in high-performance mass spectrometry, ABPP has matured to a powerful and effective proteomic platform for rapid target deconvolution as well as enzyme classification in recent years. Furthermore, stable isotope labelling of proteins and peptides, respectively, added a quantitative dimension to mass spectrometric measurements.<sup>103-107</sup> Classically, ABPP enables the direct identification and functional characterization of enzymes or enzyme families based on a sensitive and selective readout of enzyme activity irrespective of protein abundances.<sup>108-109</sup> Diverse specific activity-based probes have been developed to identify, annotate and study several major enzyme classes. These include specific probes for hydrolases and proteases, kinases, phosphatases, histone deacetylases, glycosidases and various oxidoreductases.<sup>108-109</sup> Furthermore, these selective activity-based probes have enabled selectivity profilings of bioactive molecules targeting particular enzyme families. To this end, whole cells or lysates are treated with the molecule of interest, followed by selective labelling of the remaining enzymes utilizing respective activity-based probes.<sup>110-111</sup>

In the context of a more compound-centric approach, ABPP has been widely applied for the direct target deconvolution of an individual bioactive molecule in complex proteomes under nearly native *in vivo* conditions (e.g. physiological pH, endogenous abundance levels, post-translational modifications, presence of natural binding partners, such as proteins, nucleic acids, cofactors and endogenous small molecules).<sup>112-114</sup> Synthetic modification of the molecule of interest is required to give access to a functionalized analog bearing a reporter tag. Here, detailed knowledge of the structure-activity relationship (SAR) of the molecule of interest is fundamental as the synthetic modification should not significantly alter the bioactivity of the parent compound and should not disturb the compound-protein interaction. This reporter tag enables either visualization (e.g. via a fluorophore tag) or protein enrichment (e.g. via a biotin tag utilizing its strong interaction with immobilized avidin) and subsequent downstream proteomic applications. Inevitably, the steric demand of these tags adversely affects cellular

uptake, potency and probe size. However, small chemically traceable tags have overcome these limitations. In particular, small bioorthogonal terminal alkyne tags are used. They enable the attachment of an azide-containing reporter group via copper-mediated 1,3-dipolar cycloaddition (“click chemistry”) after *in vivo* incubation and cell lysis.<sup>115-118</sup> While some bioactive small molecules are endowed with a reactive group (e.g. electrophilic moieties like Michael-acceptor systems or  $\beta$ -lactones) that form a covalent bond upon binding to the target protein active site (e.g. by reaction with nucleophilic serine or cysteine residues within the active site),<sup>112-114</sup> most bioactive compounds interact with their protein binding partners in a reversible, non-covalent manner (Affinity-based Protein Profiling, AfBPP). Besides the synthetic modification by a traceable tag these molecules must be further equipped with a photocrosslinking moiety that upon UV irradiation converts the transient probe-protein interaction into a stable, covalent linkage.<sup>114</sup> This stable linkage provides the basis for subsequent *in vitro* protein enrichment and downstream MS-based target identification.

### Types of photocrosslinking functionalities

Three major types of photocrosslinking functionalities are frequently applied: Benzophenones, aryl azides and diazirines that can be grouped in phenyl and alkyl diazirines. These functional groups form highly reactive diradicals, nitrenes and carbenes, respectively, upon photoactivation to facilitate an irreversible binding (Scheme 1.1).



**Scheme 1.1.** Three widely applied photocrosslinking groups and their reactive intermediates: Benzophenone (A), aryl azide (B) and diazirine (C), namely alkyl and trifluoromethylphenyl diazirine.

As these functional groups differ in steric bulk and photochemical properties, including crosslinking efficacy and possible side reactions – factors that can adversely affect the analysis of the respective ligand-protein interaction – the choice of photocrosslinker type represents a crucial step. Benzophenone is rather bulky and its steric demand can negatively influence the affinity of the respective photoprobe towards its biological target. Photoactivation is accomplished by UV light of relatively long wavelengths (350 – 365 nm), which is in favor of minimal damage to biological systems.<sup>119</sup> The resulting reactive triplet diradical state reacts with C-H bonds in close proximity, but relaxes back to the ground-state in the absence thereof as it is not quenched by surrounding water (Scheme 1.1 A).<sup>119-120</sup> This reversibility, however, leads to long irradiation times that are often accompanied with non-specific labelling events.<sup>121</sup>

Incorporation of an aryl azide in the molecule of interest represents a small structural perturbation provided that the parent compound already accommodates an aryl ringsystem. However, UV light of short wavelength (< 300 nm) is often required for photoactivation, which is associated with an increased risk of photolytic damage to biological molecules due to photoinduced degradative chemical transformations.<sup>122</sup> Here it should be noted that appropriate substitution of the aryl ring, in particular by electron withdrawing groups, can shift the wavelength spectrum required for photoinduction to wavelengths greater than 320 nm.<sup>122-123</sup> Upon photoactivation reactive nitrenes are formed by the loss of N<sub>2</sub>. If no suitable reaction partner is in close proximity of this reactive species, rearrangement to the dehydroazepine/ketenimine species occurs as an undesired side reaction (Scheme 1.1 B).<sup>123-124</sup> Electrophilic dehydroazepine/ketenimine can be attacked by nucleophiles, still nitrene rearrangement is often linked to low crosslinking efficiency and non-specific crosslinking events.

Owing their small size that ensures minimal perturbation of ligand-protein interactions, phenyl diazirines, particularly the trifluoromethyl derivative, and alkyl diazirines are widely applied. Upon irradiation with UV light of a wavelength of around 350 nm – a wavelength associated with minimal photolytic damage to biological systems – diazirines are converted into highly reactive carbenes by the loss of N<sub>2</sub>.<sup>124-125</sup> This reactive species is of short half-life and readily inserts into any C–H or heteroatom–H bond nearby. However, the high reactivity of the diazirine-generated carbene is accompanied by quenching events through the reaction with surrounding water, thereby reducing its crosslinking efficiency.<sup>126</sup> On the other hand, these quenching events can be seen as beneficial as it minimizes non-specific binding. Crosslinking efficiencies are further reduced due to the isomerization of the diazirine to a linear diazo isomer, which is often generated in addition to the carbene species.<sup>125</sup> This long-lived electrophilic species decomposes to form either the reactive carbene species or the carbocation that is prone to nucleophilic attack (Scheme 1.1 C).<sup>125</sup> In the case of phenyl diazirines, introduction of a trifluoromethyl group in  $\alpha$ -position to the diazirine functionality stabilizes respective diazo isomer rendering it relatively inert towards nucleophilic attack.<sup>125, 127</sup>

### Gel-based activity- and affinity-based protein profiling

In a classical gel-based ABPP and AfBPP approach, whole cells are incubated with a cell-permeable probe equipped with a terminal alkyne and a photocrosslinking moiety, if required to facilitate irreversible binding to a protein target. In the case of AfBPP experiments, this incubation step is followed by irradiation with UV light. Subsequently, cells are lysed and labelled proteins clicked to an azide-containing fluorophore reporter group. The analytical step is completed by separation of labelled proteins via SDS-PAGE and visualization by fluorescence scanning (Figure 1.4).

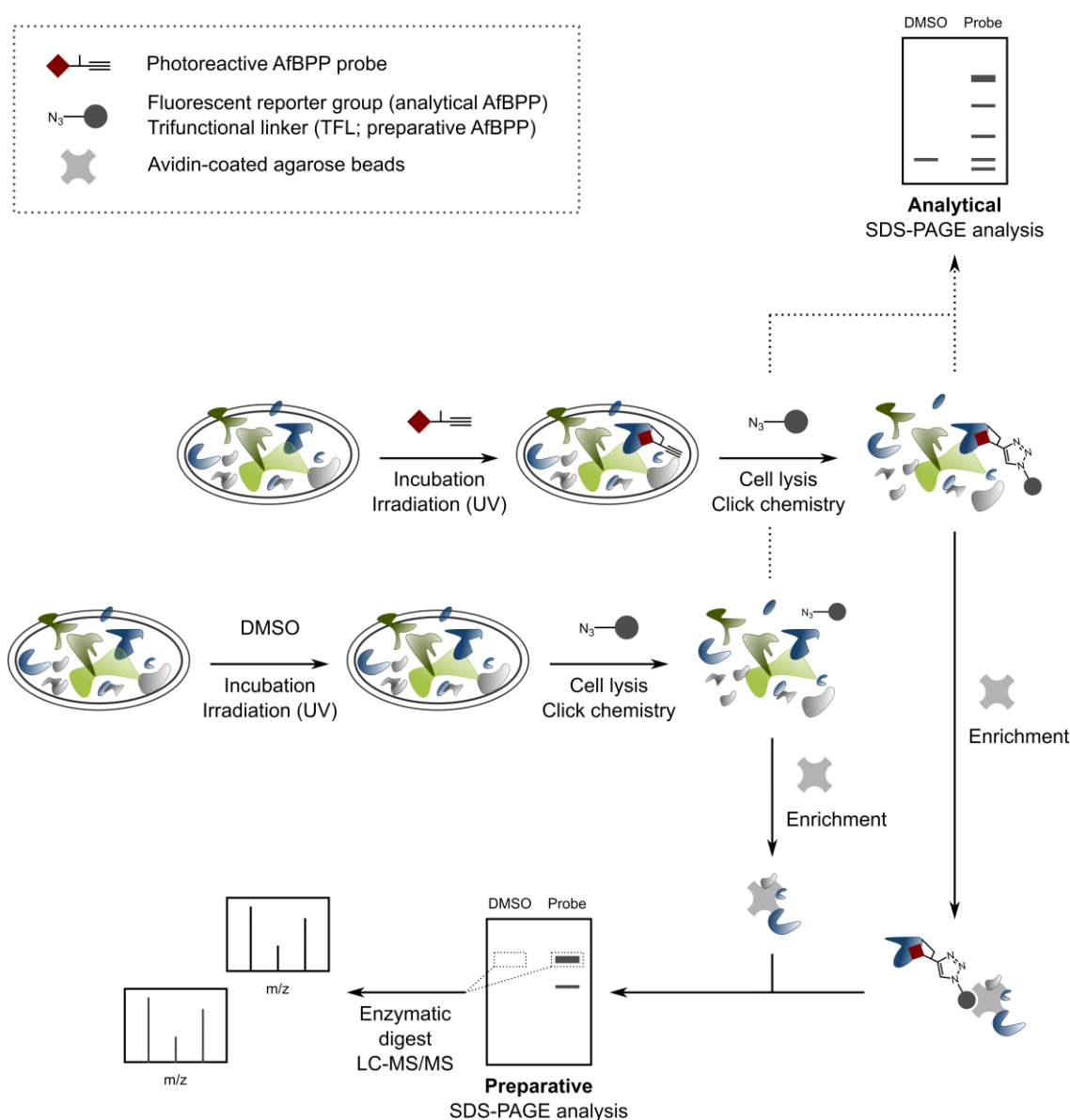


**Figure 1.4.** The concept of gel-based analytical and preparative ABPP and AfBPP.

For a mass spectrometry-based identification of potential protein binding partners, the analytical step needs to be further modified: After the initial labelling step and cell lysis, labelled proteins are clicked to a trifunctional linker,<sup>128</sup> which contains an azide for attachment via click

chemistry, a fluorophore for visualization and a biotin enrichment tag. Subsequent selective enrichment on avidin-coated beads reduces the enormous complexity of a whole proteome and is followed by separation of enriched and labelled proteins via SDS-PAGE and visualization by fluorescence scanning. Specific fluorescent bands of interest are isolated, respective proteins extracted, enzymatically digested and finally analyzed by high resolution mass spectrometry (Figure 1.4).

### Gel-free activity- and affinity-based protein profiling and quantitative proteomics

In recent years, gel-free approaches have become the gold standard in ABPP and AfBPP (Figure 1.5, 1.6). These techniques are based on the introduction of a quantitative dimension to mass spectrometric analysis by stable isotope labelling of proteins or peptides.<sup>103-107</sup> Stable isotope labels are commonly introduced into proteins or peptides metabolically or by chemical ways.<sup>107</sup> Stable isotope labelling by amino acids in cell culture (SILAC; Figure 1.5), first reported by Mann et al., represents a popular example for the metabolic labelling approach.<sup>104</sup> Here, isotopic labelling of proteins is achieved by metabolic incorporation of heavy isotopes in form of labelled auxotrophic amino acids ( $^{13}\text{C}$  and  $^{13}\text{C}^{15}\text{N}$ -labelled amino acids) during cell growth and division.

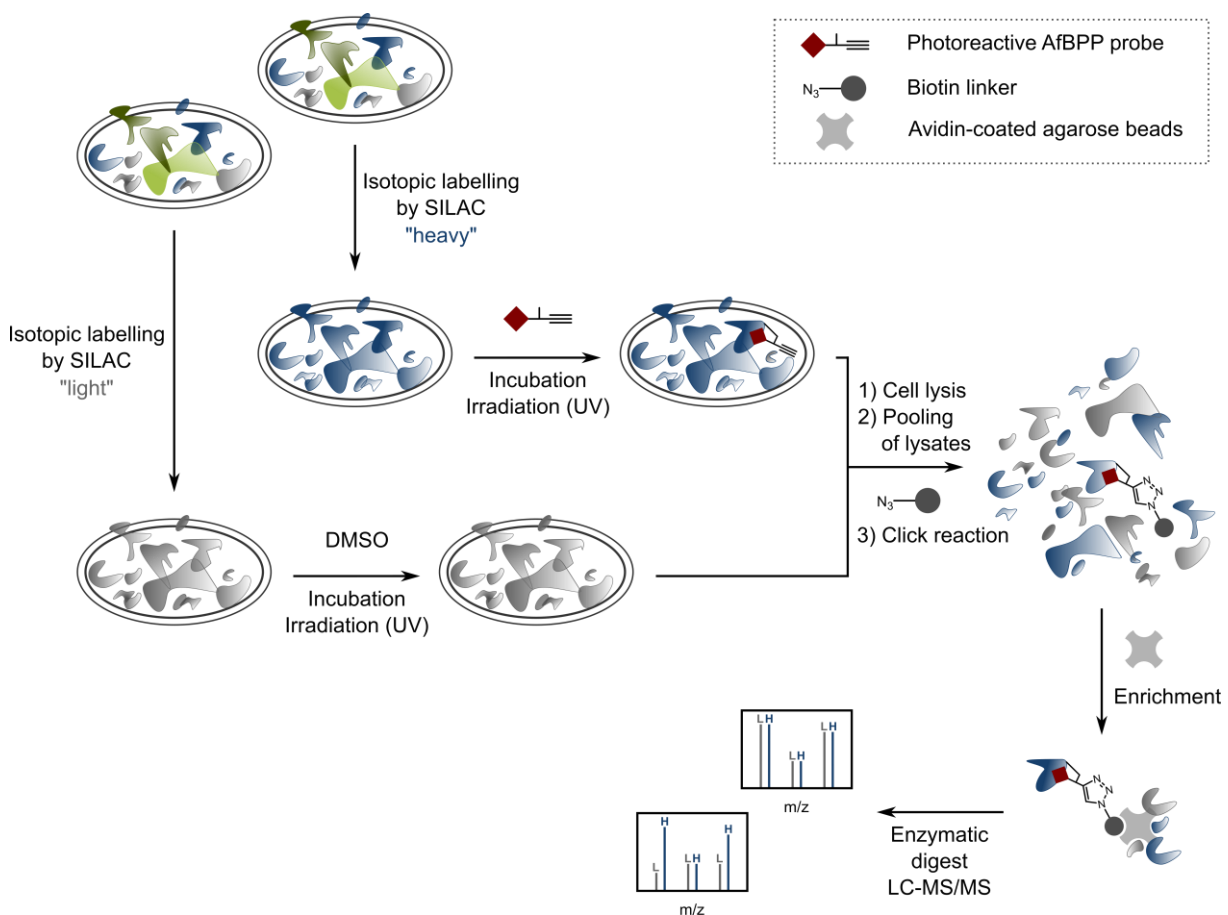


**Figure 1.5.** The concept of SILAC-based quantitative ABPP and AfBPP.

Alternatively, dimethyl labelling provides access to incorporating isotope labels in a chemical manner.<sup>103, 105</sup> This technique is employed in settings where metabolic implementation is challenging, e.g. in bacteria or tissue samples. While metabolic strategies like SILAC enable isotopic labelling at an early stage and thereby enable combination of differentially treated samples at the level of intact or lysed cells, dimethyl labelling is performed at a late stage after protein digest. Here, reagent mixtures of unlabelled and stable isotope-labelled cyanoborohydride and formaldehyde are employed to label primary amines in digested peptides, mainly at the *N*-terminus and the  $\epsilon$ -amino group of lysine.<sup>105</sup> Subsequently, differentially treated samples are combined directly before mass spectrometric measurement.

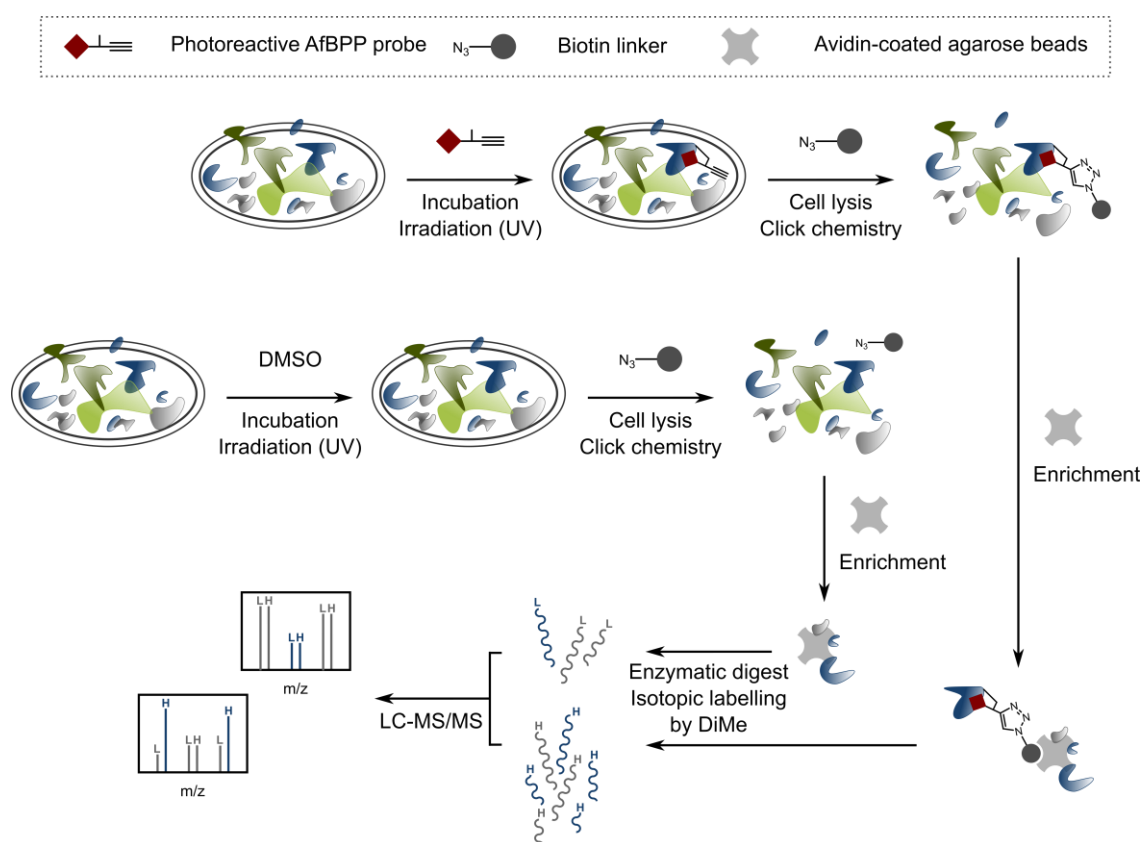


**Figure 1.6.** The concept of dimethyl labelling (DiMe)-based quantitative ABPP and AfBPP.

Label-free MS quantification represents an arising proteomic technique independent of isotopic labels. Here, quantification can be accomplished by comparing either the measured signal intensity of peptide precursor ions belonging to a protein or the number of counted fragment spectra identifying peptides of a protein.<sup>107</sup>

While these proteomic-based approaches provide powerful and effective platforms for the identification of potential protein binding partners of a bioactive molecule, the resulting target hypotheses still needs substantial proof of a direct compound-protein interaction as well as a direct link to the biological and/or pathological phenotype.



## 2. INSIGHTS INTO PHOTOCROSSLINKER-ASSOCIATED OFF-TARGET PROTEIN BINDING

The following chapter is based on data published in:

**P. Kleiner\***, W. Heydenreuter\*, M. Stahl\*, V. S. Korotkov, S. A. Sieber. A Whole Proteome Inventory of Background Photocrosslinker Binding. *Angew. Chem. Int. Ed.* **2017**, *56*, 1396. \*These authors contributed equally to this work.

W. Heydenreuter. Target identification of natural products by activity based protein profiling and a whole proteome inventory of background photocrosslinker binding. Dissertation, Technische Universität München, **2016**.

P. Kleiner, W. Heydenreuter, M. Stahl and S. A. Sieber designed experiments and interpreted results. P. Kleiner, W. Heydenreuter and V. S. Korotkov synthesized photocrosslinker probes and control compounds. P. Kleiner and W. Heydenreuter performed gel- and mass spectrometry-based labelling experiments. P. Kleiner and M. Stahl analyzed data. M. Stahl developed and created overlays and conducted bioinformatic analysis.

## 2.1. NON-SPECIFIC CROSSLINKING EVENTS IN PHOTOAFFINITY LABELLING

The concept of photoaffinity labelling (PAL) introduced by Westheimer et al. in the early 1960s<sup>129</sup> has laid the foundations for detailed studies on different types of transient, non-covalent ligand-protein interactions under native conditions, including protein-protein, nucleic acid-protein, carbohydrate-protein, peptide-protein and small molecule-protein interactions.<sup>114, 121, 126, 130-133</sup> In particular analysis of transient small molecule-protein interactions represents a prominent application of this methodology as it is frequently used in medicinal chemistry and chemical biology for the deconvolution of protein targets of bioactive molecules (AfBPP, Chapter 1.3).<sup>121, 125, 131, 133</sup>

Since Westheimer, who used diazocarbonyl derivatives of the molecule of interest as photoprobes, various photoreactive groups have been developed. Three major types are frequently applied in AfBPP: Benzophenones, aryl azides and diazirines that can be grouped in phenyl and alkyl diazirines (photocrosslinker types, Chapter 1.3). In particular alkyl diazirines enjoyed a recent revival after reports by Taunton et al.<sup>134-135</sup>, Yao et al.<sup>136-138</sup> and Cravatt et al.<sup>139-140</sup> demonstrated suitable properties thereof for successful protein labelling in AfBPP. Furthermore, the introduction of a “minimalist terminal alkyne-containing diazirine photocrosslinker” – an “all-in-one” linker containing a photoreactive diazirine moiety, a traceable terminal alkyne and a functional group – by Yao et al.<sup>138</sup> provided easy access and rapid incorporation of all functionalities required for AfBPP into the molecule of interest and thereby further encouraged their application. Recent comparative studies on different photoreactive groups with a focus on crosslinking reactivity, selectivity and efficiency, underscored the beneficial properties of alkyl diazirines.<sup>141-142</sup> In addition, these studies highlighted a general and known problem of photocrosslinker-based proteomic experiments: Ligand-independent reactivity – a phenomenon that is directly correlated to unspecific background binding. Here, photochemical properties like the reversible nature of the reactive species formation (benzophenones) or side reactions yielding less reactive electrophilic byproducts (aryl azides and diazirines) contribute to unspecific crosslinking events as they do not necessarily facilitate a crosslink within the residence time of the binary photoprobe-protein complex.<sup>141</sup> Besides these intrinsic photochemical properties, experimental parameters like high photoprobe concentrations or long irradiation times are reported to result in low selectivity and high background binding.<sup>141</sup> Consequently, optimization of experimental settings is recommended as well as competition experiments with an excess of the unmodified parental ligand to distinguish specific from non-specific labelling.<sup>135</sup> However, these competition experiments are hampered by the fact that the reversible binding of the unmodified parental ligand to its protein target is discriminated in comparison to the irreversible nature of the photoprobe-protein complex upon irradiation. Therefore, minimal probes lacking the ligand

specific structure are often used to account for non-specific photocrosslinker-associated off-target binding.<sup>138, 141</sup>

Although the phenomenon of non-specific background labelling is recognized as a major obstacle for the interpretation of AfBPP data, little is known about the nature and identity of photocrosslinker-associated off-target binding. This, however, is important given the high sensitivity of modern high resolution mass spectrometry that is capable of reporting minimal amounts of labelled proteins. Recent gel-based approaches by Park et al. identified few proteins that were associated with non-specific background binding.<sup>143-144</sup> However, it remained elusive whether these 2D-SDS-PAGE-based efforts were able to review the full spectrum of background protein binders, in particular with regard to quantitative, gel-free proteomics – the state-of-the-art technology.

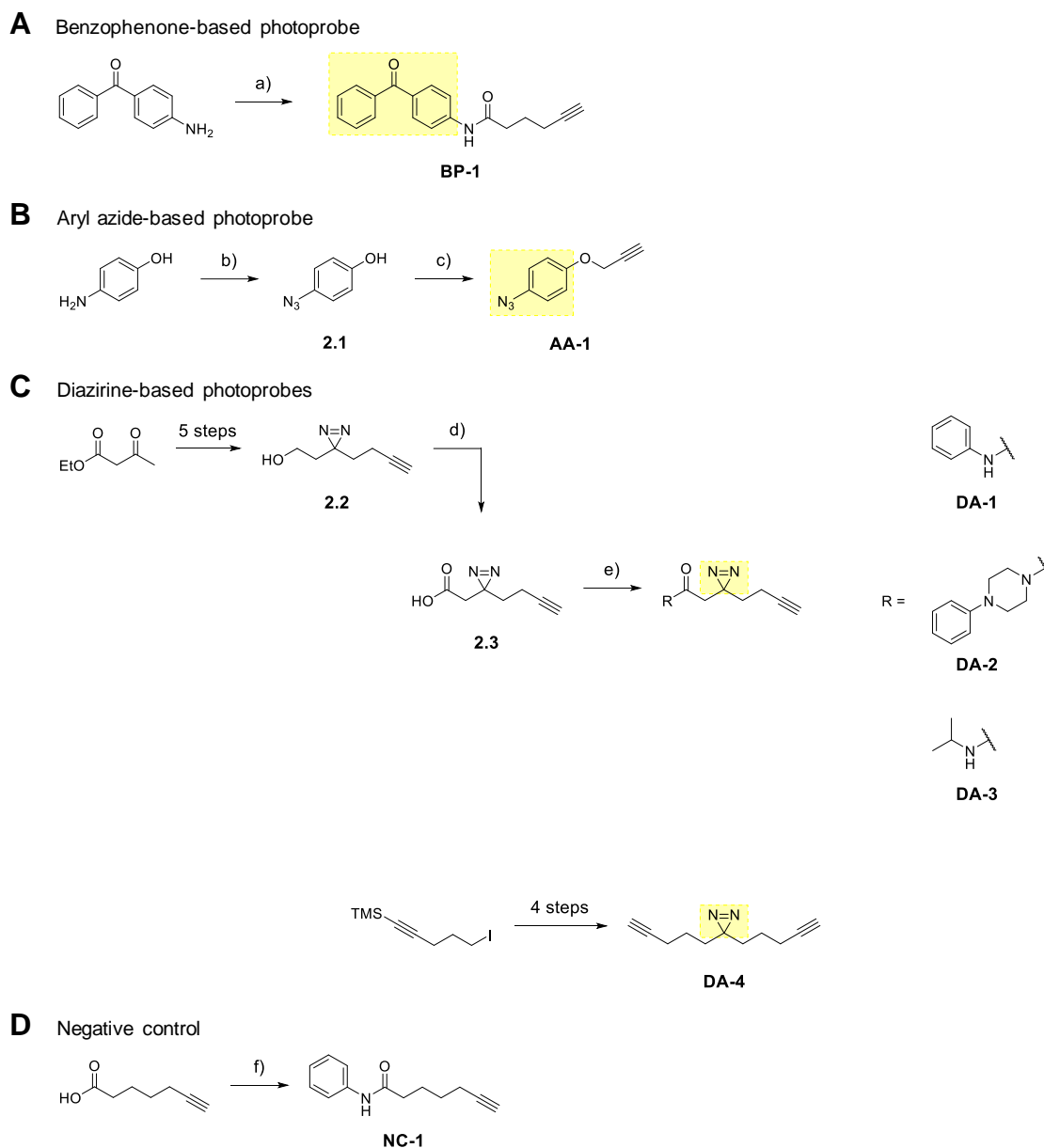
## 2.2. RESULTS AND DISCUSSION

In order to account for the characteristic features of modern quantitative, gel-free proteomics a systematic investigation of non-specific photocrosslinker-associated protein labelling profiles (photome) in different human cell lines was conducted.

To broaden the photome spectrum beyond human cell lines, the background labelling of diazirine-containing minimal photoprobes in the proteome of Gram-positive *S. aureus* is covered in Chapter 3.2.2.3.

### 2.2.1. Design and Synthesis of Minimal Photoprobes

Three widely applied photoreactive groups – benzophenone, aryl azide, and alkyl diazirine (photocrosslinker types, Chapter 1.3) – were chosen on the basis of different functionality and structural diversity. These photoreactive functionalities were incorporated into simple molecular scaffolds equipped with a terminal alkyne for subsequent downstream proteomic analysis. Due to the focus on ligand-independent reactivity, the design of these minimal photoprobes tried to reduce specific ligand-protein interactions to a minimum (Scheme 2.1). Benzophenone- and aryl azide-based minimal photoprobes **BP-1** and **AA-1**, respectively, were obtained by modification of the photoreactive aryl scaffold with a terminal alkyne tag via an amide linkage and a small aliphatic ether, respectively. Here, coupling of commercially available 4-aminobenzophenone and 5-hexynoic acid using standard peptide coupling conditions yielded **BP-1**, while direct propargylation of 4-azidophenol<sup>145</sup> (**2.1**) gave access to **AA-1** (Scheme 2.1 A, B). In order to enable a direct ligand-independent comparison, a diazirine-based minimal photoprobe (**DA-1**) was designed in a similar fashion by attaching a modified version of Yao's<sup>138</sup> “all-in-one” minimalist diazirine photocrosslinker (**2.3**) to a simple aryl scaffold (Scheme 2.1 C). This modified photocrosslinker version (**2.3**), which contains a carboxyl functionality for rapid incorporation into the scaffold of interest by robust peptide coupling, was obtained by direct oxidation of the respective hydroxyl derivative (**2.2**) originally reported by Yao et al.. In order to gain deeper insights into the off-target preferences of widely applied diazirine photocrosslinking moieties, diazirine photocrosslinker **2.3** was further embedded into various aliphatic and aromatic scaffolds. Standard peptide coupling of **2.3** with different primary and secondary amines gave access to minimal diazirine photoprobes **DA-2** and **DA-3**. **DA-4**, which was synthesized in four steps starting from 5-(iodopent-1-yn-1-yl)trimethylsilane as published previously,<sup>146</sup> completed the list of diazirine-based minimal photoprobes (Scheme 2.1 C). In addition, control probe **NC-1**, whose design is based on the **DA-1** scaffold without a photoreactive moiety, was synthesized to account for background labelling that is photocrosslinker-independent and might arise due to non-specific labelling during click reaction (Scheme 2.1 D).



**Scheme 2.1.** Design and synthesis of minimal photoprobes containing a benzophenone (**BP-1**; A), aryl azide (**AA-1**; B) or diazirine (**DA-1**, **DA-2**, **DA-3** and **DA-4**; C) photoreactive functionality as well as control probe **NC-1** (D) lacking a photoreactive moiety. Reaction conditions: a) 5-Hexynoic acid, oxalyl chloride,  $\text{NEt}_3$ , DMF, room temperature, 6 h, 69%; b) i)  $\text{NaNO}_2$ , HCl,  $\text{H}_2\text{O}$ ,  $0^\circ\text{C}$ ; ii)  $\text{NaN}_3$ ,  $0^\circ\text{C}$ , 5 h, 76%; c) NaH, propargyl bromide,  $0^\circ\text{C}$  – room temperature, 24 h, 69%; d) Jones reagent, acetone,  $0^\circ\text{C}$ , 2 h, 88%; e) amine, HOBt, EDC, DIPEA, DMF, room temperature, 16 h, 77% for **DA-1**, 89% for **DA-2** and 99% for **DA-3**; f) 6-heptynoic acid, HOBt, EDC, DIPEA, DMF, room temperature, 16 h, 92%.

### 2.2.2. Evaluation of Photocrosslinker-Associated Background Labelling by Gel-Based Affinity-Based Protein Profiling

Prior to in-depth mass spectrometry-based quantitative analysis, cell permeability as well as background labelling preferences of all minimal photoprobes were assessed by gel-based analytical AfBPP (gel-based AfBPP, Chapter 1.3). Minimal photoprobes as well as click control

probe **NC-1** were incubated with human A549 cells in situ (10  $\mu$ M; 1 h, 37°C), followed by irradiation with UV light of appropriate wavelengths (365 nm for benzophenone- and diazirine-based photoprobes, 300 nm for aryl azide-based photoprobe; 30 min, 4°C) to facilitate a covalent linkage with putative background binders. Cells were lysed, followed by click reaction with rhodamine azide and labelled proteins analyzed via SDS-PAGE. Subsequent fluorescent scanning resulted in distinct fluorescent bands for all photoprobes (Figure 2.1), in particular in the cytosolic fraction, thereby indicating sufficient cell permeability. Here it should be noted that cell lysis was performed using detergent-based lysis buffer that facilitates partial solvation of membrane proteins. Interestingly, benzophenone-based photoprobe **BP-1** revealed the strongest labelling among all probes tested. This observation is in line with previous reports that hold the reversible nature of the benzophenone-generated diradical responsible for unspecific labelling events (photochemical characteristics of benzophenone, Chapter 1.3).<sup>121, 141</sup> All diazirine-based minimal photoprobes showed moderate labelling and shared a similar labelling pattern, which indicated ligand-independent diazirine-associated protein binding in gel-based AfBPP. Among all minimal photoprobes, aryl azide probe **AA-1** revealed the slightest gel-based protein labelling. Protein binding was also observed with negative control **NC-1** lacking electrophilic or photo-inducible reactivity. Here, protein labelling might be the result of non-specific labelling during click reaction.

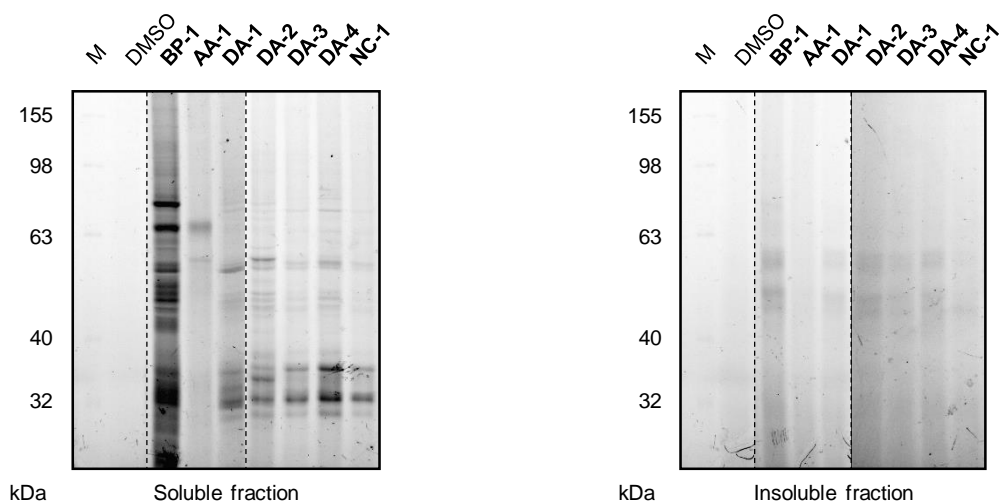


**Figure 2.1.** In situ analytical AfBPP labelling with minimal photoprobes containing a benzophenone (**BP-1**), aryl azide (**AA-1**) or diazirine (**DA-1**, **DA-2**, **DA-3** and **DA-4**) photoreactive functionality as well as control probe **NC-1** lacking a photoreactive moiety in A549 (10  $\mu$ M; incubation for 60 min, 37°C; irradiation for 30 min, 4°C).

### 2.2.3. Analysis of Photocrosslinker-Specific Protein Labelling Profiles via SILAC-Based Quantitative Proteomics

In order to introduce a quantitative and statistical dimension to the in-depth mass spectrometric analysis a gel-free approach based on the SILAC technology<sup>104</sup> was applied (SILAC-based AfBPP, Chapter 1.3). Two commonly used human cell lines, A549 and HeLa, were chosen as representative test systems and stable isotopes were metabolically introduced by cultivating cells in the presence of isotope labelled auxotrophic amino acids. In subsequent AfBPP experiments, photoprobe concentrations in the low  $\mu\text{M}$  range were used in order to reflect experimental conditions commonly applied in photocrosslinking studies. In accordance with standard AfBPP labelling procedures, isotope labelled intact cells were treated with either DMSO, minimal photoprobes (**BP-1**, **AA-1** and **DA-1**, respectively) or control probe **NC-1** (3  $\mu\text{M}$ ; 1 h, 37°C) and subsequently irradiated with UV light of appropriate wavelengths (365 nm for benzophenone- and diazirine-based photoprobes, 300 nm for aryl azide-based photoprobe; 30 min, 4°C). Cells were lysed, equal protein amounts of opposing isotopic states resulting from DMSO and probe-treated samples were pooled, followed by click reaction with biotin azide. Biotin-tagged proteins were enriched on avidin-coated beads and peptides released via digest with trypsin. Obtained peptides were measured on a high resolution LC-MS/MS instrument and analyzed using MaxQuant<sup>147</sup> software in combination with the Andromeda<sup>148</sup> search engine. Statistical evaluation (Student's *t*-test) of isotope ratios of detected proteins using Perseus<sup>149</sup> software considered proteins with high enrichment ratios ( $\log_2(\text{enrichment}) > 1$ ) and high confidence levels ( $p\text{-value} < 0.05$ ) as potential hits.

#### 2.2.3.1. Photocrosslinker-Specific Protein Labelling Profiles

In line with gel-based analysis (Chapter 2.2.2), benzophenone-based probe (**BP-1**) revealed significant enrichment of multiple proteins in both cell lines (114 in A549, 78 in HeLa; Figure 2.2). In direct comparison, protein labelling with aryl azide- (**AA-1**) and diazirine-based (**DA-1**) minimal photoprobes was less pronounced with few potential background hits in A549 (5 and 19, respectively; Figure 2.2 A), while substantial background labelling was observed in HeLa cells (46 and 85, respectively; Figure 2.2 B). Again, minor protein binding was observed with control probe **NC-1** (2 in A549, 6 in HeLa; Figure 2.2). While a clear tendency was noticeable in A549 cells with decreasing protein binding from **BP-1** to **DA-1** and **AA-1**, photocrosslinker-specific protein labelling appeared to be more evenly distributed in HeLa. These fluctuations in different cell lines are rather remarkable and yet illuminate the importance of cell-line-specific off-target analysis.

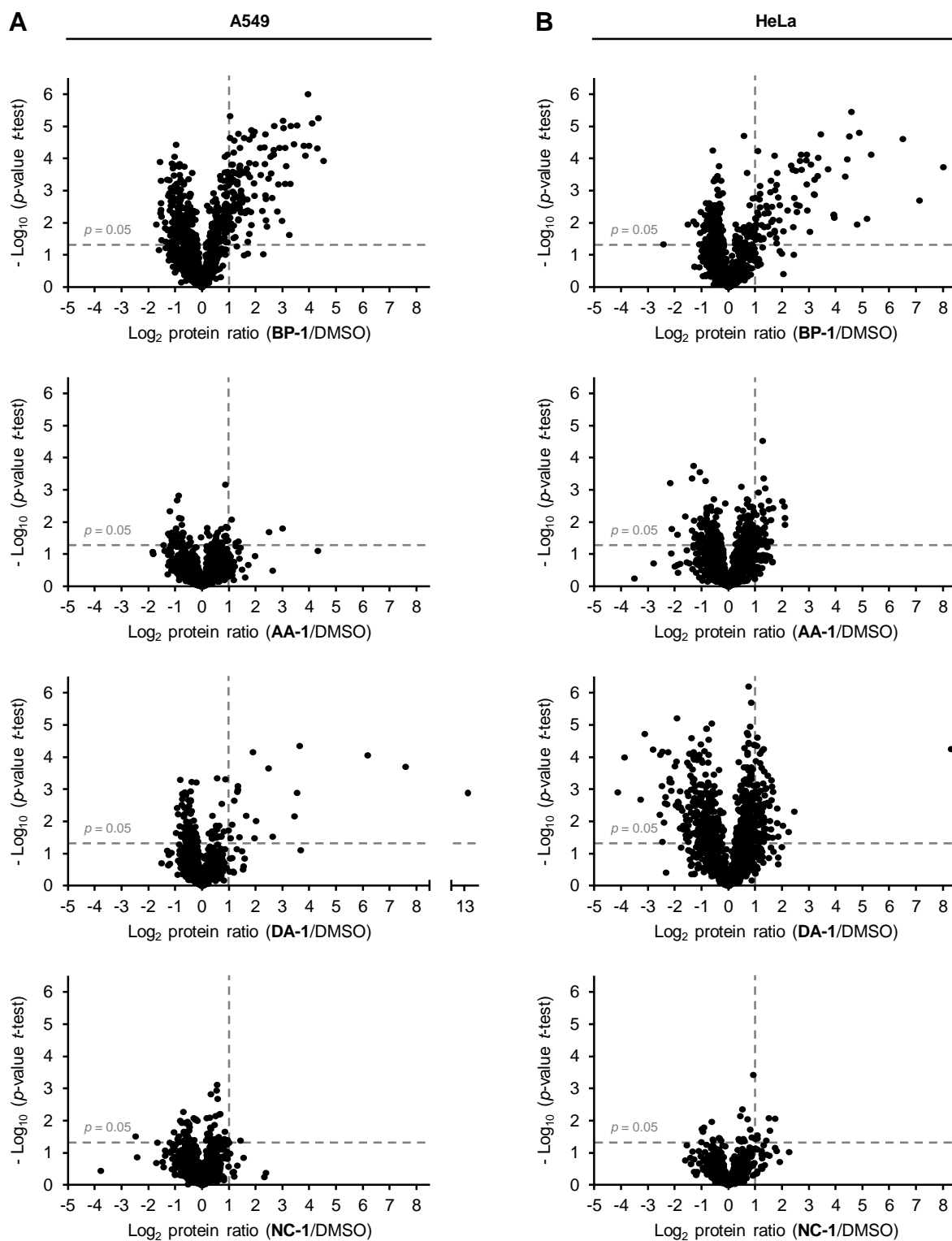


**Figure 2.2.** Photocrosslinker-associated background binding of minimal photoprobes **BP-1**, **AA-1** and **DA-1** as well as control compound **NC-1** in A549 (A) and HeLa (B) cells (3  $\mu$ M; incubation for 60 min, 37°C; irradiation for 30 min, 4°C). Volcano plots illustrate the log<sub>2</sub>-fold enrichment of proteins compared to DMSO treatment. Dashed lines represent a log<sub>2</sub>(enrichment ratio) of 1 and a *p*-value of 0.05, respectively. Data represent average values; *n* = 6 (two independent experiments in technical triplicates).

Direct comparative analysis of overlapping background proteins as illustrated by Venn representation (Figure 2.3) revealed only minimal overlap between the different photocrosslinking functionalities. Interestingly, not a single background protein was shared by all three minimal photoprobes. Given the number of identified and significantly enriched proteins, this finding illustrates that off-target binding is a specific event driven by the individual characteristics of each photocrosslinking moiety.

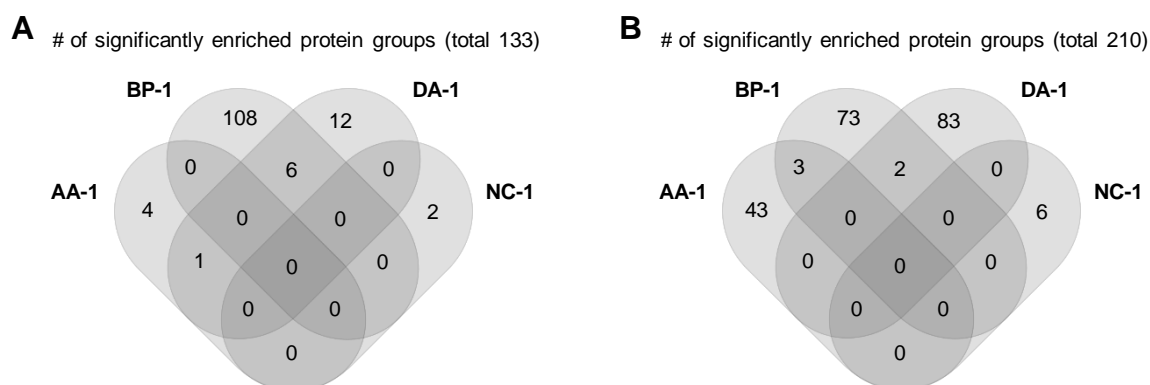


**Figure 2.3.** Venn representation of proteins that were significantly enriched by minimal photoprobes **BP-1**, **AA-1** and **DA-1** as well as control compound **NC-1** in A549 (A) and HeLa (B) cells.

### 2.2.3.2. Diazirine-Specific Protein Labelling Profiles

While previous chapter focused on the impact of the photocrosslinking functionality on background binding, a closer inspection of diazirine-specific protein labelling via structurally diverse photoprobes (**DA-1**, **DA-2**, **DA-3** and **DA-4**) revealed a significant influence of the ligand scaffold (Figure 2.4). Here, **DA-3** – a minimal diazirine-based photoprobe with little steric demand due to its short aliphatic chain – showed only slight labelling in both cell lines. A pronounced level of labelling was observed with **DA-4**, where the diazirine functionality was embedded into a linear aliphatic chain. With increasing steric demand and hydrophobicity (**DA-1** and **DA-2**) protein labelling increased in A549 and HeLa. While in A549 **DA-2** – a photoprobe containing an aryl piperazine – showed the highest protein enrichment followed by phenylic **DA-1**, protein labelling of **DA-2** was less pronounced in HeLa. This observation again stresses the importance of cell-line-specific analysis.

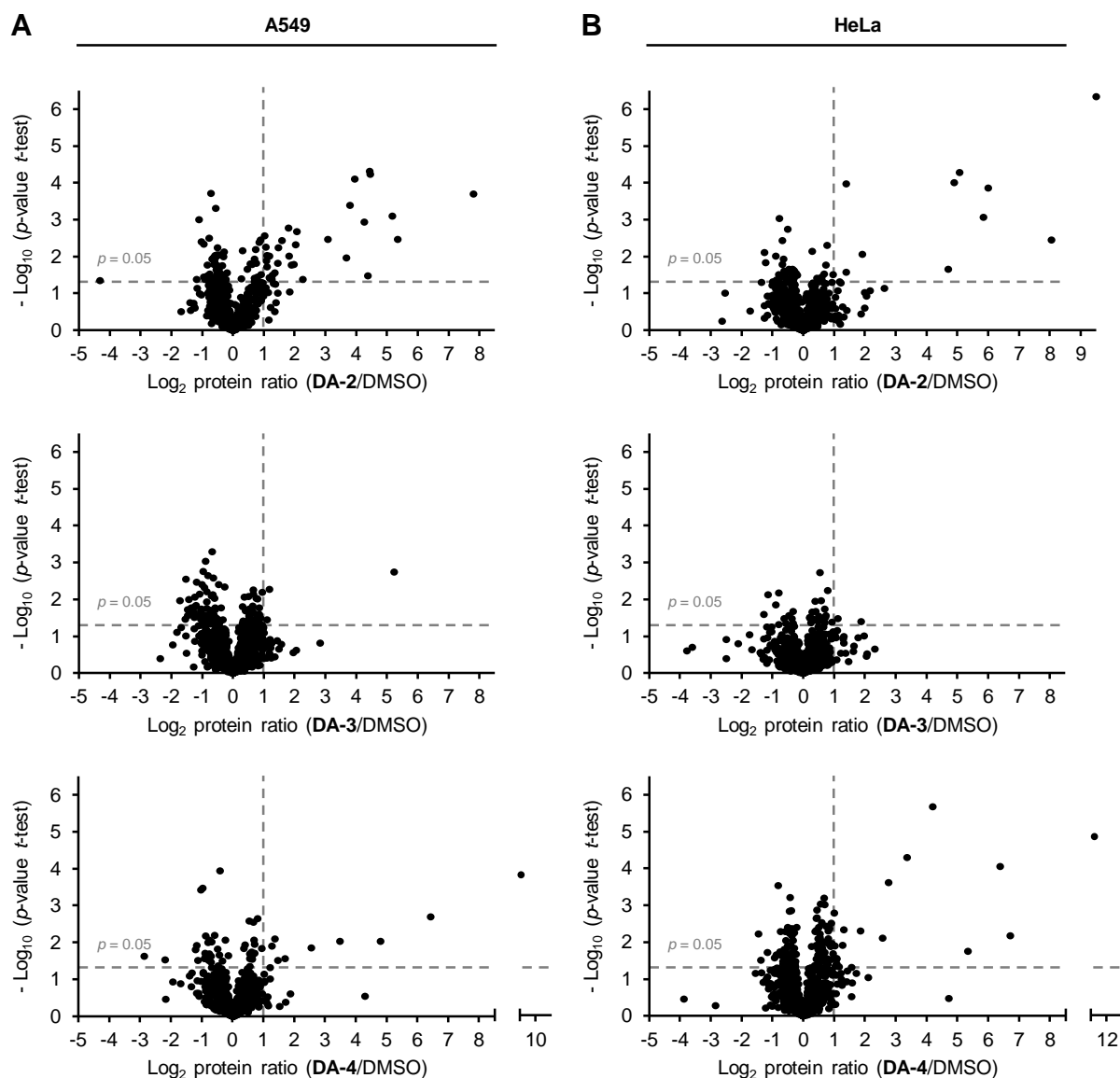


**Figure 2.4.** Photocrosslinker-associated background binding of minimal diazirine-based photoprobes **DA-2**, **DA-3** and **DA-4** in A549 (A) and HeLa (B) cells (3  $\mu$ M; incubation for 60 min, 37°C; irradiation for 30 min, 4°C). Volcano plots illustrate the log<sub>2</sub>-fold enrichment of proteins compared to DMSO treatment. Dashed lines represent a log<sub>2</sub>(enrichment ratio) of 1 and a  $p$ -value of 0.05, respectively. Data represent average values;  $n = 6$  (two independent experiments in technical triplicates). The protein labelling profile of **DA-1** is depicted in Figure 2.2.

The major influence of the ligand scaffold was further highlighted by direct comparative analysis of overlapping background proteins (Figure 2.5 A, B). In both cell lines, only minimal overlap between the different diazirine containing photoprobes was registered. Besides structural differences between respective ligand scaffolds, differences in hydrophobicity with log  $P$  values ranging from 2.2 for **DA-3** to 3.9 for **DA-4** (Figure 2.5 C) might account for diverging labelling profiles as hydrophobicity is a critical factor in cellular uptake as well as binding to hydrophobic protein segments.

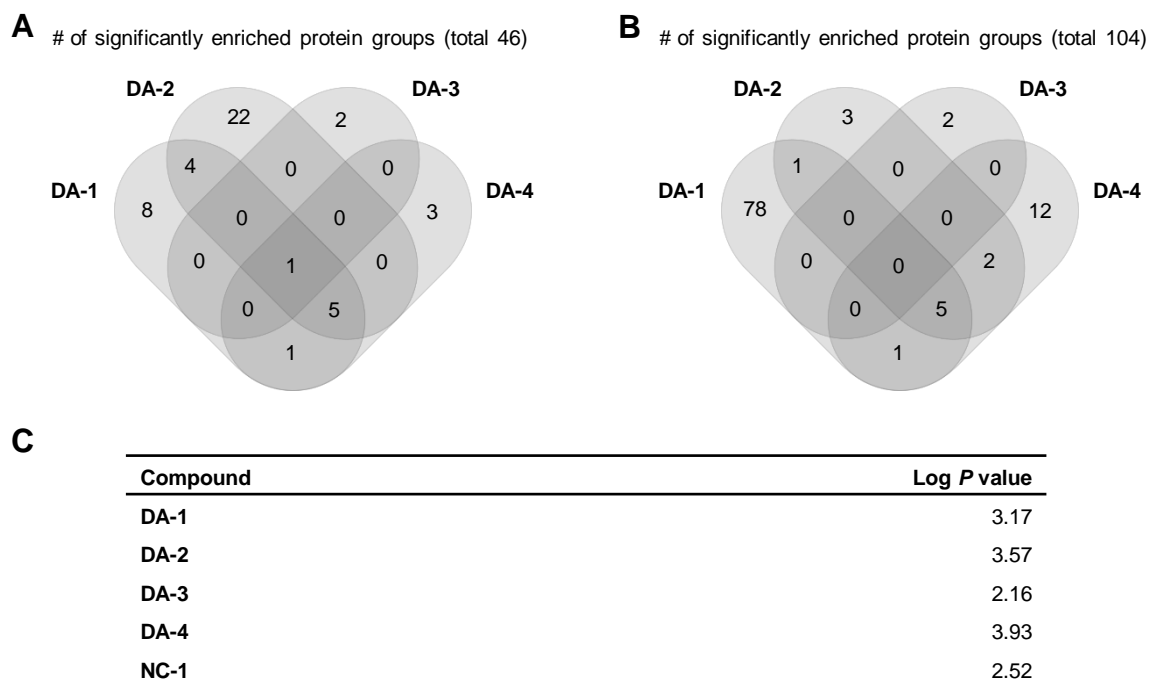


**Figure 2.5.** (A/B) Venn representation of proteins that were significantly enriched by minimal photoprobes **DA-1**, **DA-2**, **DA-3** and **DA-4** in A549 (A) and HeLa (B) cells. (C) Log *P* values of alkyl diazirine containing probes. Log *P* values were calculated using ChemBioDraw Ultra 13.0.

In order to extract ligand-independent diazirine-specific labelling from the bulk of proteins identified with each of the diazirine-based photoprobes, an overlay of diazirine-associated proteomic data was performed (Figure 2.6). To this end, logarithmized enrichment ratios of each diazirine photoprobe were merged by common majority protein IDs, summed up and normalized by the number of valid values. Thereby, ligand-specific hits were imputed with low mean of  $\log_2(\text{enrichment})$  values. In contrast, diazirine-specific hits protruded from the background noise. These overlays highlighted a collection of eight proteins for A549 cells and seven proteins for HeLa cells that were significantly enriched in a ligand-independent manner. A total of four proteins was shared among both cell lines, namely voltage-dependent anion-selective channel proteins 1 and 2 (VDAC1 and 2), cathepsin D (CTSD) and delta(3,5)-delta(2,4)-dienoyl-CoA isomerase (ECH1).

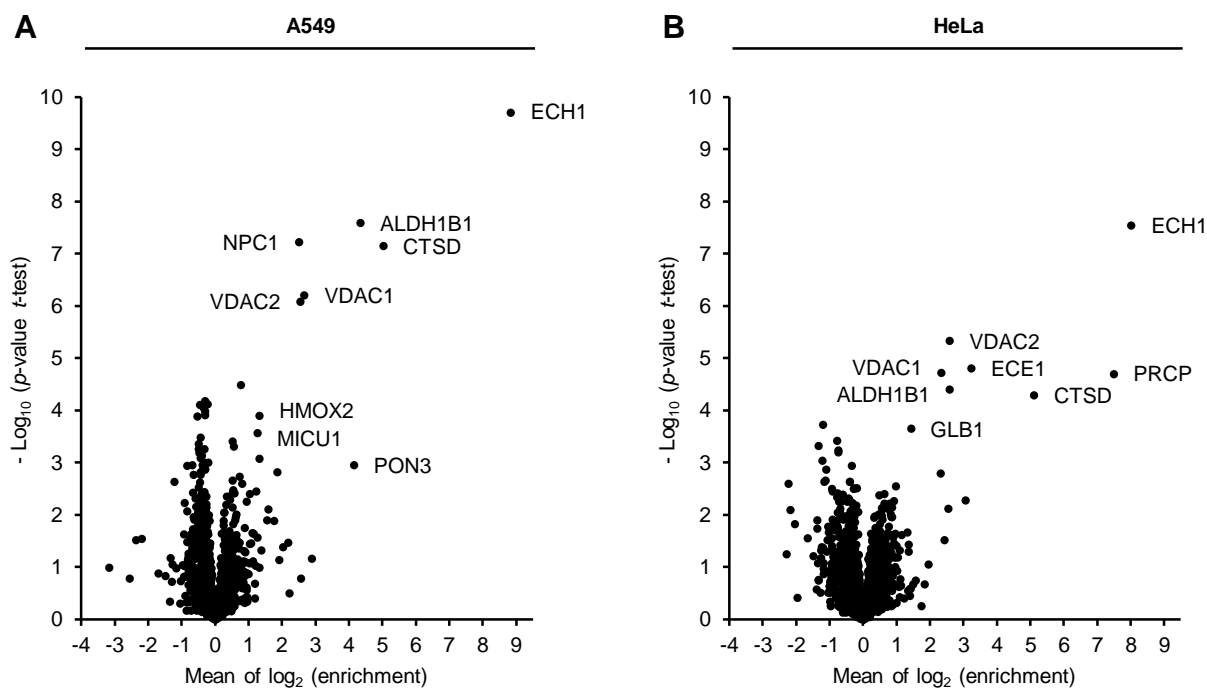


**Figure 2.6.** Combined and overlaid representation of diazirine-specific protein labelling in A549 (A) and HeLa (B) cells. The significance levels were adjusted to  $p$ -values of 0.0008 and 0.0002, respectively, by the method of Benjamini and Hochberg (FDR = 0.05).

Gene ontology (GO) annotation revealed that 291 out of 1655 proteins identified in A549 as well as 299 out of 2075 within the HeLa proteome were annotated as “intrinsic to membrane”. Importantly, several major protein hits of diazirine-based photoprobes were found among them (e.g. VDAC1 and 2, NPC1 and ECE1), thereby underscoring the general applicability of these background binding results for studies on membrane proteins.

Alignment with the Pfam protein families database<sup>150</sup> and the database of protein domains, families and functional sites (PROSITE)<sup>151</sup> grouped the set of diazirine-specific binders into three classes: (i) Channels or channel-associated proteins, e.g. voltage-dependent anion-selective channel proteins 1 and 2 (VDAC1 and 2); (ii) catabolic enzymes, e.g. cathepsin D (CTSD); and (iii) small molecule binders, e.g. aldehyde dehydrogenase X (ALDH1B1). An overview of diazirine-specific protein binders for A549 and HeLa proteomes including information about respective protein abundances, cellular functions and localizations is given in Table 2.1.

**Table 2.1.** Collection of proteins that were significantly enriched in a diazirine-dependent manner as revealed by overlaid diazirine-associated proteomic data (Figure 2.6). Selection criteria included a minimum mean  $\log_2$ (enrichment) of 1 and minimum Benjamini-Hochberg significance levels with  $p$ -values of 0.0008 (A549) and 0.0002 (HeLa; FDR = 0.05), respectively. In case of missing overlap between both cell lines, corresponding non-significant mean of  $\log_2$ (enrichment) values are marked with a \*. iBAQ (intensity-based absolute quantification) abundances<sup>152</sup> were extracted from the ProteomicsDB database<sup>153</sup>.

| Protein name  | Gene name | Cell line | Mean of $\log_2$ (ratios) | Detected x times out of 6 with probe |      |      |      | Abundance $\log_{10}$ (iBAQ) | Function                                     | Localization              |
|---|-----------|-----------|---------------------------|--------------------------------------|------|------|------|------------------------------|--|---------------------------|
|   |           |           |                           | DA-1                                 | DA-2 | DA-3 | DA-4 |                              |  |                           |
| Delta(3,5)-delta(2,4)-dienoyl-CoA isomerase         | ECH1      | A549      | 8.83                      | 6                                    | 6    | 6    | 6    | 6.56                         | beta-oxidation                               | mitochondrion, peroxisome |
|   |           | HeLa      | 8.01                      | 6                                    | 4    | 2    | 6    | 5.90                         |  |                           |
| Cathepsin D   | CTSD      | A549      | 5.04                      | 6                                    | 6    | 6    | 6    | 6.51                         | protease                                     | lysosome                  |
|   |           | HeLa      | 5.10                      | 4                                    | 4    | 2    | 6    | 5.94                         |  |                           |
| Aldehyde dehydrogenase X                            | ALDH1B1   | A549      | 4.34                      | 6                                    | 6    | 4    | 6    | 5.69                         | acetaldehyde detoxification                  | mitochondrion             |
|   |           | HeLa      | 2.57                      | 6                                    | 6    | 6    | 6    | 5.99                         |  |                           |
| Niemann-Pick C1 protein                             | NPC1      | A549      | 2.51                      | 6                                    | 6    | 6    | 6    | 5.00                         | cholesterol transporter                      | lysosome                  |
|   |           | HeLa      | 1.95*                     | 0                                    | 3    | 0    | 0    | 4.84                         |  |                           |
| Voltage-dependent anion-selective channel protein 1 | VDAC1     | A549      | 2.67                      | 6                                    | 6    | 6    | 6    | 7.14                         | hydrophilic porin                            | mitochondrion             |
|   |           | HeLa      | 2.32                      | 6                                    | 6    | 6    | 6    | 6.81                         |  |                           |
| Voltage-dependent anion-selective channel protein 2 | VDAC2     | A549      | 2.54                      | 6                                    | 6    | 6    | 6    | 6.91                         | hydrophilic porin                            | mitochondrion             |
|   |           | HeLa      | 2.57                      | 6                                    | 6    | 6    | 6    | 6.57                         |  |                           |
| Heme oxygenase 2                                    | HMOX2     | A549      | 1.33                      | 6                                    | 6    | 3    | 4    | 5.44                         | heme degradation                             | endoplasmic reticulum     |
|   |           | HeLa      | 0.55*                     | 5                                    | 3    | 4    | 3    | 5.44                         |  |                           |
| Lysosomal Pro-X carboxypeptidase                    | PRCP      | A549      | -                         | -                                    | -    | -    | -    | 4.58                         | protease                                     | lysosome                  |
|   |           | HeLa      | 7.48                      | 0                                    | 5    | 0    | 4    | 5.31                         |  |                           |
| Endothelin-converting enzyme 1                      | ECE1      | A549      | -                         | -                                    | -    | -    | -    | 4.18                         | endothelin cleavage                          | lysosome                  |
|   |           | HeLa      | 3.22                      | 4                                    | 5    | 1    | 6    | 5.32                         |  |                           |
| Calcium uptake protein 1                            | MICU1     | A549      | 1.27                      | 2                                    | 4    | 0    | 3    | 4.63                         | associated with $\text{Ca}^{2+}$ transporter | mitochondrion             |
|   |           | HeLa      | 0.37*                     | 1                                    | 2    | 1    | 3    | 4.59                         |  |                           |

Interestingly, most of the diazirine-specific protein hits are localized in the lysosome and mitochondrion, are proteins of high abundance and show a preference for small molecule binding. In particular, diverging abundance levels of certain proteins between both cells might provide an explanation for cell line-specific background binding. For example, proteins that were identified as photocrosslinker-associated protein hits in the proteome of HeLa cells only, such as endothelin-converting enzyme 1 (ECE1) and lysosomal Pro-X carboxypeptidase (PRCP), are less abundant in A549 cells. Overall, it is remarkable to notice a specific diazirine-dependent labelling profile with few distinct photome hits considering the enormous complexity of a whole proteome and the immense number of highly abundant proteins.

## **2.2.4. Evaluation of Critical Experimental Parameters on Diazirine-Associated Background Labelling by Label-Free Quantitative Proteomics**

### **2.2.4.1. Label-Free Diazirine-Specific Protein Labelling Profiles**

Label-free mass spectrometry quantification represents an arising proteomic technique independent of stable isotopic labels (label-free AfBPP, Chapter 1.3). To account for this state-of-the-art proteomic analysis method, the diazirine-dependent protein profiles were investigated in a label-free manner in A549 cells. To this end, A549 cells were incubated with a “cocktail mix” containing a mixture of all four diazirine-based photoprobes in equimolar concentrations (3  $\mu$ M per photoprobe; 1 h, 37°C) and were subsequently irradiated with UV light (365 nm; 30 min, 4°C). Cells were lysed, followed by click reaction with biotin azide and enrichment of biotin-modified proteins on avidin-coated beads. Peptides, which were released by digest with trypsin, were measured on a high resolution LC-MS/MS instrument in the label-free mode and analyzed using MaxQuant<sup>147</sup> software in combination with the Andromeda<sup>148</sup> search engine. Statistical evaluation (Student’s *t*-test) of detected proteins using Perseus<sup>149</sup> software and alignment with the diazirine-specific labelling profile from SILAC-based analysis (Chapter 2.2.3.2) revealed comparable overall results between both methods (Figure 2.7).

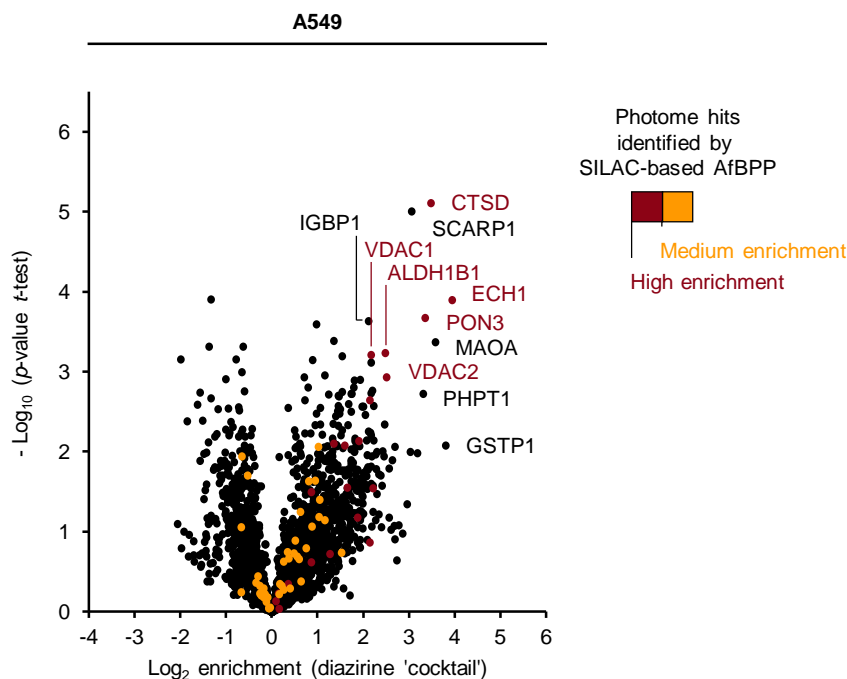


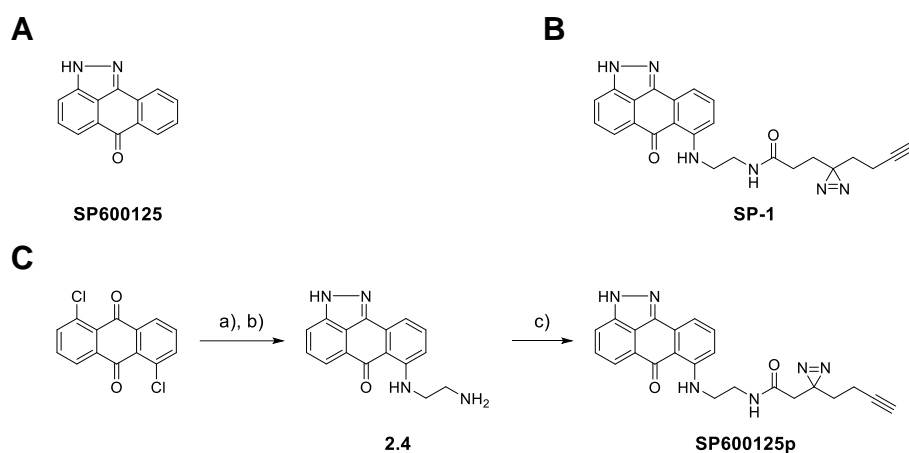
**Figure 2.7.** Photocrosslinker-associated background binding of a “cocktail mix” of minimal diazirine-based photoprobes **DA-1**, **DA-2**, **DA-3** and **DA-4** identified by gel- and label-free AfBPP in A549 cells (3  $\mu\text{M}$  per photoprobe; incubation for 60 min, 37°C; irradiation for 30 min, 4°C). Volcano plots illustrate the  $\log_2$ -fold enrichment of proteins compared to DMSO treatment. Data represent average values;  $n = 8$ . Proteins characterized as diazirine-specific hits by SILAC-AfBPP (Chapter 2.2.3.2) are highlighted in orange (selection criteria:  $0 < \log_2(\text{enrichment}) < 1$  and  $p\text{-value} < 0.05$ ) and red (selection criteria:  $\log_2(\text{enrichment}) > 1$  and  $p\text{-value} < 0.05$ ). Alignment was performed using the “match rows by name” function on the basis of Protein IDs within the Perseus software.

While most prominent photocrosslinker-associated off-targets were reported by both methods – SILAC-based and label-free AfBPP – slight differences in protein labelling profiles were detected. These deviations might be attributed to a different experimental setup using a “cocktail” approach with higher overall photoprobe concentrations as well as variations in the workflow as label-free quantification requires high protein background for optimal performance.

#### 2.2.4.2. Impact of Experimental Parameters on the Target Identification of Kinase Inhibitor **SP600125**

Critical experimental parameters in photoaffinity labelling, like irradiation times, photoprobe concentrations and competition settings, generally represent a “black box”, although their strong impact on proteomic outcomes has been noted. To address these “black box” parameters, AfBPP experiments under varying experimental conditions were performed by the example of anthrapyrazolone **SP600125** (Scheme 2.2 A), a kinase inhibitor with nanomolar potency against c-Jun N-terminal kinase (JNK)<sup>154</sup>. Corresponding photoprobe **SP600125p**, structurally similar to photoprobe **SP-1** previously reported by Yao et al. (Scheme 2.2 B).<sup>138</sup>

was synthesized by attaching diazirine-based photocrosslinker **2.3** to the anthrapyrazolone core scaffold via a short ethylenediamine linker (Scheme 2.2 C).



**Scheme 2.2.** Structure of **SP600125** (A), a nanomolar kinase inhibitor of JNK, corresponding photoprobe **SP-1** (B) previously applied by Yao et al.<sup>138</sup> and synthesis of a slightly modified photoprobe version **SP600125p** (C). Reaction conditions: a) Hydrazine monohydrate, pyridine, reflux, 18 h; b) ethylenediamine, reflux, 6 h, 22% over two steps; c) **2.3**, HOBt, EDC, DIPEA, DMF, room temperature, 16 h, 54%.

With this kinase inhibitor photoprobe in hand irradiation time-dependent studies were performed using a relatively high photoprobe concentration (compared to the nanomolar potency of parental **SP600125**) of 3  $\mu\text{M}$  to ensure sufficient saturation of background-binding proteins. The experimental workflow followed the label-free procedure established in Chapter 2.2.4.1 with varying irradiation times (5, 10, 20 and 30 min). Inspection of resulting proteomic data and alignment with the list of diazirine-associated protein hits (Chapter 2.2.4.1) revealed high background labelling at short times (5 min) that decreased with increasing irradiation time (Figure 2.8). Here, high background labelling at short irradiation times is presumably the result of incomplete proteome labelling with unspecific proteins, in particular those of high abundance, labelled first.

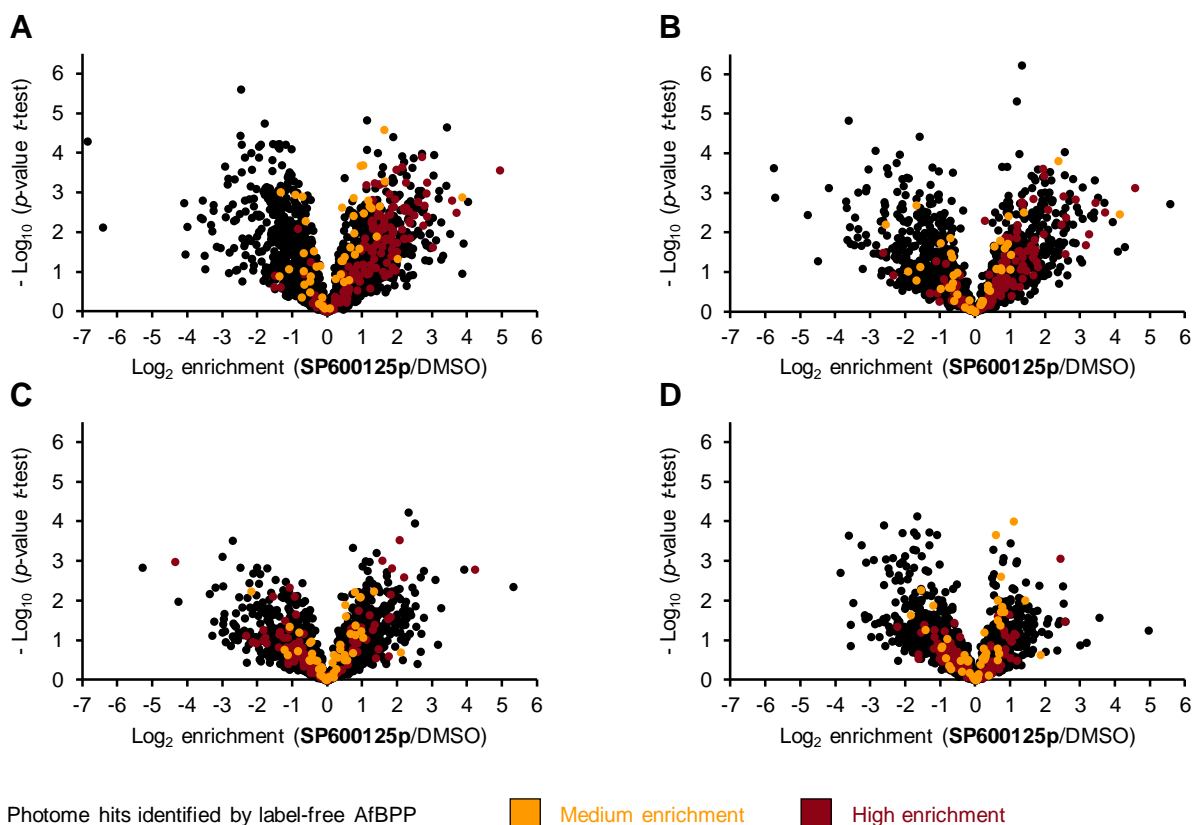


**Figure 2.8.** Protein-labelling profiles of **SP600125p** identified by gel- and label-free AfBPP in A549 cells (3  $\mu$ M; incubation for 60 min, 37°C) at different irradiation times: (A) 5 min, (B) 10 min, (C) 20 min and (D) 30 min. Volcano plots illustrate the  $\log_2$ -fold enrichment of proteins compared to DMSO treatment. Data represent average values;  $n = 8$ . Proteins characterized as diazirine-specific hits by the label-free “diazirine cocktail” approach (Chapter 2.2.4.1) are highlighted in orange (selection criteria:  $0 < \log_2(\text{enrichment}) < 1$  and  $p\text{-value} < 0.05$ ) and red (selection criteria:  $\log_2(\text{enrichment}) > 1$  and  $p\text{-value} < 0.05$ ). Alignment was performed using the “match rows by name” function on the basis of Protein IDs within the Perseus software.

Based on these findings, an irradiation time of 30 min was selected for the subsequent investigation of concentration-dependency. To this end, a label-free dose-down experiment was performed with photoprobe concentrations of 3000, 500 and 125 nM. As expected background labelling increased at higher concentrations (Figure 2.9).

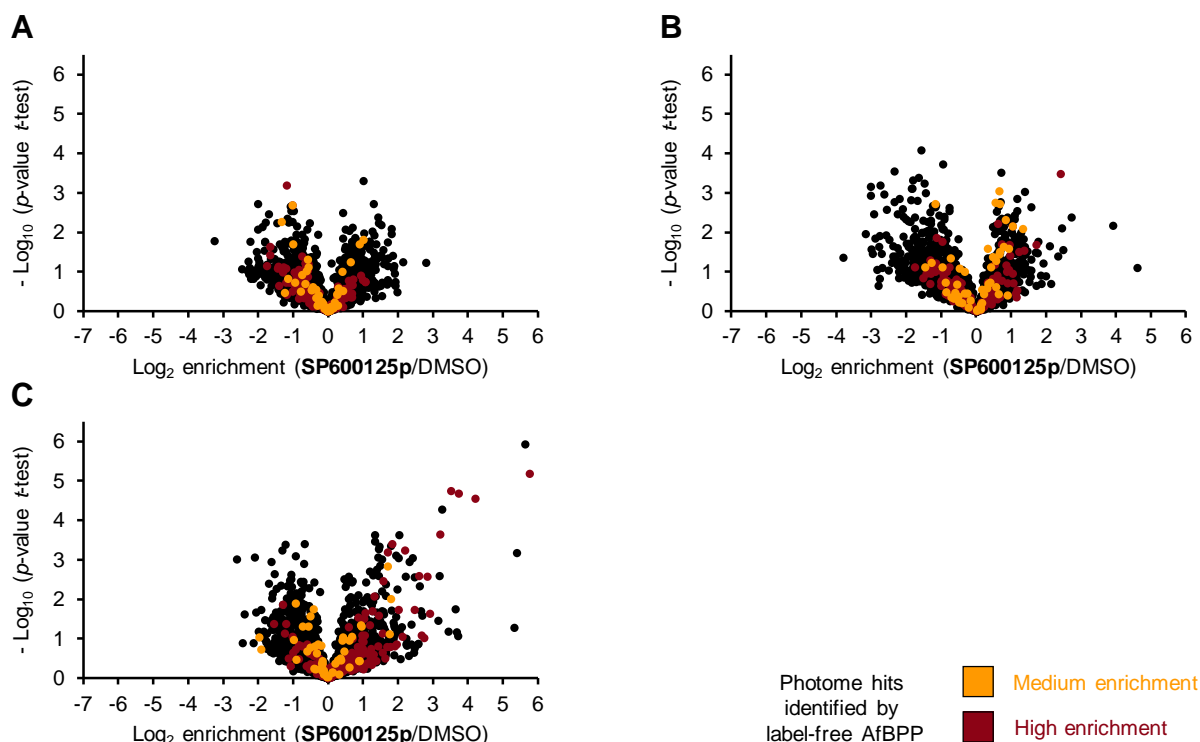


**Figure 2.9.** Protein-labelling profiles of **SP600125p** identified by gel- and label-free AfBPP in A549 cells (incubation for 60 min, 37°C; irradiation for 30 min, 4°C) at different photoprobe concentrations: (A) 125 nM, (B) 500 nM and (C) 3000 nM. Volcano plots illustrate the  $\log_2$ -fold enrichment of proteins compared to DMSO treatment. Data represent average values;  $n = 8$ . Proteins characterized as diazirine-specific hits by the label-free “diazirine cocktail” approach (Chapter 2.2.4.1) are highlighted in orange (selection criteria:  $0 < \log_2(\text{enrichment}) < 1$  and  $p\text{-value} < 0.05$ ) and red (selection criteria:  $\log_2(\text{enrichment}) > 1$  and  $p\text{-value} < 0.05$ ). Alignment was performed using the “match rows by name” function on the basis of Protein IDs within the Perseus software.

Taken together, these findings confirmed the critical impact of photolabelling parameters on photocrosslabelling experiments and indicated a preference for low photoprobe concentrations and longer irradiation times. Consequently, label-free competition studies were performed at a photoprobe concentration of 500 nM and an irradiation time of 30 min. Although, binding to an eukaryotic kinase was not confirmed within these in situ studies, competition experiments with unmodified parental **SP600125** (1/1, 1/10 and 1/100) revealed binding to several members of the carboxylase protein family (Figure 2.10). These carboxylase hits, whose labelling was concentration-dependently outcompeted, included pyruvate carboxylase (PC), propionyl carboxylase chain alpha and beta (PCCA and B) as well as methylcrotonoyl-CoA carboxylase (MCCC1). All of these enzymes harbor an ATP binding pocket, which is likely addressed by ATP-mimicking **SP600125**<sup>155</sup>. Notably, background binders were not outcompeted in these competition experiments, while competition of potential target proteins was observed at higher competition ratios.

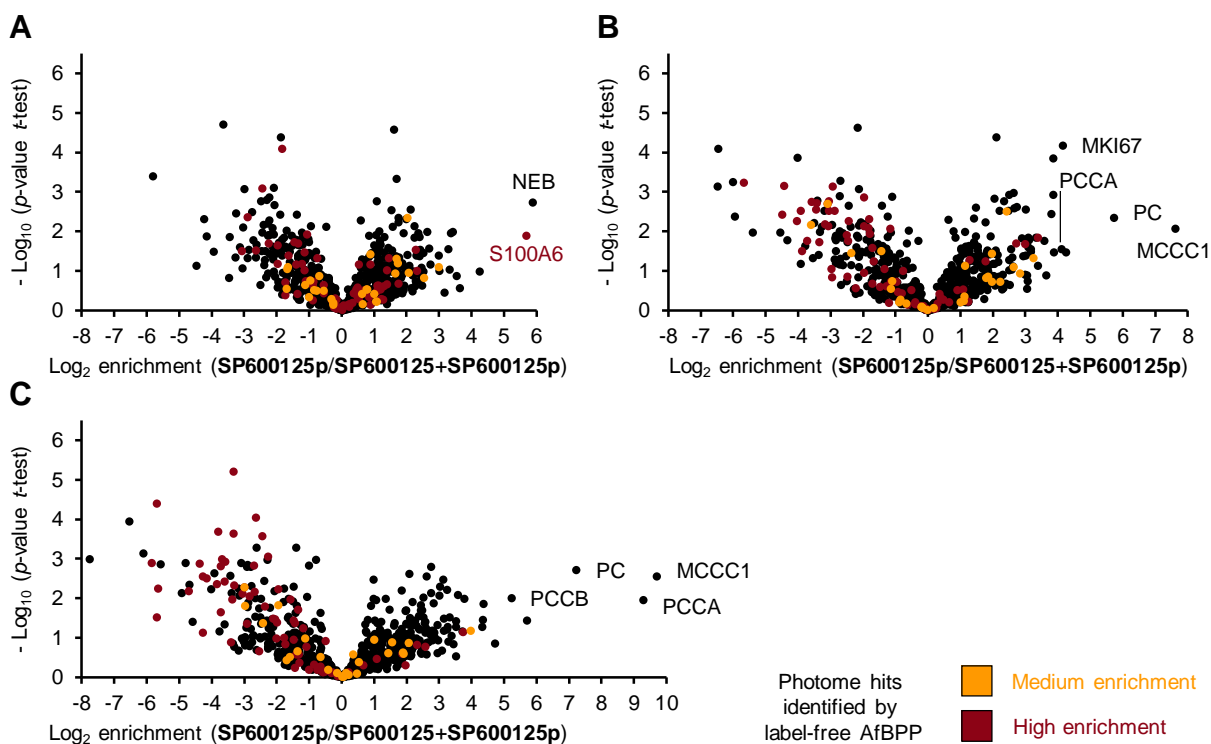
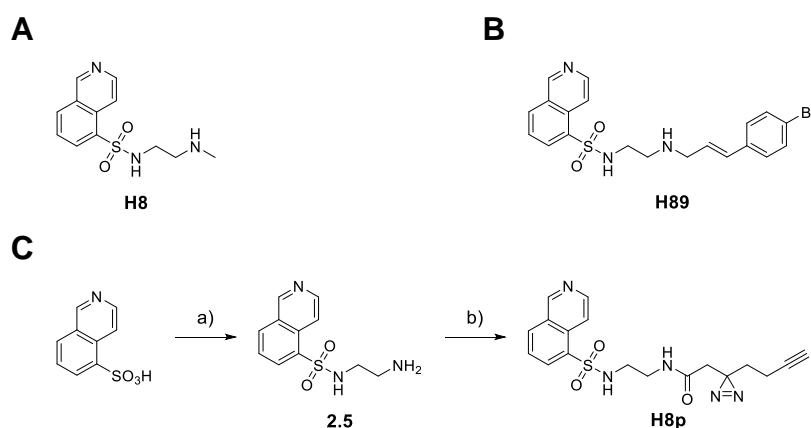


**Figure 2.10.** Protein-labelling profiles of **SP600125p** (500 nM; incubation for 60 min, 37°C; irradiation for 30 min, 4°C) in competition with unmodified parental **SP600125** (pre-incubation for 60 min, 37°C): (A) 1/1, (B) 1/10 and (C) 1/100. Volcano plots illustrate the  $\log_2$ -fold enrichment of proteins compared to competitive treatment. Data represent average values;  $n = 8$ . Proteins characterized as diazirine-specific hits by the label-free “diazirine cocktail” approach (Chapter 2.2.4.1) are highlighted in orange (selection criteria:  $0 < \log_2(\text{enrichment}) < 1$  and  $p\text{-value} < 0.05$ ) and red (selection criteria:  $\log_2(\text{enrichment}) > 1$  and  $p\text{-value} < 0.05$ ). Alignment was performed using the “match rows by name” function on the basis of Protein IDs within the Perseus software.

### 2.2.5. Proof-of-Principle Study: Target Elucidation of Reversible Protein Kinase A Inhibitor H8 via Affinity-Based Protein Profiling

With a comprehensive inventory of diazirine-associated background proteins in hand combined with fine-tuned photolabelling parameters, the general significance of these findings was demonstrated in a proof-of-principle study collaborating kinase inhibitor **H8**. Isoquinolinsulfonamide **H8** and its structurally related second-generation analogue **H89** (Scheme 2.3 A, B) are experimental inhibitors of cAMP-dependent protein kinase (PKA) with potencies in the high nanomolar range.<sup>156-158</sup> Despite their frequent use in PKA research, corresponding selectivity profiles are unknown in a cellular context and although inhibition of PKA has been validated by various studies, it is unclear whether **H8** and **H89** interfere with other cellular pathways.<sup>158</sup> In order to unravel possible unknown targets of this inhibitor class a full proteome analysis under consideration of photocrosslinker-specific background binding was conducted. The design of respective photoprobe **H8p** considered crystallographic data of the catalytic subunit of PKA in complex with **H8** and **H89**, respectively,<sup>157</sup> revealing the

methylamino ethyl unit of **H8** as a possible site for synthetic introduction of the diazirine-based photocrosslinker moiety. Here, the isoquinoline moiety occupies the ATP-binding pocket,<sup>157</sup> while the photocrosslinker unit of **H8p** should likely point away from the catalytic loop. Synthesis of **H8p** was achieved by coupling the carboxylic acid version of diazirine-based photocrosslinker (**2.3**) to readily available *N*-(2-aminoethyl)isoquinoline-5-sulfonamide (**2.5**)<sup>159</sup> (Scheme 2.3 C).



**Scheme 2.3.** Structure of kinase inhibitors of cAMP-dependent protein kinase (PKA) **H8** (A) and **H89** (B) and synthesis of corresponding photoprobe **H8p** (C). Reaction conditions: a) i)  $\text{SOCl}_2$ , DMF, reflux, 2 h; ii)  $\text{NaHCO}_3$ ,  $\text{H}_2\text{O}$ ,  $0^\circ\text{C}$ ; b) ethylenediamine,  $\text{CH}_2\text{Cl}_2$ ,  $0^\circ\text{C}$  – room temperature, 2 h, 52% over three steps; c) **2.3**, HOBt, EDC, DIPEA, DMF, room temperature, 16 h, 93%.

SILAC-based target deconvolution via AfBPP was performed according to the established protocol (Chapter 2.2.3) applying low concentrations of **H8p** ( $3\ \mu\text{M}$ ; compared to the high nanomolar potency of parental compounds **H8** und **H89**) and irradiation times of 30 minutes. Statistical evaluation of resulting proteomic data revealed a total of 30 proteins as potential protein hits that met the criteria of high enrichment ratios ( $\log_2(\text{enrichment}) > 1$ ) and high confidence levels ( $p\text{-value} < 0.05$ ; Figure 2.11). Alignment with the inventory of diazirine-associated background binders (Chapter 2.2.3.2) exposed several of these putative **H8p** hits as promiscuous. Thus, all potential hits were classified into three confidence levels (Figure 2.11): (i) Low confidence (five hits depicted in red:  $\log_2(\text{diazirine-specific enrichment}) > 1$  and  $p\text{-value} < 0.05$ ); (ii) medium confidence (six hits depicted in orange:  $0 < \log_2(\text{diazirine-specific enrichment}) < 1$  and  $p\text{-value} < 0.05$ ); and (iii) high confidence (19 hits depicted in black that were not significantly enriched in the diazirine-specific background labelling).

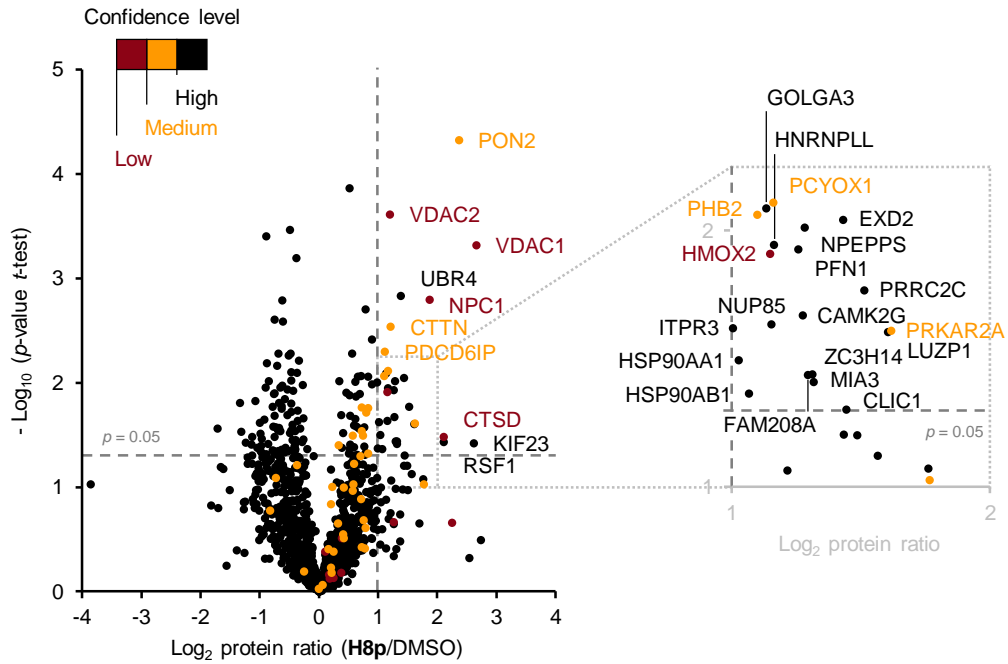


**Figure 2.11.** Protein-labelling profile of **H8p** identified by SILAC-based, gel-free AfBPP in A549 cells (3  $\mu$ M; incubation for 60 min, 37°C; irradiation for 30 min, 4°C). Volcano plots illustrate the  $\log_2$ -fold enrichment of proteins compared to DMSO treatment. Data represent average values;  $n = 6$  (two independent experiments in technical triplicates). Proteins characterized as diazirine-specific hits by SILAC-AfBPP (Chapter 2.2.3.2) are highlighted in orange (medium confidence; selection criteria:  $0 < \log_2(\text{enrichment}) < 1$  and  $p\text{-value} < 0.05$ ) and red (low confidence; selection criteria:  $\log_2(\text{enrichment}) > 1$  and  $p\text{-value} < 0.05$ ). Alignment was performed using the "match rows by name" function on the basis of Protein IDs within the Perseus software.

Importantly, the regulatory subunit of PKA (PRKAR2A) – the validated target of **H8** and **H89** – was identified as a medium confidence hit. Furthermore, alignment with the cytoscape platform<sup>160</sup> visualized potential engagements of **H8p** protein hits in cellular interaction networks (Table 2.2). Interestingly, most high confident protein hits could be associated with nucleotide binding, namely ATP/cAMP, DNA and polyadenine RNA binding (Table 2.2). This is in agreement with the spatial structure and binding mode of the core scaffold of **H8** and **H89** in eukaryotic kinases with the isoquinoline sulfonyl moiety mimicking adenosine binding.

**Table 2.2.** Overview of potential protein targets of **H8p** together with information on a potential engagement thereof in nucleotide binding and hydrolytic reactions. Confidence levels according to the alignment with diazirine-specific hits (Chapter 2.2.3.2) are indicated by color: Low confidence, red; medium, orange; high, black. \* = not significant.

| Protein name   | Gene name       | Log <sub>2</sub> (enrichment) |         | Molecular function |                  |             |                     |
|--|-----------------|-------------------------------|---------|--------------------|------------------|-------------|---------------------|
|  |                 | H8p                           | Photome | PolyA RNA binding  | ATP/cAMP binding | DNA binding | Hydrolytic activity |
| Voltage-dependent anion-selective channel protein 1            | VDAC1           | 2.66                          | 2.67    |                    |                  |             |                     |
| Kinesin-like protein KIF23                                     | KIF23           | 2.61                          | 0.32*   |                    | ■                |             |                     |
| Serum paraoxonase/arylesterase 2                               | PON2            | 2.36                          | 0.62    |                    |                  |             | ■                   |
| Remodeling and spacing factor 1                                | RSF1            | 2.10                          | 0.68*   |                    |                  |             |                     |
| Cathepsin D  | CTSD            | 2.10                          | 5.04    |                    |                  |             | ■                   |
| Niemann-Pick C1 protein  | NPC1            | 1.87                          | 2.51    |                    |                  |             |                     |
| cAMP-dependent protein kinase type II-alpha regulatory subunit | PRKAR2A         | 1.62                          | 0.70    |                    | ■                |             |                     |
| Leucine zipper protein 1                                       | LUZP1           | 1.60                          | 0.48*   |                    |                  | ■           |                     |
| Protein PRRC2C   | PRRC2C          | 1.51                          | 0.20*   | ■                  |                  |             |                     |
| Chloride intracellular channel protein 1                       | CLIC1           | 1.44                          | 0.44*   |                    |                  |             |                     |
| Exonuclease 3-5 domain containing protein 2                    | EXD2            | 1.43                          | 0.14*   |                    |                  |             | ■                   |
| E3 ubiquitin-protein ligase UBR4                               | UBR4            | 1.38                          | 0.23*   |                    |                  |             |                     |
| Melanoma inhibitory activity protein 3                         | MIA3            | 1.32                          | -0.02*  |                    |                  |             |                     |
| Zinc finger CCCH domain-containing protein 14                  | ZC3H14          | 1.31                          | -0.38   | ■                  |                  |             |                     |
| Protein FAM208A  | FAM208A         | 1.30                          | -       |                    |                  |             |                     |
| Puromycin-sensitive aminopeptidase                             | NPEPPS          | 1.28                          | 0.51*   |                    |                  |             | ■                   |
| Calcium/calmodulin-dependent protein kinase Type II gamma/beta | CAMK2G/B        | 1.27                          | 0.51*   |                    | ■                |             | ■                   |
| Profilin-1   | PFN1            | 1.26                          | 0.75*   | ■                  |                  |             |                     |
| Src substrate cactin   | CTTN, EMS1      | 1.21                          | 0.86    |                    |                  |             |                     |
| Voltage-dependent anion-selective channel protein 2            | VDAC2           | 1.20                          | 2.54    |                    |                  |             |                     |
| Heterogenous nuclear ribonucleoprotein L-like                  | HNRNPLL, HNRPLL | 1.16                          | -1.27*  | ■                  |                  |             |                     |
| Preylcysteine oxidase 1  | PCYOX1          | 1.16                          | 0.59    |                    |                  |             |                     |
| Nuclear pore complex protein Nup85                             | NUP85           | 1.15                          | -0.10*  |                    |                  |             |                     |
| Heme oxygenase 2   | HMOX2           | 1.15                          | 1.33    |                    |                  |             |                     |
| Golgin subfamily A member 3                                    | GOLGA3          | 1.13                          | 0.20*   |                    |                  |             |                     |
| Programmed cell death 6-interacting protein                    | PDCD6IP         | 1.11                          | 0.64    |                    |                  |             |                     |
| Prohibitin-2   | PHB2            | 1.10                          | 0.55    |                    |                  |             |                     |
| Heatshock protein HSP 90-beta                                  | HSP90AB1        | 1.07                          | 0.46*   | ■                  | ■                |             |                     |
| Heatshock protein HSP 90-alpha                                 | HSP90AA1, EL52  | 1.03                          | 0.34*   | ■                  | ■                |             |                     |
| Inositol 1,4,5-trisphosphate receptor type 3                   | ITPR3           | 1.01                          | 0.37*   |                    |                  |             |                     |

### 2.3. CONCLUSION AND OUTLOOK

The ligand-independent protein profiles of three commonly applied photocrosslinking functionalities – benzophenone, aryl azide and diazirine – were comprehensively illustrated. To this end, all three functionalities were embedded into simple molecular scaffolds and the photocrosslinker-specific labelling preferences of resulting minimal photoprobes were compared in two human cancer cell lines (A549 and HeLa) via quantitative, gel-free proteomics based on SILAC. Direct comparative analysis revealed superior specificity of aryl azide and diazirine functionalities compared to benzophenone. Each photocrosslinking moiety addressed a specific set of photocrosslinker-specific targets with minimal overlap among them, thereby indicating that off-target binding might be a specific event driven by the individual characteristics of each photocrosslinking moiety. In addition, in-depth analysis of diazirine-containing minimal photoprobes of differing spatial structure and hydrophobicity by state-of-the-art proteomic technologies – SILAC-based and label-free AfBPP, respectively – revealed a specific set of diazirine-specific protein hits with most being proteins of high abundance and with a preference for small-molecule binding. These diazirine-specific hits were compiled in an inventory of promiscuous proteins in order to assist the interpretation of proteomic data resulting from future photoaffinity labelling experiments as these are often hampered by false-positive hits that result from ligand-independent reactivity. Moreover, systematic variations of critical experimental parameters, including photoprobe concentration and irradiation time, indicated that AfBPP experiments might profit from longer irradiation times (20 – 30 min) as well as lower photoprobe concentrations as demonstrated with anthrapyrazolone **SP600125p**, a diazirine-based photoprobe of JNK inhibitor **SP600125**.

A proof-of-principal study collaborating a diazirine-containing photoprobe of ATP-competitive PKA inhibitor **H8** applied these fine-tuned experimental settings and illustrated the significance of the diazirine-specific off-target inventory list for the interpretation of proteomic results. While by alignment with the compilation of diazirine-associated background binders several highly enriched proteins could be exposed as promiscuous, the regulatory subunit of known target PKA as well as potential protein hits, which are associated with adenosine binding, protruded from the bulk of background binders. This data interpretation would have been challenging without the awareness and knowledge of diazirine-specific background protein labelling.

Given the sheer amount of existing proteomic data associated with photolabelling-based AfBPP experiments, mining of this readily available data might enable additional insights into ligand-independent photocrosslinker-associated off-target binding and might unearth further interdependencies in background labelling. In particular, proteomic data resulting from experiments with structurally diverse photoprobes could further enhance the significance of this off-target inventory list by covering broad chemical space.



### 3. DISCOVERY OF A SMALL MOLECULE ANTIBIOTIC ACTIVE AGAINST MULTIDRUG-RESISTANT GRAM-POSITIVE PATHOGENS

The following chapter is based on published data and data submitted for publication:

E. Kunold\*, **P. Kleiner**\*, K. Rox, M. C. Jennings, I. M. Ugur, M. Reinecke, B. Küster, I. Antes, M. Rohde, W. M. Wuest, E. Medina, S. A. Sieber. Repurposing human kinase inhibitors to create an antibiotic active against drug-resistant *Staphylococcus aureus*. Manuscript submitted for publication. \*These authors contributed equally to this work.

**P. Kleiner**, S. A. Sieber, E. Kunold. Urea motif containing compounds and derivatives thereof as antibacterial drugs. International Patent Application, PCT/EP2017/063014, **2016**.

E. Kunold, P. Kleiner and S. A. Sieber designed experiments and interpreted results. P. Kleiner performed organic synthesis and structure-activity relationship studies. E. Kunold and P. Kleiner performed gel- and mass spectrometry-based labelling experiments. E. Kunold analyzed mass spectrometry-based data and conducted bioinformatic analysis. E. Kunold and P. Kleiner performed, unless otherwise mentioned, experiments for target identification and validation. J. Lehmann and E. Ruben performed studies in mycobacteria and analyzed and interpreted related data. M. C. Jennings and W. M. Wuest performed biofilm studies and analyzed and interpreted related data. I. M. Ugur and A. Antes performed molecular docking and dynamic studies and analyzed and interpreted related data. K. Rox and E. Medina performed animal studies and analyzed and interpreted related data. K. Rox and M. Rohde performed electron microscopy studies and analyzed and interpreted related data. M. Reinecke and B. Küster performed kinobead pulldown experiments and analyzed related data.

### 3.1. REPURPOSING NON-ANTIMICROBIAL DRUGS AS ANTIBIOTICS

Given the continuing global public health crisis originated in the current antibiotic resistance crisis (antimicrobial resistance crisis, Chapter 1.1), new chemical entities that address novel, resistance-free pathways are urgently needed to combat the successive waves of resistant bacteria (history of antibiotics, Chapter 1.1.1). As the pace of discovering novel and effective antibiotics has dramatically slowed down in recent years and clinical relevant antibiotics still target a limited set of bacterial pathways (modes of action, Chapter 1.1.2), an unbiased phenotypic screening approach against *S. aureus* was performed in an attempt to identify chemical scaffolds that address novel resistance-free pathways with essential function. This was further encouraged by the recent revival of phenotypic screening approaches and the fact that these screenings have contributed in large measure to the discovery of first-in-class drugs and the exploitation of novel pathways, irrespective of whether these pathways had previously been known to be pathology-related or represented unprecedented modes of action (phenotypic screening approaches, Chapter 1.2).

The prospects of phenotypic screens are mainly affected by the variety and diversity of compounds available to screen. While there has been recent success with natural product-based platforms as natural products are endowed by nature with diverse pharmacophores and a high degree of complexity due to scaffold diversity and stereochemistry that allows to cover broad chemical space (history of antibiotics, Chapter 1.1.1), the following phenotype-driven approach deliberately focused on a selected library of kinase inhibitors with many of them approved by regulatory authorities for human use. The rationale behind this approach is that many of these inhibitors are commercial available, synthetic in origin and have optimized and well characterized pharmacokinetic and safety profiles. Furthermore, a broad range of diverse eukaryotic kinase inhibitors awaits bacterial testing and drug repurposing, an upcoming strategy that represents a shortcut to often time-consuming and financially-taxing *de novo* drug discovery procedures.<sup>161-165</sup>

Examples of repurposed eukaryotic kinase inhibitors include a recent study that mined the wealth of available small molecule kinase inhibitor libraries for bacterial kinase-selective scaffolds. In a targeted approach, compounds possessing pharmacophores with eukaryotic kinase-inhibiting attributes were repurposed as inhibitors of the penicillin-binding-protein and serine/threonine kinase-associated (PASTA) kinase PrkA of *L. monocytogenes* and mycobacterial protein kinase B (PknB), respectively.<sup>163</sup> Both enzymes represent bacterial serine/threonine kinases with high structural homology to eukaryotic protein kinases.<sup>163</sup> Furthermore, a previous study by Pfizer screened an in-house library of ATP-competitive ligands, originally compiled to target eukaryotic protein kinases, against *S. aureus* in an unbiased whole-bacterial cell assay and identified antibacterial compounds containing a eukaryotic kinase inhibitor pharmacophore.<sup>165</sup> A structurally conserved ATP-binding site – in

this case the ATP-binding site of the biotin carboxylase subunit of the enzyme acetyl-CoA carboxylase – was thought to be the bacterial site of action.<sup>165</sup> Still, the number of bacterial ATP-depending enzymes that could be targeted by existing eukaryotic kinase inhibitors is unknown and it is unclear whether these kinase inhibitor pharmacophores could exploit other proteins within the wealth of essential bacterial pathways. Recently, sorafenib (Nexavar, BAY 43-9006, *Bayer*)<sup>166</sup>, an eukaryotic kinase inhibitor approved for the treatment of advanced renal cell carcinoma (RCC), unresectable hepatocellular carcinomas (HCC) and thyroid cancer, and few derivatives thereof were shown to be effective against *S. aureus*.<sup>167-168</sup> While it is uncertain if the bacterial target of sorafenib is indeed a bacterial kinase, Roberts et al. speculated that dnaK, a chaperone involved in DNA replication, might be involved in sorafenib's antibacterial action based on structural homologies of dnaK to human protein binders of sorafenib.<sup>167</sup> In contrast, Chang et al. reported that their bactericidal sorafenib derivatives might act by inhibiting the biosynthesis of major macromolecules, causing ATP leakage, disrupting membrane integrity and forming pores within the membrane.<sup>168-169</sup>

## 3.2. RESULTS AND DISCUSSION

### 3.2.1. Antibacterial Screen of Kinase Inhibitors

As phenotypic rescreening of compound libraries originally developed to exploit eukaryotic target proteins is worthwhile exploring as highlighted by the mentioned examples of successfully repurposed eukaryotic kinase inhibitors as antibiotic entities (Chapter 3.1), an unbiased whole-bacterial cell phenotypic screening approach for antibacterial effects against *S. aureus* NCTC 8325 was performed. Out of a library of 232 commercial kinase inhibitors (Appendix 7.1), a total of nine antibiotic compounds was identified causing bacterial growth inhibition at a concentration of 30  $\mu\text{M}$ . Determination of their minimal inhibitory concentration (MIC) values revealed that two compounds of related structure, sorafenib (**SFN**), in line with previous reports (Chapter 3.1)<sup>167-168</sup>, and regorafenib (Stivarga, BAY 73-4506, *Bayer*), a second-generation derivative of sorafenib approved for the treatment of colorectal cancer and gastrointestinal stromal tumors, exhibited the highest antibacterial potencies with MIC values of 3  $\mu\text{M}$  (1.4  $\mu\text{g}/\text{mL}$ ). AZ 960 (*AstraZeneca*; MIC 30  $\mu\text{M}$ , 10.6  $\mu\text{g}/\text{mL}$ ), brivanib alaninate (BMS-582664, *Bristol-Myers Squibb*; MIC 30  $\mu\text{M}$ , 13.2  $\mu\text{g}/\text{mL}$ ), gandotinib (LY2784544, *Eli Lilly*; MIC 30  $\mu\text{M}$ , 14.1  $\mu\text{g}/\text{mL}$ ), MK-2461 (*Merck*; MIC 30  $\mu\text{M}$ , 14.9  $\mu\text{g}/\text{mL}$ ), RAF265 (CHIR-265, *Novartis*; MIC 30  $\mu\text{M}$ , 15.6  $\mu\text{g}/\text{mL}$ ), TAK-285 (*Takeda Pharmaceutical Company*; MIC 30  $\mu\text{M}$ , 16.4  $\mu\text{g}/\text{mL}$ ) and degrasyn (WP1130; MIC 30  $\mu\text{M}$ , 3.8  $\mu\text{g}/\text{mL}$ ) inhibited growth only at higher concentrations (Figure 3.1). The antibacterial spectrum of **SFN** was subsequently determined against a panel of Gram-positive and -negative bacteria (Table 3.1; Appendix 7.2). While **SFN** exhibited Gram-positive activities only, it showed activity against antibiotic sensitive and multi-resistant *S. aureus* reference strains as well as ten clinical MRSA isolates, which possess reduced susceptibilities and/or resistances against a wide range of other established antibiotics (resistance profile of clinical isolates, Appendix 7.3). The lack of cross-resistance suggests that **SFN** might address a novel target mechanism that is different from the mode of action of existing antibiotics and that **SFN** is insensitive to established staphylococcal resistance strategies. In addition, activity against mycobacteria, including challenging *M. tuberculosis* (MIC 25  $\mu\text{M}$ , 11.6  $\mu\text{g}/\text{mL}$ ), was observed.

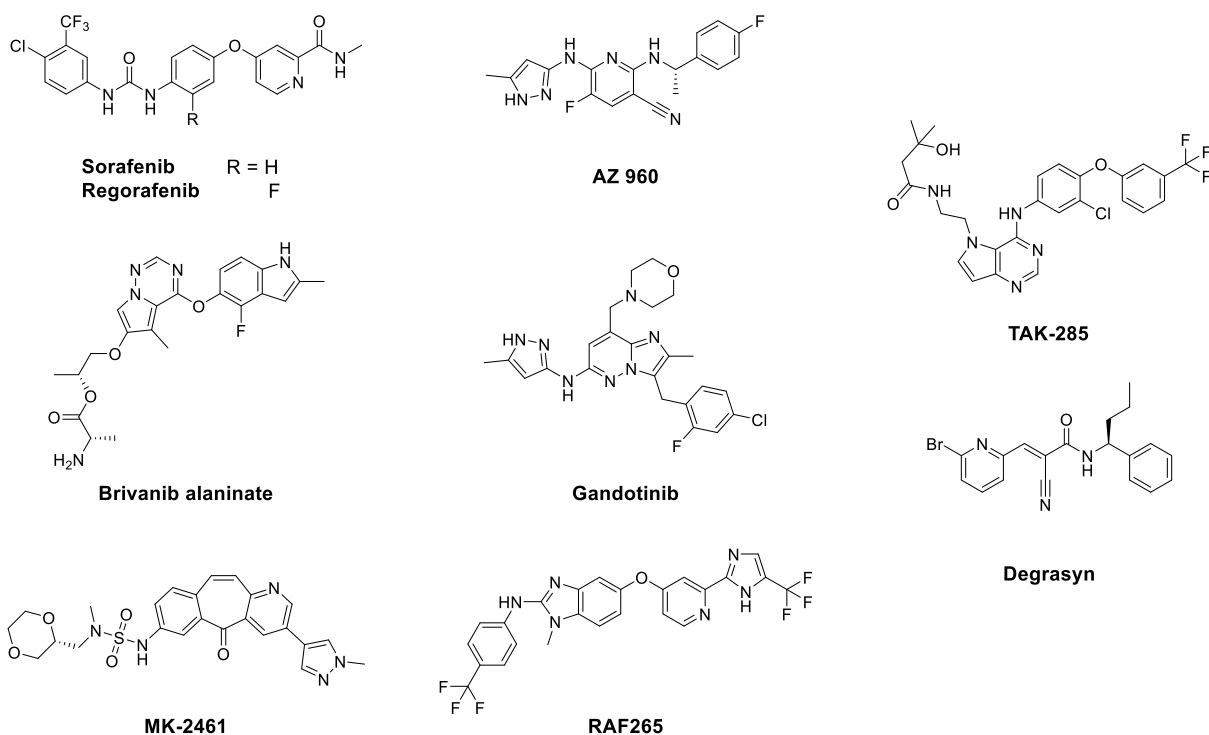


**Figure 3.1.** Non-antimicrobial drugs identified in the phenotypic screening approach against *S. aureus* NCTC 8325.

**Table 3.1.** Antibacterial spectrum of **SFN**. For further details see Appendix 7.2.

| Organism                          |                         | MIC ( $\mu\text{M}$ ) |
|-----------------------------------|-------------------------|-----------------------|
| Gram-positive                     |                         |                       |
| <i>Staphylococcus aureus</i>      | MSSA                    | 3                     |
|                                   | MRSA                    | 3 - 10                |
|                                   | MRSA, clinical isolates | 3 - 10                |
|                                   | VISA                    | 3                     |
| <i>Enterococcus faecalis</i>      | VRE                     | > 100                 |
| <i>Enterococcus faecium</i>       | VRE                     | > 100                 |
| <i>Mycobacterium tuberculosis</i> | H37Rv                   | 25                    |
| Gram-negative*                    |                         | > 100                 |

Abbreviations: MSSA, methicillin-sensitive *S. aureus*; MRSA, methicillin-resistant *S. aureus*, VISA, vancomycin-intermediate *S. aureus*; VRE, vancomycin-resistant enterococci.

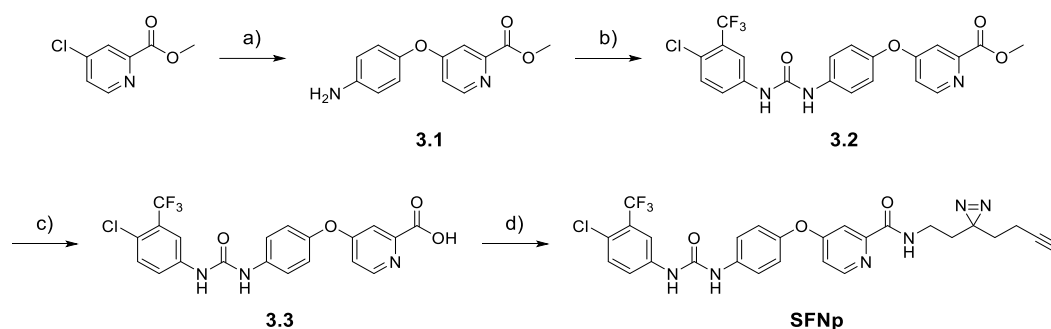
\* *A. baumannii*, *E. aerogenes*, *E. cloacae*, *E. coli*, *K. pneumoniae*, *P. aeruginosa*, *S. typhimurium*, *S. enteritidis*.

### 3.2.2. Target Deconvolution via Affinity-Based Protein Profiling

Although previous reports describing the antibacterial properties of **SFN** (Chapter 3.1),<sup>167-168</sup> target deconvolution and an in-depth mechanistic analysis of the molecular mode of action has not been conducted in detail so far. Herein, the AfBPP platform (AfBPP, Chapter 1.3) was utilized for target deconvolution on a full proteome basis that laid the foundation of further in-depth mechanistic studies.

### 3.2.2.1. Photoprobe Design and Synthesis

Proteomic target deconvolution by AfBPP is based on the synthetic modification of the **SFN** scaffold by a traceable terminal alkyne tag as well as a photocrosslinking moiety, which upon UV irradiation converts the transient probe-protein interaction into a stable, covalent linkage. As these synthetic modifications should not significantly alter the bioactivity of the parent compound and should not disturb the compound-protein interaction, detailed knowledge on the structure-activity relationship (SAR) is fundamental. Based on careful consideration of SAR data (Chapter 3.2.4) the distal methyl carboxamide moiety was identified as a modifiable part of the **SFN** scaffold and consequentially a minimalist terminal alkyne-containing diazirine photocrosslinker was introduced at this position. Synthesis was based on a modified published procedure<sup>138</sup> (Scheme 3.1) starting with the reaction of 4-aminophenol with methyl 4-chloropicolinate to access the lateral heteroaryl aryl ether moiety (**3.1**), followed by urea formation (**3.2**) with 4-chloro-3-(trifluoromethyl)phenyl isocyanate, hydrolysis of the distal methyl ester (**3.3**) and subsequent amide formation with the amine version of a “all-in-one” minimalist photocrosslinker<sup>138</sup> yielding photoprobe **SFNp**.



**Scheme 3.1.** Synthesis of sorafenib-based photoprobe **SFNp**. The photoprobe is based on the core structure of sorafenib that is synthetically equipped with a diazirine photocrosslinker and an alkyne tag required for affinity-based protein profiling (AfBPP). Reaction conditions: a) 4-Aminophenol,  $K_2CO_3$ , DMF, reflux, 47%; b) 4-chloro-3-(trifluoromethyl)phenyl isocyanate,  $CH_2Cl_2$ ,  $0^\circ C$  – room temperature, 79%; c) LiOH, THF/ $H_2O$ , room temperature, 90%; d) 2-(3-(but-3-yn-1-yl)-3H-diazirin-3-yl)ethan-1-amine<sup>138</sup>, EDC, DIEA, HOBt, DMF, room temperature, 20%.

Determination of MIC values against two different *S. aureus* strains (NCTC 8325 and USA300) confirmed that the antibacterial properties of **SFNp** were not significantly compromised compared to the parent compound as **SFNp** exhibited a MIC value ( $10\ \mu M$ ; 3.3-fold increase) slightly higher than that of **SFN** ( $3\ \mu M$ ; Chapter 3.2.1, Table 3.1) in both strains.

### 3.2.2.2. Gel-Based Affinity-Based Protein Profiling

Prior to mass spectrometry-based target identification, labelling conditions were optimized via gel-based analysis (AfBPP, Chapter 1.3). In an initial analytical labelling approach, **SFNp** was incubated with *S. aureus* NCTC 8325 cells in situ (50  $\mu$ M; 45 min, 25°C), followed by irradiation with UV light (365 nm, 30 min, 4°C) to facilitate a covalent linkage with the target protein. Mechanical disruption of bacterial cells and treatment with lysostaphin, a peptidoglycan cleaving endopeptidase, released proteins and photoprobe-labelled proteins were subsequently clicked to rhodamine-biotin azide<sup>128</sup> via the terminal alkyne tag. SDS-PAGE reduced the enormous complexity of the **SFNp**-treated proteome and successive fluorescent scanning resulted in distinct fluorescent bands (Figure 3.2 A). Furthermore, preincubation of bacterial cells with a 10-fold excess of unmodified **SFN** (0.5 mM; 45 min, 25°C) reduced overall labelling intensity of **SFNp** and specifically outcompeted distinct fluorescent bands in a competitive labelling experiment (Figure 3.2 A).

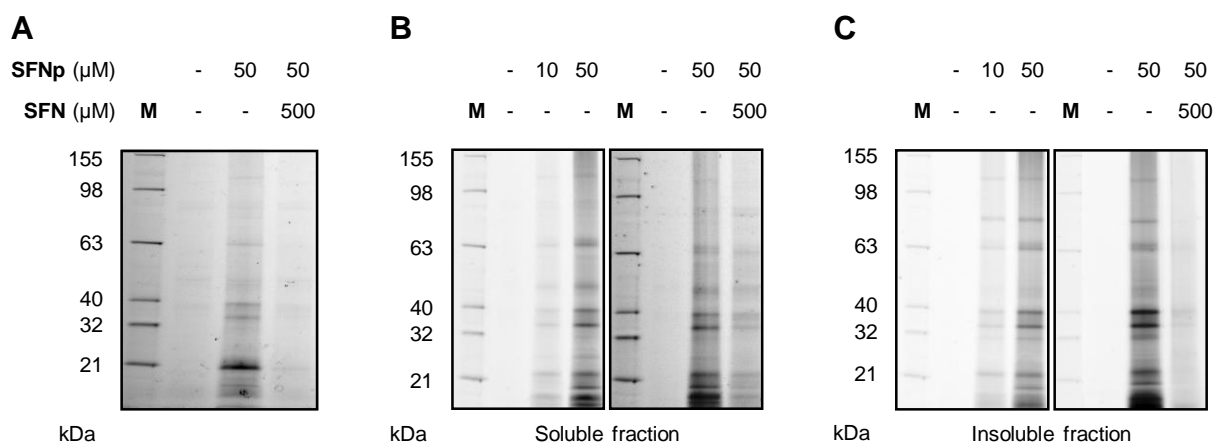


**Figure 3.2.** Gel-based analytical (A) and preparative (B, C) labelling of **SFNp**. (A) Fluorescence SDS-PAGE shows analytical labelling of *S. aureus* NCTC 8325 cells with **SFNp** (50  $\mu$ M) and competition with a 10-fold excess of **SFN** (0.5 mM). (B/C) Fluorescence SDS-PAGE shows preparative labelling of *S. aureus* NCTC 8325 cells after preincubation with DMSO or unmodified **SFN** (0.5 mM, 10-fold excess; competition) and subsequent labelling with **SFNp** (50  $\mu$ M) in soluble (B) and insoluble (C) fractions after enrichment on avidin beads.

A gel-based preparative labelling approach validated the established AfBPP protocol and confirmed sufficient labelling at photoprobe concentrations between 10 and 50  $\mu$ M as well as sufficient competition with a 10-fold excess of unmodified **SFN** in the soluble and insoluble fraction on a preparative scale (Figure 3.2 B, C). Here, labelled proteins were enriched on avidin-coated beads after photoprobe incubation (50  $\mu$ M; 45 min, 25°C), irradiation with UV light (365 nm, 30 min, 4°C), mechanical and enzymatic cell disruption and introduction of

trifunctional rhodamine-biotin azide<sup>128</sup> via click chemistry. Following preparative SDS-PAGE, distinct protein bands were visualized by fluorescent scanning (Figure 3.2 B, C).

### 3.2.2.3. Gel-Free Preparative Affinity-Based Protein Profiling

As gel-based preparative analysis resulted in multiple fluorescent bands, each encoding for several possible target proteins, a gel-free approach was consequently chosen in order to introduce a quantitative and statistical dimension to the in-depth mass spectrometric analysis (AfBPP, Chapter 1.3). Here, *S. aureus* NCTC 8325 cells were treated with **SFNp** (50  $\mu$ M; 45 min, 25°C), irradiated with UV light (365 nm, 30 min, 4°C) and lysed by mechanic and enzymatic means. Conjugation to trifunctional rhodamine-biotin azide<sup>128</sup> via click chemistry was followed by enrichment of labelled proteins on avidin-coated beads and release upon digest with trypsin. Stable isotopes were chemically incorporated at peptide level using dimethyl labelling<sup>103, 105</sup>. Isotope labelled tryptic peptides were measured on a high resolution LC-MS/MS instrument and analyzed using MaxQuant<sup>147</sup> software in combination with the Andromeda<sup>148</sup> search engine. Statistical evaluation (Student's *t*-test) of isotope ratios of detected proteins using Perseus<sup>149</sup> software considered proteins with high enrichment ratios ( $\log_2(\text{enrichment}) > 3$ ) and high confidence levels ( $p\text{-value} < 0.01$ ) as potential hits. Three control experiments were included to elucidate unspecific binding events: (i) A comparison to equally treated DMSO-control samples to determine unspecific protein binding to avidin-coated beads (Figure 3.3 A); (ii) competitive labelling by preincubation of bacterial cells with unmodified **SFN** (0.5 mM; 45 min, 25°C) and subsequent labelling with **SFNp** (50  $\mu$ M; incubation for 45 min, 25°C; irradiation at 365 nm for 30 min, 4°C) to ascertain that both compounds address the same potential target proteins (Figure 3.3 B); and (iii) a comparison to a small set of minimal photocrosslinker containing probes (**DA-1**, **DA-2** or **DA-3**, Figure 3.4 A; 50  $\mu$ M; incubation for 45 min, 25°C; irradiation at 365 nm for 30 min, 4°C)<sup>170</sup> to consider photocrosslinker-associated off-target binding (Figure 3.4).

(i) Comparing enriched proteins of **SFNp** to a DMSO control (Figure 3.3 A), only one enzyme, type I signal peptidase B (SpsB, Q2FZT7), an essential membrane-anchored serine protease involved in the staphylococcal protein secretion (Sec) pathway (Chapter 3.2.3.2),<sup>171</sup> could be revealed as a putative target in both the soluble and insoluble fraction. While SpsB was the sole protein in the soluble fraction within the selection criteria ( $\log_2(\text{enrichment ratio}) \geq 3$ ;  $p\text{-value} \leq 0.01$ ), five additional putative target proteins (uncharacterized proteins Q2G2W2, Q2FVZ5, Q2G117 and Q2FV70 as well as putative membrane protein Q2G1C5) were identified in the insoluble fraction.

(ii) Competitive labelling experiments confirmed the specificity of the sorafenib core scaffold for SpsB (Figure 3.3 B). Here, labelling and enrichment of SpsB was significantly

altered by the competition between parental **SFN** and related photoprobe **SFNp** in both the soluble and insoluble fraction. Furthermore, lytic regulatory protein (Lrp, Q2FWA8), a transmembrane protein of unknown function, was addressed by both compounds, **SFN** and **SFNp**, in the soluble fraction and competition between **SFN** and **SFNp** for four additional proteins (uncharacterized proteins Q2G117, Q2G2W2 and Q2G193 as well as putative membrane protein Q2G1C5) could be observed in the insoluble fraction.

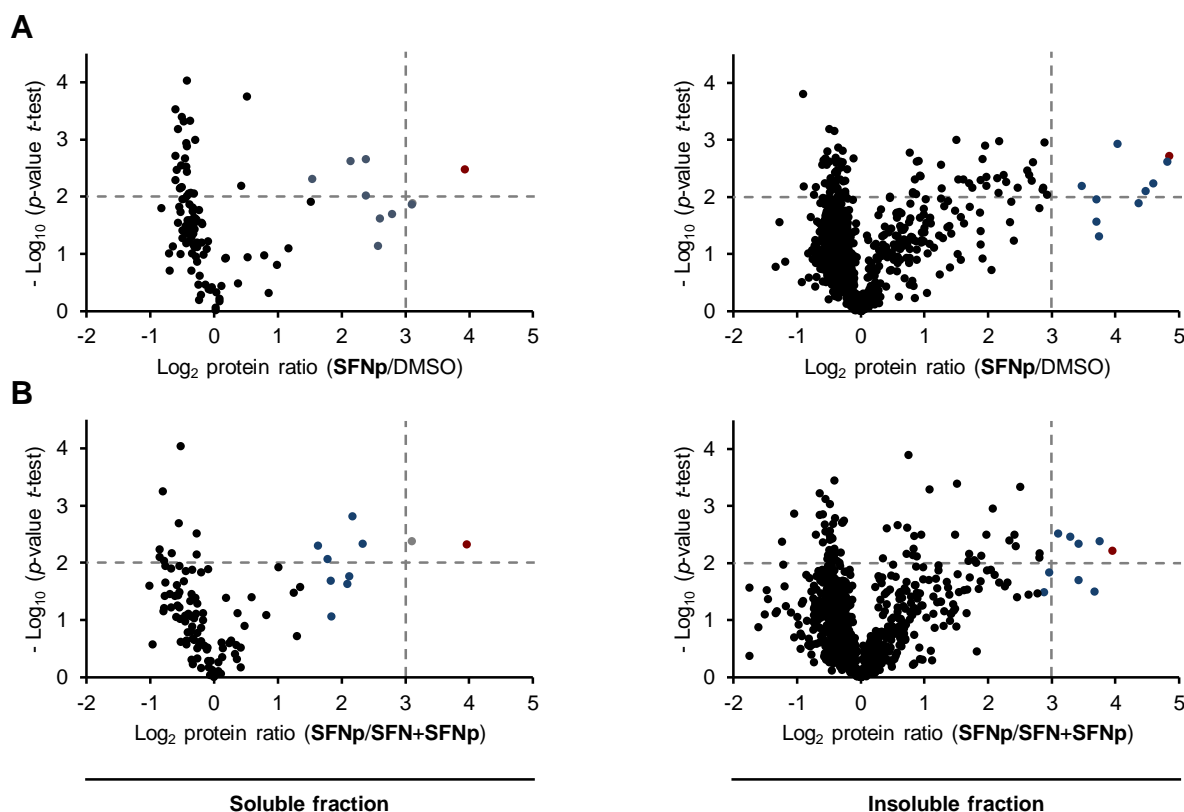


**Figure 3.3.** Target deconvolution of sorafenib by quantitative AfBPP. Volcano plots depict the  $\log_2$ -fold enrichment of proteins in the soluble and insoluble fraction after treatment of *S. aureus* NCTC 8325 cells with **SFNp** (50  $\mu\text{M}$ ) compared to DMSO (A) or to pretreatment with parental **SFN** (500  $\mu\text{M}$ ; B) in a competitive labelling experiment. Dashed lines represent a  $\log_2(\text{enrichment ratio})$  of 3 and a  $p$ -value of 0.01, respectively. The red and gray dots represent essential SpsB and lytic regulatory protein, respectively. Blue dots represent proteins that were selected for closer inspection based on their high overall enrichment ratios (Chapter 3.2.3.1, Table 3.2). Data represent average values;  $n = 3$  independent experiments performed in triplicates.

(iii) Careful consideration of photocrosslinker-associated off-target binding revealed that labelling and enrichment of SpsB by **SFNp** was not negatively influenced by background binding. Here, SpsB ranked among the most enriched proteins in **SFNp** labelling in direct comparison to each of the minimal photocrosslinker-probes (**DA-1**, **DA-2** or **DA-3**; Figure 3.4 C). Of note, all three minimal photoprobes (**DA-1**, **DA-2** or **DA-3**) exhibited modest overall

proteome labelling in *S. aureus* as shown in a gel-free quantitative as well as gel-based AfBPP approach (Figure 3.4 B, D).

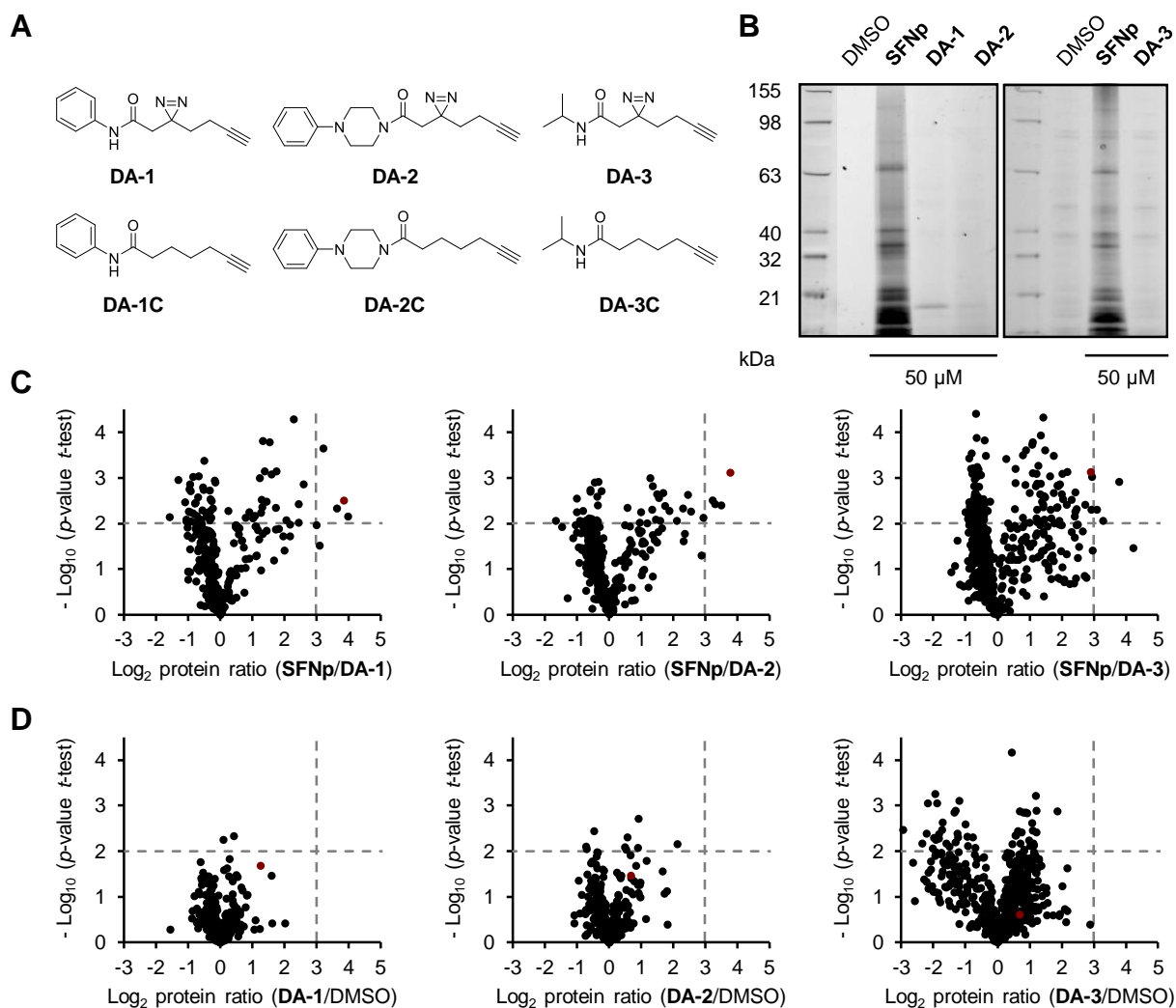


**Figure 3.4.** Photocrosslinker-associated background binding. (A) Structures of minimal photocrosslinker probes **DA-1**, **DA-2** and **DA-3** as well as corresponding control compounds **DA-1C**, **DA-2C** and **DA-3C** lacking the photoreactive diazirine moiety. (B) Comparison of gel-based labelling of **SFNp** (50  $\mu$ M) and **DA-1**, **DA-2**, **DA-3** (50  $\mu$ M) after enrichment on avidin-coated beads. (C) AfBPP of **SFNp** with consideration of photocrosslinker-associated background binding. (D) Photocrosslinker-associated background binding of **DA-1**, **DA-2** and **DA-3**. Volcano plots (C/D) illustrate the log<sub>2</sub>-fold enrichment of proteins from both – soluble and insoluble –fractions after treatment of *S. aureus* NCTC 8325 cells with minimal photocrosslinker probes **DA-1**, **DA-2** and **DA-3** (50  $\mu$ M) compared to **SFNp** (50  $\mu$ M; B) or DMSO (C) treatment. Dashed lines represent a log<sub>2</sub>(enrichment ratio) of 3 and a p-value of 0.01, respectively. The red dot represents the essential protein SpsB. Data represent average values;  $n = 3$  independent experiments performed in triplicates for **DA-1** and **DA-2** and  $n = 3$  independent experiments for **DA-3**.

Thoughtful evaluation of all implemented AfBPP experiments revealed that only SpsB consistently exhibited high enrichment ratios ( $\text{log}_2(\text{enrichment}) > 3$ ) and confidences (p-value < 0.01) in probe labelling and competition studies (Figure 3.3, red dot) and at least

8-fold less enrichment in comparison to the background-photolabelling of considered minimal photocrosslinker-probes (Figure 3.4, red dot). In addition to SpsB, 16 proteins with high enrichment ratios in labelling and competition experiments (Figure 3.3, gray and blue dots; Chapter 3.2.3.1, Table 3.2) were selected for closer inspection. Here, selection criteria defined enrichment ratios within the top ten enriched proteins for at least one of the respective experiments as substantial for closer consideration. Of note, no known protein kinase was identified using these selection criteria.

### 3.2.3. Target Validation

#### 3.2.3.1. Narrowing Down the List of Putative Target Proteins

In order to evaluate the respective role in bacterial killing for each of the selected proteins, a MIC shift assay with corresponding transposon mutants (Nebraska transposon mutant library)<sup>172</sup> was performed. Here, a MIC shift upon **SFN** treatment should be observed in comparison to the wild-type strain, when the respective protein plays a crucial part in the phenotypic effect. Only the transposon mutant of Lrp showed a moderate increase in its MIC value by 3.3-fold upon compound treatment indicating a contribution to the overall antibiotic mechanism of **SFN** (Table 3.2). Due to its essential function for *S. aureus* viability no transposon and direct knockout mutant were available for SpsB. However, the nominal essentiality of SpsB has been questioned recently, as upregulation of an ABC transporter can compensate for its essential function.<sup>173-175</sup> Here, respective ABC transporter functions as an alternative SpsB-independent secretion pathway under certain circumstances, in particular as a strategy to escape antibiotic treatment by SpsB inhibitors.<sup>173-175</sup> With regard to these reports, the antibiotic activity of **SFN** against a viable SpsB-deletion strain bearing a resistance-induced ABC transporter (ARC0001 $\Delta$ SpsB)<sup>174</sup> was determined in comparison to respective *S. aureus* wild-type strain N315. Interestingly, no MIC shift upon compound treatment was observed. However, a direct comparison between the SpsB-deletion and wild-type strain is problematic as corresponding phenotypes differ considerably. The SpsB-deletion strain is characterized by a slow growth that is constrained at phases of high cell density and accompanied by the clumping of cells – all in all, observations that indicate a general loss of fitness.

Based on the consistent results of MS-based target deconvolution by AfBPP and its importance for staphylococcal viability, further validation and in-depth mechanistic analysis focused on SpsB.

**Table 3.2.** Proteins selected for closer inspection based on AIBPP-based target deconvolution analysis. Data include information on  $\log_2$ (protein ratio) and  $-\log_{10}(p\text{-value})$  of proteins enriched in the soluble and insoluble fraction after treatment of *S. aureus* NCTC 8325 cells with **SFNP** (50  $\mu\text{M}$ ) compared to DMSO or to pretreatment with parental **SFN** (500  $\mu\text{M}$ ) in a competitive labelling experiment. In addition, MIC values against corresponding *S. aureus* USA300 transposon mutants (Nebraska Mutant Transposon Library) are reported.

| Protein name                                       | Protein ID | SFNP (50 $\mu\text{M}$ ) compared to DMSO |                              |                                |                              | SFNP (50 $\mu\text{M}$ ) in competition with SFN (500 $\mu\text{M}$ ) |                              |                                |                              | Transposon library   |                        |     |
|--|------------|---|------------------------------|--------------------------------|------------------------------|---|------------------------------|--------------------------------|------------------------------|--|------------------------|-----|
|  |            | soluble                                   | insoluble                    | soluble                        | insoluble                    | soluble   | insoluble                    | soluble                        | insoluble                    | <i>S. aureus</i> USA300 Nebraska mutant transposon library | MIC shift assay w/ SFN | N/A |
|  |            | $\log_2(\text{protein ratio})$            | $-\log_{10}(p\text{-value})$ | $\log_2(\text{protein ratio})$ | $-\log_{10}(p\text{-value})$ | $\log_2(\text{protein ratio})$  | $-\log_{10}(p\text{-value})$ | $\log_2(\text{protein ratio})$ | $-\log_{10}(p\text{-value})$ |  |                        |     |
| Signal peptidase IB                                | Q2FZT7     | 3.929                                     | 2.482                        | 4.845                          | 2.716                        | 3.957   | 2.324                        | 3.955                          | 2.219                        | N/A  | N/A                    | N/A |
| Lytic regulatory protein                           | Q2FWA8     | 3.113                                     | 1.892                        | -                              | -                            | 3.105   | 2.384                        | -                              | -                            | NE721  | 10                     | 10  |
| PTS system EIIBC component                         | Q2G1G5     | 2.376                                     | 2.022                        | 0.439                          | 1.037                        | 1.633   | 2.304                        | 0.611                          | 1.030                        | NE112  | 3                      | 3   |
| Probable quinol oxidase subunit 2                  | Q2FZJ9     | 2.139                                     | 2.622                        | 1.705                          | 2.245                        | 1.828   | 1.690                        | 1.481                          | 2.495                        | NE92   | 3                      | 3   |
| NADH dehydrogenase-like protein                    | Q2FZV7     | 1.539                                     | 2.314                        | 0.674                          | 1.262                        | 2.173   | 2.810                        | 0.581                          | 1.153                        | NE1884   | 3                      | 3   |
| ABC transporter, substrate-binding protein         | Q2G2D8     | 1.507                                     | 1.912                        | 0.110                          | 0.336                        | 1.774   | 2.062                        | 0.007                          | 0.017                        | NE1615   | 3                      | 3   |
| Probable DNA-directed RNA polymerase subunit delta | Q2FWD0     | -   | -                            | -0.530                         | 1.029                        | -   | -                            | 3.417                          | 1.706                        | NE646  | 3                      | 3   |
| Membrane protein, putative                         | Q2G1C5     | -   | -                            | 4.031                          | 2.928                        | -   | -                            | 3.287                          | 2.462                        | NE166  | 3                      | 3   |
| Uncharacterized proteins                           | Q2G2W2     | -   | -                            | 4.812                          | 2.622                        | -   | -                            | 3.424                          | 2.334                        | NE419  | 3                      | 3   |
|  | Q2FVZ5     | 2.789                                     | 1.701                        | 4.590                          | 2.242                        | 2.115   | 1.762                        | 2.955                          | 1.830                        | NE866  | 3                      | 3   |
|  | Q2G117     | -   | -                            | 4.469                          | 2.100                        | -   | -                            | 3.752                          | 2.378                        | NE323  | 3                      | 3   |
|  | Q2FV70     | -   | -                            | 3.469                          | 2.195                        | -   | -                            | 2.306                          | 1.664                        | -  | -                      | -   |
|  | Q2G193     | 2.596                                     | 1.619                        | 4.359                          | 1.891                        | 1.295   | 0.724                        | 3.097                          | 2.519                        | NE733  | 3                      | 3   |
|  | Q2FVS2     | 3.095                                     | 1.867                        | 3.697                          | 1.959                        | 2.333   | 2.335                        | 2.802                          | 2.101                        | NE1076   | 3                      | 3   |
|  | Q2FZG5     | 2.566                                     | 1.139                        | -                              | -                            | 1.841   | 1.064                        | -                              | -                            | NE1886   | 3                      | 3   |
|  | Q2FVN6     | 2.379                                     | 2.658                        | 2.704                          | 2.613                        | 2.092   | 1.635                        | 1.981                          | 1.873                        | NE291  | 3                      | 3   |
|  | Q2G2N2     | -   | -                            | 3.74259                        | 1.306                        | -   | -                            | 3.675                          | 1.505                        | NE779  | 3                      | 3   |
|  | Q2FZQ2     | -   | -                            | 3.70514                        | 1.56715                      | -   | -                            | 2.882                          | 1.486                        | NE1270   | 3                      | 3   |

### 3.2.3.2. Type I Signal Peptidase, a Putative Bacterial Target of Sorafenib

The majority of proteins predetermined to function outside the cytoplasmic membrane are generally translocated via the Sec- (secretion) pathway out of the bacterial cell. These include proteins of diverse functional roles in bacterial physiology including nutrient uptake, excretion, metabolism, cell structure, communication, virulence and bacterial defense.<sup>171, 176</sup> Here, post-translational translocation via the Sec pathway involves several steps:<sup>171, 176</sup> Preproteins containing a small *N*-terminal signal peptide as a marker for their destined translocation are directed to the membrane, bound directly to SecA, a peripheral membrane ATPase component of the Sec-machinery, and are subsequently translocated across the membrane through the SecYEG translocon channel, a process driven by the ATPase SecA. Type I signal peptidase (SpsB), a serine-endopeptidase located in the cytoplasmic membrane, removes the signal peptide during or shortly after translocation resulting in the release of the mature protein from the cytoplasmic membrane.

Within the Sec-pathway of *S. aureus*, SpsB represents an attractive antibacterial target for several reasons:<sup>171</sup> (i) SpsB is essential for bacterial virulence and viability; (ii) it is accessible as it is exposed to the bacterial cell surface; and (iii) the active site composition of SpsB significantly differs from that of human peptidases enabling selective drug design. However, developing inhibitors for type I signal peptidases, such as SpsB, is generally hampered by the fact that these enzymes do not respond to classical protease inhibitors, including inhibitors against aspartic acid, metallo, serine, and cysteine proteases.<sup>177</sup> This is due to their unconventional Ser-Lys dyad that acts by a *si*-face nucleophilic attack of its substrates in contrast to the *re*-face nucleophilic attack utilized by most classical catalytic triads.<sup>171, 178</sup> Still, distinct inhibitors of SpsB have been reported demonstrating the druggability of this enzyme. These include members of the naturally occurring polypeptides of the arylomycin family,<sup>179-181</sup> the natural cyclic depsipeptide krisynomycin<sup>182</sup>, synthetic 5S penems<sup>183-185</sup>, and several rational designed peptide substrate mimics<sup>178, 186-187</sup>. Inhibitors of SpsB mediate bacterial death either by the accumulation of unprocessed proteins jeopardizing the integrity of the cytoplasmic membrane or by the hindered secretion of extracellular proteins that are essential for viability.<sup>182, 188</sup> The antibacterial potential of these inhibitors, however, is shadowed by frequent target mutations<sup>189</sup> as well as induction of bypass pathways that restore viability upon SpsB inhibition<sup>173-175</sup>.

### 3.2.3.3. Validation of Type I Signal Peptidase as a Putative Target of Sorafenib

Introductory remark: Although medicinal chemistry and structure-relationship studies of the sorafenib scaffold are discussed in detail in Chapter 3.2.4, selected compounds are introduced within this chapter for an easier reading and a better understanding of the context. These compounds include **PK150**, the most potent **SFN** analog, as well as **SFN-C** and **PK150-C** structurally related, but antibiologically inactive analogs of **SFN** and **PK150**, respectively.

To directly demonstrate an interaction between sorafenib and SpsB, the full-length enzyme was cloned and overexpressed in *Escherichia coli* BL21(DE3)pLysS harboring a SpsB expression vector, followed by purification utilizing the Strep-tag system as previously described by Rao et al.<sup>190</sup> The identity of the purified enzyme was verified by SDS-PAGE and full protein MS. While recombinant SpsB spiked into either PBS buffer or human A549 lysate (1 mg/mL total protein concentration) was labelled by **SFNp** in an analytical labelling approach (Figure 3.5 A, B), MS-based binding studies proved to be challenging. The known limited stability of isolated SpsB as a result of self-degradation<sup>190</sup> (Figure 3.5 C; FRET-based peptidase assay, Figure 3.7 A) restricted further experiments to systems where SpsB remained in its natural membrane environment. Here, based on observations of LepB from *E. coli*,<sup>191</sup> self-cleavage is prevented as the autolysis site is physically separated from the catalytic site with both being located at opposite sides of the membrane. Indeed, the enzymatic activity was retained when endogenous SpsB was tested within its staphylococcal membrane surroundings (Figure 3.5 D; FRET-based peptidase assay, Figure 3.7 A).

A different approach, where the presence of non-ionic detergents, such as Triton X-100, increase the activity and to a limited extent the stability of SpsB (Figure 3.5 C),<sup>190</sup> probably by mimicking the hydrophobic membrane environment, was not further considered as non-ionic detergents directly interfered with **SFN** and **PK150**, the most active sorafenib analog, and adversely affected their antibacterial properties (Chapter 3.2.4.5, Figure 3.15).

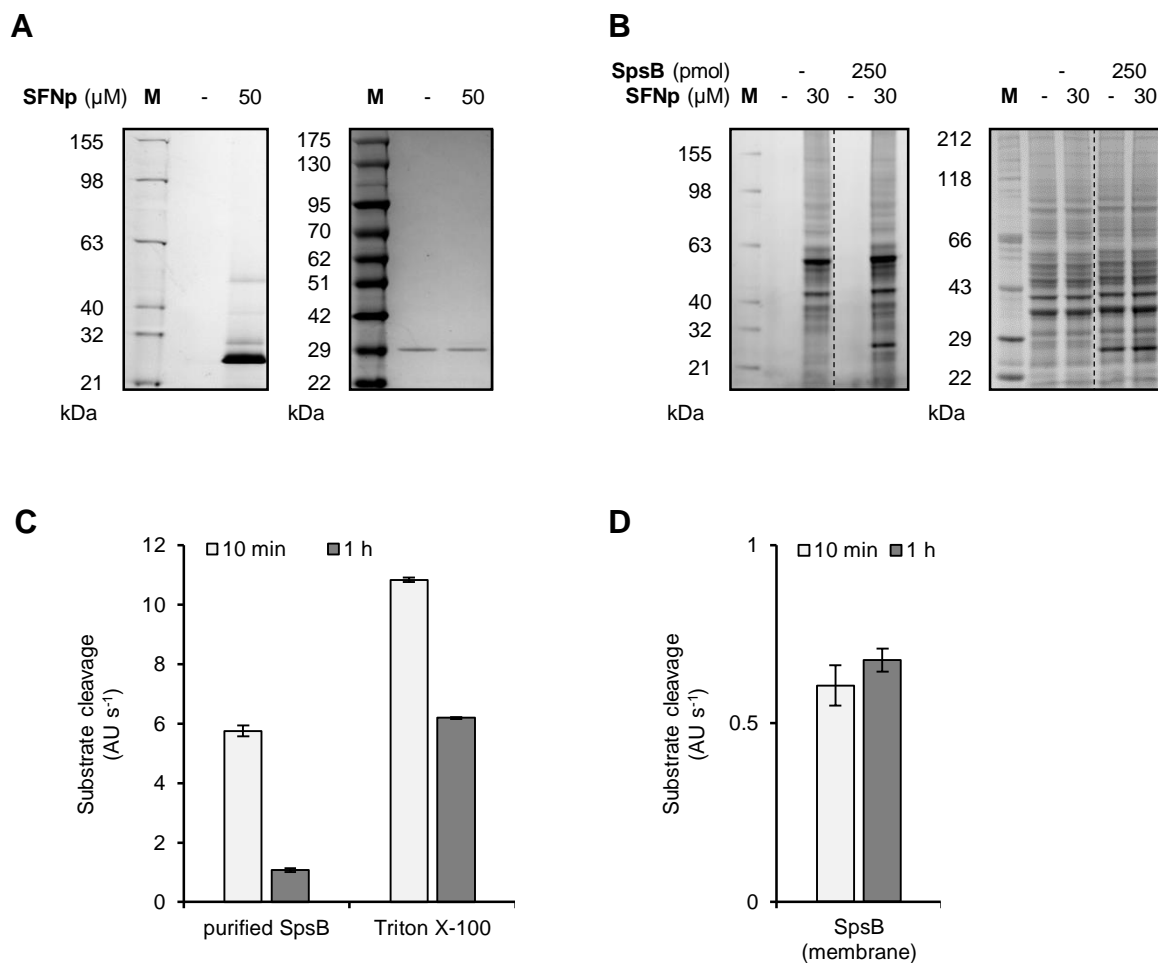


**Figure 3.5.** (A/B) Labelling of recombinant and purified SpsB spiked in either PBS buffer (5 μM final SpsB concentration; A) or human A549 lysate (1 mg/mL total protein concentration; 5, 50 and 250 pmol final SpsB amount; B) by **SFNp** (30 or 50 μM, respectively). Loading controls are represented by the coomassie-stained gels. (C) Degradation of isolated SpsB demonstrated by determining the in vitro activity of SpsB after incubation at 37°C (10 min or 1 h) by a FRET-based assay. The presence of Triton X-100 (0.5% (v/v)) prevented self-cleavage to a limited extent and stimulated activity. Data represent average values ± SD;  $n = 1$  independent experiments in triplicates. (D) Stability of endogenous SpsB within its natural *S. aureus* membrane environment (200 μg/mL total membrane protein concentration) shown by measuring the enzymatic activity after incubation at 37°C (10 min or 1 h). Data represent average values ± SD;  $n = 6$  measurements per independent replicate.

In order to illustrate an interaction with sorafenib in a membrane environment, SpsB was overexpressed in the *E. coli* expression strain and directly labelled by **SFNp** (50 μM; Figure 3.6). A competitive labelling experiment with an excess of unmodified **SFN** and **PK150** (500 μM), respectively, reduced SpsB labelling, thereby confirming that all compounds address SpsB in a similar manner.

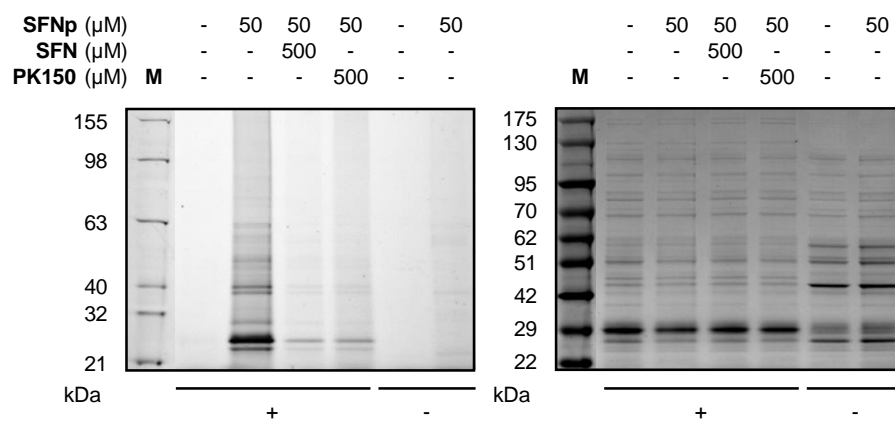


**Figure 3.6.** Labelling of *E. coli* BL21(DE3)pLysS cells harboring pET-55-DEST-SpsB (with induced (+) or not induced (-) expression of SpsB, respectively) by **SFNp** (50  $\mu\text{M}$ ) after preincubation with either DMSO or **SFN** and **PK150** (500  $\mu\text{M}$ ), respectively, in a competitive labelling approach. Loading controls are represented by the coomassie-stained gel.

The in vitro peptidase activity of SpsB can be monitored by a Förster resonance energy transfer (FRET) assay utilizing a commercially available intramolecular quenched fluorogenic peptide substrate (Figure 3.7 A).<sup>190</sup> Specificity of this synthetic substrate is generated by its sequence similarity to the signal peptide of the SceD preprotein of *Staphylococcus epidermidis*.<sup>190</sup> Arylomycin A4, a close analog of known SpsB inhibitor arylomycin A2 (SpsB inhibitors, Chapter 3.2.3.2),<sup>179, 189</sup> was used to establish the specificity of the FRET-based peptidase assay when using membrane fractions of *S. aureus* NCTC 8325 as the source of endogenous SpsB, resembling a previously published method.<sup>182</sup> Here, arylomycin A4 showed dose-dependent inhibition of substrate cleavage (Figure 3.7 B).

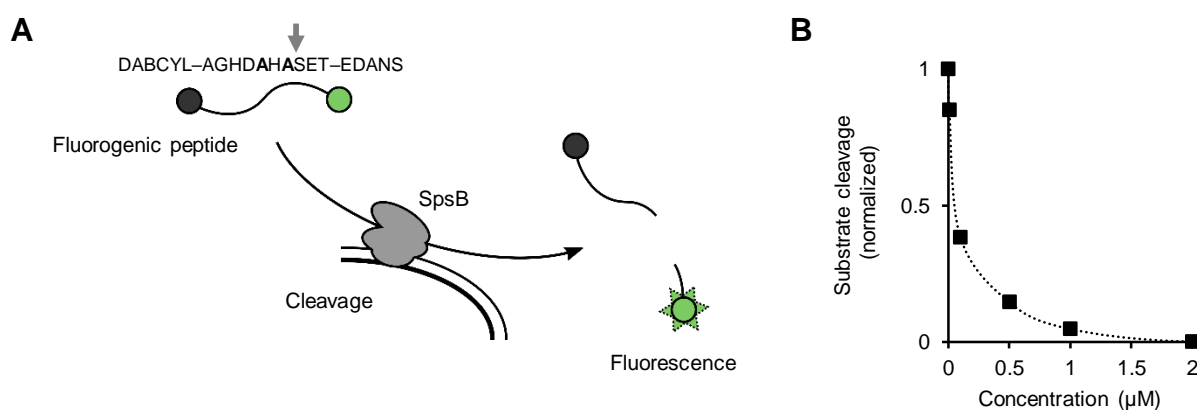


**Figure 3.7.** (A) Schematic representation of the peptidase activity assay based on Förster resonance energy transfer (FRET) that monitors the cleavage of an intramolecular quenched fluorogenic peptide substrate. The substrate is based on the signal peptide sequence of *Staphylococcus epidermidis* SceD preprotein modified with the fluorescent donor 5-((2-aminoethyl)amino)-1-naphthalenesulfonic acid (EDANS) and the quenching acceptor 4-((4-(dimethylamino)phenyl)azo)benzoic acid (DABCYL). (B) Concentration-dependent inhibition of SpsB activity by arylomycin A4 monitored by a FRET-based activity assay using

membrane fractions of *S. aureus* NCTC 8325 as the source of SpsB (200 µg/mL total membrane protein concentration). Substrate cleavage rates are normalized to DMSO-treated samples. Data represent average values ± SD; *n* = 3 independent experiments in triplicates.

To determine whether sorafenib binding affects the enzymatic activity of SpsB, the peptidase activity of isolated *S. aureus* membranes were measured after treatment with various concentrations of **SFN**. Surprisingly, **SFN** did not inhibit substrate turnover by SpsB but in contrary resulted in a significant stimulation of peptidase activity of up to 1.2-fold at a **SFN** concentration of 10 µM and 1.7-fold at saturating concentrations compared to a DMSO control (Figure 3.8 A). The ability of **SFN** to stimulate the enzymatic turnover of SpsB was confirmed using membrane fractions of the *E. coli* expression strain with induced SpsB overexpression, while *E. coli* membranes lacking SpsB expression exhibited only low substrate turnover (Figure 3.8 B). In line with its enhanced antibiotic activity **PK150** increased substrate turnover to a greater extent than **SFN** in the SpsB peptidase assay. **PK150**-activated SpsB showed an activity enhanced by 1.7-fold compared to **SFN**-activated SpsB in native *S. aureus* and induced *E. coli* membranes (at saturated concentrations). This corresponds to a 2.3 – 2.9-fold increase over base activity at saturated concentrations (Figures 3.8 A, B).

**SFN-C** and **PK150-C** – two structurally related analogs of **SFN** and **PK150**, respectively, without antibacterial activities – had no impact on the enzymatic activity of SpsB as shown by peptidase assays utilizing membrane fractions prepared from *S. aureus* (Figure 3.8 A) as well as *E. coli* with induced SpsB expression (Figure 3.8 B). Moreover, no activation was achieved with control compounds based on the small set of minimal photocrosslinkers (Figure 3.8 C; Chapter 3.2.2.3, Figure 3.4 A).

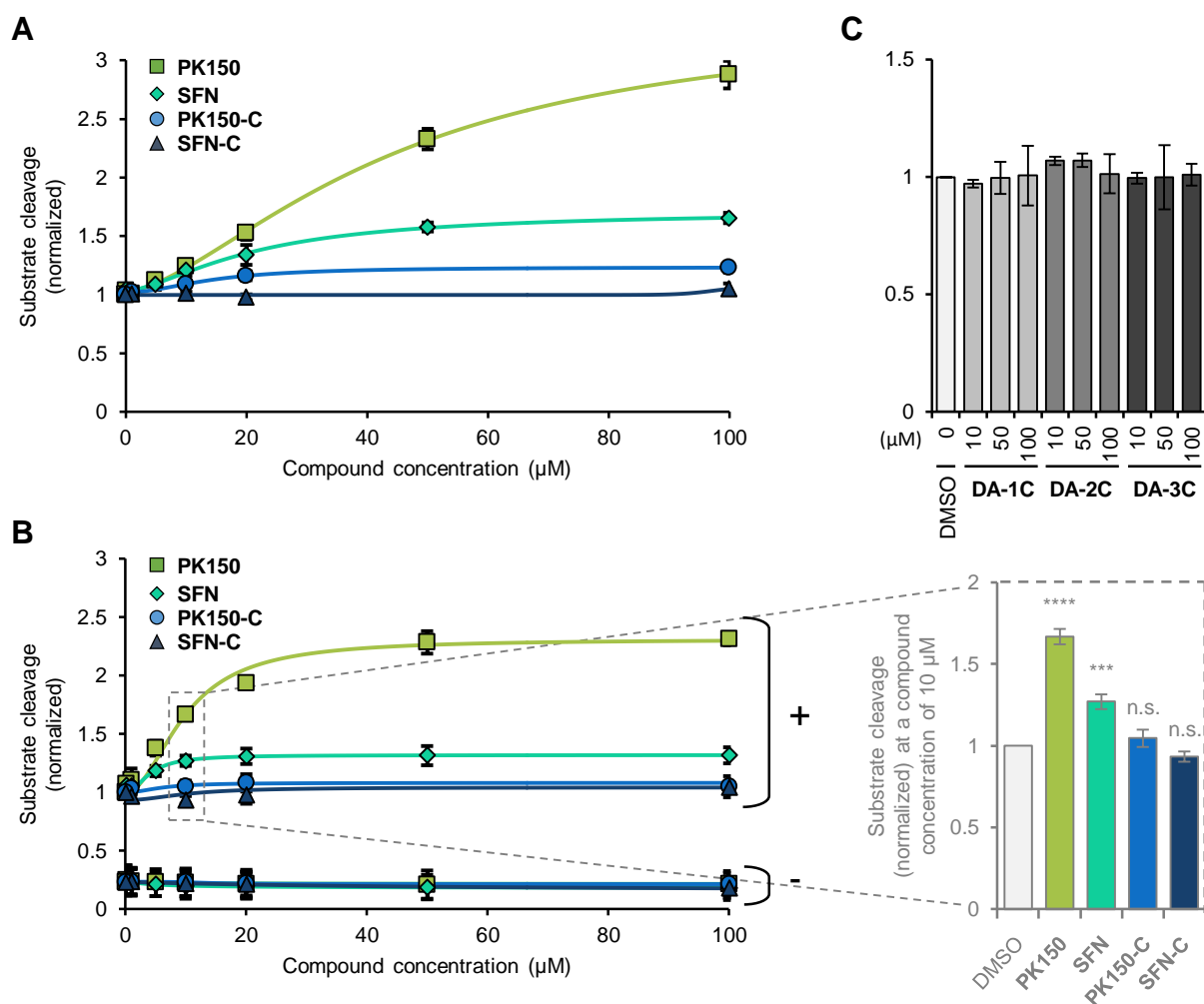


**Figure 3.8.** (A/B) Concentration-dependent influence of **SFN** and **PK150** as well as corresponding control compound **SFN-C** and **PK150-C** on the peptidase activity of membrane-bound SpsB from *S. aureus* NCTC 8325 (200 µg/mL total membrane protein concentration; A) or *E. coli* BL21(DE3)pLysS cells harboring pET-55-DEST-SpsB (50 µg/mL total membrane protein concentration; B) with either induced (+) or not induced (-) overexpression of SpsB. (C) Influence of control probes of respective minimal photocrosslinker probes **DA-1C**, **DA-2C** and **DA-3C** (Chapter 3.2.2.3, Figure 3.4 A) on the enzymatic activity of SpsB measured by a FRET-based peptidase assay with *S. aureus* NCTC 8325 membranes containing endogenous SpsB (0.2 mg/mL total membrane protein concentration). Substrate cleavage rates are normalized to DMSO-treated samples; in the case of *E. coli* membranes to DMSO-treated samples from induced membranes. Data represent average values  $\pm$  SD;  $n = 3$  independent experiments in triplicates.

Preliminary experiments exploiting an alternative purification approach to isolate SpsB in a stable conformation from the soluble fraction of the induced *E. coli* expression strain (Figure 3.9 A), showed increased peptidase activity for the purified enzyme upon **SFN** and **PK150** treatment (Figure 3.9 B). Here, the increase in substrate turnover of compound-activated SpsB was comparable to the results obtained in membrane-based assays (Figure 3.8 A, B). Although the reason for the enhanced stability of SpsB purified from the cytosolic fraction is not clear at

this stage, it is tempting to speculate that the protein takes a better conformation during overexpression compared to its equivalent purified from the insoluble fraction.

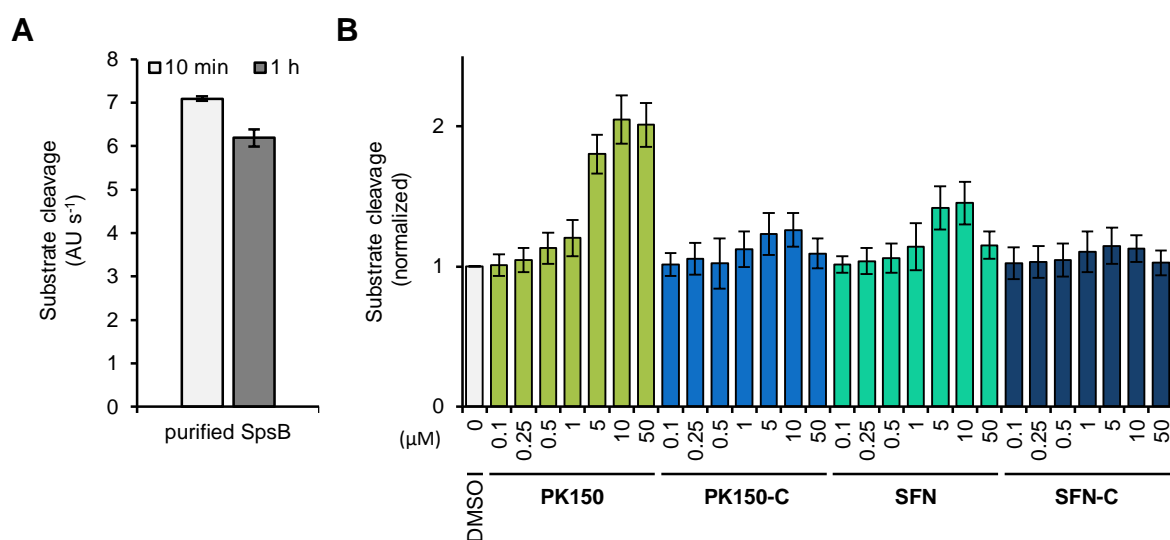


**Figure 3.9.** (A) Stability of SpsB isolated from the cytosolic fraction demonstrated by determining the enzymatic activity after incubation at 37°C (10 min or 1 h) by a FRET-based peptidase assay. Data represent average values  $\pm$  SD;  $n = 3$  independent experiments in triplicates. (B) Influence of **SFN** and **PK150** as well as corresponding control compounds **SFN-C** and **PK150-C** on the substrate turnover of fl-SpsB (0.2  $\mu$ M) purified from the cytosolic fraction of *E. coli* BL21(DE3)pLysS harboring pET-55-DEST-SpsB as determined by a FRET-based peptidase assay. Substrate cleavage rates are normalized to DMSO-treated samples. Data represent average values  $\pm$  SD;  $n = 3$  replicate experiments in triplicates.

### 3.2.4. Medicinal Chemistry – The Relationship Between Structure and Antibacterial as well as SpsB-Activating Properties

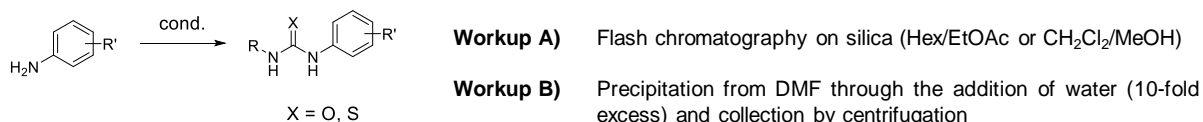
Introductory remark: The results of the structure-activity relationship study are discussed in the following using selected examples. All synthesized analogs are summarized in Appendix 7.4 together with their respective biological properties.

#### 3.2.4.1. Structure-Activity Relationship of Hit Compound Sorafenib

In order to gain a better understanding of the functional role of key structural features of sorafenib for its antibiotic properties and to explore a potential correlation between antibiotic activity and SpsB stimulation, an in-depth structure–activity relationship (SAR) study of the sorafenib scaffold was conducted. To this end, a library of 72 analogs bearing systematic variations of the **SFN** core scaffold was constructed and all derivatives were examined for their antibacterial potency and their SpsB activating properties. Here it should be noted that the spectroscopic properties of each compound in the presence and absence of fluorogenic

substrate were determined in order to identify interferences with the fluorometric readout of the FRET-based peptidase assays.

The preparation of urea and thiourea-containing compounds was generally straightforward and achieved by reaction of an amine with an isocyanate or thioisocyanate, respectively (Scheme 3.2).



**Scheme 3.2.** Synthesis of sorafenib analogs containing *N,N*-disubstituted urea or thiourea motifs from amines and isocyanates or thioisocyanates, respectively. Reaction conditions: Isocyanate or thioisocyanate, CH<sub>2</sub>Cl<sub>2</sub>, 0°C – room temperature, 13 – 98%. Reaction conditions for primary (as depicted) and secondary amines are identical.

First off, a series of urea compounds was examined that exemplified the initial chemical optimization process of the anticancer drug sorafenib:<sup>166, 192</sup> The initial 3-thienyl urea hit compound **3.4**, originally identified in a HTS screening for inhibitors of serine/threonine protein kinase Raf1 by *Bayer* and *Onyx*, further optimized compound **3.5**, bearing a 4-methyl substitution on the phenyl ring, as well as 3-amino-isoxazoles **3.6** and **3.7**, analogs with improved potency against Raf1, did neither show notable antibacterial effects against *S. aureus* NCTC 8325 nor did they had an effect on SpsB activity (Table 3.3).

Next, the structure-activity relationship of the sorafenib skeleton was explored in detail by systematic variations of structural key features, namely the 4-chloro-3-(trifluoromethyl)phenyl, the urea, and aryl heteroaryl ether moieties. All replacements explored for the lateral 4-chloro-3-(trifluoromethyl)phenyl ring resulted in a loss in antibacterial as well as SpsB-activating potency (Table 3.4) indicating that this moiety is an invariable part of the molecule. For example, aliphatic replacements for the substituted phenyl group by moieties with differing steric demand (**3.8**, **3.9** and **3.10**) were not tolerated suggesting that removing the aromatic character of this key structural feature is not favorable. Furthermore, introduction of aromatic, sterically demanding moieties (**3.11** and **3.12**) at this position caused a complete loss of biological activity. Even minor alterations of the 4-chloro and/or 3-trifluoromethyl substituents in **SFN** were not tolerated: Replacement of the trifluoromethyl substituent with a methyl moiety (**3.13**) as well as removal of the 4-chloro substituent resulting in a 3-(trifluoromethyl)phenyl analog (**3.14**) or the removal of both substituents resulting in an unsubstituted phenyl ring (**SFN-C**) affected the antibiotic properties and the ability to stimulate peptidase activity dramatically.

**Table 3.3.** Structures and biological properties of **SFN** analogs that exemplify the medicinal chemistry efforts in the development of human kinase inhibitor sorafenib. N/A = Data not available due to assay interferences.

| Compound |  | Log <i>P</i> | IC <sub>50</sub> Raf1 (μM) | MIC (μM) | SpsB activity (normalized) at 50 μM |
|----------|--|--------------|----------------------------|----------|-------------------------------------|
| 3.4      |  | 2.82         | 17                         | > 100    | N/A                                 |
| 3.5      |  | 3.25         | 1.7                        | > 100    | N/A                                 |
| 3.6      |  | 4.01         | 1.1                        | > 100    | 1.20 ± 0.10                         |
| 3.7      |  | 2.76         | 0.23                       | 100      | 1.19 ± 0.14                         |

**Table 3.4.** Structure-activity relationship study of the lateral 4-chloro-3-(trifluoromethyl)phenyl moiety. N/A = Data not available due to assay interferences.

| Compound |  | Log <i>P</i> | MIC (μM) | SpsB activity (normalized) at 50 μM |
|----------|--|--------------|----------|-------------------------------------|
| SFN      |  | 3.77         | 3        | 1.64 ± 0.12                         |
| 3.8      |  | 1.95         | > 100    | 0.99 ± 0.07                         |
| 3.9      |  | 4.17         | > 100    | 1.05 ± 0.22                         |
| 3.10     |  | 3.44         | > 100    | 1.13 ± 0.14                         |
| 3.11     |  | 3.49         | > 100    | 0.99 ± 0.09                         |
| 3.12     |  | 3.11         | > 100    | 1.07 ± 0.20                         |
| 3.13     |  | 3.07         | > 100    | 1.12 ± 0.08                         |
| 3.14     |  | 3.15         | > 100    | 1.33 ± 0.20                         |
| SFN-C    |  | 2.23         | > 100    | 1.18 ± 0.16                         |

Variations of the central urea motif showed that structural changes thereof were restricted (Table 3.5): Only conversion to a thiourea group (**3.15**) almost retained the biological properties of **SFN**, while replacement by an amide yielded analogs (**3.16** and **3.17**) that were inactive against *S. aureus*. The key role of the central urea motif was further emphasized by the observation that methylation of one of the NH-groups (**3.18**) led to a loss of biological activities.

**Table 3.5.** Structure-activity relationship study of the medial urea motif. N/A = Data not available due to assay interferences.

| Compound    |  | Log <i>P</i> | MIC (μM) | SpsB activity (normalized) at 50 μM |
|-------------|--|--------------|----------|-------------------------------------|
| <b>SFN</b>  |  | 3.77         | 3        | 1.64 ± 0.12                         |
| <b>3.15</b> |  | 4.19         | 10       | 1.58 ± 0.28                         |
| <b>3.16</b> |  | 4.07         | > 100    | 1.31 ± 0.13                         |
| <b>3.17</b> |  | 4.27         | > 100    | N/A                                 |
| <b>3.18</b> |  | 3.91         | > 100    | 1.17 ± 0.03                         |

Variations of the aryl heteroaryl ether moiety revealed this part of the molecule as an area for high optimization potential. As replacement by cyclic secondary amines resulted in several compounds with weak to moderate activities in both assays (**3.19**, **3.20**, **3.21** and **3.22**; Table 3.6), further chemical compound optimization concentrated on derivatives containing the medial *N,N'*-diphenyl urea motif of sorafenib (Table 3.7).

**Table 3.6.** Structure-activity relationship study – replacement of the aryl heteroaryl ether by cyclic secondary amines. N/A = Data not available due to assay interferences.

| Compound    |  | Log <i>P</i> | MIC (μM) | SpsB activity (normalized) at 50 μM |
|-------------|--|--------------|----------|-------------------------------------|
| <b>3.19</b> |  | 3.42         | 30       | 1.15 ± 0.20                         |
| <b>3.20</b> |  | 2.22         | > 100    | 1.06 ± 0.10                         |
| <b>3.21</b> |  | 3.97         | 10       | 1.25 ± 0.39                         |
| <b>3.22</b> |  | 4.18         | 30       | 1.56 ± 0.07                         |

Here, conversion of the distal methyl carboxamide by a methyl ester (**3.2**) was tolerated as well as complete removal thereof (**3.23**) indicating that this substituent is not crucial for antibacterial activity. Further replacement of the 4-pyridyl moiety with a phenyl ring yielded a diphenyl ether analog (**3.24**) with an improved MIC value and SpsB-activating effect. Variations of the diphenyl ether functionality (**3.25** and **3.26**) resulted in a drop in activity compared to **3.24**, however these analogs exhibited comparable or even improved antibacterial as well as SpsB-stimulating properties in comparison to hit compound **SFN**. Removal of the distal phenyl ring in **3.24** resulted in a loss of activity (**3.27** and **3.36**), but the potency of these analogs were still comparable to **SFN**. The evaluation of further analogs lacking the distal phenyl ring revealed no clear structure-activity correlation (Table 3.7). Strikingly, among all compounds of this series a 2,2-difluoro-1,3-benzodioxole analog **PK150** revealed the highest antibacterial potency with a MIC value of 0.3  $\mu\text{M}$  (0.12  $\mu\text{g/mL}$ ) against *S. aureus* NCTC 8325. In addition, **PK150** enhanced substrate turnover of SpsB with a 1.5-fold elevated activity at a compound concentration of 50  $\mu\text{M}$  compared to **SFN** (Chapter 3.2.3.3, Figure 3.8 A, B, 3.9 B). Due to its superior activity profile, compound **PK150** was selected for further in-depth analysis.

**Table 3.7.** Structure-activity relationship study of the lateral aryl heteroaryl ether moiety. N/A = Data not available due to assay interferences.

| Compound |  | Log <i>P</i> | MIC<br>( $\mu$ M) | SpsB activity<br>(normalized)<br>at 50 $\mu$ M |
|----------|--|--------------|-------------------|--|
| SFN      |  | 3.77         | 3                 | 1.64 $\pm$ 0.12                                |
| 3.2      |  | 4.31         | 3                 | 1.43 $\pm$ 0.13                                |
| 3.23     |  | 4.28         | 3                 | 1.91 $\pm$ 0.25                                |
| 3.24     |  | 5.53         | 0.5               | 2.10 $\pm$ 0.14                                |
| 3.25     |  | 6.01         | 1                 | 2.06 $\pm$ 0.05                                |
| 3.26     |  | 5.29         | 3                 | 1.86 $\pm$ 0.06                                |
| 3.27     |  | 4.04         | 3                 | 1.49 $\pm$ 0.16                                |
| 3.28     |  | 4.95         | 0.7               | 1.79 $\pm$ 0.14                                |
| 3.29     |  | 4.49         | > 100             | 1.06 $\pm$ 0.03                                |
| 3.30     |  | 4.93         | > 100             | 1.34 $\pm$ 0.21                                |
| 3.31     |  | 5.31         | 0.7               | 1.53 $\pm$ 0.20                                |
| 3.32     |  | 3.44         | 30                | 1.70 $\pm$ 0.16                                |
| 3.33     |  | 3.89         | 30                | 1.15 $\pm$ 0.21                                |
| 3.34     |  | 3.89         | > 100             | 1.28 $\pm$ 0.16                                |
| 3.35     |  | 3.22         | 100               | 1.90 $\pm$ 0.13                                |
| 3.36     |  | 3.94         | 3                 | 1.34 $\pm$ 0.29                                |
| 3.37     |  | 3.59         | 30                | 1.64 $\pm$ 0.16                                |
| PK150    |  | 4.51         | 0.3               | 2.54 $\pm$ 0.39                                |

## 3.2.4.2. Structure-Activity Relationship of PK150

Although investigation of the SAR of **PK150** identified several analogs to be more potent than hit compound **SFN**, the potency could not be further improved compared to **PK150**. Examples of analogues related to **PK150** are given in Table 3.8.

**Table 3.8.** Structure-activity relationship study of the core scaffold of **PK150**. N/A = Data not available due to assay interferences.

| Compound |  | Log <i>P</i> | MIC (μM) | SpsB activity (normalized) at 50 μM |
|----------|--|--------------|----------|-------------------------------------|
| PK150    |  | 4.51         | 0.3      | 2.54 ± 0.39                         |
| 3.38     |  | 4.91         | > 100    | 1.13 ± 0.18                         |
| 3.39     |  | 4.18         | > 100    | 1.39 ± 0.18                         |
| 3.40     |  | 3.85         | > 100    | 0.99 ± 0.13                         |
| 3.41     |  | 3.81         | 0.5      | 1.23 ± 0.05                         |
| 3.42     |  | 3.88         | 0.7      | 2.39 ± 0.23                         |
| PK150-C  |  | 2.96         | > 100    | 1.15 ± 0.01                         |
| 3.43     |  | 4.93         | 0.5      | 1.85 ± 0.44                         |
| 3.44     |  | 4.80         | > 100    | 1.43 ± 0.10                         |
| 3.45     |  | 5.01         | 3        | N/A                                 |
| 3.46     |  | 5.41         | 30       | 1.83 ± 0.41                         |
| 3.47     |  | 4.65         | > 100    | 1.39 ± 0.11                         |
| 3.48     |  | 3.79         | 10       | 1.40 ± 0.01                         |
| 3.49     |  | 4.51         | 0.5      | 1.42 ± 0.08                         |

For instance, both fluorine substituents of the benzodioxole moiety appeared to be crucial as removal thereof (**3.48**) was associated with a significant drop in both activities. The same

applied to changes in regiochemistry, however analog **3.49** almost retained the antibiotic potency of **PK150**. Furthermore, all replacements explored for the central urea motif in **PK150** resulted in analogs that were significantly less potent with the exception of a thiourea analog (**3.43**) coinciding with the observations made with regard to **SFN** (Chapter 3.2.4.1). Several aliphatic moieties as well as substituted phenyl rings were investigated as replacements for the lateral 4-chloro-3-(trifluoromethyl)phenyl ring. In line with the SAR of **SFN** (Chapter 3.2.4.1), alteration of this structural motif resulted in less potent compounds, highlighted by the fact that even removal of both substituents of the 4-chloro-3-(trifluoromethyl)phenyl moiety (**PK150-C**) abolished activities. Interestingly, the 3-chloro substituent seemed not to be vital as removal thereof (**3.42**) resulted only in a slight drop of activities. While analog **3.41** with a methyl group replacing the trifluoromethyl substituent almost retained antibiotic potency, it showed only a slight stimulation of SpsB.

### 3.2.4.3. Correlation Between Bacterial Killing and Compound-Induced SpsB Stimulation

Overall evaluation of SAR data obtained in bacterial growth inhibition assays (MIC) and FRET-based SpsB assays indicated a direct correlation between bacterial killing and compound-induced SpsB stimulation (Figure 3.10).

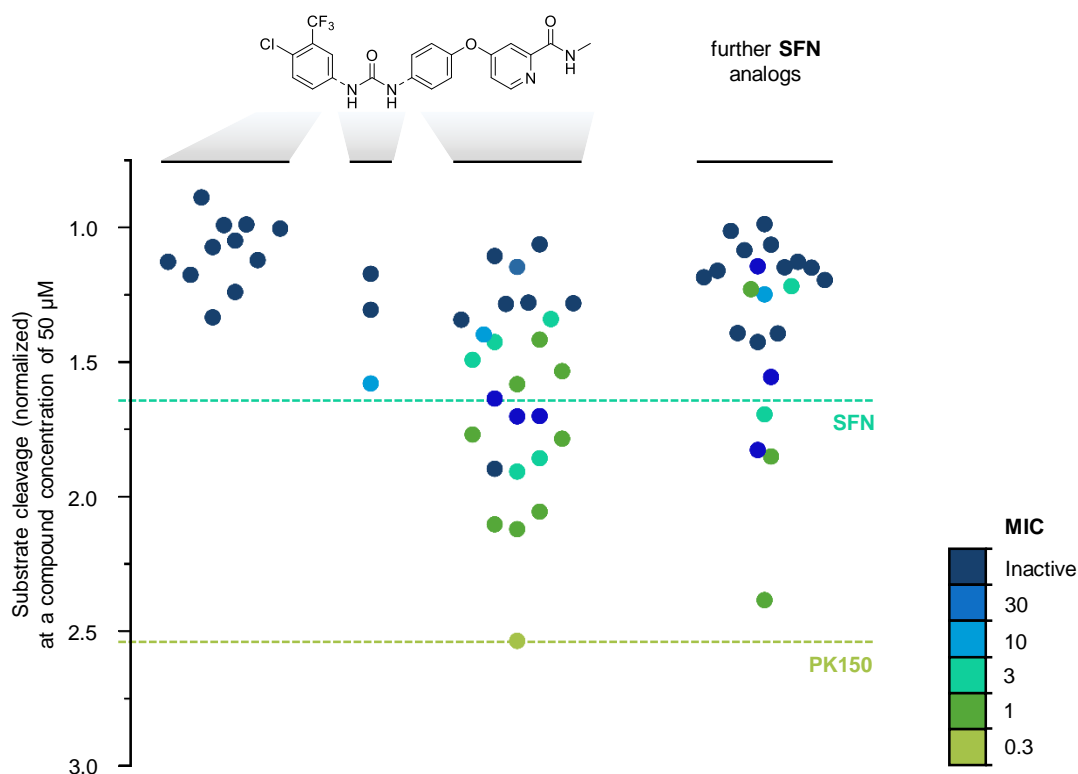


**Figure 3.10.** Structure-activity relationship study with sorafenib analogs highlighting the role of various structural key elements for the activation of SpsB (boxplot) as well as antibacterial activity (color code). Antibacterial activity was tested against *S. aureus* NCTC 8325; MIC values are represented according

to the introduced color code. SpsB activity was determined by a FRET-based peptidase activity assay using *S. aureus* NCTC 8325 membranes as the source of endogenous SpsB (0.2 mg/mL total membrane protein concentration; 50  $\mu$ M compound concentration). Substrate cleavage rates are normalized to DMSO-treated samples.

While most compounds without antibiotic activity did not enhance SpsB activity (purple and blue dots, Figure 3.10), few analogs with high antibiotic potency were not able to alter substrate turnover significantly. Interestingly, compounds **3.41** and **3.49** displayed excellent abilities to kill bacteria despite significant deficiencies in stimulating SpsB (Chapter 3.2.4.2, Table 3.8). Since **3.41** only differs in the 3-trifluoromethyl substituent of the lateral aryl ring and **3.49** is a regioisomer of **PK150**, it is tempting to speculate that these analogs share an additional target involved in the phenotypic effect with **PK150**, while the differences in antibacterial potency are related to weak effects on SpsB of these analogs.

#### 3.2.4.4. Antibacterial Characteristics of PK150

Examination of the antibacterial spectrum of **PK150** (Table 3.9; Appendix 7.2) revealed that the compound preserved potency against various MRSA strains including several clinical isolates (resistance profile of clinical isolates, Appendix 7.3), possessed improved activity against mycobacteria including *M. tuberculosis* (MIC 2  $\mu$ M, 0.93  $\mu$ g/mL) and in contrast to hit compound **SFN**, inhibited the growth of vancomycin-resistant enterococci (VRE; MIC 3  $\mu$ M; 1.0  $\mu$ g/mL). However, the compound was inactive against all tested Gram-negative bacteria.

**Table 3.9.** Antibacterial spectrum of **PK150**. For further details see Appendix 7.2.

| Organism                          |                         | MIC ( $\mu$ M) |
|-----------------------------------|-------------------------|----------------|
| Gram-positive                     |                         |                |
| <i>Staphylococcus aureus</i>      | MSSA                    | 0.3            |
|                                   | MRSA                    | 0.3 - 1        |
|                                   | MRSA, clinical isolates | 0.3            |
|                                   | VISA                    | 0.3            |
| <i>Enterococcus faecalis</i>      | VRE                     | 3              |
| <i>Enterococcus faecium</i>       | VRE                     | 1              |
| <i>Mycobacterium tuberculosis</i> | H37Rv                   | 2              |
| Gram-negative*                    |                         | > 100          |

Abbreviations: MSSA, methicillin-sensitive *S. aureus*; MRSA, methicillin-resistant *S. aureus*, VISA, vancomycin-intermediate *S. aureus*; VRE, vancomycin-resistant enterococci.

\* *A. baumannii*, *E. aerogenes*, *E. cloacae*, *E. coli*, *K. pneumoniae*, *P. aeruginosa*, *S. typhimurium*, *S. enteritidis*.

The antibacterial properties of **PK150** and **SFN** were further characterized by killing kinetic studies that revealed a rapid bactericidal killing of exponentially growing as well as stationary *S. aureus* cells in a concentration-dependent manner (Figure 3.11).

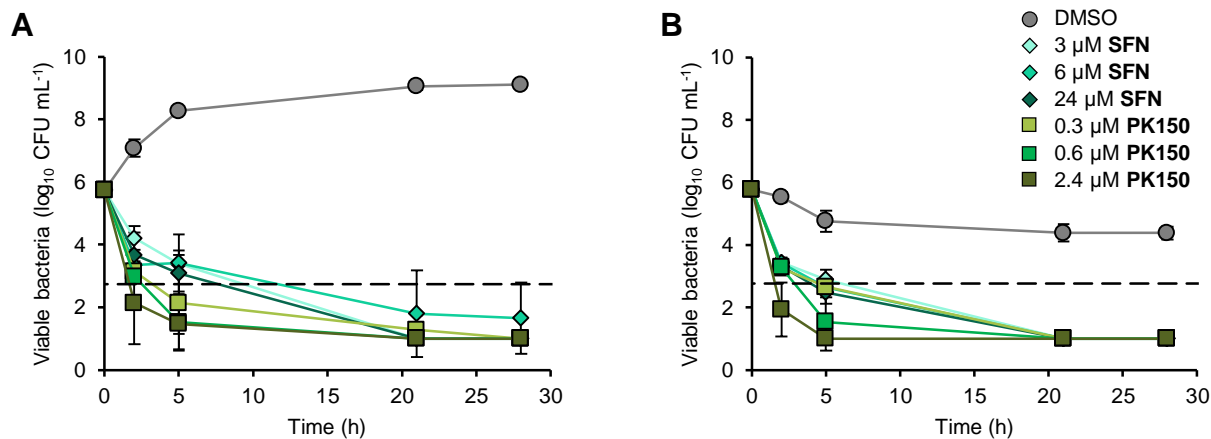


**Figure 3.11.** Time-dependent killing of exponentially growing (A) and stationary (B) *S. aureus* NCTC 8325 at different concentrations of **SFN** and **PK150**. Growth arrest of stationary bacteria was achieved by treatment with tetracycline at 2-fold MIC. Dashed lines represents 99.9% of killed bacteria. Data represent average values  $\pm$  SD;  $n = 3$  per group.

Besides its bactericidal properties, **PK150** eradicated persisters and established biofilms (persister cells and biofilm, Chapter 1.1.3). Persister cells were selected from stationary cultures of *S. aureus*, which in particular harbor large populations of persisters, under antibiotic pressure resulting from gentamicin treatment (Figure 3.12 A).<sup>193</sup> In a second independent assay format,<sup>194</sup> bacterial populations of different densities were treated with respective compounds in combination with oxacillin, which was used for persister cell selection, for 20 and 70 hours (Figure 3.12 B). In both assays **PK150** and parental sorafenib showed an effective reduction of persister cell numbers in contrast to established antibiotic ciprofloxacin as well as inactive control compounds **SFN-C** and **PK150-C**.



n.s., not significant; \*\* $p < 0.01$ , \*\*\* $p < 0.001$ , \*\*\*\* $p < 0.0001$  (Student's-test) for compound- vs. DMSO/OXA-treated groups.  $OD_{600, b.t.} = OD_{600}$  before treatment.

Furthermore, **PK150** effectively eradicated biofilms – the primary state in which *S. aureus* exists in the environment – of MSSA as well as MRSA bacteria (minimum biofilm eradication concentration (MBEC) of 12.5 – 25  $\mu\text{M}$ ; Figure 3.13).

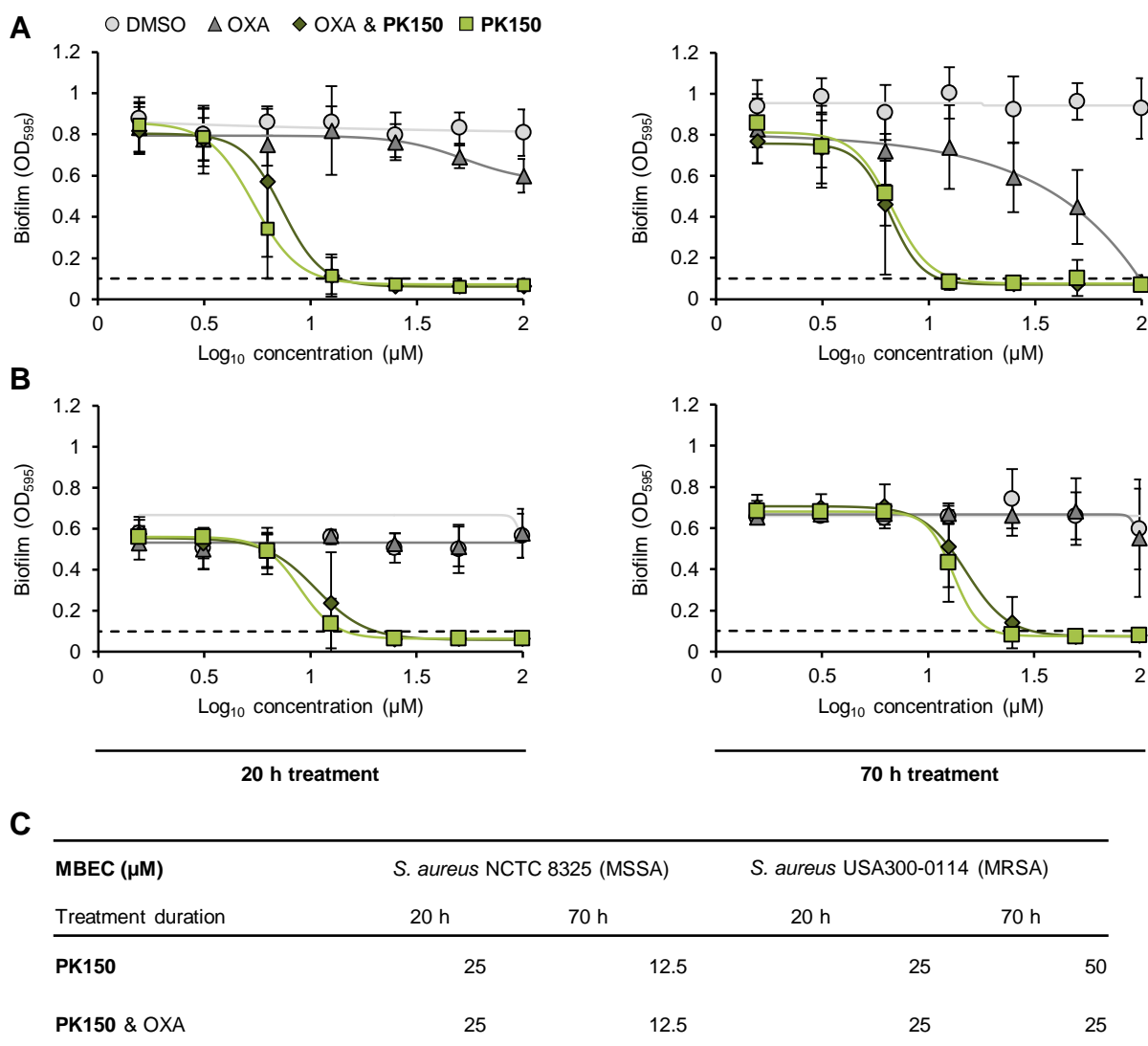


**Figure 3.13.** Eradication of *S. aureus* NCTC 8325 (A) and USA300-0114 (B) biofilms after treatment (20 h or 70 h) with DMSO, **PK150** alone or in combination with oxacillin (OXA; equimolar concentrations). The dashed line represents the minimum biofilm eradication concentration (MBEC). Data represent average values  $\pm$  SD;  $n = 9$  per group. (C) Minimum biofilm eradication concentration (MBEC) values for treatment of *S. aureus* NCTC 8325 and USA300-0114 with **PK150** alone or in combination with oxacillin (OXA; equimolar concentrations). MBEC values were defined by regrowth assays that result in an  $OD_{595}$  value of  $< 0.1$ .

Since rapid resistance development often ultimately limits the useful lifespan of promising antibiotic candidates as antibiotics in clinical settings, the resistance acquisition of **PK150** and **SFN** was tested over a period of 27 days. During serial passaging in the presence of sub-MIC levels (0.25 – 4-fold MIC) *S. aureus* bacteria showed rapid adaptation to oxacillin, which functioned as a positive control,<sup>86</sup> as well as **SFN** as seen by the reduced susceptibilities to both compounds within a few passages. In contrast, resistance did not develop to **PK150** within the experimental settings (Figure 3.14). Despite the fact that resistance development assays under artificial laboratory conditions cannot reflect clinical settings, the lack of resistance development may indicate that **PK150** addresses multiple targets thereby impeding bacterial adaptation.<sup>195</sup>

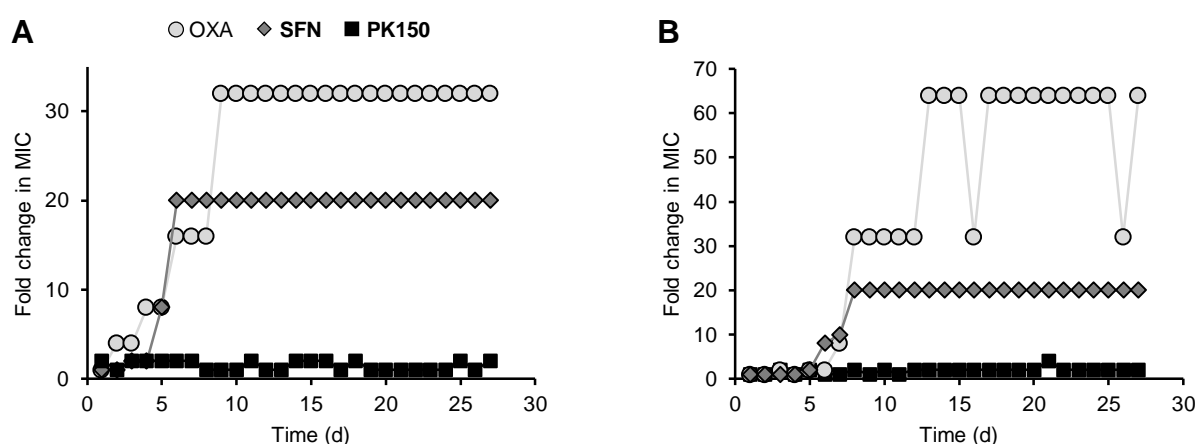


**Figure 3.14.** Resistance acquisition during serial passaging of *S. aureus* NCTC 8325 in the presence of sub-MIC levels of oxacillin, **SFN** or **PK150** as assessed in two independent experiments (A, B). For **SFN**, 20-fold MIC was the highest concentration tested (solubility limit).

### 3.2.4.5. Verification of PK150

As sorafenib is known to form aggregates that can non-specifically associate with proteins and sequester enzymes from substrate – a phenomenon known as promiscuous aggregate-based inhibition that is often associated with false-positive hits in biological assays<sup>196-197</sup> – the ability of **PK150** to form aggregates was examined by dynamic light scattering (DLS). Similar to **SFN**, **PK150** is prone to form aggregates at micromolar concentrations (critical aggregation concentration (CAC) = 10 – 25  $\mu\text{M}$ ; Figure 3.15). However, the CAC value exceeds the MIC value (Chapter 3.2.1, Table 3.1; Chapter 3.2.4.4, Table 3.9) and the concentration required for SpsB stimulation (Chapter 3.2.3.3, Figure 3.8 A, B, 3.9 B) indicating that colloidal agglomeration does not interfere with the observed effects in both assays. Tween 80, a non-ionic detergent, was able to disrupt aggregate formation as DLS signal intensities were reduced by the addition thereof (0.023% (v/v); Figure 3.15 A). However, the addition of Tween 80 (0.023% (v/v)) caused a 10-fold reduction in antibacterial potency in a detergent-

based MIC screen indicating an undesired quenching of **PK150** in solution as this shift was observed at concentrations at which no aggregates were detectable by DLS (Figure 3.15 B).

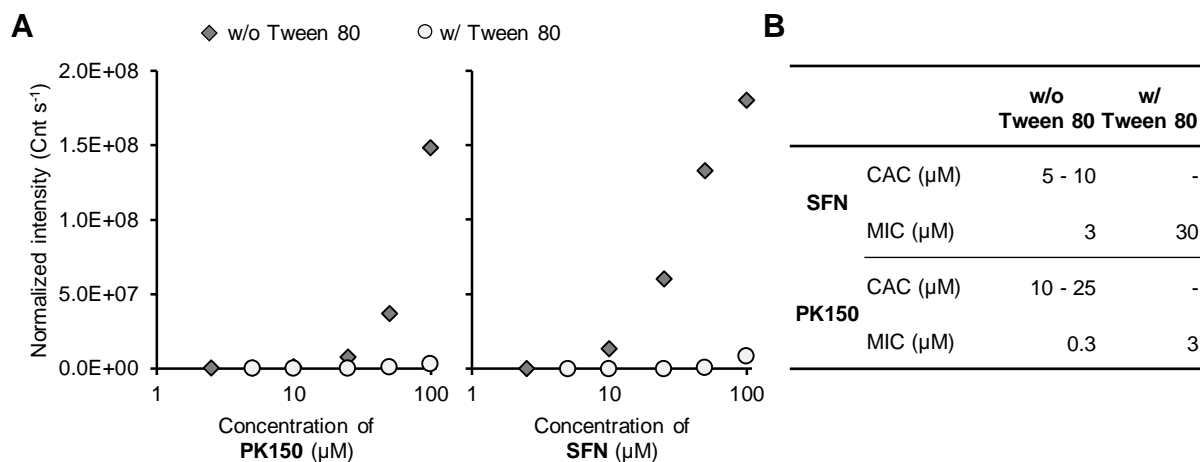


**Figure 3.15.** (A) Concentration-dependent colloidal agglomeration of **PK150** (left graph) and **SFN** (right graph). Colloidal aggregation was measured by dynamic light scattering (DLS) in the absence and presence of Tween 80 (0.023% (v/v)) in FRET assay buffer (50 mM NaPPi, pH 7.0). The figure is representative for two independent experiments. (B) Detergent-based MIC shift assay. MIC values were determined against *S. aureus* NCTC 8325 in B-medium only and B-medium supplemented with Tween 80 (0.023% (v/v)). Critical aggregation concentration (CAC) values were determined by DLS (A).

To further exclude an unspecific activation mode, **SFN** and **PK150** were tested against staphylococcal caseinolytic protease (ClpP), a tetradecameric, barrel-shaped serine protease involved in bacterial protein degradation. ClpP has been reported to be responsive to activators, such as members of the natural occurring acyldepsipeptides (ADEPs) and semisynthetic derivatives thereof.<sup>198</sup> Satisfyingly, both compounds, **SFN** and **PK150**, were unable to stimulate proteolytic turnover of ClpP (Figure 3.16).

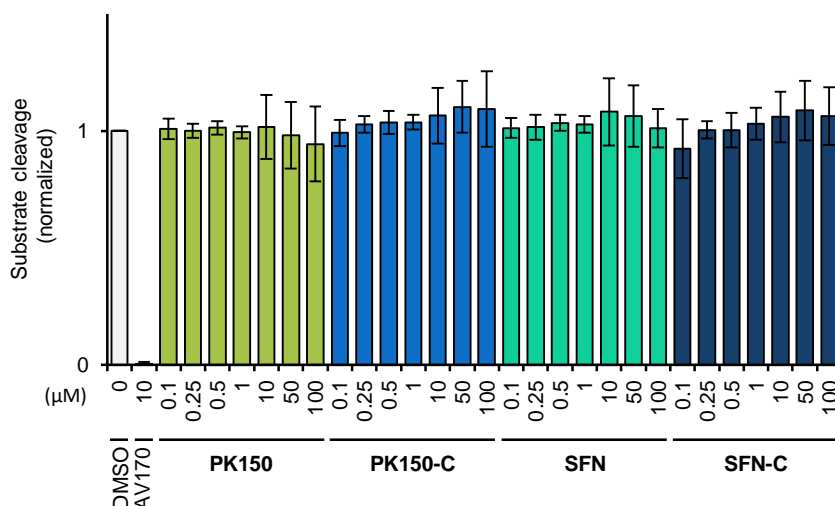


**Figure 3.16.** ClpP peptidase activity assay with *S. aureus* ClpP (1 μM final protein concentration in the presence of 200 μM fluorogenic substrate Suc-LY-AMC). AV170, an established ClpP inhibitor,<sup>199</sup> was used as control. Data is normalized to DMSO-treated samples. Data represent average values ± SD; *n* = min. 3 independent experiments in triplicates.

### 3.2.4.6. Molecular Basis of Compound-Induced SpsB Stimulation

Prior to a closer inspection of a potential contribution of SpsB stimulation to bacterial killing, the molecular basis for **PK150**-induced stimulation of SpsB activity was investigated in silico by molecular docking in combination with molecular simulation.<sup>200</sup> The recently published crystal structure of SpsB from *S. aureus* in complex with an inhibitory peptide provided the molecular basis for these simulations.<sup>178</sup> To set up the system, the bound peptide inhibitor was removed from the SpsB-peptide complex and the protein solvated in a water box in silico. Based on a refined docking pose with the best binding free energy **PK150** was found to bind in proximity to the catalytic site of SpsB with an average distance of 12 Å between its center and the C $\alpha$  carbon of the active site residues S36 and K77 (Figure 3.17 A, B). Here, the lipophilic 4-chloro-3-(trifluoromethyl)phenyl moiety inserts into a hydrophobic groove with the CF<sub>3</sub> substituent interacting with four non-polar amino acids, specifically L41, V47, V64 and V170 (average distance of 5 – 6 Å between the CF<sub>3</sub> unit and the C $\beta$  carbon of respective non-polar amino acids). In addition to these strong hydrophobic interactions, crucial hydrogen bonding between the central urea motif of **PK150** and the side chain oxygens of aspartate D147 contributes to the observed binding (average of minimum distance of 2.4 Å between the urea group hydrogens and either of the side chain oxygens of D147 during the simulation; Figure 3.17 C). These findings support SAR data (Chapter 3.2.4.2) and stress the vital role of the lipophilic CF<sub>3</sub> substituted phenyl moiety and the hydrogen bond donor character of the central urea for the binding of **PK150** into the SpsB groove.

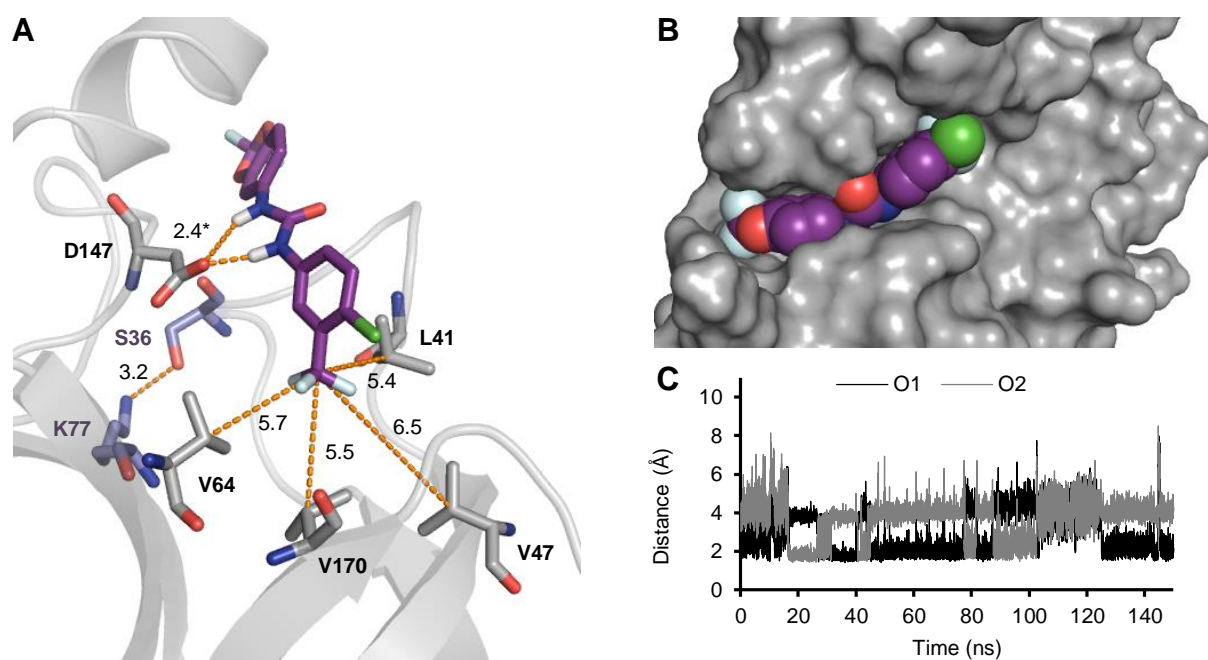


**Figure 3.17.** Binding studies by refined molecular docking and dynamic simulations. (A) Detailed representation of the binding groove within SpsB showing **PK150** (purple), essential active site residues (blue) and residues coordinating to **PK150** (gray) in stick representation. \*Average of the minimum distance between the urea group hydrogens and either of the side chain oxygens of D147 (Figure 3.17 C). (B) Surface representation of the binding groove within SpsB. **PK150** is depicted as spheres; carbon, oxygen, nitrogen, chloride and fluorine atoms are colored purple, red, blue, green and cyan, respectively. (C) Time-dependent simulation of the distance between the center of the urea group hydrogens in **PK150** and the side chain oxygens (O1, black lines; O2, gray lines) of D147.

Subsequently, the molecular basis of SpsB activation was studied by molecular dynamics (MD) simulations over a time span of 150 ns. These simulations revealed both stabilizing as well as destabilizing changes in the secondary structure of SpsB upon **PK150** binding (Figure 3.18 A). Interestingly, these structural changes result in a rigidification of the peptide substrate areas, the loop region containing the active site serine S36 and residues close to the catalytic dyad (gray, blue and green boxes; Figure 3.18 A). Importantly, following a brief initial adaption to these structural changes, the catalytic dyad remains intact upon **PK150** binding as shown by the close vicinity of both active site residues – S36 and K77 – over the course of the simulation (average distance of 3 Å between the side chain oxygen of S36 and the side chain nitrogen of K77; Figure 3.18 B).

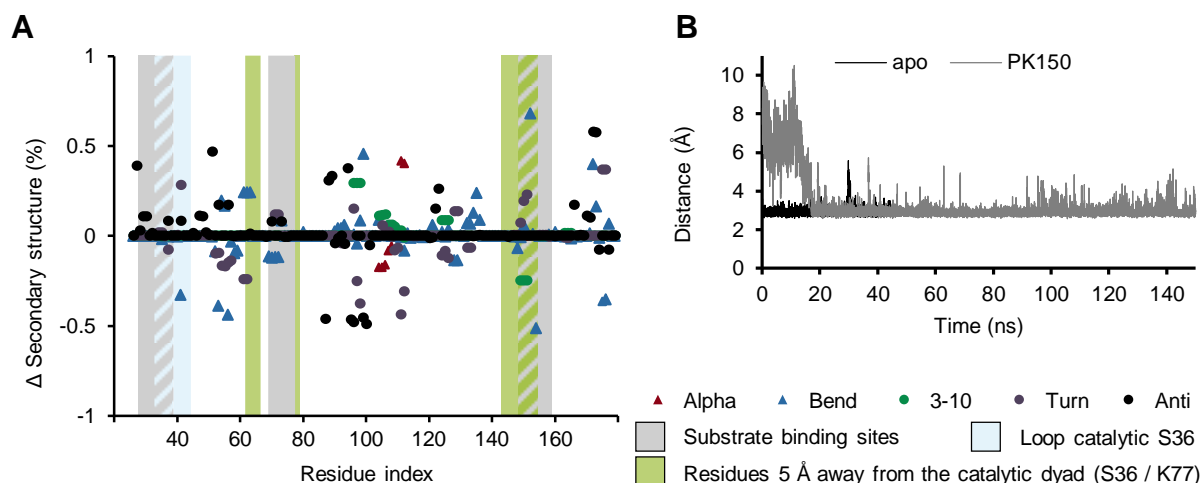


**Figure 3.18.** Molecular dynamic simulations to elucidate the mode of SpB activation. (A) Differences in secondary structure between the apo and **PK150** bound simulations (over 150 ns). Differences are given in percentage with respect to the residue index. Positive values represent stabilizing changes, while negative values represent destabilizing changes. Only secondary structure elements that differ in both simulations are considered (i.e. alpha helix, bend, 3-10 helix,  $\beta$ -turn and anti-parallel). Three critical regions of the protein are highlighted: The signal peptide binding sites (gray area), the loop involving the active site S36 (blue area) and the residues within 5 Å sphere of the catalytic dyad (green area). (B) Time-dependent simulation of the distance between side chain oxygen of active site S36 and side chain nitrogen of K77 in the apo (black lines) and **PK150** bound form (gray lines).

There is a growing recognition in the literature that changes in the local flexibility of the protein, especially around the active site, are important for the modulation of catalytic activity;<sup>201-202</sup> however the optimum amount of flexibility required for maximum activity seems to be system dependent. In the case of **PK150**-induced stimulation of SpsB activity, it seems likely that the compound induced rigidification selects an optimal dynamic state that leads to a tighter bound signal peptide-SpsB complex and as a direct result thereof to an increased catalytic activity.

### 3.2.5. Insights into the Effects of SpsB Stimulation

Based on the findings from docking and molecular dynamic stimulations that established how **PK150** enhances substrate turnover of SpsB on a molecular basis, subsequent studies focused on how external manipulation of SpsB activity might contribute to bacterial killing.

#### 3.2.5.1. Secretome and Surfome Analysis

Recently it was hypothesized on the basis of proteomic analysis of the bacterial secretome upon arylomycin treatment that inhibition of SpsB mediates bacterial cell death by the accumulation of unprocessed proteins and resulting dysbalanced membrane integrity.<sup>203-204</sup> However, little is known about how dysregulation of the finely controlled Sec translocation

machinery by overactivation of SpsB alters extracellular protein transport and thereby the secretome composition. To address this question the composition of extracellular proteins secreted upon treatment with **SFN** and **PK150** in comparison to inactive **SFN-C** and **PK150-C**, respectively, was analyzed. Here, bacterial cells were treated with sub-MIC concentrations of compound (0.5 x MIC; for inactive controls, an equimolar concentration with regard to the respective parent compound was used) to avoid contamination by the release of non-secreted proteins from the cytosol. Subsequently, secreted extracellular proteins were analyzed by label-free high resolution mass spectrometry. Under these conditions, a shift of known SpsB-dependent proteins<sup>203</sup> in samples treated with activators **SFN** and **PK150**, respectively, towards higher secretion levels was identified in direct comparison to DMSO and control compound treated samples (Figure 3.19).

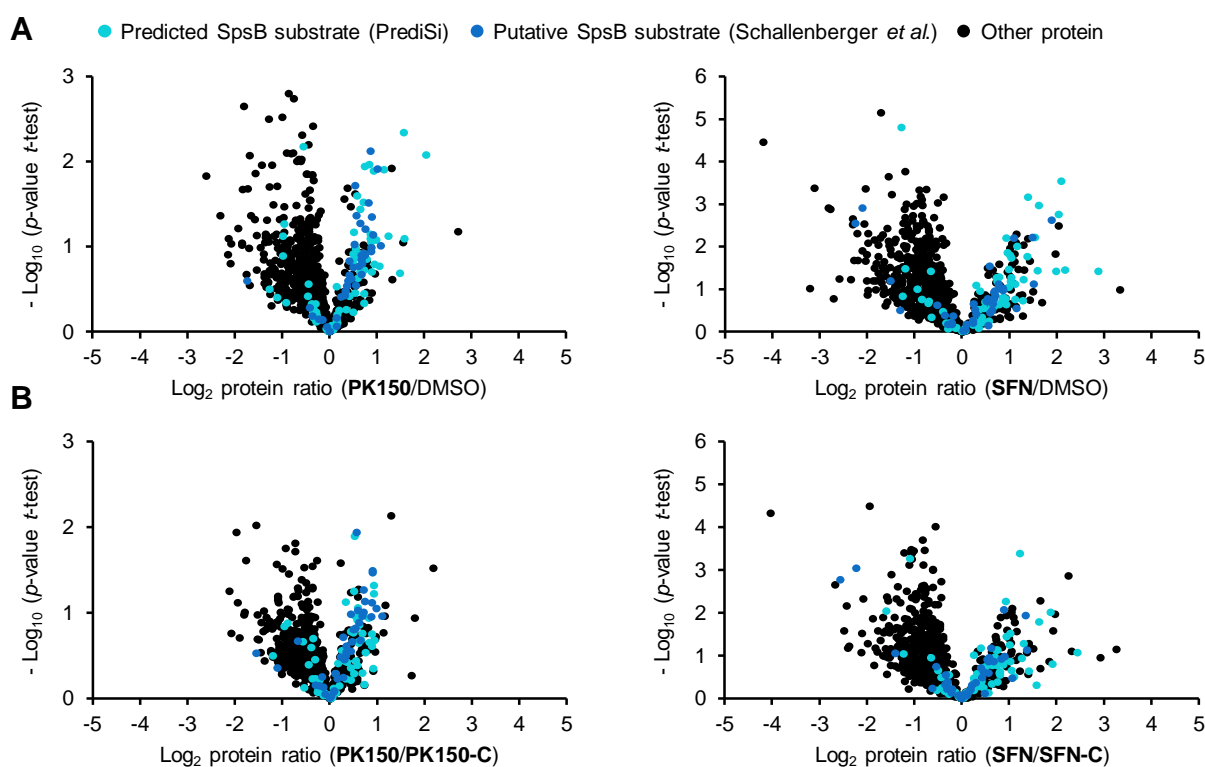


**Figure 3.19.** Secretome analysis of *S. aureus* NCTC 8325 cells treated with **PK150** (0.15  $\mu$ M, 0.5 x MIC; left panel) or **SFN** (1.5  $\mu$ M, 0.5 x MIC; right panel) compared to samples treated either with DMSO (A) or with control compounds **PK150-C** (0.15  $\mu$ M) and **SFN-C** (1.5  $\mu$ M), respectively (B). Volcano plots depict the  $\log_2$ -fold change of protein levels in the secretome. Dark blue dots represent proteins that are proposed SpsB substrates,<sup>203</sup> while light blue dots represent proteins that are predicted to have a SpsB signal peptide motif.<sup>205</sup> Data represent average values;  $n = 4$  independent experiments per group.

The observation of enhanced Sec-dependent protein export was further supported by mass spectrometry-based analysis of the surfome that revealed a reduction of SpsB-dependent proteins residing in the bacterial membrane in activator – **SFN** and **PK150** – treated samples

in direct comparison to DMSO and control compound treated samples, respectively (Figure 3.20).

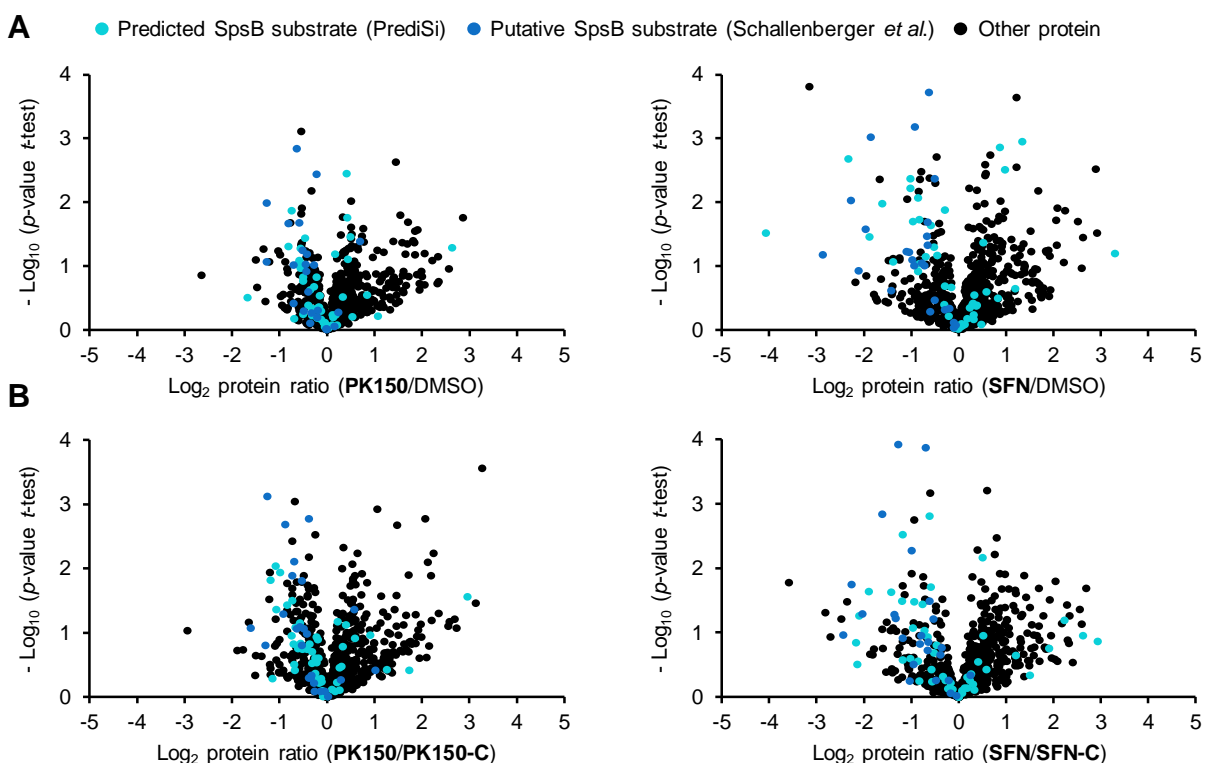


**Figure 3.20.** Surfome analysis of *S. aureus* NCTC 8325 cells treated with **PK150** (0.15  $\mu$ M, 0.5 x MIC; left panel) or **SFN** (1.5  $\mu$ M, 0.5 x MIC; right panel) compared to samples treated either with DMSO (A) or with control compounds **PK150-C** (0.15  $\mu$ M) and **SFN-C** (1.5  $\mu$ M), respectively (B). Volcano plots illustrate the  $\log_2$ -fold change of protein levels in the surfome. Dark blue dots represent proteins that are proposed SpsB substrates,<sup>203</sup> while light blue dots represent proteins that are predicted to have a SpsB signal peptide motif.<sup>205</sup> Data represent average values;  $n = 4$  independent experiments per group.

Furthermore, in-depth mining of secretome data revealed that proteins containing a peptidoglycan hydrolase (PGH) domain were present in the group of significantly enriched proteins ( $\log_2$ -fold enrichment of  $> 0.5$ ) resulting from activator induced secretomes as found by alignment with the Pfam protein families database<sup>150</sup> (Table 3.10). This accumulation of PGH domain-containing proteins was not found in secretomes resulting from control compound treatment.

**Table 3.10.** Autolysin enrichment analysis of peptidoglycan hydrolase domain-containing proteins as defined by the Pfam annotations<sup>150</sup> CHAP domain, LysM domain, amidase, transglycolase, glucosaminidase and peptidase M23 domain using Fisher's exact test among proteins with a log<sub>2</sub>-fold enrichment of > 0.5 in the secretome against the complete measured secretome as background.

| Category  | PK150/<br>DMSO                                       | PK150/<br>PK150-C | SFN/<br>DMSO  | SFN/<br>SFN-C | PK150-C/<br>DMSO | SFN-C/<br>DMSO | Secretome |
|---|--|-------------------|---------------|---------------|------------------|----------------|-----------|
|   | Proteins with log <sub>2</sub> (protein ratio) > 0.5 |                   |               |               |                  |                |           |
| Total proteins  | 83   | 72                | 121           | 112           | 46               | 45             | 806       |
| „PGH domain AND Signal Predicted/<br>AC16-responder“ proteins     | 10   | 8                 | 9             | 7             | 0                | 1              | 12        |
| Not „PGH domain AND Signal Predicted/<br>AC16-responder“ proteins | 73   | 64                | 112           | 105           | 46               | 44             | 794       |
| Fisher Exact <i>p</i> -value<br>(Secretome as background)         | <b>&lt;0.0001</b>                                    | <b>&lt;0.0001</b> | <b>0.0006</b> | <b>0.0048</b> | <b>1.0000</b>    | <b>0.5091</b>  |           |

Taken together, it is conceivable that a well-balanced depot of already translocated, but still not released preproteins is exploited upon SpsB stimulation. Likely, not a single enzyme but the total bulk of proteins that are dysregulated by **PK150** contribute to bacterial killing. Among these are peptidoglycan hydrolases that breakdown the macromolecular matrix of peptidoglycan, a major component of the dynamic structure of the bacterial cell wall. As peptidoglycan hydrolases have an important physiological role including regulation of peptidoglycan turnover during cell wall modification and growth, cell separation and autolysis, endogenous levels thereof need to be strictly balanced by the cell. Imbalanced peptidoglycan hydrolase levels represent a potential suicide mechanism as shown recently by induced expression thereof that had fatal consequences for cellular structural integrity and cell growth.<sup>206-207</sup> The observed enhanced levels of peptidoglycan hydrolases in the secretome caused by treatment with SpsB activators **SFN** and **PK150**, respectively, likely impact regulation and balance thereof and trigger suicidal autolysis by once essential peptidoglycan hydrolases. Indeed, general changes in lytic activity related to **SFN** and **PK150** treatment could be shown by zymographic analysis (Figure 3.21). Characteristic induction of hydrolytic enzymes was observed (molecular mass > 70 kDa), similar to positive control penicillin G.

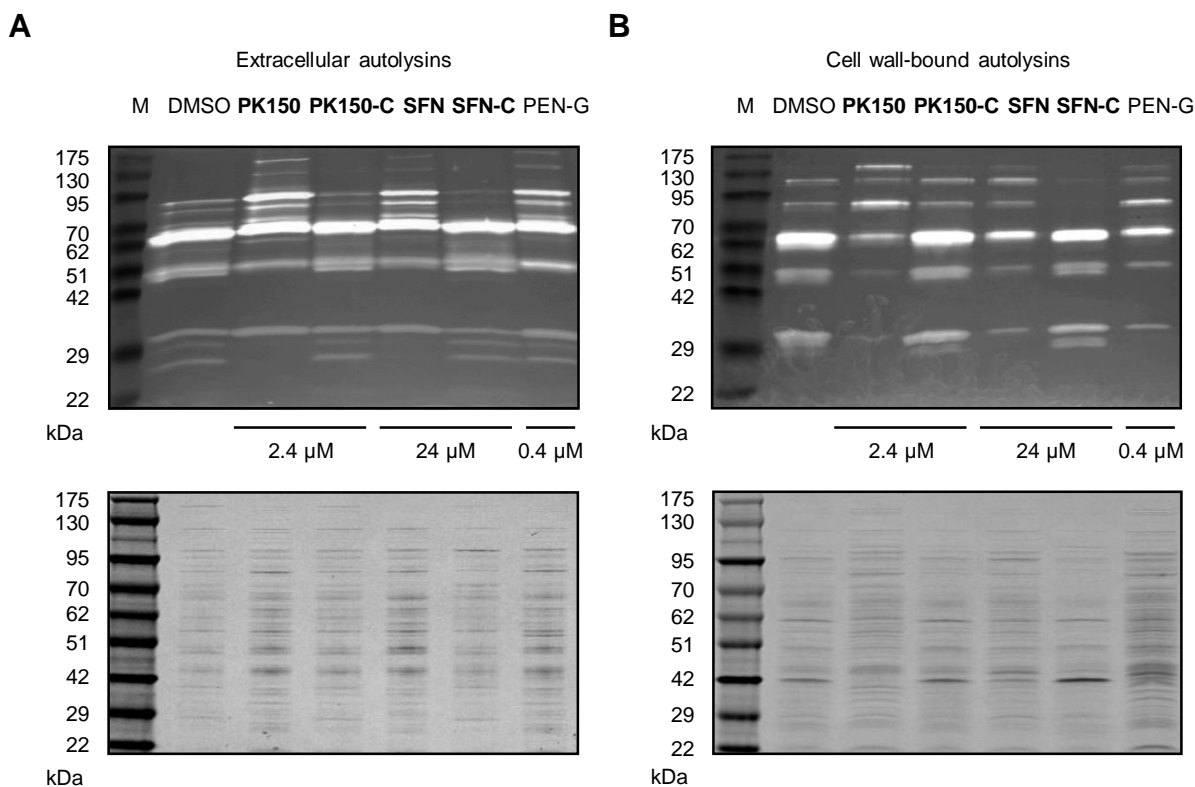


**Figure 3.21.** Zymography of *S. aureus* NCTC 8325 extracellular protein extracts (A) and cell wall-bound extracts (B) after treatment of bacterial cells with either **PK150** (2.4  $\mu$ M, 8 x MIC), **SFN** (24  $\mu$ M, 8 x MIC), penicillin G (PEN-G; 0.4  $\mu$ M, 8 x MIC) or control compounds (**PK150-C**, 2.4  $\mu$ M; **SFN-C**, 24  $\mu$ M). Clear bands indicate peptidoglycan hydrolase activity. Loading controls are represented by the coomassie-stained gels.

As antibiotic activity was observed in the prophage-cured *S. aureus* strain NCTC 8325-4, phage induction as a possible alternative mechanism can be excluded.<sup>208</sup>

### 3.2.5.2. Electron Microscopy

Field emission scanning electron microscopy (FESEM; Figure 3.22) and transmission electron microscopy (TEM; Figure 3.23) studies revealed insights into the consequences of **PK150** treatment (4 – 8 x MIC, 3 h) on *S. aureus* morphology. Here, extracellular vesicle formation at the cross-wall of dividing cells (Figure 3.22 D – F) as well as cell lysis and rupture accompanied by the extrusion of DNA containing material (Figure 3.22 D, G – I) were observed in FESEM micrographs of **PK150** treated bacteria.

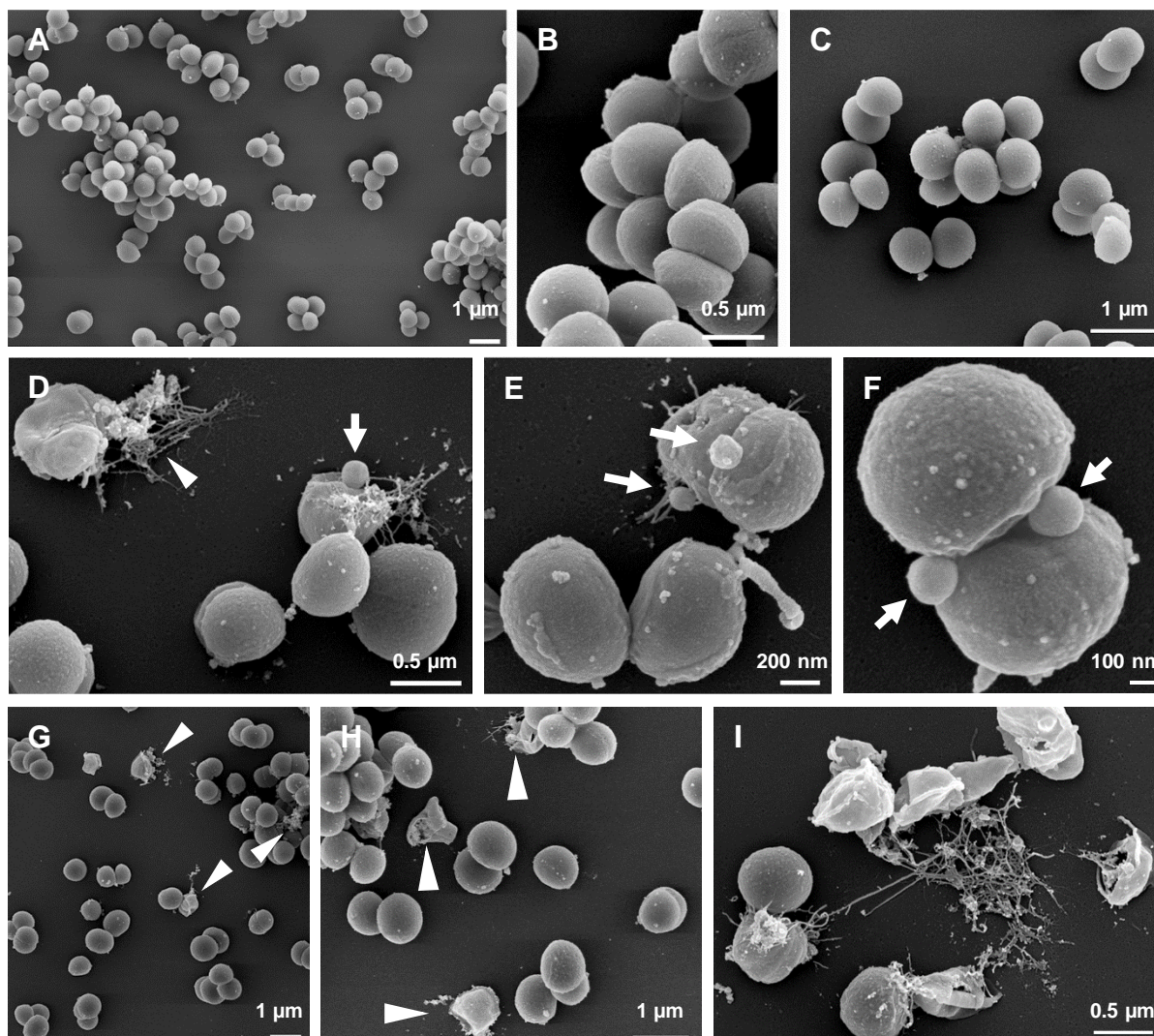


**Figure 3.22.** Field emission scanning electron micrographs (FESEM) of intact *S. aureus* NCTC 8325 cells (DMSO; A, B) and after treatment with inactive control compound **PK150-C** (2.4  $\mu$ M; C). FESEM micrographs of **PK150** (1.2  $\mu$ M, 4 x MIC, F; 2.4  $\mu$ M, 8 x MIC, D, E, G – I) treated cells with arrows highlighting extracellular vesicles formation (D – F) or cell rupture (D, G – I).

Inspection of ultrathin sections of these cells by TEM confirmed the formation of extracellular vesicles that contained two different sorts of intraluminal cargo, either DNA (Figure 3.23 C) or cytoplasmic material (CY; Figure 3.23 D). Interestingly, no peptidoglycan was observed at the sites of vesicular formation (Figure 3.23 E). Here, gaps in the cell wall (CW) seemed to enable protrusions of the cytoplasmic membrane (CM; Figure 3.23 E) that filled with intraluminal cargo. Ultimately, these protrusion seemed to burst under turgor pressure releasing the entire cytoplasmic content and leaving cell wall relicts behind (Figure 3.23 F – I).

In contrast, no morphological abnormalities, cellular defects or vesicular formations were found in FESEM and TEM micrographs of DMSO (Figure 3.22 A, B and Figure 3.23 A) and inactive **PK150-C** treated cells (2.4  $\mu$ M; Figure 3.22 C and Figure 3.23 B).

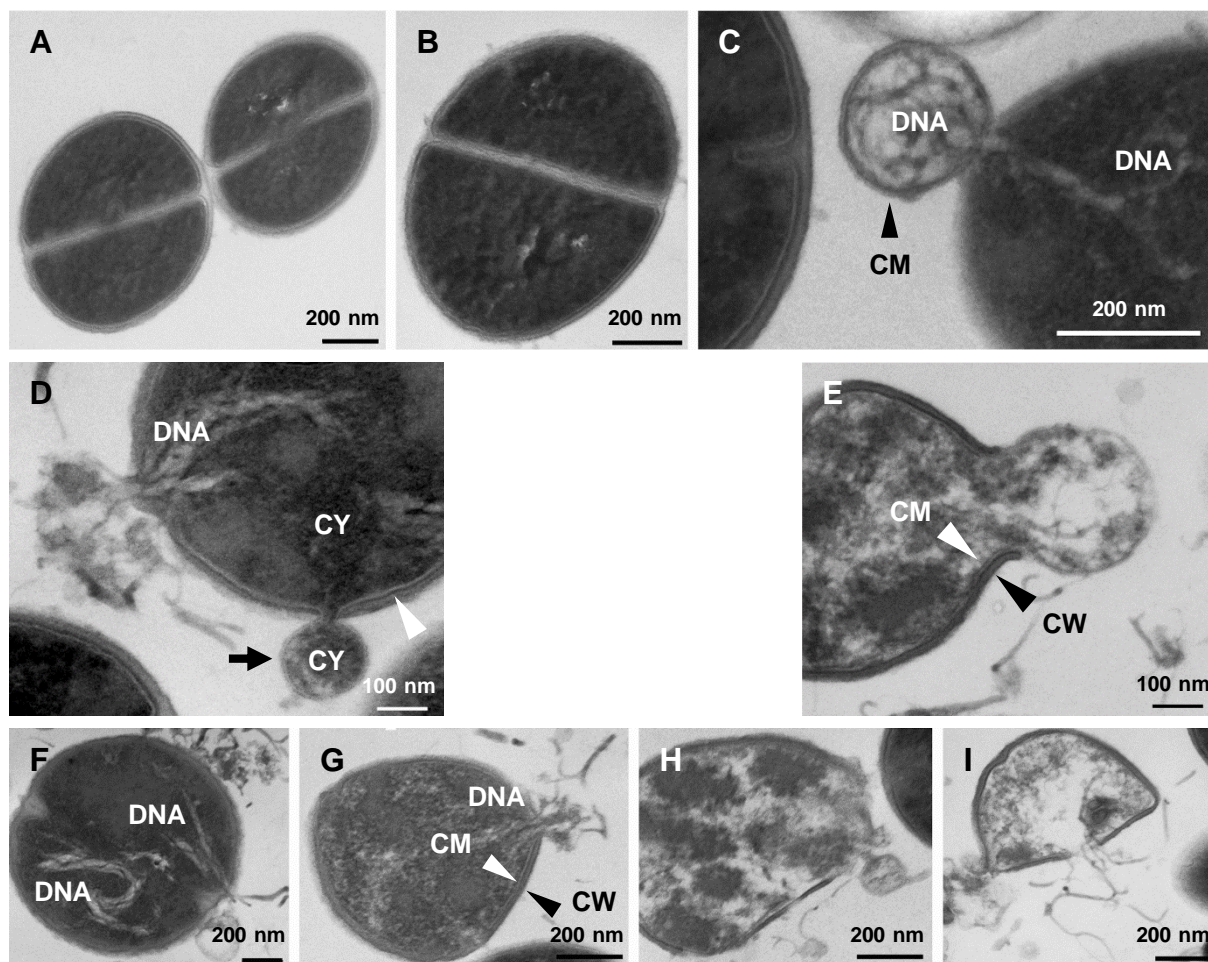


**Figure 3.23.** Transmission electron micrographs (TEM) of intact *S. aureus* NCTC 8325 cells (DMSO; A) and after treatment with inactive **PK150-C** (2.4  $\mu$ M; B). Morphological consequences after treatment with **PK150** (2.4  $\mu$ M, 8 x MIC; C – I). Arrows highlight DNA (C) or cytoplasm (CY; D) containing protrusions as well as the localization of the cytoplasmic membrane (CM) and cell wall (CW).

Of particular interest for the potential mode of action is the observation that formation sites of vesicle-like protrusions lacked peptidoglycan and were located at the septum of dividing cells, a known location of peptidoglycan hydrolase, namely autolysin, action.<sup>209-211</sup> With consideration of secretome and surfome data (Chapter 3.2.5.1) these findings indicate that imbalanced peptidoglycan breakdown by autolysins facilitates a thinning of the cell wall, thereby enabling vesicular extrusions that ultimately burst under the internal osmotic pressure.

### 3.2.6. Pharmacological Profile of PK150

#### 3.2.6.1. In Vitro Toxicological Profile of PK150

To exclude an unspecific disruption of bacterial membrane integrity via pore formation, which is often accompanied by undesired adverse effects on human blood cells, changes in membrane permeability were examined in a time-dependent manner. At their corresponding MICs **SFN** and **PK150**, respectively, affected membrane permeability barely and only at a slow

rate (Figure 3.24 A). Moreover, compound mediated hemolysis of ovine red blood cells was investigated as a reference measure of adverse effects on mammalian cell integrity. Here, **PK150** caused hemolysis of ovine erythrocytes to a limited extent, but only at concentrations well above its MIC value (Figure 3.24 B).

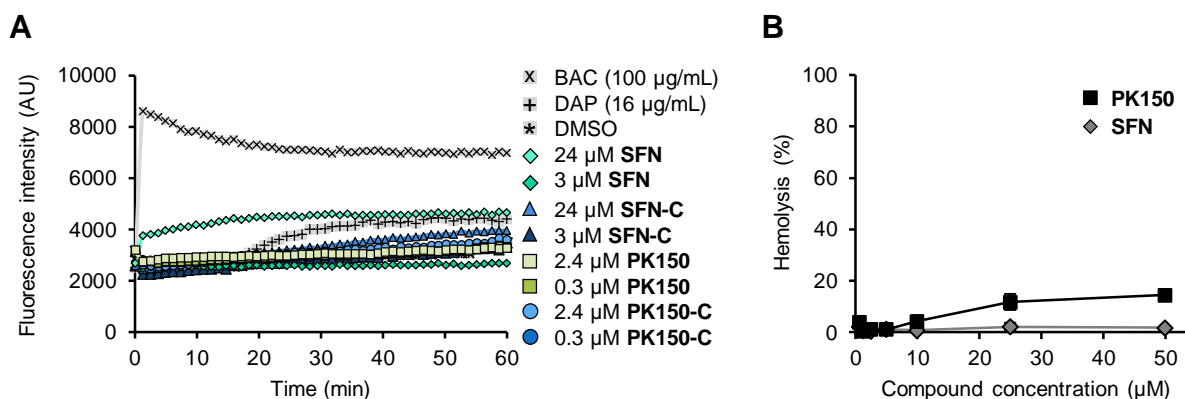


**Figure 3.24.** (A) Cell permeability assay in *S. aureus* NCTC 8325 utilizing the fluorescence of propidium iodide (PI) upon interaction with DNA as a readout. Benzalkonium chloride (BAC; 100 µg/mL) and daptomycin (DAP; 16 µg/mL + 50 µg/mL Ca<sup>2+</sup>) were used as positive controls. Data represent average measured values ± SD; *n* = 3 per group. Data is representative for three biological replicates. (B) Hemolysis of ovine erythrocytes at increasing concentrations of **SFN** and **PK150**, respectively, as a measure of the effect on red blood cell integrity. Hemolysis is normalized to negative control DMSO (hemolysis 0%) and positive control Triton X-100 (0.2% (v/v); hemolysis 100%). Data represent average values ± SD; *n* = 4 independent experiments in triplicates.

To evaluate the applicability of **PK150** as a systemic drug, its cytotoxicity and in vitro stability in plasma samples was investigated. Plasma stability studies in murine blood plasma showed excellent stability for **PK150** with no observable degradation or decline in plasma concentration after 6 hours (Figure 3.25). In addition, **PK150** possessed modest cytotoxicity against a panel of human and murine cell lines with IC<sub>50</sub> values ranging from 7 to 15 µM, thereby providing the basis for in vivo studies as demonstrated by selectivity ratios of cytotoxicity to antibiotic activity (IC<sub>50</sub> to MIC) of up to 52 (Table 3.11). However, the concentration required to eradicate biofilms with a MBEC of 12.5 µM (42-fold higher than the MIC against the same bacterium; Chapter 3.2.4.4, Figure 3.13) is in the range of cytotoxic concentrations. The resulting poor selectivity ratios of cytotoxicity to biofilm eradication (IC<sub>50</sub> to MBEC) indicate that the in vivo efficacy of biofilm eradication might be low within an acceptable dosage range.

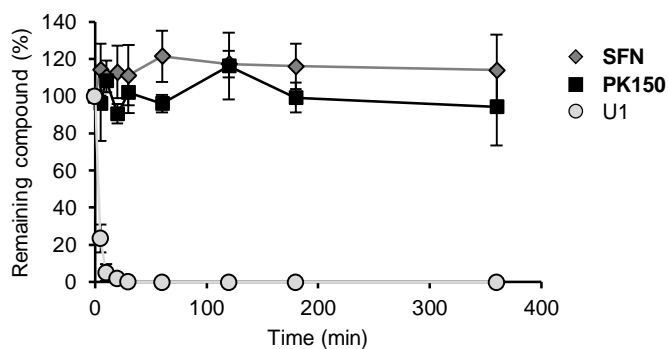


**Figure 3.25.** Stability of **SFN** and **PK150** in murine blood plasma (10  $\mu\text{M}$  compound concentration) determined by a LC-MS-based method. U1 (50  $\mu\text{M}$  compound concentration), a  $\beta$ -lactone with known low plasma stability,<sup>212</sup> was used as positive control. The time-dependent peak decline was expressed relative to 100% at  $t = 0$  min. Data represent average values  $\pm$  SD;  $n = \text{min. } 3$  independent experiments in triplicates.

**Table 3.11.** Cytotoxicity of **SFN** and **PK150** against a panel of human and murine cell lines. Selectivity ratios represent the ratios of  $\text{IC}_{50}$  (cytotoxicity) and MIC values (antibacterial activity against *S. aureus* NCTC 8325). Data represent average values;  $n = \text{min. } 3$  independent experiments in triplicates.

|   | A549          | HeLa         | HepG2        | NIH/3T3     |
|---|---------------|--------------|--------------|-------------|
| <b>SFN</b> $\text{IC}_{50}$ ( $\mu\text{M}$ )   | 19.93         | 9.52         | 1.69         | 7.56        |
| <b>SFN</b> 95% CI                               | 17.13 - 23.19 | 8.20 - 11.05 | 1.07 - 2.67  | 6.45 - 8.86 |
| <b>SFN</b> Selectivity ratio                    | 6.64          | 3.17         | 0.56         | 2.52        |
| <b>PK150</b> $\text{IC}_{50}$ ( $\mu\text{M}$ ) | 15.50         | 7.04         | 10.45        | 7.93        |
| <b>PK150</b> 95% CI                             | 12.74 - 18.86 | 5.68 - 8.73  | 6.77 - 16.13 | 6.80 - 9.24 |
| <b>PK150</b> Selectivity ratio                  | 51.67         | 23.46        | 34.83        | 26.42       |

Abbreviation: CI, confidence interval.

Due to the observed moderate cytotoxicity, the kinobeads technology<sup>213</sup> was utilized to address the question whether **PK150** still shared sorafenib's protein kinase affinities. In the presence and absence of **SFN** and **PK150**, respectively, lysates pooled from a panel of human cancer cell lines, namely K562, Colo205, SKNBE2 and MV4 11, were incubated with kinobeads that cover a vast variety of kinase inhibitors covalently attached to a solid support for competitive affinity enrichment of protein kinases. High resolution mass spectrometry-based analysis captured nearly half of the human kinome and revealed that **PK150** did not interact with any of the more than 250 observed kinases. In contrast, **SFN** showed affinity for eight human kinases, namely RET ( $K_d^{\text{app}} = 32$  nM), DDR1 ( $K_d^{\text{app}} = 86$  nM), ZAK ( $K_d^{\text{app}} = 221$  nM), FLT3 ( $K_d^{\text{app}} = 453$  nM), DDR2 ( $K_d^{\text{app}} = 610$  nM), MAPK11 ( $K_d^{\text{app}} = 1.2$   $\mu\text{M}$ ), MAPK14 ( $K_d^{\text{app}} = 8.8$   $\mu\text{M}$ ) and MAP3K1 ( $K_d^{\text{app}} = 4.3$   $\mu\text{M}$ ). The generally reduced kinase affinity of **PK150** is in line with conclusions made from co-crystal structures of human kinases B-RAF and VEGFR2 with sorafenib. Here, the distal 4-pyridyl ring of the type II kinase inhibitor occupies the highly conserved ATP-binding pocket of the kinase domain forming crucial interactions with the

conserved hinge region – a structural feature **PK150** is lacking.<sup>214-215</sup> The molecular mode of the observed toxicity of **PK150**, however, remains unknown.

### 3.2.6.2. In Vivo Pharmacokinetic Profile of PK150

Prior to the evaluation of the therapeutic potential of **PK150** in *S. aureus* infected mice, the in vivo pharmacokinetic parameters in mice (Figure 3.26) were determined following either intravenous injection (i.v.; 10 mg/kg) or oral administration via an intragastric gavage (p.o.; 10 and 20 mg/kg). While mice showed no signs of toxicity via the oral administration route at both doses, severe toxic effects were observed at i.v. dosing of 20 mg/kg. Subsequently, i.v. administration of doses higher than 10 mg/kg were excluded from further pharmacokinetic and therapeutic mouse models. After oral administration with a dosing of 10 mg/kg, **PK150** reached peak plasma levels after around 6.7 hours with a  $C_{max}$  of 1.02  $\mu\text{g/mL}$  (6.19  $\mu\text{g/mL}$  for the same dose given i.v.), while increasing the oral dose to 20 mg/kg resulted in an earlier  $T_{max}$  of around 5.3 hours with a  $C_{max}$  of 1.58  $\mu\text{g/mL}$ . Oral bioavailability was approximately 63% as reflected by the AUC values (33.61  $\mu\text{g/mL}\cdot\text{h}$  i.v. compared to 21.09  $\mu\text{g/mL}\cdot\text{h}$  p.o. at 10 mg/kg). **PK150** showed a mean half-life ranging from approximately 9.4 (20 mg/kg p.o.) to 11.7 hours (10 mg/kg i.v.). The mean residence time (MRT) increased slightly when the compound was given orally (from 10.1 h for 10 mg/kg i.v. to 13.8 h for 10 mg/kg p.o.) as did the generally low plasma clearance of **PK150**. Overall, a single dose of 20 mg/kg given via the oral administration route resulted in a 47 hour window with plasma levels of **PK150** exceeding the MIC value.

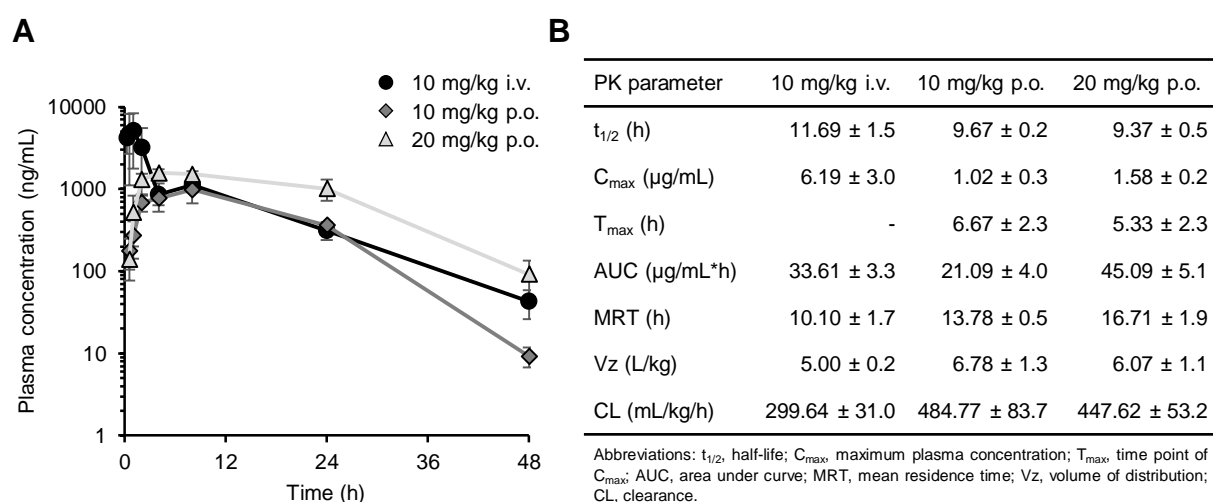


**Figure 3.26.** Pharmacokinetic analysis of **PK150** in murine plasma following oral (p.o.) or intravenous (i.v.) administration. Time-dependent changes in plasma levels (A) and pharmacokinetic parameters (B) after the administration of 10 mg/kg p.o. (diamond), 20 mg/kg p.o. (triangle) or 10 mg/kg i.v. (circle), respectively, are shown. Compound levels in plasma were determined by LC-MS/MS analysis. Data represent mean values  $\pm$  SD;  $n = 3$  per group.

### 3.2.6.3. In Vivo Pharmacodynamic Profile of PK150

Given the good bioavailability and high plasma levels that were maintained at levels above the MIC value for several hours, the oral administration route was chosen for subsequent therapeutic mouse models. Two different pharmacodynamic efficacy models were used to determine the direct effect of **PK150** on the in vivo killing of *S. aureus*: A neutropenic mouse thigh model with mice infected intramuscular with *S. aureus* ATCC 33591 (MRSA) and a bloodstream infection model with immunocompetent mice infected intravenously with *S. aureus* SH1000 (MSSA). In both models the therapeutic effect of **PK150** was assessed by measuring the reduction in CFU/g-levels in tissue and organs, respectively.

The neutropenic mouse thigh model (Figure 3.27) was sensitive to **PK150** treatment, with three doses of **PK150** at 20 mg/kg p.o. producing a 10-fold reduction in CFU/g-levels in thighs in comparison to vehicle-treated mice. The same range of reduction in bacterial load was observed in the treatment with positive control levofloxacin, with three doses at 5 mg/kg administered by intraperitoneal injection.

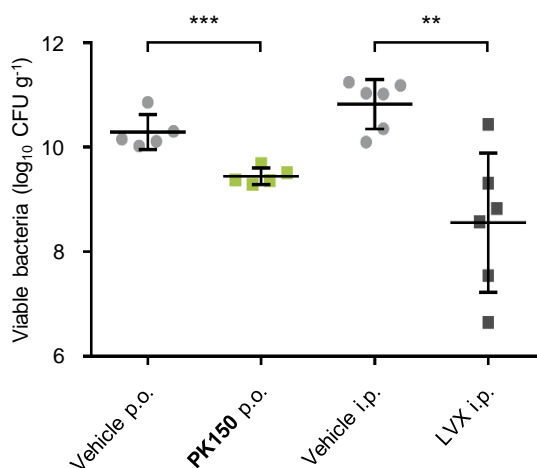


**Figure 3.27.** In vivo efficacy of **PK150** and levofloxacin (LVX) in a neutropenic mouse thigh model with mice infected intramuscular with *S. aureus* ATCC 33591. **PK150** (20 mg/kg p.o.) and corresponding vehicle were administered orally at time point 0.5, 4 and 8 h after bacterial infection; LVX (5 mg/kg) and corresponding vehicle were administered intraperitoneally at time point 2, 6 and 10 h after infection. Data are expressed as mean values  $\pm$  SD;  $n = 6$  for vehicle i.p., LVX i.p. and **PK150** p.o.;  $n = 5$  for vehicle p.o.; \*\* $p < 0.01$ ; \*\*\* $p < 0.001$  (Student's *t*-test).

The observed efficacy in the neutropenic thigh infection model was confirmed by the in vivo evaluation of **PK150** in a bloodstream infection model (Figure 3.28). Here, oral treatment with **PK150** (6 doses at 20 mg/kg administered at different intervals over a period of 6 days) starting at day 3 after intravenous *S. aureus* infection, a time point at which infected immunocompetent mice were fully symptomatic, was highly efficacious, causing an approximately 100-fold

reduction in CFU/g-levels in livers and hearts. However, no significant differences were observed in the bacterial loads in kidneys between **PK150**-treated and vehicle-treated mice.

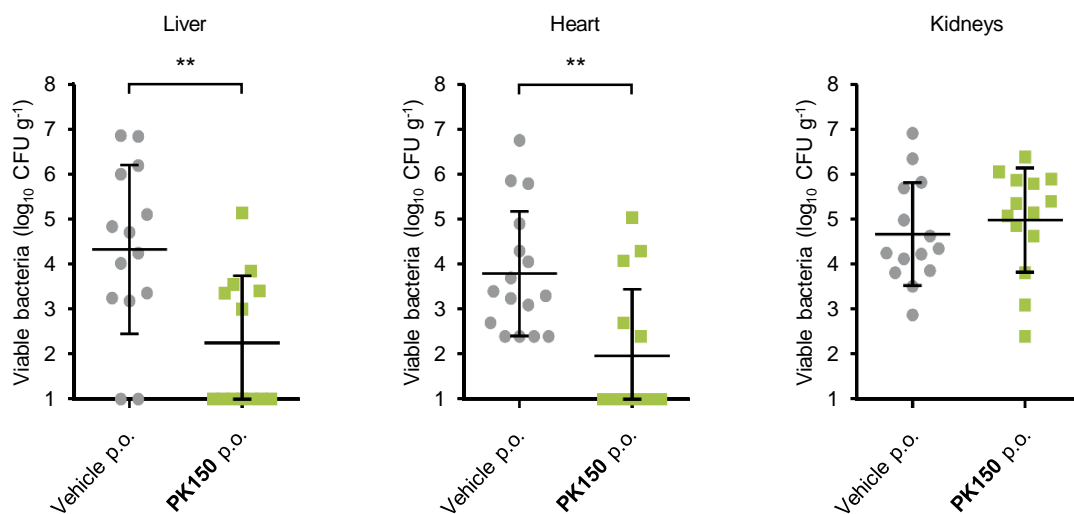


**Figure 3.28.** In vivo efficacy of **PK150** in a bloodstream infection model with immunocompetent mice infected intravenously with *S. aureus* SH1000. **PK150** (20 mg/kg p.o. per dose) and corresponding vehicle were administered twice daily on day 3 (in a 6 hour interval) followed by a single oral dose on day 4, 6 and 8 after intravenous *S. aureus* infection. Compilation data from three independent experiments are presented. Horizontal lines represent the mean values  $\pm$  SD;  $n = 14$  for vehicle and **PK150**.  $**p < 0.01$  (Student's *t*-test).

### 3.3. CONCLUSION AND OUTLOOK

A phenotypic screening approach of a library of readily available human kinase inhibitors against *S. aureus* was conducted in order to identify candidates that can be repurposed as antimicrobials. Sorafenib and structurally closely related regorafenib, two approved anticancer drugs with oral bioavailability, showed potent activity against *S. aureus*, which is in agreement with previous findings.<sup>167-168</sup> Chemical proteomic profiling in *S. aureus* utilizing a sorafenib-based photoprobe identified several potential target proteins in mass spectrometry-based gel-free AfBPP. While among those only uncharacterized lytic regulatory protein (Lrp) showed a slight effect in a MIC shift assay with respective transposon mutants, thereby indicating a contribution to the observed antibiotic effect, subsequent investigations concerning the mode of action focused on essential type I signal peptidase (SpsB), the strongest hit in all conducted proteomic experiments. Interestingly, sorafenib was found to stimulate the peptidase activity of SpsB, a membrane-anchored serine protease that processes signal peptides of preproteins translocated via the Sec secretion pathway.

In parallel, in-depth structure-activity relationship studies established structural key features within the sorafenib scaffold as hallmarks for antibacterial as well as SpsB stimulating properties. These medicinal chemistry efforts resulted in an analog – **PK150** – with a minimal inhibitory concentration of 300 nM against various multi-resistant *S. aureus* strains and in addition improved activity against mycobacteria, including *M. tuberculosis*, and vancomycin-resistant enterococci. Importantly, **PK150** was able to significantly enhance SpsB substrate turnover. Both compounds, sorafenib and **PK150**, induced rapid bactericidal killing of *S. aureus* and were found to kill dormant persister cells. Moreover, **PK150** eradicated established biofilms, a clinical challenging state of *S. aureus*, with a minimal biofilm eradication concentration of 12.5  $\mu$ M. In contrast to sorafenib, **PK150** did not show any signs of in vitro resistance acquisition in *S. aureus* over a period of 27 days.

Docking and molecular dynamic stimulations provided insights into the molecular basis of SpsB activation. Here, rigidification of the SpsB active site area upon binding of **PK150** into a defined groove likely explains the increase of catalytic activity through changes in intrinsic protein dynamics.

In depth proteomic analysis of secretome and surfome data demonstrated that overactivation of SpsB by sorafenib and **PK150** resulted in dysregulation of the finely controlled Sec translocation machinery. Altered extracellular protein transport was reflected in an accumulation of SpsB-dependent proteins in the secretome. Among those dysregulated proteins, peptidoglycan hydrolases, which play an important role in cell wall metabolism, including autolysis, were found. Electron microscopy data indicated an involvement of peptidoglycan hydrolases in the observed bursting of vesicular protrusions that probably were the result of a thinning of the cell membrane.

While it is difficult to pin down the exact mode of action to a single target enzyme and observed antibiotic effects likely result from a multi-target profile, it is conceivable that dysregulation of the secretory machinery in *S. aureus* by **PK150** contributes to bacterial killing. Even so, the polypharmacology of **PK150** is evident due to the lack of resistance acquisition and the observation that structurally close analogs of **PK150** do show effective antibacterial killing but do not impact SpsB activity. To unearth further potential protein targets a quantitative mass spectrometry-based cellular thermal shift assay (CETSA)<sup>216</sup> is currently underway that monitors ligand-induced changes in protein thermal stability. This proteomic platform does not rely on a synthetic modification of the molecule of interest and thereby enables to take the impact of even small structural changes on the biological profile into account.

While evolution from sorafenib to **PK150** was accompanied by a loss of human kinase affinity, in vitro cytotoxicity only slightly changed. Based on its antibacterial potency, its excellent in vitro as well as in vivo stability and its oral bioavailability, the in vivo efficacy of **PK150** in *S. aureus* infected mice was evaluated. These pharmacodynamic studies demonstrated that **PK150** possesses promising in vivo anti-MRSA activity.

The pharmacological evaluation of **PK150** albeit illuminated the limitations of the established diphenyl urea scaffold in terms of activity against Gram-positive pathogens only, solubility and foremost toxicity. To address these issues ongoing medicinal chemistry studies are underway.

Reducing the observed toxic effects is directly linked to a fundamental understanding of the underlying mechanism of toxicity. Therefore, investigation thereof as well as an in-depth cell culture-based structure-toxicity relationship study represent promising starting points for a rational revision of the core scaffold.

In addition to the highly lipophilic and planar character of the molecule, intermolecular urea bridging<sup>217</sup> contributes in large measure to the observed poor solubility of **PK150**. Breaking these intermolecular interactions by structural modifications, however, must consider the hydrogen bond donor character of the central urea motif as this seems to be crucial for antibiotic as well as SpsB stimulating effects. Isosters like guanidine or cyclic benzimidazole functionalities<sup>217-218</sup> might retain the hydrogen bond donor character, while they simultaneously contribute no longer to intermolecular interactions.

Provided that compound uptake is the limiting factor for expanding the antibiotic scope of the **PK150** core scaffold, a strategy to circumvent the permeability problems in Gram-negative bacteria is given by hijacking the active uptake of siderophores, small iron chelators secreted from bacteria in order to acquire essential iron from the environment. The applicability of this Trojan horse strategy was currently demonstrated by the example of Gram-positive antibiotic daptomycin, which was conjugated to a siderophore resulting in a synthetic

sideromycin with selective activity against Gram-negative *A. baumannii*.<sup>219</sup> *n*-Butyl ester derivative **3.61** (Appendix 7.4) might provide access to a respective siderophore conjugate.

Tuberculosis is the leading cause of death associated with microbial infections worldwide with an estimated 10.4 million people infected annually and at least 1.6 million associated deaths.<sup>220</sup> Although the high death toll is related to limited access to efficient treatment for a large number of people in developing countries, drug-resistant tuberculosis is a continuing threat. Given the antituberculosis properties of **PK150**, current studies are underway to access the in vivo efficiency against tuberculosis.



## 4. EXPERIMENTAL SECTION

### 4.1. ORGANIC SYNTHESIS

#### 4.1.1. General Methods and Materials

Chemical reagents and solvents were purchased from commercial suppliers (*Alfa Aesar, Carl Roth, Fluorochem, Merck, Sigma-Aldrich, TCI Europe* and *Thermo Fisher Scientific*) and used as received unless otherwise indicated. Reaction grade or anhydrous solvents (max. 0.01% water content, stored over molecular sieve under an inert atmosphere of argon) were used for all reactions. Ultrapure water (ddH<sub>2</sub>O) was generated using a Milli-Q water purifier (*Merck*).

Cooling baths [ice/water (0°C), ice/acetone (-10°C), ice/NaCl (-20°C) and dry ice/acetone (-78°C)] were used to maintain low temperatures as indicated in the experimental procedures. All temperatures were measured externally.

Reactions sensitive to air and moisture were carried out in flame-dried glassware under an inert atmosphere of argon. Yields refer to purified, dried and spectroscopically pure compounds.

Reaction progress was monitored by LC-MS (*Thermo Fisher Scientific* LCQ-Fleet ion trap mass spectrometer equipped with a hESI ion source and a *Dionex* Ultimate3000 HPLC system) and/or analytical thin layer chromatography (TLC). TLC was performed on precoated silica gel plates (60 F-254, 0.25 mm, *Merck*) with detection by UV ( $\lambda = 254$  and/or 366 nm) and/or by coloration using a phosphomolybdate (PMA) or potassium permanganate (KMnO<sub>4</sub>) TLC stain and subsequent heat treatment.

Flash column chromatography was performed on silica gel (Kieselgel 60, 0.035 – 0.070 mm, mesh 60 Å, *Merck*). Preparative thin layer chromatography (pTLC) was performed on pre-coated silica layer plates (SIL G-100 UV254, 1.00 mm, *Macherey-Nagel*). The solvent compositions reported for all chromatographic separations are on a volume/volume (v/v) basis. Common solvents for chromatography [n-hexane (Hex), ethyl acetate (EtOAc), dichloromethane (CH<sub>2</sub>Cl<sub>2</sub>) and methanol (MeOH)] were distilled prior to use.

Reversed phase HPLC (RP-HPLC) analysis was performed on a *Waters* 2695 separation module, equipped with a *Waters* PDA 2996 and a *Waters* XBridge C18 column (3.5  $\mu$ m, 4.6 x 100 mm, flow = 1.2 mL/min). For preparative scale RP-HPLC separation a *Waters* 2545 quaternary gradient module combined with a *Waters* PDA 2998 and *Waters* XBridgeTMPrep C18 (5.0  $\mu$ m, 30 x 150 mm, flow = 50 mL/min or 10  $\mu$ m, 50 x 250 mm, flow = 130 mL/min) column or a *YMC* Triart C18 (3.5  $\mu$ m, 10 x 250 mm, flow = 10 mL/min) column was used. The mobile phase for elution consisted of a gradient mixture of 0.1% (v/v) TFA in water (buffer A, HPLC grade), 0.1% (v/v) TFA in acetonitrile (buffer B, HPLC grade), water (buffer C, HPLC grade) and acetonitrile (buffer D, HPLC grade).

$^1\text{H}$  and proton-decoupled  $^{13}\text{C}$  NMR spectra were recorded on a *Bruker Avance III HD 300* (300 MHz), a *Bruker Avance I 360* (360 MHz), a *Bruker Avance III HD* (500 MHz) or a *Bruker Avance III HD* (500 MHz, equipped with a *Bruker CryoProbe* platform) at 298 K. Chemical shifts are reported in delta ( $\delta$ ) units in parts per million (ppm) relative to distinguished solvent signals [deuterated chloroform ( $\text{CDCl}_3$ )  $\delta_{\text{H}} = 7.26$  ppm and  $\delta_{\text{C}} = 77.16$  ppm; deuterated DMSO ( $\text{DMSO-d}_6$ ),  $\delta_{\text{H}} = 2.50$  ppm and  $\delta_{\text{C}} = 39.52$  ppm]. Coupling constants ( $J$ ) are reported in Hertz (Hz) and multiplicity is reported as follows: s – singlet, br s – broad singlet, d – doublet, t – triplet, q – quartet, m – multiplet or unresolved. The identity of all compounds was further verified by 2D NMR experiments.

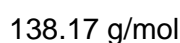
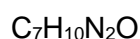
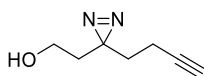
HRMS spectra were recorded in the ESI or APCI mode on a *Thermo Fisher Scientific LTQ-FT Ultra* (FT-ICR-MS) coupled with an *UltiMate 3000 HPLC* system (*Thermo Fisher Scientific*).

#### 4.1.2. Synthetic Procedures for Chapter 2: Insights into Photocrosslinker-Associated Off-Target Protein Binding

1-Hydroxyhept-6-yn-3-one,<sup>138, 221</sup> 3,3-di(pent-4-yn-1-yl)-3*H*-diazirine (**DA-4**),<sup>146</sup> 4-azidophenol (**2.1**),<sup>145</sup> 7-((2-aminoethyl)amino)dibenzo[*cd,g*]indazol-6(2*H*)-one (**2.4**)<sup>138, 222</sup> and *N*-(2-aminoethyl)isoquinoline-5-sulfonamide (**2.5**)<sup>159, 223</sup> were synthesised according to known literature procedures. The synthesis of 2-(3-(but-3-yn-1-yl)-3*H*-diazirin-3-yl)ethanol (**2.2**)<sup>138</sup> and *N*-phenylhept-6-ynamide (**NC-1**)<sup>224</sup> were based on modified literature procedures.

##### 4.1.2.1. Procedures for the Synthesis of Building Blocks

###### 2-(3-(But-3-yn-1-yl)-3*H*-diazirin-3-yl)ethanol (**2.2**)



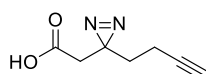
To a flask containing 1-hydroxyhept-6-yn-3-one<sup>138</sup> (851 mg, 6.80 mmol, 1.00 eq.) was added  $\text{NH}_3$  (7 M in MeOH; 14.6 mL, 102 mmol, 15.0 eq.) at  $-10^\circ\text{C}$ . The flask was sealed and the mixture was stirred at  $-10^\circ\text{C}$  for 4.5 h. Then a solution of hydroxylamine-*O*-sulfonic acid (1.00 g, 8.84 mmol, 1.30 eq.) in anhydrous MeOH (5 mL) was added dropwise at  $-10^\circ\text{C}$  and the reaction mixture was stirred at  $-10^\circ\text{C}$  for 1 h in a sealed flask. Subsequently, the reaction mixture was allowed to warm to room temperature and stirred for 16 h.  $\text{NH}_3$  was removed by gently blowing  $\text{N}_2$  through the suspension. The precipitate was removed by filtration through a syringe filter (0.45  $\mu\text{m}$  GHP acrodisc) and the precipitate was washed with several portions of anhydrous MeOH. The organic phase was treated with anhydrous  $\text{NEt}_3$  (6.97 mL, 5.09 g, 50.3 mmol, 7.40 eq.) and cooled to  $0^\circ\text{C}$ . A solution of  $\text{I}_2$  (2.24 g, 8.84 mmol, 1.30 eq.) in anhydrous MeOH (5 mL) was added dropwise at  $0^\circ\text{C}$  and the mixture was stirred at  $0^\circ\text{C}$  for 1 h.  $\text{Et}_2\text{O}$  (25 mL)

was added and the mixture was washed with brine (25 mL). The aqueous phase was extracted with Et<sub>2</sub>O (3 x 25 mL), the combined organic layers were dried over Na<sub>2</sub>SO<sub>4</sub>, filtered and the solvent was removed under reduced pressure. The residue was purified by flash column chromatography on silica (Hex/EtOAc = 9/1 – 4/1) to afford **2.2** (286 mg, 2.07 mmol, 30%) as pale yellow oil.

**TLC** (Hex/EtOAc = 4/1): R<sub>f</sub> = 0.20 [UV | KMnO<sub>4</sub>]. **<sup>1</sup>H NMR** (500 MHz, CDCl<sub>3</sub>): δ [ppm] = 3.49 (q, *J* = 6.0 Hz, 2H), 2.05 (td, *J* = 7.4, 2.6 Hz, 2H), 2.00 (t, *J* = 2.6 Hz, 1H), 1.75 – 1.65 (m, 4H), 1.44 (t, *J* = 5.2 Hz, 1H). **<sup>13</sup>C NMR** (91 MHz, CDCl<sub>3</sub>): δ [ppm] = 83.0, 69.4, 57.6, 35.7, 32.8, 26.7, 13.4.

The spectral data are consistent with those published previously.<sup>138</sup>

### 2-(3-(But-3-yn-1-yl)-3H-diazirin-3-yl)acetic acid (2.3)



C<sub>7</sub>H<sub>8</sub>N<sub>2</sub>O<sub>2</sub>  
152.15 g/mol

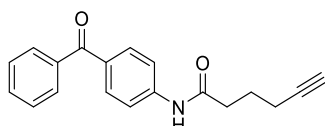
Jones reagent (2 M CrO<sub>3</sub> in H<sub>2</sub>SO<sub>4</sub> aq.; 1.30 mL, 2.60 mmol, 4.00 eq.) was added dropwise to a stirred solution of 2-(3-(but-3-yn-1-yl)-3H-diazirin-3-yl)ethanol (**2.2**) (90.0 mg, 0.651 mmol, 1.00 eq.) in acetone (5 mL) at 0°C. The reaction mixture was stirred at room temperature for 2 h and subsequently quenched with isopropanol (5 mL) and filtered over kieselgur. The filter cake was washed with acetone (3 x 5 mL). Next, the filtrate was dried over Na<sub>2</sub>SO<sub>4</sub>, filtered, concentrated and purified by flash chromatography on silica gel (Hex/EtOAc = 4/1 + 2% acetic acid) to give **2.3** (87.0 mg, 0.572 mmol, 88%) as pale yellow oil.

**TLC** (Hex/EtOAc = 4/1 + 2% acetic acid): R<sub>f</sub> = 0.29 [UV | KMnO<sub>4</sub>]. **<sup>1</sup>H NMR** (300 MHz, CDCl<sub>3</sub>): δ [ppm] = 11.44 (br s, 1H), 2.41 (s, 2H), 2.10 – 2.04 (m, 2H), 2.01 (t, *J* = 2.6 Hz, 1H), 1.80 (t, *J* = 7.3 Hz, 2H). **<sup>13</sup>C NMR** (75 MHz, CDCl<sub>3</sub>): δ [ppm] = 175.8, 82.5, 69.7, 39.6, 32.0, 25.3, 13.3.

**ESI-HRMS** (m/z): [M-H<sup>+</sup>] calcd. for C<sub>7</sub>H<sub>7</sub>N<sub>2</sub>O<sub>2</sub><sup>-</sup> 151.0513; found, 151.0513.

#### 4.1.2.2. Synthesis of Minimal Photoprobes

##### *N*-(4-Benzoylphenyl)hex-5-ynamide (BP-1)



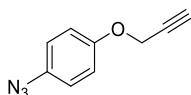
C<sub>19</sub>H<sub>17</sub>NO<sub>2</sub>  
291.35 g/mol

A solution of 5-hexynoic acid (0.500 mL, 500 mg, 4.46 mmol, 1.00 eq.) in CH<sub>2</sub>Cl<sub>2</sub> (30 mL) and DMF (0.1 mL) was cooled to 0°C and oxalyl chloride (0.520 mL, 762 mg, 6.00 mmol, 1.35 eq.) was added. The mixture was stirred at this temperature for 1 h. 4-Aminobenzophenone (880 mg, 4.46 mmol, 1.00 eq.) and Et<sub>3</sub>N (1 mL) were added. The reaction was stirred at room

temperature for 5 h and quenched by the addition of water. The mixture obtained was washed with brine and the phases were separated. The organic phase was dried over  $\text{Na}_2\text{SO}_4$ , filtered and concentrated under reduced pressure. The residue was separated by column chromatography (Hex/EtOAc = 2/1) to yield the desired product (900 mg, 3.09 mmol, 69%).

**TLC** (Hex/EtOAc = 2/1):  $R_f = 0.53$  [ $\text{KMnO}_4$ ].  **$^1\text{H NMR}$**  (360 MHz,  $\text{CDCl}_3$ ):  $\delta$  [ppm] = 8.20 – 7.92 (m, 1H), 7.82 – 7.72 (m, 4H), 7.66 (d,  $J = 8.6$  Hz, 2H), 7.61 – 7.54 (m, 1H), 7.50 – 7.43 (m, 2H), 2.54 (t,  $J = 7.3$  Hz, 2H), 2.34 – 2.25 (m, 2H), 2.00 – 1.90 (m, 3H).  **$^{13}\text{C NMR}$**  (91 MHz,  $\text{CDCl}_3$ ):  $\delta$  [ppm] = 196.0, 171.3, 142.2, 137.9, 132.9, 132.4, 131.7, 130.0, 128.4, 119.0, 83.4, 69.6, 36.1, 23.9, 17.9. **ESI-HRMS** (m/z):  $[\text{M}+\text{H}^+]$  calcd. for  $\text{C}_{19}\text{H}_{18}\text{NO}_2^+$  292.1338; found, 292.1335.

### 1-Azido-4-(prop-2-yn-1-yloxy)benzene (AA-1)



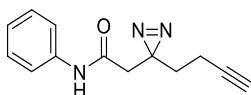
$\text{C}_9\text{H}_7\text{N}_3\text{O}$

173.18 g/mol

To a solution of 4-azidophenol (**2.1**)<sup>145</sup> (1.00 g, 7.40 mmol, 1.00 eq.) in anhydrous THF (30 mL) was added NaH (195 mg, 8.14 mmol, 1.10 eq.) at 0°C. The mixture was stirred for 30 min and propargyl bromide (673  $\mu\text{L}$ , 1.06 g, 8.88 mmol, 1.20 eq.) was added. After stirring at room temperature for 24 h, the reaction was terminated by addition of sat.  $\text{NH}_4\text{Cl}$  solution and the organic phase separated. The aqueous phase was extracted with EtOAc (2 x 20 mL), the organic fractions combined, dried over  $\text{Na}_2\text{SO}_4$ , filtered and the solvent evaporated under reduced pressure. Purification via preparative TLC (Hex/EtOAc = 7/1) yielded propargylic ether **AA-1** (0.890 g, 5.14 mmol, 69%) as a yellow oil, which solidified in the freezer.

**TLC** (Hex/EtOAc = 9/1):  $R_f = 0.11$  [UV |  $\text{KMnO}_4$ ].  **$^1\text{H NMR}$**  (300 MHz,  $\text{CDCl}_3$ ):  $\delta$  [ppm] = 6.97 (s, 4H), 4.67 (d,  $J = 2.4$  Hz, 2H), 2.53 (t,  $J = 2.4$  Hz, 1H).  **$^{13}\text{C NMR}$**  (75 MHz,  $\text{CDCl}_3$ ):  $\delta$  [ppm] = 155.0, 133.5, 120.1, 116.5, 78.5, 75.9, 56.3. **APCI-HRMS** (m/z):  $[\text{2M}+\text{H}^+]$  calcd. for  $\text{C}_{18}\text{H}_{15}\text{N}_6\text{O}_2^+$  347.1250; found, 347.1250.

### 2-(3-(But-3-yn-1-yl)-3H-diazirin-3-yl)-N-phenylacetamide (DA-1)



$\text{C}_{13}\text{H}_{13}\text{N}_3\text{O}$

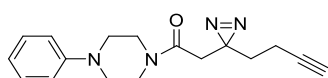
227.27 g/mol

To a mixture of **2.3** (20.0 mg, 0.131 mmol, 1.00 eq.) and aniline (14.4  $\mu\text{L}$ , 14.7 mg, 0.158 mmol, 1.20 eq.) in DMF (2 mL) were added HOBt· $\text{H}_2\text{O}$  (26.6 mg, 0.197 mmol, 1.50 eq.), EDC·HCl (37.8 mg, 0.197 mmol, 1.50 eq.) and DIEA (44.6  $\mu\text{L}$ , 33.9 mg, 0.262 mmol, 2.00 eq.). The mixture was stirred at room temperature for 16 h. Subsequently, the reaction was quenched by the addition of water (5 mL) and the mixture was extracted with EtOAc (3 x 10 mL). The

combined organic phases were washed with sat.  $\text{NH}_4\text{Cl}$  solution (20 mL), dried over  $\text{Na}_2\text{SO}_4$  and filtered. Upon solvent evaporation, the residue was purified by flash chromatography (Hex/EtOAc = 4/1) to yield **DA-1** (23.0 mg, 0.101 mmol, 77%) as a yellow solid.

**TLC** (Hex/EtOAc = 4/1):  $R_f = 0.19$  [UV |  $\text{KMnO}_4$ ].  **$^1\text{H NMR}$**  (360 MHz,  $\text{CDCl}_3$ ):  $\delta$  [ppm] = 7.59 (br s, 1H), 7.51 (d,  $J = 7.8$  Hz, 2H), 7.33 (t,  $J = 7.9$  Hz, 2H), 7.18 – 7.09 (m, 1H), 2.42 (s, 2H), 2.10 (td,  $J = 7.2, 2.6$  Hz, 2H), 2.03 (t,  $J = 2.6$  Hz, 1H), 1.82 (t,  $J = 7.2$  Hz, 2H).  **$^{13}\text{C NMR}$**  (91 MHz,  $\text{CDCl}_3$ ):  $\delta$  [ppm] = 166.2, 137.5, 129.2, 125.0, 120.4, 82.8, 69.8, 42.8, 32.1, 26.2, 13.4. **ESI-HRMS** (m/z):  $[\text{M}+\text{H}^+]$  calcd. for  $\text{C}_{13}\text{H}_{14}\text{N}_3\text{O}^+$  228.1131; found, 228.1129.

### 2-(3-(But-3-yn-1-yl)-3H-diazirin-3-yl)-1-(4-phenylpiperazin-1-yl)ethan-1-one (DA-2)

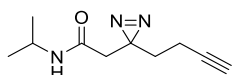


$\text{C}_{17}\text{H}_{20}\text{N}_4\text{O}$   
296.37 g/mol

To a mixture of **2.3** (20.0 mg, 0.131 mmol, 1.00 eq.) and 1-phenylpiperazine (24.0  $\mu\text{L}$ , 25.5 mg, 0.157 mmol, 1.20 eq.) in DMF (1 mL) were added HOBt· $\text{H}_2\text{O}$  (26.6 mg, 0.197 mmol, 1.50 eq.), EDC·HCl (37.8 mg, 0.197 mmol, 1.50 eq.) and DIEA (44.6  $\mu\text{L}$ , 33.9 mg, 0.262 mmol, 2.00 eq.). The mixture was stirred at room temperature for 16 h. Subsequently, the reaction was quenched by water (5 mL) and the mixture was extracted with EtOAc (3 x 10 mL). The combined organic phases were washed with sat.  $\text{NH}_4\text{Cl}$  solution (20 mL), dried over  $\text{Na}_2\text{SO}_4$  and filtered. Upon solvent evaporation, the residue was purified by flash chromatography (Hex/EtOAc = 4/1 – 3/2) to yield **DA-2** (34.6 mg, 0.117 mmol, 89%) as a pale yellow solid.

**TLC** (Hex/EtOAc = 3/2):  $R_f = 0.45$  [UV | PMA].  **$^1\text{H NMR}$**  (360 MHz,  $\text{CDCl}_3$ ):  $\delta$  [ppm] = 7.31 – 7.21 (m, 2H), 6.95 – 6.84 (m, 3H), 3.79 – 3.70 (m, 2H), 3.52 – 3.42 (m, 2H), 3.23 – 3.09 (m, 4H), 2.46 (s, 2H), 2.05 (td,  $J = 7.3, 2.6$  Hz, 2H), 1.97 (t,  $J = 2.6$  Hz, 1H), 1.77 (t,  $J = 7.3$  Hz, 2H).  **$^{13}\text{C NMR}$**  (91 MHz,  $\text{CDCl}_3$ ):  $\delta$  [ppm] = 166.6, 150.9, 129.4, 120.8, 116.8, 82.9, 69.5, 49.9, 49.5, 46.1, 41.8, 38.8, 32.1, 26.3, 13.3. **ESI-HRMS** (m/z):  $[\text{M}+\text{H}^+]$  calcd. for  $\text{C}_{17}\text{H}_{21}\text{N}_4\text{O}^+$  297.1710; found, 297.1709.

### 2-(3-(But-3-yn-1-yl)-3H-diazirin-3-yl)-N-isopropylacetamide (DA-3)

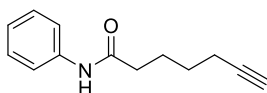


$\text{C}_{10}\text{H}_{15}\text{N}_3\text{O}$   
193.25 g/mol

To a mixture of **2.3** (20.0 mg, 0.131 mmol, 1.00 eq.) and isopropylamine (13.4  $\mu\text{L}$ , 9.28 mg, 0.157 mmol, 1.20 eq.) in DMF (1 mL) were added HOBt· $\text{H}_2\text{O}$  (26.6 mg, 0.197 mmol, 1.50 eq.), EDC·HCl (37.8 mg, 0.197 mmol, 1.50 eq.) and DIEA (44.6  $\mu\text{L}$ , 33.9 mg, 0.262 mmol, 2.00 eq.). The mixture was stirred at room temperature for 16 h. Upon solvent evaporation, the residue was purified by flash chromatography (Hex/EtOAc = 9/1 – 4/1) to yield **DA-3** (25.2 mg, 0.130 mmol, 99%) as a pale oil.

**TLC** (Hex/EtOAc = 4/1):  $R_f = 0.19$  [PMA].  **$^1\text{H NMR}$**  (360 MHz,  $\text{CDCl}_3$ ):  $\delta$  [ppm] = 5.57 (br s, 1H), 4.08 (dq,  $J = 13.2, 6.6$  Hz, 1H), 2.21 (s, 2H), 2.07 (td,  $J = 7.2, 2.6$  Hz, 2H), 2.01 (t,  $J = 2.6$  Hz, 1H), 1.76 (t,  $J = 7.2$  Hz, 2H), 1.17 (d,  $J = 6.6$  Hz, 6H).  **$^{13}\text{C NMR}$**  (91 MHz,  $\text{CDCl}_3$ ):  $\delta$  [ppm] = 166.7, 82.8, 69.6, 42.0, 41.9, 32.2, 26.1, 22.9, 13.4. **ESI-HRMS** ( $m/z$ ):  $[\text{M}+\text{H}^+]$  calcd. for  $\text{C}_{10}\text{H}_{16}\text{N}_3\text{O}^+$  194.1288; found, 194.1286.

### **N-Phenylhept-6-ynamide (NC-1)**



$\text{C}_{13}\text{H}_{15}\text{NO}$

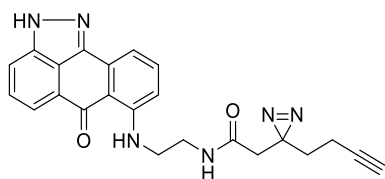
201.27 g/mol

To a mixture of 6-heptynoic acid (50.1  $\mu\text{L}$ , 50.0 mg, 0.396 mmol, 1.00 eq.) and aniline (43.3  $\mu\text{L}$ , 44.2 mg, 0.476 mmol, 1.20 eq.) in DMF (5 mL) were added HOBt· $\text{H}_2\text{O}$  (80.3 mg, 0.594 mmol, 1.50 eq.), EDC·HCl (114 mg, 0.594 mmol, 1.50 eq.) and DIEA (134  $\mu\text{L}$ , 102 mg, 0.792 mmol, 2.00 eq.). The mixture was stirred at room temperature for 16 h. Subsequently, the reaction was quenched by water (5 mL) and the mixture was extracted with  $\text{CH}_2\text{Cl}_2$  (2 x 20 mL). The combined organic phases were washed with sat.  $\text{NH}_4\text{Cl}$  solution (20 mL), dried over  $\text{Na}_2\text{SO}_4$  and filtered. Upon solvent evaporation, the residue was purified by flash chromatography (Hex/EtOAc = 4/1) to yield **NC-1** (73.3 mg, 0.364 mmol, 92%) as a yellow solid.

**TLC** (Hex/EtOAc = 4/1):  $R_f = 0.23$  [UV | PMA].  **$^1\text{H NMR}$**  (300 MHz,  $\text{CDCl}_3$ ):  $\delta$  [ppm] = 7.62 (br s, 1H), 7.51 (d,  $J = 7.8$  Hz, 2H), 7.30 (t,  $J = 7.8$  Hz, 2H), 7.09 (t,  $J = 7.4$  Hz, 1H), 2.37 (t,  $J = 7.5$  Hz, 2H), 2.22 (td,  $J = 7.0, 2.6$  Hz, 2H), 1.96 (t,  $J = 2.6$  Hz, 1H), 1.92 – 1.75 (m, 2H), 1.67 – 1.51 (m, 2H).  **$^{13}\text{C NMR}$**  (75 MHz,  $\text{CDCl}_3$ ):  $\delta$  [ppm] = 171.3, 138.0, 129.0, 124.3, 120.0, 84.1, 68.9, 37.1, 27.9, 24.7, 18.3. **ESI-HRMS** ( $m/z$ ):  $[\text{M}+\text{H}^+]$  calcd. for  $\text{C}_{13}\text{H}_{16}\text{NO}^+$  202.1226; found, 202.1224.

The spectral data are consistent with those published previously.<sup>224</sup>

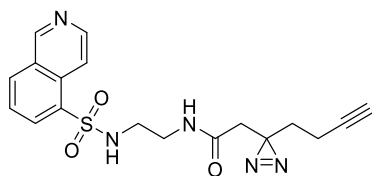
## 4.1.2.3. Synthesis of Kinase Inhibitor Photoprobes

**2-(3-(But-3-yn-1-yl)-3*H*-diazirin-3-yl)-*N*-(2-((6-oxo-2,6-dihydrodibenzo[*cd,g*]indazol-7-yl)amino)ethyl)acetamide (SP600125p)**

$C_{23}H_{20}N_6O_2$   
412.45 g/mol

To a mixture of **2.3** (20.0 mg, 0.131 mmol, 1.00 eq.) and 7-((2-aminoethyl)amino)dibenzo[*cd,g*]indazol-6(2*H*)-one (**2.4**)<sup>138, 222</sup> (43.7 mg, 0.157 mmol, 1.20 eq.) in DMF (1 mL) were added HOBt·H<sub>2</sub>O (26.6 mg, 0.197 mmol, 1.50 eq.), EDC·HCl (37.8 mg, 0.197 mmol, 1.50 eq.) and DIEA (44.6 μL, 33.9 mg, 0.262 mmol, 2.00 eq.). The mixture was stirred at room temperature for 16 h. Upon solvent evaporation, the residue was purified by flash chromatography (hexane/EtOAc = 2/3) to yield **SP600125p** (29.0 mg, 0.0703 mmol, 54%) as a red solid.

**TLC** (hexane/EtOAc = 2/3):  $R_f$  = 0.18 [UV]. **<sup>1</sup>H NMR** (500 MHz, DMSO-*d*<sub>6</sub>): δ [ppm] = 13.62 (s, 1H), 10.09 (t,  $J$  = 5.4 Hz, 1H), 8.24 (t,  $J$  = 5.4 Hz, 1H), 7.87 (d,  $J$  = 8.2 Hz, 1H), 7.80 (d,  $J$  = 7.1 Hz, 1H), 7.69 – 7.63 (m, 1H), 7.58 – 7.51 (m, 1H), 7.40 (d,  $J$  = 7.2 Hz, 1H), 6.95 (d,  $J$  = 8.2 Hz, 1H), 3.44 – 3.37 (m, 2H), 3.34 – 3.30 (m, 2H), 2.81 (t,  $J$  = 2.7 Hz, 1H), 2.25 (s, 2H), 2.04 – 1.99 (m, 2H), 1.67 (t,  $J$  = 7.5 Hz, 2H). **<sup>13</sup>C NMR** (126 MHz, DMSO-*d*<sub>6</sub>): δ [ppm] = 186.4, 167.8, 153.2, 139.4, 138.8, 135.3, 133.1, 128.6, 126.5, 121.6, 119.2, 116.0, 113.8, 111.9, 109.1, 83.2, 71.8, 41.4, 39.6, 38.0, 31.8, 26.7, 12.7. **ESI-HRMS** ( $m/z$ ) [ $M+H^+$ ] calcd. for  $C_{23}H_{21}N_6O_2^+$  413.1721; found, 413.1722.

**2-(3-(But-3-yn-1-yl)-3*H*-diazirin-3-yl)-*N*-(2-(isoquinoline-5-sulfonamido)ethyl)acetamide (H8p)**

$C_{18}H_{19}N_5O_3S$   
385.44 g/mol

To a mixture of **2.3** (20.0 mg, 0.131 mmol, 1.00 eq.) and *N*-(2-aminoethyl)isoquinoline-5-sulfonamide (**2.5**)<sup>159, 223</sup> (39.5 mg, 0.157 mmol, 1.20 eq.) in DMF (1 mL) were added HOBt·H<sub>2</sub>O (26.6 mg, 0.197 mmol, 1.50 eq.), EDC·HCl (37.8 mg, 0.197 mmol, 1.50 eq.) and DIEA (44.6 μL, 33.9 mg, 0.262 mmol, 2.00 eq.). The mixture was stirred at room temperature for 16 h. Upon solvent evaporation, the residue was purified by flash chromatography (CH<sub>2</sub>Cl<sub>2</sub>/MeOH = 98/2 – 95/5) to yield **H8p** (46.6 mg, 0.121 mmol, 93%) as a white solid.

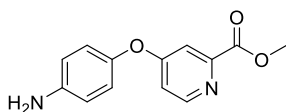
**TLC** (CH<sub>2</sub>Cl<sub>2</sub>/MeOH = 95/5): R<sub>f</sub> = 0.44 [UV | PMA]. **<sup>1</sup>H NMR** (360 MHz, CDCl<sub>3</sub>): δ [ppm] = 9.37 (br s, 1H), 8.64 (br s, 1H), 8.51 – 8.39 (m, 2H), 8.27 – 8.19 (m, 1H), 7.71 (t, *J* = 7.8 Hz, 1H), 6.75 (t, *J* = 5.7 Hz, 1H), 6.63 (t, *J* = 5.9 Hz, 1H), 3.36 (q, *J* = 5.6 Hz, 2H), 3.07 (q, *J* = 5.8 Hz, 2H), 2.23 (s, 2H), 2.04 – 1.93 (m, 3H), 1.69 (t, *J* = 7.2 Hz, 2H). **<sup>13</sup>C NMR** (91 MHz, CDCl<sub>3</sub>): δ [ppm] = 169.1, 153.0, 144.5, 134.4, 134.0, 133.6, 131.5, 129.2, 126.4, 117.7, 82.8, 69.8, 43.1, 41.2, 39.8, 32.2, 26.1, 13.4. **ESI-HRMS** (m/z) [M+H<sup>+</sup>] calcd. for C<sub>18</sub>H<sub>20</sub>N<sub>5</sub>O<sub>3</sub>S<sup>+</sup> 386.1281; found, 386.1279.

### 4.1.3. Synthetic Procedures for Chapter 3: Discovery of a Small Molecule Antibiotic Active Against Multidrug-Resistant Gram-Positive Pathogens

#### 4.1.3.1. Synthesis of Sorafenib-Based Photoprobe SFNp

The synthesis of photoprobe **SFNp** was based on a modified published procedure.<sup>138</sup> 2-(3-(But-3-yn-1-yl)-3H-diazirin-3-yl)ethan-1-amine was synthesized according to a known literature procedure.<sup>138</sup>

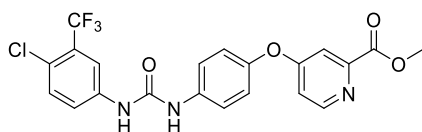
#### Methyl 4-(4-aminophenoxy)picolinate (3.1)



C<sub>13</sub>H<sub>12</sub>N<sub>2</sub>O<sub>3</sub>  
244.25 g/mol

A solution of 4-aminophenol (0.636 g, 5.83 mmol, 1.00 eq.), methyl 4-chloropicolinate (1.00 g, 5.83 mmol, 1.00 eq.) and K<sub>2</sub>CO<sub>3</sub> (1.62 g, 11.7 mmol, 2.00 eq.) in dry DMF (25 mL) was stirred at 135°C for 16 h. The reaction mixture was concentrated, EtOAc (25 mL) added and the mixture filtered over a pad of kieselgur. The filtrate was washed with H<sub>2</sub>O (25 mL) and the aqueous phase was extracted with EtOAc (3 x 25 mL). The combined organic phases were dried over Na<sub>2</sub>SO<sub>4</sub>, filtered and the solvent removed. Purification by flash column chromatography on silica (CH<sub>2</sub>Cl<sub>2</sub>/MeOH = 99/1 – 98/2) gave **3.1** (0.667 g, 2.73 mmol, 47%) as a white solid.

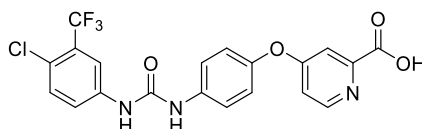
**TLC** (CH<sub>2</sub>Cl<sub>2</sub>/MeOH = 98/2): R<sub>f</sub> = 0.45 [PMA]. **<sup>1</sup>H NMR** (300 MHz, CDCl<sub>3</sub>): δ [ppm] = 8.52 (d, *J* = 5.6 Hz, 1H), 7.61 (d, *J* = 2.5 Hz, 1H), 6.95 (dd, *J* = 5.6, 2.5 Hz, 1H), 6.88 (d, *J* = 8.8 Hz, 2H), 6.71 (d, *J* = 8.8 Hz, 2H), 3.96 (s, 3H). **<sup>13</sup>C NMR** (76 MHz, CDCl<sub>3</sub>): δ [ppm] = 166.9, 165.6, 151.3, 149.8, 145.5, 144.5, 122.0, 116.5, 114.6, 113.2, 53.1. **ESI-HRMS** (m/z) [M+H<sup>+</sup>] calcd. for C<sub>13</sub>H<sub>13</sub>N<sub>2</sub>O<sub>3</sub><sup>+</sup>, 245.0921; found, 245.0918.

**Methyl 4-(4-(3-(4-chloro-3-(trifluoromethyl)phenyl)ureido)phenoxy)picolinate (3.2)**C<sub>21</sub>H<sub>15</sub>ClF<sub>3</sub>N<sub>3</sub>O<sub>4</sub>

465.81 g/mol

A solution of 4-chloro-3-(trifluoromethyl)phenyl isocyanate (600 mg, 2.71 mmol, 1.10 eq.) in dry dichloromethane (15 mL) was cooled to 0°C. After the addition of a solution of **3.1** (600 mg, 2.46 mmol, 1.00 eq.) in dry dichloromethane (3 mL) the reaction mixture was allowed to warm to room temperature and the reaction was stirred at room temperature for 20 h. The solvent was removed followed by purification by flash column chromatography on silica (CH<sub>2</sub>Cl<sub>2</sub>/MeOH = 98/2 – 96/4) to yield **3.2** (900 mg, 1.94 mmol, 79%) as a red solid.

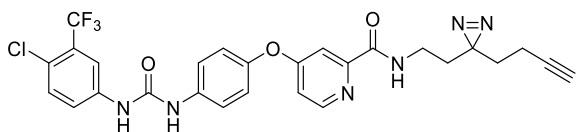
**TLC** (CH<sub>2</sub>Cl<sub>2</sub>/MeOH = 98/2): R<sub>f</sub> = 0.11 [KMnO<sub>4</sub>]. **<sup>1</sup>H NMR** (250 MHz, CDCl<sub>3</sub>): δ [ppm] = 8.74 (br s, 1H), 8.64 (br s, 1H), 8.45 (d, *J* = 5.7 Hz, 1H), 7.69 – 7.65 (m, 2H), 7.58 (dd, *J* = 8.7, 2.5 Hz, 1H), 7.48 – 7.40 (m, 2H), 7.32 (d, *J* = 8.7 Hz, 1H), 7.02 – 6.93 (m, 3H), 4.01 (s, 3H). **<sup>13</sup>C NMR** (63 MHz, CDCl<sub>3</sub>): δ [ppm] = 166.7, 166.0, 153.6, 151.4, 149.4, 148.9, 138.1, 136.8, 132.0, 128.7 (q, *J* = 31.3 Hz), 125.5 (m), 123.5, 122.8 (q, *J* = 273.3 Hz), 122.0, 121.5, 118.5 (q, *J* = 5.5 Hz), 115.1, 114.2, 53.5 (observed complexity is due to the C-F splitting). **ESI-HRMS** (m/z) [M+H<sup>+</sup>] calcd. for C<sub>21</sub>H<sub>16</sub>ClF<sub>3</sub>N<sub>3</sub>O<sub>4</sub><sup>+</sup>, 466.0776; found, 466.0771.

**4-(4-(3-(4-Chloro-3-(trifluoromethyl)phenyl)ureido)phenoxy)picolinic acid (3.3)**C<sub>20</sub>H<sub>13</sub>ClF<sub>3</sub>N<sub>3</sub>O<sub>4</sub>

451.79 g/mol

A solution of **3.2** (110 mg, 0.236 mmol, 1.00 eq.) in THF/H<sub>2</sub>O (1:1 (v/v), 10 mL) was treated with LiOH·H<sub>2</sub>O (19.8 mg, 0.472 mmol, 2.00 eq.). After being stirred at room temperature for 20 h, THF was removed in vacuo and the aqueous phase was acidified with HCl (2M, 300 μL). The aqueous phase was extracted with EtOAc (3 x 15 mL) and the combined organic phases were dried over Na<sub>2</sub>SO<sub>4</sub>, filtered and the solvent removed to give **3.3** (105 mg, 0.232 mmol, 98%) as an off-white solid that was used without further purification.

**<sup>1</sup>H NMR** (500 MHz, DMSO-d<sub>6</sub>): δ [ppm] = 9.29 (s, 1H), 9.08 (s, 1H), 8.54 (br s, 1H), 8.13 (d, *J* = 2.4 Hz, 1H), 7.68 – 7.57 (m, 4H), 7.42 (d, *J* = 2.5 Hz, 1H), 7.22 – 7.16 (m, 3H). **<sup>13</sup>C NMR** (126 MHz, DMSO-d<sub>6</sub>): δ [ppm] = 165.5, 165.4, 152.5, 150.8, 150.7, 147.7, 139.4, 137.2, 132.0, 126.7 (q, *J* = 30.5 Hz), 123.1, 122.9 (q, *J* = 273.1 Hz), 122.4 (m), 121.5, 120.5, 116.8 (q, *J* = 5.6 Hz), 114.7, 111.6 (observed complexity is due to the C-F splitting; certain peaks were picked based on HSQC data). **ESI-HRMS** (m/z) [M+H<sup>+</sup>] calcd. for C<sub>20</sub>H<sub>14</sub>ClF<sub>3</sub>N<sub>3</sub>O<sub>4</sub><sup>+</sup>, 452.0619; found, 452.0620.

***N*-(2-(3-(But-3-yn-1-yl)-3H-diazirin-3-yl)ethyl)-4-(4-(3-(4-chloro-3-(trifluoromethyl)phenyl)ureido) phenoxy)picolinamide (SFNp)**

$C_{27}H_{22}ClF_3N_6O_3$   
570.96 g/mol

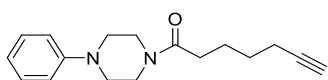
To a solution of **3.3** (23.1 mg, 0.0511 mmol, 1.00 eq.) in dry DMF (0.5 mL) was added HOBt·H<sub>2</sub>O (8.28 mg, 0.0613 mmol, 1.20 eq.), EDC·HCl (11.8 mg, 0.0613, 1.20 eq.) and DIEA (17.8 μL, 13.2 mg, 0.102 mmol, 2.00 eq.). After the addition of a solution of 2-(3-(but-3-yn-1-yl)-3H-diazirin-3-yl)ethan-1-amine<sup>138</sup> (7.71 mg, 0.0562 mmol, 1.10 eq.) in dry DMF (0.5 mL) the mixture was stirred at room temperature for 24 h. The solvent was removed and the residue was purified by flash column chromatography on silica (Hex/EtOAc = 2/3) to yield **SFNp** (17.6 mg, 0.0308 mmol, 60%) as a yellowish solid.

**TLC** (Hex/EtOAc = 2/3):  $R_f = 0.45$  [UV | KMnO<sub>4</sub>]. **<sup>1</sup>H NMR** (500 MHz, DMSO-*d*<sub>6</sub>):  $\delta$  [ppm] = 9.25 (s, 1H), 9.03 (s, 1H), 8.85 (t,  $J = 6.1$  Hz, 1H), 8.52 (d,  $J = 5.6$  Hz, 1H), 8.13 (d,  $J = 2.4$  Hz, 1H), 7.68 – 7.58 (m, 4H), 7.37 (d,  $J = 2.6$  Hz, 1H), 7.20 – 7.16 (m, 3H), 3.17 (q,  $J = 7.0$  Hz, 2H), 2.83 (t,  $J = 2.7$  Hz, 1H), 2.00 (td,  $J = 7.4, 2.7$  Hz, 2H), 1.63 (t,  $J = 7.2$  Hz, 2H), 1.59 (t,  $J = 7.4$  Hz, 2H). **<sup>13</sup>C NMR** (126 MHz, DMSO-*d*<sub>6</sub>):  $\delta$  [ppm] = 166.1, 163.3, 152.5, 152.2, 150.4, 147.8, 139.4, 137.1, 132.1, 126.7 (q,  $J = 30.3$  Hz), 123.2, 123.2 (m), 121.6, 122.9 (q,  $J = 273.3$  Hz), 120.5, 116.9 (q,  $J = 5.3$  Hz), 114.2, 108.7, 83.2, 71.9, 34.1, 32.0, 31.3, 27.3, 12.7 (observed complexity is due to the C-F splitting). **ESI-HRMS** (m/z) [M+H<sup>+</sup>] calcd. for  $C_{27}H_{23}ClF_3N_6O_3^+$ , 571.1467; found, 571.1472.

#### 4.1.3.2. Synthesis of Minimal Photocrosslinker Probes and Corresponding Control Compounds

The synthetic procedures for the preparation of 2-(3-(but-3-yn-1-yl)-3H-diazirin-3-yl)-*N*-phenylacetamide (**DA-1**), 2-(3-(but-3-yn-1-yl)-3H-diazirin-3-yl)-1-(4-phenylpiperazin-1-yl)ethan-1-one (**DA-2**) and 2-(3-(but-3-yn-1-yl)-3H-diazirin-3-yl)-*N*-isopropylacetamide (**DA-3**) are reported in Chapter 4.1.2.2. *N*-phenylhept-6-ynamide (**DA-1C**) was synthesized according to a known literature procedure.<sup>224</sup>

#### 1-(4-Phenylpiperazin-1-yl)hept-6-yn-1-one (DA-2C)



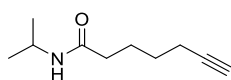
$C_{17}H_{22}N_2O$   
270.38 g/mol

1-Phenylpiperazine (291 μL, 308 mg, 1.90 mmol, 1.20 eq.) in dry DMF (8 mL) was treated with 6-heptynoic acid (200 μL, 199 mg, 1.58 mmol, 1.00 eq.), EDC·HCl (454 mg, 2.37 mmol, 1.50 eq.), HOBt (320 mg, 2.37 mmol, 1.50 eq.) and DIPEA (551 μL, 408 mg, 3.16 mmol,

2.00 eq.). The reaction mixture was stirred at room temperature for 16 h and subsequently the solvent was removed in vacuo. The residue was purified by flash column chromatography on silica (Hex/EtOAc = 1/1) to yield the desired product (217 mg, 0.803 mmol, 51%) as an off-white solid.

**TLC** (Hex/EtOAc = 1/1):  $R_f$  = 0.41 [UV | PMA].  **$^1\text{H NMR}$**  (300 MHz, DMSO- $d_6$ ):  $\delta$  [ppm] = 7.27 – 7.19 (m, 2H), 6.99 – 6.91 (m, 2H), 6.85 – 6.77 (m, 1H), 3.64 – 3.53 (m, 4H), 3.17 – 3.03 (m, 4H), 2.75 (t,  $J$  = 2.7 Hz, 1H), 2.36 (t,  $J$  = 7.4 Hz, 2H), 2.18 (td,  $J$  = 6.9, 2.7 Hz, 2H), 1.66 – 1.54 (m, 2H), 1.53 – 1.41 (m, 2H).  **$^{13}\text{C NMR}$**  (75 MHz, DMSO- $d_6$ ):  $\delta$  [ppm] = 170.4, 150.8, 128.9, 119.3, 115.8, 84.4, 71.2, 48.8, 48.3, 44.7, 40.8, 31.6, 27.6, 23.9, 17.5. **ESI-HRMS** (m/z) [ $\text{M}+\text{H}^+$ ] calcd. for  $\text{C}_{17}\text{H}_{23}\text{N}_2\text{O}^+$ , 271.1805; found, 271.1804.

#### ***N*-Isopropylhept-6-ynamide (DA-3C)**



$\text{C}_{10}\text{H}_{17}\text{NO}$

167.25 g/mol

A solution of isopropylamine (162  $\mu\text{L}$ , 112 mg, 1.90 mmol, 1.20 eq.) in dry  $\text{CH}_2\text{Cl}_2$  (8 mL) was treated with 6-heptynoic acid (200  $\mu\text{L}$ , 199 mg, 1.58 mmol, 1.00 eq.), EDC·HCl (454 mg, 2.37 mmol, 1.50 eq.), HOBt (320 mg, 2.37 mmol, 1.50 eq.) and DIPEA (551  $\mu\text{L}$ , 408 mg, 3.16 mmol, 2.00 eq.). The reaction mixture was stirred at room temperature for 16 h and subsequently citric acid (5% (v/v), 5 mL) was added. The phases were separated and the organic phase was washed with citric acid (5% (v/v), 2 x 5 mL) and saturated  $\text{NaHCO}_3$  (3 x 5 mL). The organic phase was dried over  $\text{Na}_2\text{SO}_4$ , filtered and the solvent removed in vacuo. The crude product was purified by flash column chromatography on silica (Hex/EtOAc = 1/1) to yield the desired product (172 mg, 1.03 mmol, 65%) as a colorless solid.

**TLC** (Hex/EtOAc = 1/1):  $R_f$  = 0.34 [UV | CAM].  **$^1\text{H NMR}$**  (300 MHz, DMSO- $d_6$ ):  $\delta$  [ppm] = 5.27 (s, 1H), 4.16 – 4.00 (m, 1H), 2.25 – 2.12 (m, 4H), 1.95 (t,  $J$  = 2.7 Hz, 1H), 1.80 – 1.70 (m, 2H), 1.61 – 1.50 (m, 2H), 1.15 (s, 3H), 1.13 (s, 3H).  **$^{13}\text{C NMR}$**  (75 MHz, DMSO- $d_6$ ):  $\delta$  [ppm] = 171.8, 84.3, 68.7, 41.4, 36.5, 28.1, 25.0, 23.0, 18.4. **ESI-HRMS** (m/z) [ $\text{M}+\text{H}^+$ ] calcd. for  $\text{C}_{10}\text{H}_{18}\text{NO}^+$ , 168.1383; found, 168.1383.

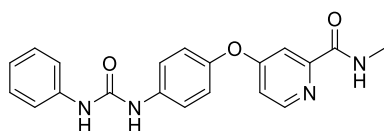
#### **4.1.3.3. Synthesis of a Sorafenib-Based Compound Library**

Isocyanates, thioisocyanates and amines used for compound library synthesis are available from commercial vendors unless otherwise indicated. Synthetic procedure for the synthesis of *compound library building blocks* are reported in Chapter 4.1.3.3.4.

#### 4.1.3.3.1. General Procedure for the Synthesis of Urea and Thiourea Containing Compounds

A solution of the corresponding isocyanate or thioisocyanate (1.10 eq.) in dry dichloromethane (3 mL) was cooled to 0°C. After the addition of the corresponding amine (1.00 eq.) the reaction mixture was allowed to warm to room temperature and the reaction was stirred at room temperature for 20 h. Individual work up and purification yielded the desired urea or thiourea containing compounds. In brief, the solvent was removed followed either by purification via flash column chromatography on silica (Hex/EtOAc or CH<sub>2</sub>Cl<sub>2</sub>/MeOH; workup A) or by the precipitation from DMF through the addition of water (10-fold excess) and collection of the product by centrifugation (17,000 x g, 10 min) (workup B).

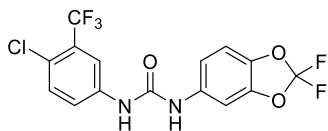
##### **N-Methyl-4-(4-(3-phenylureido)phenoxy)picolinamide (SFN-C)**



C<sub>20</sub>H<sub>18</sub>N<sub>4</sub>O<sub>3</sub>  
362.39 g/mol

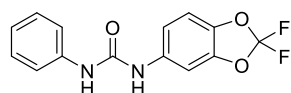
**Yield:** 63% (93.9 mg, 0.259 mmol); workup A (Hex/EtOAc = 3/2). **TLC** (Hex/EtOAc = 3/2): R<sub>f</sub> = 0.18 [UV | KMnO<sub>4</sub>]. **<sup>1</sup>H NMR** (500 MHz, DMSO-d<sub>6</sub>): δ [ppm] = 8.81 (s, 1H), 8.76 (q, J = 4.6 Hz, 1H), 8.70 (s, 1H), 8.50 (d, J = 5.6 Hz, 1H), 7.60 – 7.56 (m, 2H), 7.46 (d, J = 7.7 Hz, 2H), 7.38 (d, J = 2.5 Hz, 1H), 7.31 – 7.26 (m, 2H), 7.19 – 7.12 (m, 3H), 7.00 – 6.96 (m, 1H), 2.78 (d, J = 4.9 Hz, 3H). **<sup>13</sup>C NMR** (75 MHz, DMSO-d<sub>6</sub>): δ [ppm] = 166.1, 163.8, 152.6, 152.4, 150.4, 147.4, 139.7, 137.6, 128.8, 121.9, 121.5, 120.0, 118.3, 114.0, 108.6, 26.0. **ESI-HRMS** (m/z) [M+H<sup>+</sup>] calcd. for C<sub>20</sub>H<sub>19</sub>N<sub>4</sub>O<sub>3</sub><sup>+</sup>, 363.4152; found, 363.1450.

##### **1-(4-Chloro-3-(trifluoromethyl)phenyl)-3-(2,2-difluorobenzo[d][1,3]dioxol-5-yl)urea (PK150)**



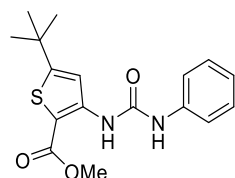
C<sub>15</sub>H<sub>8</sub>ClF<sub>5</sub>N<sub>2</sub>O<sub>3</sub>  
394.68 g/mol

**Yield:** 91% (148 mg, 0.375 mmol); workup A (CH<sub>2</sub>Cl<sub>2</sub>/MeOH = 99/1). **TLC** (CH<sub>2</sub>Cl<sub>2</sub>/MeOH = 98/2): R<sub>f</sub> = 0.57 [UV | PMA]. **<sup>1</sup>H NMR** (500 MHz, DMSO-d<sub>6</sub>): δ [ppm] = 9.22 (s, 1H), 9.07 (s, 1H), 8.09 (d, J = 2.3 Hz, 1H), 7.68 – 7.59 (m, 3H), 7.33 (d, J = 8.7 Hz, 1H), 7.12 (dd, J = 8.8, 2.2 Hz, 1H). **<sup>13</sup>C NMR** (126 MHz, DMSO-d<sub>6</sub>): δ [ppm] = 152.5, 142.8, 139.2, 137.8, 136.0, 132.0, 131.3 (t, J = 252.2 Hz), 126.7 (q, J = 30.5 Hz), 123.2, 122.8 (q, J = 273.1 Hz), 122.5 (m), 116.9 (q, J = 6.0 Hz), 114.2, 110.1, 101.7 (observed complexity is due to the C-F splitting). **ESI-HRMS** (m/z) [M+H<sup>+</sup>] calcd. for C<sub>15</sub>H<sub>9</sub>ClF<sub>5</sub>N<sub>2</sub>O<sub>3</sub><sup>+</sup>, 395.0216; found, 395.0211.

**1-(2,2-Difluorobenzo[d][1,3]dioxol-5-yl)-3-phenylurea (PK150-C)**C<sub>14</sub>H<sub>10</sub>F<sub>2</sub>N<sub>2</sub>O<sub>3</sub>

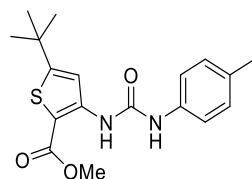
292.24 g/mol

**Yield:** 17% (38.0 mg, 0.130 mmol); workup A (Hex/EtOAc = 4/1). **TLC** (Hex/EtOAc = 4/1): R<sub>f</sub> = 0.16 [UV | PMA]. **<sup>1</sup>H NMR** (500 MHz, DMSO-d<sub>6</sub>): δ [ppm] = 8.88 (s, 1H), 8.72 (s, 1H), 7.66 (d, *J* = 2.1 Hz, 1H), 7.46 – 7.43 (m, 2H), 7.32 – 7.26 (m, 3H), 7.08 (dd, *J* = 8.7, 2.2 Hz, 1H), 7.00 – 6.95 (m, 1H). **<sup>13</sup>C NMR** (126 MHz, DMSO-d<sub>6</sub>): δ [ppm] = 152.6, 142.8, 139.5, 137.4, 136.6, 131.3 (t, *J* = 252.2 Hz), 128.8, 122.1, 118.4, 113.5, 110.1, 101.2 (observed complexity is due to the C-F splitting). **ESI-HRMS** (m/z) [M+H<sup>+</sup>] calcd. for C<sub>14</sub>H<sub>11</sub>F<sub>3</sub>N<sub>2</sub>O<sub>3</sub><sup>+</sup>, 293.0732; found, 293.0732.

**Methyl 5-(tert-butyl)-3-(3-phenylureido)thiophene-2-carboxylate (3.4)**C<sub>17</sub>H<sub>20</sub>N<sub>2</sub>O<sub>3</sub>S

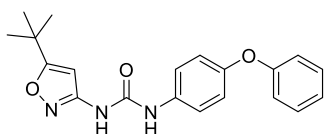
332.42 g/mol

**Yield:** 50% (78.3 mg, 0.236 mmol); workup A (Hex/EtOAc = 9/1). **TLC** (Hex/EtOAc = 9/1): R<sub>f</sub> = 0.23 [UV | KMnO<sub>4</sub>]. **<sup>1</sup>H NMR** (500 MHz, DMSO-d<sub>6</sub>): δ [ppm] = 10.01 (s, 1H), 9.54 (s, 1H), 7.86 (s, 1H), 7.50 (d, *J* = 7.6 Hz, 2H), 7.29 (t, *J* = 7.9 Hz, 2H), 7.00 (t, *J* = 7.4 Hz, 1H), 3.81 (s, 3H), 1.34 (s, 9H). **<sup>13</sup>C NMR** (126 MHz, DMSO-d<sub>6</sub>): δ [ppm] = 163.6, 163.0, 151.3, 145.4, 139.4, 128.8, 122.4, 118.5, 117.3, 104.0, 51.7, 34.8, 31.5. **ESI-HRMS** (m/z) [M+H<sup>+</sup>] calcd. for C<sub>17</sub>H<sub>21</sub>N<sub>2</sub>O<sub>3</sub>S<sup>+</sup>, 333.1267; found, 333.1270.

**Methyl 5-(tert-butyl)-3-(3-(p-tolyl)ureido)thiophene-2-carboxylate (3.5)**C<sub>18</sub>H<sub>22</sub>N<sub>2</sub>O<sub>3</sub>S

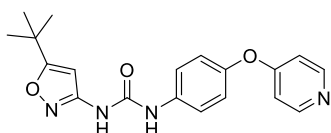
346.44 g/mol

**Yield:** 74% (121 mg, 0.349 mmol); workup A (Hex/EtOAc = 9/1). **TLC** (Hex/EtOAc = 9/1): R<sub>f</sub> = 0.24 [UV | PMA]. **<sup>1</sup>H NMR** (500 MHz, DMSO-d<sub>6</sub>): δ [ppm] = 9.89 (s, 1H), 9.49 (s, 1H), 7.86 (s, 1H), 7.38 (d, *J* = 8.4 Hz, 2H), 7.09 (d, *J* = 8.3 Hz, 2H), 3.81 (s, 3H), 2.24 (s, 3H), 1.34 (s, 9H). **<sup>13</sup>C NMR** (126 MHz, DMSO-d<sub>6</sub>): δ [ppm] = 163.6, 163.0, 151.3, 145.5, 136.8, 131.2, 129.2, 118.6, 117.3, 103.8, 51.7, 34.8, 31.5, 20.4. **ESI-HRMS** (m/z) [M+H<sup>+</sup>] calcd. for C<sub>18</sub>H<sub>23</sub>N<sub>2</sub>O<sub>3</sub>S<sup>+</sup>, 347.1424; found, 347.1426.

**1-(5-(*tert*-Butyl)isoxazol-3-yl)-3-(4-phenoxyphenyl)urea (3.6)**C<sub>20</sub>H<sub>21</sub>N<sub>3</sub>O<sub>3</sub>

351.41 g/mol

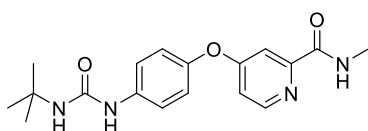
**Yield:** 83% (208 mg, 0.592 mmol); workup A (Hex/EtOAc = 4/1). **TLC** (Hex/EtOAc = 4/1): R<sub>f</sub> = 0.38 [UV | KMnO<sub>4</sub>]. **<sup>1</sup>H NMR** (500 MHz, CDCl<sub>3</sub>): δ [ppm] = 9.26 – 9.00 (m, 2H), 7.46 (d, *J* = 8.9 Hz, 2H), 7.35 – 7.29 (m, 2H), 7.10 – 7.06 (m, 1H), 7.01 – 6.96 (m, 4H), 5.98 (s, 1H), 1.35 (s, 9H). **<sup>13</sup>C NMR** (75 MHz, CDCl<sub>3</sub>): δ [ppm] = 181.4, 158.6, 157.7, 153.5, 153.1, 133.4, 129.9, 123.2, 122.4, 119.8, 118.5, 92.1, 33.0, 28.7. **ESI-HRMS** (*m/z*) [M+H<sup>+</sup>] calcd. for C<sub>20</sub>H<sub>21</sub>N<sub>3</sub>O<sub>3</sub><sup>+</sup>, 352.1656; found, 352.1658.

**1-(5-(*tert*-Butyl)isoxazol-3-yl)-3-(4-(pyridin-4-yloxy)phenyl)urea (3.7)**C<sub>19</sub>H<sub>20</sub>N<sub>4</sub>O<sub>3</sub>

352.39 g/mol

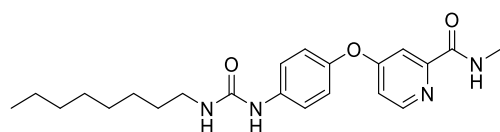
**Amine building block: BB-1** (Chapter 4.1.3.3.4)

**Yield:** 27% (21.3 mg, 0.0604 mmol); workup A (CH<sub>2</sub>Cl<sub>2</sub>/MeOH = 19/1). **TLC** (CH<sub>2</sub>Cl<sub>2</sub>/MeOH = 19/1): R<sub>f</sub> = 0.22 [UV | KMnO<sub>4</sub>]. **<sup>1</sup>H NMR** (300 MHz, CDCl<sub>3</sub>): δ [ppm] = 9.44 – 9.14 (m, 2H), 8.46 (d, *J* = 5.9 Hz, 2H), 7.57 (d, *J* = 8.9 Hz, 2H), 7.06 (d, *J* = 8.9 Hz, 2H), 6.83 (d, *J* = 6.2 Hz, 2H), 6.02 (s, 1H), 1.35 (s, 9H). **<sup>13</sup>C NMR** (75 MHz, CDCl<sub>3</sub>): δ [ppm] = 181.4, 165.2, 158.5, 152.7, 151.2, 149.8, 135.5, 121.9, 121.5, 112.0, 92.0, 32.9, 28.6. **ESI-HRMS** (*m/z*) [M+H<sup>+</sup>] calcd. for C<sub>19</sub>H<sub>21</sub>N<sub>4</sub>O<sub>3</sub><sup>+</sup>, 353.1608; found, 353.1605.

**4-(4-(3-(*tert*-Butyl)ureido)phenoxy)-*N*-methylpicolinamide (3.8)**C<sub>18</sub>H<sub>22</sub>N<sub>4</sub>O<sub>3</sub>

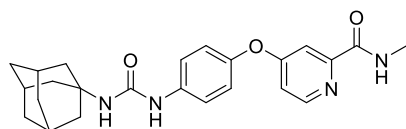
342.40 g/mol

**Yield:** 52% (72.9 mg, 0.213 mmol); workup A (CH<sub>2</sub>Cl<sub>2</sub>/MeOH = 98/2). **TLC** (CH<sub>2</sub>Cl<sub>2</sub>/MeOH = 98/2): R<sub>f</sub> = 0.26 [UV | PMA]. **<sup>1</sup>H NMR** (500 MHz, CDCl<sub>3</sub>): δ [ppm] = 8.33 (d, *J* = 5.6 Hz, 1H), 8.16 (q, *J* = 4.9 Hz, 1H), 7.82 (s, 1H), 7.60 (d, *J* = 2.5 Hz, 1H), 7.33 (d, *J* = 8.9 Hz, 2H), 6.94 – 6.88 (m, 3H), 5.64 (s, 1H), 3.00 (d, *J* = 5.1 Hz, 3H), 1.35 (s, 9H). **<sup>13</sup>C NMR** (126 MHz, CDCl<sub>3</sub>): δ [ppm] = 167.0, 165.2, 155.4, 151.7, 149.9, 147.6, 138.1, 121.3, 120.4, 114.5, 109.4, 50.5, 29.5, 26.5. **ESI-HRMS** (*m/z*) [M+H<sup>+</sup>] calcd. for C<sub>18</sub>H<sub>23</sub>N<sub>4</sub>O<sub>3</sub><sup>+</sup>, 343.1765; found, 343.1763.

***N*-methyl-4-(4-(3-octylureido)phenoxy)picolinamide (3.9)**

$C_{22}H_{30}N_4O_3$   
398.51 g/mol

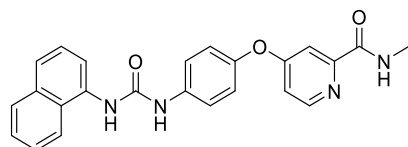
**Yield:** 35% (57.4 mg, 0.144 mmol); workup A ( $CH_2Cl_2/MeOH = 98/2$ ). **TLC** ( $CH_2Cl_2/MeOH = 98/2$ ):  $R_f = 0.25$  [UV | PMA].  **$^1H$  NMR** (500 MHz,  $DMSO-d_6$ ):  $\delta$  [ppm] = 8.75 (q,  $J = 4.7$  Hz, 1H), 8.63 (s, 1H), 8.48 (d,  $J = 5.6$  Hz, 1H), 7.53 – 7.48 (m, 2H), 7.36 (d,  $J = 2.6$  Hz, 1H), 7.11 (dd,  $J = 5.6, 2.6$  Hz, 1H), 7.09 – 7.05 (m, 2H), 6.23 (t,  $J = 5.6$  Hz, 1H), 3.07 (q,  $J = 6.7$  Hz, 2H), 2.78 (d,  $J = 4.9$  Hz, 3H), 1.46 – 1.39 (m, 2H), 1.32 – 1.21 (m, 10H), 0.89 – 0.83 (m, 3H).  **$^{13}C$  NMR** (126 MHz,  $DMSO-d_6$ ):  $\delta$  [ppm] = 166.2, 163.8, 155.2, 152.4, 150.3, 146.6, 138.6, 121.3, 119.1, 113.9, 108.6, 39.1, 31.3, 29.8, 28.8, 28.7, 26.4, 26.0, 22.1, 14.0. **ESI-HRMS** (m/z) [ $M+H^+$ ] calcd. for  $C_{22}H_{31}N_4O_3^+$ , 399.2391; found, 399.2388.

***N*-methyl-4-(4-(3-((3*s*,5*s*,7*s*)-adamantan-1-yl)ureido)phenoxy)-picolinamide (3.10)**

$C_{24}H_{28}N_4O_3$   
420.51 g/mol

**Yield:** 79% (136 mg, 0.323 mmol); workup A (Hex/EtOAc = 1/4). **TLC** (Hex/EtOAc = 1/4):  $R_f = 0.40$  [UV | PMA].  **$^1H$  NMR** (500 MHz,  $DMSO-d_6$ ):  $\delta$  [ppm] = 8.77 (q,  $J = 4.7$  Hz, 1H), 8.48 (d,  $J = 5.6$  Hz, 1H), 8.40 (s, 1H), 7.47 – 7.43 (m, 2H), 7.35 (d,  $J = 2.6$  Hz, 1H), 7.11 (dd,  $J = 5.6, 2.6$  Hz, 1H), 7.09 – 7.05 (m, 2H), 5.91 (s, 1H), 2.78 (d,  $J = 4.9$  Hz, 3H), 2.03 (br s, 3H), 1.96 – 1.91 (m, 6H), 1.63 (br s, 6H).  **$^{13}C$  NMR** (126 MHz,  $DMSO-d_6$ ):  $\delta$  [ppm] = 166.2, 163.8, 153.9, 152.4, 150.3, 146.5, 138.6, 121.4, 118.9, 113.9, 108.6, 49.9, 41.7, 36.1, 28.9, 26.0. **ESI-HRMS** (m/z) [ $M+H^+$ ] calcd. for  $C_{24}H_{29}N_4O_3^+$ , 421.2234; found, 421.2234.

The spectral data are consistent with those published previously.<sup>225</sup>

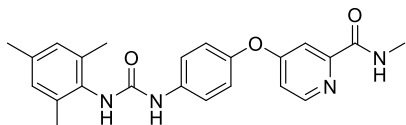
***N*-methyl-4-(4-(3-(naphthalen-1-yl)ureido)phenoxy)picolinamide (3.11)**

$C_{24}H_{20}N_4O_3$   
412.45 g/mol

**Yield:** 50% (116 mg, 0.281 mmol); workup B (additional washing step of product with  $CH_2Cl_2$ ).  **$^1H$  NMR** (500 MHz,  $DMSO-d_6$ ):  $\delta$  [ppm] = 9.22 (s, 1H), 8.82 (s, 1H), 8.79 (q,  $J = 4.6$  Hz, 1H), 8.51 (d,  $J = 5.6$  Hz, 1H), 8.14 (d,  $J = 8.4$  Hz, 1H), 8.02 (d,  $J = 7.3$  Hz, 1H), 7.94 (d,  $J = 7.9$  Hz, 1H), 7.68 – 7.59 (m, 4H), 7.58 – 7.53 (m, 1H), 7.49 (t,  $J = 7.9$  Hz, 1H), 7.40 (d,  $J = 2.6$  Hz, 1H), 7.22 – 7.17 (m, 2H), 7.15 (dd,  $J = 5.6, 2.6$  Hz, 1H), 2.79 (d,  $J = 4.9$  Hz, 3H).  **$^{13}C$  NMR** (126 MHz,  $DMSO-d_6$ ):  $\delta$  [ppm] = 166.1, 163.8, 153.0, 152.5, 150.4, 147.4, 137.7, 134.2, 133.7, 128.5,

126.0, 126.0, 125.9, 125.8, 123.1, 121.6, 121.4, 119.9, 117.6, 114.0, 108.7, 26.1. **ESI-HRMS** (m/z) [M+H<sup>+</sup>] calcd. for C<sub>24</sub>H<sub>21</sub>N<sub>4</sub>O<sub>3</sub><sup>+</sup>, 413.1608; found, 413.1607.

#### 4-(4-(3-Mesitylureido)phenoxy)-N-methylpicolinamide (3.12)

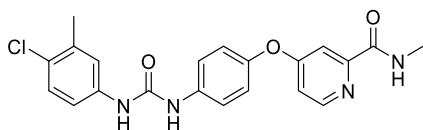


C<sub>23</sub>H<sub>24</sub>N<sub>4</sub>O<sub>3</sub>  
404.47 g/mol

**Yield:** 44% (73.8 mg, 0.182 mmol); workup B (additional washing step of product with Et<sub>2</sub>O).

**<sup>1</sup>H NMR** (500 MHz, DMSO-d<sub>6</sub>): δ [ppm] = 8.84 (br s, 1H), 8.76 (q, *J* = 4.6 Hz, 1H), 8.49 (d, *J* = 5.6 Hz, 1H), 7.65 (s, 1H), 7.59 – 7.54 (m, 2H), 7.37 (d, *J* = 2.6 Hz, 1H), 7.15 – 7.09 (m, 3H), 6.89 (s, 2H), 2.78 (d, *J* = 4.9 Hz, 3H), 2.23 (s, 3H), 2.17 (s, 6H). **<sup>13</sup>C NMR** (126 MHz, DMSO-d<sub>6</sub>): δ [ppm] = 166.1, 163.8, 153.3, 152.4, 150.3, 147.0, 138.3, 135.4, 135.0, 132.6, 128.3, 121.4, 119.5, 113.9, 108.6, 26.0, 20.5, 18.2. **ESI-HRMS** (m/z) [M+H<sup>+</sup>] calcd. for C<sub>23</sub>H<sub>25</sub>N<sub>4</sub>O<sub>3</sub><sup>+</sup>, 405.1921; found, 405.1919.

#### 4-(4-(3-(4-Chloro-3-methylphenyl)ureido)phenoxy)-N-methylpicolinamide (3.13)

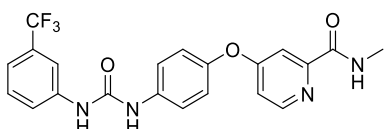


C<sub>21</sub>H<sub>19</sub>ClN<sub>4</sub>O<sub>3</sub>  
410.86 g/mol

**Yield:** 91% (154 mg, 0.375 mmol); workup B (additional washing step of product with Et<sub>2</sub>O).

**<sup>1</sup>H NMR** (500 MHz, DMSO-d<sub>6</sub>): δ [ppm] = 8.86 (s, 1H), 8.81 – 8.76 (m, 2H), 8.50 (d, *J* = 5.6 Hz, 1H), 7.57 (d, *J* = 8.9 Hz, 2H), 7.47 – 7.43 (m, 1H), 7.37 (d, *J* = 2.6 Hz, 1H), 7.33 – 7.28 (m, 2H), 7.18 – 7.13 (m, 3H), 2.78 (d, *J* = 4.9 Hz, 3H), 2.30 (s, 3H). **<sup>13</sup>C NMR** (126 MHz, DMSO-d<sub>6</sub>): δ [ppm] = 166.0, 163.8, 152.5, 152.4, 150.4, 147.5, 138.6, 137.5, 135.6, 129.0, 125.8, 121.5, 120.6, 120.1, 117.5, 114.0, 108.6, 26.0, 19.9. **ESI-HRMS** (m/z) [M+H<sup>+</sup>] calcd. for C<sub>21</sub>H<sub>20</sub>ClN<sub>4</sub>O<sub>3</sub><sup>+</sup>, 411.1218; found, 411.1216.

#### N-Methyl-4-(4-(3-(3-(trifluoromethyl)phenyl)ureido)phenoxy)picolinamide (3.14)



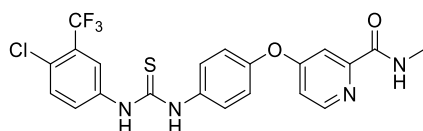
C<sub>21</sub>H<sub>17</sub>F<sub>3</sub>N<sub>4</sub>O<sub>3</sub>  
430.39 g/mol

**Yield:** 98% (172 mg, 0.400 mmol); workup A (CH<sub>2</sub>Cl<sub>2</sub>/MeOH = 98/2).

**TLC** (CH<sub>2</sub>Cl<sub>2</sub>/MeOH = 98/2): R<sub>f</sub> = 0.15 [UV | KMnO<sub>4</sub>]. **<sup>1</sup>H NMR** (500 MHz, DMSO-d<sub>6</sub>): δ [ppm] = 9.11 (s, 1H), 8.96 (s, 1H), 8.79 (q, *J* = 4.5 Hz, 1H), 8.50 (d, *J* = 5.6 Hz, 1H), 8.03 (s, 1H), 7.62 – 7.57 (m, 3H), 7.52 (t, *J* = 7.9 Hz, 1H), 7.38 (d, *J* = 2.6 Hz, 1H), 7.32 (d, *J* = 7.7 Hz, 1H), 7.20 – 7.13 (m, 3H), 2.78 (d, *J* = 4.9 Hz, 3H). **<sup>13</sup>C NMR** (126 MHz, DMSO-d<sub>6</sub>):

$\delta$  [ppm] = 166.0, 163.8, 152.6, 152.5, 150.4, 147.7, 140.6, 137.3, 130.0, 129.6 (q,  $J$  = 31.4 Hz), 124.3 (q,  $J$  = 272.6 Hz), 121.9, 121.5, 120.4, 118.2 (q,  $J$  = 3.6 Hz), 114.2 (q,  $J$  = 4.0 Hz), 114.0, 108.7, 26.0 (observed complexity is due to the C-F splitting). **ESI-HRMS** ( $m/z$ ) [ $M+H^+$ ] calcd. for  $C_{21}H_{18}F_3N_4O_3^+$ , 431.1326; found, 431.1325.

**4-(4-(3-(4-Chloro-3-(trifluoromethyl)phenyl)thioureido)phenoxy)-*N*-methylpicolinamide**  
(3.15)

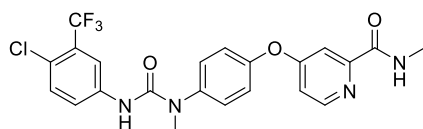


$C_{21}H_{16}ClF_3N_4O_2S$   
480.89 g/mol

**Yield:** 41% (81.0 mg, 0.168 mmol); workup B.  **$^1H$  NMR** (500 MHz,  $DMSO-d_6$ ):  $\delta$  [ppm] = 10.21 – 10.13 (m, 2H), 8.78 (q,  $J$  = 4.6 Hz, 1H), 8.53 (d,  $J$  = 5.6 Hz, 1H), 8.09 (d,  $J$  = 2.5 Hz, 1H), 7.82 (dd,  $J$  = 8.7, 2.5 Hz, 1H), 7.68 (d,  $J$  = 8.7 Hz, 1H), 7.58 (d,  $J$  = 8.8 Hz, 2H), 7.42 (d,  $J$  = 2.6 Hz, 1H), 7.23 (d,  $J$  = 8.9 Hz, 2H), 7.18 (dd,  $J$  = 5.6, 2.6 Hz, 1H), 2.79 (d,  $J$  = 4.9 Hz, 3H).  **$^{13}C$  NMR** (126 MHz,  $DMSO-d_6$ ):  $\delta$  [ppm] = 179.9, 165.6, 163.8, 152.5, 150.5, 150.1, 139.2, 136.6, 131.6, 128.6, 126.3 (d,  $J$  = 30.9 Hz), 126.0, 125.2, 122.8 (d,  $J$  = 273.3 Hz), 122.5 (q,  $J$  = 2.4 Hz), 121.2, 114.4, 108.9, 26.1 (observed complexity is due to the C-F splitting). **ESI-HRMS** ( $m/z$ ) [ $M+H^+$ ] calcd. for  $C_{21}H_{17}ClF_3N_4O_2S^+$ , 481.0707; found, 481.0709.

The spectral data are consistent with those published previously.<sup>226</sup>

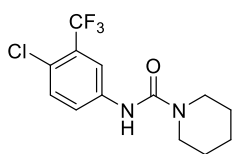
**4-(4-(3-(4-Chloro-3-(trifluoromethyl)phenyl)-1-methylureido)phenoxy)-*N*-methylpicolinamide** (3.18)



$C_{22}H_{18}ClF_3N_4O_3$   
478.86 g/mol

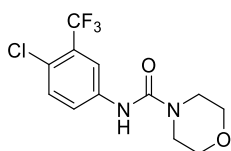
**Amine building block: BB-2** (Chapter 4.1.3.3.4)

**Yield:** 64% (79.2 mg, 0.165 mmol); workup A (Hex/EtOAc = 1/1). **TLC** (Hex/EtOAc = 1/1):  $R_f$  = 0.16 [UV | PMA].  **$^1H$  NMR** (500 MHz,  $DMSO-d_6$ ):  $\delta$  [ppm] = 8.81 (q,  $J$  = 4.6 Hz, 1H), 8.75 (s, 1H), 8.54 (d,  $J$  = 5.6 Hz, 1H), 8.06 (d,  $J$  = 2.6 Hz, 1H), 7.81 (dd,  $J$  = 8.8, 2.5 Hz, 1H), 7.58 (d,  $J$  = 8.8 Hz, 1H), 7.52 – 7.46 (m, 3H), 7.30 – 7.26 (m, 2H), 7.22 (dd,  $J$  = 5.6, 2.6 Hz, 1H), 3.31 (s, 3H), 2.79 (d,  $J$  = 4.9 Hz, 3H).  **$^{13}C$  NMR** (126 MHz,  $DMSO-d_6$ ):  $\delta$  [ppm] = 165.4, 163.8, 154.4, 152.6, 151.3, 150.5, 140.9, 139.9, 131.5, 128.7, 126.3 (q,  $J$  = 30.6 Hz), 124.4, 122.9 (q,  $J$  = 273.0 Hz), 122.5 (m), 121.6, 118.4 (q,  $J$  = 5.7 Hz), 114.5, 109.3, 37.8, 26.1 (observed complexity is due to the C-F splitting). **ESI-HRMS** ( $m/z$ ) [ $M+H^+$ ] calcd. for  $C_{22}H_{19}ClF_3N_4O_3^+$ , 479.1092; found, 479.1083.

***N*-(4-Chloro-3-(trifluoromethyl)phenyl)piperidine-1-carboxamide (3.19)**C<sub>13</sub>H<sub>14</sub>ClF<sub>3</sub>N<sub>2</sub>O

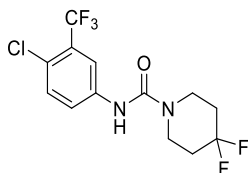
306.71 g/mol

**Yield:** 91% (138 mg, 0.450 mmol); workup A (Hex/EtOAc = 4/1). **TLC** (Hex/EtOAc = 4/1):  $R_f = 0.14$  [UV | PMA]. **<sup>1</sup>H NMR** (500 MHz, DMSO-*d*<sub>6</sub>):  $\delta$  [ppm] = 8.87 (s, 1H), 8.05 (d,  $J = 2.6$  Hz, 1H), 7.79 (dd,  $J = 8.8, 2.6$  Hz, 1H), 7.55 (d,  $J = 8.8$  Hz, 1H), 3.45 – 3.39 (m, 4H), 1.62 – 1.54 (m, 2H), 1.52 – 1.44 (m, 4H). **<sup>13</sup>C NMR** (126 MHz, DMSO-*d*<sub>6</sub>):  $\delta$  [ppm] = 154.2, 140.5, 131.6, 126.3 (q,  $J = 30.4$  Hz), 123.7, 123.0 (q,  $J = 272.9$  Hz), 121.8 (m), 117.8 (q,  $J = 5.7$  Hz), 44.6, 25.5, 24.0 (observed complexity is due to the C-F splitting). **ESI-HRMS** ( $m/z$ ) [ $M+H^+$ ] calcd. for C<sub>13</sub>H<sub>15</sub>ClF<sub>3</sub>N<sub>2</sub>O<sup>+</sup>, 307.0820; found, 307.0818.

***N*-(4-Chloro-3-(trifluoromethyl)phenyl)morpholine-4-carboxamide (3.20)**C<sub>12</sub>H<sub>12</sub>ClF<sub>3</sub>N<sub>2</sub>O<sub>2</sub>

308.69 g/mol

**Yield:** 36% (128 mg, 0.415 mmol); workup A (Hex/EtOAc = 1/1). **TLC** (Hex/EtOAc = 1/1):  $R_f = 0.21$  [UV | PMA]. **<sup>1</sup>H NMR** (500 MHz, DMSO-*d*<sub>6</sub>):  $\delta$  [ppm] = 8.95 (s, 1H), 8.05 (d,  $J = 2.6$  Hz, 1H), 7.79 (dd,  $J = 8.8, 2.5$  Hz, 1H), 7.57 (d,  $J = 8.8$  Hz, 1H), 3.63 – 3.59 (m, 4H), 3.46 – 3.42 (m, 4H). **<sup>13</sup>C NMR** (126 MHz, DMSO-*d*<sub>6</sub>):  $\delta$  [ppm] = 154.6, 140.1, 131.7, 126.4 (q,  $J = 30.4$  Hz), 123.8, 122.9 (q,  $J = 273.1$  Hz), 122.2 (m), 117.9 (q,  $J = 5.7$  Hz), 65.9, 44.1 (observed complexity is due to the C-F splitting). **ESI-HRMS** ( $m/z$ ) [ $M+H^+$ ] calcd. for C<sub>12</sub>H<sub>13</sub>ClF<sub>3</sub>N<sub>2</sub>O<sup>+</sup>, 309.0612; found, 309.0611.

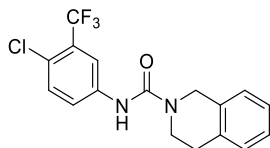
***N*-(4-Chloro-3-(trifluoromethyl)phenyl)-4,4-difluoropiperidine-1-carboxamide (3.21)**C<sub>13</sub>H<sub>12</sub>ClF<sub>5</sub>N<sub>2</sub>O

342.69 g/mol

**Yield:** 20% (27.5 mg, 0.0802 mmol); workup A (Hex/EtOAc = 4/1). **TLC** (Hex/EtOAc = 4/1):  $R_f = 0.14$  [UV | KMnO<sub>4</sub>]. **<sup>1</sup>H NMR** (500 MHz, DMSO-*d*<sub>6</sub>):  $\delta$  [ppm] = 9.10 (s, 1H), 8.04 (d,  $J = 2.6$  Hz, 1H), 7.78 (dd,  $J = 8.8, 2.5$  Hz, 1H), 7.58 (d,  $J = 8.8$  Hz, 1H), 3.62 – 3.55 (m, 4H), 2.06 – 1.93 (m, 4H). **<sup>13</sup>C NMR** (126 MHz, DMSO-*d*<sub>6</sub>):  $\delta$  [ppm] = 154.1, 140.1, 131.7, 126.3 (q,  $J = 30.5$  Hz), 123.9, 122.9 (q,  $J = 272.4$  Hz), 122.8 (q,  $J = 241.2$  Hz), 122.2 (m), 117.9 (q,  $J = 5.7$  Hz), 40.9 (t,  $J = 5.3$  Hz), 33.4 (t,  $J = 22.6$  Hz) (observed complexity is due to the C-F splitting). **ESI-HRMS** ( $m/z$ ) [ $M+H^+$ ] calcd. for C<sub>13</sub>H<sub>13</sub>ClF<sub>5</sub>N<sub>2</sub>O<sup>+</sup>, 343.0631; found, 343.0630.

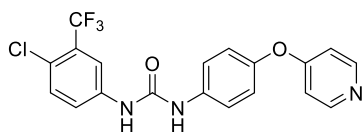
**N-(4-Chloro-3-(trifluoromethyl)phenyl)-3,4-dihydroisoquinoline-2(1H)-carboxamide**

(3.22)

 $C_{17}H_{14}ClF_3N_2O$ 

354.76 g/mol

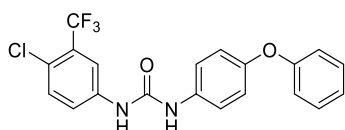
**Yield:** 85% (226 mg, 0.637 mmol); workup A (Hex/EtOAc = 4/1). **TLC** (Hex/EtOAc = 4/1):  $R_f = 0.25$  [UV | PMA].  **$^1H$  NMR** (500 MHz, DMSO- $d_6$ ):  $\delta$  [ppm] = 9.01 (s, 1H), 8.08 (d,  $J = 2.6$  Hz, 1H), 7.84 (dd,  $J = 8.8, 2.5$  Hz, 1H), 7.58 (d,  $J = 8.8$  Hz, 1H), 7.19 (s, 4H), 4.65 (s, 2H), 3.71 (t,  $J = 5.9$  Hz, 2H), 2.86 (t,  $J = 5.9$  Hz, 2H).  **$^{13}C$  NMR** (126 MHz, DMSO- $d_6$ ):  $\delta$  [ppm] = 154.5, 140.3, 134.7, 133.6, 131.6, 128.6, 126.5, 126.3, 126.3 (q,  $J = 30.5$  Hz; partially covered by other signals), 126.2, 124.0, 123.0 (q,  $J = 272.9$  Hz), 122.1, 118.0 (q,  $J = 5.7$  Hz), 45.5, 41.4, 28.3 (observed complexity is due to the C-F splitting). **ESI-HRMS** (m/z)  $[M+H]^+$  calcd. for  $C_{17}H_{15}ClF_3N_2O^+$ , 355.0820; found, 355.0819.

**1-(4-Chloro-3-(trifluoromethyl)phenyl)-3-(4-(pyridin-4-yloxy)phenyl)urea** (3.23) $C_{19}H_{13}ClF_3N_3O_2$ 

407.78 g/mol

**Amine building block: BB-1** (Chapter 4.1.3.3.4)

**Yield:** 41% (24.4 mg, 0.0598 mmol); workup A ( $CH_2Cl_2/MeOH = 19/1$ ). **TLC** ( $CH_2Cl_2/MeOH = 19/1$ ):  $R_f = 0.27$  [UV |  $KMnO_4$ ].  **$^1H$  NMR** (300 MHz,  $CDCl_3$ ):  $\delta$  [ppm] = 8.52 (s, 1H), 8.48 – 8.34 (m, 2H), 8.28 (s, 1H), 7.61 (d,  $J = 2.5$  Hz, 1H), 7.43 (dd,  $J = 8.7, 2.5$  Hz, 1H), 7.37 – 7.27 (m, 3H), 7.00 – 6.91 (m, 2H), 6.86 – 6.76 (m, 2H).  **$^{13}C$  NMR** (75 MHz,  $CDCl_3$ ):  $\delta$  [ppm] = 165.7, 153.7, 150.9, 149.5, 137.7, 135.8, 132.0, 128.7 (q,  $J = 31.1$  Hz), 125.8 (m), 123.5, 122.7 (d,  $J = 273.0$  Hz), 122.0, 121.6, 118.5 (q,  $J = 5.7$  Hz), 112.5. (observed complexity is due to the C-F splitting). **ESI-HRMS** (m/z)  $[M+H]^+$  calcd. for  $C_{19}H_{14}ClF_3N_3O_2^+$ , 408.0721; found, 408.0719.

**1-(4-Chloro-3-(trifluoromethyl)phenyl)-3-(4-phenoxyphenyl)urea** (3.24) $C_{20}H_{14}ClF_3N_2O_2$ 

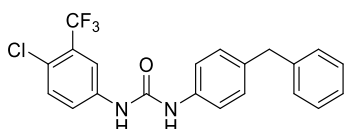
406.79 g/mol

**Yield:** 92% (203 mg, 0.499 mmol); workup B.  **$^1H$  NMR** (500 MHz, DMSO- $d_6$ ):  $\delta$  [ppm] = 9.13 (s, 1H), 8.84 (s, 1H), 8.11 (d,  $J = 2.3$  Hz, 1H), 7.66 – 7.59 (m, 2H), 7.48 (d,  $J = 8.9$  Hz, 2H), 7.36 (t,  $J = 8.0$  Hz, 2H), 7.09 (t,  $J = 7.4$  Hz, 1H), 7.02 – 6.94 (m, 4H).  **$^{13}C$  NMR** (126 MHz, DMSO- $d_6$ ):  $\delta$  [ppm] = 157.5, 152.5, 151.1, 139.4, 135.1, 132.0, 130.0, 126.7 (q,  $J = 30.5$  Hz),

123.0, 122.9, 122.9 (q,  $J = 273.0$  Hz), 122.2 (m), 120.5, 119.7, 117.7, 116.7 (q,  $J = 5.7$  Hz) (observed complexity is due to the C-F splitting). **ESI-HRMS** (m/z)  $[M+H]^+$  calcd. for  $C_{20}H_{15}ClF_3N_2O_2^+$ , 407.0769; found, 407.0770.

The spectral data are consistent with those published previously.<sup>227</sup>

### 1-(4-Benzylphenyl)-3-(4-chloro-3-(trifluoromethyl)phenyl)urea (3.25)

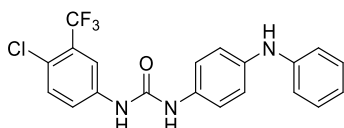


$C_{21}H_{16}ClF_3N_2O$

404.82 g/mol

**Yield:** 72% (120 mg, 0.296 mmol); workup A (Hex/EtOAc = 3/1). **TLC** (Hex/EtOAc = 3/1):  $R_f = 0.37$  [UV | PMA].  **$^1H$  NMR** (300 MHz, DMSO- $d_6$ ):  $\delta$  [ppm] = 9.13 (br s, 1H), 8.78 (br s, 1H), 8.10 (d,  $J = 2.0$  Hz, 1H), 7.66 – 7.56 (m, 2H), 7.37 (d,  $J = 8.5$  Hz, 2H), 7.32 – 7.11 (m, 7H), 3.88 (s, 2H).  **$^{13}C$  NMR** (75 MHz, DMSO- $d_6$ ):  $\delta$  [ppm] = 152.4, 141.6, 139.4, 137.1, 135.2, 132.0, 129.0, 128.6, 128.4, 126.7 (q,  $J = 30.5$  Hz), 125.9, 122.9, 122.8 (q,  $J = 273.0$  Hz), 122.1 (m), 118.9, 116.6 (q,  $J = 6.0$  Hz), 40.5 (observed complexity is due to the C-F splitting). **ESI-HRMS** (m/z)  $[M+H]^+$  calcd. for  $C_{21}H_{17}ClF_3N_2O^+$ , 405.0976; found, 405.0975.

### 1-(4-Chloro-3-(trifluoromethyl)phenyl)-3-(4-(phenylamino)phenyl)urea (3.26)

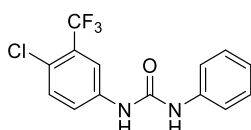


$C_{20}H_{15}ClF_3N_3O$

405.81 g/mol

**Yield:** 97% (148 mg, 0.365 mmol); workup A (Hex/EtOAc = 1/1). **TLC** (Hex/EtOAc = 1/1):  $R_f = 0.47$  [UV | PMA].  **$^1H$  NMR** (500 MHz, DMSO- $d_6$ ):  $\delta$  [ppm] = 9.08 (s, 1H), 8.64 (s, 1H), 8.12 (d,  $J = 2.3$  Hz, 1H), 8.01 (s, 1H), 7.65 – 7.57 (m, 2H), 7.34 (d,  $J = 8.8$  Hz, 2H), 7.19 (t,  $J = 7.9$  Hz, 2H), 7.04 (d,  $J = 8.8$  Hz, 2H), 6.99 (d,  $J = 7.7$  Hz, 2H), 6.75 (t,  $J = 7.3$  Hz, 1H).  **$^{13}C$  NMR** (126 MHz, DMSO- $d_6$ ):  $\delta$  [ppm] = 152.5, 144.3, 139.6, 138.2, 132.1, 132.0, 129.2, 126.7 (q,  $J = 30.5$  Hz), 122.9, 122.9 (q,  $J = 273.2$  Hz), 122.0 (m), 120.4, 118.8, 118.3, 116.6 (q,  $J = 6.3$  Hz), 115.6. **ESI-HRMS** (m/z)  $[M+H]^+$  calcd. for  $C_{20}H_{16}ClF_3N_3O^+$ , 406.0929; found, 406.0921.

### 1-(4-Chloro-3-(trifluoromethyl)phenyl)-3-phenylurea (3.27)



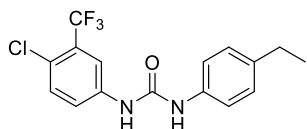
$C_{14}H_{10}ClF_3N_2O$

314.69 g/mol

**Yield:** 13% (44.0 mg, 0.140 mmol); A ( $CH_2Cl_2$ /MeOH = 99/1). **TLC** ( $CH_2Cl_2$ /MeOH = 99/1):  $R_f = 0.26$  [UV | PMA].  **$^1H$  NMR** (500 MHz, DMSO- $d_6$ ):  $\delta$  [ppm] = 9.17 (br s, 1H), 8.85 (br s, 1H),

8.11 (d,  $J = 2.3$  Hz, 1H), 7.66 – 7.59 (m, 2H), 7.46 (d,  $J = 7.6$  Hz, 2H), 7.29 (t,  $J = 7.9$  Hz, 2H), 7.00 (t,  $J = 7.4$  Hz, 1H).  $^{13}\text{C}$  NMR (126 MHz, DMSO- $d_6$ ):  $\delta$  [ppm] = 152.4, 139.4, 139.2, 132.0, 128.8, 126.7 (q,  $J = 30.5$  Hz), 123.0, 122.9 (q,  $J = 273.0$  Hz), 122.3, 122.2 (m), 118.6, 116.7 (q,  $J = 5.7$  Hz) (observed complexity is due to the C-F splitting). **ESI-HRMS** (m/z) [ $\text{M}+\text{H}^+$ ] calcd. for  $\text{C}_{14}\text{H}_{11}\text{ClF}_3\text{N}_2\text{O}^+$ , 315.0507; found, 315.0507.

#### 1-(4-Chloro-3-(trifluoromethyl)phenyl)-3-(4-ethylphenyl)urea (3.28)

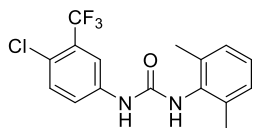


$\text{C}_{16}\text{H}_{14}\text{ClF}_3\text{N}_2\text{O}$

342.75 g/mol

**Yield:** 78% (110 mg, 0.320 mmol); workup A (Hex/EtOAc = 3/1). **TLC** (Hex/EtOAc = 3/1):  $R_f = 0.40$  [UV | PMA].  $^1\text{H}$  NMR (500 MHz, DMSO- $d_6$ ):  $\delta$  [ppm] = 9.11 (br s, 1H), 8.74 (br s, 1H), 8.10 (d,  $J = 2.4$  Hz, 1H), 7.64 – 7.58 (m, 2H), 7.36 (d,  $J = 8.5$  Hz, 2H), 7.12 (d,  $J = 8.5$  Hz, 2H), 2.54 (q,  $J = 7.6$  Hz, 2H), 1.15 (t,  $J = 7.6$  Hz, 3H).  $^{13}\text{C}$  NMR (126 MHz, DMSO- $d_6$ ):  $\delta$  [ppm] = 152.4, 139.5, 137.7, 136.8, 132.0, 128.0, 126.7 (q,  $J = 30.5$  Hz), 123.0, 122.9 (q,  $J = 273.0$  Hz), 122.1 (m), 118.8, 116.7 (q,  $J = 5.7$  Hz), 27.6, 15.8 (observed complexity is due to the C-F splitting). **ESI-HRMS** (m/z) [ $\text{M}+\text{H}^+$ ] calcd. for  $\text{C}_{16}\text{H}_{15}\text{ClF}_3\text{N}_2\text{O}^+$ , 343.0820; found, 343.0819.

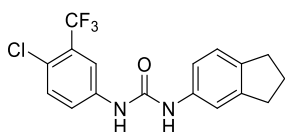
#### 1-(4-Chloro-3-(trifluoromethyl)phenyl)-3-(2,6-dimethylphenyl)urea (3.29)



$\text{C}_{16}\text{H}_{14}\text{ClF}_3\text{N}_2\text{O}$

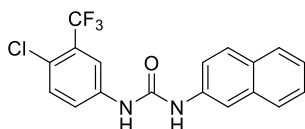
342.75 g/mol

**Yield:** 55% (77.0 mg, 0.225 mmol); workup A (Hex/EtOAc = 4/1). **TLC** (Hex/EtOAc = 4/1):  $R_f = 0.25$  [UV].  $^1\text{H}$  NMR (500 MHz, DMSO- $d_6$ ):  $\delta$  [ppm] = 9.27 (br s, 1H), 8.10 (d,  $J = 2.5$  Hz, 1H), 7.91 (br s, 1H), 7.70 – 7.62 (m, 1H), 7.58 (d,  $J = 8.8$  Hz, 1H), 7.08 (s, 3H), 2.20 (s, 6H).  $^{13}\text{C}$  NMR (126 MHz, DMSO- $d_6$ ):  $\delta$  [ppm] = 153.0, 140.0, 135.8, 134.9, 131.9, 127.8, 126.6 (q,  $J = 30.4$  Hz), 126.3, 122.9 (q,  $J = 273.0$  Hz), 122.7, 121.7, 116.5 (m), 18.2 (observed complexity is due to the C-F splitting). **ESI-HRMS** (m/z) [ $\text{M}+\text{H}^+$ ] calcd. for  $\text{C}_{16}\text{H}_{15}\text{ClF}_3\text{N}_2\text{O}^+$ , 343.0820; found, 343.0820.

**1-(4-Chloro-3-(trifluoromethyl)phenyl)-3-(2,3-dihydro-1H-inden-5-yl)urea (3.30)**C<sub>17</sub>H<sub>14</sub>ClF<sub>3</sub>N<sub>2</sub>O

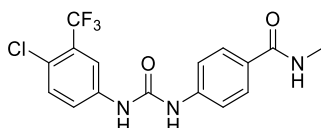
354.76 g/mol

**Yield:** 75% (199 mg, 0.561 mmol); workup A (Hex/EtOAc = 4/1). **TLC** (Hex/EtOAc = 4/1): R<sub>f</sub> = 0.10 [UV | PMA]. **<sup>1</sup>H NMR** (500 MHz, DMSO-d<sub>6</sub>): δ [ppm] = 9.08 (s, 1H), 8.67 (s, 1H), 8.13 – 8.09 (m, 1H), 7.63 – 7.57 (m, 2H), 7.38 (s, 1H), 7.16 – 7.09 (m, 2H), 2.86 – 2.76 (m, 4H), 2.00 (p, *J* = 7.4 Hz, 2H). **<sup>13</sup>C NMR** (126 MHz, DMSO-d<sub>6</sub>): δ [ppm] = 152.5, 144.3, 139.5, 137.6, 137.3, 132.0, 126.7 (q, *J* = 30.4 Hz), 124.2, 122.9, 122.9 (q, *J* = 273.2 Hz), 122.1 (m), 116.9, 116.6 (q, *J* = 5.7 Hz), 115.0, 32.6, 31.7, 25.2 (observed complexity is due to the C-F splitting). **ESI-HRMS** (m/z) [M+H<sup>+</sup>] calcd. for C<sub>17</sub>H<sub>15</sub>ClF<sub>3</sub>N<sub>2</sub>O<sup>+</sup>, 355.0820; found, 355.0818.

**1-(4-Chloro-3-(trifluoromethyl)phenyl)-3-(naphthalen-2-yl)urea (3.31)**C<sub>18</sub>H<sub>12</sub>ClF<sub>3</sub>N<sub>2</sub>O

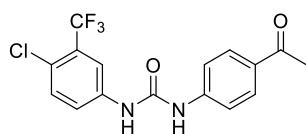
364.75 g/mol

**Yield:** 29% (43.0 mg, 0.118 mmol); workup A (Hex/EtOAc = 4/1). **TLC** (Hex/EtOAc = 3/2): R<sub>f</sub> = 0.45 [UV | PMA]. **<sup>1</sup>H NMR** (500 MHz, DMSO-d<sub>6</sub>): δ [ppm] = 9.26 (s, 1H), 9.07 (s, 1H), 8.18 (d, *J* = 2.2 Hz, 1H), 8.13 (d, *J* = 1.6 Hz, 1H), 7.87 – 7.79 (m, 3H), 7.68 – 7.61 (m, 2H), 7.52 – 7.43 (m, 2H), 7.37 (t, *J* = 7.4 Hz, 1H). **<sup>13</sup>C NMR** (126 MHz, DMSO-d<sub>6</sub>): δ [ppm] = 152.5, 139.4, 136.9, 133.7, 132.0, 129.3, 128.5, 127.5, 127.1, 126.8 (q, *J* = 30.6 Hz), 126.4, 124.2, 123.1, 122.9 (q, *J* = 273.1 Hz), 122.4 (m), 119.8, 116.8 (q, *J* = 5.7 Hz), 114.0 (observed complexity is due to the C-F splitting). **ESI-HRMS** (m/z) [M+H<sup>+</sup>] calcd. for C<sub>18</sub>H<sub>13</sub>ClF<sub>3</sub>N<sub>2</sub>O<sup>+</sup>, 365.0663; found, 365.0662.

**4-(3-(4-Chloro-3-(trifluoromethyl)phenyl)ureido)-*N*-methylbenzamide (3.32)**C<sub>16</sub>H<sub>13</sub>ClF<sub>3</sub>N<sub>3</sub>O<sub>2</sub>

371.74 g/mol

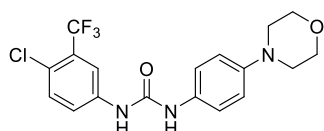
**Yield:** 64% (98.2 mg, 0.264 mmol); workup B. **<sup>1</sup>H NMR** (500 MHz, DMSO-d<sub>6</sub>): δ [ppm] = 9.25 (s, 1H), 9.10 (s, 1H), 8.31 (q, *J* = 4.2 Hz, 1H), 8.14 – 8.11 (m, 1H), 7.78 (d, *J* = 8.8 Hz, 2H), 7.66 – 7.61 (m, 2H), 7.53 (d, *J* = 8.8 Hz, 2H), 2.76 (d, *J* = 4.5 Hz, 3H). **<sup>13</sup>C NMR** (126 MHz, DMSO-d<sub>6</sub>): δ [ppm] = 166.1, 152.3, 141.8, 139.2, 132.1, 128.1, 128.0, 126.8 (q, *J* = 30.5 Hz), 123.2, 122.8 (q, *J* = 273.0 Hz), 122.5 (m), 117.6, 116.9 (q, *J* = 5.8 Hz), 26.2 (observed complexity is due to the C-F splitting). **ESI-HRMS** (m/z) [M+H<sup>+</sup>] calcd. for C<sub>16</sub>H<sub>14</sub>ClF<sub>3</sub>N<sub>3</sub>O<sub>2</sub><sup>+</sup>, 372.0721; found, 372.0717.

**1-(4-Acetylphenyl)-3-(4-chloro-3-(trifluoromethyl)phenyl)urea (3.33)**C<sub>16</sub>H<sub>12</sub>ClF<sub>3</sub>N<sub>2</sub>O<sub>2</sub>

356.73 g/mol

**Yield:** 53% (77.5 mg, 0.217 mmol); workup B (additional washing step of product with CH<sub>2</sub>Cl<sub>2</sub>).

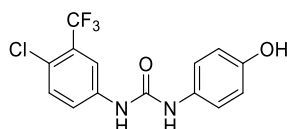
**<sup>1</sup>H NMR** (500 MHz, DMSO-d<sub>6</sub>): δ [ppm] = 9.31 – 9.25 (m, 2H), 8.11 (d, *J* = 2.2 Hz, 1H), 7.91 (d, *J* = 8.7 Hz, 2H), 7.66 – 7.57 (m, 4H), 2.52 (s, 3H). **<sup>13</sup>C NMR** (126 MHz, DMSO-d<sub>6</sub>): δ [ppm] = 196.4, 152.1, 143.9, 139.0, 132.1, 130.8, 129.7, 126.8 (q, *J* = 30.5 Hz), 123.4, 122.8 (q, *J* = 272.8 Hz), 122.7 (m), 117.6, 117.0 (q, *J* = 5.7 Hz), 26.4 (observed complexity is due to the C-F splitting). **ESI-HRMS** (m/z) [M+H<sup>+</sup>] calcd. for C<sub>16</sub>H<sub>13</sub>ClF<sub>3</sub>N<sub>2</sub>O<sub>2</sub><sup>+</sup>, 357.0612; found, 357.0607.

**1-(4-Chloro-3-(trifluoromethyl)phenyl)-3-(4-morpholinophenyl)urea (3.34)**C<sub>18</sub>H<sub>17</sub>ClF<sub>3</sub>N<sub>3</sub>O<sub>2</sub>

399.80 g/mol

**Yield:** 77% (126 mg, 0.315 mmol); workup A (CH<sub>2</sub>Cl<sub>2</sub>/MeOH = 99/1).

**TLC** (CH<sub>2</sub>Cl<sub>2</sub>/MeOH = 98/2): R<sub>f</sub> = 0.13 [UV | PMA]. **<sup>1</sup>H NMR** (500 MHz, DMSO-d<sub>6</sub>): δ [ppm] = 9.06 (s, 1H), 8.58 (s, 1H), 8.10 (d, *J* = 2.3 Hz, 1H), 7.64 – 7.56 (m, 2H), 7.32 (d, *J* = 9.0 Hz, 2H), 6.89 (d, *J* = 9.0 Hz, 2H), 3.77 – 3.69 (m, 4H), 3.06 – 2.98 (m, 4H). **<sup>13</sup>C NMR** (126 MHz, DMSO-d<sub>6</sub>): δ [ppm] = 152.5, 146.8, 139.6, 132.0, 131.4, 126.7 (q, *J* = 30.5 Hz), 122.9 (q, *J* = 272.9 Hz), 122.8, 121.9 (m), 120.1, 116.6 (q, *J* = 5.7 Hz), 115.8, 66.2, 49.1 (observed complexity is due to the C-F splitting). **ESI-HRMS** (m/z) [M+H<sup>+</sup>] calcd. for C<sub>18</sub>H<sub>18</sub>ClF<sub>3</sub>N<sub>3</sub>O<sub>2</sub><sup>+</sup>, 400.1034; found, 400.1028.

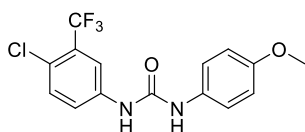
**1-(4-Chloro-3-(trifluoromethyl)phenyl)-3-(4-hydroxyphenyl)urea (3.35)**C<sub>14</sub>H<sub>10</sub>ClF<sub>3</sub>N<sub>2</sub>O<sub>2</sub>

330.69 g/mol

**Yield:** 81% (110 mg, 0.333 mmol); workup A (Hex/EtOAc = 1/1). **TLC** (Hex/EtOAc = 1/1):

R<sub>f</sub> = 0.40 [UV | PMA]. **<sup>1</sup>H NMR** (500 MHz, DMSO-d<sub>6</sub>): δ [ppm] = 9.14 (s, 1H), 9.03 (s, 1H), 8.50 (s, 1H), 8.10 (d, *J* = 2.3 Hz, 1H), 7.63 – 7.56 (m, 2H), 7.25 – 7.19 (m, 2H), 6.72 – 6.67 (m, 2H). **<sup>13</sup>C NMR** (126 MHz, DMSO-d<sub>6</sub>): δ [ppm] = 153.0, 152.7, 139.7, 132.0, 130.5, 126.7 (q, *J* = 30.4 Hz), 122.9 (q, *J* = 273.0 Hz), 122.8, 121.9 (m), 121.0, 116.6 (q, *J* = 5.6 Hz), 115.2 (observed complexity is due to the C-F splitting). **ESI-HRMS** (m/z) [M+H<sup>+</sup>] calcd. for C<sub>14</sub>H<sub>11</sub>ClF<sub>3</sub>N<sub>2</sub>O<sub>2</sub><sup>+</sup>, 331.0456; found, 331.0456.

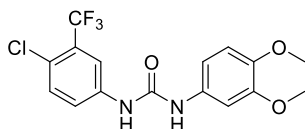
The spectral data are consistent with those published previously.<sup>228</sup>

**1-(4-Chloro-3-(trifluoromethyl)phenyl)-3-(4-methoxyphenyl)urea (3.36)**C<sub>15</sub>H<sub>12</sub>ClF<sub>3</sub>N<sub>2</sub>O<sub>2</sub>

344.72 g/mol

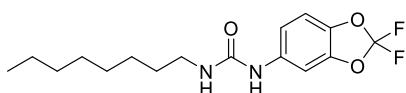
**Yield:** 40% (56.6 mg, 0.164 mmol); workup B. **<sup>1</sup>H NMR** (500 MHz, DMSO-d<sub>6</sub>): δ [ppm] = 9.08 (s, 1H), 8.64 (s, 1H), 8.10 (d, *J* = 2.2 Hz, 1H), 7.65 – 7.57 (m, 2H), 7.36 (d, *J* = 8.9 Hz, 2H), 6.87 (d, *J* = 8.9 Hz, 2H), 3.72 (s, 3H). **<sup>13</sup>C NMR** (126 MHz, DMSO-d<sub>6</sub>): δ [ppm] = 154.8, 152.6, 139.6, 132.1, 132.0, 126.7 (q, *J* = 30.5 Hz), 122.9, 122.9 (q, *J* = 273.0 Hz), 122.0, 120.6, 116.7 (q, *J* = 5.6 Hz), 114.0, 55.2. **ESI-HRMS** (m/z) [M+H<sup>+</sup>] calcd. for C<sub>15</sub>H<sub>13</sub>ClF<sub>3</sub>N<sub>2</sub>O<sub>2</sub><sup>+</sup>, 345.0612; found, 345.0608.

The spectral data are consistent with those published previously.<sup>227</sup>

**1-(4-Chloro-3-(trifluoromethyl)phenyl)-3-(3,4-dimethoxyphenyl)urea (3.37)**C<sub>16</sub>H<sub>14</sub>ClF<sub>3</sub>N<sub>2</sub>O<sub>3</sub>

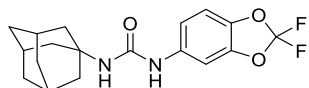
374.74 g/mol

**Yield:** 96% (147 mg, 0.392 mmol); workup A (CH<sub>2</sub>Cl<sub>2</sub>/MeOH = 99/1). **TLC** (CH<sub>2</sub>Cl<sub>2</sub>/MeOH = 98/2): R<sub>f</sub> = 0.47 [UV | PMA]. **<sup>1</sup>H NMR** (500 MHz, DMSO-d<sub>6</sub>): δ [ppm] = 9.07 (s, 1H), 8.68 (s, 1H), 8.09 (d, *J* = 2.3 Hz, 1H), 7.65 – 7.57 (m, 2H), 7.21 – 7.17 (m, 1H), 6.91 – 6.85 (m, 2H), 3.74 (s, 3H), 3.71 (s, 3H). **<sup>13</sup>C NMR** (126 MHz, DMSO-d<sub>6</sub>): δ [ppm] = 152.5, 148.7, 144.4, 139.5, 132.7, 132.0, 126.7 (q, *J* = 30.5 Hz), 123.0, 122.9 (q, *J* = 273.1 Hz), 122.1 (m), 116.7 (q, *J* = 5.7 Hz), 112.3, 110.7, 104.3, 55.8, 55.4 (observed complexity is due to the C-F splitting). **ESI-HRMS** (m/z) [M+H<sup>+</sup>] calcd. for C<sub>16</sub>H<sub>15</sub>ClF<sub>3</sub>N<sub>2</sub>O<sub>3</sub><sup>+</sup>, 375.0718; found, 375.0720.

**1-(2,2-Difluorobenzo[d][1,3]dioxol-5-yl)-3-octylurea (3.38)**C<sub>16</sub>H<sub>22</sub>F<sub>2</sub>N<sub>2</sub>O<sub>3</sub>

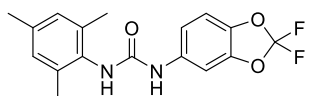
328.36 g/mol

**Yield:** 31% (59.0 mg, 0.180 mmol); workup A (Hex/EtOAc = 3/1). **TLC** (Hex/EtOAc = 3/1): R<sub>f</sub> = 0.45 [UV | PMA]. **<sup>1</sup>H NMR** (500 MHz, DMSO-d<sub>6</sub>): δ [ppm] = 8.62 (s, 1H), 7.63 (d, *J* = 2.1 Hz, 1H), 7.23 (d, *J* = 8.7 Hz, 1H), 6.96 (dd, *J* = 8.8, 2.1 Hz, 1H), 6.17 (t, *J* = 5.6 Hz, 1H), 3.05 (q, *J* = 6.8 Hz, 2H), 1.45 – 1.37 (m, 2H), 1.26 (br s, 10H), 0.84 (t, *J* = 6.9 Hz, 3H). **<sup>13</sup>C NMR** (126 MHz, DMSO-d<sub>6</sub>): δ [ppm] = 155.1, 142.8, 137.6, 136.8, 131.3 (t, *J* = 252.1 Hz), 112.6, 109.9, 100.4, 39.1, 31.3, 29.7, 28.8, 28.8, 26.4, 22.1, 14.0 (observed complexity is due to the C-F splitting). **ESI-HRMS** (m/z) [M+H<sup>+</sup>] calcd. for C<sub>16</sub>H<sub>23</sub>F<sub>2</sub>N<sub>2</sub>O<sub>3</sub><sup>+</sup>, 329.1671; found, 329.1671.

**1-((3s,5s,7s)-Adamantan-1-yl)-3-(2,2-difluorobenzo[d][1,3]dioxol-5-yl)urea (3.39)**C<sub>18</sub>H<sub>20</sub>F<sub>2</sub>N<sub>2</sub>O<sub>3</sub>

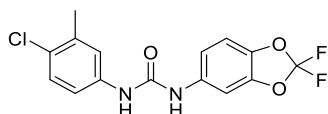
350.37 g/mol

**Yield:** 18% (36.8 mg, 0.105 mmol); workup A (Hex/EtOAc = 4/1). **TLC** (Hex/EtOAc = 4/1): R<sub>f</sub> = 0.25 [UV | PMA]. **<sup>1</sup>H NMR** (500 MHz, DMSO-d<sub>6</sub>): δ [ppm] = 8.46 (s, 1H), 7.62 – 7.59 (m, 1H), 7.22 (d, *J* = 8.7 Hz, 1H), 6.88 (dd, *J* = 8.7, 2.1 Hz, 1H), 5.90 (s, 1H), 2.02 (br s, 3H), 1.94 – 1.89 (m, 6H), 1.62 (br s, 6H). **<sup>13</sup>C NMR** (126 MHz, DMSO-d<sub>6</sub>): δ [ppm] = 153.8, 142.8, 137.6, 136.6, 131.3 (t, *J* = 251.7 Hz), 112.3, 109.9, 100.1, 50.0, 41.6, 36.0, 28.9 (observed complexity is due to the C-F splitting). **ESI-HRMS** (m/z) [M+H<sup>+</sup>] calcd. for C<sub>18</sub>H<sub>21</sub>F<sub>2</sub>N<sub>2</sub>O<sub>3</sub><sup>+</sup>, 351.1515; found, 351.1515.

**1-(2,2-Difluorobenzo[d][1,3]dioxol-5-yl)-3-mesitylurea (3.40)**C<sub>17</sub>H<sub>16</sub>F<sub>2</sub>N<sub>2</sub>O<sub>3</sub>

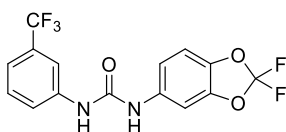
334.32 g/mol

**Yield:** 39% (74.0 mg, 0.221 mmol); workup A (Hex/EtOAc = 4/1). **TLC** (Hex/EtOAc = 3/1): R<sub>f</sub> = 0.35 [UV | PMA]. **<sup>1</sup>H NMR** (500 MHz, DMSO-d<sub>6</sub>): δ [ppm] = 8.93 (br s, 1H), 7.68 (br s, 1H), 7.65 (d, *J* = 2.1 Hz, 1H), 7.27 (d, *J* = 8.8 Hz, 1H), 7.08 (dd, *J* = 8.8, 2.1 Hz, 1H), 6.88 (s, 2H), 2.22 (s, 3H), 2.14 (s, 6H). **<sup>13</sup>C NMR** (126 MHz, DMSO-d<sub>6</sub>): δ [ppm] = 153.3, 142.8, 137.3, 137.0, 135.4, 135.1, 132.5, 131.3 (t, *J* = 251.9 Hz), 128.4, 113.1, 110.0, 100.7, 20.5, 18.2 (observed complexity is due to the C-F splitting). **ESI-HRMS** (m/z) [M+H<sup>+</sup>] calcd. for C<sub>17</sub>H<sub>17</sub>F<sub>2</sub>N<sub>2</sub>O<sub>3</sub><sup>+</sup>, 335.1202; found, 335.1201.

**1-(4-Chloro-3-methylphenyl)-3-(2,2-difluorobenzo[d][1,3]dioxol-5-yl)urea (3.41)**C<sub>15</sub>H<sub>11</sub>ClF<sub>2</sub>N<sub>2</sub>O<sub>3</sub>

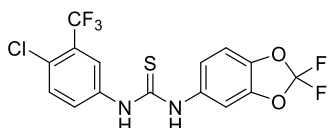
340.71 g/mol

**Yield:** 60% (84.0 mg, 0.247 mmol); workup A (Hex/EtOAc = 3/1). **TLC** (Hex/EtOAc = 2/1): R<sub>f</sub> = 0.25 [UV | PMA]. **<sup>1</sup>H NMR** (500 MHz, DMSO-d<sub>6</sub>): δ [ppm] = 8.91 (br s, 1H), 8.78 (br s, 1H), 7.65 (d, *J* = 2.1 Hz, 1H), 7.43 (br s, 1H), 7.32 – 7.29 (m, 3H), 7.08 (dd, *J* = 8.8, 2.2 Hz, 1H), 2.29 (s, 3H). **<sup>13</sup>C NMR** (126 MHz, DMSO-d<sub>6</sub>): δ [ppm] = 152.5, 142.8, 138.4, 137.5, 136.4, 135.6, 131.3 (t, *J* = 252.1 Hz), 129.0, 125.9, 120.7, 117.5, 113.7, 110.1, 101.3, 19.9 (observed complexity is due to the C-F splitting). **ESI-HRMS** (m/z) [M+H<sup>+</sup>] calcd. for C<sub>15</sub>H<sub>12</sub>F<sub>2</sub>N<sub>2</sub>O<sub>3</sub><sup>+</sup>, 341.0499; found, 341.0498.

**1-(2,2-Difluorobenzo[d][1,3]dioxol-5-yl)-3-(3-(trifluoromethyl)phenyl)urea (3.42)**C<sub>15</sub>H<sub>9</sub>F<sub>5</sub>N<sub>2</sub>O<sub>3</sub>

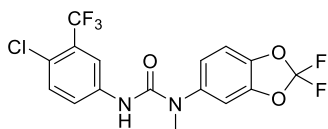
360.24 g/mol

**Yield:** 85% (149 mg, 0.414 mmol); workup A (Hex/EtOAc = 3/1). **TLC** (Hex/EtOAc = 2/1): R<sub>f</sub> = 0.29 [UV | PMA]. **<sup>1</sup>H NMR** (500 MHz, DMSO-d<sub>6</sub>): δ [ppm] = 9.09 (br s, 1H), 9.00 (br s, 1H), 8.00 (s, 1H), 7.66 (d, *J* = 2.1 Hz, 1H), 7.58 (d, *J* = 8.6 Hz, 1H), 7.51 (t, *J* = 7.9 Hz, 1H), 7.32 (d, *J* = 8.7 Hz, 2H), 7.12 (dd, *J* = 8.7, 2.2 Hz, 1H). **<sup>13</sup>C NMR** (75 MHz, DMSO-d<sub>6</sub>): δ [ppm] = 152.5, 142.8, 140.4, 137.7, 136.2, 131.3, 129.9, 129.5 (q, *J* = 31.4 Hz), 124.2 (q, *J* = 272.5 Hz), 122.0, 118.3 (q, *J* = 3.9 Hz), 114.3 (q, *J* = 4.1 Hz), 114.0, 110.0, 101.6 (observed complexity is due to the C-F splitting). **ESI-HRMS** (m/z) [M+H<sup>+</sup>] calcd. for C<sub>15</sub>H<sub>10</sub>F<sub>5</sub>N<sub>2</sub>O<sub>3</sub><sup>+</sup>, 361.0606; found, 361.0605.

**1-(4-Chloro-3-(trifluoromethyl)phenyl)-3-(2,2-difluorobenzo[d][1,3]dioxol-5-yl)thiourea (3.43)**C<sub>15</sub>H<sub>8</sub>ClF<sub>5</sub>N<sub>2</sub>O<sub>2</sub>S

410.74 g/mol

**Yield:** 74% (128 mg, 0.312 mmol); workup A (CH<sub>2</sub>Cl<sub>2</sub>/MeOH = 99/1). **TLC** (CH<sub>2</sub>Cl<sub>2</sub>/MeOH = 99/1): R<sub>f</sub> = 0.43 [UV | PMA]. **<sup>1</sup>H NMR** (500 MHz, DMSO-d<sub>6</sub>): δ [ppm] = 10.17 (s, 1H), 10.05 (s, 1H), 8.06 (d, *J* = 2.5 Hz, 1H), 7.78 (dd, *J* = 8.7, 2.5 Hz, 1H), 7.67 (d, *J* = 8.7 Hz, 1H), 7.61 (d, *J* = 2.1 Hz, 1H), 7.40 (d, *J* = 8.6 Hz, 1H), 7.14 (dd, *J* = 8.6, 2.1 Hz, 1H). **<sup>13</sup>C NMR** (126 MHz, DMSO-d<sub>6</sub>): δ [ppm] = 180.3, 142.5, 140.1, 139.1, 135.3, 131.6, 131.4 (t, *J* = 252.5 Hz), 128.9, 126.1 (q, *J* = 30.8 Hz), 125.5 (m), 122.9 (q, *J* = 5.6 Hz), 122.7 (q, *J* = 273.1 Hz), 120.7, 109.9, 107.8 (observed complexity is due to the C-F splitting). **ESI-HRMS** (m/z) [M+H<sup>+</sup>] calcd. for C<sub>15</sub>H<sub>9</sub>ClF<sub>5</sub>N<sub>2</sub>O<sub>2</sub>S<sup>+</sup>, 410.9988; found, 410.9986.

**3-(4-Chloro-3-(trifluoromethyl)phenyl)-1-(2,2-difluorobenzo[d][1,3]dioxol-5-yl)-1-methylurea (3.47)**C<sub>16</sub>H<sub>10</sub>ClF<sub>5</sub>N<sub>2</sub>O<sub>3</sub>

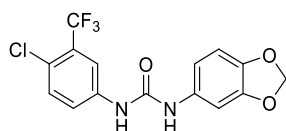
408.71 g/mol

**Amine building block: BB-3** (Chapter 4.1.3.3.4)

**Yield:** 86% (171 mg, 0.418 mmol); workup A (Hex/EtOAc = 4/1). **TLC** (Hex/EtOAc = 4/1): R<sub>f</sub> = 0.39 [UV | PMA]. **<sup>1</sup>H NMR** (500 MHz, DMSO-d<sub>6</sub>): δ [ppm] = 8.50 (s, 1H), 8.01 (d, *J* = 2.6 Hz, 1H), 7.79 (dd, *J* = 8.8, 2.5 Hz, 1H), 7.59 – 7.54 (m, 2H), 7.46 (d, *J* = 8.6 Hz, 1H), 7.21 (dd,

$J = 8.6, 2.1$  Hz, 1H), 3.24 (s, 3H).  $^{13}\text{C NMR}$  (126 MHz, DMSO- $d_6$ ):  $\delta$  [ppm] = 154.2, 143.1, 141.3, 139.7, 139.5, 131.5, 131.4 (t,  $J = 252.5$  Hz), 126.2 (q,  $J = 30.8$  Hz), 124.5, 123.6, 122.9 (q,  $J = 272.6$  Hz), 122.5, 118.6 (q,  $J = 5.5$  Hz), 110.5, 110.2, 37.9 (observed complexity is due to the C-F splitting). **ESI-HRMS** (m/z)  $[\text{M}+\text{H}^+]$  calcd. for  $\text{C}_{16}\text{H}_{11}\text{ClF}_5\text{N}_2\text{O}_3^+$ , 409.0373; found, 409.0371.

**1-(Benzo[d][1,3]dioxol-5-yl)-3-(4-chloro-3-(trifluoromethyl)phenyl)urea (3.48)**

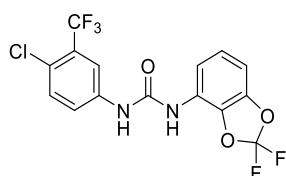


$\text{C}_{15}\text{H}_{10}\text{ClF}_3\text{N}_2\text{O}_3$

358.70 g/mol

**Yield:** 26% (37.7 mg, 0.105 mmol); workup A ( $\text{CH}_2\text{Cl}_2/\text{MeOH} = 99/1$ ). **TLC** ( $\text{CH}_2\text{Cl}_2/\text{MeOH} = 99/1$ ):  $R_f = 0.23$  [UV | PMA].  $^1\text{H NMR}$  (500 MHz, DMSO- $d_6$ ):  $\delta$  [ppm] = 9.11 (s, 1H), 8.74 (s, 1H), 8.08 (d,  $J = 2.2$  Hz, 1H), 7.64 – 7.58 (m, 2H), 7.18 (d,  $J = 2.0$  Hz, 1H), 6.84 (d,  $J = 8.3$  Hz, 1H), 6.79 (dd,  $J = 8.4, 2.0$  Hz, 1H), 5.98 (s, 2H).  $^{13}\text{C NMR}$  (126 MHz, DMSO- $d_6$ ):  $\delta$  [ppm] = 152.5, 147.2, 142.4, 139.5, 133.5, 132.0, 126.7 (q,  $J = 30.6$  Hz), 123.0, 122.9 (q,  $J = 273.1$  Hz), 122.1 (m), 116.7 (m), 111.6, 108.1, 101.4, 100.9 (observed complexity is due to the C-F splitting). **ESI-HRMS** (m/z)  $[\text{M}+\text{H}^+]$  calcd. for  $\text{C}_{15}\text{H}_{11}\text{ClF}_3\text{N}_2\text{O}_3^+$ , 359.0405; found, 359.0407.

**1-(4-Chloro-3-(trifluoromethyl)phenyl)-3-(2,2-difluorobenzo[d][1,3]dioxol-4-yl)urea (3.49)**



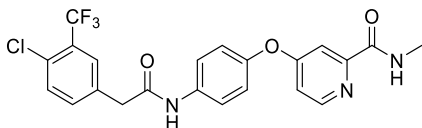
$\text{C}_{15}\text{H}_8\text{ClF}_5\text{N}_2\text{O}_3$

394.68 g/mol

**Yield:** 38% (62 mg, 0.157 mmol); workup A (Hex/EtOAc = 4/1). **TLC** (Hex/EtOAc = 4/1):  $R_f = 0.45$  [UV | PMA].  $^1\text{H NMR}$  (500 MHz, DMSO- $d_6$ ):  $\delta$  [ppm] = 9.40 (br s, 1H), 9.04 (br s, 1H), 8.09 (s, 1H), 7.66 (dd,  $J = 8.5, 1.1$  Hz, 1H), 7.65 – 7.61 (m, 2H), 7.16 (t,  $J = 8.3$  Hz, 1H), 7.11 – 7.07 (m, 1H).  $^{13}\text{C NMR}$  (126 MHz, DMSO- $d_6$ ):  $\delta$  [ppm] = 151.8, 143.1, 138.9, 133.0, 132.1, 131.0 (t,  $J = 252.5$  Hz), 126.8 (q,  $J = 30.8$  Hz), 124.5, 123.2, 123.0, 122.8, 122.8 (q,  $J = 273.1$  Hz), 116.9 (q,  $J = 5.6$  Hz), 116.5, 104.4 (observed complexity is due to the C-F splitting). **ESI-HRMS** (m/z)  $[\text{M}+\text{H}^+]$  calcd. for  $\text{C}_{15}\text{H}_9\text{ClF}_5\text{N}_2\text{O}_3^+$ , 395.0216; found, 395.0216.

#### 4.1.3.3.2. Synthesis of Derivatives Bearing Structural Variations of the Central Urea Motif

##### 4-(4-(2-(4-Chloro-3-(trifluoromethyl)phenyl)acetamido)phenoxy)-*N*-methylpicolinamide (3.16)



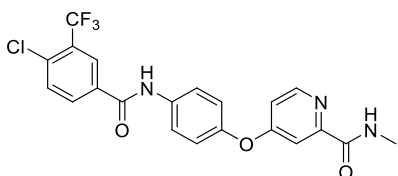
$$\text{C}_{22}\text{H}_{17}\text{ClF}_3\text{N}_3\text{O}_3$$

$$463.84 \text{ g/mol}$$

To a solution of 4-chloro-3-(trifluoromethyl)phenylacetic acid (50.0 mg, 0.210 mmol, 1.00 eq.) in dry  $\text{CH}_2\text{Cl}_2$  (4 mL) were added HOBt (42.6 mg, 0.315 mmol, 1.50 eq.), EDC·HCl (60.4 mg, 0.315 mmol, 1.50 eq.) and DIPEA (73.4  $\mu\text{L}$ , 54.3 mg, 0.420 mmol, 2.00 eq.). After the addition of 4-(4-aminophenoxy)-*N*-methylpicolinamide (61.3 mg, 0.252 mmol, 1.20 eq.) the mixture was stirred at room temperature for 20 h. The solvent was removed and the residue was purified by flash column chromatography on silica (Hex/EtOAc = 1/2) to yield the desired product (95.1 mg, 0.205 mmol, 98%) as a white solid.

**TLC** (Hex/EtOAc = 1/2):  $R_f$  = 0.25 [UV | PMA].  **$^1\text{H NMR}$**  (500 MHz, DMSO- $d_6$ ):  $\delta$  [ppm] = 10.41 (s, 1H), 8.78 (q,  $J$  = 4.5 Hz, 1H), 8.50 (d,  $J$  = 5.6 Hz, 1H), 7.86 – 7.84 (m, 1H), 7.73 – 7.69 (m, 3H), 7.67 – 7.64 (m, 1H), 7.36 (d,  $J$  = 2.5 Hz, 1H), 7.18 (d,  $J$  = 8.9 Hz, 2H), 7.13 (dd,  $J$  = 5.6, 2.6 Hz, 1H), 3.82 (s, 2H), 2.78 (d,  $J$  = 4.8 Hz, 3H).  **$^{13}\text{C NMR}$**  (126 MHz, DMSO- $d_6$ ):  $\delta$  [ppm] = 168.3, 165.9, 163.8, 152.5, 150.4, 148.5, 136.9, 136.0, 135.2, 131.5, 129.0 (m), 128.8 (q,  $J$  = 5.5 Hz), 126.3 (q,  $J$  = 30.6 Hz), 123.0 (q,  $J$  = 273.1 Hz), 121.5, 121.0, 114.1, 108.7, 41.8, 26.1 (observed complexity is due to the C-F splitting). **ESI-HRMS** (m/z) [ $\text{M}+\text{H}^+$ ] calcd. for  $\text{C}_{16}\text{H}_{10}\text{ClF}_5\text{NO}_3^+$ , 464.0983; found, 464.0984.

##### 4-(4-(4-Chloro-3-(trifluoromethyl)benzamido)phenoxy)-*N*-methylpicolinamide (3.17)



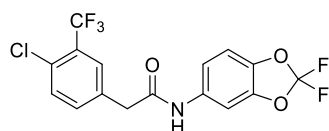
$$\text{C}_{21}\text{H}_{15}\text{ClF}_3\text{N}_3\text{O}_3$$

$$449.81 \text{ g/mol}$$

To a solution of 4-chloro-3-(trifluoromethyl)benzoic acid (100 mg, 0.445 mmol, 1.00 eq.) in dry  $\text{CH}_2\text{Cl}_2$  (8 mL) was added DIEA (155  $\mu\text{L}$ , 115 mg, 0.890 mmol, 2.00 eq.), HOBt (90.3 mg, 0.668 mmol, 1.50 eq.), EDC·HCl (128 mg, 0.668 mmol, 1.50 eq.) and 4-(4-aminophenoxy)-*N*-methyl-2-pyridinecarboxamide (130 mg, 0.534 mmol, 1.20 eq.). The reaction mixture was stirred at room temperature for 96 h and the solvent removed in vacuo. Subsequent purification by flash column chromatography on silica (Hex/EtOAc = 2/3) gave **5-010** (135 mg, 0.300 mmol, 67%) as a viscous, colorless oil.

**TLC** (Hex/EtOAc = 2/3):  $R_f = 0.38$  [UV].  **$^1\text{H NMR}$**  (500 MHz, DMSO- $d_6$ ):  $\delta$  [ppm] = 10.68 (s, 1H), 8.80 (q,  $J = 4.6$  Hz, 1H), 8.52 (d,  $J = 5.6$  Hz, 1H), 8.40 (d,  $J = 1.9$  Hz, 1H), 8.28 (dd,  $J = 8.4$ , 2.0 Hz, 1H), 7.95 (d,  $J = 8.4$  Hz, 1H), 7.92 – 7.88 (m, 2H), 7.39 (d,  $J = 2.6$  Hz, 1H), 7.29 – 7.25 (m, 2H), 7.18 (dd,  $J = 5.6$ , 2.6 Hz, 1H), 2.78 (d,  $J = 4.9$  Hz, 3H).  **$^{13}\text{C NMR}$**  (126 MHz, DMSO- $d_6$ ):  $\delta$  [ppm] = 165.8, 163.8, 163.2, 152.5, 150.5, 149.2, 136.5, 134.1, 134.0, 133.5, 132.0, 127.1 (q,  $J = 5.2$  Hz), 126.7 (q,  $J = 31.1$  Hz), 122.7 (q,  $J = 273.4$  Hz), 122.4, 121.4, 114.2, 108.8, 26.1 (observed complexity is due to the C-F splitting). **ESI-HRMS** (m/z) [ $\text{M}+\text{H}^+$ ] calcd. for  $\text{C}_{21}\text{H}_{16}\text{ClF}_3\text{N}_3\text{O}_3^+$ , 450.0827; found, 450.0827.

**2-(4-Chloro-3-(trifluoromethyl)phenyl)-*N*-(2,2-difluorobenzo[d][1,3]dioxol-5-yl)acetamide (3.44)**

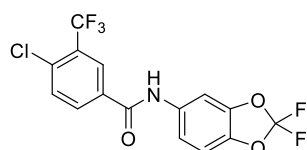


$\text{C}_{16}\text{H}_9\text{ClF}_5\text{NO}_3$   
393.69 g/mol

To a solution of 4-chloro-3-(trifluoromethyl)phenylacetic acid (50.0 mg, 0.210 mmol, 1.20 eq.) in dry  $\text{CH}_2\text{Cl}_2$  (4 mL) were added HOBT (35.5 mg, 0.263 mmol, 1.50 eq.), EDC·HCl (50.4 mg, 0.263 mmol, 1.50 eq.) and DIEA (59.5  $\mu\text{L}$ , 45.2 mg, 0.350 mmol, 2.00 eq.). After the addition of 5-amino-2,2-difluoro-1,3-benzodioxole (20.1  $\mu\text{L}$ , 30.3 mg, 0.175 mmol, 1.00 eq.) the mixture was stirred at room temperature for 20 h. The solvent was removed and the residue was purified by flash column chromatography on silica (Hex/EtOAc = 4/1) to yield the desired product (28.3 mg, 0.0719 mmol, 41%) as a white solid.

**TLC** (Hex/EtOAc = 4/1):  $R_f = 0.31$  [UV | PMA].  **$^1\text{H NMR}$**  (500 MHz, DMSO- $d_6$ ):  $\delta$  [ppm] = 10.47 (s, 1H), 7.82 (d,  $J = 1.8$  Hz, 1H), 7.76 (d,  $J = 2.0$  Hz, 1H), 7.69 (d,  $J = 8.3$  Hz, 1H), 7.65 – 7.60 (m, 1H), 7.35 (d,  $J = 8.7$  Hz, 1H), 7.25 (dd,  $J = 8.8$ , 2.1 Hz, 1H), 3.80 (s, 2H).  **$^{13}\text{C NMR}$**  (126 MHz, DMSO- $d_6$ ):  $\delta$  [ppm] = 168.5, 142.6, 138.3, 135.7, 135.2, 131.5, 131.3 (t,  $J = 252.5$  Hz), 129.0 (m), 128.9 (q,  $J = 5.2$  Hz), 126.3 (q,  $J = 30.5$  Hz), 125.9, 122.9 (q,  $J = 273.5$  Hz), 114.6, 110.2, 101.9, 41.7 (observed complexity is due to the C-F splitting). **ESI-HRMS** (m/z) [ $\text{M}+\text{H}^+$ ] calcd. for  $\text{C}_{16}\text{H}_{10}\text{ClF}_5\text{NO}_3^+$ , 394.0264; found, 394.0263.

**4-Chloro-*N*-(2,2-difluorobenzo[d][1,3]dioxol-5-yl)-3-(trifluoromethyl)benzamide (3.45)**



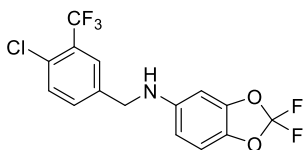
$\text{C}_{15}\text{H}_7\text{ClF}_5\text{NO}_3$   
379.67 g/mol

To a solution of 4-chloro-3-(trifluoromethyl)benzoic acid (100 mg, 0.445 mmol, 1.00 eq.) in dry  $\text{CH}_2\text{Cl}_2$  (3 mL) and dry DMF (0.1 mL) was added oxalyl chloride (57.3  $\mu\text{L}$ , 84.8 mg, 0.668 mmol, 1.50 eq.) at  $0^\circ\text{C}$ . The reaction mixture was allowed to warm to room temperature and stirred

at room temperature for 4 h. After solvent removal in vacuo the crude acyl chloride was dissolved in dry  $\text{CH}_2\text{Cl}_2$  (3 mL) and 5-amino-2,2-difluoro-1,3-benzodioxole (51.0  $\mu\text{L}$ , 77.0 mg, 0.445 mmol, 1.00 eq.) and DIEA (234  $\mu\text{L}$ , 173 mg, 1.34 mmol, 3.00 eq.) was added. The reaction mixture was stirred at room temperature for 18 h and the solvent removed in vacuo. Subsequent purification by flash column chromatography on silica (Hex/EtOAc = 4/1) gave **1-168** (69.5 mg, 0.183 mmol, 41%) as a yellowish solid.

**TLC** (Hex/EtOAc = 4/1):  $R_f$  = 0.26 [UV |  $\text{KMnO}_4$ ].  **$^1\text{H NMR}$**  (500 MHz,  $\text{DMSO-d}_6$ ):  $\delta$  [ppm] = 10.70 (s, 1H), 8.37 (d,  $J$  = 2.0 Hz, 1H), 8.25 (dd,  $J$  = 8.4, 2.1 Hz, 1H), 7.94 (d,  $J$  = 8.4 Hz, 1H), 7.88 (d,  $J$  = 2.0 Hz, 1H), 7.47 (dd,  $J$  = 8.8, 2.1 Hz, 1H), 7.42 (d,  $J$  = 8.8 Hz, 1H).  **$^{13}\text{C NMR}$**  (126 MHz,  $\text{DMSO-d}_6$ ):  $\delta$  [ppm] = 163.3, 142.5, 139.0, 135.3, 134.2, 133.7, 133.4, 132.0, 131.3 (t,  $J$  = 252.5 Hz), 127.1 (q,  $J$  = 5.3 Hz), 126.7 (q,  $J$  = 31.3 Hz), 122.7 (q,  $J$  = 273.1 Hz), 116.3, 110.1, 103.4 (observed complexity is due to the C-F splitting). **ESI-HRMS** (m/z)  $[\text{M}+\text{H}^+]$  calcd. for  $\text{C}_{15}\text{H}_8\text{ClF}_5\text{NO}_3^+$ , 380.0107; found, 380.0107.

#### ***N*-(4-Chloro-3-(trifluoromethyl)benzyl)-2,2-difluorobenzo[d][1,3]dioxol-5-amine** (3.46)



$\text{C}_{15}\text{H}_9\text{ClF}_5\text{NO}_2$

365.68 g/mol

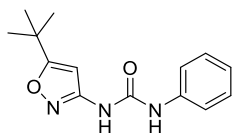
To a solution of 5-amino-2,2-difluoro-1,3-benzodioxole (66.2  $\mu\text{L}$ , 100 mg, 0.578 mmol, 1.00 eq.) in dry dichloroethane (5 mL) over molecular sieve (4 Å) was added 4-chloro-3-(trifluoromethyl)benzaldehyde (167  $\mu\text{L}$ , 242 mg, 1.16 mmol, 2.00 eq.), sodium triacetoxyborohydride (196 mg, 0.925 mmol, 1.60 eq.) and catalytic amounts of acetic acid. The reaction mixture was stirred at room temperature for 20 h. Subsequently, the reaction was quenched by the addition of saturated  $\text{NaHCO}_3$  solution (3 mL) and the aqueous phase was extracted with EtOAc (3 x 10 mL). The combined organic phases were dried over  $\text{Na}_2\text{SO}_4$ , filtered and the solvent removed in vacuo. Purification by flash column chromatography on silica (Hex/EtOAc = 9/1) gave the desired product (39.1 mg, 0.107 mmol, 51%) as a white solid.

**TLC** (Hex/EtOAc = 4/1):  $R_f$  = 0.27 [UV | PMA].  **$^1\text{H NMR}$**  (500 MHz,  $\text{DMSO-d}_6$ ):  $\delta$  [ppm] = 7.84 (d,  $J$  = 1.5 Hz, 1H), 7.70 – 7.63 (m, 2H), 7.06 (d,  $J$  = 8.7 Hz, 1H), 6.62 (d,  $J$  = 2.3 Hz, 1H), 6.60 (br s, 1H, overlapped by d), 6.30 (dd,  $J$  = 8.8, 2.3 Hz, 1H), 4.34 (s, 2H).  **$^{13}\text{C NMR}$**  (126 MHz,  $\text{DMSO-d}_6$ ):  $\delta$  [ppm] = 145.9, 143.7, 140.2, 133.9, 132.9, 131.6, 131.2 (t,  $J$  = 250.9 Hz), 128.8 (m), 126.6 (q,  $J$  = 5.2 Hz), 126.5 (q,  $J$  = 30.6 Hz), 122.9 (q,  $J$  = 273.0 Hz), 110.3, 106.6, 94.7, 45.5 (observed complexity is due to the C-F splitting). **ESI-HRMS** (m/z)  $[\text{M}+\text{H}^+]$  calcd. for  $\text{C}_{15}\text{H}_{10}\text{ClF}_5\text{NO}_2^+$ , 366.0315; found, 366.0314.

#### 4.1.3.3.3. Synthesis of Further Derivatives Not Highlighted in Chapter 3

For general experimental procedure for the synthesis of urea and thiourea containing compounds see Chapter 4.1.3.3.1.

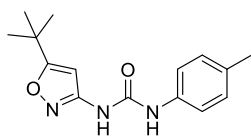
##### 1-(5-(*tert*-Butyl)isoxazol-3-yl)-3-phenylurea (3.50)



$C_{14}H_{17}N_3O_2$   
259.31 g/mol

**Yield:** 86% (160 mg, 0.617 mmol); workup A (Hex/EtOAc = 9/1). **TLC** (Hex/EtOAc = 9/1):  $R_f = 0.49$  [UV |  $KMnO_4$ ].  **$^1H$  NMR** (300 MHz,  $CDCl_3$ ):  $\delta$  [ppm] = 9.37 – 9.01 (m, 2H), 7.51 (d,  $J = 8.4$  Hz, 2H), 7.33 (t,  $J = 7.9$  Hz, 2H), 7.14 – 7.07 (m, 1H), 6.01 (s, 1H), 1.35 (s, 9H).  **$^{13}C$  NMR** (75 MHz,  $CDCl_3$ ):  $\delta$  [ppm] = 181.3, 158.7, 152.9, 138.0, 129.1, 124.2, 120.5, 92.1, 33.0, 28.7. **ESI-HRMS** (m/z) [ $M+H^+$ ] calcd. for  $C_{14}H_{18}N_3O_2^+$ , 260.1394; found, 260.1395.

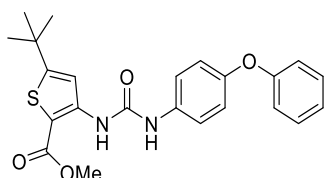
##### 1-(5-(*tert*-Butyl)isoxazol-3-yl)-3-(*p*-tolyl)urea (3.51)



$C_{15}H_{19}N_3O_2$   
273.34 g/mol

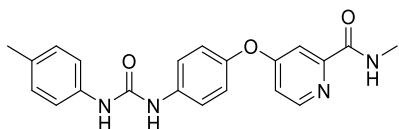
**Yield:** 92% (179 mg, 0.655 mmol); workup A (Hex/EtOAc = 9/1). **TLC** (Hex/EtOAc = 9/1):  $R_f = 0.25$  [UV |  $KMnO_4$ ].  **$^1H$  NMR** (500 MHz,  $DMSO-d_6$ ):  $\delta$  [ppm] = 9.44 (s, 1H), 8.70 (s, 1H), 7.32 (d,  $J = 8.4$  Hz, 2H), 7.10 (d,  $J = 8.3$  Hz, 2H), 6.49 (s, 1H), 2.24 (s, 3H), 1.28 (s, 9H).  **$^{13}C$  NMR** (126 MHz,  $DMSO-d_6$ ):  $\delta$  [ppm] = 180.6, 158.9, 151.8, 136.8, 131.9, 129.7, 119.0, 92.9, 32.9, 28.8, 20.8. **ESI-HRMS** (m/z) [ $M+H^+$ ] calcd. for  $C_{15}H_{20}N_3O_2^+$ , 274.1550; found, 274.1551.

##### Methyl 5-(*tert*-butyl)-3-(3-(4-phenoxyphenyl)ureido)thiophene-2-carboxylate (3.52)



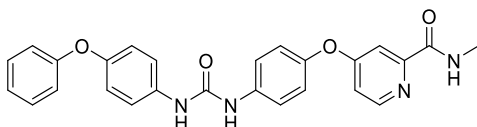
$C_{23}H_{24}N_2O_4S$   
424.51 g/mol

**Yield:** 65% (130 mg, 0.306 mmol); workup A (Hex/EtOAc = 9/1). **TLC** (Hex/EtOAc = 9/1):  $R_f = 0.10$  [UV |  $KMnO_4$ ].  **$^1H$  NMR** (300 MHz,  $CDCl_3$ ):  $\delta$  [ppm] = 9.69 (s, 1H), 7.86 (s, 1H), 7.42 – 7.36 (m, 2H), 7.36 – 7.28 (m, 3H), 7.11 – 7.05 (m, 1H), 7.04 – 6.97 (m, 4H), 3.80 (s, 3H), 1.35 (s, 9H).  **$^{13}C$  NMR** (75 MHz,  $CDCl_3$ ):  $\delta$  [ppm] = 165.3, 164.7, 157.7, 153.9, 152.4, 146.0, 133.2, 129.8, 123.6, 123.1, 120.2, 118.4, 117.2, 105.1, 51.8, 35.4, 31.9. **ESI-HRMS** (m/z) [ $M^+$ ] calcd. for  $C_{23}H_{24}N_2O_4S^+$ , 424.1457; found, 424.1458.

**N-Methyl-4-(4-(3-(*p*-tolyl)ureido)phenoxy)picolinamide (3.53)**C<sub>21</sub>H<sub>20</sub>N<sub>4</sub>O<sub>3</sub>

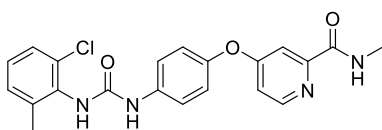
376.42 g/mol

**Yield:** 78% (121 mg, 0.321 mmol); workup B (additional washing step of product with CH<sub>2</sub>Cl<sub>2</sub>). **<sup>1</sup>H NMR** (500 MHz, DMSO-d<sub>6</sub>): δ [ppm] = 8.76 (br s, 2H), 8.59 (s, 1H), 8.50 (d, *J* = 5.6 Hz, 1H), 7.59 – 7.54 (m, 2H), 7.38 (d, *J* = 2.6 Hz, 1H), 7.35 (d, *J* = 8.4 Hz, 2H), 7.17 – 7.13 (m, 3H), 7.09 (d, *J* = 8.3 Hz, 2H), 2.79 (d, *J* = 4.9 Hz, 3H), 2.24 (s, 3H). **<sup>13</sup>C NMR** (126 MHz, DMSO-d<sub>6</sub>): δ [ppm] = 166.1, 163.8, 152.6, 152.4, 150.4, 147.3, 137.7, 137.1, 130.7, 129.2, 121.5, 119.9, 118.4, 114.0, 108.6, 26.0, 20.4. **ESI-HRMS** (*m/z*) [*M*+*H*<sup>+</sup>] calcd. for C<sub>21</sub>H<sub>21</sub>N<sub>4</sub>O<sub>3</sub><sup>+</sup>, 377.1608; found, 377.1606.

**N-Methyl-4-(4-(3-(4-phenoxyphenyl)ureido)phenoxy)picolinamide (3.54)**C<sub>26</sub>H<sub>22</sub>N<sub>4</sub>O<sub>4</sub>

454.49 g/mol

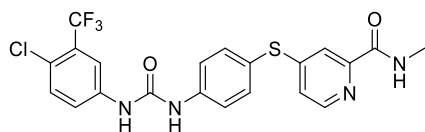
**Yield:** 65% (121 mg, 0.266 mmol); workup B (additional washing step of product with CH<sub>2</sub>Cl<sub>2</sub>). **<sup>1</sup>H NMR** (500 MHz, DMSO-d<sub>6</sub>): δ [ppm] = 8.80 (s, 1H), 8.76 (q, *J* = 4.7 Hz, 1H), 8.73 (s, 1H), 8.50 (d, *J* = 5.6 Hz, 1H), 7.60 – 7.56 (m, 2H), 7.51 – 7.47 (m, 2H), 7.39 – 7.34 (m, 3H), 7.18 – 7.13 (m, 3H), 7.11 – 7.07 (m, 1H), 7.01 – 6.94 (m, 4H), 2.79 (d, *J* = 4.9 Hz, 3H). **<sup>13</sup>C NMR** (126 MHz, DMSO-d<sub>6</sub>): δ [ppm] = 166.1, 163.8, 157.7, 152.7, 152.4, 150.7, 150.4, 147.4, 137.7, 135.7, 129.9, 122.8, 121.5, 120.0, 119.9, 119.8, 117.6, 114.0, 108.6, 26.0. **ESI-HRMS** (*m/z*) [*M*+*H*<sup>+</sup>] calcd. for C<sub>26</sub>H<sub>23</sub>N<sub>4</sub>O<sub>4</sub><sup>+</sup>, 455.1714; found, 455.1712.

**4-(4-(3-(2-Chloro-6-methylphenyl)ureido)phenoxy)-N-methylpicolinamide (3.55)**C<sub>21</sub>H<sub>19</sub>ClN<sub>4</sub>O<sub>3</sub>

410.86 g/mol

**Yield:** 63% (111 mg, 0.270 mmol); workup A (CH<sub>2</sub>Cl<sub>2</sub>/MeOH = 97/3). **TLC** (CH<sub>2</sub>Cl<sub>2</sub>/MeOH = 97/3): R<sub>f</sub> = 0.26 [UV | KMnO<sub>4</sub>]. **<sup>1</sup>H NMR** (300 MHz, DMSO-d<sub>6</sub>): δ [ppm] = 9.38 (br s, 1H), 8.77 (q, *J* = 4.5 Hz, 1H), 8.49 (d, *J* = 5.7 Hz, 1H), 8.34 (br s, 1H), 7.59 (d, *J* = 9.0 Hz, 2H), 7.39 – 7.33 (m, 2H), 7.27 – 7.22 (m, 1H), 7.19 (d, *J* = 7.7 Hz, 1H), 7.16 – 7.11 (m, 3H), 2.78 (d, *J* = 4.9 Hz, 3H), 2.27 (s, 3H). **<sup>13</sup>C NMR** (75 MHz, DMSO-d<sub>6</sub>): δ [ppm] = 166.1, 163.8, 152.9, 152.4, 150.4, 147.1, 138.6, 138.2, 134.1, 132.0, 129.0, 127.2, 126.8, 121.4, 119.6, 113.9, 108.7, 26.0, 18.6. **ESI-HRMS** (*m/z*) [*M*+*H*<sup>+</sup>] calcd. for C<sub>21</sub>H<sub>20</sub>ClN<sub>4</sub>O<sub>3</sub><sup>+</sup>, 411.1218; found, 411.1218.

**4-((4-(3-(4-Chloro-3-(trifluoromethyl)phenyl)ureido)phenyl)thio)-N-methylpicolinamide**  
(3.56)

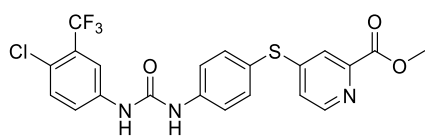


$C_{21}H_{16}ClF_3N_4O_2S$   
480.89 g/mol

**Amine building block: BB-4** (Chapter 4.1.3.3.4)

**Yield:** 57% (56.6 mg, 0.118 mmol); workup B.  **$^1H$  NMR** (500 MHz, DMSO- $d_6$ ):  $\delta$  [ppm] = 9.30 (s, 1H), 9.23 (s, 1H), 8.74 (q,  $J$  = 4.5 Hz, 1H), 8.39 (d,  $J$  = 5.3 Hz, 1H), 8.13 (d,  $J$  = 2.4 Hz, 1H), 7.70 – 7.61 (m, 4H), 7.58 – 7.50 (m, 3H), 7.23 (dd,  $J$  = 5.3, 2.0 Hz, 1H), 2.76 (d,  $J$  = 4.8 Hz, 3H).  **$^{13}C$  NMR** (126 MHz, DMSO- $d_6$ ):  $\delta$  [ppm] = 163.8, 152.4, 152.3, 150.2, 148.3, 141.5, 139.1, 136.5, 132.1, 126.8 (q,  $J$  = 30.5 Hz), 123.3, 122.8 (q,  $J$  = 273.2 Hz), 122.6 (m), 122.0, 119.9, 119.5, 117.3, 117.0 (q,  $J$  = 5.7 Hz), 26.0 (observed complexity is due to the C-F splitting). **ESI-HRMS** (m/z) [ $M+H^+$ ] calcd. for  $C_{21}H_{17}ClF_3N_4O_2S^+$ , 481.0707; found, 481.0705.

**Methyl 4-((4-(3-(4-chloro-3-(trifluoromethyl)phenyl)ureido)phenyl)thio)picolinate** (3.57)

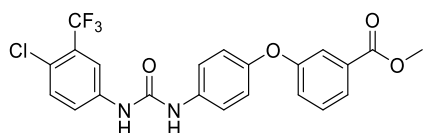


$C_{21}H_{15}ClF_3N_3O_3S$   
481.87 g/mol

**Amine building block: BB-5** (Chapter 4.1.3.3.4)

**Yield:** 68% (109 mg, 0.226 mmol); workup B.  **$^1H$  NMR** (500 MHz, DMSO- $d_6$ ):  $\delta$  [ppm] = 10.47 – 10.20 (m, 2H), 8.50 (d,  $J$  = 5.2 Hz, 1H), 8.09 (d,  $J$  = 2.3 Hz, 1H), 7.82 (dd,  $J$  = 8.7, 2.3 Hz, 1H), 7.74 – 7.67 (m, 3H), 7.64 – 7.58 (m, 3H), 7.28 (dd,  $J$  = 5.2, 1.9 Hz, 1H), 3.83 (s, 3H).  **$^{13}C$  NMR** (126 MHz, DMSO- $d_6$ ):  $\delta$  [ppm] = 165.0, 152.3, 152.2, 149.6, 147.6, 141.5, 139.1, 136.4, 132.1, 126.8 (q,  $J$  = 30.7 Hz), 123.3, 123.0, 122.8 (q,  $J$  = 272.6 Hz), 122.6 (m), 120.4, 119.9, 119.3, 117.0 (m), 52.6 (observed complexity is due to the C-F splitting). **ESI-HRMS** (m/z) [ $M+H^+$ ] calcd. for  $C_{21}H_{16}ClF_3N_3O_3S^+$ , 482.0548; found, 482.0547.

**Methyl 3-(4-(3-(4-chloro-3-(trifluoromethyl)phenyl)ureido)phenoxy)benzoate** (3.58)



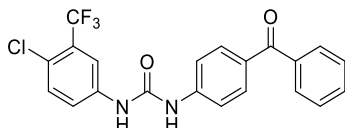
$C_{22}H_{16}ClF_3N_2O_4$   
464.83 g/mol

**Amine building block: BB-6** (Chapter 4.1.3.3.4)

**Yield:** 91% (1.40 g, 3.01 mmol); workup A ( $CH_2Cl_2/MeOH$  = 99/1). **TLC** ( $CH_2Cl_2/MeOH$  = 98/2):  $R_f$  = 0.28 [UV | PMA].  **$^1H$  NMR** (250 MHz,  $CDCl_3$ ):  $\delta$  [ppm] = 7.78 – 7.72 (m, 1H), 7.69 (br s, 1H), 7.60 – 7.55 (m, 2H), 7.45 (br s, 1H), 7.41 – 7.27 (m, 3H), 7.20 – 7.09 (m, 3H), 6.92 – 6.84

(m, 2H), 3.89 (s, 3H).  $^{13}\text{C NMR}$  (63 MHz,  $\text{CDCl}_3$ ):  $\delta$  [ppm] = 167.1, 157.6, 153.9, 153.6, 137.2, 133.1, 132.1, 131.9, 130.1, 128.9 (q,  $J = 31.6$  Hz), 126.4 (m), 124.6, 124.1, 123.6, 123.4, 122.6 (q,  $J = 273.3$  Hz), 120.0, 119.2, 119.1 (m), 52.5 (observed complexity is due to the C-F splitting). **ESI-HRMS** (m/z)  $[\text{M}+\text{H}^+]$  calcd. for  $\text{C}_{22}\text{H}_{17}\text{ClF}_3\text{N}_2\text{O}_4^+$ , 465.0824; found, 465.0825.

### 1-(4-Benzoylphenyl)-3-(4-chloro-3-(trifluoromethyl)phenyl)urea (3.59)

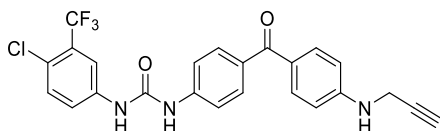


$\text{C}_{21}\text{H}_{14}\text{ClF}_3\text{N}_2\text{O}_2$

418.80 g/mol

**Yield:** 70% (121 mg, 0.289 mmol); workup B.  $^1\text{H NMR}$  (500 MHz,  $\text{DMSO-d}_6$ ):  $\delta$  [ppm] = 9.35 (s, 1H), 9.31 (s, 1H), 8.13 (d,  $J = 2.3$  Hz, 1H), 7.77 – 7.69 (m, 4H), 7.68 – 7.62 (m, 5H), 7.56 (t,  $J = 7.6$  Hz, 2H).  $^{13}\text{C NMR}$  (126 MHz,  $\text{DMSO-d}_6$ ):  $\delta$  [ppm] = 194.5, 152.1, 143.8, 139.0, 137.7, 132.2, 132.1, 131.4, 130.4, 129.3, 128.5, 126.8 (q,  $J = 30.6$  Hz), 123.4, 122.8 (m), 122.8 (q,  $J = 272.8$  Hz), 117.6, 117.0 (q,  $J = 5.6$  Hz) (observed complexity is due to the C-F splitting). **ESI-HRMS** (m/z)  $[\text{M}+\text{H}^+]$  calcd. for  $\text{C}_{21}\text{H}_{15}\text{ClF}_3\text{N}_2\text{O}_2^+$ , 419.0769; found, 419.0766.

### 1-(4-Chloro-3-(trifluoromethyl)phenyl)-3-(4-(4-(prop-2-yn-1-ylamino)benzoyl)phenyl)urea (3.60)

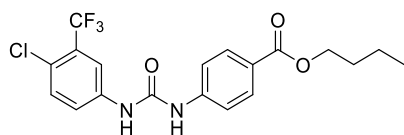


$\text{C}_{24}\text{H}_{17}\text{ClF}_3\text{N}_2\text{O}_2$

471.86 g/mol

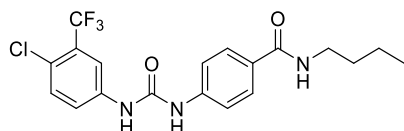
**Amine building block: BB-7** (Chapter 4.1.3.3.4)

**Yield:** 55% (51.7 mg, 0.110 mmol); workup A (Hex/EtOAc = 4/1). **TLC** (Hex/EtOAc = 1/1):  $R_f = 0.23$  [UV | PMA].  $^1\text{H NMR}$  (500 MHz,  $\text{DMSO-d}_6$ ):  $\delta$  [ppm] = 9.28 (s, 1H), 9.24 (s, 1H), 8.13 (d,  $J = 2.2$  Hz, 1H), 7.67 – 7.59 (m, 8H), 6.98 (t,  $J = 5.9$  Hz, 1H), 6.71 (d,  $J = 8.7$  Hz, 2H), 3.98 (dd,  $J = 5.8, 2.2$  Hz, 2H), 3.16 (t,  $J = 2.3$  Hz, 1H).  $^{13}\text{C NMR}$  (126 MHz,  $\text{DMSO-d}_6$ ):  $\delta$  [ppm] = 192.6, 152.2, 151.7, 142.5, 139.1, 132.1, 132.1, 132.0, 130.6, 126.7 (q,  $J = 30.4$  Hz), 125.3, 123.3, 122.8 (q,  $J = 273.2$  Hz), 122.6 (m), 117.5, 117.0 (q,  $J = 5.7$  Hz), 111.6, 81.4, 73.5, 31.6 (observed complexity is due to the C-F splitting). **ESI-HRMS** (m/z)  $[\text{M}+\text{H}^+]$  calcd. for  $\text{C}_{24}\text{H}_{18}\text{ClF}_3\text{N}_2\text{O}_2^+$ , 472.1034; found, 472.1032.

**Butyl 4-(3-(4-chloro-3-(trifluoromethyl)phenyl)ureido)benzoate (3.61)**C<sub>19</sub>H<sub>18</sub>ClF<sub>3</sub>N<sub>2</sub>O<sub>3</sub>

414.81 g/mol

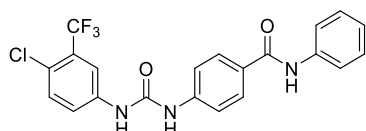
**Yield:** 93% (200 mg, 0.482 mmol); workup B. **<sup>1</sup>H NMR** (500 MHz, DMSO-d<sub>6</sub>): δ [ppm] = 9.32 – 9.24 (m, 2H), 8.12 (d, *J* = 2.2 Hz, 1H), 7.89 (d, *J* = 8.8 Hz, 2H), 7.67 – 7.58 (m, 4H), 4.24 (t, *J* = 6.5 Hz, 2H), 1.72 – 1.63 (m, 2H), 1.46 – 1.37 (m, 2H), 0.93 (t, *J* = 7.4 Hz, 3H). **<sup>13</sup>C NMR** (126 MHz, DMSO-d<sub>6</sub>): δ [ppm] = 165.4, 152.1, 143.9, 139.0, 132.1, 130.4, 126.8 (q, *J* = 30.8 Hz), 123.3, 123.2, 122.8 (q, *J* = 273.0 Hz), 122.7 (m), 117.7, 117.0 (q, *J* = 5.5 Hz), 64.0, 30.3, 18.8, 13.7 (observed complexity is due to the C-F splitting). **ESI-HRMS** (*m/z*) [M+H]<sup>+</sup> calcd. for C<sub>19</sub>H<sub>19</sub>ClF<sub>3</sub>N<sub>2</sub>O<sub>3</sub><sup>+</sup>, 415.1031; found, 415.1032.

***N*-Butyl-4-(3-(4-chloro-3-(trifluoromethyl)phenyl)ureido)benzamide (3.62)**C<sub>19</sub>H<sub>19</sub>ClF<sub>3</sub>N<sub>3</sub>O<sub>2</sub>

413.83 g/mol

**Amine building block:** **BB-8.1** and **BB-8.2** (Chapter 4.1.3.3.4)

**Yield:** 59% (99.8 mg, 0.241 mmol); workup B (additional washing step of product with CH<sub>2</sub>Cl<sub>2</sub>). **<sup>1</sup>H NMR** (500 MHz, DMSO-d<sub>6</sub>): δ [ppm] = 9.25 (s, 1H), 9.11 (s, 1H), 8.31 (t, *J* = 5.6 Hz, 1H), 8.12 (d, *J* = 2.1 Hz, 1H), 7.79 (d, *J* = 8.8 Hz, 2H), 7.66 – 7.61 (m, 2H), 7.53 (d, *J* = 8.8 Hz, 2H), 3.24 (q, *J* = 7.0 Hz, 2H), 1.53 – 1.46 (m, 2H), 1.36 – 1.28 (m, 2H), 0.90 (t, *J* = 7.4 Hz, 3H). **<sup>13</sup>C NMR** (126 MHz, DMSO-d<sub>6</sub>): δ [ppm] = 165.6, 152.3, 141.8, 139.2, 132.1, 128.3, 128.1, 126.8 (q, *J* = 30.5 Hz), 123.2, 122.8 (q, *J* = 273.1 Hz), 122.5 (m), 117.5, 116.9 (q, *J* = 5.8 Hz), 38.8, 31.4, 19.7, 13.8 (observed complexity is due to the C-F splitting). **ESI-HRMS** (*m/z*) [M+H]<sup>+</sup> calcd. for C<sub>19</sub>H<sub>20</sub>ClF<sub>3</sub>N<sub>3</sub>O<sub>2</sub><sup>+</sup>, 414.1191; found, 414.1189.

**4-(3-(4-Chloro-3-(trifluoromethyl)phenyl)ureido)-*N*-phenylbenzamide (3.63)**C<sub>21</sub>H<sub>15</sub>ClF<sub>3</sub>N<sub>3</sub>O<sub>2</sub>

433.82 g/mol

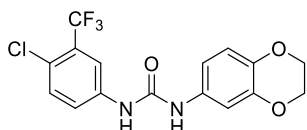
**Amine building block:** **BB-9** (Chapter 4.1.3.3.4)

**Yield:** 37% (65.6 mg, 0.151 mmol); workup B (additional washing step of product with CH<sub>2</sub>Cl<sub>2</sub>). **<sup>1</sup>H NMR** (500 MHz, DMSO-d<sub>6</sub>): δ [ppm] = 10.11 (s, 1H), 9.28 (s, 1H), 9.20 (s, 1H), 8.13 (d, *J* = 2.3 Hz, 1H), 7.94 (d, *J* = 8.7 Hz, 2H), 7.77 (d, *J* = 7.7 Hz, 2H), 7.69 – 7.59 (m, 4H), 7.34 (t, *J* = 7.9 Hz, 2H), 7.08 (t, *J* = 7.4 Hz, 1H). **<sup>13</sup>C NMR** (126 MHz, DMSO-d<sub>6</sub>): δ [ppm] = 164.9, 152.2, 142.4, 139.3, 139.1, 132.1, 128.8, 128.6, 128.2, 126.8 (q, *J* = 30.5 Hz), 123.5, 123.3,

122.8 (q,  $J = 273.0$  Hz), 122.6 (m), 120.3, 117.6, 117.0 (q,  $J = 5.5$  Hz) (observed complexity is due to the C-F splitting). **ESI-HRMS** (m/z)  $[M+H^+]$  calcd. for  $C_{21}H_{16}ClF_3N_3O_2^+$ , 434.0878; found, 434.0875.

### 1-(4-Chloro-3-(trifluoromethyl)phenyl)-3-(2,3-dihydrobenzo[*b*][1,4]dioxin-6-yl)urea

(3.64)



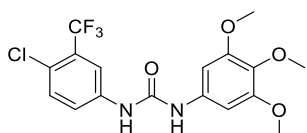
$C_{16}H_{12}ClF_3N_2O_3$

372.73 g/mol

**Yield:** 21% (31.8 mg, 0.0853 mmol); workup A ( $CH_2Cl_2/MeOH = 99/1$ ).

**TLC** ( $CH_2Cl_2/MeOH = 99/1$ ):  $R_f = 0.25$  [UV | PMA].  **$^1H$  NMR** (500 MHz,  $DMSO-d_6$ ):  $\delta$  [ppm] = 9.07 (s, 1H), 8.64 (s, 1H), 8.07 (d,  $J = 2.3$  Hz, 1H), 7.65 – 7.54 (m, 2H), 7.07 (d,  $J = 2.4$  Hz, 1H), 6.85 – 6.73 (m, 2H), 4.25 – 4.15 (m, 4H).  **$^{13}C$  NMR** (126 MHz,  $DMSO-d_6$ ):  $\delta$  [ppm] = 152.4, 143.1, 139.5, 138.8, 132.8, 132.0, 126.7 (q,  $J = 30.6$  Hz), 123.0, 122.9 (q,  $J = 273.1$  Hz), 122.1 (m), 116.9, 116.7 (q,  $J = 6.0$  Hz), 112.1, 108.0, 64.2, 63.9 (observed complexity is due to the C-F splitting). **ESI-HRMS** (m/z)  $[M+H^+]$  calcd. for  $C_{16}H_{13}ClF_3N_2O_3^+$ , 373.0561; found, 373.0564.

### 1-(4-Chloro-3-(trifluoromethyl)phenyl)-3-(3,4,5-trimethoxyphenyl)urea (3.65)



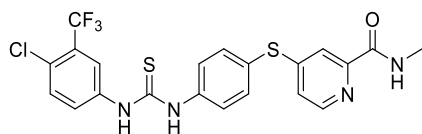
$C_{17}H_{16}ClF_3N_2O_4$

404.77 g/mol

**Yield:** 98% (163 mg, 0.402 mmol); workup A ( $CH_2Cl_2/MeOH = 99/1$ ).

**TLC** ( $CH_2Cl_2/MeOH = 98/2$ ):  $R_f = 0.21$  [UV | PMA].  **$^1H$  NMR** (500 MHz,  $DMSO-d_6$ ):  $\delta$  [ppm] = 9.10 (s, 1H), 8.79 (s, 1H), 8.09 (d,  $J = 2.4$  Hz, 1H), 7.67 – 7.58 (m, 2H), 6.80 (s, 2H), 3.75 (s, 6H), 3.61 (s, 3H).  **$^{13}C$  NMR** (126 MHz,  $DMSO-d_6$ ):  $\delta$  [ppm] = 152.9, 152.4, 139.4, 135.3, 132.8, 132.0, 126.7 (q,  $J = 30.6$  Hz), 123.2, 122.9 (q,  $J = 273.1$  Hz), 122.3 (m), 116.8 (q,  $J = 5.6$  Hz), 96.4, 60.1, 55.7 (observed complexity is due to the C-F splitting). **ESI-HRMS** (m/z)  $[M+H^+]$  calcd. for  $C_{17}H_{17}ClF_3N_2O_4^+$ , 405.0824; found, 405.0828.

**4-((4-(3-(4-Chloro-3-(trifluoromethyl)phenyl)thioureido)phenyl)thio)-N-methylpicolinamide (3.66)**

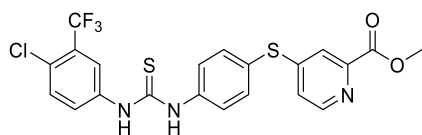


$C_{21}H_{16}ClF_3N_4OS_2$   
496.95 g/mol

**Amine building block: BB-4** (Chapter 4.1.3.3.4)

**Yield:** 42% (165 mg, 0.332 mmol); workup B.  **$^1H$  NMR** (500 MHz,  $CDCl_3$ ):  $\delta$  [ppm] = 8.91 (s, 1H), 8.78 (s, 1H), 8.31 (d,  $J$  = 5.3 Hz, 1H), 8.14 (d,  $J$  = 4.8 Hz, 1H), 7.73 – 7.69 (m, 2H), 7.65 – 7.61 (m, 1H), 7.56 (d,  $J$  = 8.6 Hz, 2H), 7.52 (d,  $J$  = 8.6 Hz, 2H), 7.45 (d,  $J$  = 9.3 Hz, 1H), 7.24 (dd,  $J$  = 5.3, 1.9 Hz, 1H), 2.96 (d,  $J$  = 5.1 Hz, 3H).  **$^{13}C$  NMR** (126 MHz,  $CDCl_3$ ):  $\delta$  [ppm] = 179.8, 165.1, 153.2, 149.4, 147.8, 139.7, 137.1, 136.4, 131.9, 129.1 (m), 129.0, 128.8 (q,  $J$  = 31.6 Hz), 125.5, 125.3, 123.6 (m), 123.2, 122.5 (q,  $J$  = 273.2 Hz), 118.2, 26.5 (observed complexity is due to the C-F splitting). **ESI-HRMS** (m/z)  $[M+H^+]$  calcd. for  $C_{21}H_{17}ClF_3N_4OS_2^+$ , 497.0479; found, 497.0477.

**Methyl 4-((4-(3-(4-chloro-3-(trifluoromethyl)phenyl)thioureido)phenyl)thio)picolinate (3.67)**

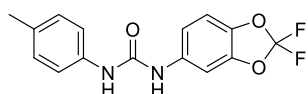


$C_{21}H_{15}ClF_3N_3O_2S_2$   
497.94 g/mol

**Amine building block: BB-5** (Chapter 4.1.3.3.4)

**Yield:** 64% (109 mg, 0.219 mmol); workup B (additional washing step of product with  $Et_2O$ ).  **$^1H$  NMR** (500 MHz,  $DMSO-d_6$ ):  $\delta$  [ppm] = 10.36 (s, 1H), 10.28 (s, 1H), 8.50 (d,  $J$  = 5.2 Hz, 1H), 8.09 (d,  $J$  = 2.4 Hz, 1H), 7.82 (dd,  $J$  = 8.7, 2.4 Hz, 1H), 7.74 – 7.68 (m, 3H), 7.64 – 7.58 (m, 3H), 7.28 (dd,  $J$  = 5.2, 1.9 Hz, 1H), 3.83 (s, 3H).  **$^{13}C$  NMR** (126 MHz,  $DMSO-d_6$ ):  $\delta$  [ppm] = 179.7, 164.9, 151.5, 149.7, 147.7, 141.2, 139.0, 135.7, 131.7, 128.6, 126.3 (q,  $J$  = 29.8 Hz), 125.4, 124.5, 123.2, 122.7 (q,  $J$  = 273.1 Hz), 122.5, 122.4 (m), 120.7, 52.6 (observed complexity is due to the C-F splitting). **ESI-HRMS** (m/z)  $[M+H^+]$  calcd. for  $C_{21}H_{16}ClF_3N_3O_2S_2^+$ , 498.0319; found, 498.0321.

**1-(2,2-Difluorobenzo[d][1,3]dioxol-5-yl)-3-(p-tolyl)urea (3.68)**

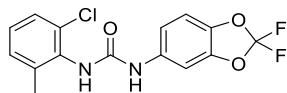


$C_{15}H_{12}F_2N_2O_3$   
306.27 g/mol

**Yield:** 63% (131 mg, 0.428 mmol); workup A (Hex/ $EtOAc$  = 4/1). **TLC** (Hex/ $EtOAc$  = 3/1):  $R_f$  = 0.32 [UV | PMA].  **$^1H$  NMR** (500 MHz,  $DMSO-d_6$ ):  $\delta$  [ppm] = 8.83 (s, 1H), 8.61 (s, 1H), 7.66

(d,  $J = 2.1$  Hz, 1H), 7.34 – 7.28 (m, 3H), 7.10 – 7.04 (m, 3H), 2.24 (s, 3H).  $^{13}\text{C NMR}$  (126 MHz, DMSO- $d_6$ ):  $\delta$  [ppm] = 152.6, 142.8, 137.4, 136.9, 136.7, 131.3 (t,  $J = 252.2$  Hz), 130.9, 129.2, 118.5, 113.4, 110.1, 101.1, 20.4 (observed complexity is due to the C-F splitting). **ESI-HRMS** ( $m/z$ ) [ $M+H^+$ ] calcd. for  $\text{C}_{15}\text{H}_{13}\text{F}_2\text{N}_2\text{O}_3^+$ , 307.0889; found, 307.0887.

### 1-(2-Chloro-6-methylphenyl)-3-(2,2-difluorobenzo[d][1,3]dioxol-5-yl)urea (3.69)

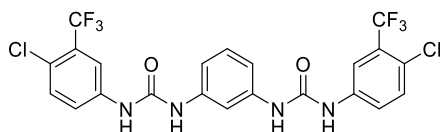


$\text{C}_{15}\text{H}_{11}\text{ClF}_2\text{N}_2\text{O}_3$

340.71 g/mol

**Yield:** 82% (162 mg, 0.475 mmol); workup B.  $^1\text{H NMR}$  (500 MHz, DMSO- $d_6$ ):  $\delta$  [ppm] = 9.11 (s, 1H), 8.02 (s, 1H), 7.65 (d,  $J = 2.1$  Hz, 1H), 7.37 – 7.33 (m, 1H), 7.29 (d,  $J = 8.7$  Hz, 1H), 7.25 – 7.17 (m, 2H), 7.11 (dd,  $J = 8.8, 2.1$  Hz, 1H), 2.25 (s, 3H).  $^{13}\text{C NMR}$  (126 MHz, DMSO- $d_6$ ):  $\delta$  [ppm] = 152.8, 142.8, 138.7, 137.3, 136.9, 133.8, 132.0, 131.3 (t,  $J = 252.0$  Hz), 129.1, 127.4, 126.9, 113.2, 110.0, 100.9, 18.6 (observed complexity is due to the C-F splitting). **ESI-HRMS** ( $m/z$ ) [ $M+H^+$ ] calcd. for  $\text{C}_{15}\text{H}_{12}\text{ClF}_2\text{N}_2\text{O}_3^+$ , 341.0499; found, 341.0501.

### 1,1'-(1,3-Phenylene)bis(3-(4-chloro-3-(trifluoromethyl)phenyl)urea (3.70)



$\text{C}_{22}\text{H}_{14}\text{Cl}_2\text{F}_6\text{N}_4\text{O}_2$

551.27 g/mol

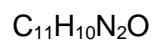
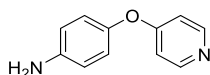
A solution of 4-chloro-3-(trifluoromethyl)phenyl isocyanate (339 mg, 1.53 mmol, 2.20 eq.) in dry dichloromethane (10 mL) was cooled to  $0^\circ\text{C}$ . After the addition of *m*-phenylenediamine (75.0 mg, 0.694 mmol, 1.00 eq.) the reaction mixture was allowed to warm to room temperature and the reaction was stirred at room temperature for 20 h. The solvent was removed followed by the precipitation from DMF through the addition of water (10fold excess) and collection of the product by centrifugation (17,000 x g, 10 min). The product was washed with  $\text{Et}_2\text{O}$  (2 x 1 mL) and collected by centrifugation (17,000 x g, 10 min) to yield 192 mg (0.348 mmol, 50%) of an off-white solid.

$^1\text{H NMR}$  (500 MHz, DMSO- $d_6$ ):  $\delta$  [ppm] = 9.08 (s, 2H), 8.92 (s, 2H), 8.14 (s, 2H), 7.74 (t,  $J = 2.0$  Hz, 1H), 7.61 (d,  $J = 1.4$  Hz, 4H), 7.22 – 7.17 (m, 1H), 7.09 (dd,  $J = 7.9, 2.0$  Hz, 2H).  $^{13}\text{C NMR}$  (126 MHz, DMSO- $d_6$ ):  $\delta$  [ppm] = 152.3, 139.7, 139.4, 132.0, 129.2, 126.7 (q,  $J = 30.5$  Hz), 123.0, 122.8 (q,  $J = 273.0$  Hz), 122.3 (m), 116.7 (q,  $J = 5.7$  Hz), 112.5, 108.6. **ESI-HRMS** ( $m/z$ ) [ $M+H^+$ ] calcd. for  $\text{C}_{22}\text{H}_{15}\text{Cl}_2\text{F}_6\text{N}_4\text{O}_2^+$ , 551.0471; found, 551.0486.

#### 4.1.3.3.4. Synthesis of Compound Library Building Blocks

4-((4-Aminophenyl)thio)-*N*-methylpicolinamide (**BB-4**)<sup>229</sup> and 4-aminobenzanilide (**BB-9**)<sup>230</sup> were synthesized according to known literature procedures.

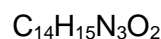
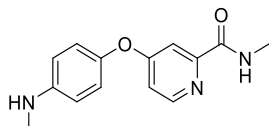
#### 4-(Pyridin-4-yloxy)aniline (BB-1)



To a solution of 4-chloropyridine hydrochloride (1.00 g, 6.67 mmol, 1.00 eq.) in DMF (12 mL), 4-aminophenol (0.728 g, 6.67 mmol, 1.00 eq.) was added, followed by  $\text{K}_2\text{CO}_3$  (1.84 g, 13.3 mmol, 2.00 eq.). After being stirred under reflux for 20 hours, the solvent was removed. The crude product was purified by flash column chromatography (Hex/EtOAc = 3/2, 2% diethyl amine) to yield a brown solid (0.0962 g, 0.517 mmol, 8%).

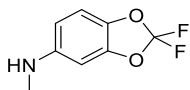
**TLC** (Hex/EtOAc = 3/2, 2% diethyl amine):  $R_f = 0.15$  [UV |  $\text{KMnO}_4$ ].  **$^1\text{H NMR}$**  (500 MHz,  $\text{CDCl}_3$ ):  $\delta$  [ppm] = 8.42 (dd,  $J = 4.8, 1.6$  Hz, 2H), 6.92 – 6.87 (m, 2H), 6.81 (dd,  $J = 4.8, 1.6$  Hz, 2H), 6.74 – 6.70 (m, 2H).  **$^{13}\text{C NMR}$**  (75 MHz,  $\text{CDCl}_3$ ):  $\delta$  [ppm] = 166.0, 151.1, 145.8, 144.3, 122.1, 116.4, 111.7. **ESI-HRMS** ( $m/z$ ) [ $\text{M}+\text{H}^+$ ] calcd. for  $\text{C}_{11}\text{H}_{11}\text{N}_2\text{O}^+$ , 187.0866; found, 187.0865.

#### *N*-Methyl-4-(4-(methylamino)phenoxy)picolinamide (BB-2)



A solution of 4-(4-aminophenoxy)-*N*-methyl-2-pyridine carboxamide (319 mg, 1.31 mmol, 1.00 eq.) in dry MeOH (5 mL) was treated with sodium methoxide (354 mg, 6.55 mmol, 5.00 eq.) and *para*-formaldehyde (397 mg, 13.1 mmol, 10.0 eq.). The reaction mixture was stirred at room temperature for 16 h, sodium borohydride (149 mg, 3.93 mmol, 3.00 eq.) was added and the mixture stirred at 40°C for 4 h. The reaction mixture was filtered and the solvent removed in vacuo. The residue was dissolved in EtOAc (20 mL) and the organic phase was washed with brine (20 mL). The organic phase was dried over  $\text{Na}_2\text{SO}_4$ , filtered and the solvent was removed. The residue was purified by flash column chromatography on silica (Hex/EtOAc = 1/1) to yield **BB-2** (139 mg, 0.540 mmol, 41%) as a yellow oil.

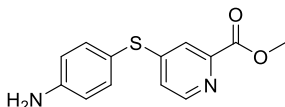
**TLC** (Hex/EtOAc = 1/1):  $R_f = 0.22$  [UV | PMA].  **$^1\text{H NMR}$**  (300 MHz,  $\text{CDCl}_3$ ):  $\delta$  [ppm] = 8.32 (d,  $J = 5.6$  Hz, 1H), 7.99 (br s, 1H), 7.67 (d,  $J = 2.6$  Hz, 1H), 6.95 – 6.88 (m, 3H), 6.66 – 6.59 (m, 2H), 3.00 (d,  $J = 5.1$  Hz, 3H), 2.85 (s, 3H).  **$^{13}\text{C NMR}$**  (75 MHz,  $\text{CDCl}_3$ ):  $\delta$  [ppm] = 167.5, 164.8, 152.2, 149.6, 147.4, 144.8, 122.0, 113.8, 113.6, 110.0, 31.2, 26.2. **ESI-HRMS** ( $m/z$ ) [ $\text{M}+\text{H}^+$ ] calcd. for  $\text{C}_{14}\text{H}_{16}\text{N}_3\text{O}_2^+$ , 258.1237; found, 258.1237.

**2,2-Difluoro-*N*-methylbenzo[*d*][1,3]dioxol-5-amine (BB-3)**C<sub>8</sub>H<sub>7</sub>F<sub>2</sub>NO<sub>2</sub>

187.15 g/mol

A solution of 2,2-difluorobenzo[*d*][1,3]dioxol-5-amine (150  $\mu$ L, 227 mg, 1.31 mmol, 1.00 eq.) in dry MeOH (5 mL) was treated with sodium methoxide (354 mg, 6.55 mmol, 5.00 eq.) and *para*-formaldehyde (397 mg, 13.1 mmol, 10.0 eq.). The reaction mixture was stirred at room temperature for 16 h, sodium borohydride (149 mg, 3.93 mmol, 3.00 eq.) was added and the mixture stirred at 40°C for 4 h. The reaction mixture was filtered and the solvent removed in vacuo. The residue was dissolved in EtOAc (20 mL) and the organic phase was washed with brine (20 mL). The organic phase was dried over Na<sub>2</sub>SO<sub>4</sub>, filtered and the solvent was removed. The residue was purified by flash column chromatography on silica (Hex/EtOAc = 4/1) to yield the desired product (145 mg, 0.775 mmol, 59%) as a brown oil.

**TLC** (Hex/EtOAc = 4/1): R<sub>f</sub> = 0.34 [UV | PMA]. **<sup>1</sup>H NMR** (300 MHz, CDCl<sub>3</sub>):  $\delta$  [ppm] = 6.85 (d, *J* = 8.6 Hz, 1H), 6.37 (d, *J* = 2.3 Hz, 1H), 6.23 (dd, *J* = 8.6, 2.4 Hz, 1H), 2.81 (s, 3H). **<sup>13</sup>C NMR** (75 MHz, CDCl<sub>3</sub>):  $\delta$  [ppm] = 146.4, 144.9, 136.0, 131.9 (t, *J* = 252.9 Hz), 109.8, 106.3, 95.0, 31.5. **ESI-HRMS** (*m/z*) [M+H<sup>+</sup>] calcd. for C<sub>8</sub>H<sub>8</sub>F<sub>2</sub>NO<sub>2</sub><sup>+</sup>, 188.0518; found, 188.0517.

**Methyl 4-((4-aminophenyl)thio)picolinate (BB-5)**C<sub>13</sub>H<sub>12</sub>N<sub>2</sub>O<sub>2</sub>S

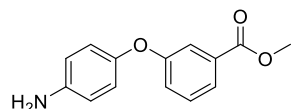
260.31 g/mol

A solution of 4-aminothiophenol (364 mg, 2.91 mmol, 1.00 eq.), methyl 4-chloropicolinate (500 mg, 2.91 mmol, 1.00 eq.) and K<sub>2</sub>CO<sub>3</sub> (804 mg, 5.82 mmol, 2.00 eq.) in dry DMF (7 mL) was stirred at 135°C for 16 h. H<sub>2</sub>O (20 mL) was added and the mixture was extracted with EtOAc (3 x 40 mL). The organic phase was washed with brine (2 x 40 mL), dried over Na<sub>2</sub>SO<sub>4</sub>, filtered and the solvent removed. Purification by flash column chromatography on silica (CH<sub>2</sub>Cl<sub>2</sub>/MeOH = 98/2) gave **BB-5** (169 mg, 0.649 mmol, 22%) as a brown solid.

**TLC** (CH<sub>2</sub>Cl<sub>2</sub>/MeOH = 98/2): R<sub>f</sub> = 0.22 [UV | PMA]. **<sup>1</sup>H NMR** (500 MHz, CDCl<sub>3</sub>):  $\delta$  [ppm] = 8.40 (d, *J* = 5.3 Hz, 1H), 7.77 (d, *J* = 1.9 Hz, 1H), 7.35 – 7.30 (m, 2H), 7.00 (dd, *J* = 5.3, 1.9 Hz, 1H), 6.76 – 6.72 (m, 2H), 3.96 (s, 3H). **<sup>13</sup>C NMR** (126 MHz, CDCl<sub>3</sub>):  $\delta$  [ppm] = 165.8, 154.8, 149.2, 148.6, 147.5, 137.5, 122.8, 121.5, 116.3, 115.0, 53.1. **ESI-HRMS** (*m/z*) [M+H<sup>+</sup>] calcd. for C<sub>13</sub>H<sub>13</sub>N<sub>2</sub>O<sub>2</sub>S<sup>+</sup>, 261.0692; found, 261.0690.

**Methyl 3-(4-aminophenoxy)benzoate (BB-6)**

The synthesis of **BB-6** was based on a previously published procedure.<sup>231</sup>

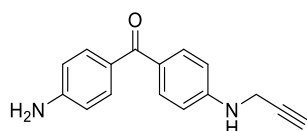


$C_{14}H_{13}NO_3$   
243.26 g/mol

1-Fluoro-4-nitrobenzene (0.752 mL, 1.00 g, 7.09 mmol, 1.00 eq.) in dry DMF (12 mL) was treated with methyl 3-hydroxybenzoate (1.08 g, 7.09 mmol, 1.00 eq.) and  $K_2CO_3$  (1.96 g, 14.2 mmol, 2.00 eq.). The reaction mixture was stirred at 135°C for 14 h and quenched by the addition of  $H_2O$  (20 mL). The aqueous phase was extracted with EtOAc (3 x 25 mL) and the combined organic phases were dried over  $Na_2SO_4$ , filtered and the solvent removed in vacuo. The crude product was used without further purification and characterization.

To a solution of crude methyl 3-(4-nitrophenoxy)benzoate in EtOAc (25 mL) palladium on carbon (10% wt, 0.300 g) was added. The mixture was stirred at room temperature under an atmosphere of hydrogen for 5 h. Subsequently, the mixture was filtered through a pad of kieselgur and the solvent was removed to give **BB-6** (1.70 g, 7.00 mmol, 99%) as a white solid.

$^1H$  NMR (250 MHz,  $CDCl_3$ ):  $\delta$  [ppm] = 7.69 (dt,  $J$  = 7.7, 1.3 Hz, 1H), 7.61 – 7.52 (m, 1H), 7.34 (t,  $J$  = 7.9 Hz, 1H), 7.13 (ddd,  $J$  = 8.2, 2.6, 1.0 Hz, 1H), 6.91 – 6.83 (m, 2H), 6.73 – 6.65 (m, 2H), 3.88 (s, 3H), 3.63 (s, 2H).  $^{13}C$  NMR (63 MHz,  $CDCl_3$ ):  $\delta$  [ppm] = 166.7, 159.0, 148.0, 143.1, 131.6, 129.5, 123.2, 121.8, 121.2, 117.8, 116.3, 52.1. **ESI-HRMS** (m/z) [ $M+H^+$ ] calcd. for  $C_{14}H_{14}NO_3^+$ , 244.0968; found, 244.0966.

**(4-Aminophenyl)(4-(prop-2-yn-1-ylamino)phenyl)methanone (BB-7)**

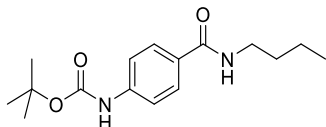
$C_{16}H_{14}N_2O$   
250.30 g/mol

A solution of 4,4'-diaminobenzophenone (500 mg, 2.36 mmol, 1.00 eq.) in dry DMF (5 mL) was treated with  $K_2CO_3$  (359 mg, 2.60 mmol, 1.10 eq.) and propargyl bromide (20% wt in toluene; 351  $\mu$ L, 3.26 mmol, 1.00 eq.). The reaction mixture was stirred at 50°C for 16 h. Subsequently, the solvent was removed and the residue dissolved in EtOAc (20 mL). The organic phase was washed with brine (20 mL), dried over  $Na_2SO_4$ , filtered and the solvent was removed. Flash column chromatography on silica (Hex/EtOAc = 1/1, 2% diethyl amine) yielded **BB-7** (227 mg, 0.907 mmol, 38%) as a yellow solid.

**TLC** (Hex/EtOAc = 1/1, 2% diethyl amine):  $R_f$  = 0.44 [UV | PMA].  $^1H$  NMR (500 MHz,  $DMSO-d_6$ ):  $\delta$  [ppm] = 7.52 (d,  $J$  = 8.7 Hz, 2H), 7.46 (d,  $J$  = 8.6 Hz, 2H), 6.76 (t,  $J$  = 6.0 Hz, 1H), 6.68 (d,  $J$  = 8.7 Hz, 2H), 6.59 (d,  $J$  = 8.6 Hz, 2H), 5.91 (s, 2H), 3.96 (dd,  $J$  = 6.0, 2.4 Hz, 2H), 3.13 (t,  $J$  = 2.4 Hz, 1H).  $^{13}C$  NMR (75 MHz,  $DMSO-d_6$ ):  $\delta$  [ppm] = 192.1, 152.7, 150.8, 131.9, 131.4,

126.5, 125.2, 112.4, 111.4, 81.5, 73.3, 31.7. **ESI-HRMS** (m/z) [M+H<sup>+</sup>] calcd. for C<sub>16</sub>H<sub>15</sub>N<sub>2</sub>O<sup>+</sup>, 251.1179; found, 251.1178.

**tert-Butyl (4-(butylcarbamoyl)phenyl)carbamate (BB-8.1)**

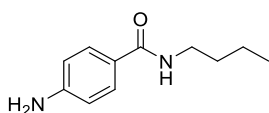


C<sub>16</sub>H<sub>24</sub>N<sub>2</sub>O<sub>3</sub>  
292.38 g/mol

To a solution of *N*-*tert*-butoxycarbonyl-4-aminobenzoic acid (300 mg, 1.26 mmol, 1.00 eq.) in dry DMF (10 mL) were added EDC·HCl (242 mg, 1.26 mmol, 1.00 eq.), DMAP (15.4 mg, 0.126 mmol, 0.100 eq.) and 1-butylamine (125 μL, 92.2 mg, 1.26 mmol, 1.00 eq.). The reaction mixture was stirred at room temperature for 24 h. The solvent was removed in vacuo and the residue was purified by flash column chromatography on silica (Hex/EtOAc = 1/1) to yield **BB-8.1** (258 mg, 0.882 mmol, 70%) as a white solid.

**TLC** (Hex/EtOAc = 1/1): R<sub>f</sub> = 0.45 [UV | PMA]. **<sup>1</sup>H NMR** (300 MHz, DMSO-d<sub>6</sub>): δ [ppm] = 9.58 (s, 1H), 8.25 (t, *J* = 5.6 Hz, 1H), 7.74 (d, *J* = 8.8 Hz, 2H), 7.50 (d, *J* = 8.8 Hz, 2H), 3.22 (q, *J* = 6.9 Hz, 2H), 1.54 – 1.43 (m, 11H), 1.38 – 1.24 (m, 2H), 0.89 (t, *J* = 7.3 Hz, 3H). **<sup>13</sup>C NMR** (75 MHz, DMSO-d<sub>6</sub>): δ [ppm] = 165.5, 152.6, 142.0, 128.1, 127.9, 117.0, 79.4, 38.8, 31.4, 28.1, 19.7, 13.7. **ESI-HRMS** (m/z) [M+H<sup>+</sup>] calcd. for C<sub>16</sub>H<sub>25</sub>N<sub>2</sub>O<sub>3</sub><sup>+</sup>, 293.1860; found, 293.1857.

**4-Amino-*N*-butylbenzamide (BB-8.2)**



C<sub>11</sub>H<sub>16</sub>N<sub>2</sub>O  
192.26 g/mol

*tert*-Butyl (4-(butylcarbamoyl)phenyl)carbamate (**BB-8.1**; 240 mg, 0.821 mmol, 1.00 eq.) was dissolved in dry CH<sub>2</sub>Cl<sub>2</sub> (7 mL) and treated with TFA (3 mL). The reaction mixture was stirred at room temperature for 5 h. Subsequently, the solvent was removed in vacuo, the residue dissolved in CH<sub>2</sub>Cl<sub>2</sub> (20 mL) and the organic phase washed with aqueous NaOH (2M, 20 mL). The organic phase was dried over Na<sub>2</sub>SO<sub>4</sub>, filtered and the solvent removed in vacuo to yield the desired product (156 mg, 0.811 mmol, 99%) as an off-white solid. **BB-8.2** was used without further purification.

**<sup>1</sup>H NMR** (300 MHz, CDCl<sub>3</sub>): δ [ppm] = 7.62 – 7.55 (m, 2H), 6.68 – 6.61 (m, 2H), 6.01 (br s, 1H), 3.46 – 3.37 (m, 2H), 1.63 – 1.51 (m, 2H), 1.46 – 1.32 (m, 2H), 0.94 (t, *J* = 7.3 Hz, 3H). **<sup>13</sup>C NMR** (75 MHz, CDCl<sub>3</sub>): δ [ppm] = 167.4, 149.5, 128.7, 124.6, 114.3, 39.8, 32.0, 20.3, 13.9. **ESI-HRMS** (m/z) [M+H<sup>+</sup>] calcd. for C<sub>11</sub>H<sub>17</sub>N<sub>2</sub>O<sup>+</sup>, 193.1335; found, 193.1333.

The spectral data are consistent with those published previously.<sup>232</sup>

## 4.2. BIOCHEMISTRY

### 4.2.1. General Methods and Materials

#### 4.2.1.1. Cell Culture

Cell culture media and supplements were purchased from commercial suppliers. A549 and HeLa cells were cultured in Dulbecco's Modified Eagle Medium (DMEM high glucose, 4.5 g/L; *Sigma Life Science*) supplemented with 10% fetal bovine serum (*Sigma Life Science*) and 2 mM L-glutamine (PAA). NIH/3T3 cells were cultured in Dulbecco's Modified Eagle Medium (DMEM high glucose; *Sigma Life Science*) supplemented with 10% fetal bovine serum (*Sigma Life Science*) and 4 mM L-glutamine (PAA). HepG2 cells were cultured in RPMI-1640 medium (*Sigma Life Science*) supplemented with 10% fetal bovine serum (*Sigma Life Science*) and 2 mM L-glutamine (PAA). All cells were maintained at 37°C in a humidified 5% CO<sub>2</sub> atmosphere. Cells were detached with trypsin-EDTA (*Thermo Fisher Scientific*).

For SILAC-based experiments, A549 and HeLa cells were passaged six times in SILAC-DMEM (*gibco, Life Technologies*) supplemented with 10% dialyzed fetal bovine serum (*Sigma Life Science*) and 2 mM L-glutamine (PAA) as well as 214 µM [<sup>13</sup>C<sub>6</sub>, <sup>15</sup>N<sub>4</sub>] L-arginine·HCl and 419 µM [<sup>13</sup>C<sub>6</sub>, <sup>15</sup>N<sub>2</sub>] L-lysine·2 HCl (*Cambridge Isotope Laboratories*) resulting in “heavy” cells or [<sup>13</sup>C<sub>6</sub>] L-arginine·HCl and [4,4,5,5-D<sub>4</sub>] L-lysine·2 HCl (*Cambridge Isotope Laboratories*) in corresponding molarities resulting in “light” cells.

Cell counting was conducted with a mixture of cell suspension and trypan blue (1:1 (v/v)) in a *Neubauer* improved cell counting chamber.

For cryostock preparation, cell were grown to 90% confluence, detached with trypsin-EDTA, and concentrated to 1 – 2 million cells/mL (600 x g, 5 min). The concentrated cell suspension was aliquoted and transferred to sterile cryogenic vials, followed by the addition of glycerol (9:1 (v/v)). Cells were frozen slowly by reducing the temperature at approximately 1°C per minute using a cryo-freezing container (Cryo 1°C Cooler; *VWR*). Frozen cells were stored at a liquid nitrogen tank (-196°C).

#### 4.2.1.2. Bacterial Strains and Culture Media

Commercially available strains were obtained from the following suppliers: Institute Pasteur, France (*Listeria monocytogenes* EGD-e; *Staphylococcus aureus* NCTC 8325, *S. aureus* Mu 50), American Type Culture Collection ATCC, USA (*Bacillus subtilis* 168, *Enterococcus faecalis* OG1RF/ATCC 47077, *E. faecalis* V583/ATCC 700802, *S. aureus* USA300 FPR3757, *S. aureus* ATCC 33591, *S. aureus* ATCC 33592), Deutsche Sammlung von Mikroorganismen und Zellkulturen DSMZ, Germany (*Acinetobacter baumannii* DSM-30007; *Enterobacter aerogenes* DSM-30053, *E. cloacae* subsp. *cloacae* DSM-30054, *Enterococcus faecium* DSM-

20477, *E. faecium* DSM-17050, *Pseudomonas aeruginosa* DSM-19882, *Klebsiella pneumoniae* DSM-30104) and Belgian Coordinated Collections of Microorganisms/Laboratory of microbiology BCCM/LMG, Belgium (*Listeria monocytogenes* F2365). Clinical *S. aureus* isolates (BK95395, BK97296, IS050678, IS050611, VA417350, VA418879, VA402923, VA412350, VA409044, VA402525) were a kind gift from Prof. Dr. Markus Gerhard (Institute of Medical Microbiology and Immunology, Technische Universität München, Germany). *S. aureus* NCTC 8325-4 was a kind gift from PD Dr. Knut Ohlsen (Institute for Molecular Infection Biology IMIB, Julius-Maximilians-Universität Würzburg, Germany). *S. aureus* N315 and ARC0001ΔSpsB<sup>174</sup> were a kind gift from Prof. Dr. Floyd Romesberg (The Scripps Research Institute, La Jolla, CA, USA). *Escherichia coli* CFT073 was a kind gift from Dr. Guiseppe Magistro (Department of Urology, Hospital of the Ludwig-Maximilians-Universität München, Germany). *S. aureus* Newman was a kind gift from Prof. Dr. Olaf Schneewind (The University of Chicago, Chicago, IL, USA). *Salmonella typhimurium* LT2 and TA100 were a kind gift from the Institute of Biochemistry, Genetics and Microbiology (University of Regensburg, Germany). Nebraska Transposon Mutant Library (NTML) was kindly provided by the Network on Antimicrobial Resistance in *Staphylococcus aureus* (NARSA; Medical Center, University of Nebraska, USA).

Experiments involving *Mycobacterium tuberculosis* H37Rv, *M. smegmatis* mc<sup>2</sup> 155 and *M. bovis* BCG strains were performed by Dr. Johannes Lehmann in the laboratories of Prof. Dr. Eric Rubin, Department of Immunology and Infectious Diseases, Harvard School of Public Health, Boston, MA, USA.

Unless otherwise stated B-medium (10 g/L casein peptone, 5 g/L NaCl, 5 g/L yeast extract, 1 g/L K<sub>2</sub>HPO<sub>4</sub>, pH 7.5) was used for cultivation of all *S. aureus* strains. For cultivation of transposon mutants, B-medium was supplemented with erythromycin (5 µg/mL). LB-medium (Lysogeny Broth; 10 g/L casein peptone, 5 g/L NaCl, 5 g/L yeast extract, pH 7.5) was used for cultivation of *B. subtilis*, *E. coli* and *S. typhimurium* strains. BHB-medium (Brain Heart Infusion; 7.5 g/L brain infusion, 10 g/L heart infusion, 10 g/L casein peptone, 5 g/L NaCl, 2.5 g/L Na<sub>2</sub>HPO<sub>4</sub>, 2 g/L glucose, pH 7.4) was used for cultivation of *L. monocytogenes*, *K. pneumoniae*, *A. baumannii*, *E. aerogenes*, *E. cloacae* and *E. faecalis*. TSB-medium (Tryptic Soy Broth; 7 g/L casein peptone (pancreas hydrolysate), 3 g/L soy peptone (papain hydrolysate), 2.5 g/L K<sub>2</sub>HPO<sub>4</sub>, 5 g/L NaCl, 2.5 g/L glucose, pH 7.3) was used for cultivation of *E. faecium*. 7H9-medium (Middlebrook 7H9 broth; 4.7 g/L 7H9 powder (0.5 g/L ammonium sulfate, 2.5 g/L Na<sub>2</sub>HPO<sub>4</sub>, 1 g/L KH<sub>2</sub>PO<sub>4</sub>, 0.5 g/L L-glutamic acid, 0.1 g/L sodium citrate, 0.05 g/L MgSO<sub>4</sub>, 0.04 g/L ferric ammonium citrate, 1 mg/L pyridoxine, 1 mg/L ZnSO<sub>4</sub>, 1 mg/L CuSO<sub>4</sub>, 0.5 mg/L CaCl<sub>2</sub>, 0.5 mg/L biotin), 2 mL/L glycerol, 2.5 mL/L 20% Tween 80, 5 g/L BSA (fraction V), 2 g/L dextrose, 850 mg/L NaCl, 3 mg/L catalase) was used for *M. bovis* and

*M. smegmatis* and 7H9-OADC-medium (7H9-medium supplemented with 25 mg/L oleic acid) for *M. tuberculosis*.

For cryostock preparation, fresh culture medium was inoculated (1:100) from the respective bacterial overnight culture (37°C, 200 rpm, 14 h) and incubated (37°C, 200 rpm) until the bacterial culture was in late log or stationary phase. Subsequently, bacteria were harvested by centrifugation (6,000 x g, 4°C, 10 min) and viable bacteria resuspended in fresh culture medium (max. one fourth of the original culture volume). Resulting bacterial suspension was aliquoted and transferred to sterile cryogenic vials, followed by the addition of glycerol (1:1 (v/v)). Bacterial cells were frozen in liquid nitrogen and stored at -80°C.

Overnight cultures were prepared by inoculating fresh culture medium from the respective cryostock (1:1000 (v/v)) and subsequent overnight incubation (37°C, 200 rpm, 14 h).

#### **4.2.2. Proteomics – Chapter 2: Insights into Photocrosslinker-Associated Off-Target Protein Binding**

##### **4.2.2.1. Analytical In Situ Affinity-Based Protein Profiling**

For analytical labelling, cells were seeded in 6-well plates (Nunc 6-well plate; *Thermo Fisher Scientific*) and grown to 90% confluence. After suction of the medium and washing with PBS, respective compound (10 µM; final DMSO concentration of 0.1%) in PBS (1 mL) were added. After incubation (37°C, 5% CO<sub>2</sub>, 1 h), the cells were irradiated with the appropriate UV lamps (*Philips* TL-D BLB UV lamps, 365 nm – diazirine and benzophenone containing probes; *Luzchem* LZC-UVB lamps, 300 nm – aryl azide containing probes) with ice cooling for 30 min. Cells were detached with a cell scraper, washed with PBS and lysed in lysis buffer (100 µL; 1% (v/v) NP40 and 1% (w/v) sodium deoxycholate in PBS; 4°C, 15 min). Following centrifugation (20,000 x g, 4°C, 15 min) the soluble fraction (supernatant) and insoluble fraction (pellet) were separated and the pellet resuspended in PBS (88 µL) followed by homogenization by sonication (10% intensity, 15 s; Sonopuls HD 2070 ultrasonic rod, *Bandelin electronic*). Both fractions were supplemented with 0.20 mM rhodamine-azide (10 mM stock in DMSO; *Base Click*; Rh-N<sub>3</sub>), 1.0 mM TCEP (52 mM stock in ddH<sub>2</sub>O) and 0.10 mM TBTA ligand (1.67 mM stock in 80% *tert*-BuOH and 20% DMSO). Samples were gently vortexed and the cycloaddition was initiated by the addition of 1.0 mM CuSO<sub>4</sub> (50 mM stock in ddH<sub>2</sub>O). After incubation at room temperature for 1 h, 2x SDS loading buffer (100 µL; 1:1 (v/v)) was added and the samples heated at 95°C for 10 min. For gel electrophoresis, 50 µL were applied per gel-lane on a SDS-PAGE gel (10% acrylamide). Fluorescence was recorded using a *Fujifilm* LAS 4000 luminescent image analyser with a *Fujinon* VRF43LMD3 lens and a 575DF20 filter.

#### 4.2.2.2. Preparative In Situ Affinity-Based Protein Profiling with Quantification via SILAC

“Heavy” and “light” A549 and HeLa cells were plated out on 15 cm dishes (*Sarstedt*) and grown (37°C, 5% CO<sub>2</sub>) to 90% confluence. The cells were washed with PBS, and either “heavy” or “light” cells were treated (37°C, 5% CO<sub>2</sub>, 1 h) with compound (3 μM) and the other isotopic label with the corresponding amount of DMSO (final DMSO concentration of 0.1%) in PBS (10 mL). Following irradiation with the appropriate UV lamps (*Philips* TL-D BLB UV lamps, 365 nm – diazirine and benzophenone containing probes; *Luzchem* LZC-UVB lamps, 300 nm – aryl azide containing probes) with ice cooling for 30 min, cells were detached with a cell scraper, washed with PBS and lysed in lysis buffer (1 mL; 1% (v/v) NP40 and 1% (w/v) sodium deoxycholate in PBS; 4°C, 15 min). Protein concentrations of the lysed cells were measured using a BCA assay kit (Roti Quant, *Carl Roth*) and equal protein amounts resulting from “heavy” or “light” cells incubated with probe and corresponding DMSO control of the opposite label were pooled and adjusted to a final volume of 1880 μL with PBS. The lysates, containing cytosolic and membrane proteins, were supplemented with 0.20 mM azide-PEG<sub>3</sub>-biotin conjugate (10 mM stock in DMSO; *Jena Bioscience*), 0.52 mM TCEP (52 mM stock in ddH<sub>2</sub>O) and 0.050 mM TBTA ligand (1.67 mM stock in 80% *tert*-BuOH and 20% DMSO). Samples were gently vortexed and the cycloaddition was initiated by the addition of 0.50 mM CuSO<sub>4</sub> (50 mM stock in ddH<sub>2</sub>O). The reaction mixtures were incubated at room temperature for 1 h. Proteins were precipitated by the addition of a 4-fold volume excess of acetone (8 mL) and incubated at -20°C overnight. Precipitated proteins were collected by centrifugation (16,000 x g, 4°C, 15 min), the supernatant discarded and the protein pellet washed two times with pre-chilled methanol (500 μL). Resuspension was achieved by sonication (10% intensity, 15 s; Sonopuls HD 2070 ultrasonic rod; *Bandelin electronic*). Subsequently, protein pellets were dissolved in 0.4% (w/v) SDS in PBS (1 mL) at room temperature by sonication (10% intensity, 15 s; Sonopuls HD 2070 ultrasonic rod; *Bandelin electronic*). For enrichment, avidin-agarose beads (50 μL; *Sigma-Aldrich*) were prepared by washing three times with 0.4% (w/v) SDS in PBS (1 mL). Protein solutions were added to the conditioned avidin-agarose beads and incubated under continuous inverting at 20 rpm and room temperature for 1 h. The beads were washed three times with 0.4% (w/v) SDS in PBS (1 mL), twice with 6 M urea in water (1 mL), and three times with PBS (1 mL). Here, all centrifugation steps were conducted at 400 x g for 2 min at room temperature. The proteins were reduced, alkylated and tryptically digested on-bead: The beads were resuspended in X-buffer (200 μL; 7 M urea, 2 M thiourea in 20 mM Hepes buffer pH 7.5), 1 mM DTT (1 M stock in ddH<sub>2</sub>O) was added, and incubated under gentle mixing at 25°C for 45 min. For alkylation 5.5 mM iodoacetamide (550 mM stock in ddH<sub>2</sub>O) were added and incubated under gentle mixing at room temperature for 30 min. The alkylation was stopped by the addition of 4 mM DTT (1 M stock in ddH<sub>2</sub>O) and incubation at

room temperature for 30 min under gentle mixing. For digest, 2.5 µg/mL LysC (0.5 mg/mL stock in ddH<sub>2</sub>O; *Wacko*) were added and the mixture incubated under gentle mixing at room temperature for 2 h. 50 mM TEAB buffer (600 µL) and trypsin (1.5 µL; 0.5 mg/mL stock; sequencing grade, modified; *Promega*) were added. The reaction was incubated overnight at 37°C and stopped by the addition of formic acid (0.1% final concentration). The resulting peptides were desalted and concentrated using SepPak C18 Vac cartridges (*Waters*): The C18 material was pre-treated with MeCN (1 mL), ddH<sub>2</sub>O/0.5% TFA (1 mL), 80% MeCN/0.5% FA (1 mL) and ddH<sub>2</sub>O/0.1% TFA (2 mL) prior to sample loading. The beads were pelleted and the peptide solution loaded to the cartridges. Peptides bound to the cartridges were washed with ddH<sub>2</sub>O/0.1% TFA (3 mL) and ddH<sub>2</sub>O/0.5% FA (1 mL) and eluted with 80% MeCN/0.5% FA (750 µL). The peptides were dried and stored at -80°C.

#### 4.2.2.3. Preparative In Situ Affinity-Based Protein Profiling with Label-Free Quantification

A549 cells were plated out on 15 cm dishes (*Sarstedt*) and grown (37°C, 5% CO<sub>2</sub>) to approximately 90% confluence. The medium was removed and the cells were washed with PBS. For competitive labelling experiments cells were pre-treated (37°C, 5% CO<sub>2</sub>, 1 h) with varying concentrations of **SP600125** (0.5 µM – competition 1/1; 5 µM – competition 1/10; 50 µM – competition 1/100) in PBS (10 mL). Subsequently, **SP600125p** (0.5 µM) was added and the cells were further incubated (37°C, 5% CO<sub>2</sub>) for 1 h. For all other labelling experiments, cells were treated (37°C, 5% CO<sub>2</sub>, 1 h) in either a “cocktail” approach containing a mixture of all diazirine containing minimal probes (**DA-1**, **DA-2**, **DA-3** and **DA-4**) in equal concentrations (final concentration of each probe 3 µM), **SP600125** in varying concentrations (0.125 µM, 0.5 µM and 3 µM) or DMSO (final DMSO concentrations of 0.1 – 1%) in PBS (10 mL). Following irradiation with appropriate UV lamps (*Philips* TL-D BLB UV lamps, 365 nm) on ice for 30 min (or 5, 10 and 20 min for time-dependent irradiation experiments with 0.5 µM **SP600125p**), cells were detached with a cell scraper, washed with PBS and lysed in lysis buffer (1 mL; 1% (v/v) NP40 and 1% (w/v) sodium deoxycholate in PBS; 4°C, 15 min). Protein concentrations of the lysed cells were measured using a BCA assay kit (Roti Quant; *Carl Roth*) and equal protein amounts were pooled and adjusted to a final volume of 500 µL. The lysates, containing cytosolic and membrane proteins, were supplemented with 0.20 mM azide-PEG<sub>3</sub>-biotin conjugate (10 mM stock in DMSO; *Jena Bioscience*), 0.52 mM TCEP (52 mM stock in ddH<sub>2</sub>O) and 0.050 mM TBTA ligand (1.67 mM stock in 80% *tert*-BuOH and 20% DMSO). Samples were gently vortexed and the cycloaddition was initiated by the addition of 0.50 mM CuSO<sub>4</sub> (50 mM stock in ddH<sub>2</sub>O). The reaction mixtures were incubated at room temperature for 1 h. Proteins were precipitated by the addition of a 4-fold volume excess of acetone (2 mL) and incubated at -20°C overnight. Precipitated proteins were collected by centrifugation

(16,000 x g, 15 min), the supernatant discarded and the protein pellet washed two times with pre-chilled methanol (200  $\mu$ L). Resuspension was achieved by sonication (10% intensity, 15 s; Sonopuls HD 2070 ultrasonic rod, *Bandelin electronic*). Subsequently, protein pellets were dissolved in 0.4% (w/v) SDS in PBS (1 mL) at room temperature by sonication (10% intensity, 15 s; Sonopuls HD 2070 ultrasonic rod; *Bandelin electronic*). For enrichment, avidin-agarose beads (50  $\mu$ L; *Sigma-Aldrich*) were prepared by washing three times with 0.4% (w/v) SDS in PBS (1 mL). Protein solutions were added to the conditioned avidin-agarose beads and incubated under continuous inverting at 20 rpm and room temperature for 1 h. The beads were washed three times with 0.4% (w/v) SDS in PBS (1 mL) and five times with PBS (1 mL). Here, all centrifugation steps were conducted at 400 x g for 2 min at room temperature. The proteins were reduced, alkylated and tryptically digested on-bead. Therefore, digestion buffer I (25  $\mu$ L; 5 ng/ $\mu$ L trypsin (0.5 mg/mL stock; sequencing grade, modified, *Promega*), 2 M urea, 1 mM DTT in 50 mM Tris-HCl buffer pH 8.0) was added to the beads and incubated at 25°C for 30 min. Then, digestion buffer II (100  $\mu$ L; 2 M urea, 5 mM iodoacetamide in 50 mM Tris-HCl buffer pH 8.0) was added to the beads, followed by incubation in the dark under gentle mixing at 25°C overnight. The reaction was stopped by the addition of formic acid (1% final concentration). The resulting peptides were desalted and concentrated using SepPak C18 Vac cartridges (*Waters*): The C18 material was pre-treated with MeCN (1 mL), 80% MeCN/0.5% FA (0.5 mL) and ddH<sub>2</sub>O/0.1% TFA (3 mL) prior to sample loading. The beads were pelleted and the peptide solution loaded to the cartridges. Peptides bound to the cartridges were washed with ddH<sub>2</sub>O/0.1% TFA (3 mL) and ddH<sub>2</sub>O/0.5% FA (0.25 mL) and eluted three times with 80% MeCN/0.5% FA (0.25 mL). The peptides were dried and stored at -80°C. All labelling experiments were performed in at least triplicate runs.

#### **4.2.2.4. Mass Spectrometry Setup and Settings**

Prior to LC-MS/MS measurements all peptide samples were reconstituted in ddH<sub>2</sub>O/1% FA (30  $\mu$ L), filtered using centrifugal filters (modified Nylon, 0.45  $\mu$ m, low protein binding; *VWR*) and transferred into LC-MS sample vials.

##### **4.2.2.4.1. Mass Spectrometry Setup and Settings for SILAC-Based Quantification**

Nanoflow LC-MS/MS analysis was performed with an UltiMate 3000 Nano HPLC system (*Thermo Fisher Scientific*) coupled to an Orbitrap Fusion (*Thermo Fisher Scientific*). Peptides were loaded on a trap column (Acclaim C18 PepMap100 75  $\mu$ m ID x 2 cm; *Thermo Fisher Scientific*), washed for 10 min with 0.1% FA and then transferred to an analytical column (Acclaim C18 PepMap RSLC, 75  $\mu$ m ID x 15 cm; *Thermo Fisher Scientific*) followed by separation using a 125 min gradient from 3% to 40% (120 min from 3% to 25% and 5 min to

40%) MeCN in 0.1% FA and 5% DMSO at a flow rate of 200 nL/min. Peptides were ionised using a nanospray source at 1.9 kV and a capillary temperature of 275°C. Orbitrap Fusion was operated in a top speed data-dependent mode with a cycle time of 3 s. Full scan acquisition (scan range of 300 – 1700 m/z) was performed in the orbitrap at a resolution of 120000 (at m/z 200) and with an automatic gain control ion target value of 4e5. Monoisotopic precursor selection as well as dynamic exclusion of 60 s were enabled. Internal calibration was performed using the ion signal of fluoranthene cations (EASY-ETD/IC source). Most intense precursors with charge states of 2 – 7 and intensities greater than 5e3 were selected for fragmentation. Isolation was performed in the quadrupole using a window of 1.6 m/z. Ions were collected to a target of 1e2 for a maximum injection time of 250 ms with “inject ions for all available parallelizable time” enabled (“universal” method, Eliuk et al., *Thermo Fisher Scientific* Poster Note PN40914). Fragments were generated using higher-energy collisional dissociation (HCD) and detected in the ion trap at a rapid scan rate.

#### **4.2.2.4.2. Mass Spectrometry Setup and Settings for Label-Free Quantification**

The LC-MS/MS setup and settings for label-free quantification were identical as applied for SILAC-based experiments (Chapter 4.2.2.4.1), with the following changes: HPLC gradient of 152 min (non-linear 5% to 32% MeCN over 115 min without DMSO), 300 nL/min; EASY-spray source with variable voltage; Acclaim Pepmap RSLC C18 column (75 µm x 50 cm; *Thermo Fisher Scientific*); 0.1% TFA loading buffer; scan range of 300 – 1500 m/z; MS<sup>1</sup> AGC-target of 2e5; MS<sup>2</sup> AGC-target of 1e4; and max. MS<sup>2</sup> injection time of 50 ms.

#### **4.2.2.5. Bioinformatics**

##### **4.2.2.5.1. Analysis of SILAC-Based Experiments**

Raw files were analysed using MaxQuant<sup>147</sup> software (version 1.5.1.2) with Andromeda<sup>148</sup> as the integrated search engine. Analysis included carbamidomethylation of cysteines as a fixed modification and oxidation of methionines and acetylation of protein N-termini as variable modifications. Trypsin was specified as the proteolytic enzyme with N-terminal cleavage to proline and two missed cleavages allowed. Precursor mass tolerance was set to 4.5 ppm (main search) and fragment mass tolerance to 0.5 Da. Searches were performed against the Uniprot database for *Homo sapiens* (taxon identifier: 9606, downloaded on 24.11.2014, including isoforms). The second peptide identification option was enabled. False discovery rate determination was carried out using a decoy database and thresholds were set to 1% FDR both at peptide-spectrum match and at protein levels. “I = L”, “requantification” and “match between runs” (0.7 min match and 20 min alignment time windows) options were enabled. Quantification of SILAC pairs was carried out based on unique peptides only using “Arg6” and

“Lys4” as “light” and “Arg10” and “Lys8” as “heavy” isotope identifiers requiring a minimum ratio count of 2. For raw files resulting from label switched experiments, the isotope identifiers were defined in reverse order resulting in ratios probe vs. DMSO. The mass spectrometry proteomics data have been deposited to the ProteomeXchange Consortium via the PRIDE<sup>233</sup> partner repository with the dataset identifier PXD004009.

Statistical analysis was performed with Perseus<sup>149</sup> software (version 1.5.1.6). Two biological replicates (forward SILAC + SILAC label switch) with three technical replicates each were used for statistics. The MaxQuant result table proteinGroups.txt was used for further analysis. Putative contaminants, reverse hits and only identified by site hits were removed. SILAC ratios were  $\log_2$ -transformed, hits with less than 3 valid values removed, the remaining ratios z-score normalised and  $-\log_{10}(p\text{-values})$  were obtained by a two-sided one sample Student's *t*-test over six replicates.

Diazirine overlays were generated from post-MaxQuant file merges. Protein groups with identical gene names within one file were excluded from analyses. A list with their identifiers and quantification results can be found at <http://www.oc2.ch.tum.de> (section Research / Resources / Data) in a supplementary Excel sheet. The proteinGroups.txt files were then compared by majority protein ID. In detail, to target the protein inference problem, an overlap of at least one majority protein ID was sufficient to account for a merge of respective protein groups. The program codes for redundancy checking and the merge can be found at [www.oc2.ch.tum.de](http://www.oc2.ch.tum.de) (section Research / Resources / Bioinformatics). Thus, for each combined protein group a maximum of 24 quantification values (six replicates x four probes) can be obtained. Putative contaminants, reverse sequences, only identified by site hits and protein groups with two or less valid values were filtered out. After  $\log_2$  transformation and z-score normalisation, the mean over all logarithmized ratios  $a$  with the respective sample size  $n$  was determined according to the principle of the geometric mean  $g$  (equation 1).

$$\log_2(g) = \log_2\left(\sqrt[n]{\prod_{i=1}^n a_i}\right) = \frac{1}{n} \sum_{i=1}^n \log_2(a_i) \quad (1)$$

Based on this mathematical operation, photocrosslinker-specific targets are summed up over all samples, while scaffold-specific protein groups reside in the noise. Additionally,  $p$ -values were gathered for each protein group from one-sample Student's *t*-tests against 0. The initial significance level of  $p = 0.05$  was adjusted by the multiple testing correction method of Benjamini and Hochberg (FDR = 0.05). Finally, the  $-\log_{10}$  of  $p$ -values were plotted against the  $\log_2$  of geometric mean  $g$ .

#### 4.2.2.5.2. Analysis of Label-Free Experiments

Raw files were analyzed using MaxQuant<sup>147</sup> software (version 1.5.3.8) with Andromeda<sup>148</sup> as the integrated search engine. Separate runs were performed for each distinct experiment (e.g. **SP600125p** AfBPP labelling at different photoprobe concentrations). Search parameters were adopted from SILAC analysis as described in Chapter 4.2.2.5.1, but without setting labels and without enabling the "requantify" option. LFQ was switched on with a (LFQ) minimum ratio count of 1. LFQ intensities were further analyzed with Perseus<sup>149</sup> software (version 1.5.3.2) as described in Chapter 4.2.2.5.1. Replicate groups were annotated and each experiment (e.g. **SP600125p** AfBPP labelling at 500 nM) was analyzed separately. Only proteins with two valid values in each group were used for missing value imputation from normal distribution (width: 0.3, down-shift: 1.8, total matrix). Finally, two-sample Student's *t*-tests including Benjamini-Hochberg multiple testing correction (FDR = 0.05) were performed. Proteins with the GOCC term "intrinsic to membrane" were denoted as membrane proteins.

### 4.2.3. Proteomics – Chapter 3: Discovery of a Small Molecule Antibiotic Active Against Multidrug-Resistant Gram-Positive Pathogens

#### 4.2.3.1. Target Deconvolution via Affinity-Based Protein Profiling

##### 4.2.3.1.1. General Experiment Procedure for Affinity-Based Protein Profiling

B-medium (100 mL) was inoculated (1:10) from a bacterial overnight culture (37°C, 200 rpm, 14 h). After incubation (37°C, 200 rpm) for 7 h, bacterial cells were harvested (6,000 x g, 4°C, 10 min), washed with PBS and viable bacterial cells were resuspended in PBS to a theoretical OD<sub>600</sub> of 40. For competition experiments, bacterial cells (0.5 mL aliquots) were preincubated (25°C, 700 rpm, 45 min) with **SFN** (0.5 mM) or DMSO only (final concentration of DMSO 1% during preincubation). After preincubation **SFNp** (10 or 50 µM) or minimal photoprobes (**DA-1**, **DA-2** or **DA-3**; 50 µM) or DMSO (final total concentration of DMSO 2%) were added, followed by incubation (25°C, 700 rpm) for 45 min. Subsequently, samples were diluted with PBS (5 mL final volume), transferred to petri dishes (5 cm radius; *Sarstedt*) and irradiated (*Philips* TL-D BLB UV lamps, 365 nm) for 30 min with ice cooling. Bacteria were harvested (6,000 x g, 4°C, 10 min) and washed with PBS. Cell pellets were resuspended in PBS (0.5 mL) containing a protease inhibitor cocktail (cOmplete Mini, EDTA-free, *Roche Diagnostics*) and lysed (6 x 5,500 rpm, 15 s, 2 min cooling breaks on ice after each run; Precellys Glass/Ceramic Kit SK38 2.0 mL tubes; Precellys 24 Homogenizer, *Bertin Technologies*). 300 µL of the lysate were transferred to 1.5 mL microcentrifuge tubes (*Eppendorf*) and treated (37°C, 700 rpm, 20 min) with 8 µg/mL lysostaphin (from *S. staphylolyticus*, *Sigma-Aldrich*). Separation of soluble and insoluble fraction was performed by centrifugation (21,000 x g, 4°C, 1 h). The insoluble fraction was washed twice with PBS using an ultrasonic rod (10% intensity, 10 s;

Sonopuls HD 2070, *Bandelin electronic*) for resuspension. Note that no separation of soluble and insoluble fractions was done for the investigation of analytical labelling (Chapter 3.2.2.2, Figure 3.2 A) and LC-MS/MS analysis of minimal photoprobes (**DA-1**, **DA-2** and **DA-3**; Chapter 3.2.2.3, Figure 3.4 C, D). Protein concentrations were determined using the *Pierce BCA Protein assay kit (Thermo Fisher Scientific, Pierce Biotechnology)* and samples normalized to equal protein amounts. For click chemistry, 300  $\mu$ L of the normalized soluble and insoluble fractions were treated with 60  $\mu$ M trifunctional linker (TFL, 10 mM stock in DMSO)<sup>128</sup>, 1 mM TCEP (52 mM stock in ddH<sub>2</sub>O), and 0.1 mM TBTA ligand (1.67 mM stock in 80% *tert*-BuOH and 20% DMSO). Samples were gently vortexed and the cycloaddition was initiated by the addition of 1 mM CuSO<sub>4</sub> (50 mM stock in ddH<sub>2</sub>O). The reaction mixtures were incubated at room temperature for 1 h. Proteins were precipitated by the addition of a 4-fold volume excess of acetone and incubated at -20°C overnight. Precipitated proteins were collected by centrifugation (16,900 x g, 4°C, 15 min), the supernatant discarded and the protein pellet washed twice with pre-chilled methanol (1 mL). Resuspension was achieved by sonication (10% intensity, 15 s; Sonopuls HD 2070 ultrasonic rod, *Bandelin electronic*). Subsequently, protein pellets were resuspended in 0.4% (w/v) SDS in PBS (0.5 mL) at room temperature by sonication (10% intensity, 15 s; Sonopuls HD 2070 ultrasonic rod, *Bandelin electronic*). For enrichment, avidin-agarose beads (50  $\mu$ L; *Sigma-Aldrich*) were prepared by washing three times with 0.4% (w/v) SDS in PBS (1 mL). Protein solutions were added to the conditioned avidin-agarose beads and incubated under continuous inverting at 20 rpm and RT for 1 h. Subsequently, the beads were washed three times with 0.4% (w/v) SDS in PBS (1 mL), two times with 6 M urea in water (1 mL) and three times with PBS (1 mL). All centrifugation steps were conducted at 400 x g for 2 min at room temperature.

#### **4.2.3.1.2. Gel-Based Analytical In Situ Affinity-Based Protein Profiling**

For gel-based analysis, protein samples were mixed (1:1 (v/v)) with 2x SDS loading buffer (125 mM Tris-HCl, 20% (v/v) glycerol, 4% (w/v) SDS, 0.005% (w/v) bromophenol blue, 10% (v/v) 2-mercaptoethanol) and separated by SDS-PAGE on a 4 – 12% Bis-Tris gel with 1x MOPS SDS Running Buffer (NuPAGE, *Thermo Fisher Scientific*). BenchMark Fluorescent Protein Standard (*Life Technologies*) and Pink Color Protein Standard II (prestained, *SERVA*) were used as size markers. An ImageQuant Las-4000 image reader (*GE Healthcare*) equipped with a *Fujinon* VRF43LMD3 lens and a 575DF20 filter was used for visualization of fluorescence labelled and enriched bands. Additionally, gels were stained with Coomassie brilliant blue.

#### 4.2.3.1.3. Gel-Free Preparative In Situ Affinity-Based Protein Profiling with Quantification via Dimethyl Labelling

For quantitative mass spectrometric analyses, avidin-beads with bound proteins (Chapter 4.2.3.1.1) were resuspended in denaturation buffer (200  $\mu$ L; 7 M urea, 2 M thiourea in 20 mM pH 7.5 HEPES buffer). Proteins were reduced on-bead with 5 mM TCEP (1 M stock in ddH<sub>2</sub>O) at 37°C for 1 h. Subsequent alkylation was performed with 10 mM iodoacetamide (IAA, 1 M stock in ddH<sub>2</sub>O) at 25°C for 30 min in the dark. Alkylation was quenched by the addition of 10 mM dithiothreitol (DTT; 1 M stock in ddH<sub>2</sub>O) and incubation at 25°C for 30 min. For digest, 2.5 ng/ $\mu$ L Lys-C (0.5 mg/mL stock in ddH<sub>2</sub>O; *Wacko*) was added to each sample, followed by incubation at 25°C for 2 h. Subsequently, the samples were diluted 1:4 with 50 mM TEAB buffer and digested with 3.75 ng/ $\mu$ L trypsin (0.5 mg/mL stock; sequencing grade, modified; *Promega*) at 37°C overnight. The reaction was stopped by adding formic acid (FA) to a final concentration of 0.5% (final pH 2 – 3). Peptides were desalted and labelled by stable isotope dimethyl labelling on-column using 50 mg SepPak C18 Vac cartridges (*Waters*). SepPak C18 cartridges were equilibrated with acetonitrile (1 mL), elution buffer (1 mL; 80% ACN, 0.5% FA) and three times ddH<sub>2</sub>O/0.5% FA (1 mL). Subsequently, protein samples were loaded by gravity flow, washed five times with ddH<sub>2</sub>O/0.5% FA (1 mL) and labelled with 5 mL of the respective dimethyl labelling solution. The following solutions were used: 30 mM NaBH<sub>3</sub>CN, 0.2% CH<sub>2</sub>O, 10 mM NaH<sub>2</sub>PO<sub>4</sub>, 35 mM Na<sub>2</sub>HPO<sub>4</sub>, pH 7.5 (“light” isotope (L)); 30 mM NaBH<sub>3</sub>CN, 0.2% CD<sub>2</sub>O, 10 mM NaH<sub>2</sub>PO<sub>4</sub>, 35 mM Na<sub>2</sub>HPO<sub>4</sub>, pH 7.5 (“medium” isotope (M)) and 30 mM NaBHD<sub>3</sub>CN, 0.2% <sup>13</sup>CD<sub>2</sub>O, 10 mM NaH<sub>2</sub>PO<sub>4</sub>, 35 mM Na<sub>2</sub>HPO<sub>4</sub>, pH 7.5 (“heavy” isotope (H)). For technical replicates isotopic labels were permuted. Labelled peptides were washed three times with ddH<sub>2</sub>O/0.5% FA (1 mL) and eluted with elution buffer (0.75 mL; 80% ACN, 0.5% FA). Differentially labelled peptides were mixed according to respective replicates for quantification and lyophilized using a vacuum centrifuge.

#### 4.2.3.1.4. Mass Spectrometry Setup and Settings

Prior to LC-MS/MS measurements all peptide samples were reconstituted in ddH<sub>2</sub>O/0.5% FA (50  $\mu$ L), filtered using centrifugal filters (modified Nylon, 0.45  $\mu$ m, low protein binding; *VWR*) and transferred into LC-MS sample vials.

Nanoflow LC-MS/MS analysis was performed with an UltiMate 3000 Nano HPLC system (*Thermo Fisher Scientific*) coupled to an Orbitrap Fusion (*Thermo Fisher Scientific*). Peptides were loaded on a trap column (Acclaim C18 PepMap100 75  $\mu$ m ID x 2 cm; *Thermo Fisher Scientific*), washed for 10 min with 0.1% FA and then transferred to an analytical column (Acclaim C18 PepMap RSLC, 75  $\mu$ m ID x 15 cm; for **DA-1** and **DA-2** experiments: 75  $\mu$ m ID x 50 cm; *Thermo Fisher Scientific*) followed by separation using a 120 min gradient from

3% to 25% ACN in 0.1% FA and 5% DMSO at 200 nL/min flow rate (for **DA-1** and **DA-2** experiments: 105 min gradient from 5% to 22% and a 10 min step from 22% to 32% ACN in 0.1% FA at 300 nL/min flow rate). LTQ Orbitrap Fusion was operated in a 3 second top speed data-dependent mode. Full scan acquisition was performed in the orbitrap at a resolution of 120000 and an ion target of 4e5 (for **DA-1** and **DA-2** experiments: 2e5) in a scan range of 300 – 1700 m/z (for **DA-1** and **DA-2** experiments: 2e5 and 300 – 1500 m/z). Monoisotopic precursor selection as well as dynamic exclusion for 60 s were enabled. Precursors with charge states of 2 – 7 and intensities greater than 5e3 were selected for fragmentation. Isolation was performed in the quadrupole using a window of 1.6 m/z. Precursors were collected to a target of 1e2 for a maximum injection time of 250 with “inject ions for all available parallelizable time” enabled (for **DA-1** and **DA-2** experiments: 1e4 AGC target and 50 ms maximum injection time). Fragments were generated using higher-energy collisional dissociation (HCD) and detected in the ion trap at a rapid scan rate. Internal calibration was performed using the ion signal of fluoranthene cations (EASY-ETD/IC source).

#### **4.2.3.1.5. Bioinformatics – Analysis of Affinity-Based Protein Profiling Experiments Based on Quantification via Dimethyl Labelling**

Raw files were analysed using MaxQuant<sup>147</sup> software (version 1.5.1.2) with Andromeda<sup>148</sup> as the integrated search engine. Analysis included the following parameters: Carbamidomethylation of cysteines as fixed and oxidation of methionine as dynamic modifications, trypsin/P as the proteolytic enzyme, 4.5 ppm for precursor mass tolerance (main search ppm) and 0.5 Da for fragment mass tolerance (ITMS MS/MS tolerance). Searches were performed against the Uniprot database for *S. aureus* NCTC 8325 (taxon identifier: 93061, downloaded on 02.12.2014; please note that SpsB (Q2FZT7) is not correctly annotated in the Uniprot Fasta-file as amino acids 1 – 36 are missing). Quantification was performed using following settings: DimethLys0, DimethNter0 (“light” isotopes), DimethLys4, DimethNter4 (“medium” isotopes) and DimethLys8, DimethNter8 (“heavy” isotopes) with a maximum of four labelled amino acids. “I = L”, “requantify” and “match between runs” (default settings) options were enabled. Identification was done with at least 2 unique peptides and quantification only with unique peptides. The mass spectrometry proteomics data have been deposited to the ProteomeXchange Consortium via the PRIDE<sup>233</sup> partner repository with the dataset identifier PXD008070.

For statistical analysis with Perseus<sup>149</sup> (version 1.5.3.2), three biological replicates consisting of three technical replicates each were analyzed for **SFNp**, competition experiments of **SFN** vs. **SFNp** and background labelling experiments with **DA-1** and **DA-2**. For **DA-3**, three biological replicates were prepared and analyzed. Putative contaminants, reverse hits and

proteins identified by side only were removed. Normalized protein ratios were  $\log_2(x)$  transformed and filtered to contain at least one valid value within the technical replicates. Ratios were z-score normalized within replicates and average values of technical replicates were calculated. Mean differences in enrichment and respective *p*-values were obtained by a two sided one sample *t*-test over the three biological replicates.

#### 4.2.3.2. Surfome and Secretome Analysis

##### 4.2.3.2.1. Experimental Procedure for the Preparation of Secretome Samples

Secretome analysis is based on a procedure published by Schallenberger et al..<sup>203</sup>

For preparation of overnight cultures, B-medium (50 mL) was inoculated from a respective cryostock (1:100) and incubated (37°C, 200 rpm) for 16 h. The overnight culture was diluted with fresh B-medium to an OD<sub>600</sub> of 0.1 (40 mL per biological replicate). After 5 h of growth (37°C, 200 rpm) OD<sub>600</sub> values were determined, bacterial cells harvested (3,000 x g, 4°C, 15 min) and washed with PBS. Viable bacterial cells were resuspended in fresh B-medium to a cell density of  $1.5 \times 10^9$  CFU/mL and aliquoted to samples of a final volume of 10 mL. Next, bacterial cells were incubated (37°C, 200 rpm, 1.5 h) with **SFN** or **SFN-C** (1.5 μM, 0.5 x MIC), **PK150** or **PK150-C** (0.15 μM, 0.5 x MIC) or DMSO in 50 mL falcon tubes (*Sarstedt*). OD<sub>600</sub> values were determined and serial dilutions plated on agar plates for cell number determination. Bacterial cells were pelleted by centrifugation (3,000 x g, 15 min and 6,000 x g, 5 min). The resulting pellets were saved for surfome analysis (Chapter 4.2.3.2.2). The resulting supernatants were filtered (0.22 μM filter, *VWR*) and proteins precipitated by the addition of 10% (w/v) trichloroacetic acid followed by overnight incubation at 4°C. Precipitated proteins were collected by centrifugation (9,000 x g, 15 min) and washed two times with 90% acetone. Protein pellets were dried in the open air and dissolved in 8 M urea in Tris buffer (50 mM, pH 8.0). Protein concentrations were determined using the *Pierce BCA Protein assay kit* (*Thermo Fisher Scientific, Pierce Biotechnology*) and samples normalized to equal protein amounts – no reduction in cell numbers was observed at a concentration of 0.5 x MIC as determined by CFU/mL. Proteins were reduced with 10 mM TCEP (1 M stock in ddH<sub>2</sub>O) at 37°C for 1 h. Subsequent alkylation was performed with 12.5 mM iodoacetamide (IAA; 1 M stock in ddH<sub>2</sub>O) at 25°C for 30 min in the dark. Alkylation was quenched by the addition of 12.5 mM dithiothreitol (DTT; 1 M stock in ddH<sub>2</sub>O) and incubation at 25°C for 30 min. For digest, 2.5 ng/μL Lys-C (0.5 mg/mL stock in ddH<sub>2</sub>O; *Wacko*) was added to each sample, followed by incubation at 25°C for 2 h. Subsequently, the samples were diluted 1:5 with 50 mM TEAB buffer and digested with 3.75 ng/μL trypsin (0.5 mg/mL stock; sequencing grade, modified; *Promega*) at 37°C overnight. The reaction was stopped by adding formic acid (FA) to a final concentration of 0.5% (final pH 2 – 3). Peptides were desalted on-column using 50 mg SepPak

C18 Vac cartridges (*Waters*). SepPak C18 cartridges were equilibrated with acetonitrile (1 mL), elution buffer (1 mL; 80% ACN, 0.5% FA) and three times ddH<sub>2</sub>O/0.5% FA (1 mL). Subsequently, protein samples were loaded by gravity flow, washed three times with ddH<sub>2</sub>O/0.5% FA (1 mL), eluted with elution buffer (0.5 mL, 80% ACN, 0.5% FA) and lyophilized using a centrifugal vacuum concentrator (*Eppendorf*).

#### 4.2.3.2.2. Experimental Procedure for the Preparation of Surfome Samples

Surfome analysis is based on a procedure published by Ventura et al.<sup>234</sup>

Bacterial cell pellets resulting from secretome analysis (Chapter 4.2.3.2.1) were washed three times with 50 mM Tris-HCl pH 7.4 (centrifugation at 3,000 x g, 4°C, 15 min) and carefully resuspended in hydrolysis buffer (0.4 mL; 50 mM Tris-HCl pH 7.4, 0.6 M sucrose). OD<sub>600</sub> values were adjusted to equal turbidity and equal volumes with hydrolysis buffer (50 mM Tris-HCl pH 7.4, 0.6 M sucrose). Surface proteins were shaved with trypsin (15 µg; 0.5 mg/mL stock; sequencing grade, modified; *Promega*) at 37°C for 25 min under continuous inverting at 20 rpm. The digest was stopped by cooling on ice for 5 min. Supernatants were collected by centrifugation (1,000 x g, 4°C, 15 min) and filtrated (0.22 µm mesh; *VWR*) in order to eliminate residual bacterial cells. Protein concentrations were determined using the *Pierce* BCA Protein assay kit (*Thermo Fisher Scientific, Pierce Biotechnology*) and samples normalized to equal protein amounts. Proteins were reduced with 10 mM TCEP (1 M stock in ddH<sub>2</sub>O) at 37°C for 1 h. Subsequent alkylation was performed with 12.5 mM iodoacetamide (IAA; 1 M stock in ddH<sub>2</sub>O) at 25°C for 30 min in the dark. Alkylation was quenched by the addition of 12.5 mM dithiothreitol (DTT; 1 M stock in ddH<sub>2</sub>O) and incubation at 25°C for 30 min. For digest, 2.5 ng/µL Lys-C (0.5 mg/mL stock in ddH<sub>2</sub>O; *Wako*) was added to each sample, followed by incubation at 25°C for 2 h. Subsequently, the samples were diluted 1:5 with 50 mM TEAB buffer and digested with 3.75 ng/µL trypsin (0.5 mg/mL stock; sequencing grade, modified; *Promega*) at 37°C overnight. The reaction was stopped by adding formic acid (FA) to a final concentration of 0.5% (final pH 2 – 3). Peptides were desalted on-column using 50 mg SepPak C18 Vac cartridges (*Waters*). SepPak C18 cartridges were equilibrated with acetonitrile (1 mL), elution buffer (1 mL; 80% ACN, 0.5% FA) and three times ddH<sub>2</sub>O/0.5% FA (1 mL). Subsequently, protein samples were loaded by gravity flow, washed three times with ddH<sub>2</sub>O/0.5% FA (1 mL), eluted with elution buffer (0.5 mL, 80% ACN, 0.5% FA) and lyophilized using a centrifugal vacuum concentrator (*Eppendorf*).

#### 4.2.3.2.3. Mass Spectrometry Setup and Settings

Prior to LC-MS/MS measurements all peptide samples were reconstituted in ddH<sub>2</sub>O/0.5% FA (50 µL), filtered using centrifugal filters (modified Nylon, 0.45 µm, low protein binding; VWR) and transferred into LC-MS sample vials.

Nanoflow LC-MS/MS analysis was performed with an UltiMate 3000 Nano HPLC system (*Thermo Fisher Scientific*) coupled to an Orbitrap Fusion (*Thermo Fisher Scientific*). Peptides were loaded on a trap column (Acclaim C18 PepMap100 75 µm ID x 2 cm; *Thermo Fisher Scientific*), washed for 10 min with 0.1% FA and then transferred to an analytical column (Acclaim C18 PepMap RSLC, 75 µm ID x 50 cm) followed by separation using a 105 min gradient from 5% to 22% and a final 10 min step from 22% to 32% ACN in 0.1% FA at 300 nL/min flow rate. LTQ Orbitrap Fusion was operated in a 3 second top speed data-dependent mode. Full scan acquisition was performed in the orbitrap at a resolution of 120000 and an ion target of 2e5 in a scan range of 300 - 1500 m/z. Monoisotopic precursor selection as well as dynamic exclusion for 60 s were enabled. Precursors with charge states of 2 – 7 and intensities greater than 5e3 were selected for fragmentation. Isolation was performed in the quadrupole using a window of 1.6 m/z. Precursors were collected to a target of 1e4 for a maximum injection time of 50 with “inject ions for all available parallelizable time”. Fragments were generated using higher-energy collisional dissociation (HCD) and detected in the ion trap at a rapid scan rate. Internal calibration was performed using the ion signal of fluoranthene cations (EASY-ETD/IC source).

#### 4.2.3.2.4. Bioinformatics – Analysis of Secretome and Surfome Data

Raw files were analysed using MaxQuant<sup>147</sup> software (version 1.5.1.2) with Andromeda<sup>148</sup> as the integrated search engine. Analysis included the following parameters: Carbamidomethylation of cysteines as fixed and oxidation of methionine as dynamic modifications, trypsin/P as the proteolytic enzyme, 4.5 ppm for precursor mass tolerance (main search ppm) and 0.5 Da for fragment mass tolerance (ITMS MS/MS tolerance). Searches were performed against the Uniprot database for *S. aureus* NCTC 8325 (taxon identifier: 93061, downloaded on 08.05.2014). Quantification was performed using MaxQuant's LFQ algorithm. The “I = L”, “requantify” and “match between runs” (default settings) options were enabled. Identification was done with at least 2 unique peptides and quantification only with unique peptides. The mass spectrometry proteomics data have been deposited to the ProteomeXchange Consortium via the PRIDE<sup>233</sup> partner repository with the dataset identifier PXD008070.

For statistical analysis with Perseus<sup>149</sup> (version 1.5.1.6), four biological replicates were analyzed. Putative contaminants, reverse hits and proteins, identified by side only, were

removed. LFQ intensities were  $\log_2(x)$  transformed and filtered to contain minimum three valid values in at least one condition. Missing values were imputed on the basis of a normal distribution (width = 0.3, down-shift = 1.8). *P*-values were obtained by a two sided two-sample *t*-test over the three biological replicates.

Annotation enrichment analysis was performed by alignment with the database for annotation, visualization and integrated discovery (DAVID; v6.8). Proteins with an accumulation of  $\log_2$ -fold > 0.5 in secretomes for compound- vs. control-treated samples were selected for analysis and the complete measured secretome was used as background.

Peptidoglycan hydrolase domain-containing proteins were annotated using the Pfam protein family database<sup>150</sup> via the entries PF05257 (CHAP domain), PF01510 and PF01520 (*N*-acetylmuramoyl-L-alanine amidase), PF01464 (transglycosylase SLT domain), PF06737 (transglycosylase-like domain), PF01832 (mannosyl-glycoprotein endo-beta-*N*-acetylglucosaminidase) and PF01551 (peptidase family M23). Enrichment analysis was performed manually via a Fisher's Exact test.<sup>235-236</sup>

#### **4.2.3.3. Kinase Selectivity Profiling via the Kinobead Technology**

Kinobead selectivity profiling experiments were performed by Maria Reinecke in the laboratories of Prof. Dr. Bernhard Küster, Chair of Proteomics and Bioanalytics, Technische Universität München, Germany.

##### **4.2.3.3.1. Experimental Procedure of the Preparation of Kinobead Samples**

Kinobeads selectivity profiling of sorafenib and **PK150** was performed as described previously.<sup>213</sup> Briefly, 5 mg of a protein mixture of four cancer cell lines (K562, Colo205, SKNBE2 and MV4 11) were incubated (end-over-end shaker, 4°C, 45 min) with compound dilutions in DMSO (3 nM, 10 nM, 30 nM, 100 nM, 300 nM, 1  $\mu$ M, 3  $\mu$ M, 30  $\mu$ M). DMSO was used as control. After preincubation the mixtures were incubated (end-over-end shaker, 4°C, 30 min) with kinobeads (35  $\mu$ l settled beads). After washing, bound proteins were eluted with LDS sample buffer (NuPAGE, *Invitrogen*) containing DTT (50 mM). For the calculation of a correction factor, the flowthrough of the DMSO control was incubated with fresh beads for a second time (pull-down of pull-down). Reduced eluates were alkylated with chloroacetamide (55 mM) and the proteins were desalted and concentrated by a short electrophoresis on a 4 – 12% NuPAGE gel (*Invitrogen*). In-gel digestion was performed according to the standard protocol.

#### 4.2.3.3.2. Mass Spectrometry Setup and Settings

Peptides generated by in-gel trypsin digestion were analyzed via LC-MS/MS on a Dionex Ultimate3000 nano HPLC coupled online to an Orbitrap HF (*Thermo Fisher Scientific*) mass spectrometer. Peptides were delivered to a trap column (100  $\mu\text{m}$  x 2 cm, packed in house with Reprosil-Gold C18 ODS-3 5  $\mu\text{m}$  resin, *Dr. Maisch HPLC*) at a flow rate of 5  $\mu\text{L}/\text{min}$  in solvent  $A_0$  (0.1% FA in HPLC grade  $\text{H}_2\text{O}$ ). Peptides were then separated on an analytical column (75  $\mu\text{m}$  x 40 cm, packed in house with Reprosil-Gold C18 3  $\mu\text{m}$  resin, *Dr. Maisch HPLC*) using a 52 min gradient ranging from 5 – 33% solvent B (0.1% FA, 5% DMSO in ACN) in solvent  $A_1$  (0.1% FA, 5% DMSO in HPLC grade  $\text{H}_2\text{O}$ ) at a flow rate of 300 nL/min. The mass spectrometer was operated in data-dependent mode, automatically switching between MS and  $\text{MS}^2$  spectra.  $\text{MS}^1$  spectra were acquired at a resolution of 60,000 (at  $m/z$  200) in the Orbitrap using a maximum injection time of 10 ms and an AGC target value of  $3e6$ . Up to 12 peptide precursors were isolated (isolation width of 1.7 Th, maximum injection time of 75 ms, AGC value of  $2e5$ ) and fragmented by HCD using 25% CE and analyzed in the Orbitrap at a resolution of 15,000. The dynamic exclusion duration of fragmented precursor ions was set to 30 s.

#### 4.2.3.3.3. Bioinformatics – Analysis of Kinobeads Selectivity Profiling Data

Peptide and protein quantification was performed using MaxQuant<sup>147</sup> software (version 1.5.3.30) by searching the tandem MS data against all canonical protein sequences as annotated in the Swissprot reference database (20193 entries, downloaded 22.03.2016, annotated in-house with Pfam domains) using the embedded search engine Andromeda<sup>148</sup>. Carbamidomethylated cysteine was used as a fixed modification, phosphorylation of serine, threonine and tyrosine, oxidation of methionine, and N-terminal protein acetylation as variable modifications. Trypsin/P was specified as the proteolytic enzyme and up to two missed cleavage sites were allowed. Label-free quantification and match between runs were enabled within the MaxQuant<sup>147</sup> software. Search results were filtered for a minimal length of seven amino acids, 1% peptide and protein FDR as well as common contaminants and reverse identifications.

For competition binding assays,  $\text{EC}_{50}$  values were determined based on the LFQ intensity ratio to the DMSO control for every single dose point by nonlinear regression with variable slope using an in-house pipeline.<sup>237</sup>  $K_d^{\text{app}}$  was then calculated by multiplying the  $\text{EC}_{50}$  with a correction factor for each protein. The correction factor  $r$  for a protein is defined as the ratio of the amount of protein captured from two consecutive pull-downs of the same DMSO control lysate.<sup>238</sup> Targets of the inhibitors were annotated manually. A protein was considered as target if the resulting binding curve showed a sigmoidal curve shape with a dose-dependent decrease of binding to the beads. Furthermore, unique peptides and MS/MS-counts as well as peptide

and MS/MS behavior with increasing dosage were taken into account. Proteins, which only showed an effect at the highest inhibitor concentration were not annotated as target.

#### **4.2.4. Biochemical Procedures and Microbiology – Chapter 3: Discovery of a Small Molecule Antibiotic Active Against Multidrug-Resistant Gram-Positive Pathogens**

All kinase inhibitors within the screened library are available from commercial vendors (*SelleckChem* and *Sigma-Aldrich*). *SelleckChem*'s kinase inhibitor library was a kind gift from Prof. Dr. Bernhard Küster, Chair of Proteomics and Bioanalytics, Technische Universität München, Germany. Arylomycin A4 was a kind gift from Prof. Dr. Stephanie Grond, Chair of Organic Chemistry and Natural Product Analytics, Eberhard Karls Universität Tübingen, Germany.

##### **4.2.4.1. Minimum Inhibitory Concentration Assay**

The minimum inhibitory concentration (MIC) represents the lowest concentration of an antibiotic that inhibits the visible growth of a microorganism after 24 h incubation, and was obtained by a 96-well plate-based assay (transparent Nunc flat-bottomed 96-well plate; *Thermo Fisher Scientific*) with serial dilutions of the compounds tested. In case of *S. aureus*, B-medium was inoculated from a bacterial overnight culture (1:100) and incubated (37°C, 200 rpm) until the culture reached an OD<sub>600</sub> of 0.4 – 0.6. Bacteria were diluted in fresh medium to a cell number of 10<sup>5</sup> CFU/mL. For all other bacterial species tested, medium was inoculated from corresponding bacterial overnight cultures (1:10000) and directly used for testing. Compounds at various concentrations were added to diluted bacterial cultures (1:100, 100 µL/well final volume; final assay concentration of DMSO from compound stocks 1%) in triplicates. A growth control containing DMSO only and a sterile control containing fresh medium were included. After incubation (37°C, 200 rpm, 16 – 24 h), the dilution series was analysed for microbial growth, usually indicated by turbidity and/or a pellet of bacteria at the bottom of the well. The lowest concentration within the dilution series at which no growth of bacteria could be observed by eye was defined as the MIC of the compound. MIC values were determined by three independent experiments.

For transposon mutants, precultures were grown in the presence of erythromycin (5 µg/mL), whereas the MIC assay itself was performed without erythromycin to avoid interfering effects.

For *M. bovis* and *M. tuberculosis* strains, the MIC value was determined as follows: A culture of stationary phase growing bacteria was diluted to a final OD<sub>600</sub> of 0.001 in 7H9-medium (7H9-medium for *M. bovis* and 7H9-OADC for *M. tuberculosis*; note that for MIC determination medium did not contain Tween 80). Diluted bacteria (100 µL/well) were added

to the wells of a sterile 96-well microtitre plate containing two-fold serial dilutions of compound in growth medium (100 µL/well) Control wells were prepared with culture medium and bacterial suspension only. The microtitre plates were sealed with a water impermeable membrane and incubated at 37°C. To determine the growth of mycobacteria a 0.02% resazurin solution (100 µL/well) was added (after 5 – 7 days for *M. tuberculosis*). A color change from purple to pink within 2 to 4 days indicated viable cells, while purple colored wells suggested no bacterial growth. MIC values were determined by three independent experiments.

Please note that microbiological experiments involving mycobacteria were performed by Dr. Johannes Lehmann and/or Shoko Minami in the laboratories of Prof. Dr. Eric Rubin, Department of Immunology and Infectious Diseases, Harvard School of Public Health, Boston, USA.

#### 4.2.4.2. Cloning, Expression and Purification of Full-Length SpsB

For cloning the *Invitrogen* Gateway Technology (*Life Technologies Corp.*) was used. The SpsB gene was amplified by PCR from *S. aureus* NCTC 8325 (taxid: 93061) using genomic DNA as template and the Phusion High-Fidelity DNA Polymerase (*New England Biolabs*) according to the manufacturer's instruction. Genomic DNA was prepared using the peqGOLD Bacterial DNA Kit (*VWR Peqlab*) according to the manufacturer's instruction, but with lysostaphin (0.1 mg/mL, from *S. staphylolyticus*, *Sigma-Aldrich*) instead of lysozyme. Primers (*Eurofins Genomics*) were designed based on the GenBank entry CP000253.1, in which the rare ATA (coding the amino acid isoleucine) codon was exchanged to TTA (coding the amino acid leucine) and the sequences were equipped with *attB1*- and *attB2*-sites for Gateway cloning. The PCR product was integrated into the donor vector pDONR207 (*Invitrogen*) using the BP Clonase II Enzyme Mix (*Thermo Fisher Scientific*) and subsequently transformed into chemically competent *E. coli* TOP10 (*Invitrogen*). Plasmid DNA was purified using the E.Z.N.A. Plasmid Mini Kit I (*Omega Bio-tek*). fl-SpsB was cloned into the destination vector pET-55-DEST (*Novagen*) by the LR Clonase II Enzyme Mix (*Thermo Fisher Scientific*) and transformed into chemically competent *E. coli* BL21(DE3)pLysS (*Promega*). Plasmid DNA was purified and the sequence verified via Sanger sequencing (*GATC Biotech*).

Primer sequences for the cloning of fl-SpsB are as follows – *AttB1*- and *attB2*-sequences are underlined; the TEV cleavage site sequence is presented in italics; the replacement of the rare ATA- to TTA-codon is highlighted in bold letters; and capital letters indicate consensus sequence with the SpsB genetic code (with the exception of the replacement of ATA by TTA):

Forward: 5'-ggggacaagtttgtacaaaaagcaggcttgagaatctttattttcagggcAAAAAGAA  
TTATTGGAATGGATTATT-3'

Reverse: 5'-ggggaccactttgtacaagaagctgggtgTTAATTTTTAGTATTTTCAGGatt-3'

Plasmids used for the cloning of fl-SpsB:

pDONR207: *rrnB* T2, *rrnB* T1, *attP1*, *ccdB*, Cm<sup>R</sup>, *attP2*, Gm<sup>R</sup>, pUC ori, Gateway donor vector (*Invitrogen*).

pDONR207-fl-SpsB: *rrnB* T2, *rrnB* T1, *attL1*, *attL2*, Gm<sup>R</sup>, pUC ori, fl-SpsB cloned into *attP1* and *attP2* sites of pDONR207, entry clone.

pET-55-DEST: *attR1*, *ccdB*, Cm<sup>R</sup>, *attR2*, Amp<sup>R</sup>, *lacI*, pUC ori, T7 promoter, *Strep*-tag II sequence (N-terminal), Gateway Nova destination vector (*Invitrogen*).

pET-55-DEST-fl-SpsB: *attB1*, *attB2*, Amp<sup>R</sup>, *lacI*, pUC ori, T7 promoter, *Strep*-tag II sequence (N-terminal), fl-SpsB cloned into *attR1* and *attR2* sites of pET-55-DEST, expression clone.

Expression and purification protocols were adapted from Rao et al.<sup>190</sup> *E. coli* BL21(DE3)pLysS harboring pET-55-DEST-fl-SpsB were grown (37°C, 200 rpm) in LB-medium to an OD<sub>600</sub> of 0.5 – 0.6. To induce overexpression, isopropyl β-D-1-thiogalactosidase (IPTG; 0.5 mM) was added. After incubation (22°C, 200 rpm, 3 h) cells were harvested by centrifugation (5,000 x g, 4°C, 10 min) and washed with PBS.

For purification of the recombinant protein from the insoluble fraction, cells were resuspended in Tris-HCl (50 mM, pH 8; supplemented with 20% sucrose and a protease inhibitor cocktail (cOmplete Mini, EDTA-free; *Roche Diagnostics*)), treated with DNase I (5 μg/mL; *AppliChem*) and lysed via high-pressure homogenization (1.7 kbar) and ultrasonication (80% intensity, ice-cooling, 5 min; Sonopuls HD 2070 ultrasonic rod; *Bandelin electronic*). Cell debris was removed by centrifugation (12,000 x g, 4°C, 10 min) and the insoluble fraction containing recombinant fl-SpsB was obtained by centrifugation of the supernatant (45,000 x g, 4°C, 2 h). The resulting membrane pellet was resuspended in binding buffer (100 mM Tris, 150 mM NaCl, 1 mM EDTA and 0.5% Triton X-100), centrifuged (10,000 x g, 4°C, 5 min) to remove insoluble contaminations and the resulting supernatant transferred onto a StrepTrap HP column (*GE Healthcare Life Sciences*). The column was washed with eight column volumes washing buffer (100 mM Tris, 150 mM NaCl, 1 mM EDTA and Triton X-100 (0.05% (v/v))) and eluted with washing buffer containing d-desthiobiotin (2.5 mM, *IBA*).

For purification of the recombinant protein from the cytosolic fraction, the supernatant of the 2 h centrifugation step (45,000 x g, 4°C, 2 h) was directly injected onto a StrepTrap HP column (*GE Healthcare Life Sciences*). Purification was performed as described above with the exception that Triton X-100 was not supplemented to the buffers.

#### 4.2.4.3. Preparation of Membrane Fractions from the *Escherichia Coli* SpsB Expression Strain and *Staphylococcus Aureus* NCTC 8325

For preparation of *E. coli* membrane fractions, growth and induction of BL21(DE3)pLysS cells harboring pET-55-DEST-fl-SpsB were performed as described in Chapter 4.2.4.2.

For preparation of *S. aureus* NCTC 8325 membrane fractions, cells were grown (37°C, 200 rpm) in B-medium to stationary phase after inoculation from a respective overnight culture (1:100).

The preparation of membrane fractions was adapted from Therien et al.<sup>182</sup> *E. coli* and *S. aureus* cells were harvested (12,000 x g, 4°C, 10 min) and lysed using a bead beater homogenizer (6 x 5500 rpm, 15 s, 2 min cooling breaks on ice after each run; Precellys Ceramic Kit CK01L, 7.0 mL tubes; Precellys 24 Homogenizer; *Bertin Technologies*). The lysate was centrifuged (12,000 x g, 4°C, 10 min) to remove intact cells and debris. Membranes were collected from the resulting supernatant (39,000 x g, 4°C, 75 min) and resuspended in cold sodium phosphate buffer (50 mM, pH 7.5). Protein concentrations were determined using the Pierce BCA Protein assay kit (*Thermo Fisher Scientific, Pierce Biotechnology*).

#### 4.2.4.4. FRET-Based In Vitro Peptidase Activity Assay

SpsB activities were measured by a FRET-based peptidase assay as described by Rao et al.<sup>190</sup> A synthetic peptide based on known SpsB substrate SceD modified by 4-(4-dimethylaminophenylazo)benzoic acid (DABCYL) and 5-((2-aminoethyl)amino)-1-naphthalene sulfonic acid (EDANS) was used as a fluorogenic substrate (DABCYL-AGHDAHASET-EDANS, *AnaSpec*). Assays were performed with membranes from induced and not induced *E. coli* BL21(DE3)pLysS harboring pET-55-DEST-fl-SpsB (50 µg/mL total membrane protein concentration; Chapter 4.2.4.3), membranes from *S. aureus* NCTC 8325 (200 µg/mL total membrane protein concentration; Chapter 4.2.4.3) or purified fl-SpsB (0.2 µM protein concentration; purified from the soluble fraction; Chapter 4.2.4.2) in sodium phosphate buffer (50 mM, pH 7.5).

Membranes containing endogenous or recombinant SpsB (100 µL/well final volume; sodium phosphate buffer, 50 mM, pH 7.5; opaque Nunc flat-bottomed 96-well plate; *Thermo Fisher Scientific*) were treated (37°C, 5 min) with varying concentrations of the respective compound or DMSO (final assay concentration of DMSO from compound stocks 1%). For SpsB stability assays, *S. aureus* NCTC 8325 membranes or recombinant SpsB were incubated at 37°C for 10 min or 1 h prior to substrate addition. After addition of the fluorogenic substrate (10 µM final substrate concentration; final DMF concentration from substrate stock 1%) fluorescence turnover was monitored by a *Tecan* Infinite 200Pro plate reader (340 nm

excitation and 510 nm emission wavelengths, fluorescence top reading mode) at 37°C. Initial substrate cleavage velocities were determined (linear range), normalized to DMSO-treated samples (for *E. coli*, data was normalized to DMSO-treated samples of induced membranes) and plotted against respective compound concentrations. Curves were fitted by the nonlinear Hill1 function ( $y=START+(END-START)*x^n/(k^n+x^n)$ ; OriginPro 9.1G, *OriginLab*). *P*-values for substrate turnover enhancement were determined for compound concentrations of 10 µM using an unpaired parametric *t*-test.

#### 4.2.4.5. Cell Permeability Assay

For determination of cell wall permeability,<sup>239</sup> *S. aureus* NCTC 8325 was grown to an OD<sub>600</sub> of 0.4 to 0.5, harvested (6,000 x g, 10 min) and washed with 5 mM HEPES-NaOH (pH 7.2) and 5 mM glucose. Pellets were resuspended in the same buffer to an OD<sub>600</sub> of 0.4, aliquots a 100 µL were transferred to a 96-well plate (opaque Nunc flat-bottomed 96-well plate; *Thermo Fisher Scientific*) and incubated (37°C, 15 min) with propidium iodide (10 µM). During incubation fluorescence (535 nm excitation and 617 nm emission wavelength) was measured at 37°C with a *Tecan* Infinite M200 Pro microplate reader to ensure that propidium iodide had been fully integrated into bacterial membranes. After the addition of compounds, the measurement was continued for 1 h. Benzalkonium chloride (BAC; 100 µg/mL) and daptomycin (DAP; 16 µg/mL with 50 µg/mL CaCl<sub>2</sub>) were used as positive controls.

#### 4.2.4.6. Bacterial Killing Kinetics

Time-kill experiments were performed as described by Smith and Romesberg.<sup>188</sup> Briefly, an overnight culture of *S. aureus* NCTC 8325 was diluted to an OD<sub>600</sub> of 0.025 and grown (37°C, 200 rpm) to mid-logarithmic phase (OD<sub>600</sub> = 0.4 – 0.5). Subsequently, cells were diluted to 1x10<sup>6</sup> CFU/mL in B-medium and aliquoted a 3 mL in 15 mL falcon tubes (*Sarstedt*) containing DMSO, **SFN** (24, 6 and 3 µM final concentration) or **PK150** (0.24, 0.6 and 0.3 µM final concentration). Cells were incubated (37°C, 200 rpm), serially diluted and plated on agar plates at indicated time points for the determination of viable cell numbers (CFU/mL). Additionally, time-kill experiments were performed with stationary-phase bacteria in the presence of tetracycline (bacteriostatic translational inhibitor; 1 µM) to arrest cell growth.

#### 4.2.4.7. Persister Cell Assay

Two assays with different experimental conditions were performed to corroborate effects of **PK150** treatment on persisters.

Persister cell assay I was based on a procedure by Conlon et al.<sup>193</sup> and Kim et al.<sup>194</sup>, with slight modifications. TSB-medium (17 g/L casein peptone, pancreas hydrolysate, 3 g/L soy peptone (papain hydrolysate), 2.5 g/L di-potassium hydrogen phosphate, 5 g/L sodium chloride, 2.5 g/L glucose monohydrate, pH 7.3 ± 0.2; CASO Broth, *Carl Roth*) was inoculated (1:1000) with *S. aureus* NCTC 8325 cells from an exponentially growing culture ( $OD_{600} = 0.4 - 0.5$ ) and incubated (37°C, 200 rpm) for 15 h. Cells were serially diluted and plated on agar plates to determine viable cell numbers before treatment. Persisters were prepared by treatment (37°C, 200 rpm, 4 h) with gentamicin (20 µg/mL, 40 x MIC). A H<sub>2</sub>O-treated control culture was incubated in parallel. Persisters and control cells were washed three times with PBS (5,000 x g, 5 min) and diluted to an  $OD_{600}$  of 4 in PBS. Serial dilutions were prepared for determination of CFU/mL on agar plates. **PK150** (2.4 µM, 8 x MIC), **SFN** (24 µM, 8 x MIC) or ciprofloxacin (5 µg/mL, 20 x MIC) were added to 10 mL aliquots of diluted persisters in 100 mL flasks (1:1000; final assay concentration of DMSO from compound stocks 1%) and incubated (37°C, 200 rpm) for 70 h. At indicated time points, samples (1 mL) were withdrawn and corresponding bacteria harvested (10,000 x g, 3 min), washed with PBS (1 mL) and resuspended in PBS (1 or 0.1 mL) for the determination of CFU/mL by plating serial dilutions on agar plates. Three biological replicates were prepared and means, standard deviations and *p*-values (unpaired parametric *t*-test) were determined with Prism (GraphPadPrism v6.05, GraphPad Software).

Persister cell assay II was based on a procedure by Springer et al.<sup>240</sup> Briefly, TSB-medium (50 mL in 250 mL culture flasks) was inoculated (1:1000) with an overnight culture of *S. aureus* NCTC 8325 and grown (37°C, 200 rpm) to an  $OD_{600}$  of 4 or 11 (20 h). Serial dilutions were prepared and plated on agar plates to determine viable cell numbers of the inoculum. The cultures were aliquoted a 1 mL and treated with either oxacillin (OXA; 30 µg/mL, 30 x MIC) combined with ciprofloxacin (CIPRO; 5 µg/mL, 20 x MIC) or combined with compounds to be tested (**PK150** or **PK150-C**, 2.4 µM, 8 x MIC; **SFN** or **SFN-C**, 24 µM, 8 x MIC) or compounds to be tested only (37°C, 200 rpm, 20 or 70 h). Cells were harvested, washed two times with PBS (10,000 x g, 3 min), serially diluted and plated on agar plates for determination of surviving cell numbers.

#### 4.2.4.8. Biofilm Eradication and Inhibition Assay

Biofilm studies were performed by Dr. Megan C. Jennings and Prof. Dr. William M. Wuest at the Department of Chemistry, Temple University, Philadelphia, USA.

For determination of minimum biofilm eradication concentrations (MBEC), overnight cultures of *S. aureus* NCTC 8325 and USA300-0114 in TSB-medium (17 g/L casein peptone, pancreas hydrolysate, 3 g/L soy peptone (papain hydrolysate), 2.5 g/L di-potassium hydrogen phosphate, 5 g/L sodium chloride, 2.5 g/L glucose monohydrate, pH 7.3 ± 0.2; CASO Broth, *Carl Roth*) were diluted (1:100) in fresh TSB-medium on a 96-well plate (200 µL/well; flat-bottomed 96-well plate, *BD Biosciences*, BD 351172). Bacteria were incubated (37°C, 24 h) to establish biofilms. After 24 h, the wells were emptied and a pre-mixed solution of TSB-media and compound stock solution was added to each well (maximum DMSO concentration 2% for single compounds and 4% for combination of **PK150** and oxacillin). Plates were incubated at 37°C for 20 or 70 h, then the media from each well was removed and biofilms washed three times with PBS (200 µL) to remove planktonic cells. Biofilms were regrown overnight at 37°C in fresh medium (200 µL). An aliquot of 100 µL of the supernatant from each well was transferred to a fresh 96-well flat bottomed plate and the OD<sub>600</sub> at 595 nm was measured using a plate reader (POLARstar Omega; *BMG Labtech*). Concentrations of compound yielding a regrown OD<sub>600</sub> of less than 0.1 corresponded to the MBEC. Three biological replicates in technical triplicates ( $n = 9$ ) were prepared for each concentration of compound as well as positive (cetyl pyridinium chloride and PQ-11,11)<sup>241-242</sup> and negative controls (DMSO). Cetylpyridinium chloride showed full eradication of biofilms at 50 µM for NCTC 8325 (MSSA) and USA300-0114 (MRSA) and PQ-11,11 at 50 µM for NCTC 8325 (MSSA) and 200 µM for USA300-0114 (MRSA). Averages and standard deviations (SD) were calculated with GraphPadPrism (v6.05, GraphPad Software) across all replicates.

Prior to MBIC determination, MIC values in TSB-medium were determined (in contrast to standard MIC conditions in B-medium; Chapter 4.2.4.1). To this end, overnight cultures were diluted to 10<sup>6</sup> CFU/mL in TSB-medium and 100 µL thereof added into each well of a U-bottomed 96-well plate (*BD Biosciences*, BD 351177) containing 100 µL compound in TSB-medium (maximum DMSO concentration 2% for single compounds and 4% for combination of **PK150** and oxacillin). Plates were incubated at 37°C for 72 h and evaluated visually for bacterial growth. The MIC was determined as the lowest concentration of compound resulting in no bacterial growth visible to the eye, based on the majority of three trials. Positive and negative controls were conducted for each trial. For **PK150**, MIC values were 0.78 and 1.56 µM for *S. aureus* NCTC 8325 and USA300-0114, respectively.

For MBIC determination, sub-MIC concentrations of compounds were used. Overnight cultures of *S. aureus* NCTC 8325 and USA300-0114 in TSB-medium were diluted in fresh TSB-medium (1:100) and 100  $\mu$ L thereof were added to each well of a flat-bottomed 96-well plate (*BD Biosciences*, BD 351172) already containing different concentration of compounds in TSB-medium (100  $\mu$ L; maximum DMSO concentration 2%). Plates were incubated at 37°C for 24 h. After emptying the wells and a washing step with ddH<sub>2</sub>O (200  $\mu$ L), the wells were dried first for 3 h at 37°C and then at room temperature overnight. Wells were then incubated at room temperature for 10 min with 1% (w/v) crystal violet. Excess crystal violet was removed by submerging plates in fresh tap water until the run off was colorless. Plates were then again dried at room temperature. Crystal violet was re-dissolved with 95% ethanol, and 100  $\mu$ L thereof were transferred to a new flat-bottom 96-well plate for absorbance measurements at 595 nm. Controls corresponding to each test concentration were performed. Three biological replicates were performed. No biofilm inhibition could be observed for sub-MIC concentrations of **PK150**.

#### 4.2.4.9. Resistance Development Assay

The procedure for assessing resistance development was adapted from Ling et al.<sup>86</sup> For resistance development by sequential passaging, exponential growing *S. aureus* NCTC 8325 was diluted (1:100) in MH-medium (1 mL; 2 g/L beef infusion solids, 17.5 g/L casein hydrolysate, 1.5 g/L starch, pH 7.4) containing various concentration of **SFN**, **PK150** or ofloxacin as positive control as well as DMSO or 0.1 M NaOH as growth controls (final assay concentration of DMSO from compound stocks 1%). Bacteria were incubated (37°C, 200 rpm) and passaged in 24 h intervals in the presence of **SFN**, **PK150** or ofloxacin at different concentrations (0.25, 0.5, 1, 2 and 4 x MIC). Cultures from the second highest concentrations that allowed growth ( $OD_{600} \geq 3$ ) were diluted 1:100 into fresh MH-medium (1 mL) containing different concentrations of the respective antimicrobial (0.25, 0.5, 1, 2 and 4 x MIC). If a shift in MIC levels was observed, concentrations of the respective antimicrobial were adjusted accordingly for subsequent passaging. This serial passaging was repeated for 27 days and in two independent biological replicates. The MIC shifts were calculated by dividing the respective daily MICs by the initial MIC on day 1.

#### 4.2.4.10. Zymography

Procedures for the preparation of extracellular and cell-bound autolysin extracts were adapted from Mani et al.<sup>243</sup> and Huff et al.<sup>244</sup> B-medium was inoculated (1:1000) from an overnight culture of *S. aureus* NCTC 8325 (37°C, 200 rpm, overnight) and bacterial cells grown (37°C, 200 rpm, 8 h) to an  $OD_{600}$  of 4 to 4.5. Cells were harvested (3,000 x g, 15 min) and washed

with PBS to remove secreted proteins. The cell density was adjusted to an OD<sub>600</sub> of 1.6 in B-medium. Cells were treated (37°C, 1.5 h) with respective compounds (**PK150** and **PK150-C**, 2.4 µM; **SFN** and **SFN-C**, 24 µM; penicillin G, 0.4 µM). Cells were harvested (3,000 x g, 4°C, 15 min) and saved for the extraction of cell wall-bound lytic proteins. Supernatants were filtrated (0.2 µm, VWR), concentrated 100x by ultrafiltration with 10 kDa filters (*Amicon* YM-10) and used for the analysis of extracellular proteins. Cell wall-bound enzymes were extracted by a freeze-thaw method. Here, harvested cells were washed with cold water, then with potassium hydrogen phosphate buffer (0.01 M, pH 7) and resuspended in the same buffer. The cell suspension was frozen at -80°C for 1 h and thawed at 37°C for 10 min. This cycle was repeated and cells were stored overnight at -80°C. After thawing at 37°C supernatants were collected by centrifugation (13,300 x g, 4°C, 10 min). Concentrations of protein extracts were determined by Bradford assay (*Roti-Quant*, *Carl Roth*) and adjusted to equal protein amounts.

Zymography for the analysis of lytic activities of protein extracts were based on SDS-PAGE using 10% gels containing *S. aureus* NCTC 8325 as substrate cells. The protocol for the preparation of gels and performing SDS-PAGE was adapted from Vaz et al.<sup>245-246</sup> For the preparation of substrate cells, *S. aureus* NCTC 8325 was grown (37°C, 200 rpm) to an OD<sub>600</sub> of 1 in B-medium. Cells were harvested (6,000 x g, 15 min), washed with water and autoclaved in water (121°C, 15 min). The autoclaved cells were harvested by centrifugation (15,050 x g, 15 min). Pellets were kept at -20°C overnight, resuspended in water and lyophilized at -80°C. Substrate cells were resuspended in water and added to resolving gels before addition of TEMED (0.2% (w/v) final concentration). Subsequently, gels were prepared according to standard procedures. Samples of prepared extracellular (11 µg) and cell wall-bound protein extracts (3 µg) were loaded on zymogram gels. After SDS-PAGE in Tris-glycine-SDS-buffer, gels were rinsed with water and washed three times with water (room temperature, gentle agitation, 15 min) to remove SDS. Gels were subsequently incubated (37°C, gentle agitation, overnight) in renaturation buffer (50 mM Tris-HCl, pH 7.5, 0.1% (v/v) Triton X-100, 10 mM calcium chloride, 10 mM magnesium chloride). Afterwards gels were stained (room temperature, 1 h) with methylene blue solution (0.1% (w/v) methylene blue in 0.01% (w/v) potassium hydroxide) and destained with water overnight. In addition, the same samples were analyzed on 4 – 12% Bis-Tris gels with 1x MOPS SDS Running Buffer (*NuPAGE*, *Thermo Fisher Scientific*). Pink Color Protein Standard II protein size marker (prestained, *SERVA*) was used.

#### 4.2.4.11. ClpP Peptidase Assay

*S. aureus* ClpP (100  $\mu$ L/well final volume; 1  $\mu$ M final protein concentration in 100 mM HEPES pH 7.0, 100 mM NaCl)<sup>199</sup> was treated (32°C, 15 min) with varying concentrations of the respective compound or DMSO (final assay concentration of DMSO from compound stocks 1%) in triplicates (opaque Nunc 96-well flat bottom, *Thermo Fisher Scientific*). Subsequently, preheated fluorogenic peptide Suc-LY-AMC (succinyl-Leu-Tyr-4-aminomethylcumarin; 1  $\mu$ L, 200  $\mu$ M final substrate concentration) was added and the fluorescence signal increase monitored (380 nm excitation and 440 nm emission wavelength) using a *Tecan Infinite M200Pro* plate reader. The initial slopes were calculated with OriginPro 9.1G (*OriginLab*) based on fluorescence over time plots via linear regression using a time range from 600 to 2000 s. All data were recorded in triplicates and in at least three independent experiments. Averages and standard deviations were calculated with GraphPadPrism (v6.05; *GraphPad Software*).

#### 4.2.4.12. Cytotoxicity Assay

MTT assays were performed in 96-well plates (transparent Nunc flat-bottomed 96-well plate; *Thermo Fisher Scientific*). A549, HeLa and HepG2 cells were seeded at a density of 4000 cells/well, whereas NIH/3T3 cells were seeded at a density of 2000 cells/well. Cells were grown (37°C, humidified 5% CO<sub>2</sub> atmosphere, 24 h) to 30 – 40% confluence. The medium was removed and the cells were treated with varying concentrations of the respective compound or DMSO in full growth media (100  $\mu$ L/well; final assay concentration of DMSO from compound stocks 0.1%) in triplicates. After incubation (37°C, humidified 5% CO<sub>2</sub> atmosphere, 24 h) thiazolyl blue tetrazolium bromide (20  $\mu$ L; 5 mg/mL in PBS; *Sigma-Aldrich*) was added to the cells, followed by incubation (37°C, humidified 5% CO<sub>2</sub> atmosphere, 4 h) until complete consumption was observed. After removal of the medium, the resulting formazan was dissolved in DMSO (200  $\mu$ L) and the optical density was measured at 570 nm with background subtraction at 630 nm by a *Tecan Infinite M200 Pro*. MTT data were obtained from at least three independent experiments with triplicate runs for each concentration. All measured values were normalized to values resulting from DMSO-treated samples (100% cell viability). IC<sub>50</sub> values and 95% confidence intervals were calculated with GraphPadPrism (v5.03, *GraphPad Software*) across all replicates.

#### 4.2.4.13. Hemolysis Assay

The hemolysis protocol was adapted from Blazyk et al.<sup>247</sup> and Nüsslein et al.<sup>248</sup> Hemolysis at different antibiotic concentrations was determined by using a suspension of erythrocytes collected from the blood of an adult sheep (w/ heparin; *elocin-lab*). Fresh sheep blood

(w/ heparin) was centrifuged (2,000 x g, 20 min), the supernatant removed and erythrocytes washed five times with PBS (1:1). Subsequently, an erythrocyte suspension with 50% hematocrit was prepared and stored at 4°C for further use. Hemolysis at different compound concentrations was determined by using a 5% suspension of erythrocytes in PBS (400 µL final volume; final assay concentration of DMSO from compound stocks 1%). Complete hemolysis was determined by adding 0.2% (v/v) Triton X-100, while DMSO functioned as the zero-hemolysis control. After incubation (37°C, 400 rpm, 30 min), the suspension was centrifuged (10,000 x g, 10 min) and the absorbance of the supernatant (1:4 dilution with PBS; 100 µL) was measured at 414 nm at a *Tecan* Infinite M200 Pro. Hemolysis was determined in four independent experiments with triplicate runs for each concentration. Averages and standard deviations were calculated across all four experiments after normalization to 0% hemolysis (DMSO) and 100% hemolysis (Triton X-100, 0.2% (v/v)).

#### 4.2.4.14. In Vitro Stability in Murine Blood Plasma

The in vitro stability of **SFN** and **PK150** was tested by a LC-MS-based method. Murine blood plasma (mouse plasma w/ lithium heparin, sterile filtered; *biowest*, S2162-010) was used as a 1:1 dilution with potassium phosphate buffer (0.1 M, pH 7.4). U1, a β-lactone with known low plasma stability,<sup>212</sup> was used as positive control. For plasma stability testing, compounds were diluted 1:100 to a final concentration of 10 µM (50 µM in the case of U1, final assay concentration of DMSO from compound stocks 1%) into pre-warmed plasma at 37°C. The initial sample was taken immediately after compound addition (time point 0 min). In the following, the mixture was incubated (37°C, 600 rpm) and additional samples were withdrawn at certain time points (5, 10, 20, 30, 60, 120, 240 and 360 min). Directly after withdrawal, samples were quenched by the addition of pre-chilled acetonitrile (1:1 (v/v)) and stored at -20°C. Prior to LC-MS analysis, samples were centrifuged to pellet proteins (17,000 x g, 5 min) and supernatants were filtered through modified nylon centrifugal filters (0.45 µM, *VWR*). Quantitative LC-MS analysis was performed using a LCQ-Fleet Ion Trap Mass Spectrometer (*Thermo Fisher Scientific*) equipped with an APCI ion source and a *Dionex* Ultimate3000 HPLC system using a *Waters* Xbridge BEH130 C18-reverse phase column (5 µM 4.6 x 100 mm). Data analysis was performed using XCalibur software (*Thermo Fisher Scientific*). Briefly, ion peaks from single ion monitoring mass detection were integrated and peak areas at the time point 0 min were set to 100%. The time-dependent peak decline was expressed relative to 100% at t = 0 min. Plasma stability was determined in at least three independent experiments.

#### 4.2.5. In Vivo Animal Studies – Chapter 3: Discovery of a Small Molecule Antibiotic Active Against Multidrug-Resistant Gram-Positive Pathogens

All animal studies were carried out by Dr. Katharina Rox and Prof. Dr. Eva Medina at the Helmholtz-Zentrum für Infektionsforschung, Braunschweig, Germany.

##### 4.2.5.1. General Information

For pharmacokinetic and pharmacodynamic experiments, outbred male CD-1 mice (*Charles River*, Netherlands), 4 weeks old, were used. For efficacy experiments, pathogen-free 9-week old female C57BL/6J mice were purchased from Harlan-Winkelmann (*Envigo*, Netherlands). The animal studies were conducted in accordance with the recommendations of the European Community (Directive 86/609/EEC, 24 November 1986). All animal procedures were performed in strict accordance with the German regulations of the Society for Laboratory Animal Science (GV-SOLAS) and the European Health Law of the Federation of Laboratory Animal Science Associations (FELASA). Animals were excluded from further analysis if sacrifice was necessary according to the human endpoints established by the ethical board. All experiments were approved by the ethical board of the Niedersächsisches Landesamt für Verbraucherschutz und Lebensmittelsicherheit, Oldenburg, Germany (LAVES; permit No. 33.9-42502-04-13/1195 and 33.19-42502-04-15/1857).

##### 4.2.5.2. Pharmacokinetic Study

**PK150** was dissolved in 55% PEG-400, 15% *N*-methyl pyrrolidon, 20% dimethyl sulfoxide and 10% ethanol. Mice were administered **PK150** by intragastric gavage at 10 and 20 mg/kg or intravenously at 10 mg/kg. About 20  $\mu$ L of whole blood was collected serially from the lateral tail vein at time points 0.5, 1, 2, 4, 8 and 24 h post administration. Additionally, about 20  $\mu$ L of whole blood was collected at time point 0.25 h after i.v. administration. After 48 h mice were sacrificed and blood was collected from the heart. Whole blood was collected into *Eppendorf* tubes coated with 0.5 M EDTA and immediately centrifuged (13,000 rpm, 4°C, 10 min). The plasma was transferred into a new *Eppendorf* tube and then stored at -80°C for further analysis.

All PK plasma samples were analyzed via HPLC-MS/MS using an *Agilent* 1290 HPLC system equipped with a diode array UV detector and coupled to an *AB Sciex* QTrap 6500 mass spectrometer. First, a calibration curve was prepared by spiking different concentrations of **PK150** into mouse plasma. The lower limit of quantification was 25 ng/mL, the upper limit of quantification was 2000 ng/mL and the lower limit of qualification was 10 ng/mL. Caffeine was used as an internal standard. In addition, quality control samples (QCs) were prepared at 25, 100, 500 and 2000 ng/mL. 7.5  $\mu$ L of a plasma sample (calibration samples, QCs or PK

samples) was extracted with 37.5  $\mu\text{L}$  of acetonitrile containing 12.5 ng/mL of caffeine as internal standard for 5 min at 2000 rpm on an *Eppendorf* MixMate vortex mixer. Then samples were centrifuged (13,000 rpm, 5 min). Supernatants were transferred to standard HPLC-glass vials. HPLC conditions were as follows: Column: *Agilent* Zorbax Eclipse Plus C18, 50 x 2.1 mm, 1.8  $\mu\text{m}$ ; temperature: 30°C; injection volume: 1  $\mu\text{L}$ ; flow rate: 700  $\mu\text{L}/\text{min}$ ; solvent A: water + 0.1% FA; solvent B: ACN + 0.1% FA; gradient: 99% A at 0 min, 99% - 90% A from 0.1 min to 1.00 min, 90% - 50% A from 1.00 min to 1.50 min, 50% - 0% A from 1.50 min to 5.50 min, 0% A until 6.00 min, then 99% A post-run for 2 min; UV detection: 190 - 400 nm. Mass spectrometric conditions were as follows: Scan type: MRM, positive mode; Q1 and Q3 masses for caffeine and **PK150** are as follows:

|                      |                      |                   |                    |  |
|----------------------|----------------------|-------------------|--------------------|--|
| <b>PK150</b>         | Q1 mass (Da) 394.898 |                   |                    |  |
| Q3 mass (Da) 196.100 | time (msec) 50       | CE (volts) 31.000 | CXP (volts) 6.000  |  |
| Q3 mass (Da) 174.100 | time (msec) 50       | CE (volts) 31.000 | CXP (volts) 4.000  |  |
| caffeine             | Q1 mass (Da) 195.116 |                   |                    |  |
| Q3 mass (Da) 138.100 | time (msec) 50       | CE (volts) 27.000 | CXP (volts) 10.000 |  |
| Q3 mass (Da) 110.100 | time (msec) 50       | CE (volts) 31.000 | CXP (volts) 6.000  |  |

Peak areas of each sample and of the corresponding internal standard were analyzed using MultiQuant 3.0 software (*AB Sciex*). Peak areas of the respective sample of **PK150** were normalized to the internal standard peak area. For **PK150**  $m/z$  394.898  $\rightarrow$  196.100 was used for quantification and  $m/z$  394.898  $\rightarrow$  174.100 was used for qualification. For caffeine  $m/z$  195.116  $\rightarrow$  138.100 was used for quantification and  $m/z$  195.116  $\rightarrow$  110.100 was used for qualification. Peaks of PK samples were quantified using the calibration curve. The accuracy of the calibration curve was determined using QCs independently prepared on different days (accuracy: 98.77 - 114.60%). PK parameters were determined using a non-compartmental analysis with PKSolver.<sup>249</sup>

#### 4.2.5.3. Pharmacodynamic Efficacy Study Using a Neutropenic Thigh Infection Model

*S. aureus* ATCC 33591 (MRSA) was used to evaluate the antimicrobial effect of **PK150** in a neutropenic thigh infection model. CD-1 mice were rendered neutropenic by intraperitoneal administration of cyclophosphamide of 150 mg/kg on day -4 and of 100 mg/kg on day -1 prior to infection. On the day of infection mice were infected i.m. with  $7.2 \times 10^5$  CFU/mL *S. aureus*

ATCC 33591 (30  $\mu$ L into each posterior thigh muscle). 20 mg/kg **PK150** dissolved in 55% PEG-400, 15% *N*-methyl pyrrolidon, 20% dimethyl sulfoxide and 10% ethanol and an equally prepared vehicle as sham treatment were administered p.o. 30 min, 4 h and 8 h post infection. In addition, 5 mg/kg levofloxacin (as positive control) dissolved in phosphate buffered saline and an equally prepared vehicle as sham treatment were administered i.p. 2 h, 6 h and 10 h post infection. Mice were sacrificed 24 h post infection and the posterior thigh muscles were aseptically removed, weighted and homogenized in PBS (3 mL). The amount of viable bacteria was determined after plating 10-fold serial dilutions on BHI agar plates following overnight incubation at 37°C. Results were expressed as log<sub>10</sub> CFU/g of muscle. Tukey's test was performed to test for outliers and two-sided Student's *t*-test was used as significance test.

#### 4.2.5.4. Efficacy Experiment Mimicking a *Staphylococcus Aureus* Bloodstream Infection

The antimicrobial efficacy of **PK150** was determined in a murine model of *S. aureus* bloodstream infection. Mice were intravenously infected with  $4 \times 10^7$  CFU of *S. aureus* SH1000 and treated with 20 mg/kg **PK150** (dissolved in 55% PEG-400, 15% *N*-methyl pyrrolidon, 20% dimethyl sulfoxide and 10% ethanol) or vehicle (55% PEG-400, 15% *N*-methyl pyrrolidon, 20% dimethyl sulfoxide and 10% ethanol) starting at day 3 post inoculation. **PK150** and vehicle was administered p.o. twice on day 3 after infection (at 6 h interval) followed by a single oral dose on day 4, 6 and 8 after infection. Mice were sacrificed on day 9 and CFU of *S. aureus* were determined in liver, kidneys and heart by plating in serial dilutions. Two-sided Student's *t*-test was used as significance test.

#### 4.2.6. Further Experimental Procedures – Chapter 3: Discovery of a Small Molecule Antibiotic Active Against Multidrug-Resistant Gram-Positive Pathogens

##### 4.2.6.1. Colloidal Aggregation Determination by Dynamic Light Scattering

The critical agglomeration concentration (CAC) represents the concentration at which small molecules begin to self-aggregate into a suspension of colloid-like aggregates. This transition point is characterized by an abrupt increase in dynamic light scattering (DLS) intensity with increasing compound concentration. Here, DLS was used for detecting the presence of soluble aggregates at different concentrations of **SFN** and **PK150**, respectively, in 50 mM NaPPi buffer (pH 7). The compounds were delivered from concentrated DMSO stocks into freshly filtered 50 mM NaPPi buffer (pH 7) at room temperature (final assay concentration of DMSO from compound stocks 1%). When Tween 80 (0.023% (v/v)) was present, it was added to the buffer prior to the compound. Measurements were performed using a DynaPro NanoStar Dynamic

Light Scattering reader (*Wyatt Technology*) equipped with a 662.3 nm laser. All measurements were performed at 37°C. Data were obtained from three measurements of the same sample, each with a total measurement time of 50 s – 10 acquisitions, 5 s each. The lowest concentration in the dilution series at which the DLS intensity started to distinguish from the solvent background was defined as the critical agglomeration concentration (CAC).

#### 4.2.6.2. Molecular Docking and Dynamic Simulations

Molecular docking and dynamic simulations were performed by Dr. Ilke Ugur and Prof. Dr. Iris Antes, Theoretical Chemical Biology and Protein Modelling Group, Technische Universität München, Germany.

Residue numbers refer to the genomic sequence of *S. aureus* NCTC 8325 SpsB and is based on the entire extracellular region of the protein (residue index 26 – 191).

Molecular docking and dynamic simulations are based on the crystal structure of SpsB in complex with an inhibitor peptide (PDB code 4WVJ).<sup>178</sup> For the preparation of the systems, the bound peptide inhibitor was removed and the protein was solvated in a water box using the tleap module of the Amber15<sup>250</sup> software package by applying a 12 Å buffer region around protein atoms (yielding a model consisting of ~30,000 atoms).

Molecular dynamic simulations were performed using the ff03<sup>251</sup>, GAFF<sup>252</sup> and TIP3P<sup>253</sup> force field parameters for the solute, **PK150**, and solvent, respectively. Missing bonded parameters for the probe were obtained using the antechamber package<sup>254</sup> of Amber15, with the RESP charges calculated by the Gaussian09<sup>255</sup> software. Prior to the minimization of the models, the density of the systems was adjusted to 1 g/cm<sup>3</sup> using an in-house python script. Hydrogens and heavy atoms were minimized consecutively using the SANDER module of Amber15. Periodic boundary conditions were applied. Long-range electrostatic interactions were calculated using the particle mesh Ewald method<sup>256</sup>. A non-bonded cutoff of 12 Å and a time step of 1 fs were used. The systems were heated up to 300 K in the NVT ensemble using a stepwise fashion as performed previously.<sup>257-258</sup> The SHAKE algorithm was used to constraint all bonds involving hydrogens.<sup>259</sup> The production runs were performed in the NPT ensemble for 150 ns and 100 ns for the **PK150** bound complex and the apo-protein, respectively. The cuda-enabled graphics processing units (GPUS) version of the pmemd module of Amber15 was used.<sup>260-261</sup>

A stepwise and comparative protocol was followed to find the binding site of the probe. Two plausible binding sites were detected using surface-based analysis and analyzing their distances to the active site. The probe was docked to these two grooves separately, using the DynaDock approach of an in-house modeling program DynaCell.<sup>200</sup> The docking was

performed in two steps; broad sampling and the molecular dynamic based energy refinement of the selected poses. The energetically-highest ranked five poses (total of ten poses coming from two different binding sites) were further simulated up to 5 ns using the same simulation scheme introduced above. The Molecular Mechanics-Generalized Born Surface Area approach (MMGBSA)<sup>262</sup> was applied to calculate the binding free energies of these ten complexes. The pose with the lowest binding free energy was chosen for further analysis. For the MMGBSA calculations, three distinct production runs (starting with different velocities) were performed on each equilibrated structure to yield 20 ns simulation time in total (time step 1 fs, a total of 225,000 complex frames (3 x 75,000)). The MMGBSA.py module<sup>263</sup> of Amber15<sup>264</sup> was used to combine these frames and calculate the binding free energy. The contribution of the solvent was computed with Generalized Born Surface Area (GBSA) with a probe radius of 1.4 Å and the 'mbondi2' radii set<sup>265</sup> using the modified GB model introduced by Case et al..<sup>266-267</sup> The entropic contributions to the free energy of binding were not included in the calculation scheme as it has been shown that such costly computations do not significantly improve the results.<sup>268-270</sup>

#### 4.2.6.3. Electron Microscopy

Electron microscopy studies were performed by Dr. Katharina Rox and Prof. Dr. Manfred Rohde at Helmholtz-Zentrum für Infektionsforschung, Braunschweig, Germany.

For sample preparation, fresh LB-medium was inoculated from a *S. aureus* NCTC 8325 overnight culture (37°C, 120 rpm, overnight) and diluted to an OD<sub>600</sub> of 0.03. Bacterial cells were grown (37°C, 120 rpm) to an OD<sub>600</sub> of around 0.5 and treated (37°C, 120 rpm, 3 h) with DMSO, **PK150** (2.4 µM final concentration for TEM and 2.4 µM and 1.2 µM for FESEM) and **PK150-C** (2.4 µM final concentration), respectively. Subsequently, bacterial cells were fixed as described for FESEM or TEM procedures.

For FESEM, bacteria were fixed with 5% formaldehyde and 2% glutaraldehyde in growth medium and washed with TE buffer (10 mM Tris, 2 mM EDTA, pH 6.9). Samples were dehydrated in a graded series of acetone (10, 30, 50, 70, 90 and 100%) on ice for 10 min for each step. Samples in the 100% acetone step were allowed to reach room temperature before another change in 100% acetone. Samples were then subjected to critical-point drying with liquid CO<sub>2</sub> (CPD 030, *Bal-Tec*). Dried samples were coated with a gold/palladium (80/20) film by sputter coating (SCD 500, *Bal-Tec*) before examination in a field emission scanning electron microscope *Zeiss Merlin* using the *Everhart Thornley* HESE2-detector and the inlens SE-detector in a 25:75 ratio at an acceleration voltage of 5 kV. Images were recorded with *Zeiss SEMSmart V5.05* and contrast and brightness were adjusted with *Adobe Photoshop CS5*.

For TEM, bacteria were fixed with 5% formaldehyde and 2% glutaraldehyde in growth medium, washed with TE buffer and further fixed with 1% osmium tetroxide in TE buffer at room temperature for 1 h. After a washing step with TE buffer samples were dehydrated with 10%, 30% and 50% acetone on ice before incubation in 70% acetone with 2% uranyl acetate at 7°C overnight. Samples were further dehydrated with 90% and 100% acetone on ice, allowed to reach room temperature and further dehydrated with 100% acetone. Subsequently, samples were infiltrated with the epoxy resin Low Viscosity resin (*Agar Scientific*). After polymerisation at 75°C for 2 days ultrathin sections were cut with a diamond knife, collected onto butvar-coated 300 mesh grids, and counterstained with 4% aqueous uranyl acetate for 4 min. Samples were imaged in a *Zeiss* TEM 910 at an acceleration voltage of 80 kV and at calibrated magnifications. Images were recorded digitally at calibrated magnifications with a Slow-Scan CCD-Camera (*ProScan*, 1024 x 1024) with ITEM-Software (*Olympus Soft Imaging Solutions*). Contrast and brightness were adjusted with *Adobe Photoshop CS5*.

## 5. BILIOGRAPHY

1. Laxminarayan, R.; Duse, A.; Wattal, C.; Zaidi, A. K. M.; Wertheim, H. F. L.; Sumpradit, N.; Vlieghe, E.; Hara, G. L.; Gould, I. M.; Goossens, H.; Greko, C.; So, A. D.; Bigdeli, M.; Tomson, G.; Woodhouse, W.; Ombaka, E.; Peralta, A. Q.; Qamar, F. N.; Mir, F.; Kariuki, S.; Bhutta, Z. A.; Coates, A.; Bergstrom, R.; Wright, G. D.; Brown, E. D.; Cars, O. Antibiotic resistance - the need for global solutions. *Lancet Infect. Dis.* **2013**, *13* (12), 1057-98.
2. European Centre for Disease Prevention and Control (ECDC) and European Medicines Agency (EMA). ECDC/EMA joint technical report - The bacterial challenge: Time to react - A call to narrow the gap between multidrug-resistant bacteria in the EU and development of new antibacterial agents. *ECDC* **2009**, Stockholm. Available from: [ecdc.europa.eu/sites/portal/files/media/en/publications/Publications/0909\\_TER\\_The\\_Bacterial\\_Challenge\\_Time\\_to\\_React.pdf](http://ecdc.europa.eu/sites/portal/files/media/en/publications/Publications/0909_TER_The_Bacterial_Challenge_Time_to_React.pdf)
3. Centers for Disease Control and Prevention (CDC). Antibiotic resistance threats in the United States, 2013. *CDC* **2013**, Atlanta. Available from: [cdc.gov/drugresistance/threat-report-2013/pdf/ar-threats-2013-508.pdf](http://cdc.gov/drugresistance/threat-report-2013/pdf/ar-threats-2013-508.pdf)
4. Chen, L.; Todd, R.; Kiehlbauch, J.; Walters, M.; Kallen, A. Notes from the field: Pan-resistant New Delhi metallo- $\beta$ -lactamase-producing *Klebsiella pneumoniae* - Washoe County, Nevada, 2016. *MMWR Morb. Mortal Wkly. Rep.* **2017**, *66* (1), 33.
5. Alekshun, M. N.; Levy, S. B. Molecular mechanisms of antibacterial multidrug resistance. *Cell* **2007**, *128* (6), 1037-1050.
6. World Health Organization (WHO). Antimicrobial resistance: Global report on surveillance 2014. *WHO* **2014**, Geneva. Available from: [apps.who.int/iris/bitstream/10665/112642/1/9789241564748\\_eng.pdf](http://apps.who.int/iris/bitstream/10665/112642/1/9789241564748_eng.pdf)
7. World Health Organization (WHO). WHO Model Lists of Essential Medicines. *WHO* **2017**, Geneva. Available from: [who.int/medicines/publications/essentialmedicines/20th\\_EML2017\\_FINAL\\_amendedAug2017.pdf](http://who.int/medicines/publications/essentialmedicines/20th_EML2017_FINAL_amendedAug2017.pdf)
8. Livermore, D. M.  $\beta$ -Lactamases in laboratory and clinical resistance. *Clin. Microbiol. Rev.* **1995**, *8* (4), 557-84.
9. Castañeda-García, A.; Blázquez, J.; Rodríguez-Rojas, A. Molecular mechanisms and clinical impact of acquired and intrinsic fosfomycin resistance. *Antibiotics (Basel)* **2013**, *2* (2), 217-36.
10. Spanu, T.; De Angelis, G.; Cipriani, M.; Pedruzzi, B.; D'Inzeo, T.; Cataldo, M. A.; Sganga, G.; Tacconelli, E. In vivo emergence of tigecycline resistance in multidrug-resistant *Klebsiella pneumoniae* and *Escherichia coli*. *Antimicrob. Agents Chemother.* **2012**, *56* (8), 4516-8.

11. Lewis, J. S.; Owens, A.; Cadena, J.; Sabol, K.; Patterson, J. E.; Jorgensen, J. H.; Jorgensen, J. H. Emergence of daptomycin resistance in *Enterococcus faecium* during daptomycin therapy. *Antimicrob. Agents Chemother.* **2005**, *49* (4), 1664-5.
12. Falagas, M. E.; Kasiakou, S. K.; Saravolatz, L. D. Colistin: The revival of polymyxins for the management of multidrug-resistant Gram-negative bacterial infections. *Clin. Infect. Dis.* **2005**, *40* (9), 1333-41.
13. Lim, L. M.; Ly, N.; Anderson, D.; Yang, J. C.; Macander, L.; Jarkowski, A.; Forrest, A.; Bulitta, J. B.; Tsuji, B. T.; Tsuji, B. T. Resurgence of colistin: A review of resistance, toxicity, pharmacodynamics, and dosing. *Pharmacotherapy* **2010**, *30* (12), 1279-91.
14. Long, S. W.; Olsen, R. J.; Mehta, S. C.; Palzkill, T.; Cernoch, P. L.; Perez, K. K.; Musick, W. L.; Rosato, A. E.; Musser, J. M. PBP2a mutations causing high-level ceftaroline resistance in clinical methicillin-resistant *Staphylococcus aureus* isolates. *Antimicrob. Agents Chemother.* **2014**, *58* (11), 6668-74.
15. Endimiani, A.; Perez, F.; Bonomo, R. A. Cefepime: A reappraisal in an era of increasing antimicrobial resistance. *Expert Rev. Anti. Infect. Ther.* **2008**, *6* (6), 805-24.
16. Aminov, R. I. A brief history of the antibiotic era: Lessons learned and challenges for the future. *Front. Microbiol.* **2010**, *1*, 134.
17. Fleming, A. On the antibacterial action of cultures of a penicillium, with special reference to their use in the isolation of *B. influenzae*. *Br. J. Exp. Pathol.* **1929**, *10* (3), 226-36.
18. Lyddiard, D.; Jones, G. L.; Greatrex, B. W. Keeping it simple: Lessons from the golden era of antibiotic discovery. *FEMS Microbiol. Lett.* **2016**, *363* (8), fnw084.
19. Domagk, G. Ein Beitrag zur Chemotherapie der bakteriellen Infektionen. *Dtsch. Med. Wochenschr.* **1935**, *61* (7), 250-53.
20. Walsh, C. T.; Wencewicz, T. A. Prospects for new antibiotics: A molecule-centered perspective. *J. Antibiot.* **2014**, *67* (1), 7-22.
21. World Health Organization (WHO). Global priority list of antibiotic-resistant bacteria to guide research, discovery, and development of new antibiotics. *WHO* **2017**, Geneva. Available from: [who.int/medicines/publications/WHO-PPL-Short\\_Summary\\_25Feb-ET\\_NM\\_WHO.pdf](http://who.int/medicines/publications/WHO-PPL-Short_Summary_25Feb-ET_NM_WHO.pdf)
22. Butler, M. S.; Blaskovich, M. A. T.; Cooper, M. A. Antibiotics in the clinical pipeline at the end of 2015. *J. Antibiot. (Tokyo)* **2017**, *70* (1), 3-24.
23. Ventola, C. L. The antibiotic resistance crisis: Part 1: Causes and threats. *P & T* **2015**, *40* (4), 277-83.
24. Payne, D. J.; Gwynn, M. N.; Holmes, D. J.; Pompliano, D. L. Drugs for bad bugs: Confronting the challenges of antibacterial discovery. *Nat. Rev. Drug Discov.* **2007**, *6* (1), 29-40.

25. Projan, S. J. Why is big Pharma getting out of antibacterial drug discovery? *Curr. Opin. Microbiol.* **2003**, 6 (5), 427-30.
26. Green, D. W. The bacterial cell wall as a source of antibacterial targets. *Expert Opin. Ther. Targets* **2002**, 6 (1), 1-20.
27. Hurdle, J. G.; O'Neill, A. J.; Chopra, I.; Lee, R. E. Targeting bacterial membrane function: An underexploited mechanism for treating persistent infections. *Nat. Rev. Microbiol.* **2011**, 9 (1), 62-75.
28. Chopra, I. Bacterial RNA polymerase: A promising target for the discovery of new antimicrobial agents. *Curr. Opin. Investig. Drugs* **2007**, 8 (8), 600-7.
29. Wilson, D. N. Ribosome-targeting antibiotics and mechanisms of bacterial resistance. *Nat. Rev. Microbiol.* **2014**, 12 (1), 35-48.
30. Bermingham, A.; Derrick, J. P. The folic acid biosynthesis pathway in bacteria: Evaluation of potential for antibacterial drug discovery. *BioEssays* **2002**, 24 (7), 637-48.
31. Fleming, A. Chemotherapy yesterday, today and tomorrow - the Linacre Lecture 1946. Cambridge Univ. Pr. **2014**.
32. Barber, M. Staphylococcal infection due to penicillin-resistant strains. *Br. Med. J.* **1947**, 2 (4534), 863-5.
33. Sengupta, S.; Chattopadhyay, M. K.; Grossart, H.-P. The multifaceted roles of antibiotics and antibiotic resistance in nature. *Front. Microbiol.* **2013**, 4, 47.
34. Uttley, A. C.; Collins, C. H.; Naidoo, J.; George, R. C. Vancomycin-resistant enterococci. *Lancet* **1988**, 331 (8575-6), 57-8.
35. Murray, B. E. Vancomycin-resistant enterococcal infections. *N. Engl. J. Med.* **2000**, 342 (10), 710-21.
36. Levine, D. P. Vancomycin: A history. *Clin. Infect. Dis.* **2006**, 42 (Supplement 1), S5-12.
37. Lewis, K. Platforms for antibiotic discovery. *Nat. Rev. Drug Discov.* **2013**, 12 (5), 371-87.
38. Palumbi, S. R. Humans as the world's greatest evolutionary force. *Science* **2001**, 293 (5536), 1786-90.
39. Bloom, B. R.; Murray, C. J. L. Tuberculosis: Commentary on a reemergent killer. *Science* **1992**, 257 (5073), 1055-64.
40. Honoré, N.; Cole, S. T. Streptomycin resistance in mycobacteria. *Antimicrob. Agents Chemother.* **1994**, 38 (2), 238-42.
41. Chopra, I.; Roberts, M. Tetracycline antibiotics: Mode of action, applications, molecular biology, and epidemiology of bacterial resistance. *Microbiol. Mol. Biol. Rev.* **2001**, 65 (2), 232-60.
42. Sanders, E.; Foster, M. T.; Scott, D. Group A beta-hemolytic streptococci resistant to erythromycin and lincomycin. *N. Engl. J. Med.* **1968**, 278 (10), 538-40.
43. Jevons, M. P. Celbenin-resistant staphylococci. *Br. Med. J.* **1961**, 1 (5219), 124.

44. Smith, J. T. Penicillinase and ampicillin resistance in a strain of *Escherichia coli*. *J. Gen. Microbiol.* **1963**, 30 (2), 299-306.
45. Ronald, A. R.; Turck, M.; Petersdorf, R. G. A critical evaluation of nalidixic acid in urinary-tract infections. *N. Engl. J. Med.* **1966**, 275 (20), 1081-9.
46. Kresken, M.; Wiedemann, B., Development of resistance to nalidixic acid and the fluoroquinolones after the introduction of norfloxacin and ofloxacin. *Antimicrob. Agents Chemother.* **1988**, 32 (8), 1285-8.
47. Gonzales, R. D.; Schreckenberger, P. C.; Graham, M. B.; Kelkar, S.; DenBesten, K.; Quinn, J. P. Infections due to vancomycin-resistant *Enterococcus faecium* resistant to linezolid. *Lancet* **2001**, 357 (9263), 1179.
48. Tsiodras, S.; Gold, H. S.; Sakoulas, G.; Eliopoulos, G. M.; Wennersten, C.; Venkataraman, L.; Moellering, R. C.; Ferraro, M. J. Linezolid resistance in a clinical isolate of *Staphylococcus aureus*. *Lancet* **2001**, 358 (9277), 207-8.
49. Gentry, D. R.; McCloskey, L.; Gwynn, M. N.; Rittenhouse, S. F.; Scangarella, N.; Shawar, R.; Holmes, D. J. Genetic characterization of Vga ABC proteins conferring reduced susceptibility to pleuromutilins in *Staphylococcus aureus*. *Antimicrob. Agents Chemother.* **2008**, 52 (12), 4507-9.
50. McNeil, J. C.; Hulten, K. G.; Kaplan, S. L.; Mason, E. O. Decreased susceptibilities to retapamulin, mupirocin, and chlorhexidine among *Staphylococcus aureus* isolates causing skin and soft tissue infections in otherwise healthy children. *Antimicrob. Agents Chemother.* **2014**, 58 (5), 2878-83.
51. Goldstein, E. J. C.; Citron, D. M.; Sears, P.; Babakhani, F.; Sambol, S. P.; Gerding, D. N. Comparative susceptibilities to fidaxomicin (OPT-80) of isolates collected at baseline, recurrence, and failure from patients in two phase III trials of fidaxomicin against *Clostridium difficile* infection. *Antimicrob. Agents Chemother.* **2011**, 55 (11), 5194-9.
52. Andries, K.; Villellas, C.; Coeck, N.; Thys, K.; Gevers, T.; Vranckx, L.; Lounis, N.; de Jong, B. C.; Koul, A. Acquired resistance of *Mycobacterium tuberculosis* to bedaquiline. *PLOS ONE* **2014**, 9 (7), e102135.
53. Blair, J. M. A.; Webber, M. A.; Baylay, A. J.; Ogbolu, D. O.; Piddock, L. J. V. Molecular mechanisms of antibiotic resistance. *Nat. Rev. Microbiol.* **2014**, 13 (1), 42-51.
54. Nikaido, H. Multidrug resistance in bacteria. *Annu. Rev. Biochem.* **2009**, 78, 119-46.
55. Nikaido, H., Prevention of drug access to bacterial targets: Permeability barriers and active efflux. *Science* **1994**, 264 (5157), 382-8.
56. Levy, S. B. Active efflux mechanisms for antimicrobial resistance. *Antimicrob. Agents Chemother.* **1992**, 36 (4), 695-703.
57. Wright, G. Bacterial resistance to antibiotics: Enzymatic degradation and modification. *Adv. Drug Deliv. Rev.* **2005**, 57 (10), 1451-70.

58. Mendes, R. E.; Deshpande, L. M.; Jones, R. N. Linezolid update: Stable in vitro activity following more than a decade of clinical use and summary of associated resistance mechanisms. *Drug Resist. Updat.* **2014**, *17* (1-2), 1-12.
59. Courvalin, P. Transfer of antibiotic resistance genes between Gram-positive and Gram-negative bacteria. *Antimicrob. Agents Chemother.* **1994**, *38* (7), 1447-51.
60. Wright, G. D. The antibiotic resistome: The nexus of chemical and genetic diversity. *Nat. Rev. Microbiol.* **2007**, *5* (3), 175-86.
61. Perry, J. A.; Westman, E. L.; Wright, G. D. The antibiotic resistome: What's new? *Curr. Opin. Microbiol.* **2014**, *21*, 45-50.
62. Ruiz, J.; Pons, M. J.; Gomes, C. Transferable mechanisms of quinolone resistance. *Int. J. Antimicrob. Agents* **2012**, *40* (3), 196-203.
63. Forsberg, K. J.; Reyes, A.; Wang, B.; Selleck, E. M.; Sommer, M. O. A.; Dantas, G. The shared antibiotic resistome of soil bacteria and human pathogens. *Science* **2012**, *337* (6098), 1107-11.
64. Witte, W. Selective pressure by antibiotic use in livestock. *Int. J. Antimicrob. Agents* **2000**, *16*, 19-24.
65. McManus, P. S.; Stockwell, V. O.; Sundin, G. W.; Jones, A. L. Antibiotic use in plant agriculture. *Annu. Rev. Phytopathol.* **2002**, *40* (1), 443-65.
66. Heuer, H.; Schmitt, H.; Smalla, K. Antibiotic resistance gene spread due to manure application on agricultural fields. *Curr. Opin. Microbiol.* **2011**, *14* (3), 236-43.
67. Li, D.; Yang, M.; Hu, J.; Zhang, J.; Liu, R.; Gu, X.; Zhang, Y.; Wang, Z. Antibiotic-resistance profile in environmental bacteria isolated from penicillin production wastewater treatment plant and the receiving river. *Environ. Microbiol.* **2009**, *11* (6), 1506-17.
68. Li, D.; Yu, T.; Zhang, Y.; Yang, M.; Li, Z.; Liu, M.; Qi, R. Antibiotic resistance characteristics of environmental bacteria from an oxytetracycline production wastewater treatment plant and the receiving river. *Appl. Environ. Microbiol.* **2010**, *76* (11), 3444-51.
69. Moore, A. M.; Munck, C.; Sommer, M. O. A.; Dantas, G. Functional metagenomic investigations of the human intestinal microbiota. *Front. Microbiol.* **2011**, *2*, 188.
70. Tong, S. Y. C.; Davis, J. S.; Eichenberger, E.; Holland, T. L.; Fowler, V. G. Jr. *Staphylococcus aureus* infections: Epidemiology, pathophysiology, clinical manifestations, and management. *Clin. Microbiol. Rev.* **2015**, *28* (3), 603-61.
71. Rice, L. B. Federal funding for the study of antimicrobial resistance in nosocomial pathogens: No ESKAPE. *J. Infect. Dis.* **2008**, *197* (8), 1079-81.
72. DeLeo, F. R.; Otto, M.; Kreiswirth, B. N.; Chambers, H. F. Community-associated methicillin-resistant *Staphylococcus aureus*. *Lancet* **2010**, *375* (9725), 1557-68.

73. Chambers, H. F. The changing epidemiology of *Staphylococcus aureus*? *Emerg. Infect. Dis.* **2001**, 7 (2), 178-82.
74. Hiramatsu, K.; Hanaki, H.; Ino, T.; Yabuta, K.; Oguri, T.; Tenover, F. C. Methicillin-resistant *Staphylococcus aureus* clinical strain with reduced vancomycin susceptibility. *J. Antimicrob. Chemother.* **1997**, 40 (1), 135-6.
75. Chang, S.; Sievert, D. M.; Hageman, J. C.; Boulton, M. L.; Tenover, F. C.; Downes, F. P.; Shah, S.; Rudrik, J. T.; Pupp, G. R.; Brown, W. J.; Cardo, D.; Fridkin, S. K. Infection with vancomycin-resistant *Staphylococcus aureus* containing the vanA resistance gene. *N. Engl. J. Med.* **2003**, 348 (14), 1342-7.
76. Srinivasan, A.; Dick, J. D.; Perl, T. M. Vancomycin resistance in staphylococci. *Clin. Microbiol. Rev.* **2002**, 15 (3), 430-8.
77. Lister, J. L.; Horswill, A. R. *Staphylococcus aureus* biofilms: Recent developments in biofilm dispersal. *Front. Cell. Infect. Microbiol.* **2014**, 4, 178.
78. Scherr, T. D.; Heim, C. E.; Morrison, J. M.; Kielian, T. Hiding in plain sight: Interplay between staphylococcal biofilms and host immunity. *Front. Immunol.* **2014**, 5, 37.
79. de la Fuente-Núñez, C.; Reffuveille, F.; Fernández, L.; Hancock, R. E. W. Bacterial biofilm development as a multicellular adaptation: Antibiotic resistance and new therapeutic strategies. *Curr. Opin. Microbiol.* **2013**, 16 (5), 580-9.
80. Darouiche, R. O. Treatment of infections associated with surgical implants. *N. Engl. J. Med.* **2004**, 350 (14), 1422-9.
81. Waters, E. M.; Rowe, S. E.; O'Gara, J. P.; Conlon, B. P. Convergence of *Staphylococcus aureus* persister and biofilm research: Can biofilms be defined as communities of adherent persister cells? *PLOS Pathog.* **2016**, 12 (12), e1006012.
82. Harms, A.; Maisonneuve, E.; Gerdes, K. Mechanisms of bacterial persistence during stress and antibiotic exposure. *Science* **2016**, 354 (6318), aaf4268.
83. Balaban, N. Q.; Merrin, J.; Chait, R.; Kowalik, L.; Leibler, S. Bacterial persistence as a phenotypic switch. *Science* **2004**, 305 (5690), 1622-5.
84. Keren, I.; Kaldalu, N.; Spoering, A.; Wang, Y.; Lewis, K. Persister cells and tolerance to antimicrobials. *FEMS Microbiol. Lett.* **2004**, 230 (1), 13-8.
85. Bigger, J. Treatment of staphylococcal infections with penicillin by intermittent sterilisation. *Lancet* **1944**, 244 (6320), 497-500.
86. Ling, L. L.; Schneider, T.; Peoples, A. J.; Spoering, A. L.; Engels, I.; Conlon, B. P.; Mueller, A.; Schäberle, T. F.; Hughes, D. E.; Epstein, S.; Jones, M.; Lazarides, L.; Steadman, V. A.; Cohen, D. R.; Felix, C. R.; Fetterman, K. A.; Millett, W. P.; Nitti, A. G.; Zullo, A. M.; Chen, C.; Lewis, K. A new antibiotic kills pathogens without detectable resistance. *Nature* **2015**, 517 (7535), 455-9.

87. Zipperer, A.; Konnerth, M. C.; Laux, C.; Berscheid, A.; Janek, D.; Weidenmaier, C.; Burian, M.; Schilling, N. A.; Slavetinsky, C.; Marschal, M.; Willmann, M.; Kalbacher, H.; Schitteck, B.; Brötz-Oesterhelt, H.; Grond, S.; Peschel, A.; Krismer, B. Human commensals producing a novel antibiotic impair pathogen colonization. *Nature* **2016**, *535* (7613), 511-6.
88. Moffat, J. G.; Vincent, F.; Lee, J. A.; Eder, J.; Prunotto, M. Opportunities and challenges in phenotypic drug discovery: An industry perspective. *Nat. Rev. Drug. Discov.* **2017**, *16* (8), 531-43.
89. Drews, J. Drug discovery: A historical perspective. *Science* **2000**, *287* (5460), 1960-4.
90. Swinney, D. C.; Anthony, J. How were new medicines discovered? *Nat. Rev. Drug. Discov.* **2011**, *10* (7), 507-19.
91. Roemer, T.; Davies, J.; Giaever, G.; Nislow, C. Bugs, drugs and chemical genomics. *Nat. Chem. Biol.* **2012**, *8* (1), 46-56.
92. Schirle, M.; Bantscheff, M.; Kuster, B. Mass spectrometry-based proteomics in preclinical drug discovery. *Chem. Biol.* **2012**, *19* (1), 72-84.
93. Schenone, M.; Dancik, V.; Wagner, B. K.; Clemons, P. A. Target identification and mechanism of action in chemical biology and drug discovery. *Nat. Chem. Biol.* **2013**, *9* (4), 232-40.
94. Lee, J.; Bogoy, M. Target deconvolution techniques in modern phenotypic profiling. *Curr. Opin. Chem. Biol.* **2013**, *17* (1), 118-26.
95. Rix, U.; Superti-Furga, G. Target profiling of small molecules by chemical proteomics. *Nat. Chem. Biol.* **2009**, *5* (9), 616-24.
96. Kam, C. M.; Abuelyaman, A. S.; Li, Z.; Hudig, D.; Powers, J. C. Biotinylated isocoumarins, new inhibitors and reagents for detection, localization, and isolation of serine proteases. *Bioconjugate Chem.* **1993**, *4* (6), 560-7.
97. Abuelyaman, A. S.; Hudig, D.; Woodard, S. L.; Powers, J. C. Fluorescent derivatives of diphenyl [1-(N-peptidylamino)alkyl]phosphonate esters: Synthesis and use in the inhibition and cellular localization of serine proteases. *Bioconjugate Chem.* **1994**, *5* (5), 400-5.
98. Liu, Y.; Patricelli, M. P.; Cravatt, B. F. Activity-based protein profiling: The serine hydrolases. *Proc. Natl. Acad. Sci. U. S. A.* **1999**, *96* (26), 14694-9.
99. Speers, A. E.; Adam, G. C.; Cravatt, B. F. Activity-based protein profiling in vivo using a copper(I)-catalyzed azide-alkyne [3 + 2] cycloaddition. *J. Am. Chem. Soc.* **2003**, *125* (16), 4686-7.
100. Speers, A. E.; Cravatt, B. F. Profiling enzyme activities in vivo using click chemistry methods. *Chem. Biol.* **2004**, *11* (4), 535-46.

101. Sadaghiani, A. M.; Verhelst, S. H. L.; Bogyo, M. Tagging and detection strategies for activity-based proteomics. *Curr. Opin. Chem. Biol.* **2007**, *11* (1), 20-8.
102. Greenbaum, D.; Medzihradzky, K. F.; Burlingame, A.; Bogyo, M. Epoxide electrophiles as activity-dependent cysteine protease profiling and discovery tools. *Chem. Biol.* **2000**, *7* (8), 569-81.
103. Hsu, J. L.; Huang, S. Y.; Chow, N. H.; Chen, S. H. Stable isotope dimethyl labeling for quantitative proteomics. *Anal. Chem.* **2003**, *75* (24), 6843-52.
104. Ong, S.-E.; Blagoev, B.; Kratchmarova, I.; Kristensen, D. B.; Steen, H.; Pandey, A.; Mann, M. Stable isotope labeling by amino acids in cell culture, SILAC, as a simple and accurate approach to expression proteomics. *Mol. Cell. Proteomics* **2002**, *1* (5), 376-86.
105. Boersema, P. J.; Raijmakers, R.; Lemeer, S.; Mohammed, S.; Heck, A. J. R. Multiplex peptide stable isotope dimethyl labeling for quantitative proteomics. *Nat. Protoc.* **2009**, *4* (4), 484-94.
106. Ong, S.-E.; Mann, M. Mass spectrometry-based proteomics turns quantitative. *Nat. Chem. Biol.* **2005**, *1* (5), 252-62.
107. Bantscheff, M.; Schirle, M.; Sweetman, G.; Rick, J.; Kuster, B. Quantitative mass spectrometry in proteomics: A critical review. *Anal. Bioanal. Chem.* **2007**, *389* (4), 1017-31.
108. Evans, M. J.; Cravatt, B. F. Mechanism-based profiling of enzyme families. *Chem. Rev.* **2006**, *106* (8), 3279-301.
109. Barglow, K. T.; Cravatt, B. F. Activity-based protein profiling for the functional annotation of enzymes. *Nat. Methods* **2007**, *4* (10), 822-27.
110. Greenbaum, D. C.; Arnold, W. D.; Lu, F.; Hayrapetian, L.; Baruch, A.; Krumrine, J.; Toba, S.; Chehade, K.; Brömme, D.; Kuntz, I. D.; Bogyo, M. Small molecule affinity fingerprinting. *Chem. Biol.* **2002**, *9* (10), 1085-94.
111. Leung, D.; Hardouin, C.; Boger, D. L.; Cravatt, B. F. Discovering potent and selective reversible inhibitors of enzymes in complex proteomes. *Nat. Biotechnol.* **2003**, *21* (6), 687-91.
112. Drahl, C.; Cravatt, B. F.; Sorensen, E. J. Protein-reactive natural products. *Angew. Chem. Int. Ed.* **2005**, *44* (36), 5788-809.
113. Böttcher, T.; Pitscheider, M.; Sieber, S. A. Natural products and their biological targets: Proteomic and metabolomic labeling strategies. *Angew. Chem. Int. Ed.* **2010**, *49* (15), 2680-98.
114. Su, Y.; Ge, J.; Zhu, B.; Zheng, Y. G.; Zhu, Q.; Yao, S. Q. Target identification of biologically active small molecules via in situ methods. *Curr. Opin. Chem. Biol.* **2013**, *17* (5), 768-75.

115. Huisgen, R. 1,3-Dipolar cycloadditions: Past and future. *Angew. Chem. Int. Ed.* **1963**, *2* (10), 565-98.
116. Rostovtsev, V. V.; Green, L. G.; Fokin, V. V.; Sharpless, K. B. A stepwise Huisgen cycloaddition process: Copper(I)-catalyzed regioselective ligation of azides and terminal alkynes. *Angew. Chem. Int. Ed.* **2002**, *41* (14), 2596-9.
117. Tornøe, C. W.; Christensen, C.; Meldal, M. Peptidotriazoles on solid phase: [1,2,3]-Triazoles by regiospecific copper(I)-catalyzed 1,3-dipolar cycloadditions of terminal alkynes to azides. *J. Org. Chem.* **2002**, *67* (9), 3057-64.
118. Sletten, E. M.; Bertozzi, C. R. Bioorthogonal chemistry: Fishing for selectivity in a sea of functionality. *Angew. Chem. Int. Ed.* **2009**, *48* (38), 6974-98.
119. Dormán, G.; Prestwich, G. D. Benzophenone photophores in biochemistry. *Biochemistry* **1994**, *33* (19), 5661-73.
120. Galardy, R. E.; Craig, L. C.; Printz, M. P. Benzophenone triplet: A new photochemical probe of biological ligand-receptor interactions. *Nat. New Biol.* **1973**, *242* (117), 127-8.
121. Smith, E.; Collins, I. Photoaffinity labeling in target- and binding-site identification. *Future Med. Chem.* **2015**, *7* (2), 159-83.
122. Geiger, M. W.; Elliot, M. M.; Karacostas, V. D.; Moricone, T. J.; Salmon, J. B.; Sideli, V. L.; Onge, M. A. S. Aryl azides as protein photolabels: Absorption spectral properties and quantum yields of photodissociation. *Photochem. Photobiol.* **1984**, *40* (4), 545-8.
123. Knowles, J. R. Photogenerated reagents for biological receptor-site labeling. *Acc. Chem. Res.* **1972**, *5* (4), 155-60.
124. Tanaka, Y.; Bond, M. R.; Kohler, J. J. Photocrosslinkers illuminate interactions in living cells. *Mol. BioSyst.* **2008**, *4* (6), 473-80.
125. Das, J. Aliphatic diazirines as photoaffinity probes for proteins: Recent developments. *Chem. Rev.* **2011**, *111* (8), 4405-17.
126. Dubinsky, L.; Krom, B. P.; Meijler, M. M. Diazirine based photoaffinity labeling. *Bioorg. Med. Chem.* **2012**, *20* (2), 554-70.
127. Brunner, J.; Senn, H.; Richards, F. M. 3-Trifluoromethyl-3-phenyldiazirine: A new carbene generating group for photolabeling reagents. *J. Biol. Chem.* **1980**, *255* (8), 3313-8.
128. Eirich, J.; Burkhart, J. L.; Ullrich, A.; Rudolf, G. C.; Vollmar, A.; Zahler, S.; Kazmaier, U.; Sieber, S. A.; Fürst, R.; Zahler, S. Pretubulysin derived probes as novel tools for monitoring the microtubule network via activity-based protein profiling and fluorescence microscopy. *Mol. BioSyst.* **2012**, *8* (8), 2067-75.
129. Singh, A.; Thornton, E. R.; Westheimer, F. H. Photolysis of diazoacetylchymotrypsin. *J. Biol. Chem.* **1962**, *237* (9), 3006-8.

130. Chowdhry, V.; Westheimer, F. H. Photoaffinity labeling of biological systems. *Annu. Rev. Biochem.* **1979**, *48* (1), 293-325.
131. Lapinsky, D. J.; Johnson, D. S. Recent developments and applications of clickable photoprobes in medicinal chemistry and chemical biology. *Future Med. Chem.* **2015**, *7* (16), 2143-71.
132. Leslie, B. J.; Hergenrother, P. J.; Stults, J. T.; Lyons, D. E.; Siems, W. F.; Crouch, G. J.; Barr, R.; Facemyer, K. C.; Cremona, C. R.; Gehlsen, K.; Drewe, J.; Tseng, B.; Cai, S. X.; Kasibhatla, S. R.; Meggio, F.; Totzke, F.; Schächtele, C.; Lerman, A. S.; Carnero, A.; Wan, Y.; Gray, N.; Meijer, L. Identification of the cellular targets of bioactive small organic molecules using affinity reagents. *Chem. Soc. Rev.* **2008**, *37* (7), 1347-60.
133. Lapinsky, D. J. Tandem photoaffinity labeling-bioorthogonal conjugation in medicinal chemistry. *Bioorg. Med. Chem.* **2012**, *20* (21), 6237-47.
134. MacKinnon, A. L.; Garrison, J. L.; Hegde, R. S.; Taunton, J. Photo-leucine incorporation reveals the target of a cyclodepsipeptide inhibitor of cotranslational translocation. *J. Am. Chem. Soc.* **2007**, *129* (47), 14560-1.
135. MacKinnon, A. L.; Taunton, J. Target identification by diazirine photo-cross-linking and click chemistry. *Curr. Protoc. Chem. Biol.* **2009**, *1*, 55-73.
136. Shi, H.; Cheng, X.; Sze, S. K.; Yao, S. Q. Proteome profiling reveals potential cellular targets of staurosporine using a clickable cell-permeable probe. *Chem. Commun.* **2011**, *47* (40), 11306-8.
137. Shi, H.; Zhang, C.-J.; Chen, G. Y. J.; Yao, S. Q. Cell-based proteome profiling of potential dasatinib targets by use of affinity-based probes. *J. Am. Chem. Soc.* **2012**, *134* (6), 3001-14.
138. Li, Z.; Hao, P.; Li, L.; Tan, C. Y.; Cheng, X.; Chen, G. Y.; Sze, S. K.; Shen, H. M.; Yao, S. Q. Design and synthesis of minimalist terminal alkyne-containing diazirine photo-crosslinkers and their incorporation into kinase inhibitors for cell- and tissue-based proteome profiling. *Angew. Chem. Int. Ed.* **2013**, *52* (33), 8551-6.
139. Parker, C. G.; Galmozzi, A.; Wang, Y.; Correia, B. E.; Sasaki, K.; Joslyn, C. M.; Kim, A. S.; Cavallaro, C. L.; Lawrence, R. M.; Johnson, S. R.; Narvaiza, I.; Saez, E.; Cravatt, B. F. Ligand and target discovery by fragment-based screening in human cells. *Cell* **2017**, *168* (3), 527-541.e29.
140. Kambe, T.; Correia, B. E.; Niphakis, M. J.; Cravatt, B. F. Mapping the protein interaction landscape for fully functionalized small-molecule probes in human cells. *J. Am. Chem. Soc.* **2014**, *136* (30), 10777-82.
141. Sakurai, K.; Ozawa, S.; Yamada, R.; Yasui, T.; Mizuno, S. Comparison of the reactivity of carbohydrate photoaffinity probes with different photoreactive groups. *ChemBioChem* **2014**, *15* (10), 1399-403.

142. Bush, J. T.; Walport, L. J.; McGouran, J. F.; Leung, I. K. H.; Berridge, G.; van Berkel, S. S.; Basak, A.; Kessler, B. M.; Schofield, C. J. The Ugi four-component reaction enables expedient synthesis and comparison of photoaffinity probes. *Chem. Sci.* **2013**, *4* (11), 4115-20.
143. Park, J.; Koh, M.; Koo, J. Y.; Lee, S.; Park, S. B. Investigation of specific binding proteins to photoaffinity linkers for efficient deconvolution of target protein. *ACS Chem. Biol.* **2016**, *11* (1), 44-52.
144. Park, H.; Koo, J. Y.; Srikanth, Y. V. V.; Oh, S.; Lee, J.; Park, J.; Park, S. B. Nonspecific protein labeling of photoaffinity linkers correlates with their molecular shapes in living cells. *Chem. Commun.* **2016**, *52* (34), 5828-31.
145. Tan, X.; Kong, L.; Dai, H.; Cheng, X.; Liu, F.; Tschierske, C. Triblock polyphiles through click chemistry: Self-assembled thermotropic cubic phases formed by micellar and monolayer vesicular aggregates. *Chem. Eur. J.* **2013**, *19* (48), 16303-13.
146. Heydenreuter, W.; Kunold, E.; Sieber, S. A., Alkynol natural products target ALDH2 in cancer cells by irreversible binding to the active site. *Chem. Commun.* **2015**, *51* (87), 15784-7.
147. Cox, J.; Mann, M., MaxQuant enables high peptide identification rates, individualized p.p.b.-range mass accuracies and proteome-wide protein quantification. *Nat. Biotechnol.* **2008**, *26* (12), 1367-72.
148. Cox, J.; Neuhauser, N.; Michalski, A.; Scheltema, R. A.; Olsen, J. V.; Mann, M. Andromeda: A peptide search engine integrated into the MaxQuant environment. *J. Proteome Res.* **2011**, *10* (4), 1794-805.
149. Tyanova, S.; Temu, T.; Sinitcyn, P.; Carlson, A.; Hein, M. Y.; Geiger, T.; Mann, M.; Cox, J. The Perseus computational platform for comprehensive analysis of (prote)omics data. *Nat. Meth.* **2016**, *13* (9), 731-40.
150. Finn, R. D.; Coggill, P.; Eberhardt, R. Y.; Eddy, S. R.; Mistry, J.; Mitchell, A. L.; Potter, S. C.; Punta, M.; Qureshi, M.; Sangrador-Vegas, A.; Salazar, G. A.; Tate, J.; Bateman, A. The Pfam protein families database: Towards a more sustainable future. *Nucleic Acids Res.* **2016**, *44* (D1), D279-D285.
151. Sigrist, C. J. A.; De Castro, E.; Cerutti, L.; Cuče, B. A.; Hulo, N.; Bridge, A.; Bougueleret, L.; Xenarios, I. New and continuing developments at PROSITE. *Nucleic Acids Res.* **2013**, *41* (D1), D344-7.
152. Schwanhäusser, B.; Busse, D.; Li, N.; Dittmar, G.; Schuchhardt, J.; Wolf, J.; Chen, W.; Selbach, M. Global quantification of mammalian gene expression control. *Nature* **2011**, *473* (7347), 337-42.
153. Wilhelm, M.; Schlegl, J.; Hahne, H.; Gholami, A. M.; Lieberenz, M.; Savitski, M. M.; Ziegler, E.; Butzmann, L.; Gessulat, S.; Marx, H.; Mathieson, T.; Lemeer, S.;

- Schnatbaum, K.; Reimer, U.; Wenschuh, H.; Mollenhauer, M.; Slotta-Huspenina, J.; Boese, J. H.; Bantscheff, M.; Gerstmair, A.; Faerber, F.; Kuster, B. Mass-spectrometry-based draft of the human proteome. *Nature* **2014**, *509* (7502), 582-7.
154. Bennett, B. L.; Sasaki, D. T.; Murray, B. W.; O'Leary, E. C.; Sakata, S. T.; Xu, W.; Leisten, J. C.; Motiwala, A.; Pierce, S.; Satoh, Y.; Bhagwat, S. S.; Manning, A. M.; Anderson, D. W. SP600125, an anthrapyrazolone inhibitor of Jun N-terminal kinase. *Proc. Natl. Acad. Sci. U. S. A.* **2001**, *98* (24), 13681-6.
155. Scapin, G.; Patel, S. B.; Lisnock, J.; Becker, J. W.; LoGrasso, P. V. The structure of JNK3 in complex with small molecule inhibitors. *Chem. Biol.* **2003**, *10* (8), 705-12.
156. Hidaka, H.; Inagaki, M.; Kawamoto, S.; Sasaki, Y. Isoquinolinesulfonamides, novel and potent inhibitors of cyclic nucleotide dependent protein kinase and protein kinase C. *Biochemistry* **1984**, *23* (21), 5036-41.
157. Engh, R. A.; Girod, A.; Kinzel, V.; Huber, R.; Bossemeyer, D. Crystal structures of catalytic subunit of cAMP-dependent protein kinase in complex with isoquinolinesulfonyl protein kinase inhibitors H7, H8, and H89. *J. Biol. Chem.* **1996**, *271* (42), 26157-64.
158. Lochner, A.; Moolman, J. A. The many faces of H89: A review. *Cardiovasc. Drug Rev.* **2006**, *24* (3-4), 261-74.
159. Morikawa, A.; Sone, T.; Asano, T. 5-Isoquinolinesulfonamide derivatives. 1. Synthesis and vasodilatory activity of *N*-(2-guanidinoethyl)-5-isoquinolinesulfonamide derivatives. *J. Med. Chem.* **1989**, *32* (1), 42-6.
160. Shannon, P.; Markiel, A.; Ozier, O.; Baliga, N. S.; Wang, J. T.; Ramage, D.; Amin, N.; Schwikowski, B.; Ideker, T. Cytoscape: A software environment for integrated models of biomolecular interaction networks. *Genome Res.* **2003**, *13* (11), 2498-504.
161. Ashburn, T. T.; Thor, K. B., Drug repositioning: Identifying and developing new uses for existing drugs. *Nat. Rev. Drug Discov.* **2004**, *3* (8), 673-83.
162. Chong, C. R.; Sullivan, D. J. New uses for old drugs. *Nature* **2007**, *448* (7154), 645-6.
163. Schaenzer, A. J.; Wlodarchak, N.; Drewry, D. H.; Zuercher, W. J.; Rose, W. E.; Striker, R.; Sauer, J. D. A screen for kinase inhibitors identifies antimicrobial imidazopyridine aminofurazans as specific inhibitors of the *Listeria monocytogenes* PASTA kinase PrkA. *J. Biol. Chem.* **2017**, *292* (41), 17037-45.
164. Wlodarchak, N.; Teachout, N.; Procknow, R.; Beczkiewicz, J.; Schaenzer, A.; Satyshur, K.; Pavelka, M.; Zuercher, B.; Drewry, D.; Sauer, J.-D.; Striker, R. Repurposed kinase inhibitors and  $\beta$ -lactams as a novel therapy for antibiotic resistant bacteria. *bioRxiv* 199422.
165. Miller, J. R.; Dunham, S.; Mochalkin, I.; Banotai, C.; Bowman, M.; Buist, S.; Dunkle, B.; Hanna, D.; Harwood, H. J.; Huband, M. D.; Karnovsky, A.; Kuhn, M.; Limberakis, C.; Liu, J. Y.; Mehrens, S.; Mueller, W. T.; Narasimhan, L.; Ogden, A.; Ohren, J.; Prasad, J. V.

- N. V.; Shelly, J. A.; Skerlos, L.; Sulavik, M.; Thomas, V. H.; VanderRoest, S.; Wang, L.; Wang, Z.; Whitton, A.; Zhu, T.; Stover, C. K. A class of selective antibacterials derived from a protein kinase inhibitor pharmacophore. *Proc. Natl. Acad. Sci. U. S. A.* **2009**, *106* (6), 1737-42.
166. Wilhelm, S.; Carter, C.; Lynch, M.; Lowinger, T.; Dumas, J.; Smith, R. A.; Schwartz, B.; Simantov, R.; Kelley, S. Discovery and development of sorafenib: A multikinase inhibitor for treating cancer. *Nat. Rev. Drug Discov.* **2006**, *5* (10), 835-44.
167. Roberts, J. L.; Tavallai, M.; Nourbakhsh, A.; Fidanza, A.; Cruz-Luna, T.; Smith, E.; Siembida, P.; Plamondon, P.; Cycon, K. A.; Doern, C. D.; Booth, L.; Dent, P. GRP78/Dna K is a target for Nexavar/Stivarga/Votrient in the treatment of human malignancies, viral infections and bacterial diseases. *J. Cell. Physiol.* **2015**, *230* (10), 2552-78.
168. Chang, H. C.; Huang, Y. T.; Chen, C. S.; Chen, Y. W.; Huang, Y. T.; Su, J. C.; Teng, L. J.; Shiau, C. W.; Chiu, H. C. In vitro and in vivo activity of a novel sorafenib derivative SC5005 against MRSA. *J. Antimicrob. Chemother.* **2016**, *71* (2), 449-59.
169. Shiau, C.-W.; Chiu, H.-C. Substituted malonamides and their use as antibacterial drugs. International patent application: WO2017028745 A1, PCT/CN2016/094855, **2017**.
170. Kleiner, P.; Heydenreuter, W.; Stahl, M.; Korotkov, V. S.; Sieber, S. A. A whole proteome inventory of background photocrosslinker binding. *Angew. Chem. Int. Ed.* **2017**, *56* (5), 1396-401.
171. Rao, S.; De Waelheyns, E.; Economou, A.; Anné, J. Antibiotic targeting of the bacterial secretory pathway. *Biochim. Biophys. Acta.* **2014**, *1843* (8), 1762-83.
172. Fey, P. D.; Endres, J. L.; Yajjala, V. K.; Widhelm, T. J.; Boissy, R. J.; Bose, J. L.; Bayles, K. W. A genetic resource for rapid and comprehensive phenotype screening of nonessential *Staphylococcus aureus* genes. *mBio* **2013**, *4* (1), e00537-12.
173. Craney, A.; Romesberg, F. E. A putative Cro-like repressor contributes to arylomycin resistance in *Staphylococcus aureus*. *Antimicrob. Agents Chemother.* **2015**, *59* (6), 3066-74.
174. Craney, A.; Dix, M. M.; Adhikary, R.; Cravatt, B. F.; Romesberg, F. E. An alternative terminal step of the general secretory pathway in *Staphylococcus aureus*. *mBio* **2015**, *6* (4), e01178-15.
175. Morisaki, J. H.; Smith, P. A.; Date, S. V.; Kajihara, K. K.; Truong, C. L.; Modrusan, Z.; Yan, D.; Kang, J.; Xu, M.; Shah, I. M.; Mintzer, R.; Kofoed, E. M.; Cheung, T. K.; Arnott, D.; Koehler, M. F. T.; Heise, C. E.; Brown, E. J.; Tan, M.-W.; Hazenbos, W. L. W. A putative bacterial ABC transporter circumvents the essentiality of signal peptidase. *mBio* **2016**, *7* (5), e00412-16.
176. Auclair, S. M.; Bhanu, M. K.; Kendall, D. A. Signal peptidase I: Cleaving the way to mature proteins. *Protein Sci.* **2012**, *21* (1), 13-25.

177. Ekici, Ö. D.; Paetzel, M.; Dalbey, R. E. Unconventional serine proteases: Variations on the catalytic Ser/His/Asp triad configuration. *Protein Sci.* **2008**, *17* (12), 2023-37.
178. Ting, Y. T.; Harris, P. W. R.; Batot, G.; Brimble, M. A.; Baker, E. N.; Young, P. G. Peptide binding to a bacterial signal peptidase visualized by peptide tethering and carrier-driven crystallization. *IUCrJ* **2016**, *3* (1), 10-9.
179. Schimana, J.; Gebhardt, K.; Höltzel, A.; Schmid, D. G.; Süssmuth, R.; Müller, J.; Pukall, R.; Fiedler, H.-P. Arylomycins A and B, new biaryl-bridged lipopeptide antibiotics produced by *Streptomyces* sp. Tue 6075. I. Taxonomy, fermentation, isolation and biological activities. *J. Antibiot. (Tokyo)* **2002**, *55* (6), 565-70.
180. Kulanthaivel, P.; Kreuzman, A. J.; Strege, M. A.; Belvo, M. D.; Smitka, T. A.; Clemens, M.; Swartling, J. R.; Minton, K. L.; Zheng, F.; Angleton, E. L.; Mullen, D.; Jungheim, L. N.; Klimkowski, V. J.; Nicas, T. I.; Thompson, R. C.; Peng, S.-B. Novel lipoglycopeptides as inhibitors of bacterial signal peptidase I. *J. Biol. Chem.* **2004**, *279* (35), 36250-8.
181. Tan, Y. X.; Romesberg, F. E. Latent antibiotics and the potential of the arylomycins for broad-spectrum antibacterial activity. *MedChemComm.* **2012**, *3* (8), 916-25.
182. Therien, A. G.; Huber, J. L.; Wilson, K. E.; Beaulieu, P.; Caron, A.; Claveau, D.; Deschamps, K.; Donald, R. G. K.; Galgoci, A. M.; Gallant, M.; Gu, X.; Kevin, N. J.; Lafleur, J.; Leavitt, P. S.; Lebeau-Jacob, C.; Lee, S. S.; Lin, M. M.; Michels, A. A.; Ogawa, A. M.; Painter, R. E.; Parish, C. A.; Park, Y.-W.; Benton-Perdomo, L.; Petcu, M.; Phillips, J. W.; Powles, M. A.; Skorey, K. I.; Tam, J.; Tan, C. M.; Young, K.; Wong, S.; Waddell, S. T.; Miesel, L. Broadening the spectrum of  $\beta$ -lactam antibiotics through inhibition of signal peptidase type I. *Antimicrob. Agents Chemother.* **2012**, *56* (9), 4662-70.
183. Allsop, A.; Brooks, G.; Edwards, P. D.; Kaura, A. C.; Southgate, R. Inhibitors of bacterial signal peptidase: A series of 6-(substituted oxyethyl)penems. *J. Antibiot. (Tokyo)* **1996**, *49* (9), 921-8.
184. Hu, X.; Kim, N.; Grinius, L.; Morris, C.; Wallace, C.; Mieling, G.; Demuth, T. Synthesis of (5S)-tricyclic penems as novel and potent inhibitors of bacterial signal peptidases. *Synthesis* **2003**, *2003* (11), 1732-8.
185. Harris, D. A.; Powers, M. E.; Romesberg, F. E. Synthesis and biological evaluation of penem inhibitors of bacterial signal peptidase. *Bioorg. Med. Chem. Lett.* **2009**, *19* (14), 3787-90.
186. Bruton, G.; Huxley, A.; O'Hanlon, P.; Orlek, B.; Eggleston, D.; Humphries, J.; Readshaw, S.; West, A.; Ashman, S.; Brown, M.; Moore, K.; Pope, A.; O'Dwyer, K.; Wang, L. Lipopeptide substrates for SpsB, the *Staphylococcus aureus* type I signal peptidase: Design, conformation and conversion to  $\alpha$ -ketoamide inhibitors. *Eur. J. Med. Chem.* **2003**, *38* (4), 351-6.

187. Buzder-Lantos, P.; Bockstael, K.; Anné, J.; Herdewijn, P. Substrate based peptide aldehyde inhibits bacterial type I signal peptidase. *Bioorg. Med. Chem. Lett.* **2009**, *19* (10), 2880-3.
188. Smith, P. A.; Romesberg, F. E. Mechanism of action of the arylomycin antibiotics and effects of signal peptidase I inhibition. *Antimicrob. Agents Chemother.* **2012**, *56* (10), 5054-60.
189. Smith, P. A.; Roberts, T. C.; Romesberg, F. E. Broad-spectrum antibiotic activity of the arylomycin natural products is masked by natural target mutations. *Chem. Biol.* **2010**, *17* (11), 1223-31.
190. Rao, S.; Bockstael, K.; Nath, S.; Engelborghs, Y.; Anné, J.; Geukens, N. Enzymatic investigation of the *Staphylococcus aureus* type I signal peptidase SpsB - implications for the search for novel antibiotics. *FEBS J.* **2009**, *276* (12), 3222-34.
191. Wang, Y.; Bruckner, R.; Stein, R. L. Regulation of signal peptidase by phospholipids in membrane: Characterization of phospholipid bilayer incorporated *Escherichia coli* signal peptidase. *Biochemistry* **2004**, *43*, 265-70.
192. Smith, R. A.; Barbosa, J.; Blum, C. L.; Bobko, M. A.; Caringal, Y. V.; Dally, R.; Johnson, J. S.; Katz, M. E.; Kennure, N.; Kingery-Wood, J.; Lee, W.; Lowinger, T. B.; Lyons, J.; Marsh, V.; Rogers, D. H.; Swartz, S.; Walling, T.; Wild, H. Discovery of heterocyclic ureas as a new class of raf kinase inhibitors: Identification of a second generation lead by a combinatorial chemistry approach. *Bioorg. Med. Chem. Lett.* **2001**, *11* (20), 2775-8.
193. Conlon, B. P.; Nakayasu, E. S.; Fleck, L. E.; LaFleur, M. D.; Isabella, V. M.; Coleman, K.; Leonard, S. N.; Smith, R. D.; Adkins, J. N.; Lewis, K. Activated ClpP kills persisters and eradicates a chronic biofilm infection. *Nature* **2013**, *503* (7476), 365-70.
194. Kim, W.; Conery, A. L.; Rajamuthiah, R.; Fuchs, B. B.; Ausubel, F. M.; Mylonakis, E. Identification of an antimicrobial agent effective against methicillin-resistant *Staphylococcus aureus* persisters using a fluorescence-based screening strategy. *PLOS ONE* **2015**, *10* (6), e0127640.
195. Silver, L. L. Challenges of antibacterial discovery. *Clin. Microbiol. Rev.* **2011**, *24* (1), 71-109.
196. McGovern, S. L.; Helfand, B. T.; Feng, B.; Shoichet, B. K. A specific mechanism of nonspecific inhibition. *J. Med. Chem.* **2003**, *46* (20), 4265-72.
197. Owen, S. C.; Doak, A. K.; Wassam, P.; Shoichet, M. S.; Shoichet, B. K. Colloidal aggregation affects the efficacy of anticancer drugs in cell culture. *ACS Chem. Biol.* **2012**, *7* (8), 1429-35.
198. Brötz-Oesterhelt, H.; Beyer, D.; Kroll, H. P.; Endermann, R.; Ladel, C.; Schroeder, W.; Hinzen, B.; Raddatz, S.; Paulsen, H.; Henninger, K.; Bandow, J. E.; Sahl, H. G.;

- Labischinski, H. Dysregulation of bacterial proteolytic machinery by a new class of antibiotics. *Nat. Med.* **2005**, *11* (10), 1082-7.
199. Hackl, M. W.; Lakemeyer, M.; Dahmen, M.; Glaser, M.; Pahl, A.; Lorenz-Baath, K.; Menzel, T.; Sievers, S.; Böttcher, T.; Antes, I.; Waldmann, H.; Sieber, S. A. Phenyl esters are potent inhibitors of caseinolytic protease P and reveal a stereogenic switch for deoligomerization. *J. Am. Chem. Soc.* **2015**, *137* (26), 8475-83.
200. Antes, I. DynaDock: A novel molecular dynamics-based algorithm for protein-peptide docking including receptor flexibility. *Proteins* **2010**, *78* (5), 1084-104.
201. Eisenmesser, E. Z.; Millet, O.; Labeikovsky, W.; Korzhnev, D. M.; Wolf-Watz, M.; Bosco, D. A.; Skalicky, J. J.; Kay, L. E.; Kern, D. Intrinsic dynamics of an enzyme underlies catalysis. *Nature* **2005**, *438* (7064), 117-21.
202. McAuley, M.; Timson, D. J. Modulating mobility: A paradigm for protein engineering? *Appl. Biochem. Biotechnol.* **2017**, *181* (1), 83-90.
203. Schallenberger, M. A.; Niessen, S.; Shao, C.; Fowler, B. J.; Romesberg, F. E. Type I signal peptidase and protein secretion in *Staphylococcus aureus*. *J. Bacteriol.* **2012**, *194* (10), 2677-86.
204. Craney, A.; Romesberg, F. E. The inhibition of type I bacterial signal peptidase: Biological consequences and therapeutic potential. *Bioorg. Med. Chem. Lett.* **2015**, *25* (21), 4761-6.
205. Hiller, K.; Grote, A.; Scheer, M.; Munch, R.; Jahn, D. PrediSi: Prediction of signal peptides and their cleavage positions. *Nucleic Acids Res.* **2004**, *32*, W375-9.
206. Frankel, M. B.; Hendrickx, A. P. A.; Missiakas, D. M.; Schneewind, O. LytN, a murein hydrolase in the cross-wall compartment of *Staphylococcus aureus*, is involved in proper bacterial growth and envelope assembly. *J. Biol. Chem.* **2011**, *286* (37), 32593-605.
207. Chao, M. C.; Kieser, K. J.; Minami, S.; Mavrici, D.; Aldridge, B. B.; Fortune, S. M.; Alber, T.; Rubin, E. J. Protein complexes and proteolytic activation of the cell wall hydrolase RipA regulate septal resolution in mycobacteria. *PLOS Pathogens* **2013**, *9* (2), e1003197.
208. Bæk, K. T.; Frees, D.; Renzoni, A.; Barras, C.; Rodriguez, N.; Manzano, C.; Kelley, W. L. Genetic variation in the *Staphylococcus aureus* 8325 strain lineage revealed by whole-genome sequencing. *PLOS ONE* **2013**, *8* (9), e77122.
209. Lee, E. Y.; Choi, D. Y.; Kim, D. K.; Kim, J. W.; Park, J. O.; Kim, S.; Kim, S. H.; Desiderio, D. M.; Kim, Y. K.; Kim, K. P.; Gho, Y. S. Gram-positive bacteria produce membrane vesicles: Proteomics-based characterization of *Staphylococcus aureus*-derived membrane vesicles. *Proteomics* **2009**, *9* (24), 5425-36.
210. Pinho, M. G.; Kjos, M.; Veening, J. W. How to get (a)round: Mechanisms controlling growth and division of coccoid bacteria. *Nat. Rev. Microbiol.* **2013**, *11* (9), 601-14.

211. Brown, L.; Wolf, J. M.; Prados-Rosales, R.; Casadevall, A. Through the wall: Extracellular vesicles in Gram-positive bacteria, mycobacteria and fungi. *Nat. Rev. Microbiol.* **2015**, *13* (10), 620-30.
212. Weinandy, F.; Lorenz-Baath, K.; Korotkov, V. S.; Böttcher, T.; Sethi, S.; Chakraborty, T.; Sieber, S. A. A  $\beta$ -lactone-based antivirulence drug ameliorates *Staphylococcus aureus* skin infections in mice. *ChemMedChem.* **2014**, *9* (4), 710-3.
213. Médard, G.; Pachi, F.; Ruprecht, B.; Klaeger, S.; Heinzlmeir, S.; Helm, D.; Qiao, H.; Ku, X.; Wilhelm, M.; Kuehne, T.; Wu, Z.; Dittmann, A.; Hopf, C.; Kramer, K.; Kuster, B. Optimized chemical proteomics assay for kinase inhibitor profiling. *J. Proteome Res.* **2015**, *14* (3), 1574-86.
214. Wan, P. T. C.; Garnett, M. J.; Roe, S. M.; Lee, S.; Niculescu-Duvaz, D.; Good, V. M.; Project, C. G.; Jones, C. M.; Marshall, C. J.; Springer, C. J.; Barford, D.; Marais, R. Mechanism of activation of the RAF-ERK signaling pathway by oncogenic mutations of B-RAF. *Cell* **2004**, *116* (6), 855-67.
215. Wu, P.; Nielsen, T. E.; Clausen, M. H. FDA-approved small-molecule kinase inhibitors. *Trends Pharmacol. Sci.* **2015**, *36* (7), 422-39.
216. Savitski, M. M.; Reinhard, F. B. M.; Franken, H.; Werner, T.; Savitski, M. F.; Eberhard, D.; Molina, D. M.; Jafari, R.; Dovega, R. B.; Klaeger, S.; Kuster, B.; Nordlund, P.; Bantscheff, M.; Drewes, G. Tracking cancer drugs in living cells by thermal profiling of the proteome. *Science* **2014**, *346* (6205), 1255784.
217. Jagtap, A. D.; Kondekar, N. B.; Sadani, A. A.; Chern, J.-W. Ureas: Applications in drug design. *Curr. Med. Chem.* **2017**, *24* (6), 622-51.
218. Meanwell, N. A. Synopsis of some recent tactical application of bioisosteres in drug design. *J. Med. Chem.* **2011**, *54* (8), 2529-91.
219. Ghosh, M.; Miller, P. A.; Möllmann, U.; Claypool, W. D.; Schroeder, V. A.; Wolter, W. R.; Suckow, M.; Yu, H.; Li, S.; Huang, W.; Zajicek, J.; Miller, M. J. Targeted antibiotic delivery: Selective siderophore conjugation with daptomycin confers potent activity against multidrug resistant *Acinetobacter baumannii* both in vitro and in vivo. *J. Med. Chem.* **2017**, *60* (11), 4577-83.
220. World Health Organization (WHO). WHO Global Tuberculosis Report 2017. *WHO* **2017**, Geneva. Available from: [apps.who.int/iris/bitstream/10665/259366/1/9789241565516-eng.pdf](https://apps.who.int/iris/bitstream/10665/259366/1/9789241565516-eng.pdf)
221. Hayakawa, K.; Yodo, M.; Ohsuki, S.; Kanematsu, K. Novel bicycloannulation via tandem vinylation and intramolecular Diels-Alder reaction of five-membered heterocycles: A new approach to construction of psoralen and azapsoralen. *J. Am. Chem. Soc.* **1984**, *106* (22), 6735-40.

222. Showalter, H. D. H.; Johnson, J. L.; Hoftiezer, J. M.; Turner, W. R.; Werbel, L. M.; Leopold, W. R.; Shillis, J. L.; Jackson, R. C.; Elslager, E. F. Anthrapyrazole anticancer agents: Synthesis and structure-activity relationships against murine leukemias. *J. Med. Chem.* **1987**, *30* (1), 121-31.
223. Ricouart, A.; Gesquiere, J. C.; Tartar, A.; Sergheraert, C. Design of potent protein kinases inhibitors using the bisubstrate approach. *J. Med. Chem.* **1991**, *34* (1), 73-8.
224. Conti, P.; Tamborini, L.; Pinto, A.; Sola, L.; Ettari, R.; Mercurio, C.; De Micheli, C. Design and synthesis of novel isoxazole-based HDAC inhibitors. *Eur. J. Med. Chem.* **2010**, *45* (9), 4331-8.
225. Hwang, S. H.; Weckler, A. T.; Zhang, G.; Morisseau, C.; Nguyen, L. V.; Fu, S. H.; Hammock, B. D. Synthesis and biological evaluation of sorafenib- and regorafenib-like sEH inhibitors. *Bioorg. Med. Chem. Lett.* **2013**, *23* (13), 3732-7.
226. Yao, J.; Chen, J.; He, Z.; Sun, W.; Xu, W. Design, synthesis and biological activities of thiourea containing sorafenib analogs as antitumor agents. *Bioorg. Med. Chem.* **2012**, *20* (9), 2923-9.
227. Zhang, L.; Darko, A. K.; Johns, J. I.; McElwee-White, L. Catalytic oxidative carbonylation of arylamines to ureas with  $W(CO)_6/I_2$  as catalyst. *Eur. J. Org. Chem.* **2011**, *2011* (31), 6261-8.
228. Džolić, Z. R.; Perković, I.; Pavelić, S. K.; Sedić, M.; Ilić, N.; Schols, D.; Zorc, B. Design, synthesis, and cytostatic activity of novel pyrazine sorafenib analogs. *Med. Chem. Res.* **2016**, *25* (12), 2729-41.
229. Huang, T. T.; Huang, Y. C.; Qing, X. Y.; Xia, Y.; Luo, X.; Ye, T. H.; Yu, L. T. Synthesis and biological evaluation of novel *N*-methyl-picolinamide-4-thiol derivatives as potential antitumor agents. *Molecules* **2012**, *17* (6), 6317-30.
230. Rodríguez, F.; Rozas, I.; Kaiser, M.; Brun, R.; Nguyen, B.; Wilson, W. D.; García, R. N.; Dardonville, C. New bis(2-aminoimidazoline) and bisguanidine DNA minor groove binders with potent in vivo antitrypanosomal and antiplasmodial activity. *J. Med. Chem.* **2008**, *51* (4), 909-23.
231. Khire, U. R.; Bankston, D.; Barbosa, J.; Brittelli, D. R.; Caringal, Y.; Carlson, R.; Dumas, J.; Gane, T.; Heald, S. L.; Hibner, B.; Johnson, J. S.; Katz, M. E.; Kennure, N.; Kingery-Wood, J.; Lee, W.; Liu, X.-G.; Lowinger, T. B.; McAlexander, I.; Monahan, M.-K.; Natero, R.; Renick, J.; Riedl, B.; Rong, H.; Sibley, R. N.; Smith, R. A.; Wolanin, D. Omega-carboxypyridyl substituted ureas as Raf kinase inhibitors. *Bioorg. Med. Chem. Lett.* **2004**, *14* (3), 783-6.
232. Chen, Y.; Kamlet, A. S.; Steinman, J. B.; Liu, D. R. A biomolecule-compatible visible-light-induced azide reduction from a DNA-encoded reaction-discovery system. *Nature Chem.* **2011**, *3* (2), 146-53.

233. Vizcaíno, J. A.; Csordas, A.; del-Toro, N.; Dianes, J. A.; Griss, J.; Lavidas, I.; Mayer, G.; Perez-Riverol, Y.; Reisinger, F.; Ternent, T.; Xu, Q.-W.; Wang, R.; Hermjakob, H. 2016 update of the PRIDE database and its related tools. *Nucleic Acids Res.* **2016**, *44* (D1), D447-56.
234. Ventura, C. L.; Malachowa, N.; Hammer, C. H.; Nardone, G. A.; Robinson, M. A.; Kobayashi, S. D.; DeLeo, F. R. Identification of a novel *Staphylococcus aureus* two-component leukotoxin using cell surface proteomics. *PLOS ONE* **2010**, *5* (7), e11634.
235. Pasztor, L.; Ziebandt, A.-K.; Nega, M.; Schlag, M.; Haase, S.; Franz-Wachtel, M.; Madlung, J.; Nordheim, A.; Heinrichs, D. E.; Götz, F. Staphylococcal major autolysin (Atl) is involved in excretion of cytoplasmic proteins. *J. Biol. Chem.* **2010**, *285* (47), 36794-803.
236. Sharma, A. K.; Kumar, S.; K, H.; Dhakan, D. B.; Sharma, V. K. Prediction of peptidoglycan hydrolases- a new class of antibacterial proteins. *BMC Genomics* **2016**, *17*, 411.
237. Bantscheff, M.; Eberhard, D.; Abraham, Y.; Bastuck, S.; Boesche, M.; Hobson, S.; Mathieson, T.; Perrin, J.; Raida, M.; Rau, C.; Reader, V.; Sweetman, G.; Bauer, A.; Bouwmeester, T.; Hopf, C.; Kruse, U.; Neubauer, G.; Ramsden, N.; Rick, J.; Kuster, B.; Drewes, G. Quantitative chemical proteomics reveals mechanisms of action of clinical ABL kinase inhibitors. *Nat. Biotechnol.* **2007**, *25*, 1035-44.
238. Lemeer, S.; Zörgiebel, C.; Ruprecht, B.; Kohl, K.; Kuster, B. Comparing immobilized kinase inhibitors and covalent ATP probes for proteomic profiling of kinase expression and drug selectivity. *J. Proteome Res.* **2013**, *12* (4), 1723-31.
239. Okano, A.; Isley, N. A.; Boger, D. L. Peripheral modifications of [Ψ[CH<sub>2</sub>NH]Tpg<sub>4</sub>]vancomycin with added synergistic mechanisms of action provide durable and potent antibiotics. *Proc. Natl. Acad. Sci. U. S. A.* **2017**, *114* (26), E5052-61.
240. Springer, M. T.; Singh, V. K.; Cheung, A. L.; Donegan, N. P.; Chamberlain, N. R. Effect of clpP and clpC deletion on persister cell number in *Staphylococcus aureus*. *J. Med. Microbiol.* **2016**, *65* (8), 848-57.
241. Jennings, M. C.; Ator, L. E.; Paniak, T. J.; Minbiole, K. P. C.; Wuest, W. M. Biofilm-eradicating properties of quaternary ammonium amphiphiles: Simple mimics of antimicrobial peptides. *ChemBioChem.* **2014**, *15* (15), 2211-5.
242. Mitchell, M. A.; Iannetta, A. A.; Jennings, M. C.; Fletcher, M. H.; Wuest, W. M.; Minbiole, K. P. C. Scaffold-hopping of multicationic amphiphiles yields three new classes of antimicrobials. *ChemBioChem.* **2015**, *16* (16), 2299-303.
243. Mani, N.; Tobin, P.; Jayaswal, R. K. Isolation and characterization of autolysis-defective mutants of *Staphylococcus aureus* created by Tn917-lacZ mutagenesis. *J. Bacteriol.* **1993**, *175* (5), 1493-9.

244. Huff, E.; Silverman, C. S.; Adams, N. J.; Awkard, W. S. Extracellular cell wall lytic enzyme from *Staphylococcus aureus*: Purification and partial characterization. *J. Bacteriol.* **1970**, *103* (3), 761-9.
245. Atilano, M. L.; Pereira, P. M.; Vaz, F.; Catalão, M. J.; Reed, P.; Grilo, I. R.; Sobral, R. G.; Ligoxygakis, P.; Pinho, M. G.; Filipe, S. R. Bacterial autolysins trim cell surface peptidoglycan to prevent detection by the *Drosophila* innate immune system. *eLife* **2014**, *3*, e02277.
246. Vaz, F.; Filipe, S. R. Preparation and analysis of crude autolytic enzyme extracts from *Staphylococcus aureus*. *Bio-protocol* **2015**, e1687.
247. Blazyk, J.; Wiegand, R.; Klein, J.; Hammer, J.; Epand, R. M.; Epand, R. F.; Maloy, W. L.; Kari, U. P. A novel linear amphipathic beta-sheet cationic antimicrobial peptide with enhanced selectivity for bacterial lipids. *J. Biol. Chem.* **2001**, *276* (30), 27899-906.
248. Nusslein, K.; Arnt, L.; Rennie, J.; Owens, C.; Tew, G. N. Broad-spectrum antibacterial activity by a novel abiogenic peptide mimic. *Microbiology* **2006**, *152* (7), 1913-8.
249. Zhang, Y.; Huo, M.; Zhou, J.; Xie, S. PKSolver: An add-in program for pharmacokinetic and pharmacodynamic data analysis in Microsoft Excel. *Comput. Methods. Programs Biomed.* **2010**, *99* (3), 306-14.
250. Case, D. A., Berryman, J.T., Betz, R.M., Cerutti, D.S., Cheatham, T.E. III, Darden, T. A., Duke, R.E., Giese, T. J., Gohlke, H., Goetz, A.W., et al. Amber 2015. *University of California, San Francisco* **2015**.
251. Duan, Y.; Wu, C.; Chowdhury, S.; Lee, M. C.; Xiong, G.; Zhang, W.; Yang, R.; Cieplak, P.; Luo, R.; Lee, T.; Caldwell, J.; Wang, J.; Kollman, P. A point-charge force field for molecular mechanics simulations of proteins based on condensed-phase quantum mechanical calculations. *J. Comput. Chem.* **2003**, *24* (16), 1999-2012.
252. Wang, J.; Wolf, R. M.; Caldwell, J. W.; Kollman, P. A.; Case, D. A. Development and testing of a general amber force field. *J. Comput. Chem.* **2004**, *25* (9), 1157-74.
253. Jorgensen, W. L.; Chandrasekhar, J.; Madura, J. D.; Impey, R. W.; Klein, M. L. Comparison of simple potential functions for simulating liquid water. *J. Chem. Phys.* **1983**, *79* (2), 926-35.
254. Wang, J.; Wang, W.; Kollman, P. A.; Case, D. A. Automatic atom type and bond type perception in molecular mechanical calculations. *J. Mol. Graph. Model.* **2006**, *25* (2), 247-60.
255. Frisch, M. J., Trucks, G. W.; Schlegel, H. B., Scuseria, G. E., Robb, M. A., Cheeseman, J. R., Scalmani, G., Barone, V., Petersson, G. A., Nakatsuji, H., et al. Gaussian 09, Revision A.02. *Gaussian Inc., Wallingford CT* **2009**.
256. Essmann, U.; Perera, L.; Berkowitz, M. L.; Darden, T.; Lee, H.; Pedersen, L. G. A smooth particle mesh Ewald method. *J. Chem. Phys.* **1995**, *103* (19), 8577-93.

257. Marcinowski, M.; Rosam, M.; Seitz, C.; Elferich, J.; Behnke, J.; Bello, C.; Feige, M. J.; Becker, C. F. W.; Antes, I.; Buchner, J. Conformational selection in substrate recognition by Hsp70 chaperones. *J. Mol. Biol.* **2013**, *425* (3), 466-74.
258. Schneider, M.; Rosam, M.; Glaser, M.; Patronov, A.; Shah, H.; Back, K. C.; Daake, M. A.; Buchner, J.; Antes, I. BiPPred: Combined sequence- and structure-based prediction of peptide binding to the Hsp70 chaperone BiP. *Proteins* **2016**, *84* (10), 1390-407.
259. Ryckaert, J.-P.; Ciccotti, G.; Berendsen, H. J. C. Numerical integration of the cartesian equations of motion of a system with constraints: Molecular dynamics of n-alkanes. *J. Comput. Phys.* **1977**, *23* (3), 327-41.
260. Götz, A. W.; Williamson, M. J.; Xu, D.; Poole, D.; Le Grand, S.; Walker, R. C. Routine microsecond molecular dynamics simulations with AMBER on GPUs. 1. Generalized Born. *J. Chem. Theory Comput.* **2012**, *8* (5), 1542-55.
261. Salomon-Ferrer, R.; Götz, A. W.; Poole, D.; Le Grand, S.; Walker, R. C. Routine microsecond molecular dynamics simulations with AMBER on GPUs. 2. Explicit solvent particle Mesh Ewald. *J. Chem. Theory Comput.* **2013**, *9* (9), 3878-88.
262. Srinivasan, J.; Cheatham, T. E. III; Cieplak, P.; Kollman, P. A.; Case, D. A. Continuum solvent studies of the stability of DNA, RNA, and phosphoramidate–DNA helices. *J. Biomol. Struct. Dyn.* **1998**, *16* (3), 671-82.
263. Miller, B. R.; McGee, T. D.; Swails, J. M.; Homeyer, N.; Gohlke, H.; Roitberg, A. E. MMPBSA.py: An efficient program for end-state free energy calculations. *J. Chem. Theory Comput.* **2012**, *8* (9), 3314-21.
264. Hornak, V.; Abel, R.; Okur, A.; Strockbine, B.; Roitberg, A.; Simmerling, C. Comparison of multiple Amber force fields and development of improved protein backbone parameters. *Proteins* **2006**, *65* (3), 712-25.
265. Srinivasan, J.; Trevathan, M. W.; Beroza, P.; Case, D. A. Application of a pairwise generalized Born model to proteins and nucleic acids: Inclusion of salt effects. *Theoretica Chimica Acta* **1999**, *101* (6), 426-34.
266. Onufriev, A.; Bashford, D.; Case, D. A. Modification of the generalized Born model suitable for macromolecules. *J. Phys. Chem. B*, **2000**, *104* (15), 3712–20.
267. Onufriev, A.; Bashford, D.; Case, D. A. Exploring protein native states and large-scale conformational changes with a modified generalized born model. *Proteins* **2004**, *55* (2), 383-94.
268. Genheden, S. MM/GBSA and LIE estimates of host–guest affinities: Dependence on charges and solvation model. *J. Comput. Aided Mol. Des.* **2011**, *25* (11), 1085-93.
269. Genheden, S.; Ryde, U. Comparison of the efficiency of the LIE and MM/GBSA methods to calculate ligand-binding energies. *J. Chem. Theory Comput.* **2011**, *7* (11), 3768-78.

270. Hou, T.; Wang, J.; Li, Y.; Wang, W. Assessing the performance of the MM/PBSA and MM/GBSA methods. 1. The accuracy of binding free energy calculations based on molecular dynamics simulations. *J. Chem. Inf. Model.* **2011**, *51* (1), 69-82.

**6. LIST OF ABBREVIATIONS, ACRONYMS AND SYMBOLS**

|                                 |  |                    |   |
|---------------------------------|--|--------------------|---|
| ABPP                            | activity-based protein profiling                   | ddH <sub>2</sub> O | purified water (resistivity $\geq 18. \beta$ M $\Omega$ cm) |
| Ac                              | acetyl-  | DIC                | <i>N,N</i> -diisopropylcarbodiimide                         |
| AfBPP                           | affinity-based protein profiling                   | DIEA               | <i>N,N</i> -diisopropylethylamine (Hünig's base)            |
| ALDH1B1                         | aldehyde dehydrogenase X                           | DiMe               | dimethyl labelling  |
| AMR                             | antimicrobial resistance                           | DMF                | dimethylformamide   |
| APCI                            | atmospheric-pressure chemical ionization           | DMSO               | dimethylsulfoxid  |
| ATP                             | adenosine triphosphate                             | DNA                | deoxyribonucleic acid                                       |
| AUC                             | area under curve                                   | DTT                | dithiothreitol  |
| BAC                             | benzalkonium chloride                              | ECE1               | endothelin-converting enzyme 1                              |
| BHB                             | Bushnell Haas broth                                | ECH1               | delta(3,5)-delta(2,4)-dienoyl-CoA isomerase                 |
| brine                           | saturated aqueous sodium chloride                  | EDC                | 1-ethyl-3-(3-dimethylamino propyl)carbodiimide              |
| <i>n</i> -BuLi                  | <i>n</i> -butyllithium                             | eDNA               | extracellular DNA   |
| <i>tert</i> -BuLi               | <i>tert</i> -butyllithium                          | EDTA               | sodium ethylenediaminetetraacetat                           |
| °C                              | Grad Celsius                                       | e.g.               | exempli gratia; for example                                 |
| calcd.                          | calculated   | eq.                | equivalent(s)   |
| cf.                             | confer; compare                                    | EM                 | electron microscopy   |
| CID                             | collision-induced dissociation                     | ESI                | electrospray-ionization                                     |
| CIPRO                           | ciprofloxacin                                      | ETD                | electron-transfer dissociation                              |
| CH <sub>2</sub> Cl <sub>2</sub> | dichloromethane                                    | et al.             | et alii; and others   |
| CL                              | clearance  | Et <sub>2</sub> O  | diethyl ether   |
| CM                              | cytoplasmic membrane                               | EtCl <sub>2</sub>  | dichloroethane  |
| C <sub>max</sub>                | maximum plasma concentration                       | EtOAc              | ethyl acetate   |
| CTSD                            | cathepsin D  | EtOH               | ethanol   |
| CW                              | cell wall  | FA                 | formic acid   |
| EDANS                           | 5-((2-aminoethyl)amino)-1-naphthalenesulfonic acid | FRET               | Förster resonance energy transfer                           |
| FESEM                           | field emission scanning electron microscopy        | FESEM              | field emission scanning electron microscopy                 |
| Da                              | Dalton   | GENTA              | gentamicin  |
| DABCYL                          | 4-((4-(dimethylamino)phenyl)azo) benzoic acid      | GO                 | gene ontology   |
| DAP                             | daptomycin   |                    |   |

|                  |  |        |  |
|------------------|--|--------|--|
| GOCC             | gene ontology cellular component                   | MeCN   | acetonitrile   |
| HCC              | hepatocellular carcinoma                           | MeOH   | methanol   |
| HCD              | higher-energy collisional dissociation             | MIC    | minimal inhibitory concentration                             |
| HEPES            | 4-(2-hydroxyethyl)-1-piperazineethanesulfonic acid | MRSA   | methicillin-resistant <i>Staphylococcus aureus</i>           |
| hESI             | heated electrospray ionization                     | MRT    | mean residence time  |
| HGT              | horizontal gene transfer                           | MS     | mass spectrometry  |
| HOBt             | 1-hydroxybenzotriazol                              | MS/MS  | tandem mass spectrometry                                     |
| HPLC             | high performance liquid chromatography             | MSSA   | methicillin-sensitive <i>Staphylococcus aureus</i>           |
| HRMS             | high resolution mass spectrometry                  | MTT    | 3-(4,5-dimethylthiazol-2-yl)-2,5-diphenyltetrazolium bromide |
| Hz               | Hertz  | MW     | molecular weight   |
| iBAQ             | intensity-based absolute quantification            | NDM    | New Dehli metallo- $\beta$ -lactamase                        |
| IC               | ion chromatography                                 | NMR    | nuclear magnetic resonance                                   |
| IC <sub>50</sub> | half maximal inhibitory concentration              | o/n    | overnight  |
| i.m.             | intramuscular                                      | OD     | optical density  |
| i.p.             | intra peritoneum; intraperitoneal                  | OXA    | oxacillin  |
| i.v.             | intra vena; intravenously                          | PAGE   | polyacrylamide gel electrophoresis                           |
| <i>J</i>         | coupling constant in Hertz (Hz)                    | PAL    | photoaffinity labelling                                      |
| JNK              | c-Jun N-terminal kinase                            | PBP    | penicillin-binding protein                                   |
| K                | Kelvin   | PBS    | phosphate buffered saline                                    |
| LB               | lysogeny broth                                     | PC     | pyruvate carboxylase   |
| LC               | liquid chromatography                              | PCCA/B | propionyl carboxylase chain alpha and beta                   |
| LFQ              | label-free quantification                          | PCR    | polymerase chain reaction                                    |
| Log <i>P</i>     | logarithm of the partition coefficient             | PDD    | phenotypic drug discovery                                    |
| LVX              | levofloxacin                                       | PenG   | penicillin G   |
| LysC             | endoproteinase Lys-C                               | PGH    | peptidoglycan hydrolase                                      |
| m/z              | mass to charge ration                              | PIA    | polysaccharide intercellular adhesion                        |
| MCC1             | methylcrotonyl carboxylase                         | PNAG   | polymeric <i>N</i> -acetyl-glucosamine                       |
| MDR              | multidrug resistance                               |        |  |

|           |  |           |  |
|-----------|--|-----------|--|
| p.o.      | per oral; orally   | TEM       | transmission electron microscopy                           |
| ppm       | parts per million  |           |  |
| PRCP      | lysosomal Pro-X carboxypeptidase                           | TFA       | trifluoroacetic acid                                       |
| PROSITE   | database of protein domains, families and functional sites | TFL       | trifunctional linker                                       |
| RCC       | renal cell carcinoma                                       | THF       | tetrahydrofuran  |
| $R_f$     | reference value  | TLC       | thin layer chromatography                                  |
| RP        | reversed phase   | $t_{max}$ | time point of $C_{max}$                                    |
| RP-HPLC   | reversed phase high performance liquid chromatography      | TMS       | trimethylsilyl   |
| rpm       | rounds per minute  | TRIS      | tris(hydroxymethyl)aminomethane                            |
| rt        | room temperature   | $t_R$     | retention time   |
| SDS       | sodium dodecylsulfate                                      | UV        | ultraviolet  |
| SILAC     | stable isotope labelling with amino acids in cell culture  | VDAC 1/2  | voltage-dependent anion-selective channel proteins 1 and 2 |
| subsp.    | subspecies   | VISA      | vancomycin-intermediate <i>Staphylococcus aureus</i>       |
| $t_{1/2}$ | half life  | VRE       | vancomycin-resistant enterococci                           |
| TAMRA     | tetramethylrhodamine                                       | VRSA      | vancomycin-resistant <i>Staphylococcus aureus</i>          |
| TBAF      | tetra- <i>n</i> -butylammonium fluoride                    | vs.       | versus   |
| TBS       | <i>tert</i> -butyl-dimethylsilyl                           | $V_z$     | volume of distribution                                     |
| TBTA      | tris[(1-benzyl-1H-1,2,3-triazol-4-yl)methyl]amin)          | WHO       | World Health Organization                                  |
| TCEP      | tris(2-carboxyethyl)phosphine                              | $\delta$  | chemical shift in ppm                                      |
| TEAB      | tetraethylammonium bicarbonate                             |           |  |



## 7. APPENDICES

### 7.1. Kinase Inhibitor Library

| Kinase Inhibitor       | MIC ( $\mu\text{M}$ ) | Mw (g/mol) | CAS No.      | Supplier           |
|------------------------|-----------------------|------------|--------------|--------------------|
| A66                    | > 30                  | 393.53     | 1166227-08-2 | Selleck Chemicals  |
| A-674563               | > 30                  | 358.44     | 552325-73-2  | Selleck Chemicals  |
| A-769662               | > 30                  | 360.39     | 844499-71-4  | Selleck Chemicals  |
| AEE788                 | > 30                  | 440.58     | 497839-62-0  | Selleck Chemicals  |
| Afatinib               | > 30                  | 485.94     | 439081-18-2  | Selleck Chemicals  |
| AG-490                 | > 30                  | 294.30     | 133550-30-8  | Selleck Chemicals  |
| AMG 900                | > 30                  | 503.58     | 945595-80-2  | Selleck Chemicals  |
| AMG-208                | > 30                  | 383.40     | 1002304-34-8 | Selleck Chemicals  |
| Amuvatinib             | > 30                  | 447.51     | 850879-09-3  | Selleck Chemicals  |
| AP24534                | > 30                  | 532.56     | 943319-70-8  | Selleck Chemicals  |
| Apatinib               | > 30                  | 493.58     | 811803-05-1  | Selleck Chemicals  |
| AS252424               | > 30                  | 305.28     | 900515-16-4  | Selleck Chemicals  |
| AS604850               | > 30                  | 285.22     | 648449-76-7  | Selleck Chemicals  |
| AS-605240              | > 30                  | 257.27     | 648450-29-7  | Selleck Chemicals  |
| AS703026               | > 30                  | 431.20     | 1236699-92-5 | Selleck Chemicals  |
| AT7519                 | > 30                  | 382.24     | 844442-38-2  | Selleck Chemicals  |
| AT7867                 | > 30                  | 337.85     | 857531-00-1  | Selleck Chemicals  |
| AT9283                 | > 30                  | 381.43     | 896466-04-9  | Selleck Chemicals  |
| Aurora A Inhibitor I   | > 30                  | 588.07     | 1158838-45-9 | Selleck Chemicals  |
| AX20017                | > 30                  | 264.34     | 329221-38-7  | Vitas-M Laboratory |
| Axitinib               | > 30                  | 386.47     | 319460-85-0  | Selleck Chemicals  |
| AZ 960                 | 30                    | 354.36     | 905586-69-8  | Selleck Chemicals  |
| AZD1480                | > 30                  | 348.77     | 935666-88-9  | Selleck Chemicals  |
| AZD5438                | > 30                  | 371.46     | 602306-29-6  | Selleck Chemicals  |
| AZD7762                | > 30                  | 362.42     | 860352-01-8  | Selleck Chemicals  |
| AZD8055                | > 30                  | 465.54     | 1009298-09-2 | Selleck Chemicals  |
| AZD8330                | > 30                  | 461.23     | 869357-68-6  | Selleck Chemicals  |
| AZD8931                | > 30                  | 473.93     | 848942-61-0  | Selleck Chemicals  |
| Barasertib             | > 30                  | 507.56     | 722544-51-6  | Selleck Chemicals  |
| BEZ235                 | > 30                  | 469.54     | 915019-65-7  | Selleck Chemicals  |
| BGT226 (NVP-BGT226)    | > 30                  | 650.60     | 1245537-68-1 | Selleck Chemicals  |
| BI 2536                | > 30                  | 521.65     | 755038-02-9  | Selleck Chemicals  |
| BI6727                 | > 30                  | 618.81     | 755038-65-4  | Selleck Chemicals  |
| BIRB 796               | > 30                  | 527.66     | 285983-48-4  | Selleck Chemicals  |
| Bisindolylmaleimid III | > 30                  | 384.43     | 137592-43-9  | Enzo Lifesciences  |
| BIX 02188              | > 30                  | 426.51     | 1094614-84-2 | Selleck Chemicals  |
| BIX 02189              | > 30                  | 440.54     | 1094614-85-3 | Selleck Chemicals  |
| BKM-120                | > 30                  | 410.39     | 1202777-78-3 | Selleck Chemicals  |
| BMS 777607             | > 30                  | 512.89     | 1196681-44-3 | Selleck Chemicals  |
| BMS 794833             | > 30                  | 468.84     | 1174046-72-0 | Selleck Chemicals  |
| BMS-599626             | > 30                  | 567.01     | 8173837-23-1 | Selleck Chemicals  |
| Bosutinib (SKI-606)    | > 30                  | 530.45     | 380843-75-4  | Selleck Chemicals  |

## Appendix

| Kinase Inhibitor                         | MIC ( $\mu\text{M}$ ) | Mw (g/mol) | CAS No.      | Supplier          |
|--|-----------------------|------------|--------------|-------------------|
| Brivanib (BMS-540215)                    | > 30                  | 370.38     | 649735-46-6  | Selleck Chemicals |
| Brivanib alaninate (BMS-582664)          | 30                    | 441.46     | 649735-63-7  | Selleck Chemicals |
| BS-181 hydrochloride                     | > 30                  | 416.99     | N/A          | Selleck Chemicals |
| CAL-101                                  | > 30                  | 415.42     | 870281-82-6  | Selleck Chemicals |
| Canertinib (CI-1033)                     | > 30                  | 485.94     | 267243-28-7  | Selleck Chemicals |
| CCT128930                                | > 30                  | 341.84     | 885499-61-6  | Selleck Chemicals |
| CCT129202                                | > 30                  | 497.02     | 942947-93-5  | Selleck Chemicals |
| Cediranib (AZD2171)                      | > 30                  | 450.51     | 288383-20-0  | Selleck Chemicals |
| CHIR-99021                               | > 30                  | 465.34     | 252917-06-9  | Selleck Chemicals |
| CI-1040 (PD184352)                       | > 30                  | 478.66     | 212631-79-3  | Selleck Chemicals |
| CP-724714                                | > 30                  | 469.53     | 537705-08-1  | Selleck Chemicals |
| Crenolanib (CP-868569)                   | > 30                  | 443.54     | 670220-88-9  | Selleck Chemicals |
| Crizotinib (PF-02341066)                 | > 30                  | 450.34     | 877399-52-5  | Selleck Chemicals |
| CUDC-101                                 | > 30                  | 434.49     | 1012054-59-9 | Selleck Chemicals |
| CX-4945                                  | > 30                  | 349.77     | 1009820-21-6 | Selleck Chemicals |
| CYC116                                   | > 30                  | 368.46     | 693228-63-6  | Selleck Chemicals |
| Cyt387                                   | > 30                  | 414.46     | 1056634-68-4 | Selleck Chemicals |
| Dacomitinib (PF-00299804)                | > 30                  | 469.94     | 1110813-31-4 | Selleck Chemicals |
| Danuserib (PHA-739358)                   | > 30                  | 474.55     | 827318-97-8  | Selleck Chemicals |
| Danuserib (PHA-739358)                   | > 30                  | 413.49     | 503468-95-9  | Selleck Chemicals |
| Dasatinib                                | > 30                  | 488.01     | 302962-49-8  | Selleck Chemicals |
| DCC-2036                                 | > 30                  | 553.59     | 1020172-07-9 | Selleck Chemicals |
| Deforolimus (MK-8669)                    | > 30                  | 990.21     | 572924-54-0  | Selleck Chemicals |
| Degrasyn (WP1130)                        | 10                    | 384.27     | 856243-80-6  | Selleck Chemicals |
| Dinaciclib (SCH-727965)                  | > 30                  | 396.49     | 779353-01-4  | Selleck Chemicals |
| Dovitinib (BGJ-398, CHIR-258, TKI-258, ) | > 30                  | 392.43     | 405169-16-6  | Selleck Chemicals |
| ENMD-2076                                | > 30                  | 525.56     | 934353-76-1  | Selleck Chemicals |
| Enzastaurin                              | > 30                  | 515.60     | 170364-57-5  | Selleck Chemicals |
| Erlotinib Hydrochloride                  | > 30                  | 429.90     | 183319-69-9  | Selleck Chemicals |
| Everolimus (RAD001)                      | > 30                  | 958.22     | 159351-69-6  | Selleck Chemicals |
| Fasudil (HA-1077)                        | > 30                  | 327.83     | 105628-07-7  | Enzo Lifesciences |
| Flavopiridol (Alvocidib)                 | > 30                  | 401.84     | 146426-40-6  | Selleck Chemicals |
| Flavopiridol hydrochloride               | > 30                  | 438.30     | 131740-09-5  | Selleck Chemicals |
| Galunisertib (LY-2157299)                | > 30                  | 369.42     | 700874-72-2  | Selleck Chemicals |
| Gandotinib (LY2784544)                   | 30                    | 469.94     | 1229236-86-5 | Selleck Chemicals |
| GDC-0879                                 | > 30                  | 334.37     | 905281-76-7  | Selleck Chemicals |
| GDC-0941                                 | > 30                  | 513.64     | 957054-30-7  | Selleck Chemicals |
| GDC-0980                                 | > 30                  | 498.60     | 1032754-93-0 | Selleck Chemicals |
| Gefitinib (Iressa)                       | > 30                  | 446.90     | 184475-35-2  | Selleck Chemicals |
| GSK1059615                               | > 30                  | 333.36     | 958852-01-1  | Selleck Chemicals |
| GSK1070916                               | > 30                  | 507.63     | 942918-07-2  | Selleck Chemicals |
| GSK1120212                               | > 30                  | 615.39     | 871700-17-3  | Selleck Chemicals |
| GSK1838705A                              | > 30                  | 532.57     | 1116235-97-2 | Selleck Chemicals |
| GSK2126458                               | > 30                  | 505.50     | 1086062-66-9 | Selleck Chemicals |
| GSK461364                                | > 30                  | 543.60     | 929095-18-1  | Selleck Chemicals |

| Kinase Inhibitor                 | MIC ( $\mu\text{M}$ ) | Mw (g/mol) | CAS No.      | Supplier          |
|----------------------------------|-----------------------|------------|--------------|-------------------|
| GSK690693                        | > 30                  | 425.48     | 37174-76-0   | Selleck Chemicals |
| H-89                             | > 30                  | 519.28     | 130964-39-5  | Enzo Lifesciences |
| Hesperadin                       | > 30                  | 516.65     | 422513-13-1  | Selleck Chemicals |
| HMN-214                          | > 30                  | 424.47     | 173529-46-9  | Selleck Chemicals |
| IC-87114 (PIK-293)               | > 30                  | 397.43     | 371242-69-2  | Selleck Chemicals |
| Imatinib (STI571)                | > 30                  | 493.60     | 152459-95-5  | Selleck Chemicals |
| Imatinib Mesylate                | > 30                  | 589.71     | 220127-57-1  | Selleck Chemicals |
| Indirubin                        | > 30                  | 262.26     | 479-41-4     | Selleck Chemicals |
| Irbinitinib (ONT-380, ARRY-380 ) | > 30                  | 480.52     | 937263-43-9  | Selleck Chemicals |
| JNJ-38877605                     | > 30                  | 377.35     | 943540-75-8  | Selleck Chemicals |
| JNJ-7706621                      | > 30                  | 394.36     | 443797-96-4  | Selleck Chemicals |
| Ki8751                           | > 30                  | 469.41     | 228559-41-9  | Selleck Chemicals |
| KRN 633                          | > 30                  | 416.86     | 286370-15-8  | Selleck Chemicals |
| KU-0063794                       | > 30                  | 465.54     | 938440-64-3  | Selleck Chemicals |
| KU-55933                         | > 30                  | 395.49     | 587871-26-9  | Selleck Chemicals |
| KU-60019                         | > 30                  | 547.67     | 925701-49-1  | Selleck Chemicals |
| KW 2449                          | > 30                  | 332.40     | 1000669-72-6 | Selleck Chemicals |
| KX2-391                          | > 30                  | 431.53     | 897016-82-9  | Selleck Chemicals |
| Lapatinib Ditosylate             | > 30                  | 925.46     | 388082-77-7  | Selleck Chemicals |
| LDN193189                        | > 30                  | 406.48     | 1062368-24-4 | Selleck Chemicals |
| Lenvatinib (E7080)               | > 30                  | 426.85     | 417716-92-8  | Selleck Chemicals |
| Linifanib (ABT-869)              | > 30                  | 375.40     | 796967-16-3  | Selleck Chemicals |
| Linsitinib (OSI-906)             | > 30                  | 421.49     | 867160-71-2  | Selleck Chemicals |
| LY2228820                        | > 30                  | 612.74     | 862507-23-1  | Selleck Chemicals |
| LY2603618                        | > 30                  | 436.30     | 911222-45-2  | Selleck Chemicals |
| LY294002                         | > 30                  | 307.34     | 154447-36-6  | Selleck Chemicals |
| Masitinib (AB1010)               | > 30                  | 498.64     | 790299-79-5  | Selleck Chemicals |
| MGCD-265                         | > 30                  | 517.60     | 875337-44-3  | Selleck Chemicals |
| Milciclib (PHA-848125)           | > 30                  | 460.57     | 802539-81-7  | Selleck Chemicals |
| Mitoxantrone                     | > 30                  | 444.48     | 65271-80-9   | Selleck Chemicals |
| MK-2206                          | > 30                  | 480.39     | 1032350-13-2 | Selleck Chemicals |
| MK-2461                          | 30                    | 495.55     | 917879-39-1  | Selleck Chemicals |
| MK-5108 (VX-689)                 | > 30                  | 461.94     | 1010085-13-8 | Selleck Chemicals |
| MLN-0128 (INK-128)               | > 30                  | 309.33     | 1224844-38-5 | Selleck Chemicals |
| MLN-8054                         | > 30                  | 476.86     | 869363-13-3  | Selleck Chemicals |
| MLN8237                          | > 30                  | 518.92     | 1028486-01-2 | Selleck Chemicals |
| Motesanib Diphosphate            | > 30                  | 569.44     | 857876-30-3  | Selleck Chemicals |
| Mubritinib                       | > 30                  | 468.47     | 366017-09-6  | Selleck Chemicals |
| Neratinib                        | > 30                  | 557.04     | 698387-09-6  | Selleck Chemicals |
| Nilotinib                        | > 30                  | 529.52     | 641571-10-0  | Selleck Chemicals |
| NVP-ADW742                       | > 30                  | 453.58     | 475488-23-4  | Selleck Chemicals |
| NVP-BHG712                       | > 30                  | 503.48     | 940310-85-0  | Selleck Chemicals |
| NVP-BSK805 dihydrochloride       | > 30                  | 563.47     | 1092499-93-8 | Selleck Chemicals |
| NVP-TAE684                       | > 30                  | 614.20     | 761439-42-3  | Selleck Chemicals |
| ON-01910                         | > 30                  | 473.47     | 1225497-78-8 | Selleck Chemicals |

## Appendix

| Kinase Inhibitor           | MIC ( $\mu\text{M}$ ) | Mw (g/mol) | CAS No.      | Supplier          |
|----------------------------|-----------------------|------------|--------------|-------------------|
| Orantinib (SU6668, TSU-68) | > 30                  | 310.35     | 252916-29-3  | Selleck Chemicals |
| OSI027                     | > 30                  | 406.44     | 936890-98-1  | Selleck Chemicals |
| OSI-420                    | > 30                  | 415.87     | 183320-51-6  | Selleck Chemicals |
| OSI-930                    | > 30                  | 443.44     | 728033-96-3  | Selleck Chemicals |
| Pazopanib Hydrochloride    | > 30                  | 473.98     | 635702-64-6  | Selleck Chemicals |
| PCI-32765                  | > 30                  | 440.50     | 936563-96-1  | Selleck Chemicals |
| PD0325901                  | > 30                  | 482.19     | 391210-10-9  | Selleck Chemicals |
| PD0332991                  | > 30                  | 447.53     | 571190-30-2  | Selleck Chemicals |
| PD153035 hydrochloride     | > 30                  | 396.67     | 183322-45-4  | Selleck Chemicals |
| PD318088                   | > 30                  | 561.09     | 391210-00-7  | Selleck Chemicals |
| PD98059                    | > 30                  | 267.28     | 167869-21-8  | Selleck Chemicals |
| Pelitinib                  | > 30                  | 467.92     | 257933-82-7  | Selleck Chemicals |
| PF-00562271 (PF-562271)    | > 30                  | 507.49     | 717907-75-0  | Selleck Chemicals |
| PF-03814735                | > 30                  | 474.48     | 942487-16-3  | Selleck Chemicals |
| PF-04217903                | > 30                  | 372.38     | 956905-27-4  | Selleck Chemicals |
| PF-04691502                | > 30                  | 425.48     | 1013101-36-4 | Selleck Chemicals |
| PF-04691502                | > 30                  | 425.48     | 1013101-36-4 | Selleck Chemicals |
| PF-05212384                | > 30                  | 615.73     | 1197160-78-3 | Selleck Chemicals |
| PH-797804                  | > 30                  | 477.30     | 586379-66-0  | Selleck Chemicals |
| PH-797804                  | > 30                  | 477.30     | 586379-66-0  | Selleck Chemicals |
| PHA-680632                 | > 30                  | 501.62     | 398493-79-3  | Selleck Chemicals |
| PHA-793887                 | > 30                  | 361.48     | 718630-59-2  | Selleck Chemicals |
| Phenformin hydrochloride   | > 30                  | 241.72     | 834-28-6     | Selleck Chemicals |
| PI-103                     | > 30                  | 348.36     | 371935-74-9  | Selleck Chemicals |
| PIK-293                    | > 30                  | 397.43     | 900185-01-5  | Selleck Chemicals |
| PIK-294                    | > 30                  | 489.53     | 900185-02-6  | Selleck Chemicals |
| PIK-75 Hydrochloride       | > 30                  | 488.74     | 372196-77-5  | Selleck Chemicals |
| PIK-90                     | > 30                  | 351.36     | 677338-12-4  | Selleck Chemicals |
| PIK-93                     | > 30                  | 389.88     | 593960-11-3  | Selleck Chemicals |
| PLX-4720                   | > 30                  | 413.83     | 918505-84-7  | Selleck Chemicals |
| PP121                      | > 30                  | 319.36     | 1092788-83-4 | Selleck Chemicals |
| PP242                      | > 30                  | 308.34     | 1092351-67-1 | Selleck Chemicals |
| Quercetin (Sophoretin)     | > 30                  | 302.24     | 117-39-5     | Selleck Chemicals |
| Quizartinib                | > 30                  | 560.67     | 950769-58-1  | Selleck Chemicals |
| R406                       | > 30                  | 628.63     | 841290-81-1  | Selleck Chemicals |
| R406 (free base)           | > 30                  | 470.45     | 841290-80-0  | Selleck Chemicals |
| R935788                    | > 30                  | 624.42     | 1025687-58-4 | Selleck Chemicals |
| RAF265 (CHIR-265)          | 30                    | 518.41     | 927880-90-8  | Selleck Chemicals |
| Raf265 derivative          | > 30                  | 504.39     | N/A          | Selleck Chemicals |
| Rapamycin (Sirolimus)      | > 30                  | 914.17     | 53123-88-9   | Selleck Chemicals |
| Regorafenib (Bay 73-4506)  | 3                     | 482.82     | 755037-03-7  | Selleck Chemicals |
| Roscovitine (CYC202)       | > 30                  | 354.45     | 186692-46-6  | Selleck Chemicals |
| Ruxolitinib (INCB018424)   | > 30                  | 306.37     | 941678-49-5  | Selleck Chemicals |
| Saracatinib (AZD0530)      | > 30                  | 542.03     | 379231-04-6  | Selleck Chemicals |
| SB 202190                  | > 30                  | 331.34     | 152121-30-7  | Selleck Chemicals |

| Kinase Inhibitor                        | MIC ( $\mu\text{M}$ ) | Mw (g/mol) | CAS No.      | Supplier           |
|---|-----------------------|------------|--------------|--------------------|
| SB 203580                               | > 30                  | 377.43     | 152121-47-6  | Selleck Chemicals  |
| SB 216763                               | > 30                  | 371.22     | 280744-09-4  | Selleck Chemicals  |
| SB 431542                               | > 30                  | 384.39     | 301836-41-9  | Selleck Chemicals  |
| SB 525334                               | > 30                  | 343.42     | 356559-20-1  | Selleck Chemicals  |
| SB202190 (FHPI)                         | > 30                  | 331.34     | 152121-30-7  | Sigma-Aldrich      |
| Selumetinib (AZD6244)                   | > 30                  | 457.68     | 606143-52-6  | Selleck Chemicals  |
| SGI-1776                                | > 30                  | 405.42     | 1025065-69-3 | Selleck Chemicals  |
| SGX-523                                 | > 30                  | 359.41     | 1022150-57-7 | Selleck Chemicals  |
| SNS-032 (BMS-387032)                    | > 30                  | 380.53     | 345627-80-7  | Selleck Chemicals  |
| SNS-314 Mesylate                        | > 30                  | 527.04     | 1057249-41-8 | Selleck Chemicals  |
| Sorafenib Tosylate (Bay 43-9006)        | 3                     | 637.03     | 475207-59-1  | Selleck Chemicals  |
| Sotrastaurin (NVP-AEB071)               | > 30                  | 438.48     | 425637-18-9  | Selleck Chemicals  |
| SP600125                                | > 30                  | 220.23     | 129-56-6     | Selleck Chemicals  |
| SU11274 (PKI-SU11274)                   | > 30                  | 568.09     | 658084-23-2  | Selleck Chemicals  |
| Sunitinib Malate                        | > 30                  | 532.56     | 341031-54-7  | Selleck Chemicals  |
| TAK-285                                 | 30                    | 547.96     | 871026-44-7  | Selleck Chemicals  |
| TAK-733                                 | > 30                  | 504.23     | 1035555-63-5 | Selleck Chemicals  |
| TAK-901                                 | > 30                  | 504.64     | 934541-31-8  | Selleck Chemicals  |
| Tandutinib (MLN518)                     | > 30                  | 562.70     | 387867-13-2  | Selleck Chemicals  |
| Telatinib                               | > 30                  | 409.83     | 332012-40-5  | Selleck Chemicals  |
| Temsirolimus                            | > 30                  | 1030.29    | 162635-04-3  | Selleck Chemicals  |
| TG100-115                               | > 30                  | 346.34     | 677297-51-7  | Selleck Chemicals  |
| TG101209                                | > 30                  | 509.67     | 936091-14-4  | Selleck Chemicals  |
| TG-101348 (SAR-302503)                  | > 30                  | 524.68     | 936091-26-8  | Selleck Chemicals  |
| TGX-221                                 | > 30                  | 364.44     | 663619-89-4  | Selleck Chemicals  |
| Tivantinib (ARQ-197)                    | > 30                  | 369.42     | 905854-02-6  | Selleck Chemicals  |
| Tivozanib (AV-951)                      | > 30                  | 454.86     | 475108-18-0  | Selleck Chemicals  |
| Tofacitinib citrate (CP-690550 citrate) | > 30                  | 312.37     | 540737-29-9  | Selleck Chemicals  |
| Tozasertib (VX-680, MK-0457)            | > 30                  | 464.59     | 639089-54-6  | Vitas-M Laboratory |
| TSU-68                                  | > 30                  | 310.35     | 252916-29-3  | Selleck Chemicals  |
| Tyrphostin 23                           | > 30                  | 186.17     | 118409-57-7  | Sigma-Aldrich      |
| U0126-EtOH                              | > 30                  | 426.56     | 1173097-76-1 | Selleck Chemicals  |
| Vandetanib                              | > 30                  | 475.35     | 443913-73-3  | Selleck Chemicals  |
| Vargatef (BIBF1120)                     | > 30                  | 539.62     | 928326-83-4  | Selleck Chemicals  |
| Vatalanib                               | > 30                  | 419.73     | 212141-51-0  | Selleck Chemicals  |
| Vemurafenib (PLX-4032, R-7204)          | > 30                  | 489.92     | 918504-65-1  | Selleck Chemicals  |
| Vinorelbine (Navelbine)                 | > 30                  | 778.93     | 71486-22-1   | Selleck Chemicals  |
| VX-680                                  | > 30                  | 464.59     | 639089-54-6  | Selleck Chemicals  |
| VX-702                                  | > 30                  | 404.32     | 479543-46-9  | Selleck Chemicals  |
| VX-745                                  | > 30                  | 436.26     | 209410-46-8  | Selleck Chemicals  |
| WAY-600                                 | > 30                  | 494.59     | 1062159-35-6 | Selleck Chemicals  |
| Wortmannin                              | > 30                  | 428.43     | 19545-26-7   | Selleck Chemicals  |
| WYE-125132                              | > 30                  | 519.60     | 1144068-46-1 | Selleck Chemicals  |
| WYE-354                                 | > 30                  | 495.53     | 1062169-56-5 | Selleck Chemicals  |
| WYE-687                                 | > 30                  | 528.61     | 1062161-90-3 | Selleck Chemicals  |

## Appendix

---

| <b>Kinase Inhibitor</b> | <b>MIC (<math>\mu\text{M}</math>)</b> | <b>Mw (g/mol)</b> | <b>CAS No.</b> | <b>Supplier</b>   |
|-------------------------|---------------------------------------|-------------------|----------------|-------------------|
| WZ3146                  | > 30                                  | 464.95            | 1214265-56-1   | Selleck Chemicals |
| WZ4002                  | > 30                                  | 494.97            | 1213269-23-8   | Selleck Chemicals |
| WZ8040                  | > 30                                  | 481.01            | 1214265-57-2   | Selleck Chemicals |
| XL147                   | > 30                                  | 448.52            | 956958-53-5    | Selleck Chemicals |
| XL184                   | > 30                                  | 501.51            | 849217-68-1    | Selleck Chemicals |
| XL765                   | > 30                                  | 599.66            | 1123889-87-1   | Selleck Chemicals |
| XL880 (GSK1363089)      | > 30                                  | 632.65            | 849217-64-7    | Selleck Chemicals |
| ZM 336372               | > 30                                  | 389.45            | 208260-29-1    | Selleck Chemicals |
| ZM-447439               | > 30                                  | 513.59            | 331771-20-1    | Selleck Chemicals |
| ZSTK474                 | > 30                                  | 417.41            | 475110-96-4    | Selleck Chemicals |

## 7.2. Antibacterial Profile of Sorafenib and PK150

| Organsim  | Strain                   |            | MIC ( $\mu\text{M}$ ) |             |     |
|---|--------------------------|------------|-----------------------|-------------|-----|
|   |                          |            | SFN                   | PK150       |     |
| <b>Gram-positive</b>                              |                          |            |                       |             |     |
| <i>Staphylococcus aureus</i>                      | ATCC 33591               | MRSA       | N/A                   | 0.76 - 1.58 |     |
|   | ATCC 33592               | MRSA       | 10                    | 0.3         |     |
|   | DSM-18827                | MRSA       | 3                     | 0.3 - 1     |     |
|   | Newman                   |            | 3                     | 0.3         |     |
|   | NCTC 8325                |            | 3                     | 0.3         |     |
|   | NCTC 8325-4              |            | 3                     | 0.3         |     |
|   | Mu 50                    | MRSA, VISA | 3                     | 0.3         |     |
|   | SH1000                   |            | N/A                   | 0.76 - 1.58 |     |
|   | USA300 FPR3757           | MRSA       | 3 - 10                | 0.3         |     |
|   | N315                     |            | 3 - 10                | 0.3         |     |
|   | ARC0001 $\Delta$ SpsB    |            | 3 - 10                | 0.3         |     |
|   | clinical isolates        | BK95395    | MRSA                  | 3 - 10      | 0.3 |
|   |                          | BK97296    | MRSA                  | 3 - 10      | 0.3 |
|   |                          | IS050678   | MRSA                  | 3 - 10      | 0.3 |
|   |                          | IS050611   | MRSA                  | 3 - 10      | 0.3 |
|   |                          | VA417350   | MRSA                  | 3 - 10      | 0.3 |
|   |                          | VA418879   | MRSA                  | 3 - 10      | 0.3 |
|   |                          | VA402923   | MRSA                  | 3 - 10      | 0.3 |
|   |                          | VA412350   | MRSA                  | 3 - 10      | 0.3 |
| VA409044  |                          | MRSA       | 3 - 10                | 0.3         |     |
| <i>Bacillus subtilis</i>                          | 168                      |            | 5                     | 1           |     |
| <i>Enterococcus faecalis</i>                      | ATCC 47077               |            | > 100                 | 3           |     |
|   | ATCC 700802              | VRE        | > 100                 | 3           |     |
| <i>Enterococcus faecium</i>                       | DSM-17050                | VRE        | > 100                 | 1           |     |
|   | DSM-20477                |            | > 100                 | 1           |     |
| <i>Listeria monocytogenes</i>                     | EGD-e                    |            | 3                     | 0.3         |     |
|   | F2365                    |            | 3                     | 0.3         |     |
| <i>Mycobacterium bovis</i>                        | BCG                      |            | 12.5                  | 3           |     |
| <i>Mycobacterium smegmatis</i>                    | mc <sup>2</sup> 155      |            | 50                    | 6           |     |
| <i>Mycobacterium tuberculosis</i>                 | H37Rv                    |            | 25                    | 2           |     |
| <b>Gram-negative</b>                              |                          |            |                       |             |     |
| <i>Acinetobacter baumannii</i>                    | DSM-30007                |            | >100                  | >100        |     |
| <i>Enterobacter aerogenes</i>                     | DSM-30053                |            | >100                  | >100        |     |
| <i>Enterobacter cloacae</i> subsp. <i>cloacae</i> | DSM-30054                |            | >100                  | >100        |     |
| <i>Escherichia coli</i>                           | CFT073                   |            | >100                  | >100        |     |
| <i>Klebsiella pneumoniae</i>                      | DSM-30104                |            | >100                  | >100        |     |
| <i>Pseudomonas aeruginosa</i>                     | DSM-19882                |            | >100                  | >100        |     |
| <i>Salmonella typhimurium</i>                     | LT2                      |            | >100                  | >100        |     |
|   | TA100                    |            | >100                  | >100        |     |
| <i>Salmonella enteritidis</i>                     | veterinary isolate (dog) |            | >100                  | >100        |     |

## 7.3. Resistance Profile of Clinical Isolates

|                             | VA402525 |   | VA409044 |   | VA412350 |   | VA402923 |   | VA418879 |   |
|-----------------------------|----------|---|----------|---|----------|---|----------|---|----------|---|
|                             | MIC      |   | MIC      |   | MIC      |   | MIC      |   | MIC      |   |
| Penicillin-G                | ≥ 0.5    | R |
| Ampicillin/<br>Amoxicillin  |          | R |          | R |          | R |          | R |          | R |
| Oxacillin                   | ≥ 4      | R | ≥ 4      | R | ≥ 4      | R | ≥ 4      | R | ≥ 4      | R |
| Ampicillin<br>+Sulbactam    |          | R |          | R |          | R |          | R |          | R |
| Piperacillin                |          | R |          | R |          | R |          | R |          | R |
| Piperacillin<br>+Tazobactam |          | R |          | R |          | R |          | R |          | R |
| Cefazolin                   |          | R |          | R |          | R |          | R |          | R |
| Cefuroxim                   |          | R |          | R |          | R |          | R |          | R |
| Imipenem                    |          | R |          | R |          | R |          | R |          | R |
| Erythromycin                | ≥ 8      | R | ≤ 0.25   | S | ≤ 0.25   | S | ≤ 0.25   | S | ≥ 8      | R |
| Clindamycin                 | ≤ 0.25   | S | ≥ 8      | R |
| Cotrimoxazol                | ≤ 10     | S |
| Gentamicin                  | ≤ 0.5    | S |
| Tobramycin                  | ≤ 1      | S | ≤ 1      | S | ≤ 1      | S | ≤ 1      | S | ≤ 1      | S |
| Teicoplanin                 | ≤ 0.5    | S |
| Vancomycin                  | 1        | S | ≤ 0.5    | S | ≤ 0.5    | S | 1        | S | ≤ 0.5    | S |
| Ciprofloxacin               |          | R |          | S |          | S |          | R |          | R |
| Levofloxacin                | 4        | R | 0.25     | S | 0.25     | S | ≥ 8      | R | ≥ 8      | R |
| Moxifloxacin                | 2        | R | ≤ 0.25   | S | ≤ 0.25   | S | ≥ 8      | R | 4        | R |
| Tetracycline                | ≤ 1      | S | ≤ 1      | S | ≤ 1      | S | ≤ 1      | S | ≤ 1      | S |
| Rifampicin                  | ≤ 0.5    | S |
| Fosfomycin                  | ≤ 8      | S | ≤ 8      | S | ≤ 8      | S | ≤ 8      | S | ≤ 8      | S |
| Linezolid                   | 2        | S | 2        | S | 2        | S | 2        | S | 2        | S |
| Mupirocin                   | ≤ 2      | S | ≤ 2      | S | ≤ 2      | S | ≤ 2      | S | ≤ 2      | S |
| Fusidinsäure                | ≤ 0.5    | S | ≤ 0.5    | S | 16       | I | ≤ 0.5    | S | ≤ 0.5    | S |

MIC, Minimum inhibitory concentration (µg/mL); CL, Classification; S, Susceptible I, Intermediate; R, Resistant

|                             | VA417350 |   | IS050611 |   | BK097296 |   | IS050678 |   | BK095395 |   |
|-----------------------------|----------|---|----------|---|----------|---|----------|---|----------|---|
|                             | MIC      |   | MIC      |   | MIC      |   | MIC      |   | MIC      |   |
| Penicillin-G                | ≥ 0.5    | R |
| Ampicillin/<br>Amoxicillin  |          | R |          | R |          | R |          | R |          | R |
| Oxacillin                   | ≥ 4      | R | ≥ 4      | R | ≥ 4      | R | ≥ 4      | R | ≥ 4      | R |
| Ampicillin<br>+Sulbactam    |          | R |          | R |          | R |          | R |          | R |
| Piperacillin                |          | R |          | R |          | R |          | R |          | R |
| Piperacillin<br>+Tazobactam |          | R |          | R |          | R |          | R |          | R |
| Cefazolin                   |          | R |          | R |          | R |          | R |          | R |
| Cefuroxim                   |          | R |          | R |          | R |          | R |          | R |
| Imipenem                    |          | R |          | R |          | R |          | R |          | R |
| Erythromycin                | ≥ 8      | R | ≥ 8      | R | ≥ 8      | R | ≥ 8      | R | ≥ 8      | R |
| Clindamycin                 | ≤ 0.25   | S | ≥ 8      | R | ≤ 0.25   | S | ≤ 0.25   | R | ≥ 8      | R |
| Cotrimoxazol                | ≤ 10     | S |
| Gentamicin                  | 8        | R | ≤ 0.5    | S | 4        | R | ≤ 0.5    | S | ≤ 0.5    | S |
| Tobramycin                  | 2        | R | ≥ 16     | R | 2        | R | ≤ 1      | S | ≤ 1      | S |
| Teicoplanin                 | ≤ 0.5    | S |
| Vancomycin                  | 1        | S | 1        | S | 1        | S | ≤ 0.5    | S | ≤ 0.5    | S |
| Ciprofloxacin               |          | R |          | R |          | R |          | S |          | R |
| Levofloxacin                | 4        | R | ≥ 8      | R | 4        | R | 0.25     | S | ≥ 8      | R |
| Moxifloxacin                | 2        | R | 4        | R | 2        | R | ≤ 0.25   | S | 4        | R |
| Tetracycline                | ≥ 16     | R | ≤ 1      | S | ≥ 16     | R | ≥ 16     | R | ≤ 1      | S |
| Rifampicin                  | ≤ 0.5    | S |
| Fosfomycin                  | ≤ 8      | S | ≤ 8      | S | ≤ 8      | S | ≤ 8      | S | ≤ 8      | S |
| Linezolid                   | 2        | S | 2        | S | 4        | S | 2        | S | 2        | S |
| Mupirocin                   | ≤ 2      | S | ≤ 2      | S | ≤ 2      | S | ≤ 2      | S | ≤ 2      | S |
| Fusidinsäure                | ≥ 32     | R | ≤ 0.5    | S | ≥ 32     | R | ≤ 0.5    | S | ≤ 0.5    | S |

MIC, Minimum inhibitory concentration (µg/mL); CL, Classification; S, Susceptible I, Intermediate; R, Resistant

## 7.4. Library of Sorafenib and PK150 Analogs

| Compound no. | Structure | MIC<br><i>S. aureus</i><br>NCTC 8325 ( $\mu\text{M}$ ) | Log <i>P</i><br>predicted with<br>ChemBioDraw 13 | SpsB activity (normalized) at certain compound concentration ( $\mu\text{M}$ ) |        |        |        |        |        |
|--------------|-----------|--|--|--|--------|--------|--------|--------|--------|
|              |           |  |  | 100  |        | 50     |        | 10     |        |
|              |           |  |  | mean   | SD     | mean   | SD     | mean   | SD     |
| SFN          |           | 3  | 3.77   | 1.6863   | 0.2235 | 1.6350 | 0.1198 | 1.2498 | 0.0723 |
| SFNp         |           | 10   | 5.24   | N/A  | N/A    | N/A    | N/A    | N/A    | N/A    |
| SFN-C        |           | > 100  | 2.23   | 1.0982   | 0.0813 | 1.1761 | 0.1641 | 0.9903 | 0.0750 |
| PK150        |           | 0.3  | 4.51   | 3.0132   | 0.8017 | 2.5361 | 0.3858 | 1.3302 | 0.1192 |
| PK150-C      |           | > 100  | 2.96   | 1.2527   | 0.1716 | 1.1492 | 0.0097 | 0.9949 | 0.0460 |
| 3.2          |           | 3  | 4.31   | 1.7691   | 0.1055 | 1.4268 | 0.1289 | 1.2705 | 0.0329 |
| 3.4          |           | > 100  | 2.82   | N/A  | N/A    | N/A    | N/A    | N/A    | N/A    |
| 3.5          |           | > 100  | 3.25   | N/A  | N/A    | N/A    | N/A    | N/A    | N/A    |
| 3.6          |           | > 100  | 4.01   | 1.1113   | 0.1067 | 1.1955 | 0.0974 | 1.0583 | 0.1022 |
| 3.7          |           | 100  | 2.76   | 1.1603   | 0.0954 | 1.1860 | 0.1434 | 1.0507 | 0.0711 |
| 3.8          |           | > 100  | 1.95   | 1.0453   | 0.0382 | 0.9890 | 0.0730 | 0.9573 | 0.0300 |
| 3.9          |           | > 100  | 4.17   | 0.9263   | 0.2153 | 1.0495 | 0.2168 | 0.9752 | 0.0380 |
| 3.10         |           | > 100  | 3.44   | 1.0013   | 0.1020 | 1.1281 | 0.1385 | 1.0344 | 0.1059 |
| 3.11         |           | > 100  | 3.49   | 1.0346   | 0.0158 | 0.9926 | 0.0873 | 1.0225 | 0.0383 |
| 3.12         |           | > 100  | 3.11   | 1.0881   | 0.0783 | 1.0737 | 0.2019 | 0.9467 | 0.0493 |
| 3.13         |           | > 100  | 3.07   | 1.0867   | 0.0501 | 1.1215 | 0.0815 | 1.0616 | 0.0822 |
| 3.14         |           | > 100  | 3.15   | 1.3440   | 0.0971 | 1.3347 | 0.2011 | 1.2122 | 0.0989 |

| Compound no. | Structure | MIC<br><i>S. aureus</i><br>NCTC 8325 ( $\mu\text{M}$ ) | Log <i>P</i><br>predicted with<br>ChemBioDraw 13 | SpsB activity (normalized) at certain compound concentration ( $\mu\text{M}$ ) |        |        |        |        |        |
|--------------|-----------|--|--|--|--------|--------|--------|--------|--------|
|              |           |  |  | 100  |        | 50     |        | 10     |        |
|              |           |  |  | mean   | SD     | mean   | SD     | mean   | SD     |
| 3.15         |           | 10   | 4.19   | 1.5465   | 0.1245 | 1.5804 | 0.2827 | 1.2064 | 0.0164 |
| 3.16         |           | > 100  | 4.07   | 1.2278   | 0.0535 | 1.3060 | 0.1314 | 1.1894 | 0.2087 |
| 3.17         |           | > 100  | 4.27   | N/A  | N/A    | N/A    | N/A    | N/A    | N/A    |
| 3.18         |           | > 100  | 3.91   | 1.2975   | 0.1015 | 1.1725 | 0.0331 | 1.0038 | 0.1738 |
| 3.19         |           | 30   | 3.42   | 1.2898   | 0.2085 | 1.1451 | 0.1990 | 1.0871 | 0.0953 |
| 3.20         |           | > 100  | 2.22   | 1.1440   | 0.1737 | 1.0648 | 0.0988 | 1.0040 | 0.0801 |
| 3.21         |           | 10   | 3.97   | 1.1931   | 0.0652 | 1.2492 | 0.3929 | 1.0488 | 0.0609 |
| 3.22         |           | 30   | 4.18   | 1.4821   | 0.2230 | 1.5561 | 0.0650 | 1.1617 | 0.1052 |
| 3.23         |           | 3  | 4.28   | 2.1078   | 0.0691 | 1.9074 | 0.2495 | 1.2088 | 0.0865 |
| 3.24         |           | 0.5  | 5.53   | 2.1084   | 0.1442 | 2.1036 | 0.1438 | 1.3129 | 0.0434 |
| 3.25         |           | 1  | 6.01   | 1.7584   | 0.1711 | 2.0561 | 0.0539 | 1.2015 | 0.1409 |
| 3.26         |           | 3  | 5.29   | 1.8722   | 0.1176 | 1.8582 | 0.0640 | 1.3184 | 0.1033 |
| 3.27         |           | 3  | 4.04   | 1.2413   | 0.1913 | 1.4925 | 0.1551 | 1.0986 | 0.0246 |
| 3.28         |           | 0.7  | 4.95   | 1.3616   | 0.1292 | 1.7855 | 0.1356 | 1.1959 | 0.1384 |
| 3.29         |           | > 100  | 4.49   | 1.1006   | 0.0090 | 1.0634 | 0.0256 | 1.1666 | 0.1408 |
| 3.30         |           | > 100  | 4.93   | 1.1804   | 0.0781 | 1.3436 | 0.2113 | 1.2341 | 0.1492 |
| 3.31         |           | 0.7  | 5.31   | 1.4739   | 0.1201 | 1.5339 | 0.2019 | 1.2645 | 0.0850 |

| Compound no. | Structure | MIC<br><i>S. aureus</i><br>NCTC 8325 (μM) | Log P<br>predicted with<br>ChemBioDraw 13 | SpsB activity (normalized) at certain compound concentration (μM) |        |        |        |        |        |
|--------------|-----------|---|---|---|--------|--------|--------|--------|--------|
|              |           |   |   | 100   |        | 50     |        | 10     |        |
|              |           |   |   | mean  | SD     | mean   | SD     | mean   | SD     |
| 3.32         |           | 30  | 3.44                                      | 1.9776  | 0.0927 | 1.7020 | 0.1641 | 1.1132 | 0.0781 |
| 3.33         |           | 30  | 3.89                                      | 0.9591  | 0.0497 | 1.1473 | 0.2050 | 1.1536 | 0.0610 |
| 3.34         |           | > 100                                     | 3.89                                      | 1.9481  | 0.1210 | 1.2845 | 0.1647 | 1.0193 | 0.0464 |
| 3.35         |           | 100                                       | 3.22                                      | 2.5451  | 0.3008 | 1.8971 | 0.1347 | 1.1080 | 0.0946 |
| 3.36         |           | 3   | 3.94                                      | 1.1948  | 0.0545 | 1.3407 | 0.2931 | 1.1474 | 0.1009 |
| 3.37         |           | 30  | 3.59                                      | 2.1095  | 0.2146 | 1.6358 | 0.1606 | 1.1304 | 0.0807 |
| 3.38         |           | > 100                                     | 4.91                                      | 1.1561  | 0.1246 | 1.1280 | 0.1839 | 1.2404 | 0.0487 |
| 3.39         |           | > 100                                     | 4.18                                      | 1.3772  | 0.1604 | 1.3941 | 0.1771 | 1.1047 | 0.1503 |
| 3.40         |           | > 100                                     | 3.85                                      | 1.2065  | 0.2329 | 0.9882 | 0.1342 | 1.0129 | 0.2169 |
| 3.41         |           | 0.5                                       | 3.81                                      | 1.1718  | 0.1545 | 1.2301 | 0.0476 | 1.1548 | 0.0687 |
| 3.42         |           | 0.7                                       | 3.88                                      | 1.7190  | 0.1372 | 2.3855 | 0.2336 | 1.2742 | 0.1402 |
| 3.43         |           | 0.5                                       | 4.93                                      | 2.5479  | 0.2589 | 1.8510 | 0.4356 | 1.2110 | 0.0551 |
| 3.44         |           | > 100                                     | 4.80                                      | 1.3031  | 0.0051 | 1.4262 | 0.0984 | 1.0779 | 0.0733 |
| 3.45         |           | 3   | 5.01                                      | N/A   | N/A    | N/A    | N/A    | N/A    | N/A    |
| 3.46         |           | 30  | 5.41                                      | 2.0428  | 0.2634 | 1.8269 | 0.4115 | 1.1742 | 0.1743 |
| 3.47         |           | > 100                                     | 4.65                                      | 1.4052  | 0.2373 | 1.3931 | 0.1094 | 1.1203 | 0.1064 |
| 3.48         |           | 10  | 3.79                                      | 1.3675  | 0.0799 | 1.3986 | 0.0103 | 1.1945 | 0.0085 |

| Compound no. | Structure | MIC<br><i>S. aureus</i><br>NCTC 8325 ( $\mu\text{M}$ ) | Log <i>P</i><br>predicted with<br>ChemBioDraw 13 | SpsB activity (normalized) at certain compound concentration ( $\mu\text{M}$ ) |        |        |        |        |        |
|--------------|-----------|--|--|--|--------|--------|--------|--------|--------|
|              |           |  |  | 100  |        | 50     |        | 10     |        |
|              |           |  |  | mean   | SD     | mean   | SD     | mean   | SD     |
| 3.49         |           | 0.5  | 4.51   | 1.0820   | 0.1712 | 1.4174 | 0.0783 | 1.2468 | 0.0475 |
| 3.50         |           | > 100  | 2.52   | 1.0656   | 0.1364 | 1.1497 | 0.2692 | 0.8851 | 0.0269 |
| 3.51         |           | > 100  | 2.96   | 1.0562   | 0.0721 | 1.1609 | 0.1473 | 0.9844 | 0.0217 |
| 3.52         |           | > 100  | 4.30   | N/A  | N/A    | N/A    | N/A    | N/A    | N/A    |
| 3.53         |           | > 100  | 2.66   | 0.9395   | 0.1265 | 0.8883 | 0.0986 | 1.0903 | 0.1406 |
| 3.54         |           | > 100  | 3.72   | 1.1643   | 0.0967 | 1.2403 | 0.1386 | 1.1378 | 0.1080 |
| 3.55         |           | > 100  | 3.07   | 1.1488   | 0.1459 | 1.0041 | 0.0580 | 0.9707 | 0.1430 |
| 3.56         |           | 1  | 4.50   | N/A  | N/A    | N/A    | N/A    | N/A    | N/A    |
| 3.57         |           | 3  | 5.05   | N/A  | N/A    | N/A    | N/A    | N/A    | N/A    |
| 3.58         |           | 0.5  | 5.47   | 1.6816   | 0.0293 | 1.5831 | 0.1252 | 1.3476 | 0.0338 |
| 3.59         |           | 1  | 5.61   | N/A  | N/A    | N/A    | N/A    | N/A    | N/A    |
| 3.60         |           | 30.0   | 5.13   | N/A  | N/A    | N/A    | N/A    | N/A    | N/A    |
| 3.61         |           | 0.6  | 5.31   | 2.0252   | 0.0889 | 2.1215 | 0.2488 | 1.2764 | 0.1079 |
| 3.62         |           | > 100  | 4.76   | 1.5446   | 0.1835 | 1.2798 | 0.1667 | 1.2093 | 0.1186 |
| 3.63         |           | > 100  | 5.03   | 0.9936   | 0.0971 | 1.1061 | 0.2157 | 1.0950 | 0.0593 |
| 3.64         |           | > 100  | 3.65   | 1.1890   | 0.0638 | 1.2828 | 0.1254 | 1.1470 | 0.0819 |
| 3.65         |           | 30   | 3.49   | 2.4241   | 0.2097 | 1.7007 | 0.2366 | 1.1769 | 0.0486 |

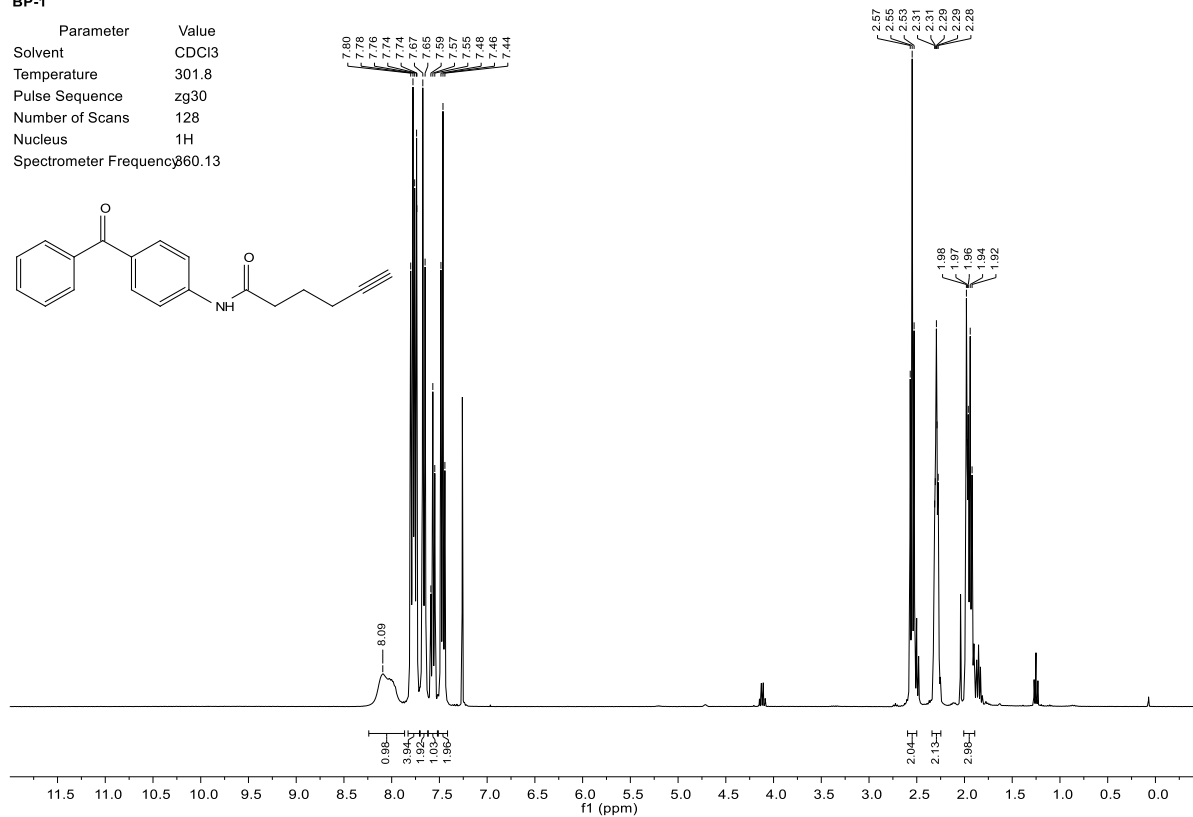
# Appendix

| Compound no. | Structure | MIC<br><i>S. aureus</i><br>NCTC 8325 (μM) | Log P<br>predicted with<br>ChemBioDraw 13 | SpsB activity (normalized) at certain compound concentration (μM) |        |        |        |        |        |
|--------------|-----------|---|---|---|--------|--------|--------|--------|--------|
|              |           |   |   | 100   |        | 50     |        | 10     |        |
|              |           |   |   | mean  | SD     | mean   | SD     | mean   | SD     |
| 3.66         |           | 3   | 4.92                                      | 1.3866  | 0.0561 | 1.2184 | 0.0258 | 1.1888 | 0.0241 |
| 3.67         |           | > 100                                     | 5.47                                      | N/A   | N/A    | N/A    | N/A    | N/A    | N/A    |
| 3.68         |           | > 100                                     | 3.40                                      | 1.0930  | 0.1150 | 1.0853 | 0.1002 | 1.0204 | 0.0312 |
| 3.69         |           | > 100                                     | 3.81                                      | 0.9481  | 0.0527 | 1.0141 | 0.1434 | 0.9670 | 0.0434 |
| 3.70         |           | 1   | 6.06                                      | 1.7420  | 0.0674 | 1.7698 | 0.1908 | 1.5341 | 0.0510 |
| DA-1         |           | > 100                                     | 2.22                                      | N/A   | N/A    | N/A    | N/A    | N/A    | N/A    |
| DA-1C        |           | > 100                                     | 2.64                                      | 1.0058  | 0.1278 | 0.9954 | 0.0679 | 0.9703 | 0.0166 |
| DA-2         |           | > 100                                     | 2.64                                      | N/A   | N/A    | N/A    | N/A    | N/A    | N/A    |
| DA-2C        |           | > 100                                     | 3.05                                      | 1.0131  | 0.0838 | 1.0706 | 0.0287 | 1.0685 | 0.0174 |
| DA-3         |           | > 100                                     | 1.53                                      | N/A   | N/A    | N/A    | N/A    | N/A    | N/A    |
| DA-3C        |           | > 100                                     | 1.95                                      | 1.0093  | 0.0457 | 0.9981 | 0.1373 | 0.9947 | 0.0231 |

## 7.5. Selected $^1\text{H}$ and $^{13}\text{C}$ NMR Spectra – Chapter 2: Insights into Photocrosslinker-Associated Off-Target Protein Binding

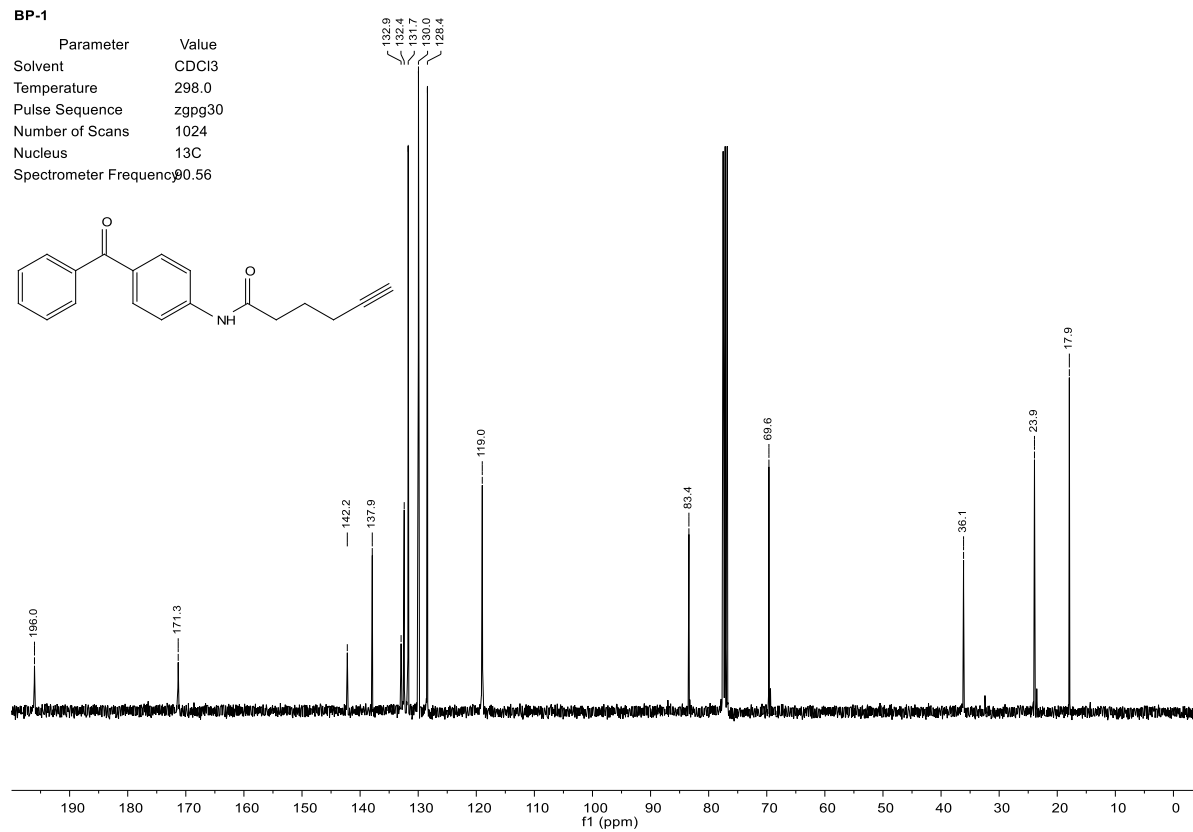
BP-1

| Parameter              | Value           |
|------------------------|-----------------|
| Solvent                | $\text{CDCl}_3$ |
| Temperature            | 301.8           |
| Pulse Sequence         | zg30            |
| Number of Scans        | 128             |
| Nucleus                | $^1\text{H}$    |
| Spectrometer Frequency | 360.13          |



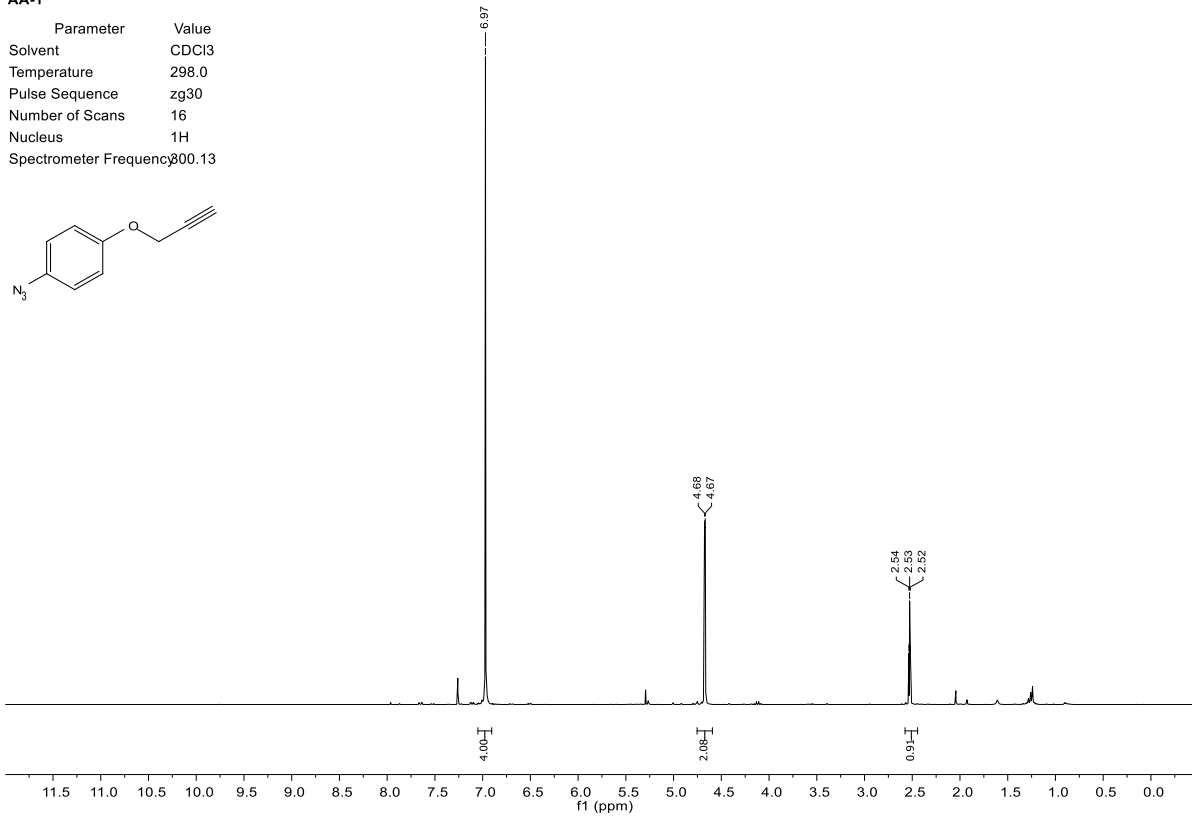
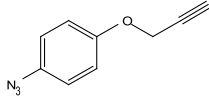
BP-1

| Parameter              | Value           |
|------------------------|-----------------|
| Solvent                | $\text{CDCl}_3$ |
| Temperature            | 298.0           |
| Pulse Sequence         | zgpg30          |
| Number of Scans        | 1024            |
| Nucleus                | $^{13}\text{C}$ |
| Spectrometer Frequency | 90.56           |



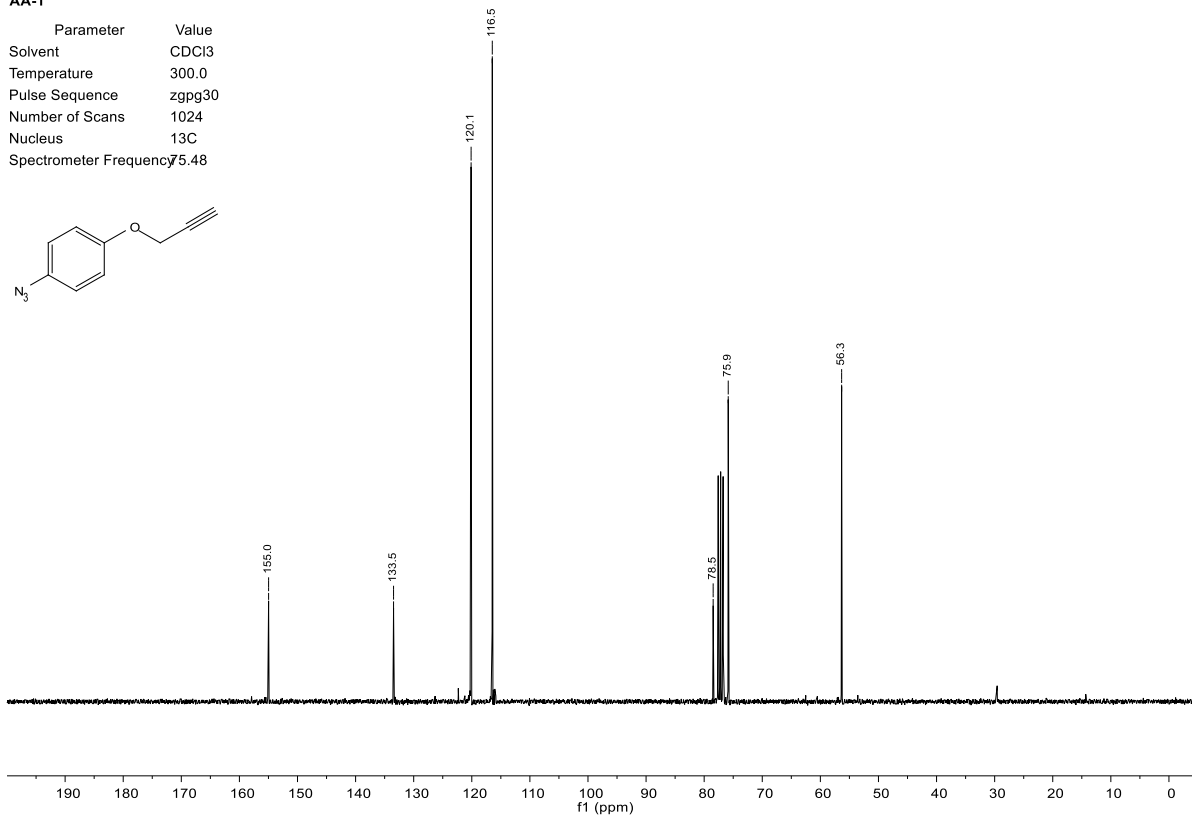
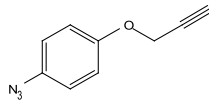
AA-1

| Parameter              | Value             |
|------------------------|-------------------|
| Solvent                | CDCl <sub>3</sub> |
| Temperature            | 298.0             |
| Pulse Sequence         | zg30              |
| Number of Scans        | 16                |
| Nucleus                | <sup>1</sup> H    |
| Spectrometer Frequency | 300.13            |



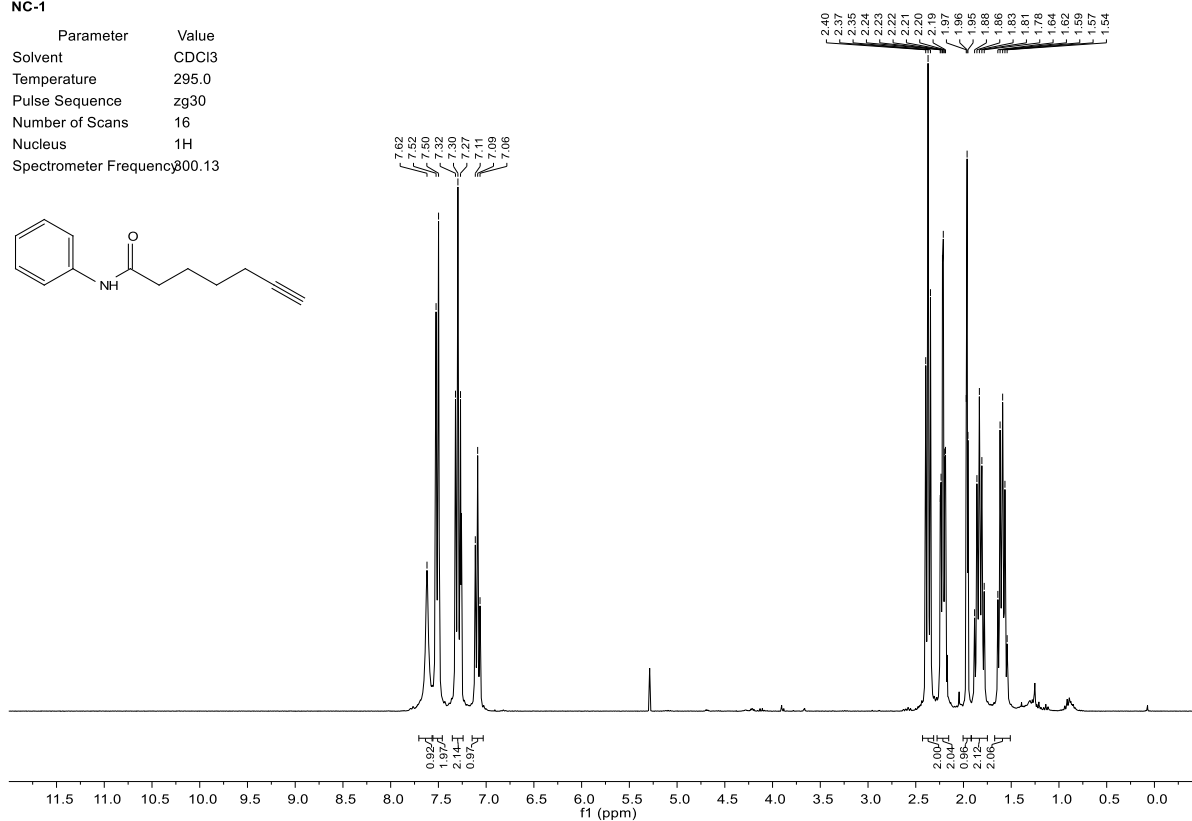
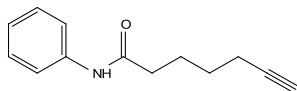
AA-1

| Parameter              | Value             |
|------------------------|-------------------|
| Solvent                | CDCl <sub>3</sub> |
| Temperature            | 300.0             |
| Pulse Sequence         | zgpg30            |
| Number of Scans        | 1024              |
| Nucleus                | <sup>13</sup> C   |
| Spectrometer Frequency | 75.48             |



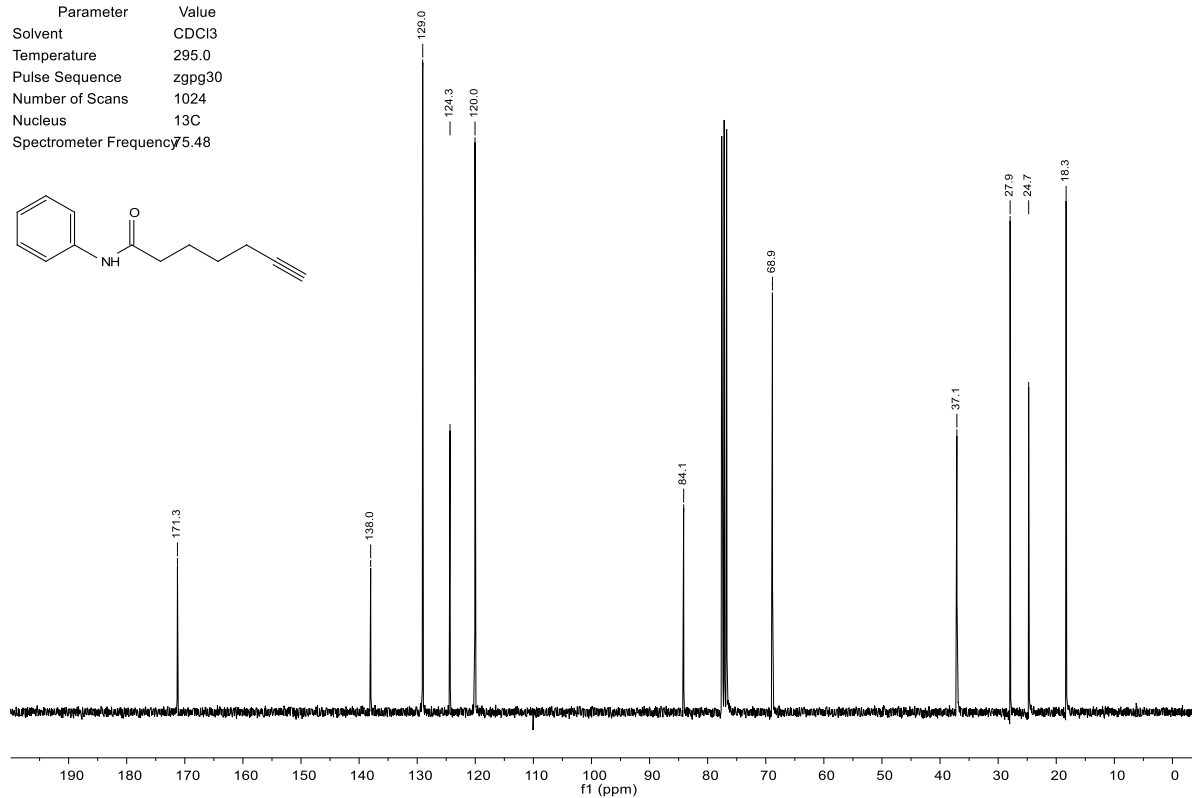
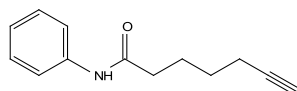
NC-1

| Parameter              | Value             |
|------------------------|-------------------|
| Solvent                | CDCl <sub>3</sub> |
| Temperature            | 295.0             |
| Pulse Sequence         | zg30              |
| Number of Scans        | 16                |
| Nucleus                | <sup>1</sup> H    |
| Spectrometer Frequency | 300.13            |



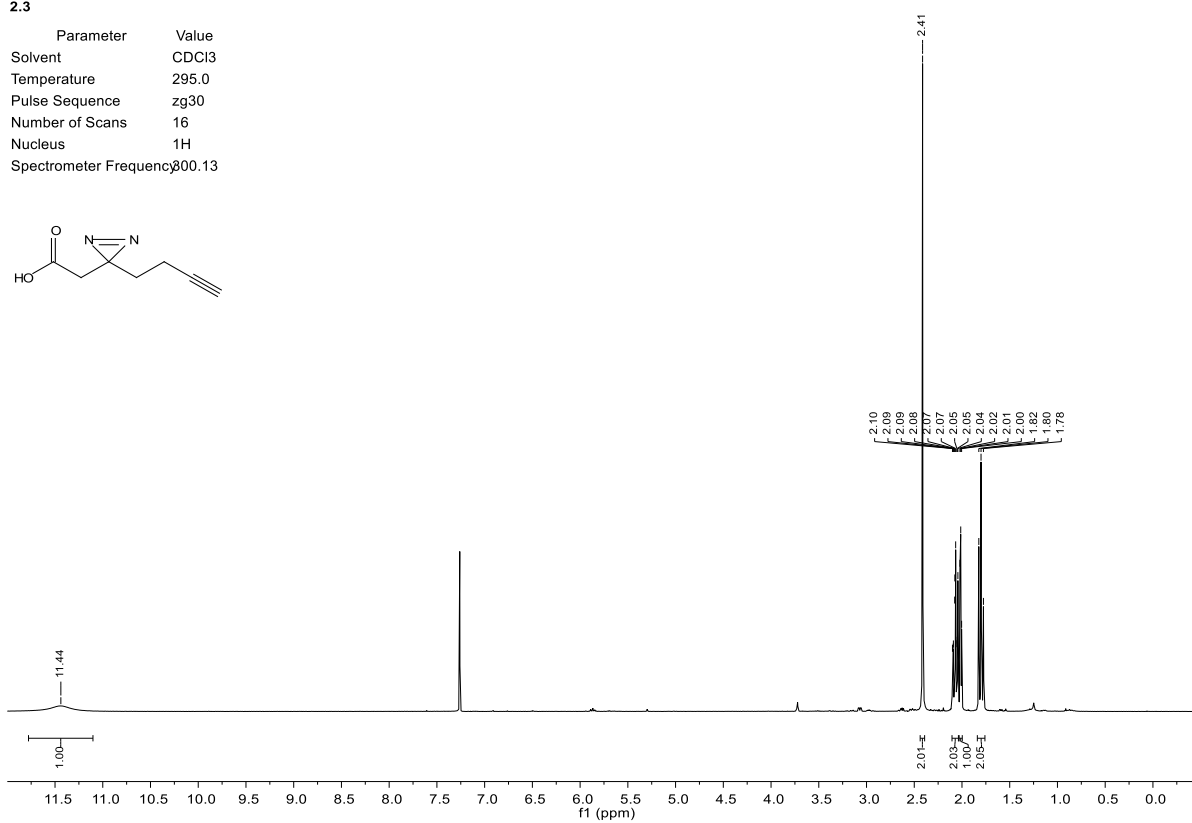
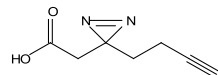
NC-1

| Parameter              | Value             |
|------------------------|-------------------|
| Solvent                | CDCl <sub>3</sub> |
| Temperature            | 295.0             |
| Pulse Sequence         | zgpg30            |
| Number of Scans        | 1024              |
| Nucleus                | <sup>13</sup> C   |
| Spectrometer Frequency | 75.48             |



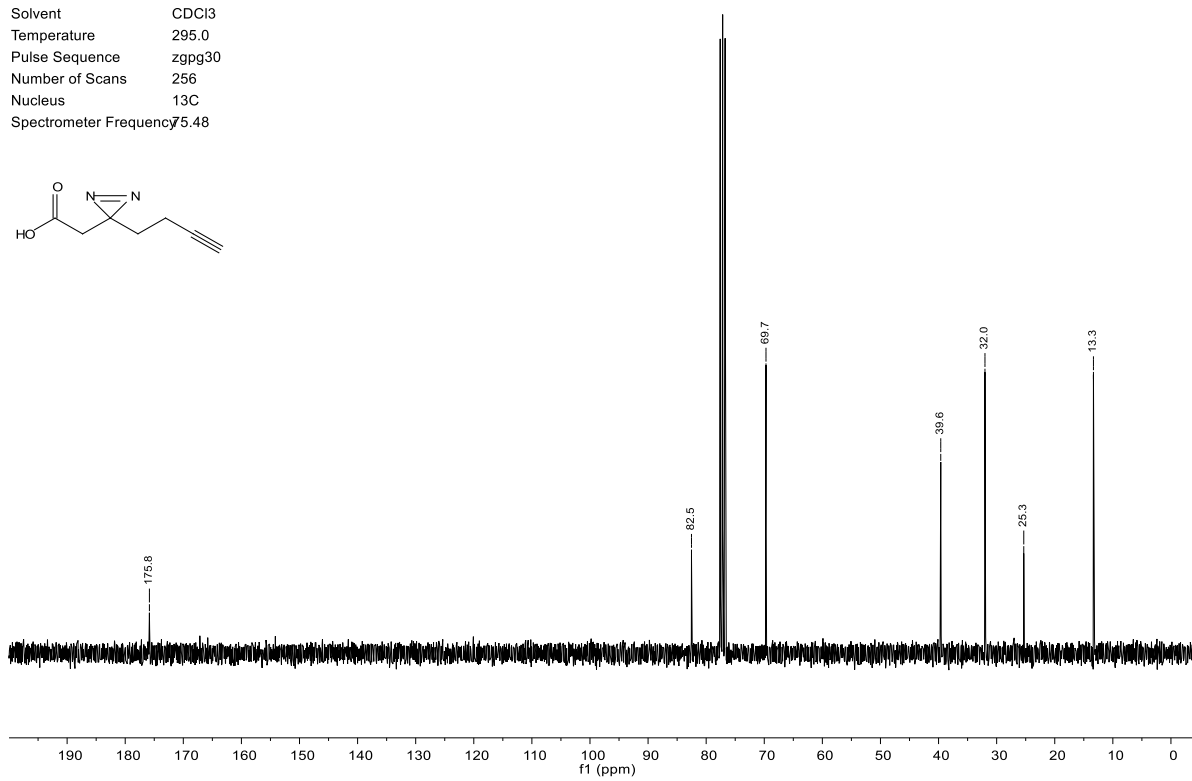
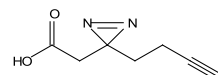
2.3

| Parameter              | Value             |
|------------------------|-------------------|
| Solvent                | CDCl <sub>3</sub> |
| Temperature            | 295.0             |
| Pulse Sequence         | zg30              |
| Number of Scans        | 16                |
| Nucleus                | <sup>1</sup> H    |
| Spectrometer Frequency | 300.13            |



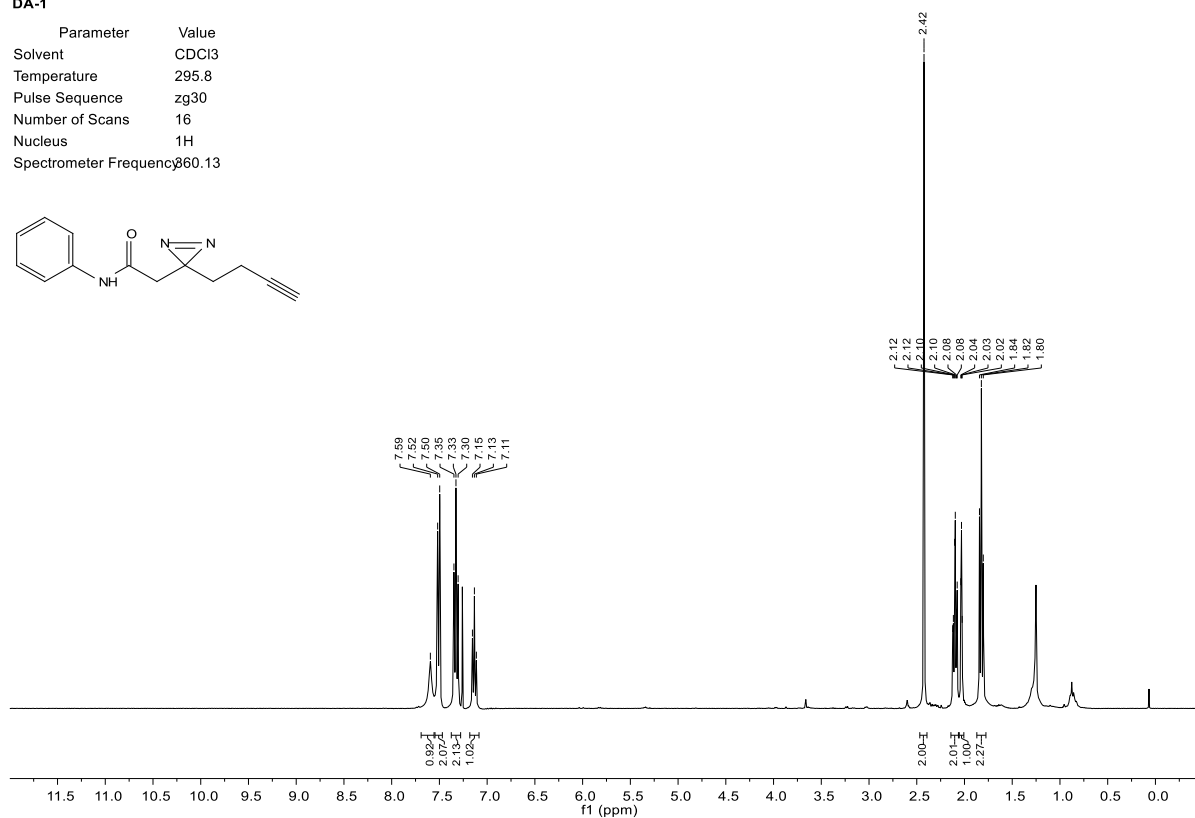
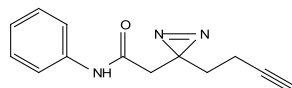
2.3

| Parameter              | Value             |
|------------------------|-------------------|
| Solvent                | CDCl <sub>3</sub> |
| Temperature            | 295.0             |
| Pulse Sequence         | zgpg30            |
| Number of Scans        | 256               |
| Nucleus                | <sup>13</sup> C   |
| Spectrometer Frequency | 75.48             |



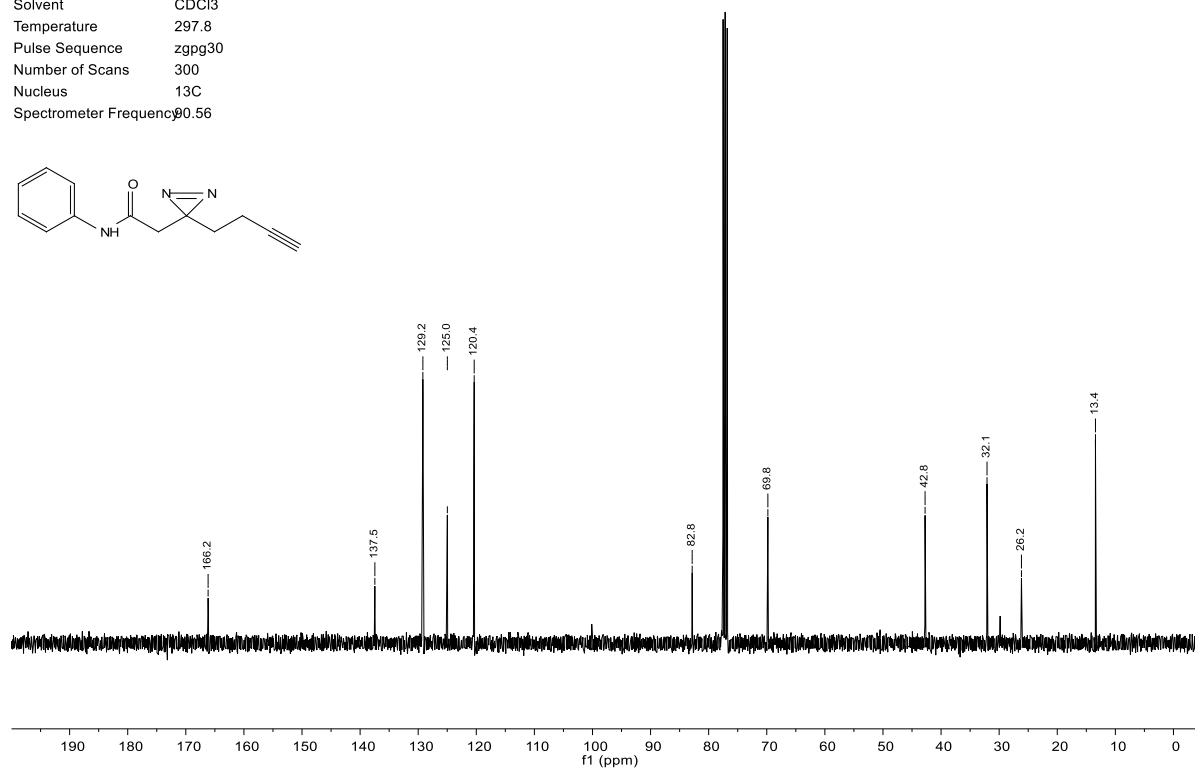
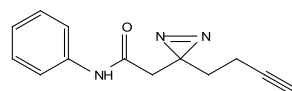
## DA-1

| Parameter              | Value             |
|------------------------|-------------------|
| Solvent                | CDCl <sub>3</sub> |
| Temperature            | 295.8             |
| Pulse Sequence         | zg30              |
| Number of Scans        | 16                |
| Nucleus                | <sup>1</sup> H    |
| Spectrometer Frequency | 860.13            |



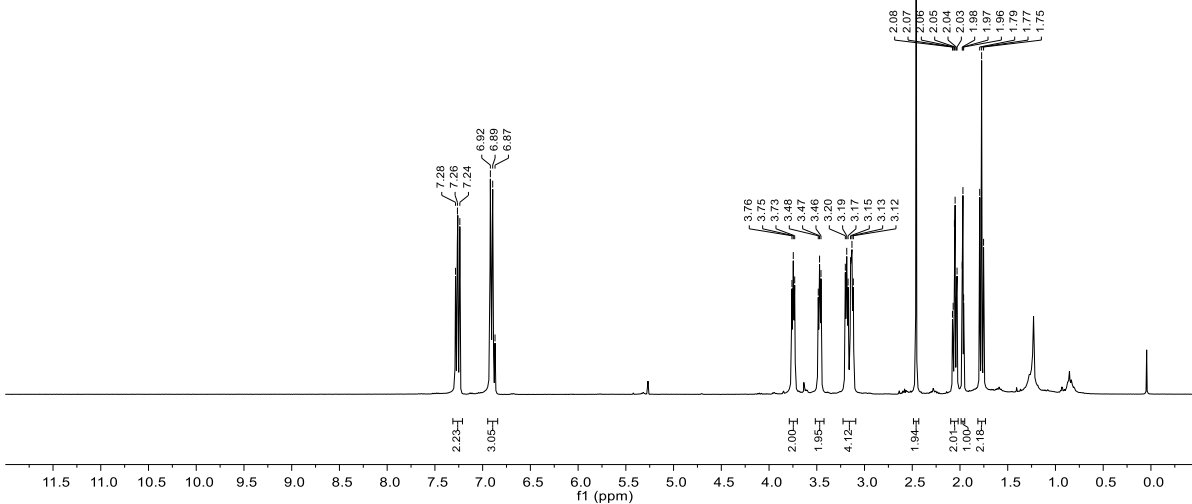
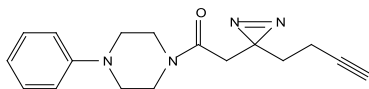
## DA-1

| Parameter              | Value             |
|------------------------|-------------------|
| Solvent                | CDCl <sub>3</sub> |
| Temperature            | 297.8             |
| Pulse Sequence         | zgpg30            |
| Number of Scans        | 300               |
| Nucleus                | <sup>13</sup> C   |
| Spectrometer Frequency | 90.56             |



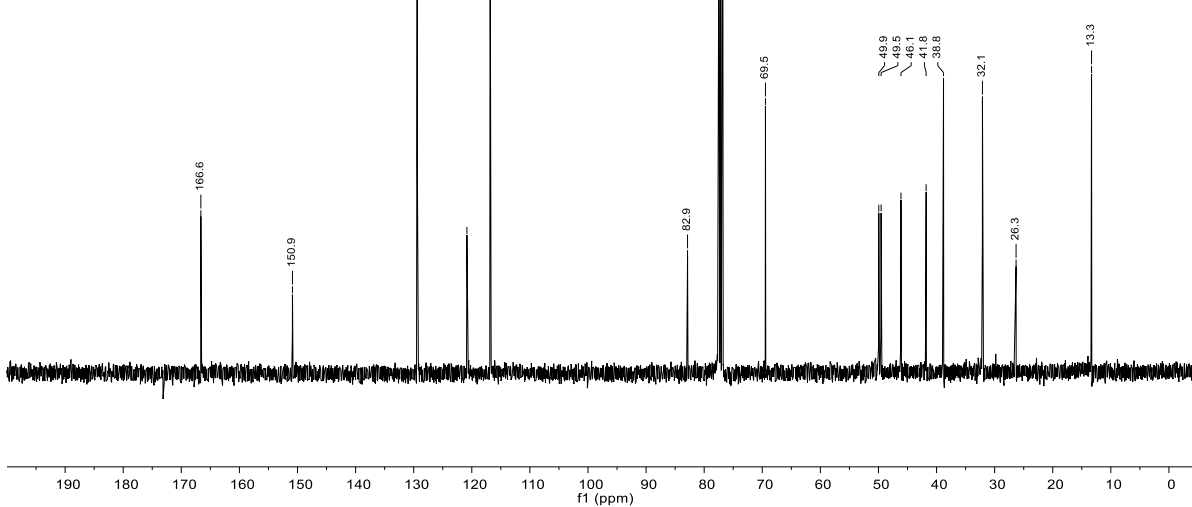
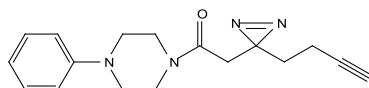
DA-2

| Parameter              | Value             |
|------------------------|-------------------|
| Solvent                | CDCl <sub>3</sub> |
| Temperature            | 296.2             |
| Pulse Sequence         | zg30              |
| Number of Scans        | 16                |
| Nucleus                | <sup>1</sup> H    |
| Spectrometer Frequency | 360.13            |



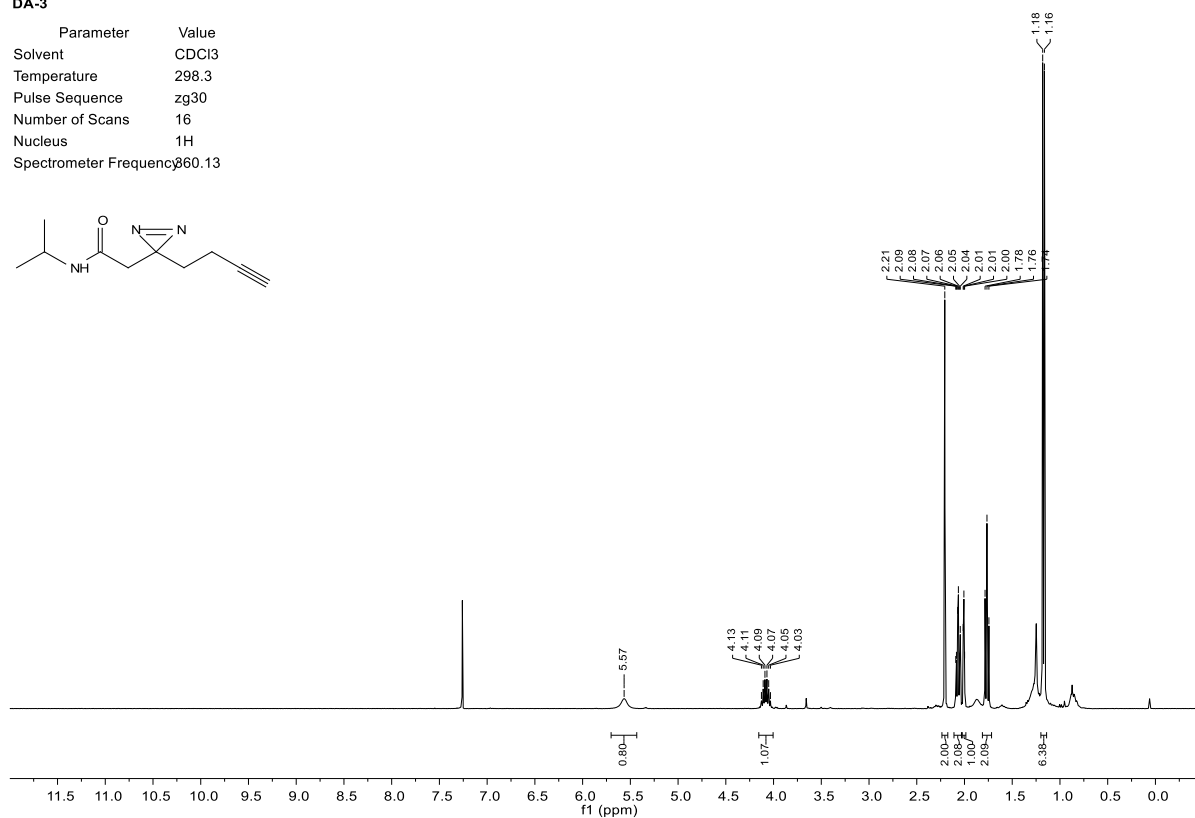
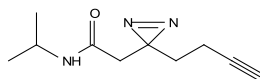
DA-2

| Parameter              | Value             |
|------------------------|-------------------|
| Solvent                | CDCl <sub>3</sub> |
| Temperature            | 298.0             |
| Pulse Sequence         | zgpg30            |
| Number of Scans        | 300               |
| Nucleus                | <sup>13</sup> C   |
| Spectrometer Frequency | 90.56             |



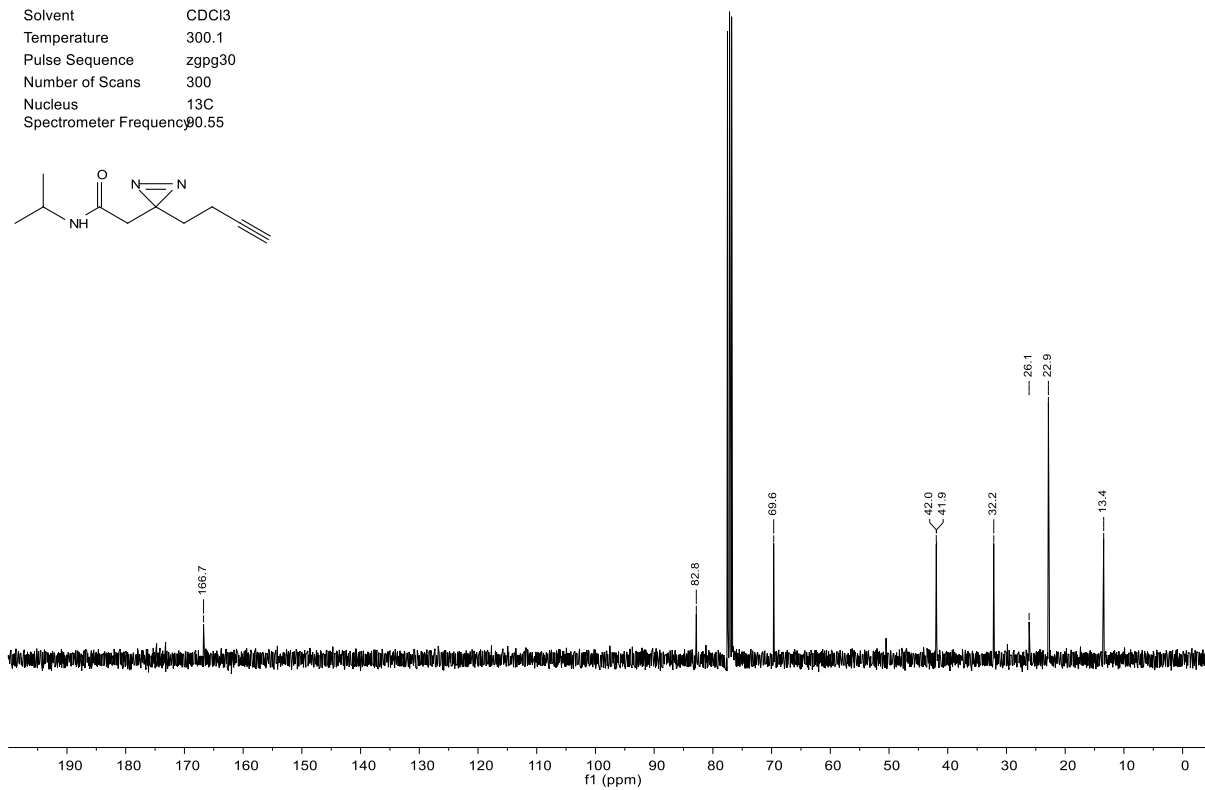
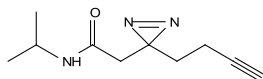
## DA-3

| Parameter              | Value             |
|------------------------|-------------------|
| Solvent                | CDCl <sub>3</sub> |
| Temperature            | 298.3             |
| Pulse Sequence         | zg30              |
| Number of Scans        | 16                |
| Nucleus                | <sup>1</sup> H    |
| Spectrometer Frequency | 360.13            |



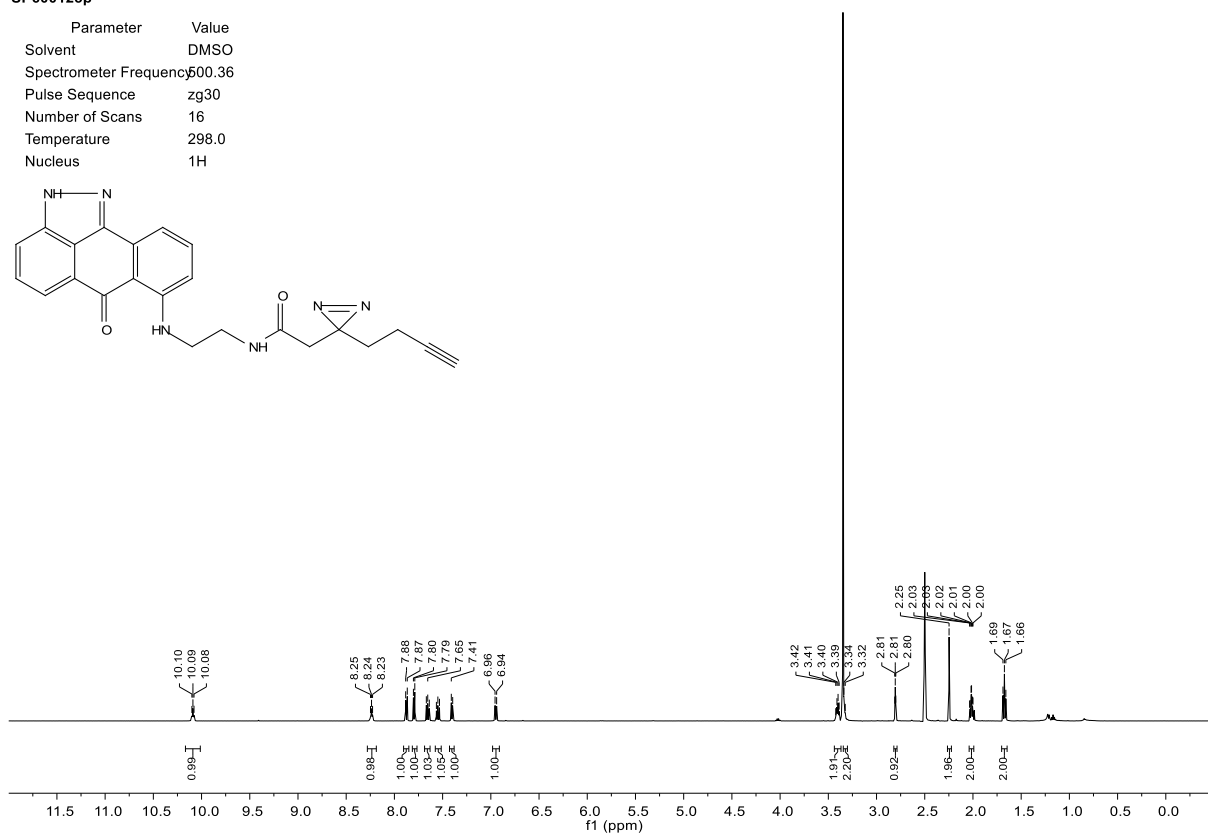
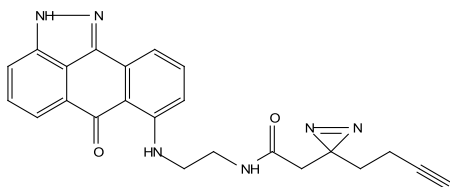
## DA-3

| Parameter              | Value             |
|------------------------|-------------------|
| Solvent                | CDCl <sub>3</sub> |
| Temperature            | 300.1             |
| Pulse Sequence         | zgpg30            |
| Number of Scans        | 300               |
| Nucleus                | <sup>13</sup> C   |
| Spectrometer Frequency | 90.55             |



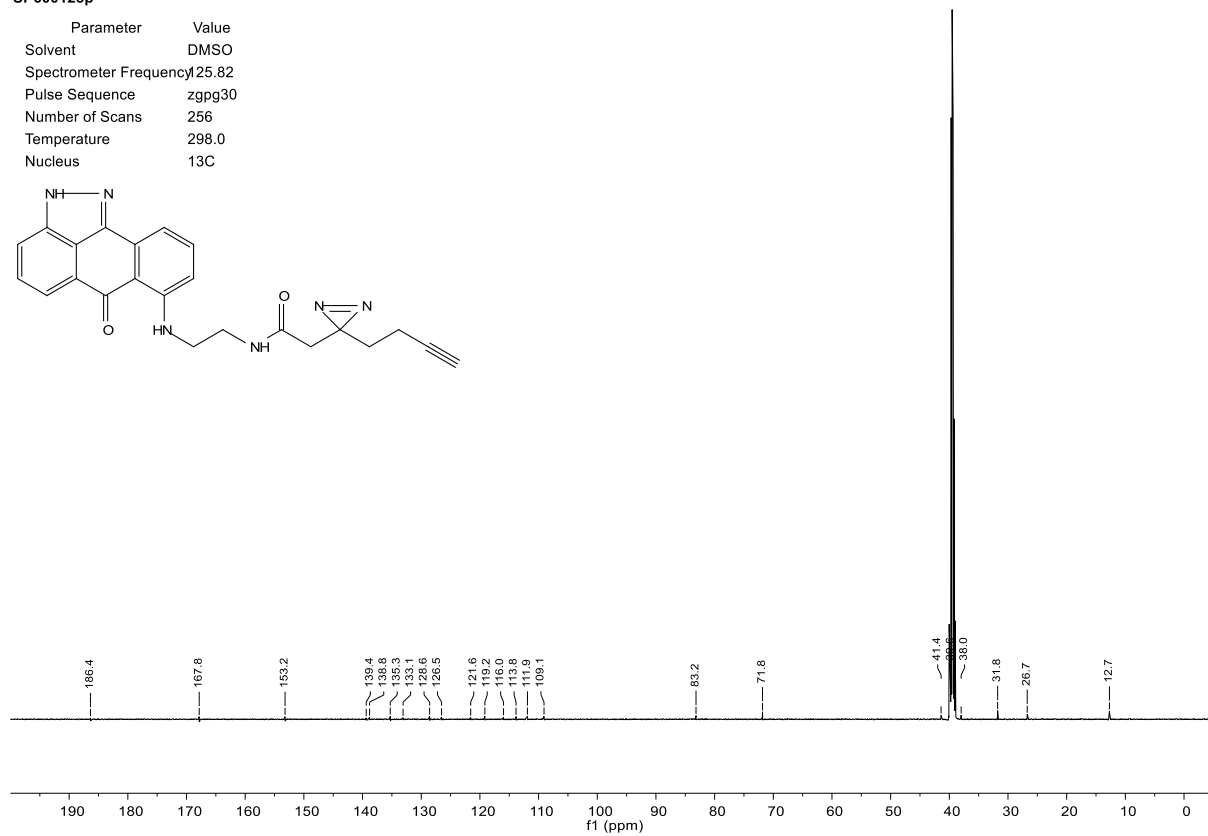
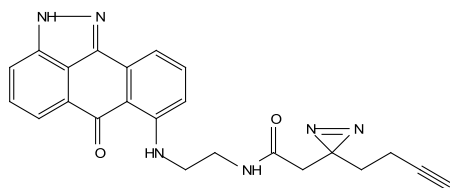
SP600125p

| Parameter              | Value          |
|------------------------|----------------|
| Solvent                | DMSO           |
| Spectrometer Frequency | 500.36         |
| Pulse Sequence         | zg30           |
| Number of Scans        | 16             |
| Temperature            | 298.0          |
| Nucleus                | <sup>1</sup> H |



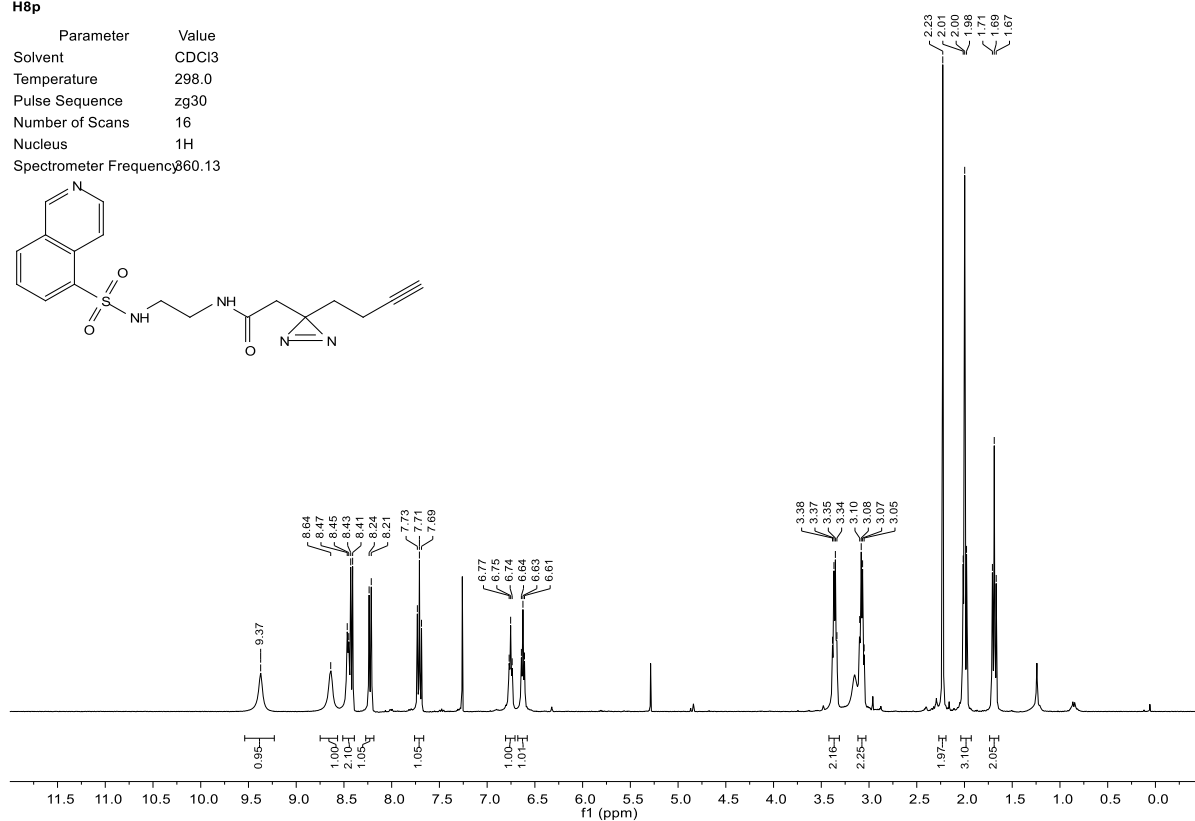
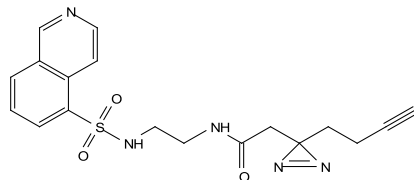
SP600125p

| Parameter              | Value           |
|------------------------|-----------------|
| Solvent                | DMSO            |
| Spectrometer Frequency | 125.82          |
| Pulse Sequence         | zgpg30          |
| Number of Scans        | 256             |
| Temperature            | 298.0           |
| Nucleus                | <sup>13</sup> C |



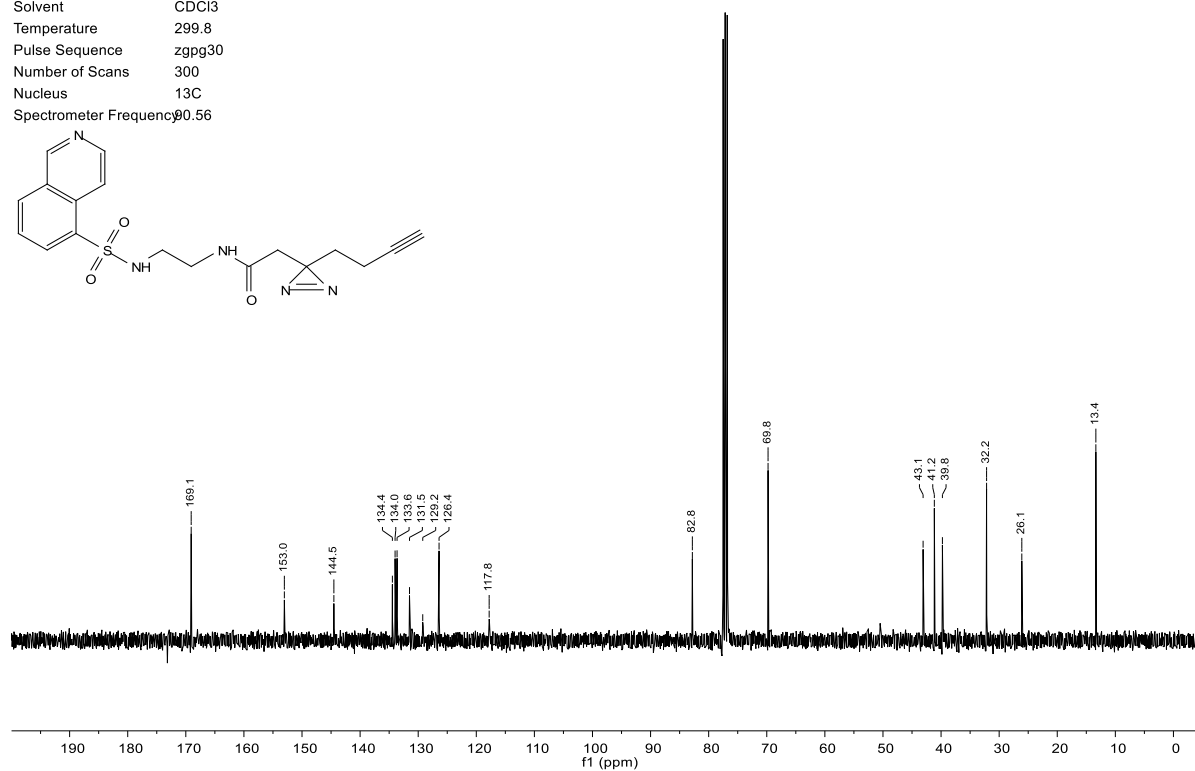
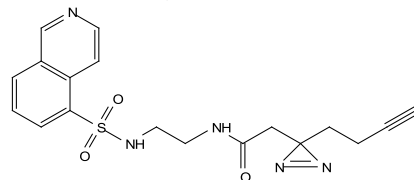
H8p

| Parameter              | Value             |
|------------------------|-------------------|
| Solvent                | CDCl <sub>3</sub> |
| Temperature            | 298.0             |
| Pulse Sequence         | zg30              |
| Number of Scans        | 16                |
| Nucleus                | <sup>1</sup> H    |
| Spectrometer Frequency | 360.13            |



H8p

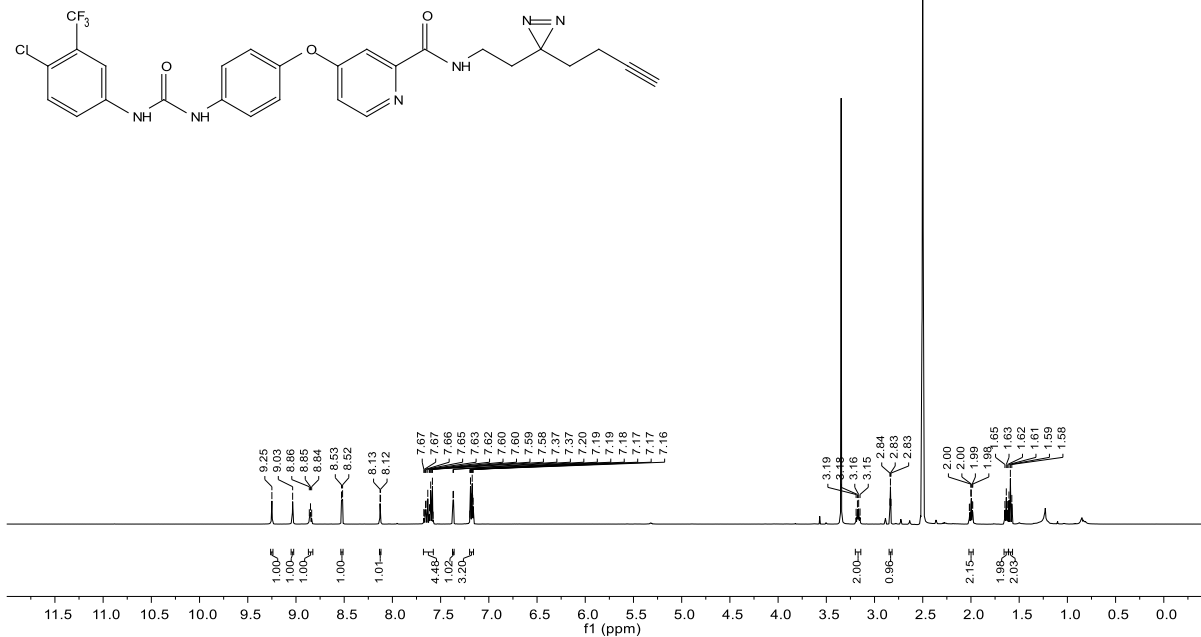
| Parameter              | Value             |
|------------------------|-------------------|
| Solvent                | CDCl <sub>3</sub> |
| Temperature            | 299.8             |
| Pulse Sequence         | zpgg30            |
| Number of Scans        | 300               |
| Nucleus                | <sup>13</sup> C   |
| Spectrometer Frequency | 90.56             |



## 7.6. Selected $^1\text{H}$ and $^{13}\text{C}$ NMR Spectra – Chapter 3: Discovery of a Small Molecule Antibiotic Active Against Multidrug-Resistant Gram-Positive Pathogens

SFNp

| Parameter              | Value        |
|------------------------|--------------|
| Solvent                | DMSO         |
| Spectrometer Frequency | 500.36       |
| Pulse Sequence         | zg30         |
| Number of Scans        | 128          |
| Temperature            | 298.0        |
| Nucleus                | $^1\text{H}$ |



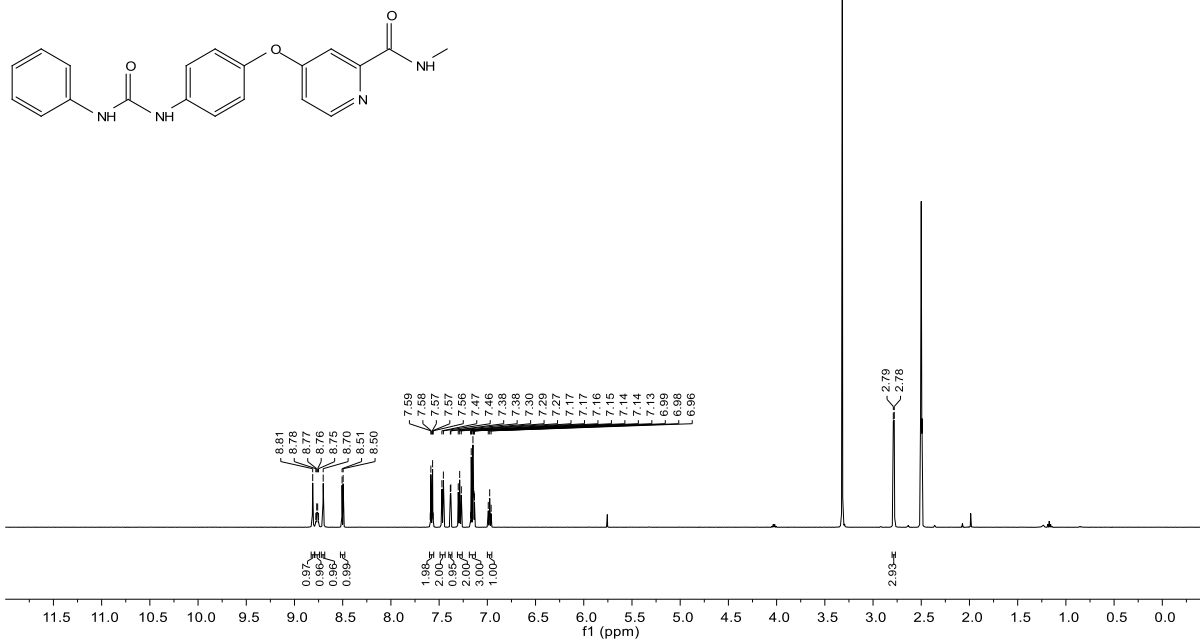
SFNp

| Parameter              | Value           |
|------------------------|-----------------|
| Solvent                | DMSO            |
| Spectrometer Frequency | 25.82           |
| Pulse Sequence         | zgpg30          |
| Number of Scans        | 512             |
| Temperature            | 298.0           |
| Nucleus                | $^{13}\text{C}$ |



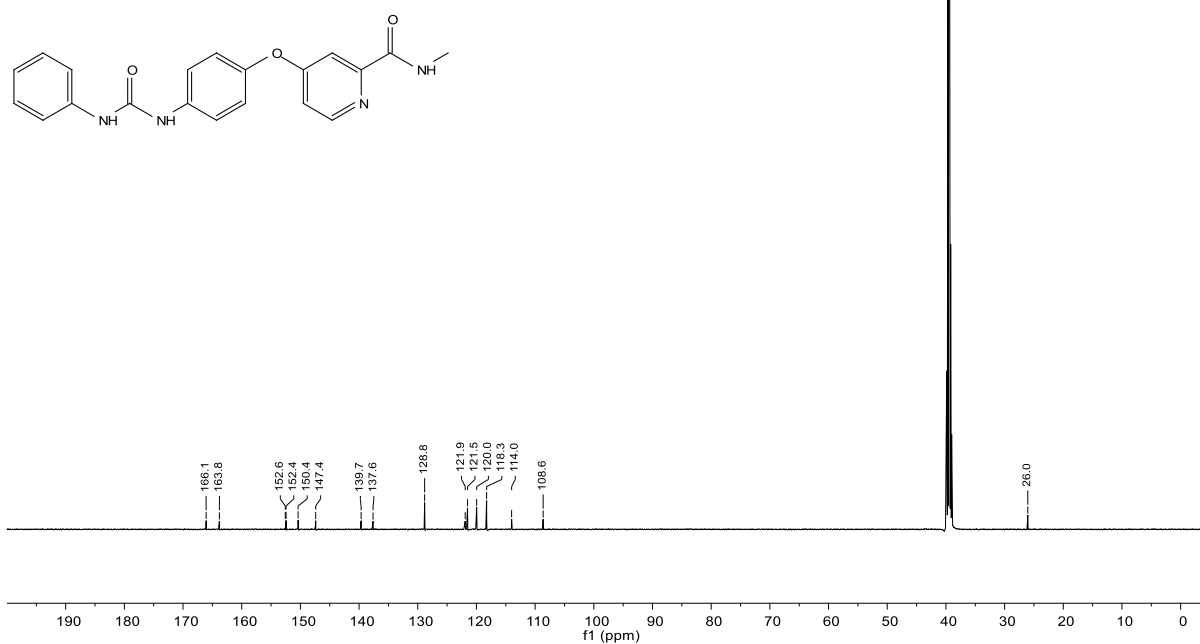
## SFN-C

| Parameter              | Value          |
|------------------------|----------------|
| Solvent                | DMSO           |
| Spectrometer Frequency | 500.13         |
| Pulse Sequence         | zg30           |
| Number of Scans        | 16             |
| Temperature            | 298.0          |
| Nucleus                | <sup>1</sup> H |



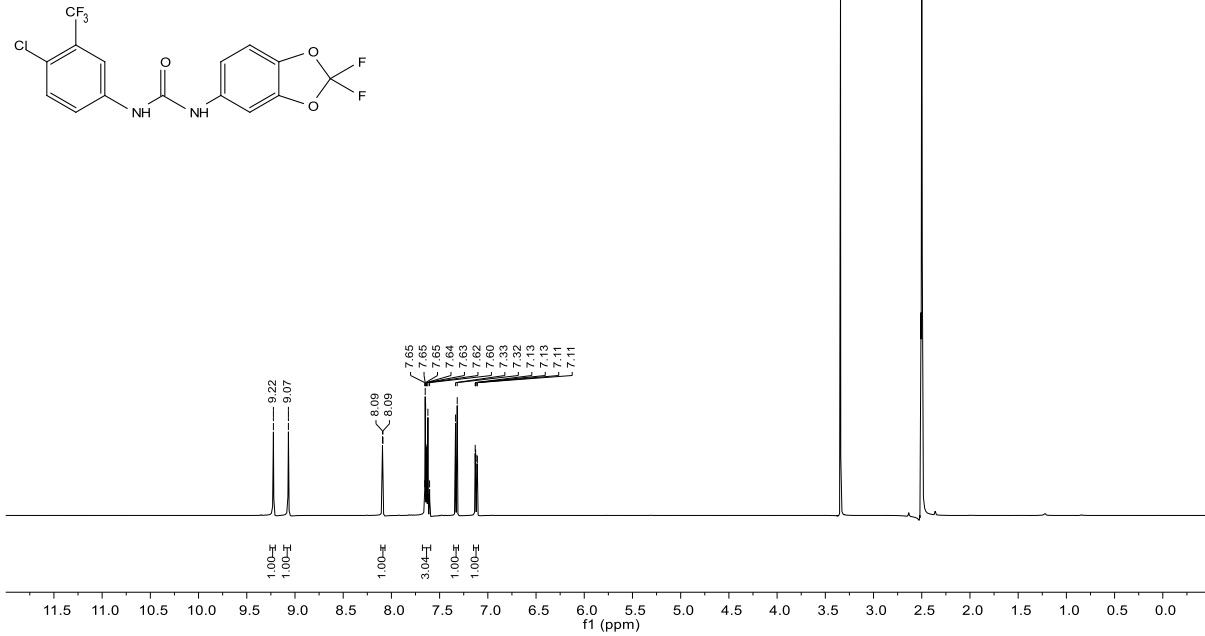
## SFN-C

| Parameter              | Value           |
|------------------------|-----------------|
| Solvent                | DMSO            |
| Spectrometer Frequency | 125.82          |
| Pulse Sequence         | zgpg30          |
| Number of Scans        | 256             |
| Temperature            | 299.8           |
| Nucleus                | <sup>13</sup> C |



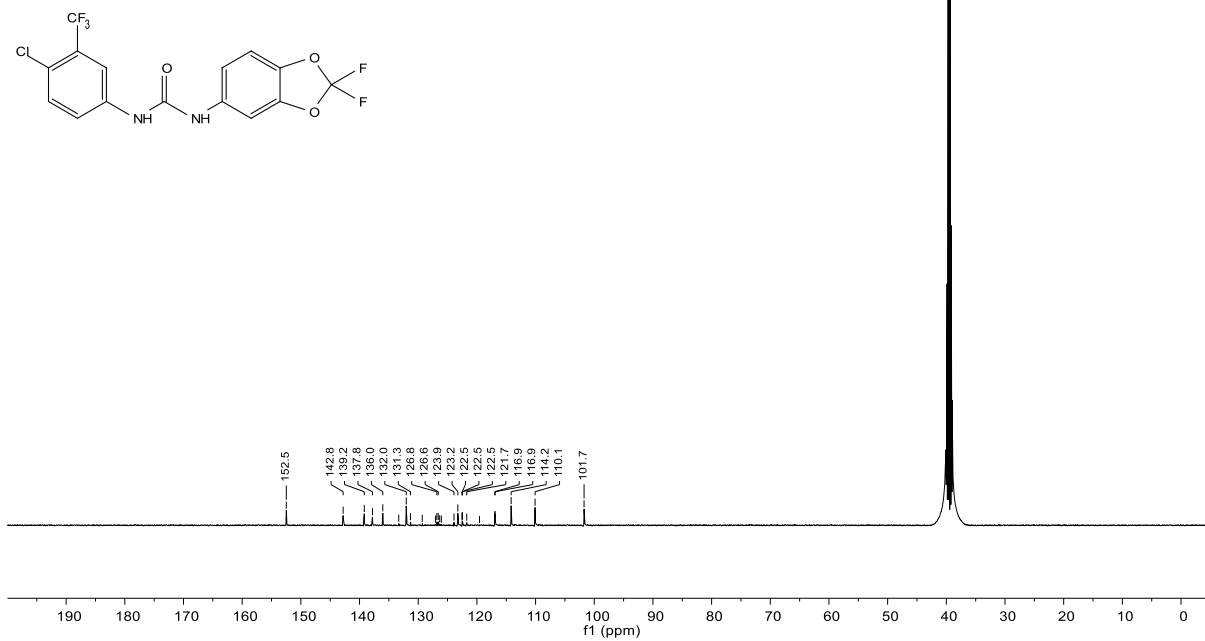
PK150

| Parameter              | Value          |
|------------------------|----------------|
| Solvent                | DMSO           |
| Spectrometer Frequency | 500.36         |
| Pulse Sequence         | zg30           |
| Number of Scans        | 16             |
| Temperature            | 299.9          |
| Nucleus                | <sup>1</sup> H |



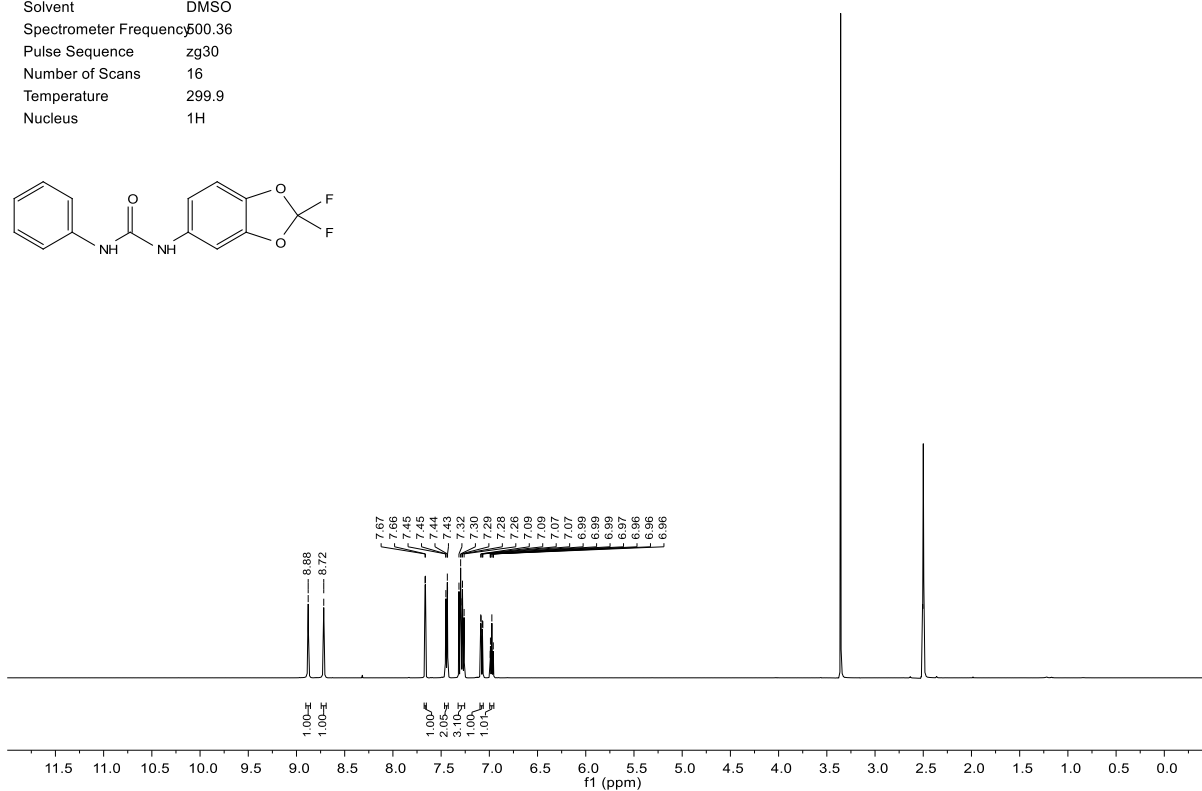
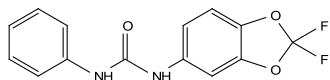
PK150

| Parameter              | Value           |
|------------------------|-----------------|
| Solvent                | DMSO            |
| Spectrometer Frequency | 125.82          |
| Pulse Sequence         | zgpg30          |
| Number of Scans        | 256             |
| Temperature            | 299.9           |
| Nucleus                | <sup>13</sup> C |



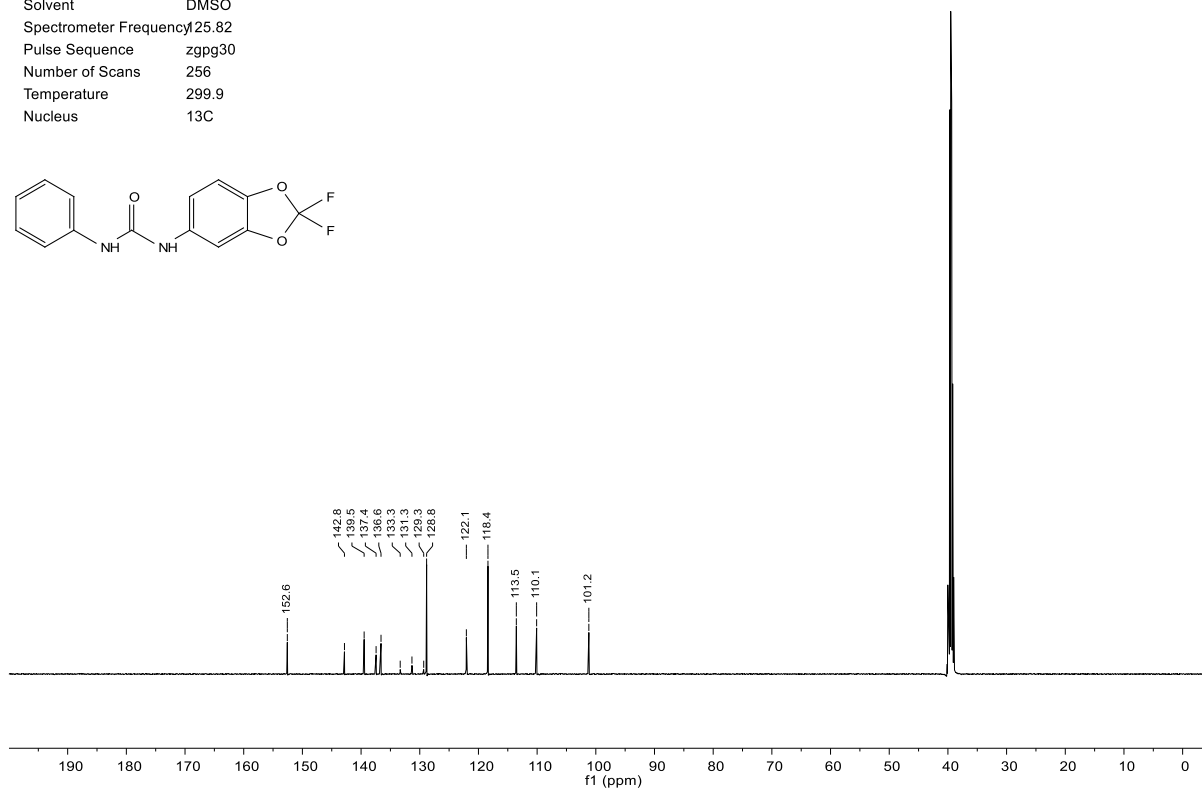
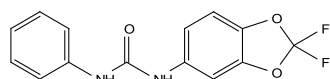
## PK150-C

| Parameter              | Value          |
|------------------------|----------------|
| Solvent                | DMSO           |
| Spectrometer Frequency | 500.36         |
| Pulse Sequence         | zg30           |
| Number of Scans        | 16             |
| Temperature            | 299.9          |
| Nucleus                | <sup>1</sup> H |



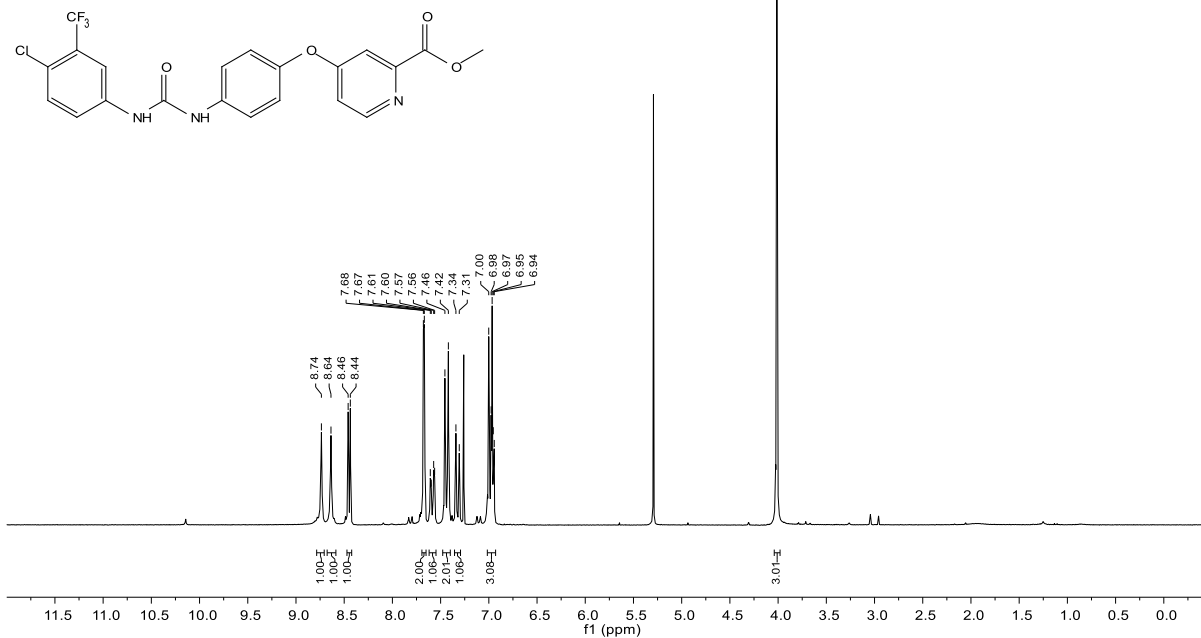
## PK150-C

| Parameter              | Value           |
|------------------------|-----------------|
| Solvent                | DMSO            |
| Spectrometer Frequency | 125.82          |
| Pulse Sequence         | zgpg30          |
| Number of Scans        | 256             |
| Temperature            | 299.9           |
| Nucleus                | <sup>13</sup> C |



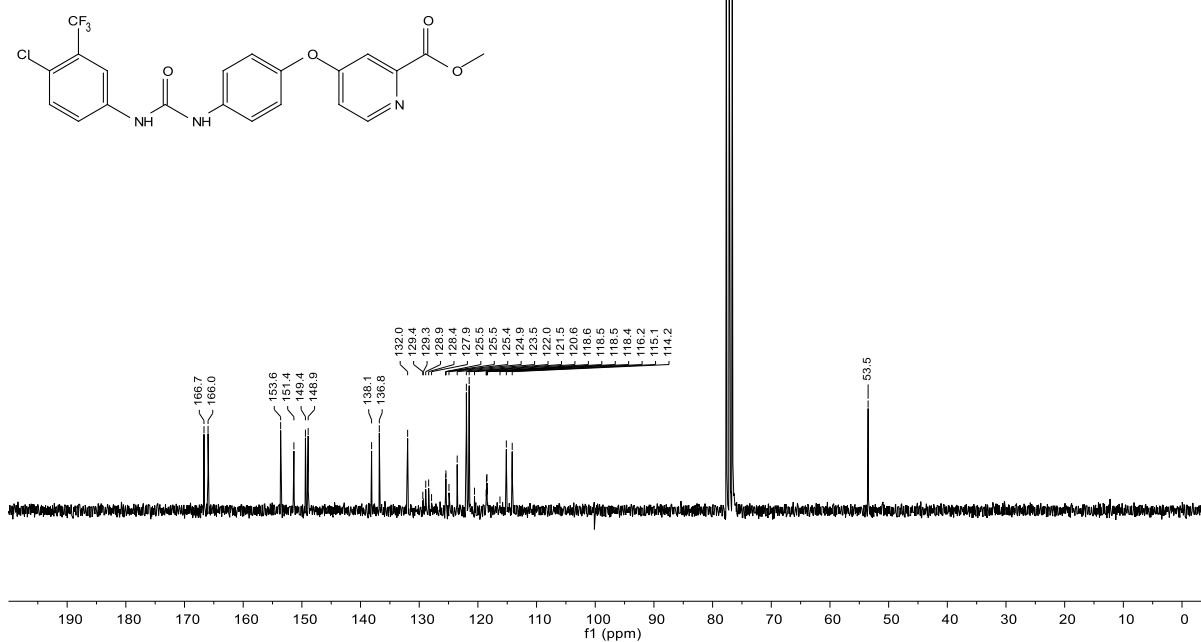
3.2

| Parameter              | Value             |
|------------------------|-------------------|
| Solvent                | CDCl <sub>3</sub> |
| Spectrometer Frequency | 250.13            |
| Pulse Sequence         | zg30              |
| Number of Scans        | 16                |
| Temperature            | 300.0             |
| Nucleus                | <sup>1</sup> H    |



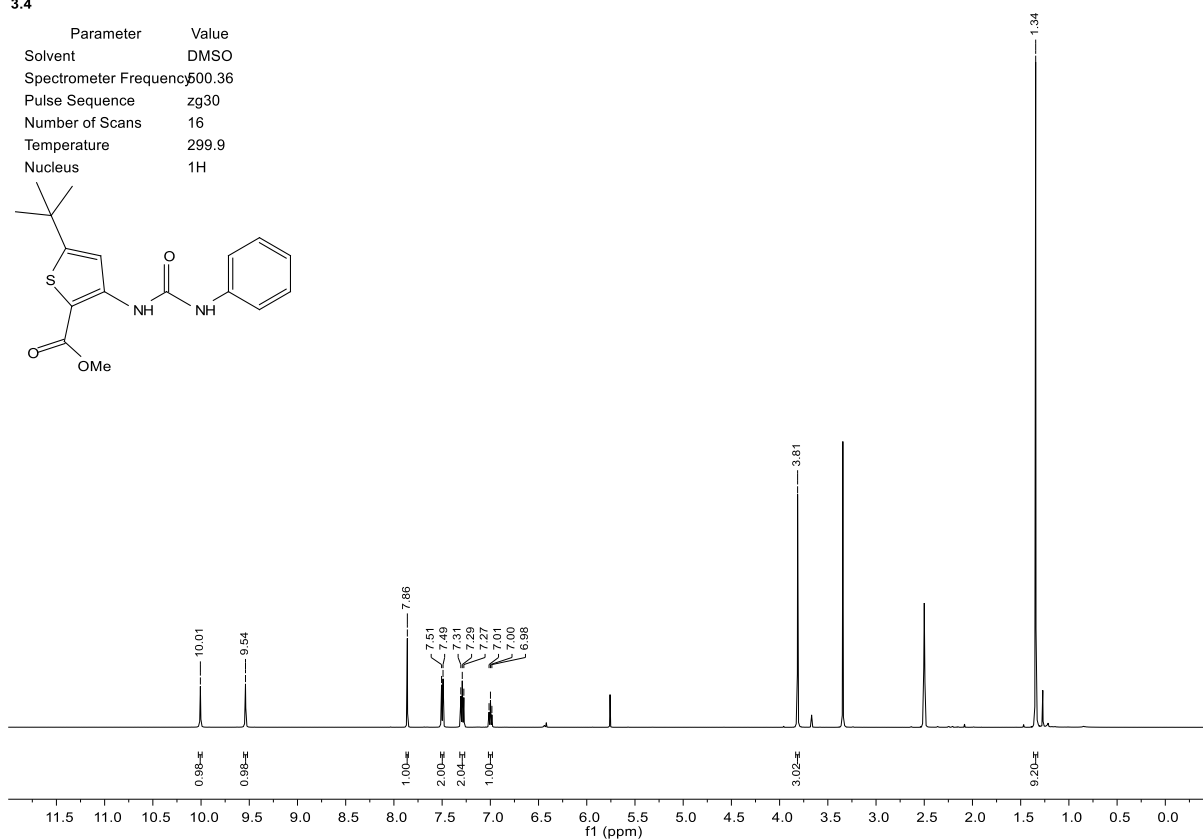
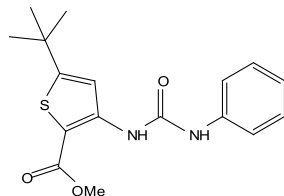
3.2

| Parameter              | Value             |
|------------------------|-------------------|
| Solvent                | CDCl <sub>3</sub> |
| Spectrometer Frequency | 62.90             |
| Pulse Sequence         | zgpg30            |
| Number of Scans        | 1024              |
| Temperature            | 300.0             |
| Nucleus                | <sup>13</sup> C   |



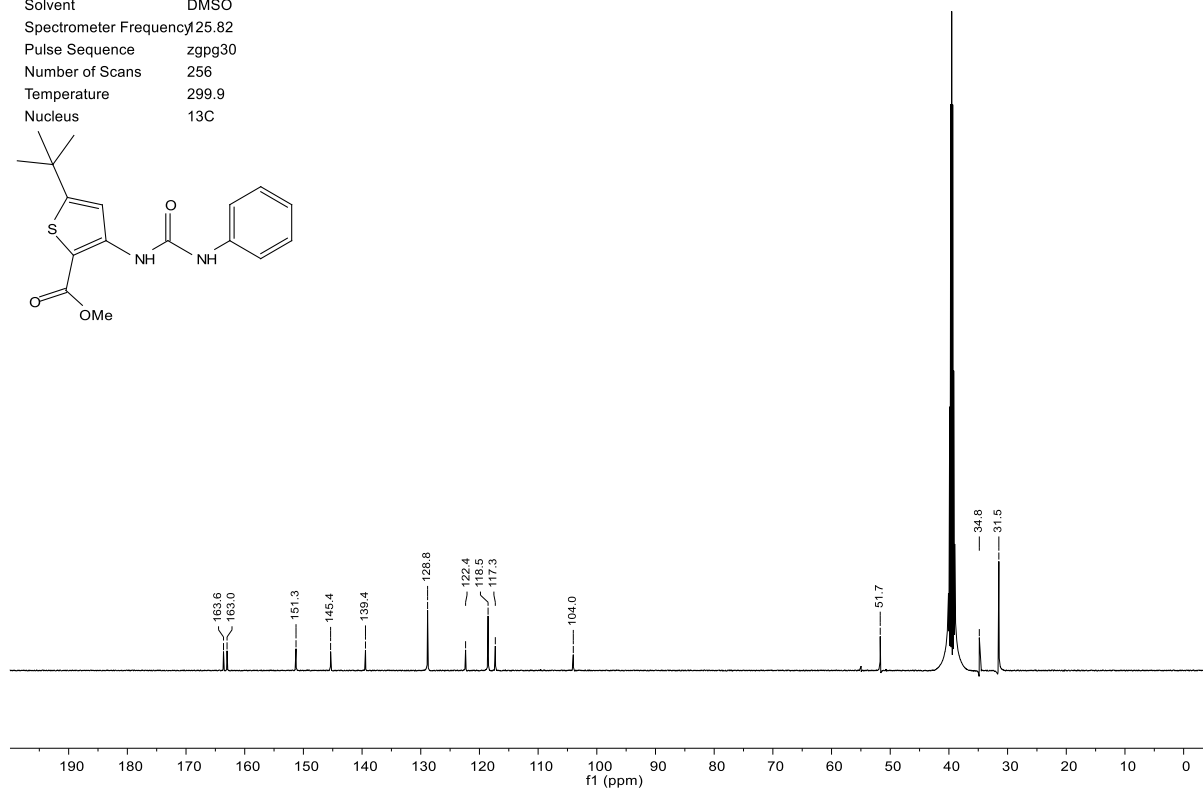
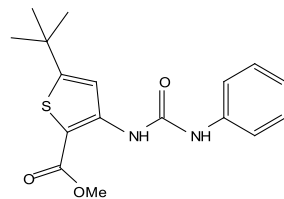
3.4

| Parameter              | Value        |
|------------------------|--------------|
| Solvent                | DMSO         |
| Spectrometer Frequency | 500.36       |
| Pulse Sequence         | zg30         |
| Number of Scans        | 16           |
| Temperature            | 299.9        |
| Nucleus                | $^1\text{H}$ |



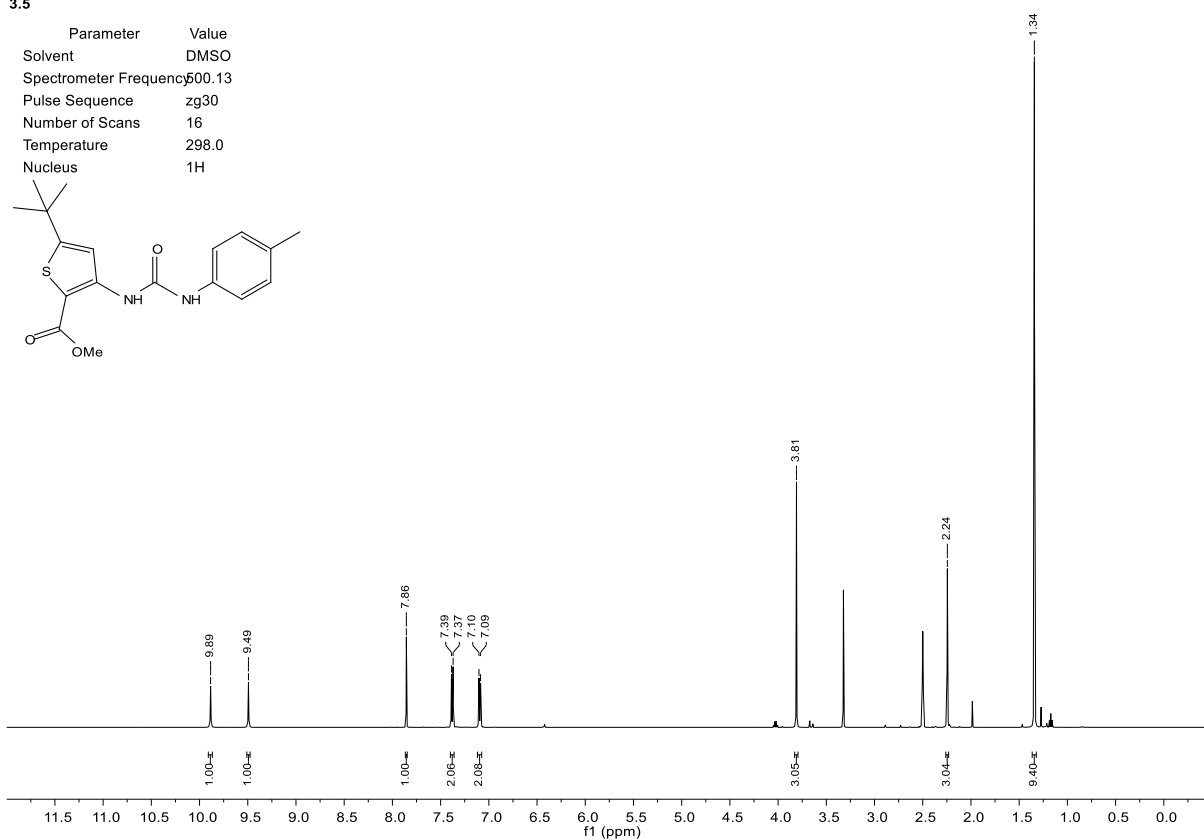
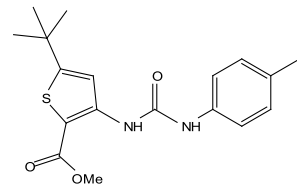
3.4

| Parameter              | Value           |
|------------------------|-----------------|
| Solvent                | DMSO            |
| Spectrometer Frequency | 125.82          |
| Pulse Sequence         | zgpg30          |
| Number of Scans        | 256             |
| Temperature            | 299.9           |
| Nucleus                | $^{13}\text{C}$ |



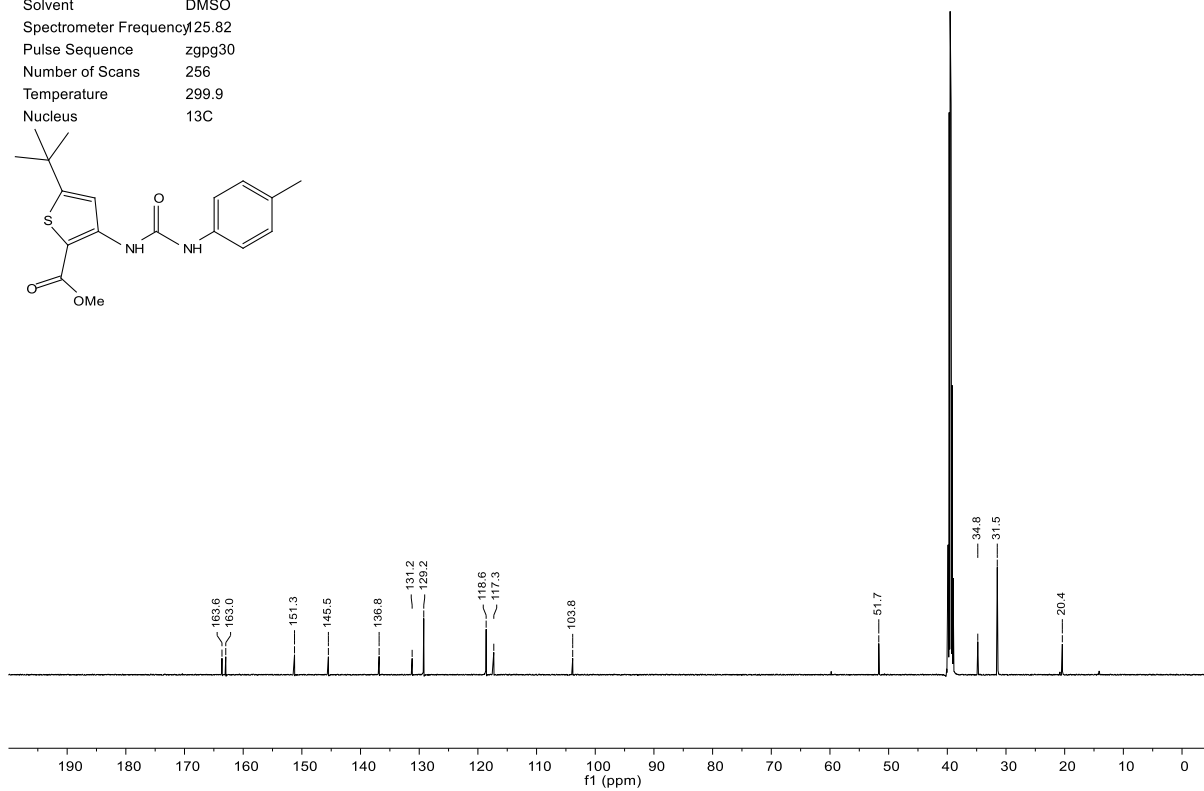
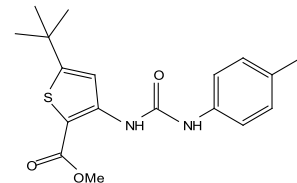
3.5

| Parameter              | Value        |
|------------------------|--------------|
| Solvent                | DMSO         |
| Spectrometer Frequency | 500.13       |
| Pulse Sequence         | zg30         |
| Number of Scans        | 16           |
| Temperature            | 298.0        |
| Nucleus                | $^1\text{H}$ |



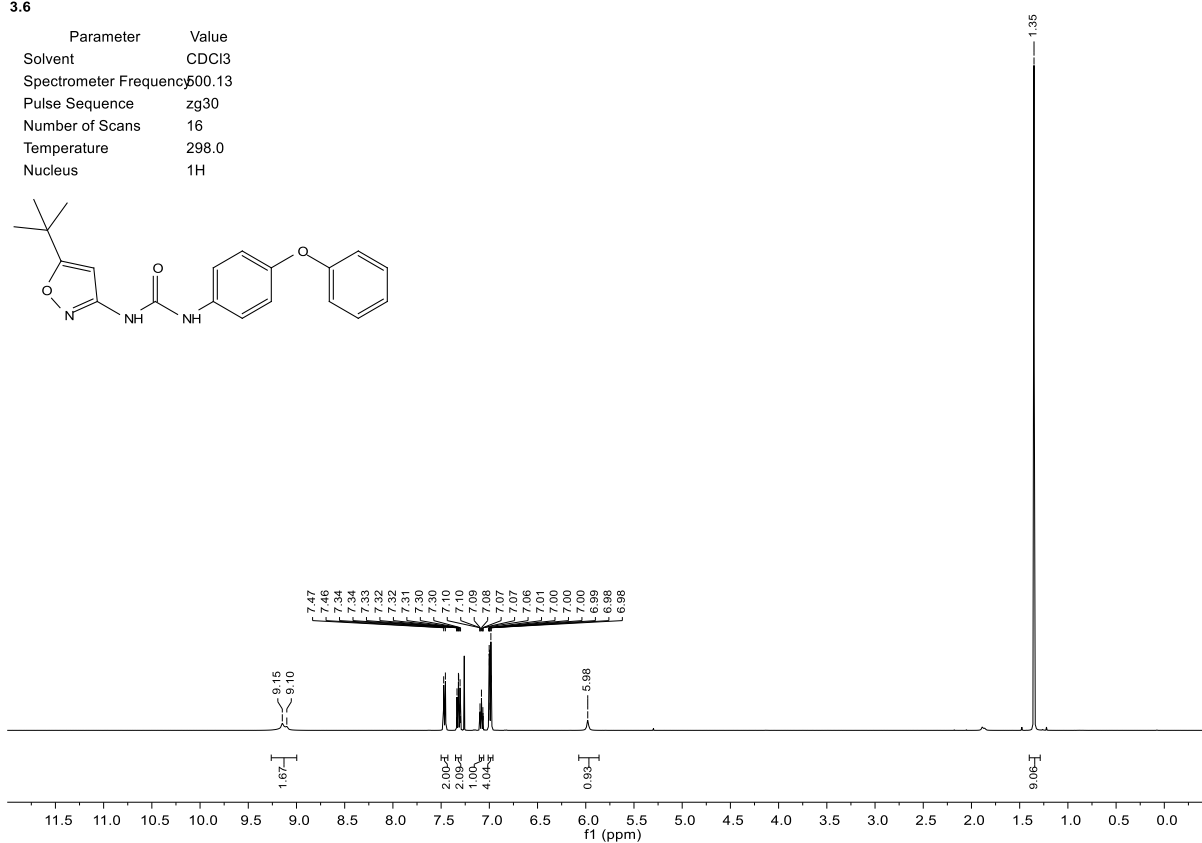
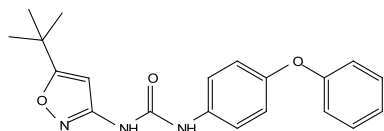
3.5

| Parameter              | Value           |
|------------------------|-----------------|
| Solvent                | DMSO            |
| Spectrometer Frequency | 125.82          |
| Pulse Sequence         | zgpg30          |
| Number of Scans        | 256             |
| Temperature            | 299.9           |
| Nucleus                | $^{13}\text{C}$ |



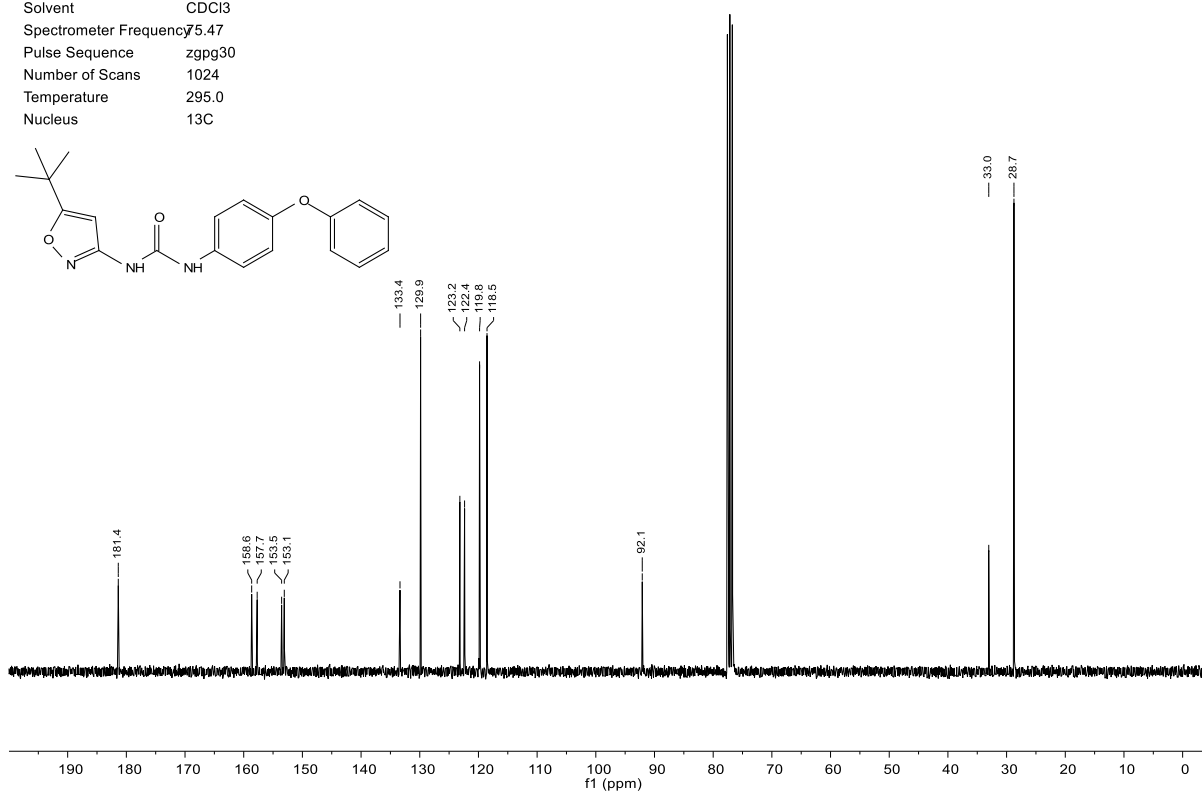
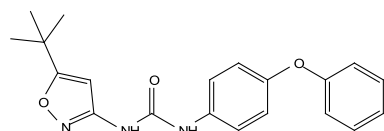
3.6

| Parameter              | Value             |
|------------------------|-------------------|
| Solvent                | CDCl <sub>3</sub> |
| Spectrometer Frequency | 500.13            |
| Pulse Sequence         | zg30              |
| Number of Scans        | 16                |
| Temperature            | 298.0             |
| Nucleus                | <sup>1</sup> H    |



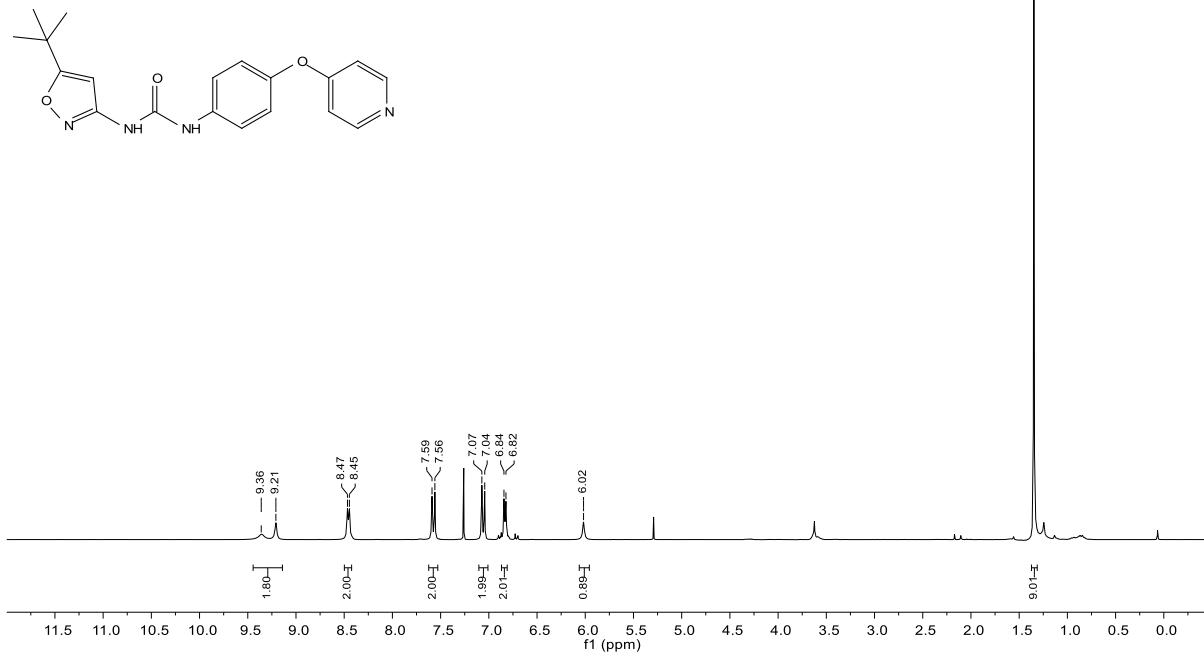
3.6

| Parameter              | Value             |
|------------------------|-------------------|
| Solvent                | CDCl <sub>3</sub> |
| Spectrometer Frequency | 75.47             |
| Pulse Sequence         | zgpg30            |
| Number of Scans        | 1024              |
| Temperature            | 295.0             |
| Nucleus                | <sup>13</sup> C   |



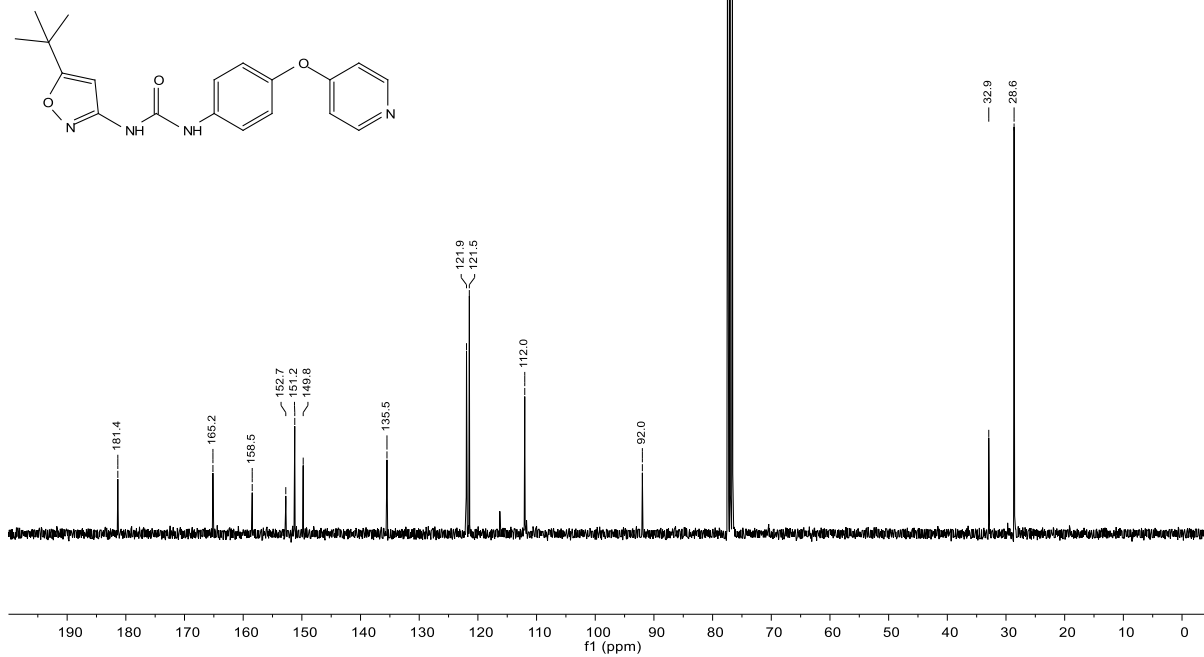
3.7

| Parameter              | Value             |
|------------------------|-------------------|
| Solvent                | CDCl <sub>3</sub> |
| Spectrometer Frequency | 300.13            |
| Pulse Sequence         | zg30              |
| Number of Scans        | 16                |
| Temperature            | 295.0             |
| Nucleus                | <sup>1</sup> H    |



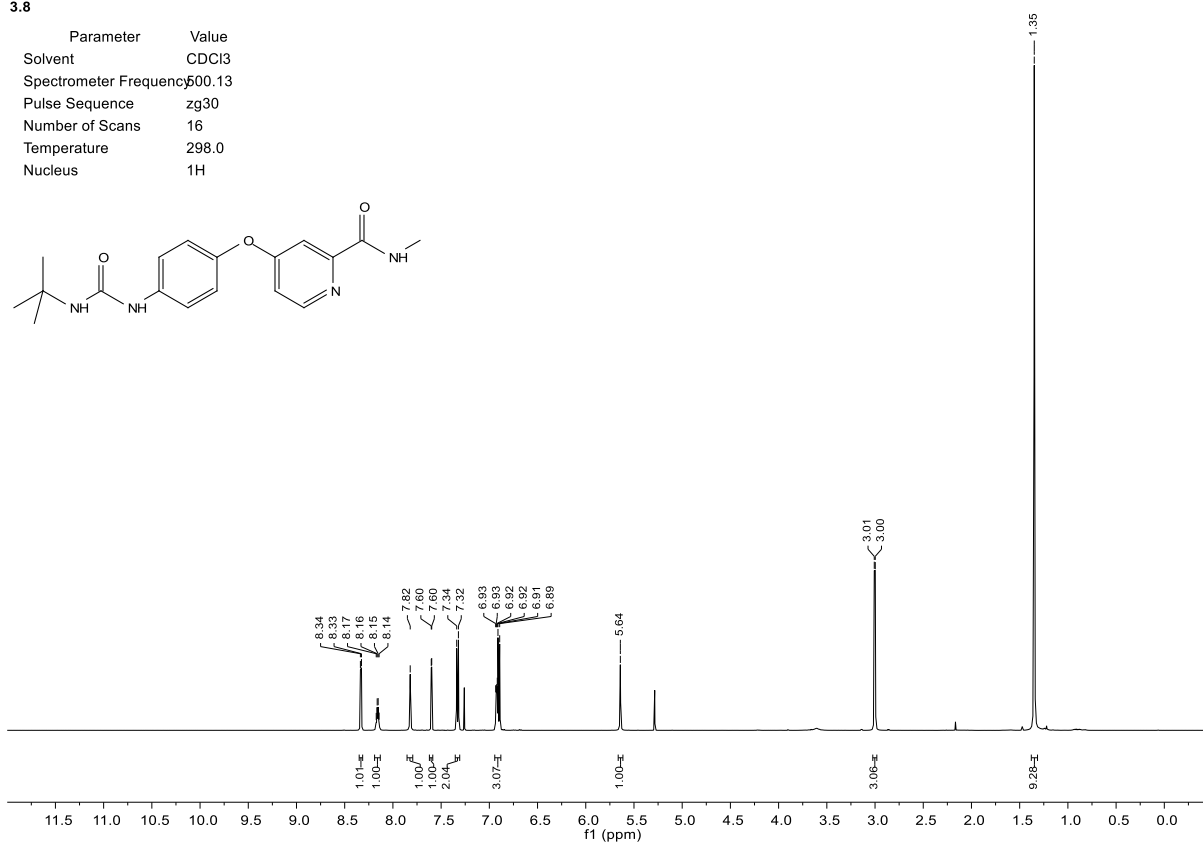
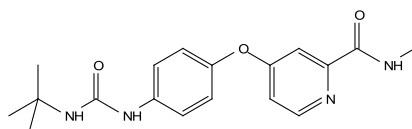
3.7

| Parameter              | Value             |
|------------------------|-------------------|
| Solvent                | CDCl <sub>3</sub> |
| Spectrometer Frequency | 75.47             |
| Pulse Sequence         | zgpg30            |
| Number of Scans        | 1024              |
| Temperature            | 295.0             |
| Nucleus                | <sup>13</sup> C   |



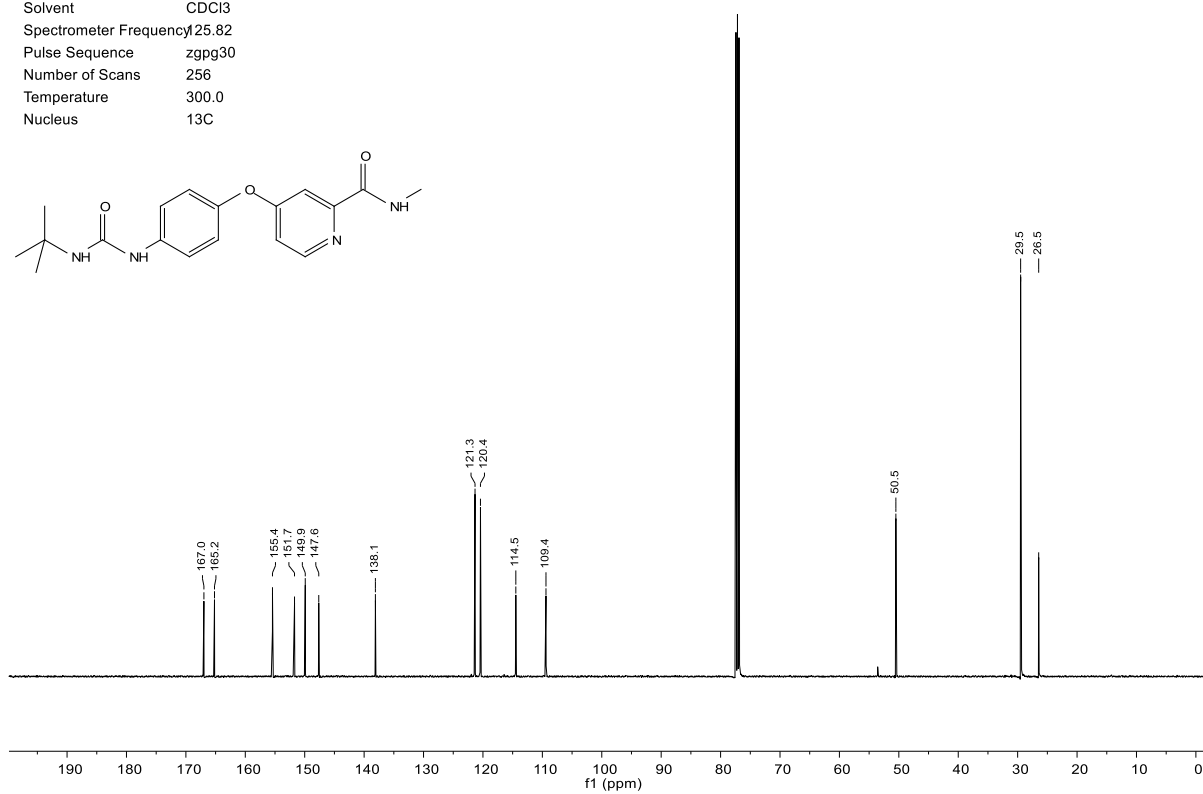
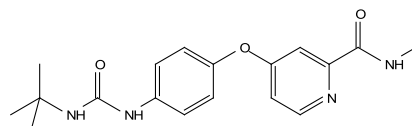
3.8

| Parameter              | Value             |
|------------------------|-------------------|
| Solvent                | CDCl <sub>3</sub> |
| Spectrometer Frequency | 500.13            |
| Pulse Sequence         | zg30              |
| Number of Scans        | 16                |
| Temperature            | 298.0             |
| Nucleus                | <sup>1</sup> H    |



3.8

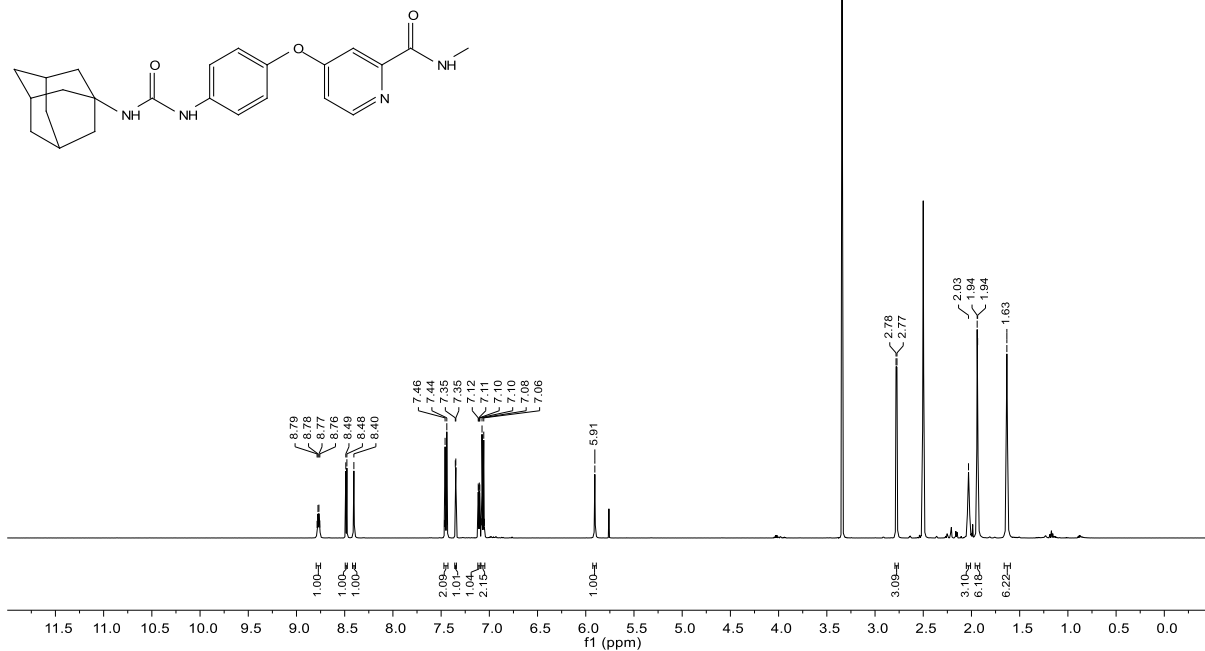
| Parameter              | Value             |
|------------------------|-------------------|
| Solvent                | CDCl <sub>3</sub> |
| Spectrometer Frequency | 125.82            |
| Pulse Sequence         | zgpg30            |
| Number of Scans        | 256               |
| Temperature            | 300.0             |
| Nucleus                | <sup>13</sup> C   |





3.10

| Parameter              | Value          |
|------------------------|----------------|
| Solvent                | DMSO           |
| Spectrometer Frequency | 500.36         |
| Pulse Sequence         | zg30           |
| Number of Scans        | 16             |
| Temperature            | 299.9          |
| Nucleus                | <sup>1</sup> H |



3.10

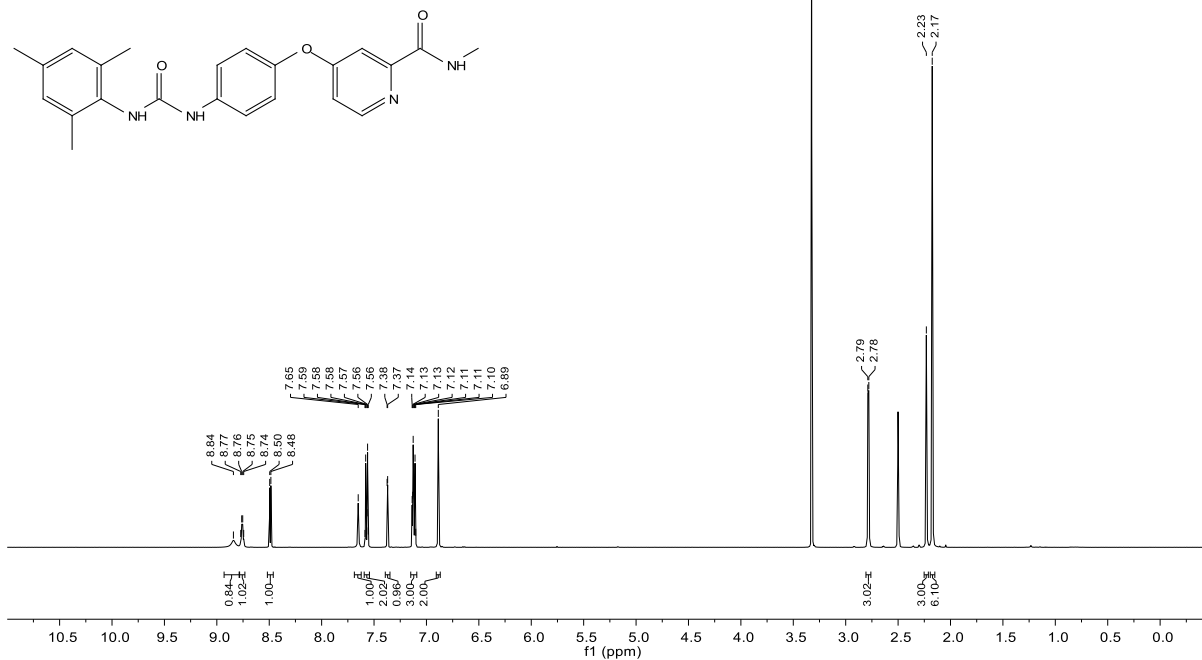
| Parameter              | Value           |
|------------------------|-----------------|
| Solvent                | DMSO            |
| Spectrometer Frequency | 125.82          |
| Pulse Sequence         | zgpg30          |
| Number of Scans        | 256             |
| Temperature            | 299.8           |
| Nucleus                | <sup>13</sup> C |





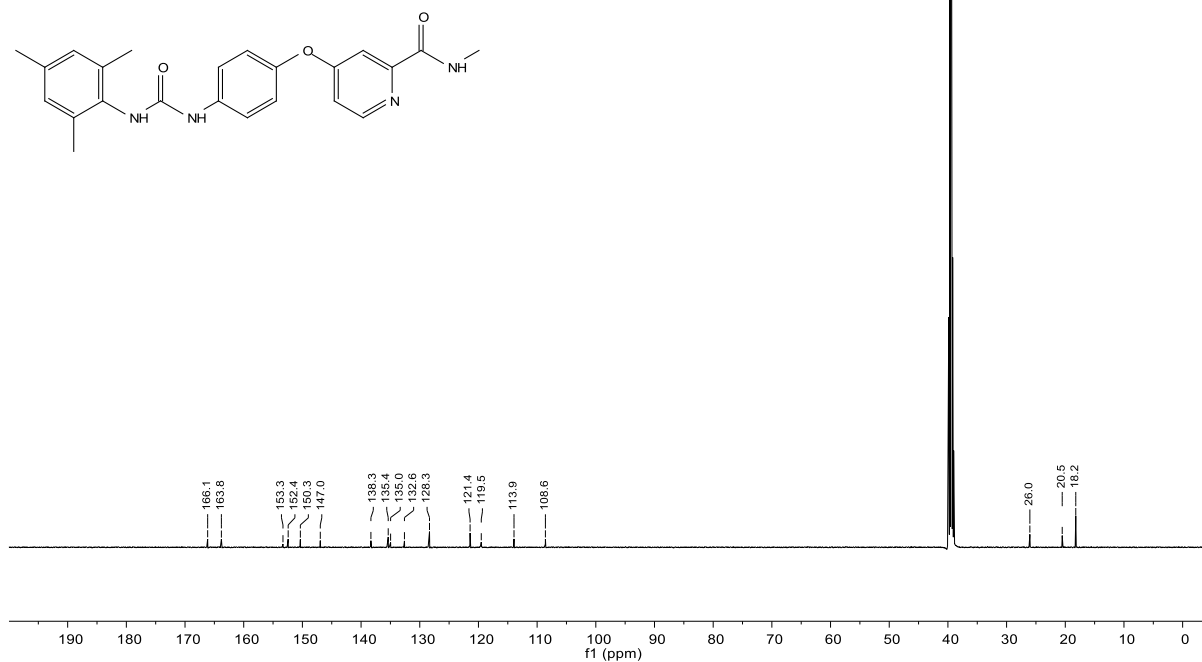
## 3.12

| Parameter              | Value          |
|------------------------|----------------|
| Solvent                | DMSO           |
| Spectrometer Frequency | 500.13         |
| Pulse Sequence         | zg30           |
| Number of Scans        | 16             |
| Temperature            | 298.0          |
| Nucleus                | <sup>1</sup> H |



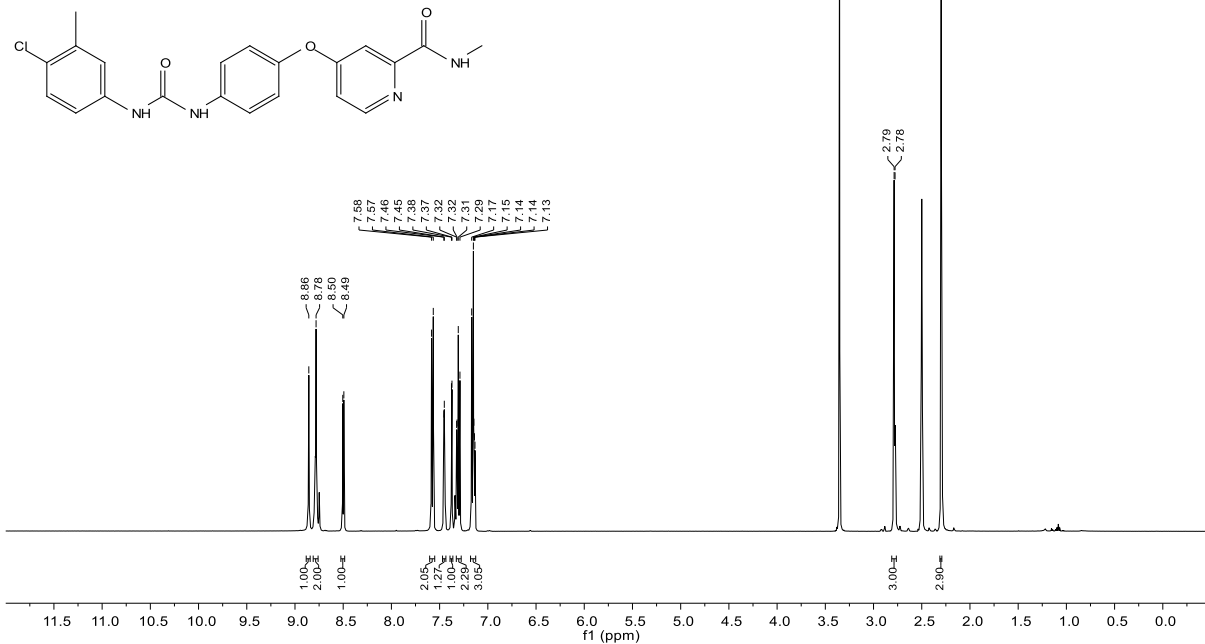
## 3.12

| Parameter              | Value           |
|------------------------|-----------------|
| Solvent                | DMSO            |
| Spectrometer Frequency | 125.82          |
| Pulse Sequence         | zgpg30          |
| Number of Scans        | 256             |
| Temperature            | 300.0           |
| Nucleus                | <sup>13</sup> C |



3.13

| Parameter              | Value          |
|------------------------|----------------|
| Solvent                | DMSO           |
| Spectrometer Frequency | 500.36         |
| Pulse Sequence         | zg30           |
| Number of Scans        | 16             |
| Temperature            | 299.8          |
| Nucleus                | <sup>1</sup> H |



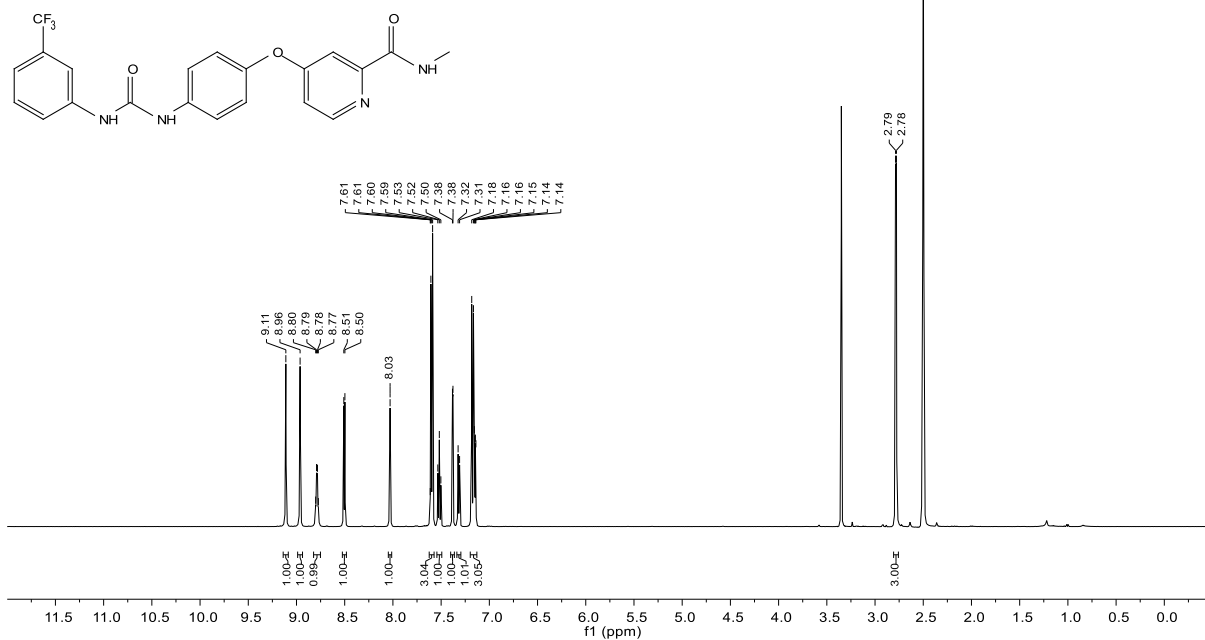
3.13

| Parameter              | Value           |
|------------------------|-----------------|
| Solvent                | DMSO            |
| Spectrometer Frequency | 125.82          |
| Pulse Sequence         | zgpg30          |
| Number of Scans        | 256             |
| Temperature            | 299.9           |
| Nucleus                | <sup>13</sup> C |



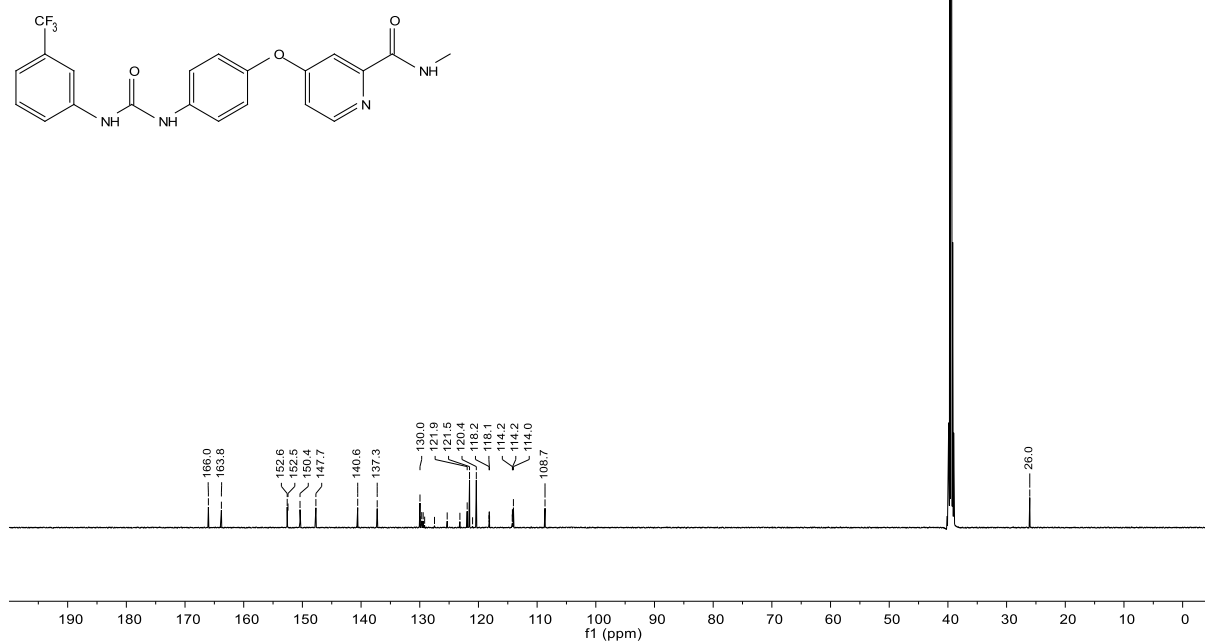
3.14

| Parameter              | Value          |
|------------------------|----------------|
| Solvent                | DMSO           |
| Spectrometer Frequency | 500.36         |
| Pulse Sequence         | zg30           |
| Number of Scans        | 16             |
| Temperature            | 299.9          |
| Nucleus                | <sup>1</sup> H |



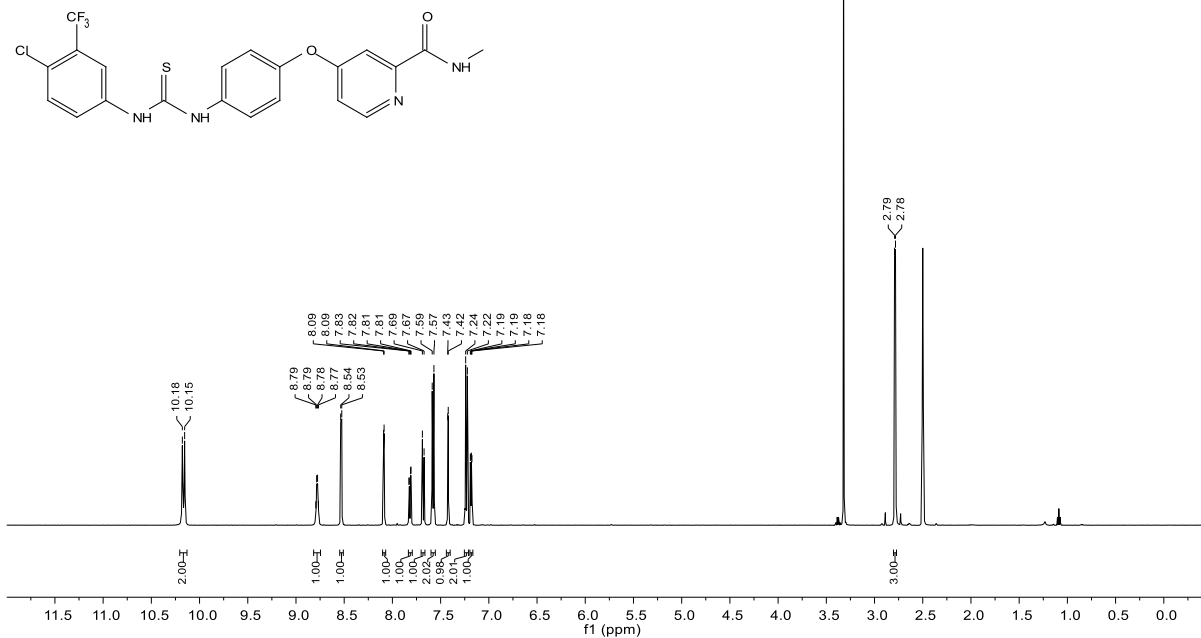
3.14

| Parameter              | Value           |
|------------------------|-----------------|
| Solvent                | DMSO            |
| Spectrometer Frequency | 125.82          |
| Pulse Sequence         | zgpg30          |
| Number of Scans        | 256             |
| Temperature            | 299.9           |
| Nucleus                | <sup>13</sup> C |



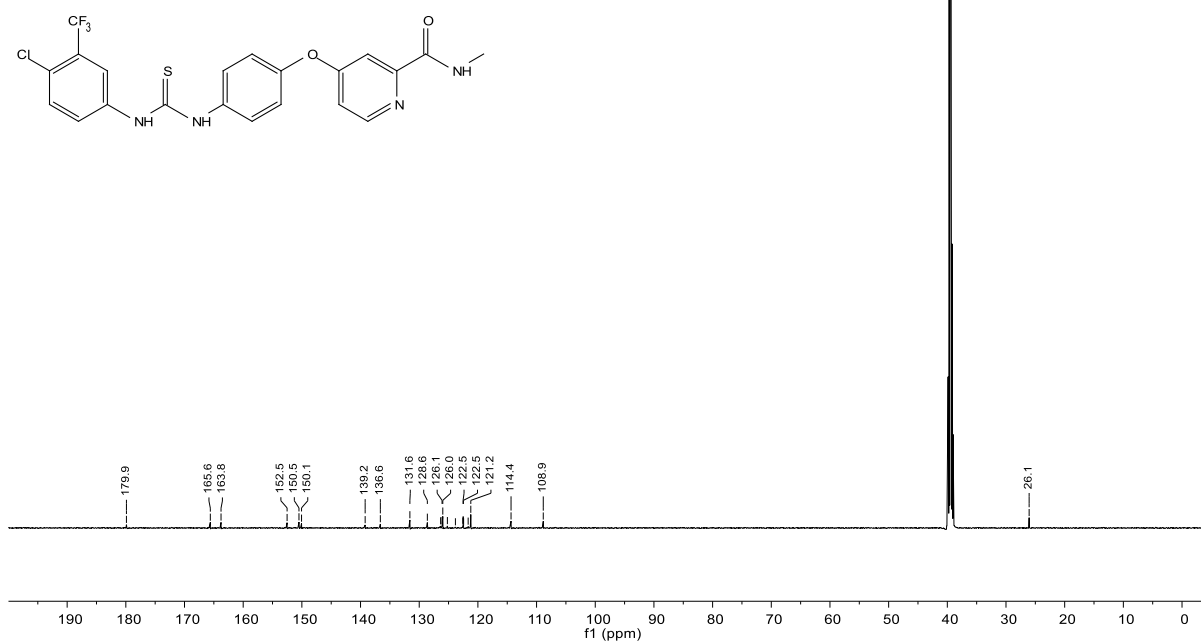
3.15

| Parameter              | Value          |
|------------------------|----------------|
| Solvent                | DMSO           |
| Spectrometer Frequency | 500.13         |
| Pulse Sequence         | zg30           |
| Number of Scans        | 16             |
| Temperature            | 298.0          |
| Nucleus                | <sup>1</sup> H |



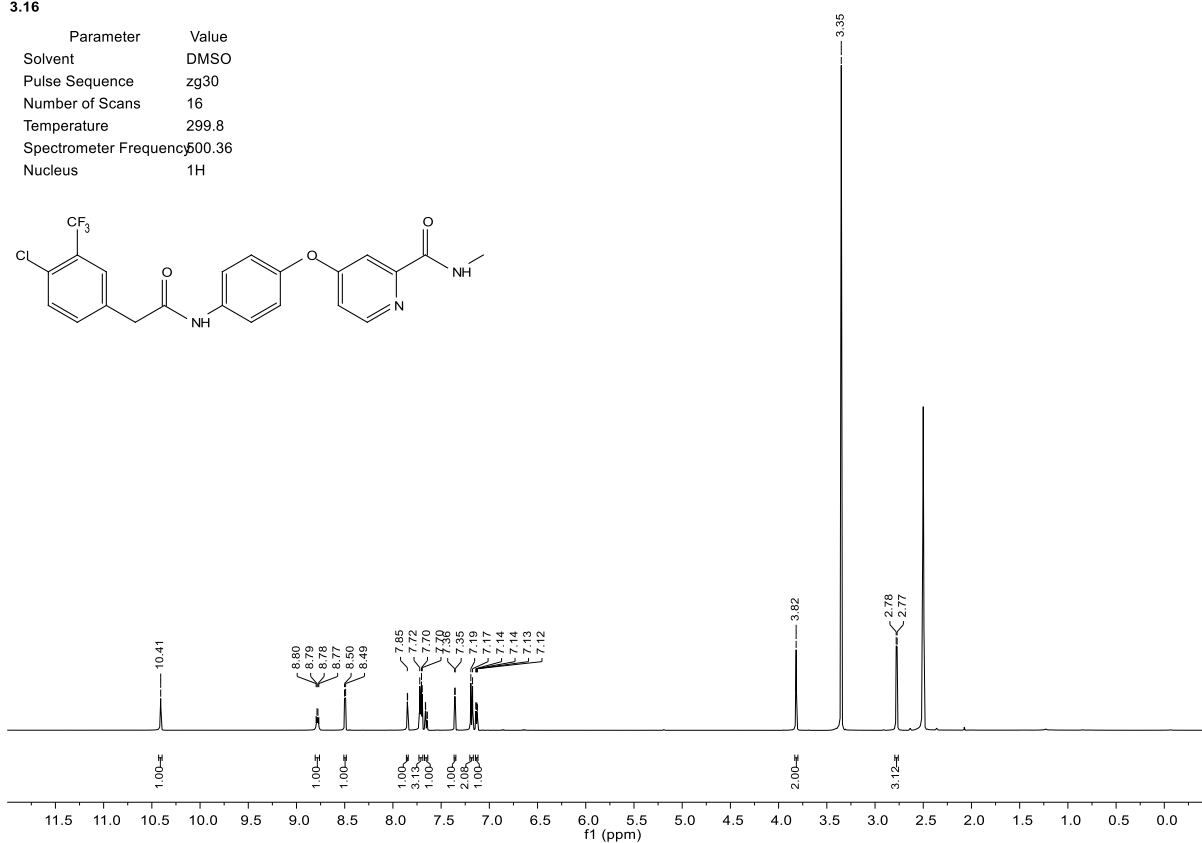
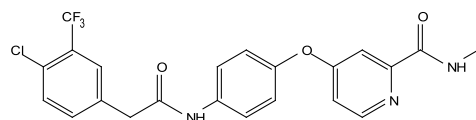
3.15

| Parameter              | Value           |
|------------------------|-----------------|
| Solvent                | DMSO            |
| Spectrometer Frequency | 125.82          |
| Pulse Sequence         | zgpg30          |
| Number of Scans        | 256             |
| Temperature            | 300.0           |
| Nucleus                | <sup>13</sup> C |



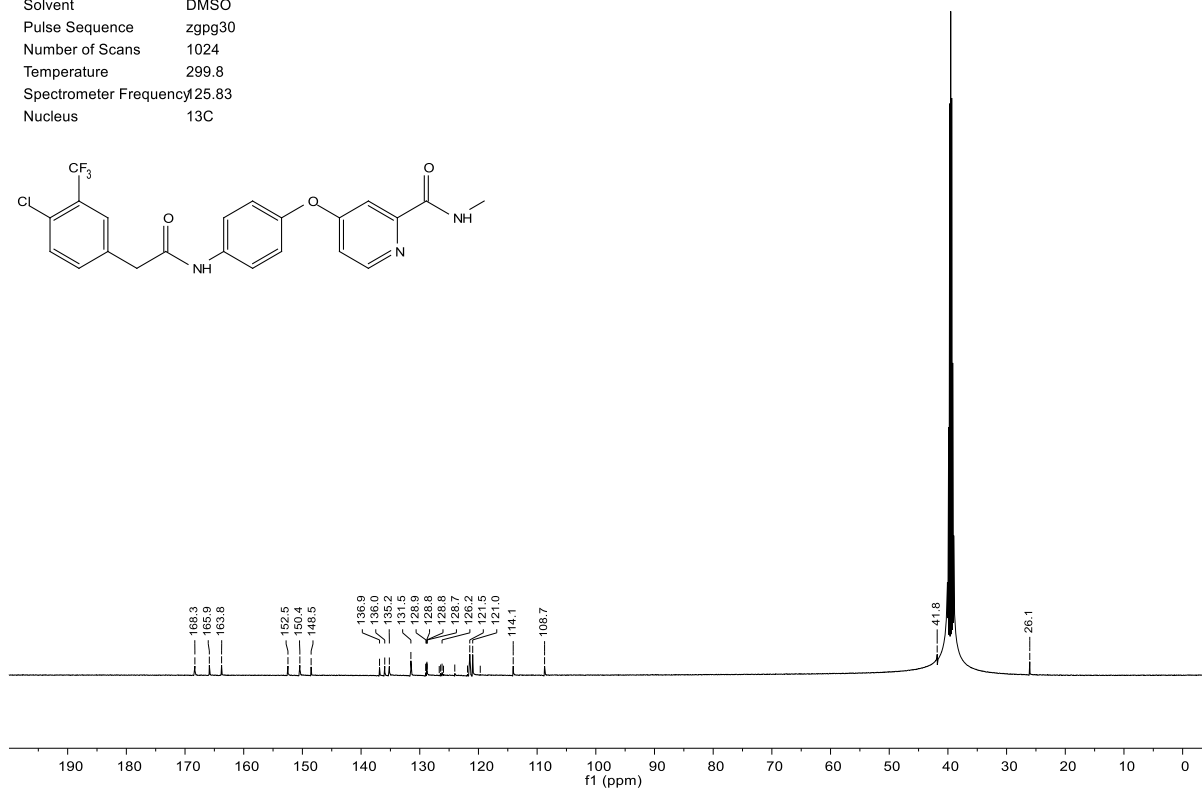
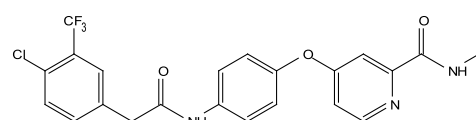
3.16

| Parameter              | Value          |
|------------------------|----------------|
| Solvent                | DMSO           |
| Pulse Sequence         | zg30           |
| Number of Scans        | 16             |
| Temperature            | 299.8          |
| Spectrometer Frequency | 500.36         |
| Nucleus                | <sup>1</sup> H |



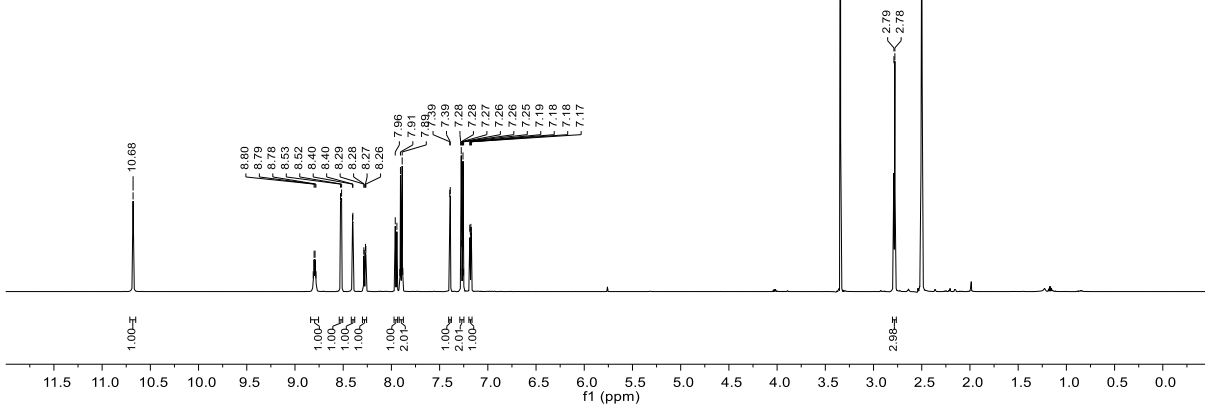
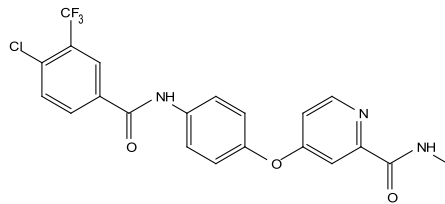
3.16

| Parameter              | Value           |
|------------------------|-----------------|
| Solvent                | DMSO            |
| Pulse Sequence         | zgpg30          |
| Number of Scans        | 1024            |
| Temperature            | 299.8           |
| Spectrometer Frequency | 125.83          |
| Nucleus                | <sup>13</sup> C |



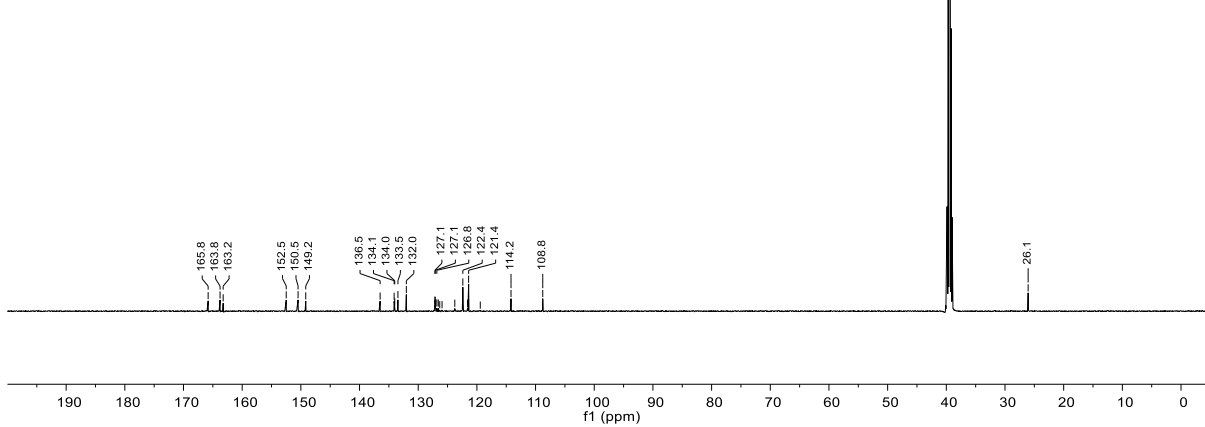
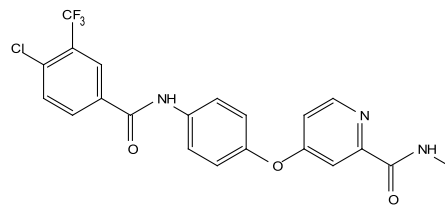
3.17

| Parameter              | Value          |
|------------------------|----------------|
| Solvent                | DMSO           |
| Spectrometer Frequency | 500.36         |
| Pulse Sequence         | zg30           |
| Number of Scans        | 16             |
| Temperature            | 299.9          |
| Nucleus                | <sup>1</sup> H |



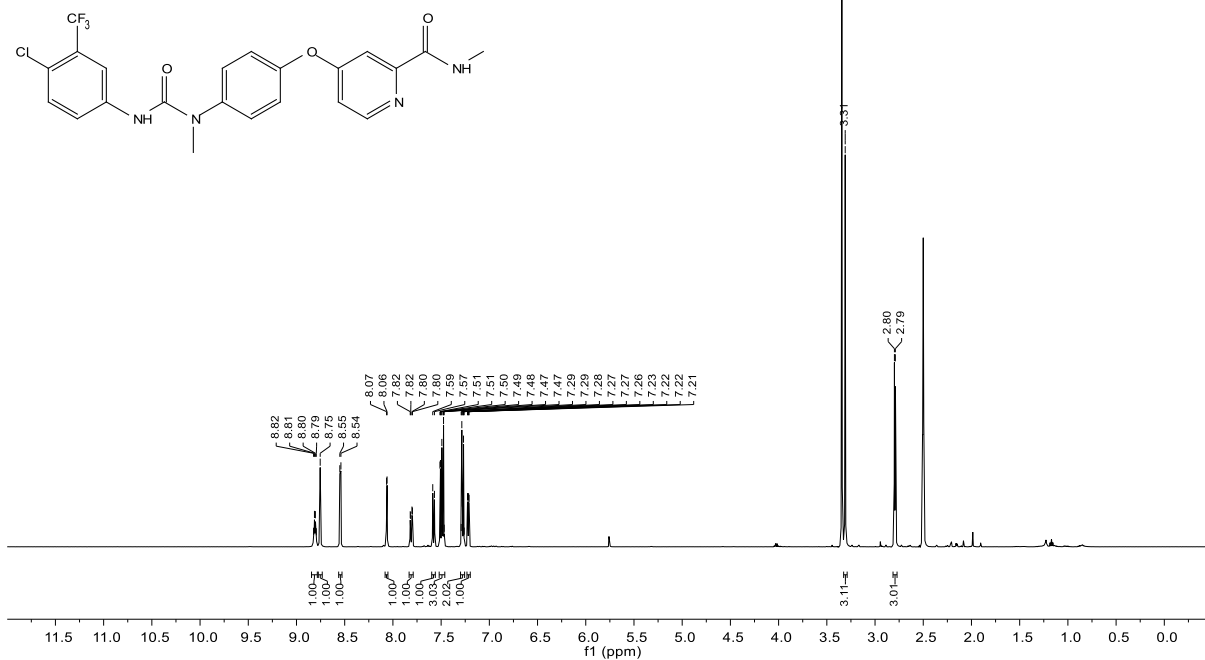
3.17

| Parameter              | Value           |
|------------------------|-----------------|
| Solvent                | DMSO            |
| Spectrometer Frequency | 125.82          |
| Pulse Sequence         | zgpg30          |
| Number of Scans        | 256             |
| Temperature            | 299.9           |
| Nucleus                | <sup>13</sup> C |



3.18

| Parameter              | Value          |
|------------------------|----------------|
| Solvent                | DMSO           |
| Spectrometer Frequency | 500.36         |
| Pulse Sequence         | zg30           |
| Number of Scans        | 16             |
| Temperature            | 299.9          |
| Nucleus                | <sup>1</sup> H |



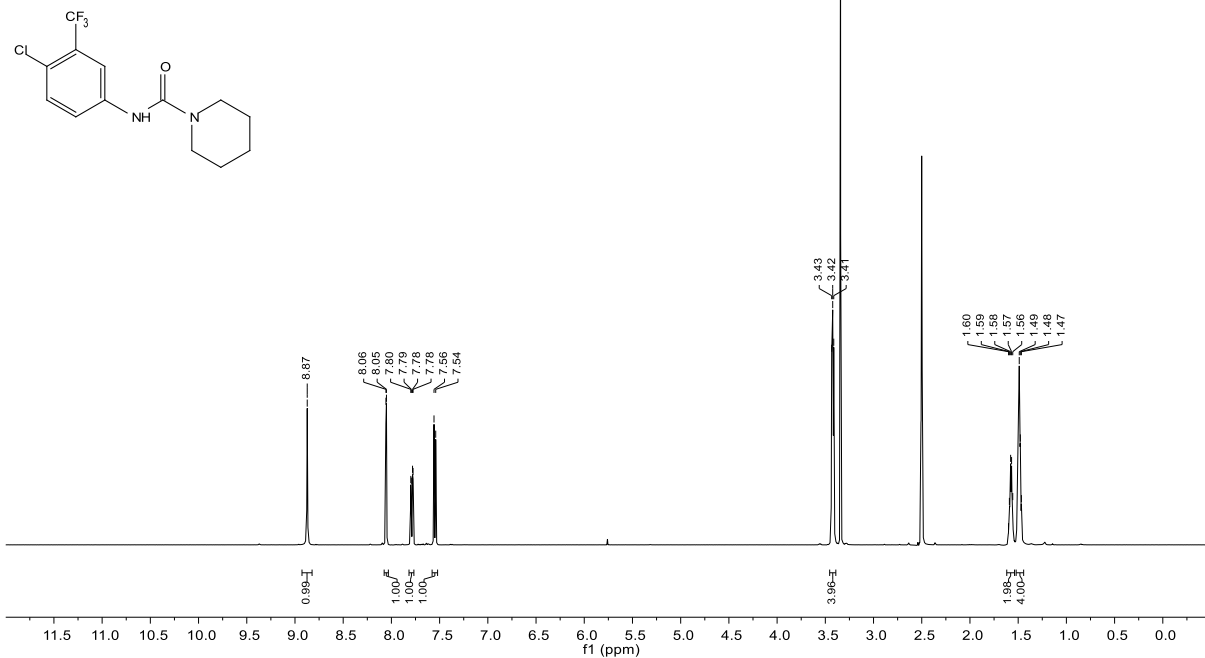
3.18

| Parameter              | Value           |
|------------------------|-----------------|
| Solvent                | DMSO            |
| Spectrometer Frequency | 125.82          |
| Pulse Sequence         | zgpg30          |
| Number of Scans        | 256             |
| Temperature            | 299.9           |
| Nucleus                | <sup>13</sup> C |



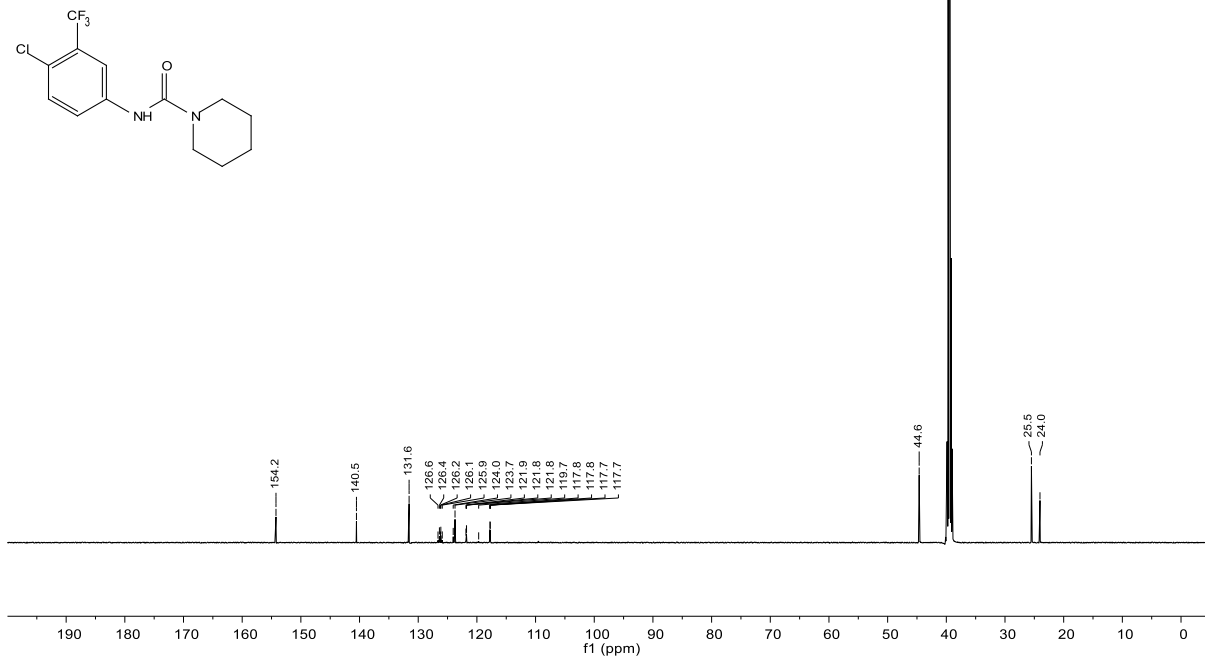
3.19

| Parameter              | Value          |
|------------------------|----------------|
| Solvent                | DMSO           |
| Spectrometer Frequency | 500.36         |
| Pulse Sequence         | zg30           |
| Number of Scans        | 16             |
| Temperature            | 299.9          |
| Nucleus                | <sup>1</sup> H |



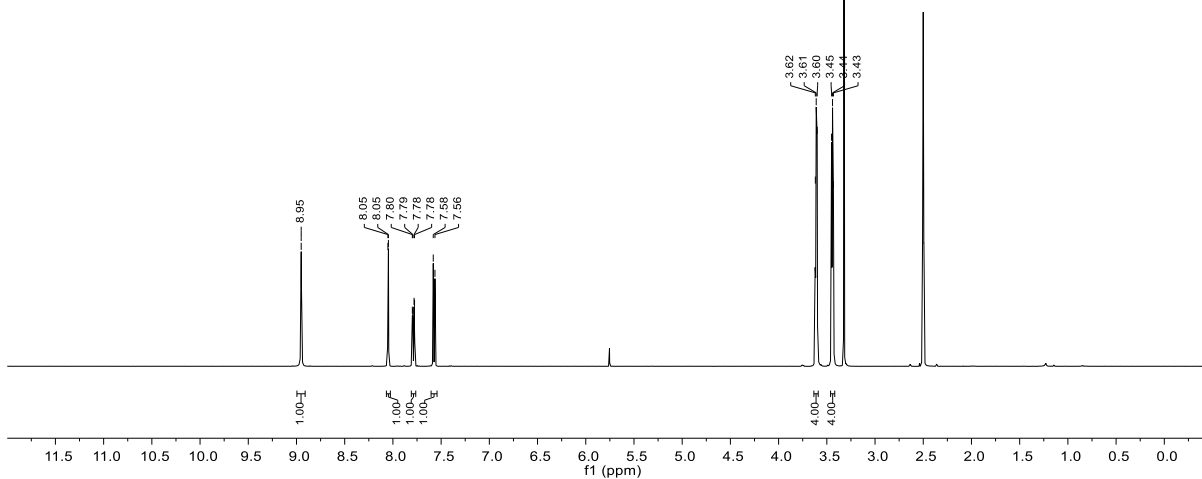
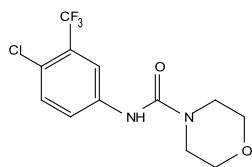
3.19

| Parameter              | Value           |
|------------------------|-----------------|
| Solvent                | DMSO            |
| Spectrometer Frequency | 125.82          |
| Pulse Sequence         | zgpg30          |
| Number of Scans        | 256             |
| Temperature            | 299.9           |
| Nucleus                | <sup>13</sup> C |



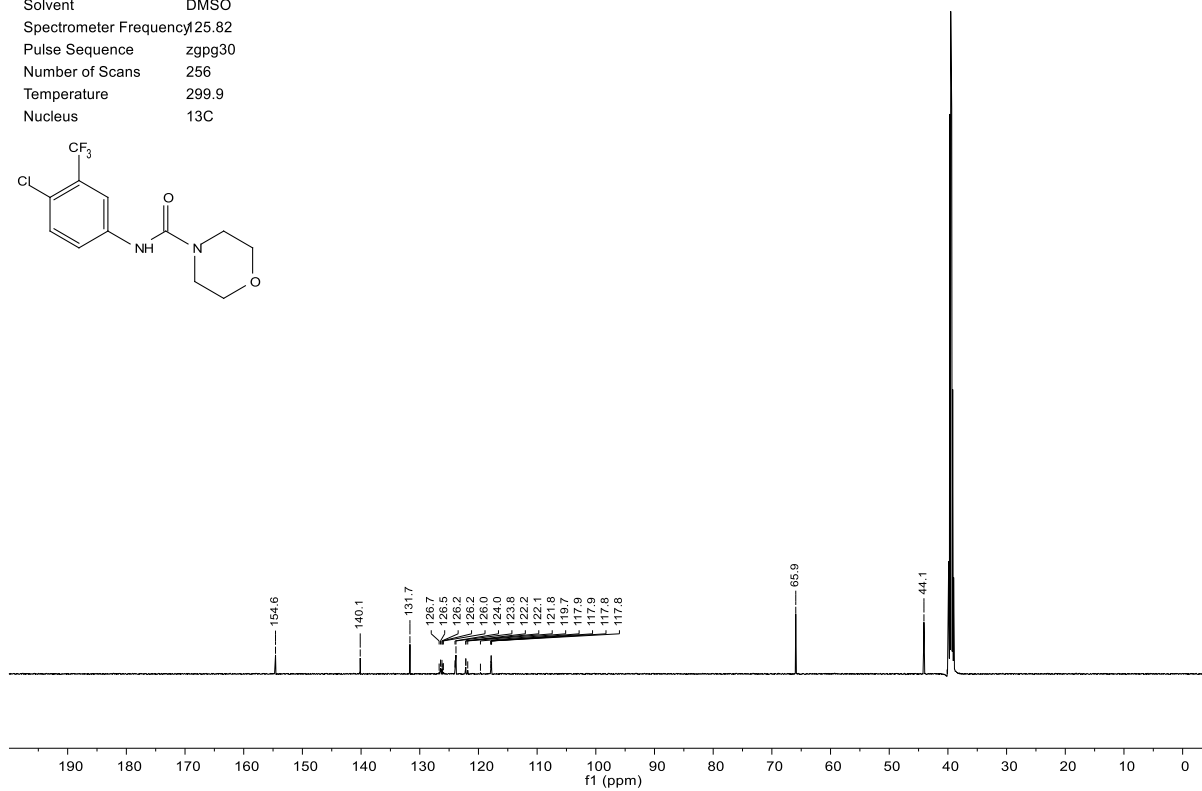
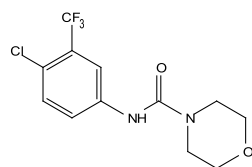
## 3.20

| Parameter              | Value          |
|------------------------|----------------|
| Solvent                | DMSO           |
| Spectrometer Frequency | 500.13         |
| Pulse Sequence         | zg30           |
| Number of Scans        | 16             |
| Temperature            | 298.0          |
| Nucleus                | <sup>1</sup> H |



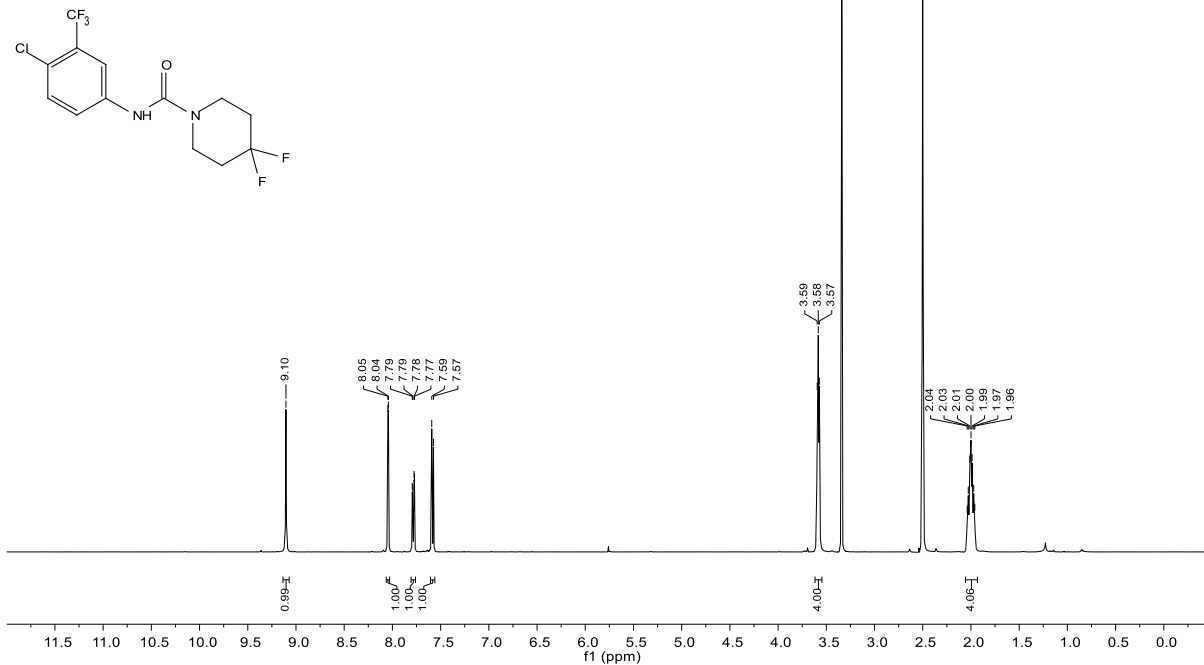
## 3.20

| Parameter              | Value           |
|------------------------|-----------------|
| Solvent                | DMSO            |
| Spectrometer Frequency | 125.82          |
| Pulse Sequence         | zgpg30          |
| Number of Scans        | 256             |
| Temperature            | 299.9           |
| Nucleus                | <sup>13</sup> C |



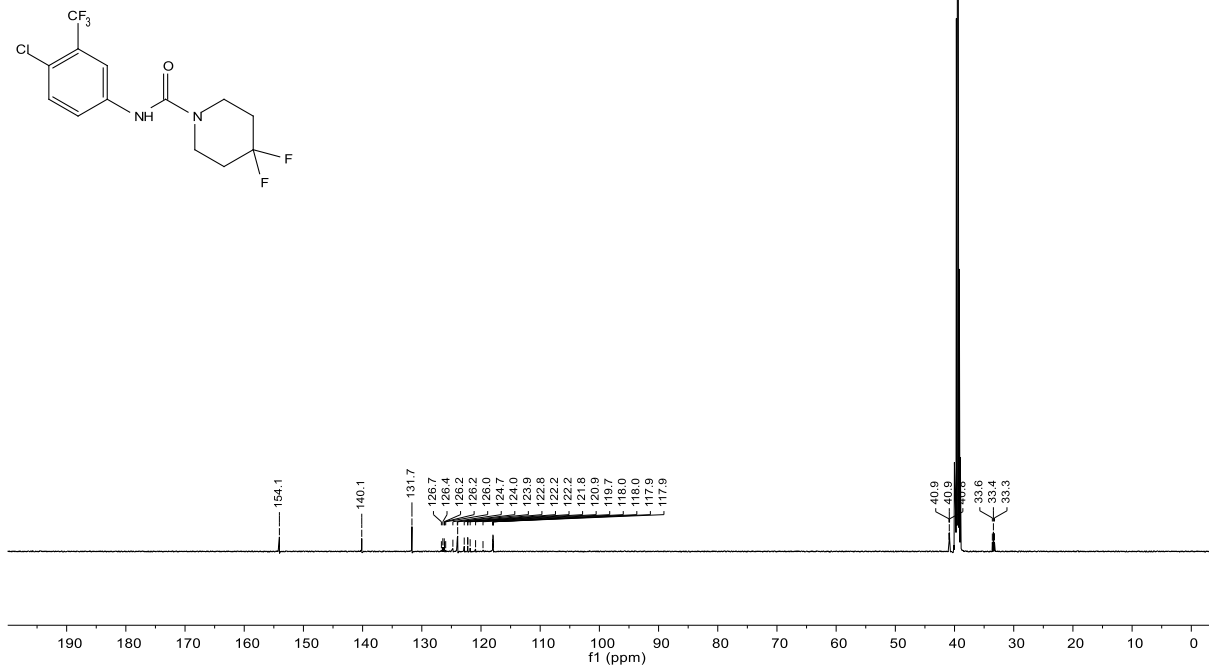
## 3.21

| Parameter              | Value        |
|------------------------|--------------|
| Solvent                | DMSO         |
| Spectrometer Frequency | 500.36       |
| Pulse Sequence         | zg30         |
| Number of Scans        | 16           |
| Temperature            | 299.9        |
| Nucleus                | $^1\text{H}$ |



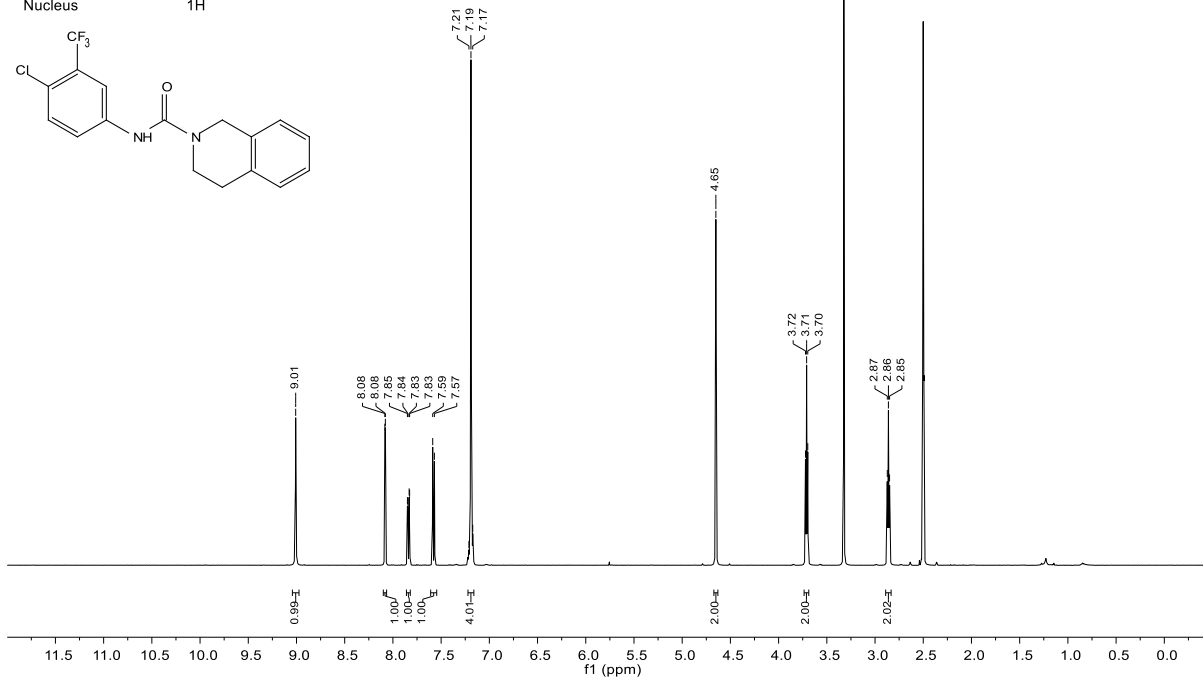
## 3.21

| Parameter              | Value           |
|------------------------|-----------------|
| Solvent                | DMSO            |
| Spectrometer Frequency | 125.82          |
| Pulse Sequence         | zgpg30          |
| Number of Scans        | 256             |
| Temperature            | 299.9           |
| Nucleus                | $^{13}\text{C}$ |



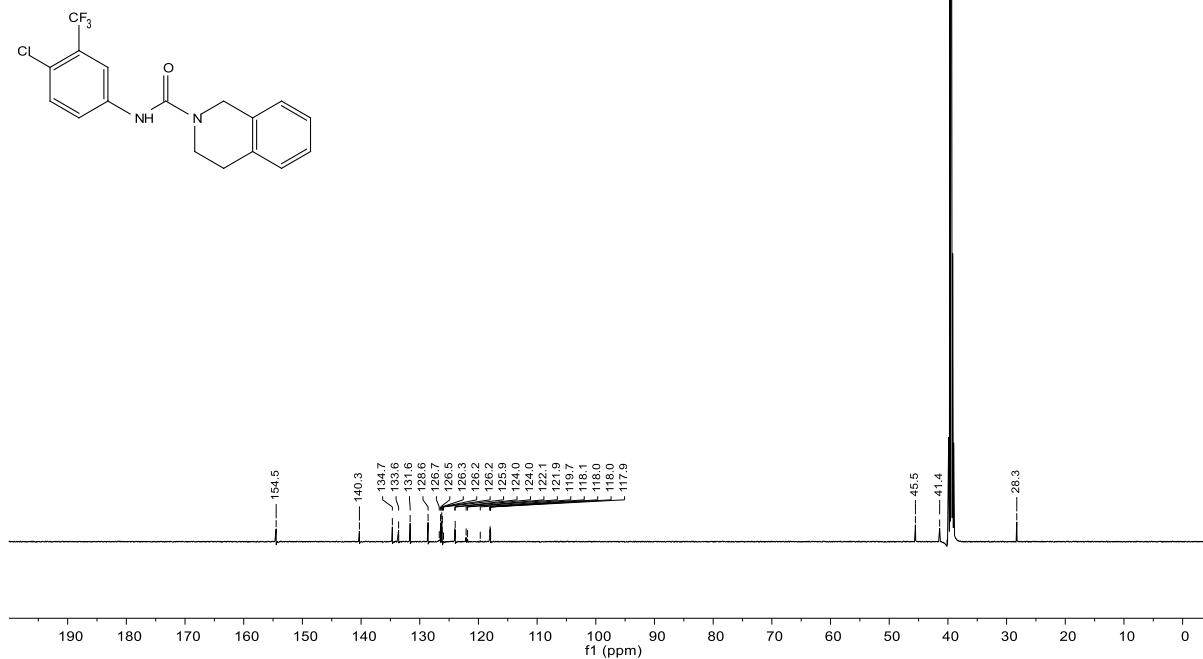
## 3.22

| Parameter              | Value          |
|------------------------|----------------|
| Solvent                | DMSO           |
| Spectrometer Frequency | 500.13         |
| Pulse Sequence         | zg30           |
| Number of Scans        | 16             |
| Temperature            | 298.0          |
| Nucleus                | <sup>1</sup> H |



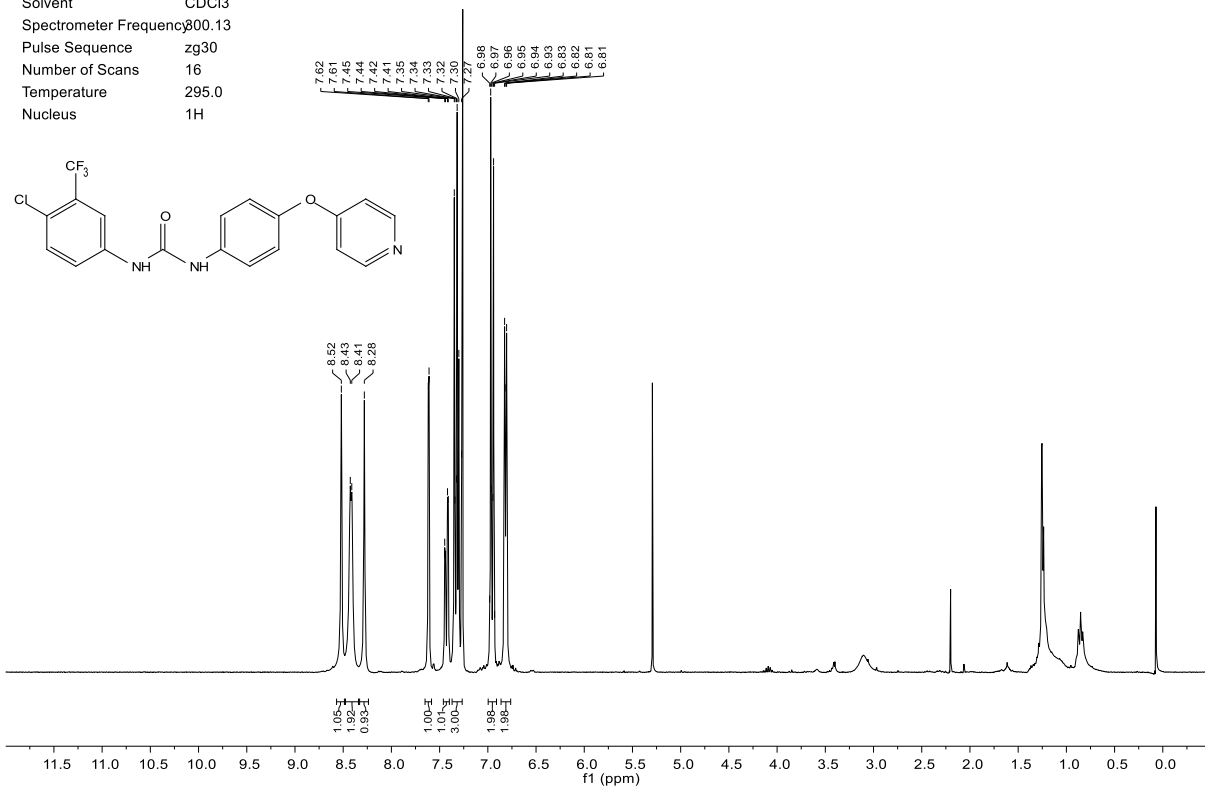
## 3.22

| Parameter              | Value           |
|------------------------|-----------------|
| Solvent                | DMSO            |
| Spectrometer Frequency | 125.82          |
| Pulse Sequence         | zgpg30          |
| Number of Scans        | 256             |
| Temperature            | 299.8           |
| Nucleus                | <sup>13</sup> C |



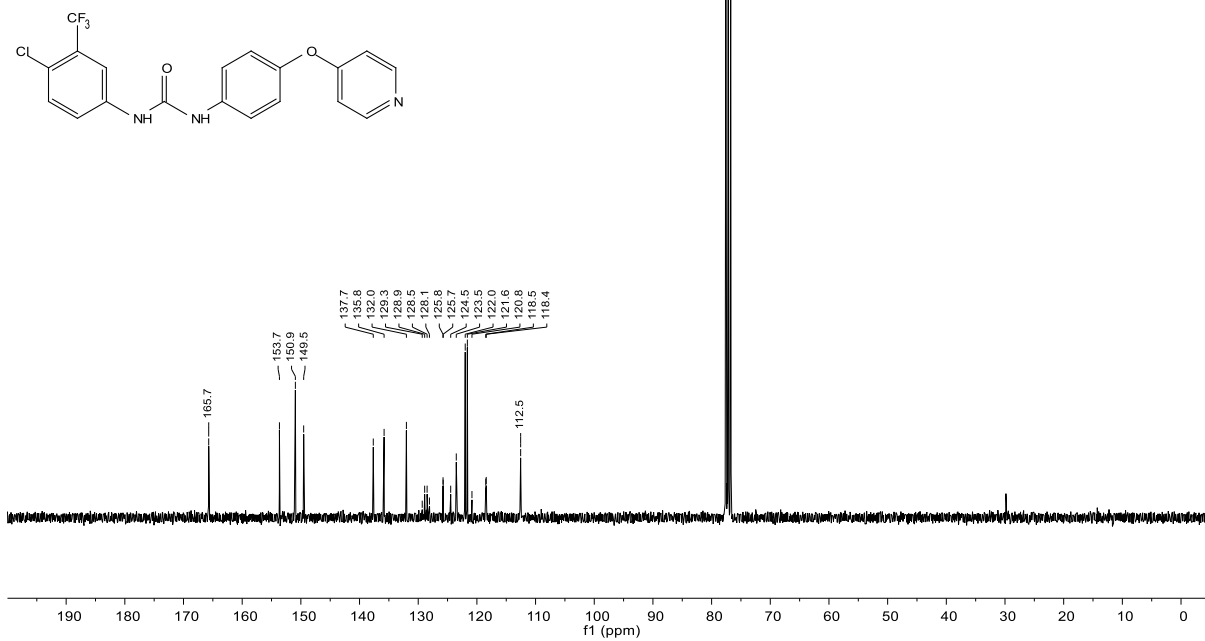
3.23

| Parameter              | Value             |
|------------------------|-------------------|
| Solvent                | CDCl <sub>3</sub> |
| Spectrometer Frequency | 300.13            |
| Pulse Sequence         | zg30              |
| Number of Scans        | 16                |
| Temperature            | 295.0             |
| Nucleus                | <sup>1</sup> H    |



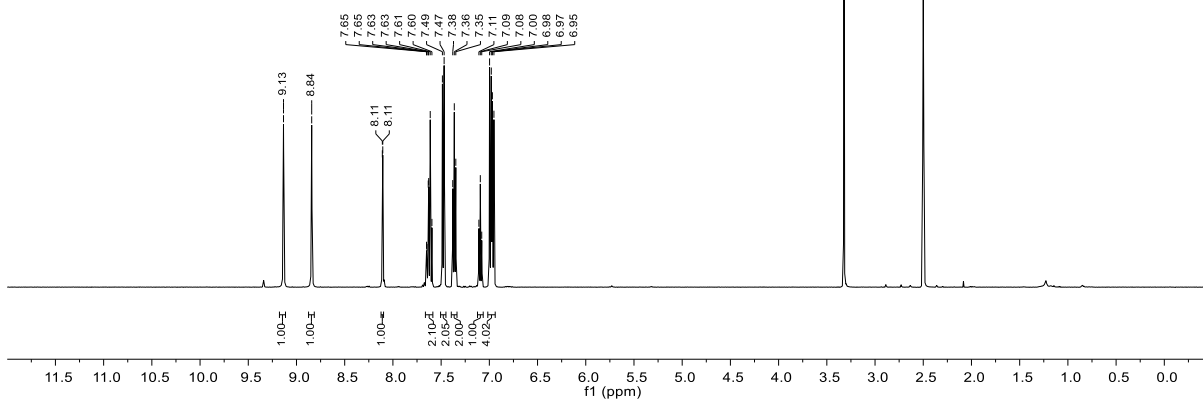
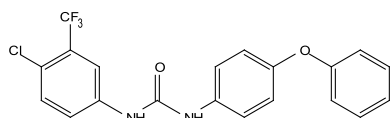
3.23

| Parameter              | Value             |
|------------------------|-------------------|
| Solvent                | CDCl <sub>3</sub> |
| Spectrometer Frequency | 75.47             |
| Pulse Sequence         | zgpg30            |
| Number of Scans        | 1024              |
| Temperature            | 295.0             |
| Nucleus                | <sup>13</sup> C   |



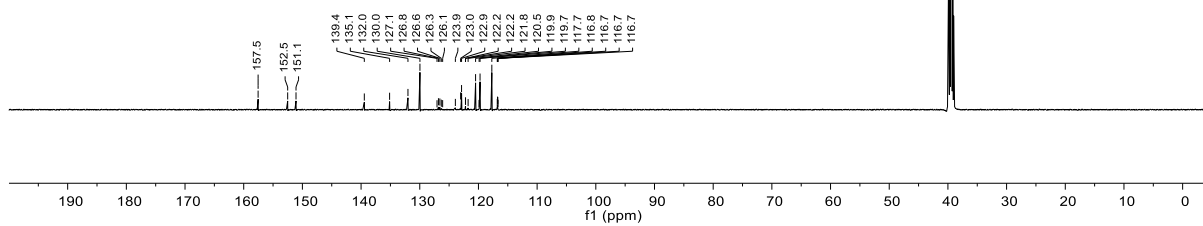
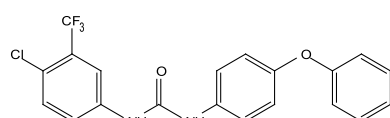
## 3.24

| Parameter              | Value          |
|------------------------|----------------|
| Solvent                | DMSO           |
| Spectrometer Frequency | 500.13         |
| Pulse Sequence         | zg30           |
| Number of Scans        | 16             |
| Temperature            | 298.0          |
| Nucleus                | <sup>1</sup> H |



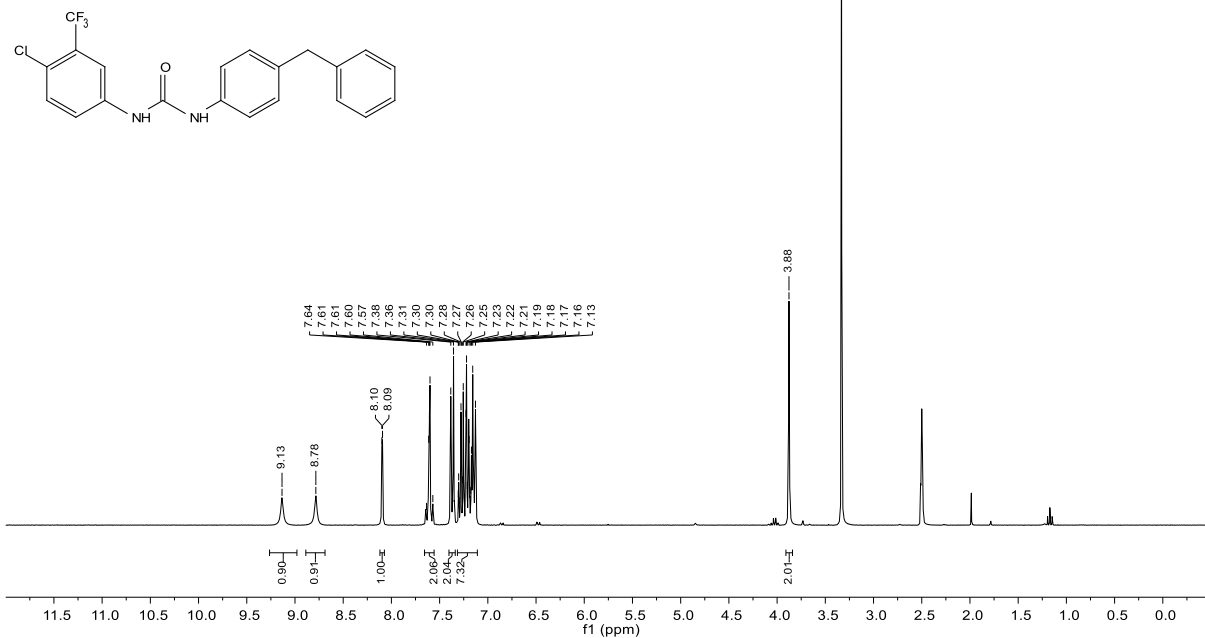
## 3.24

| Parameter              | Value           |
|------------------------|-----------------|
| Solvent                | DMSO            |
| Spectrometer Frequency | 125.82          |
| Pulse Sequence         | zgpg30          |
| Number of Scans        | 256             |
| Temperature            | 300.0           |
| Nucleus                | <sup>13</sup> C |



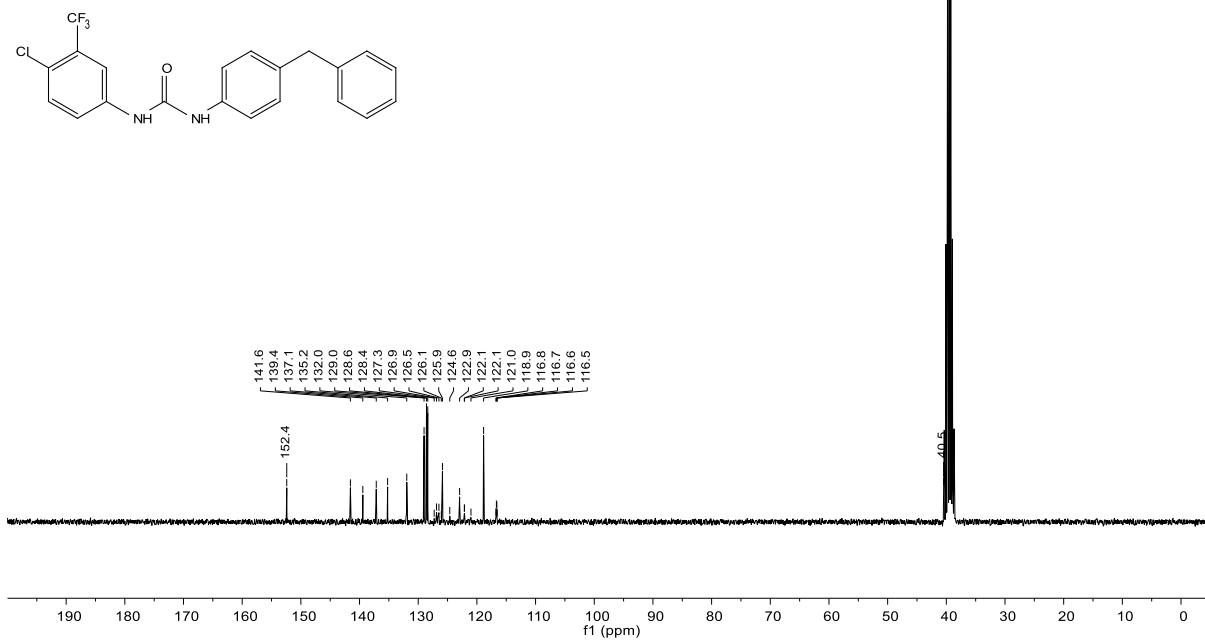
3.25

| Parameter              | Value          |
|------------------------|----------------|
| Solvent                | DMSO           |
| Spectrometer Frequency | 300.13         |
| Pulse Sequence         | zg30           |
| Number of Scans        | 16             |
| Temperature            | 298.0          |
| Nucleus                | <sup>1</sup> H |



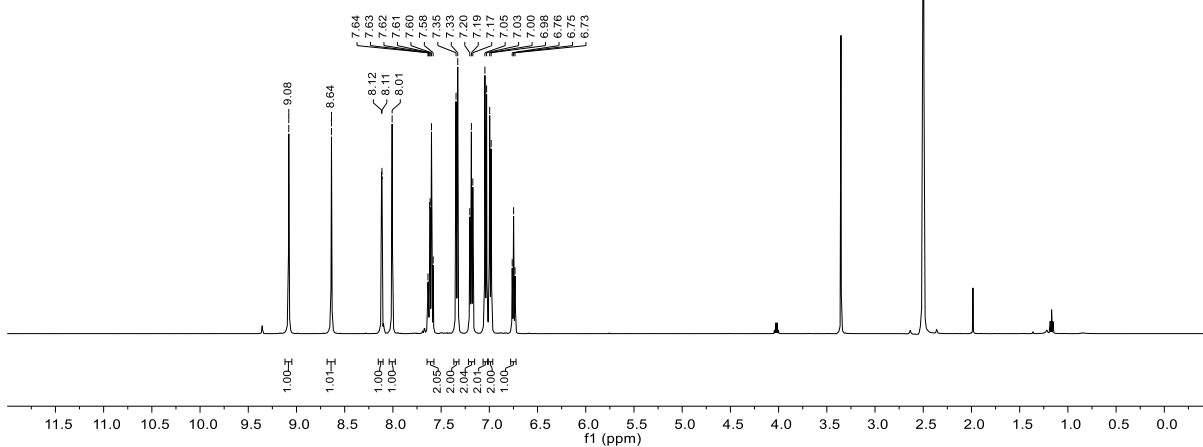
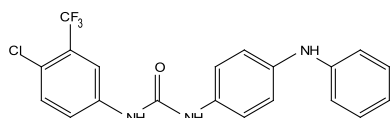
3.25

| Parameter              | Value           |
|------------------------|-----------------|
| Solvent                | DMSO            |
| Spectrometer Frequency | 75.47           |
| Pulse Sequence         | zgpg30          |
| Number of Scans        | 1024            |
| Temperature            | 298.0           |
| Nucleus                | <sup>13</sup> C |



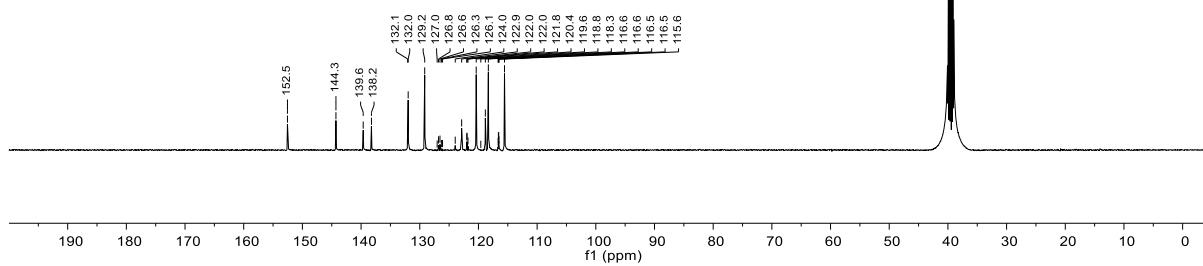
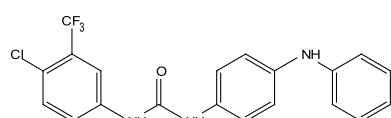
## 3.26

| Parameter              | Value        |
|------------------------|--------------|
| Solvent                | DMSO         |
| Spectrometer Frequency | 500.36       |
| Pulse Sequence         | zg30         |
| Number of Scans        | 16           |
| Temperature            | 299.9        |
| Nucleus                | $^1\text{H}$ |



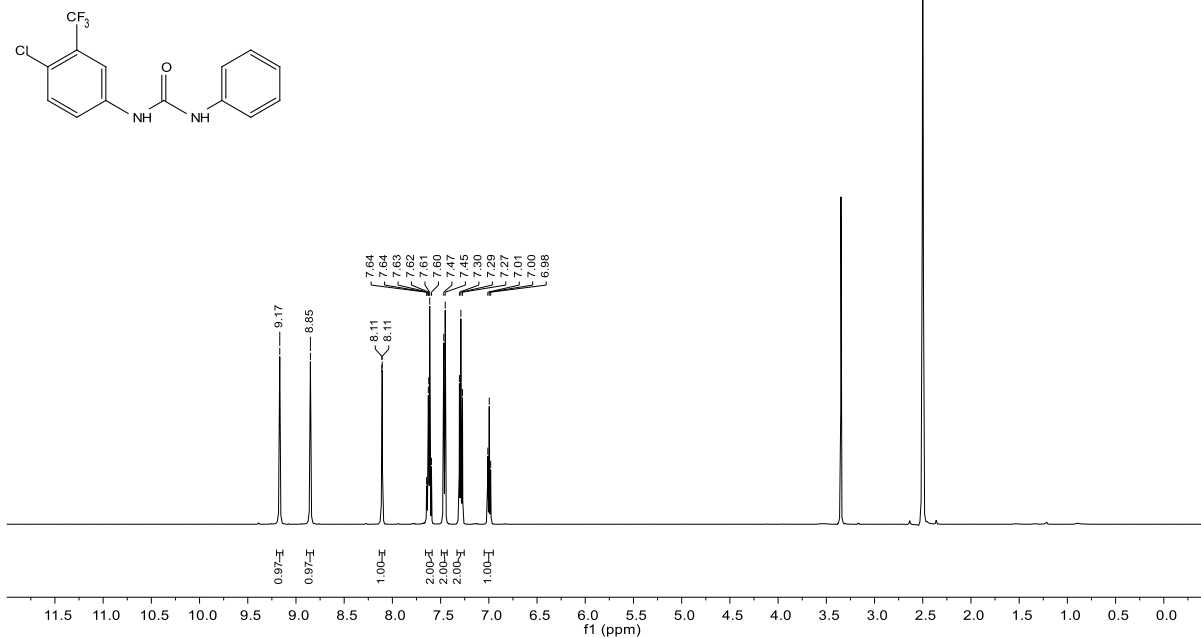
## 3.26

| Parameter              | Value           |
|------------------------|-----------------|
| Solvent                | DMSO            |
| Spectrometer Frequency | 125.82          |
| Pulse Sequence         | zgpg30          |
| Number of Scans        | 256             |
| Temperature            | 299.8           |
| Nucleus                | $^{13}\text{C}$ |



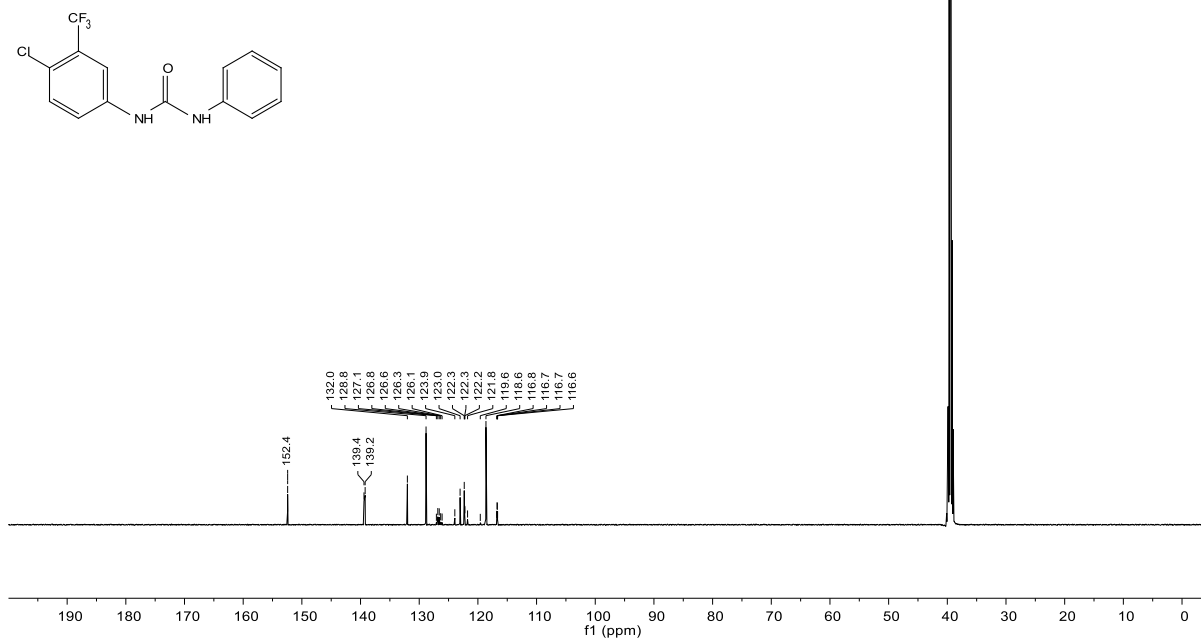
## 3.27

| Parameter              | Value        |
|------------------------|--------------|
| Solvent                | DMSO         |
| Spectrometer Frequency | 500.36       |
| Pulse Sequence         | zg30         |
| Number of Scans        | 16           |
| Temperature            | 299.8        |
| Nucleus                | $^1\text{H}$ |



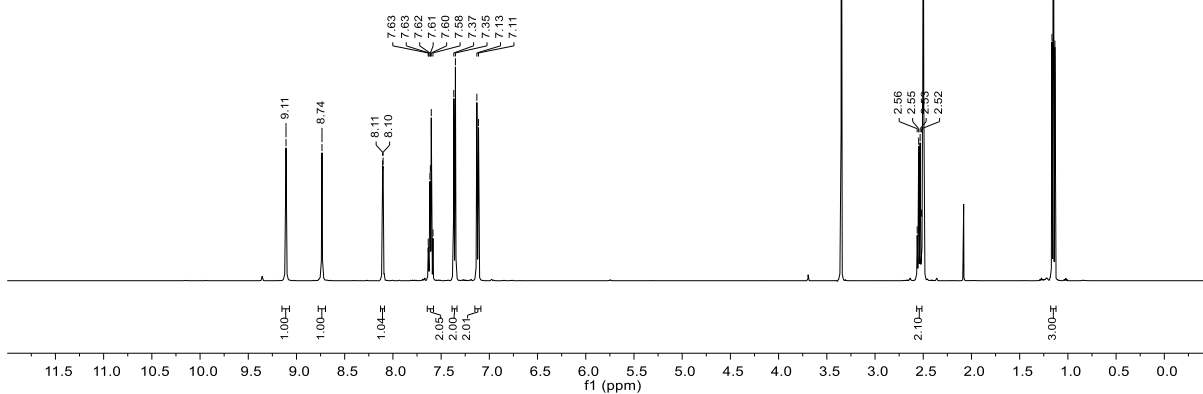
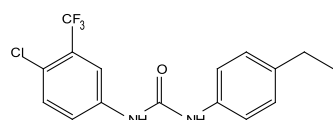
## 3.27

| Parameter              | Value           |
|------------------------|-----------------|
| Solvent                | DMSO            |
| Spectrometer Frequency | 125.82          |
| Pulse Sequence         | zgpg30          |
| Number of Scans        | 256             |
| Temperature            | 299.9           |
| Nucleus                | $^{13}\text{C}$ |



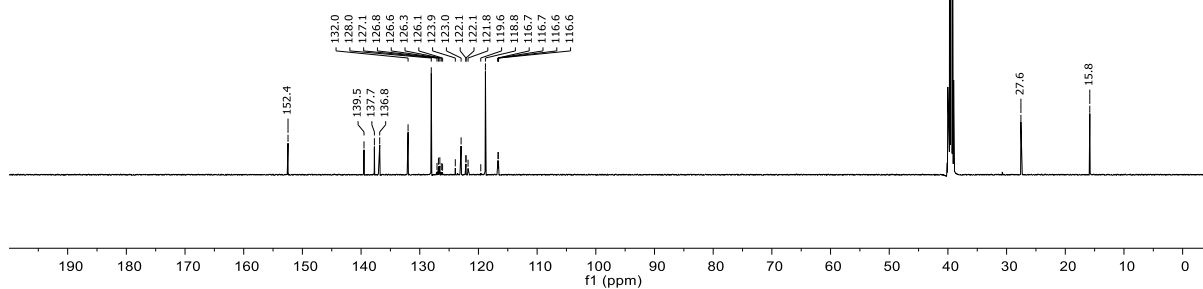
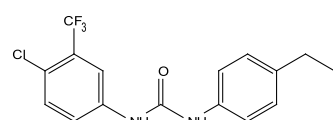
3.28

| Parameter              | Value          |
|------------------------|----------------|
| Solvent                | DMSO           |
| Spectrometer Frequency | 500.36         |
| Pulse Sequence         | zg30           |
| Number of Scans        | 16             |
| Temperature            | 299.9          |
| Nucleus                | <sup>1</sup> H |



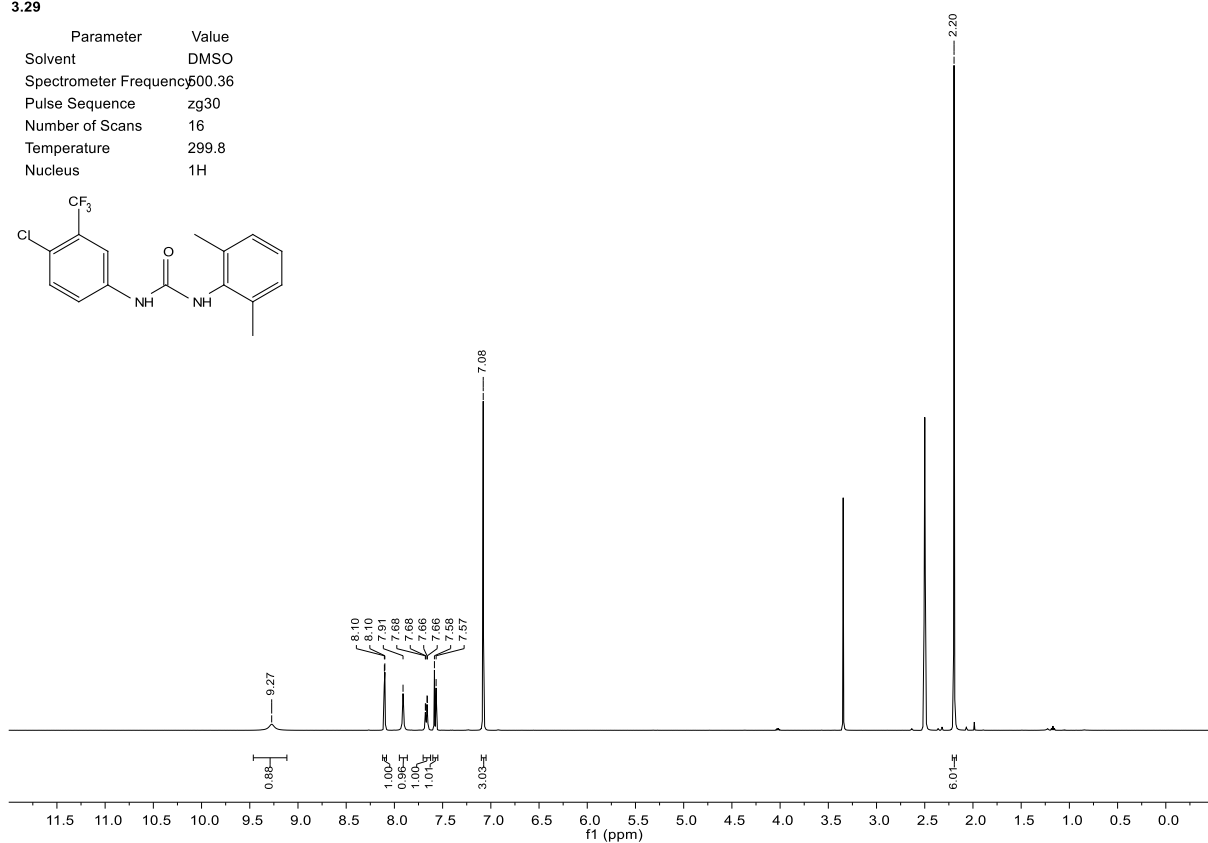
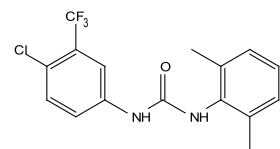
3.28

| Parameter              | Value           |
|------------------------|-----------------|
| Solvent                | DMSO            |
| Spectrometer Frequency | 125.82          |
| Pulse Sequence         | zgpg30          |
| Number of Scans        | 256             |
| Temperature            | 299.9           |
| Nucleus                | <sup>13</sup> C |



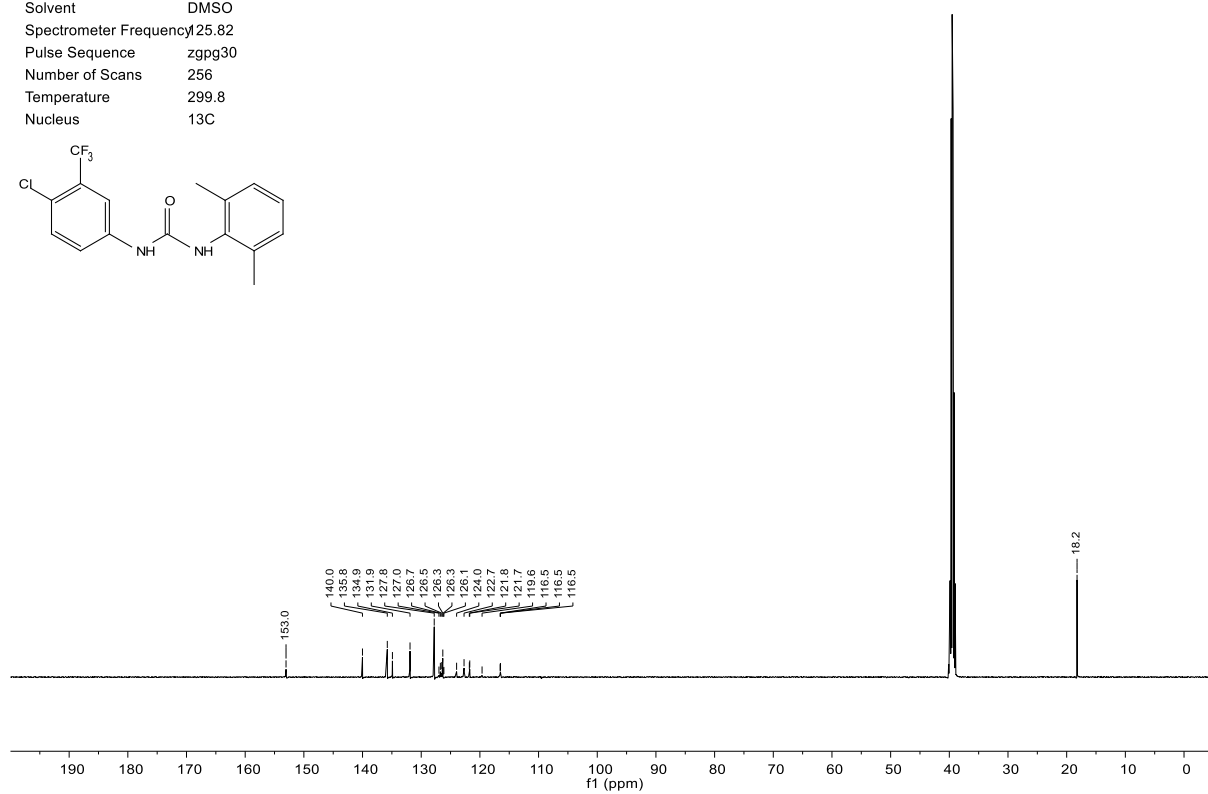
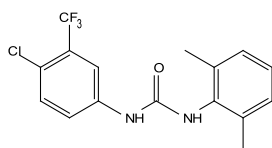
3.29

| Parameter              | Value          |
|------------------------|----------------|
| Solvent                | DMSO           |
| Spectrometer Frequency | 500.36         |
| Pulse Sequence         | zg30           |
| Number of Scans        | 16             |
| Temperature            | 299.8          |
| Nucleus                | <sup>1</sup> H |



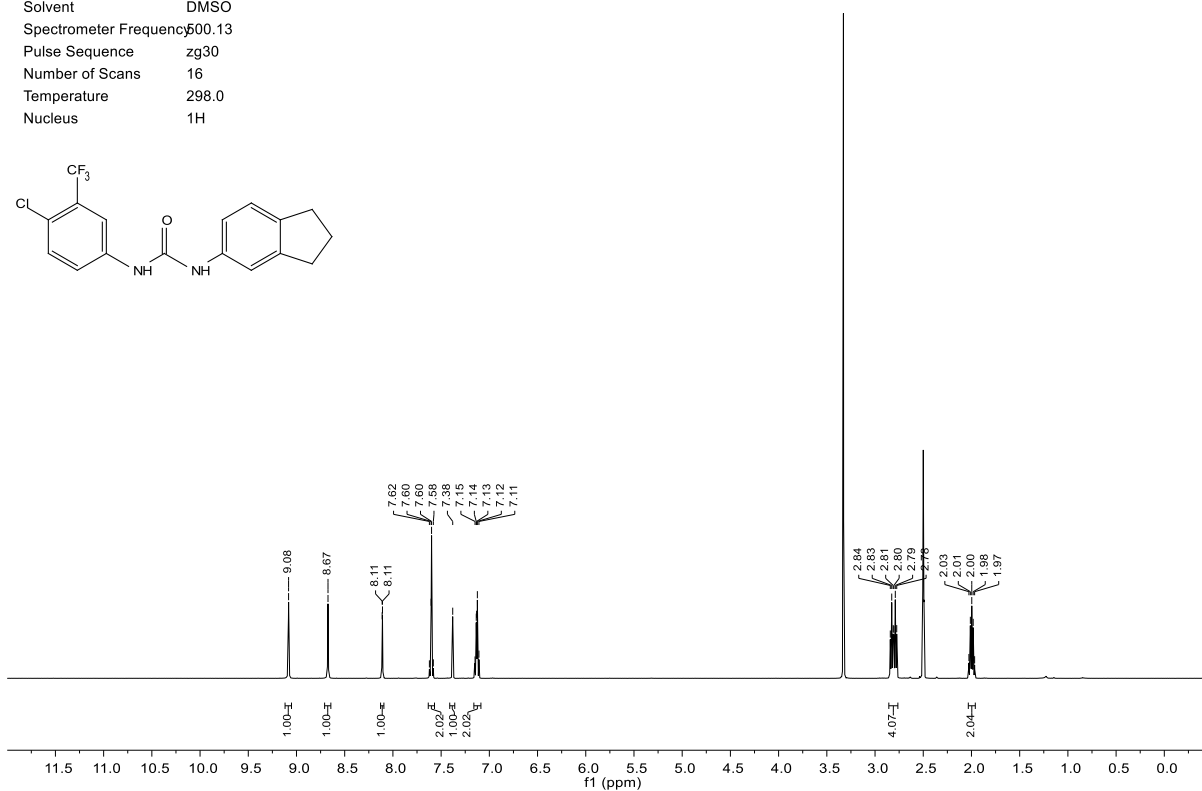
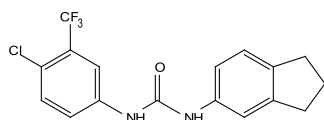
3.29

| Parameter              | Value           |
|------------------------|-----------------|
| Solvent                | DMSO            |
| Spectrometer Frequency | 125.82          |
| Pulse Sequence         | zgpg30          |
| Number of Scans        | 256             |
| Temperature            | 299.8           |
| Nucleus                | <sup>13</sup> C |



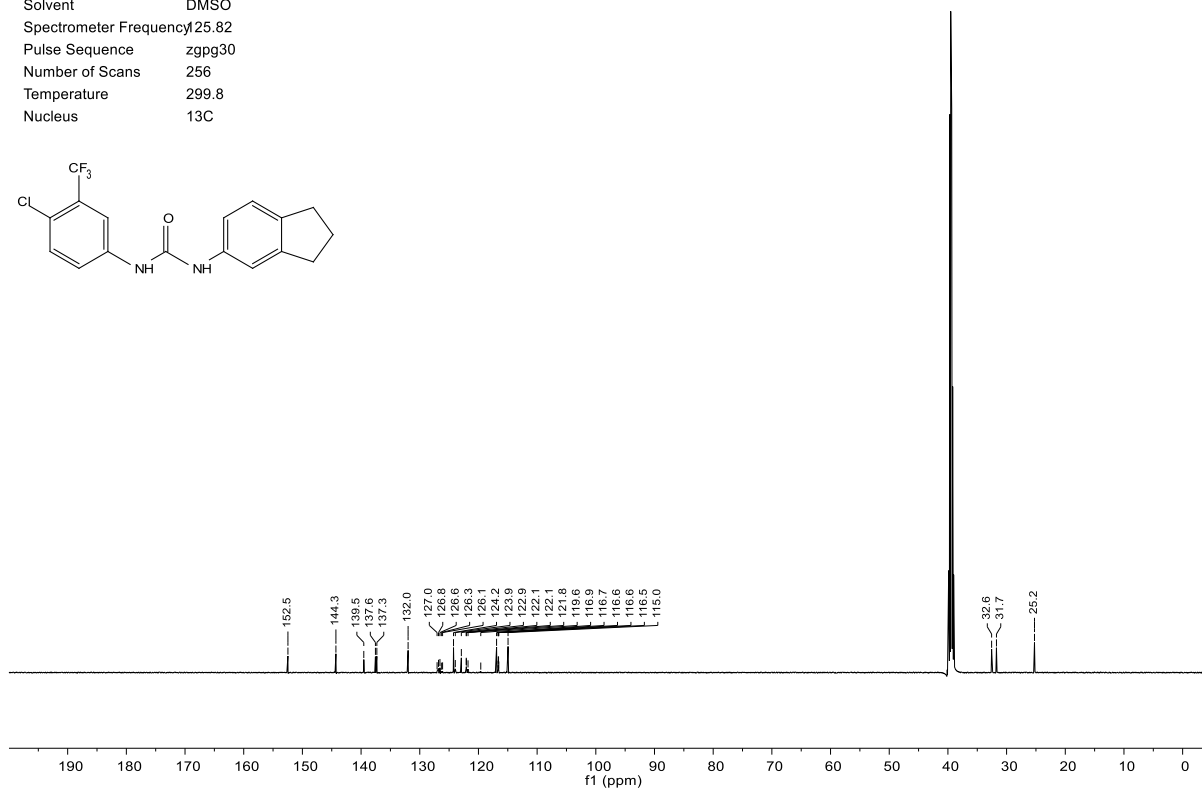
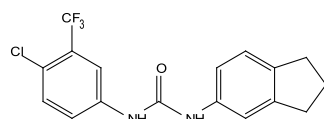
## 3.30

| Parameter              | Value          |
|------------------------|----------------|
| Solvent                | DMSO           |
| Spectrometer Frequency | 500.13         |
| Pulse Sequence         | zg30           |
| Number of Scans        | 16             |
| Temperature            | 298.0          |
| Nucleus                | <sup>1</sup> H |



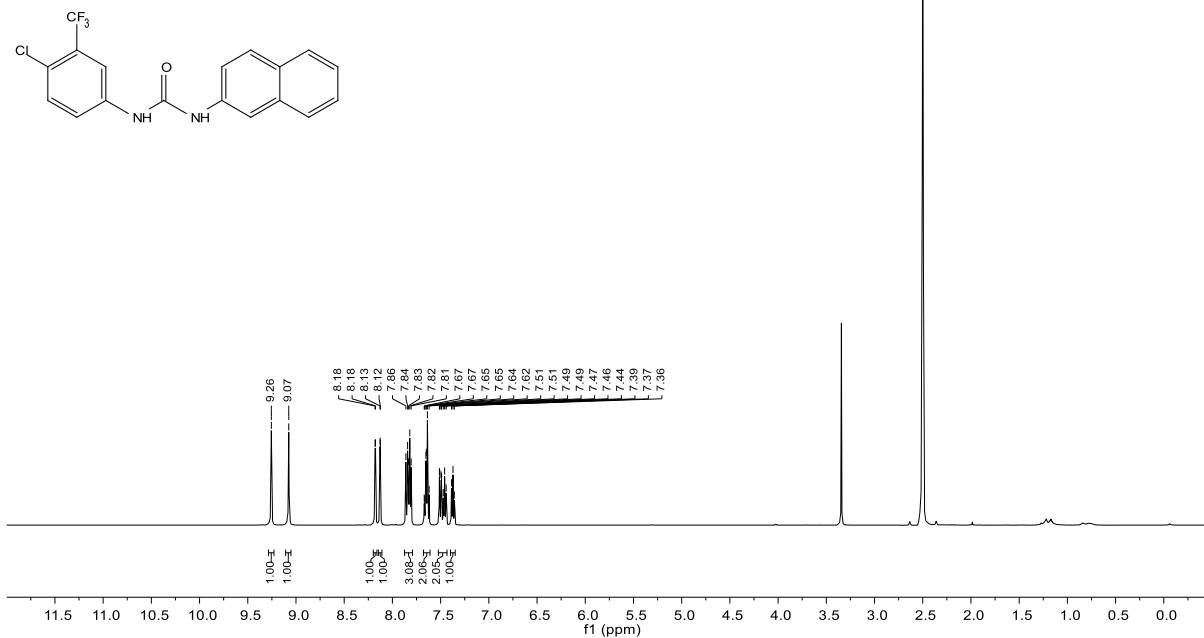
## 3.30

| Parameter              | Value           |
|------------------------|-----------------|
| Solvent                | DMSO            |
| Spectrometer Frequency | 125.82          |
| Pulse Sequence         | zgpg30          |
| Number of Scans        | 256             |
| Temperature            | 299.8           |
| Nucleus                | <sup>13</sup> C |



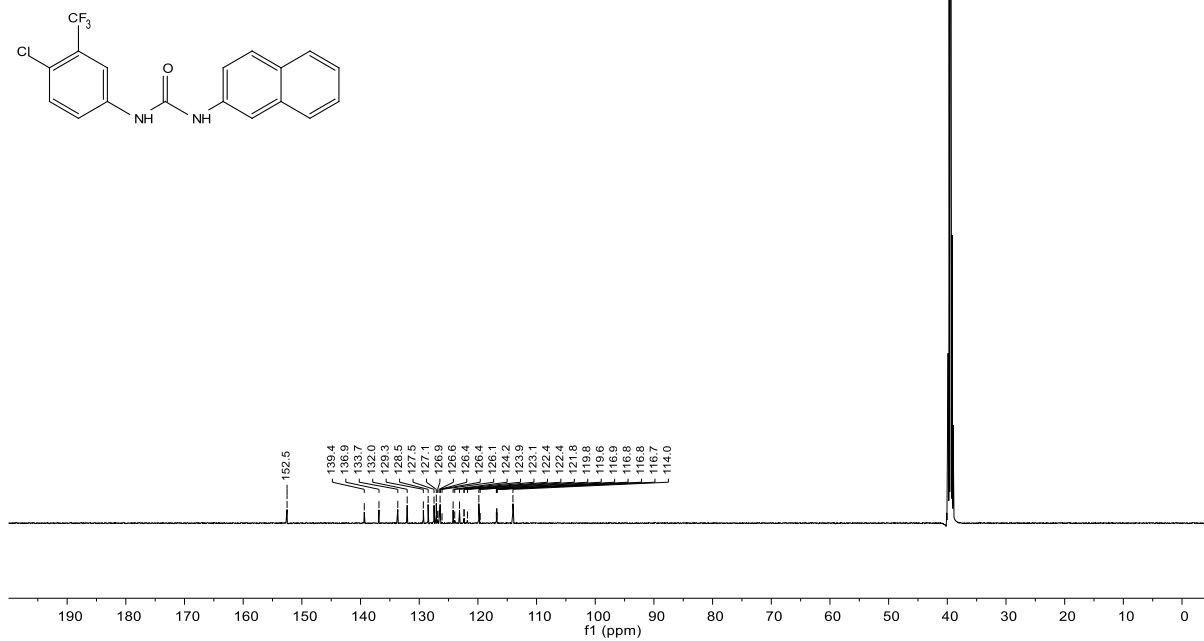
3.31

| Parameter              | Value        |
|------------------------|--------------|
| Solvent                | DMSO         |
| Spectrometer Frequency | 500.36       |
| Pulse Sequence         | zg30         |
| Number of Scans        | 16           |
| Temperature            | 299.9        |
| Nucleus                | $^1\text{H}$ |



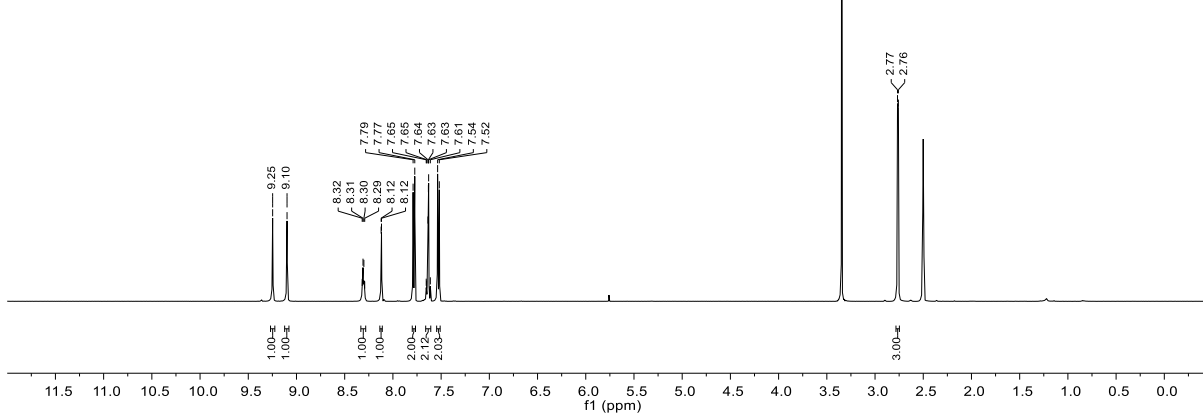
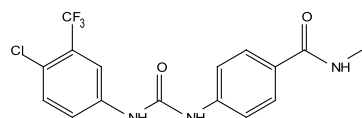
3.31

| Parameter              | Value           |
|------------------------|-----------------|
| Solvent                | DMSO            |
| Spectrometer Frequency | 125.82          |
| Pulse Sequence         | zgpg30          |
| Number of Scans        | 256             |
| Temperature            | 299.9           |
| Nucleus                | $^{13}\text{C}$ |



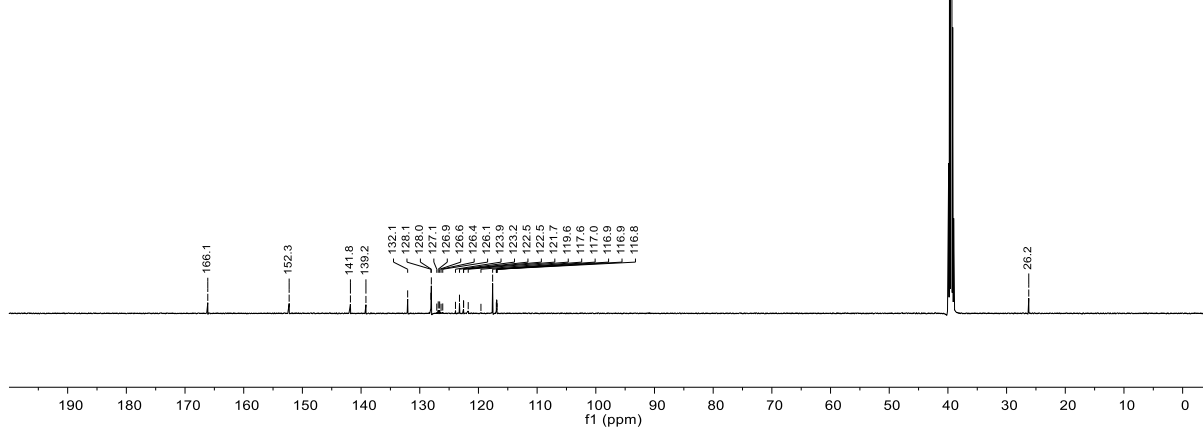
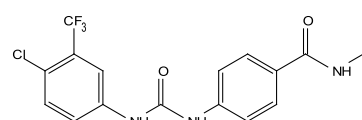
3.32

| Parameter              | Value          |
|------------------------|----------------|
| Solvent                | DMSO           |
| Spectrometer Frequency | 500.36         |
| Pulse Sequence         | zg30           |
| Number of Scans        | 16             |
| Temperature            | 299.9          |
| Nucleus                | <sup>1</sup> H |



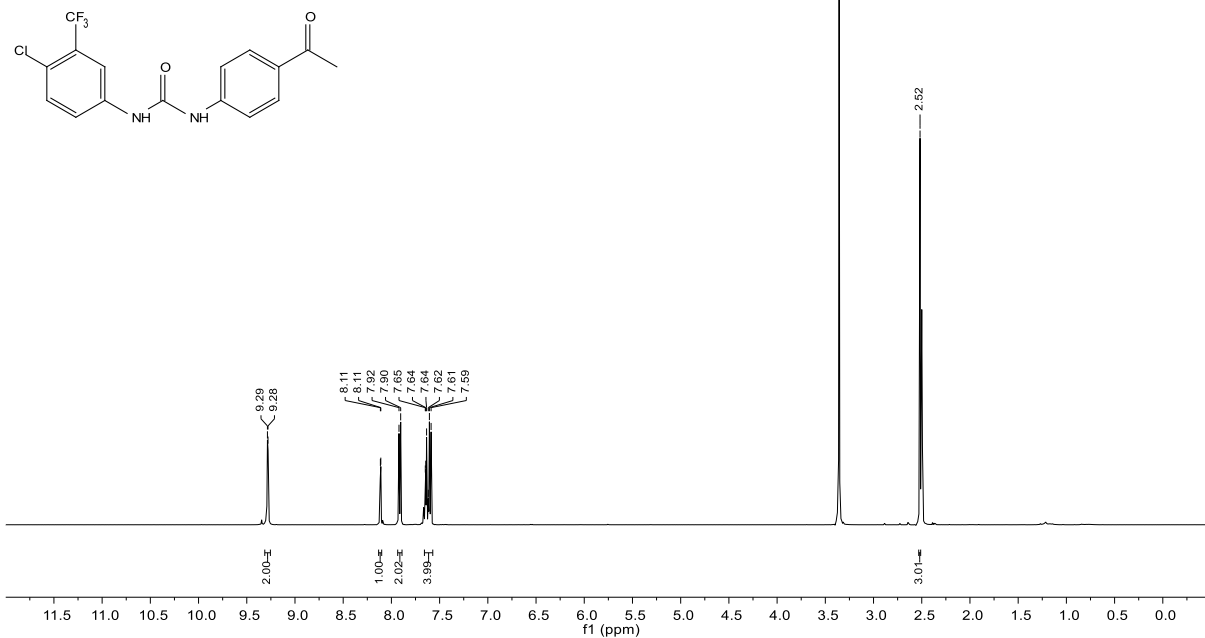
3.32

| Parameter              | Value           |
|------------------------|-----------------|
| Solvent                | DMSO            |
| Spectrometer Frequency | 125.82          |
| Pulse Sequence         | zgpg30          |
| Number of Scans        | 256             |
| Temperature            | 299.9           |
| Nucleus                | <sup>13</sup> C |



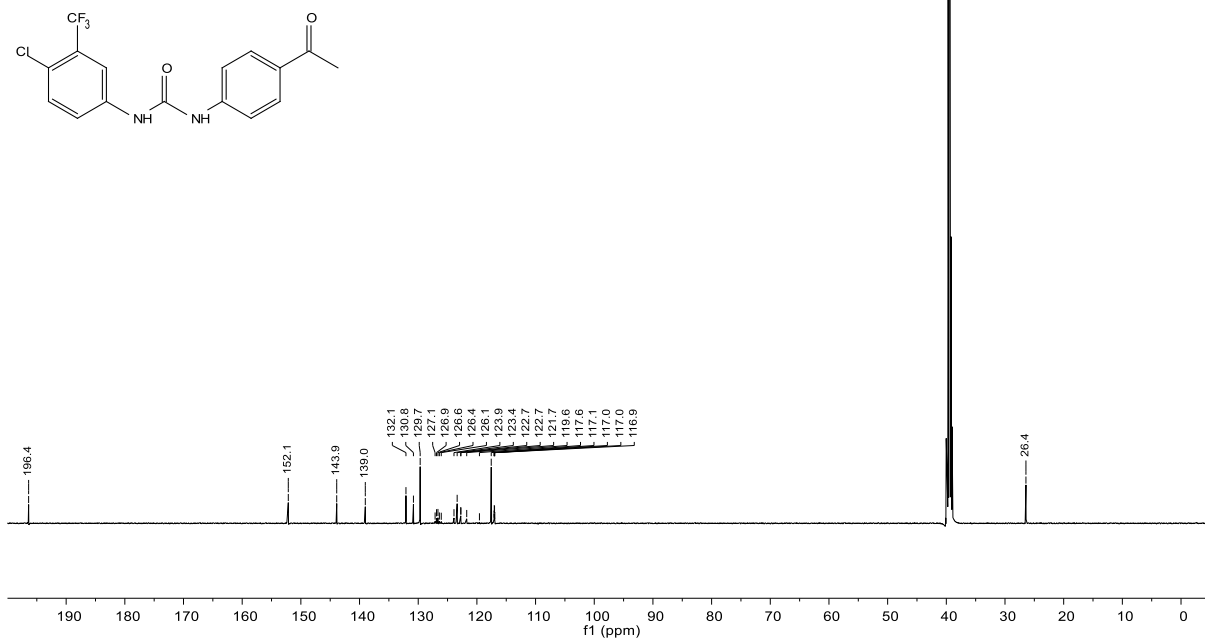
3.33

| Parameter              | Value          |
|------------------------|----------------|
| Solvent                | DMSO           |
| Spectrometer Frequency | 500.36         |
| Pulse Sequence         | zg30           |
| Number of Scans        | 16             |
| Temperature            | 299.8          |
| Nucleus                | <sup>1</sup> H |



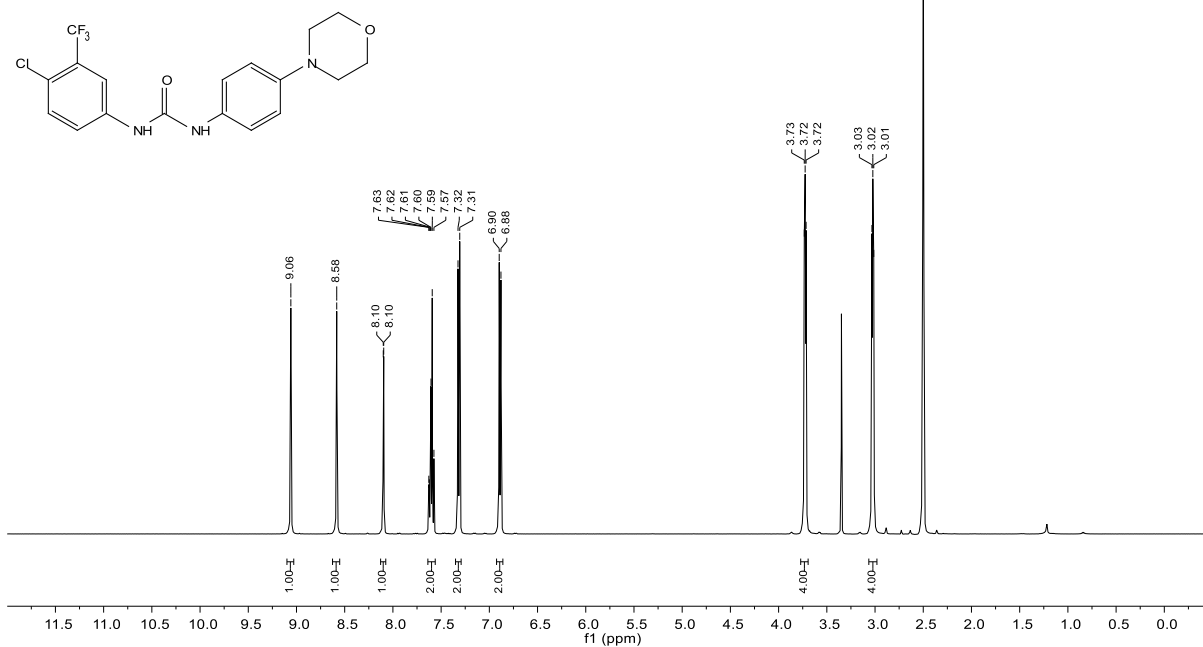
3.33

| Parameter              | Value           |
|------------------------|-----------------|
| Solvent                | DMSO            |
| Spectrometer Frequency | 125.82          |
| Pulse Sequence         | zgpg30          |
| Number of Scans        | 256             |
| Temperature            | 299.8           |
| Nucleus                | <sup>13</sup> C |



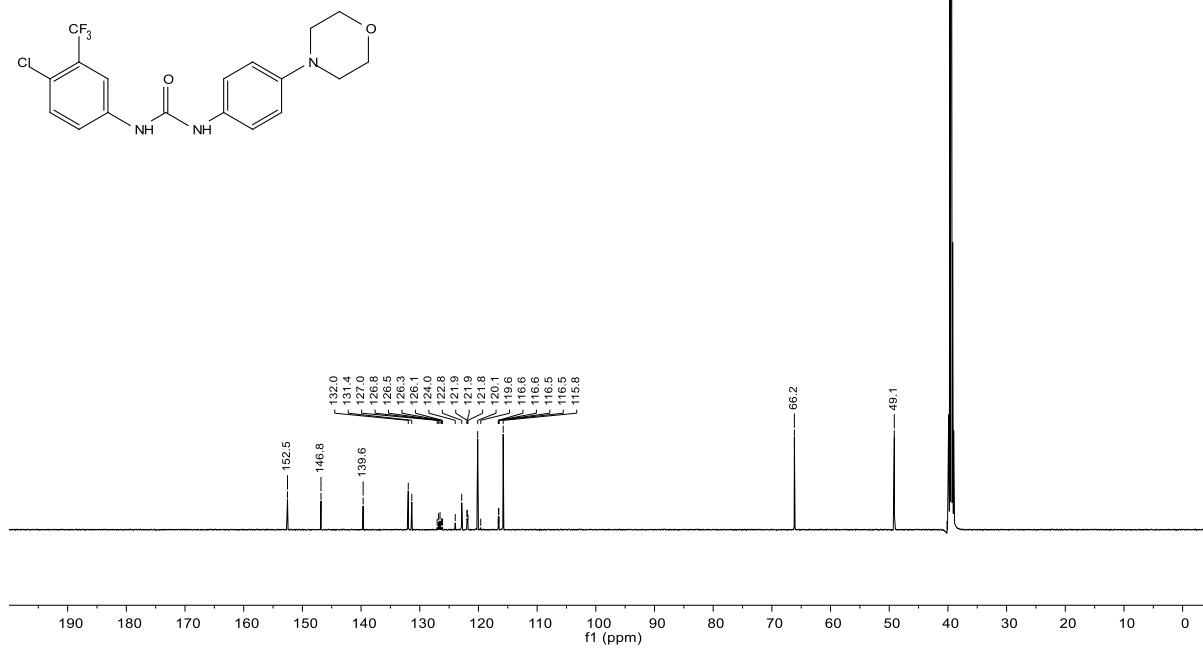
3.34

| Parameter              | Value          |
|------------------------|----------------|
| Solvent                | DMSO           |
| Spectrometer Frequency | 500.36         |
| Pulse Sequence         | zg30           |
| Number of Scans        | 16             |
| Temperature            | 299.9          |
| Nucleus                | <sup>1</sup> H |



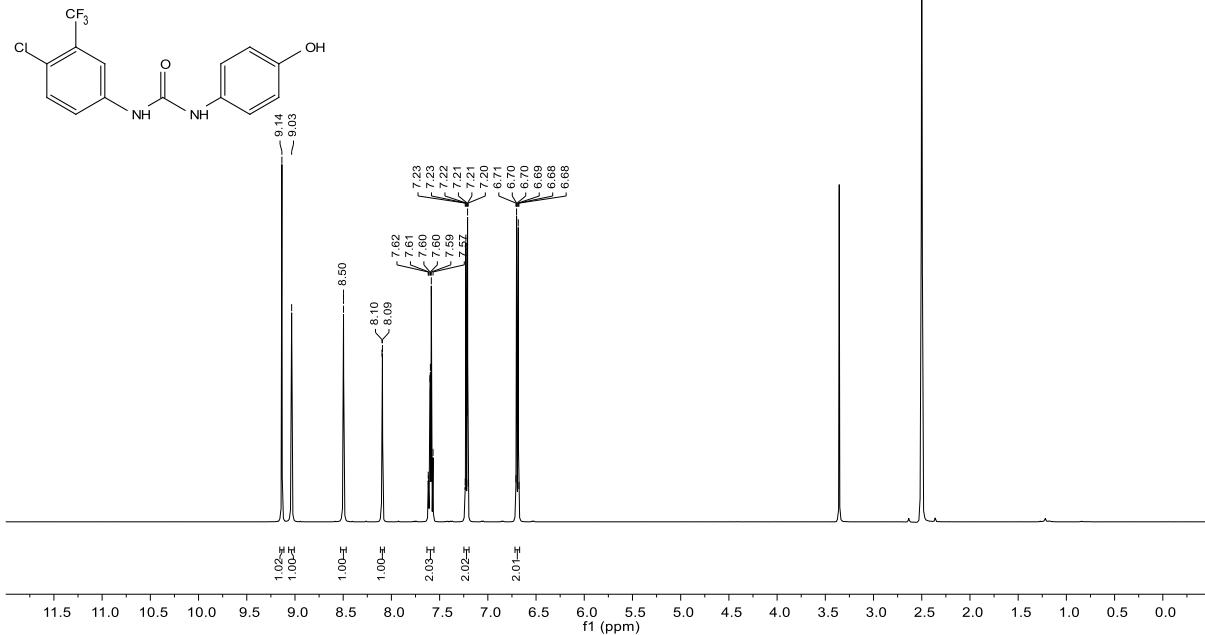
3.34

| Parameter              | Value           |
|------------------------|-----------------|
| Solvent                | DMSO            |
| Spectrometer Frequency | 125.82          |
| Pulse Sequence         | zgpg30          |
| Number of Scans        | 256             |
| Temperature            | 299.8           |
| Nucleus                | <sup>13</sup> C |



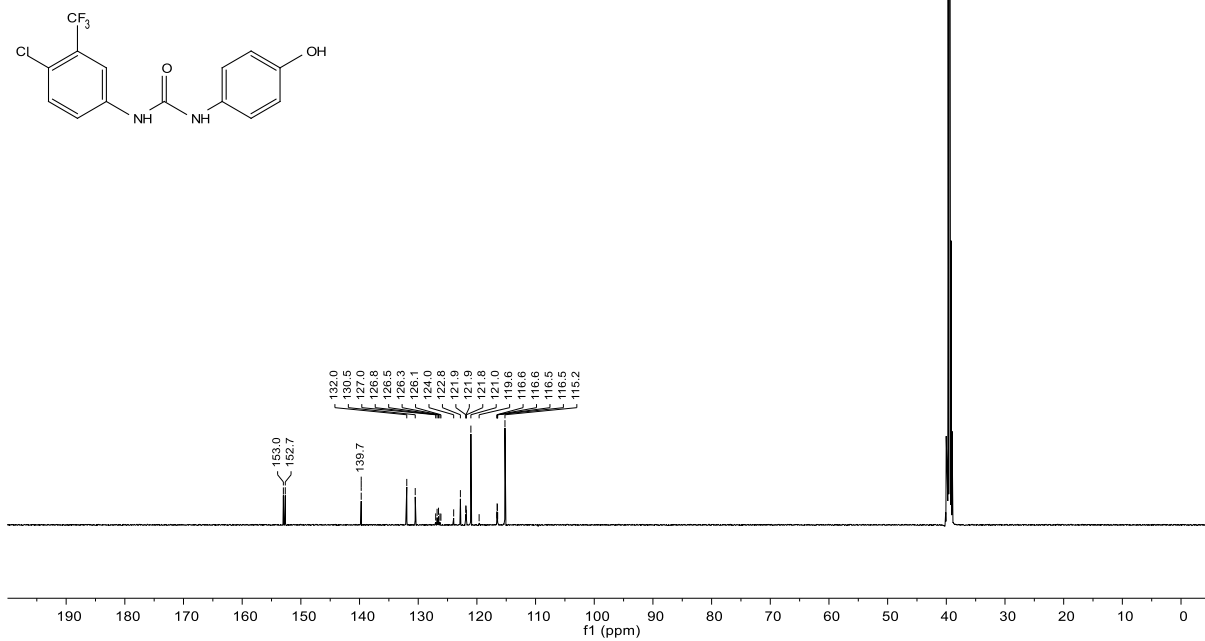
3.35

| Parameter              | Value          |
|------------------------|----------------|
| Solvent                | DMSO           |
| Spectrometer Frequency | 500.36         |
| Pulse Sequence         | zg30           |
| Number of Scans        | 16             |
| Temperature            | 299.9          |
| Nucleus                | <sup>1</sup> H |



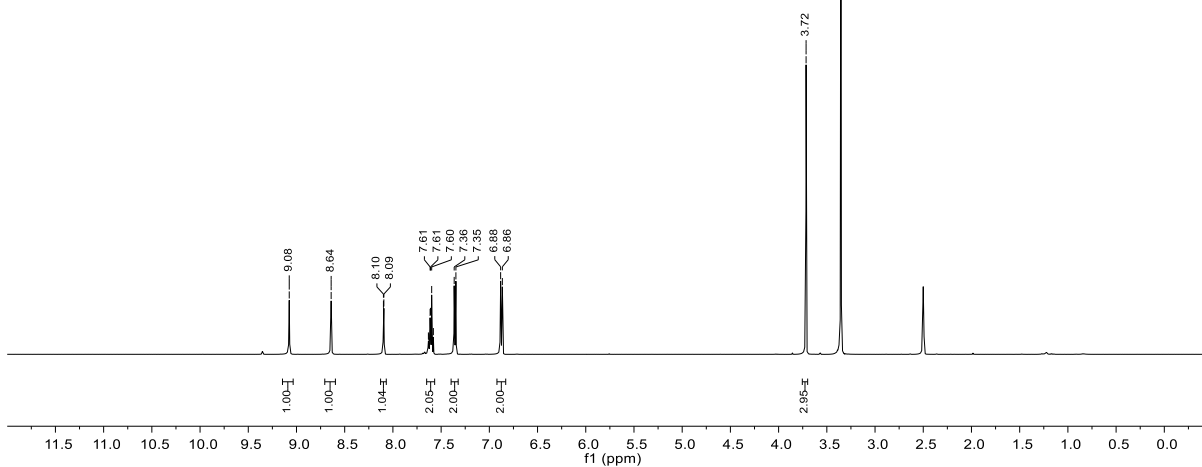
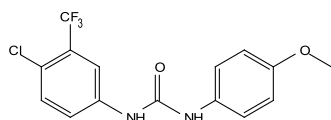
3.35

| Parameter              | Value           |
|------------------------|-----------------|
| Solvent                | DMSO            |
| Spectrometer Frequency | 125.82          |
| Pulse Sequence         | zgpg30          |
| Number of Scans        | 256             |
| Temperature            | 299.9           |
| Nucleus                | <sup>13</sup> C |



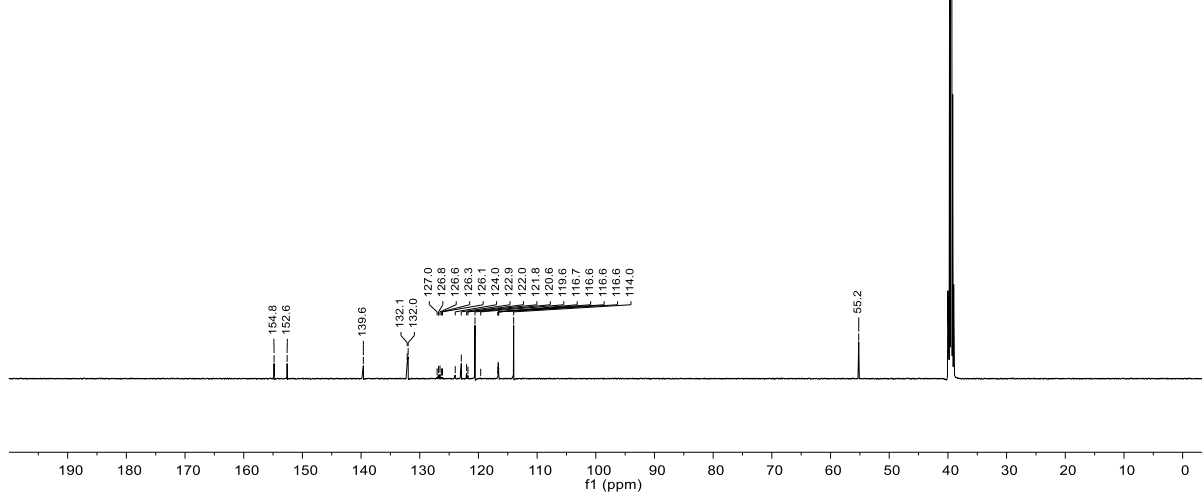
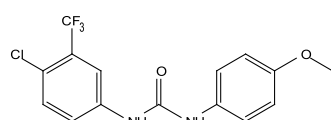
## 3.36

| Parameter              | Value          |
|------------------------|----------------|
| Solvent                | DMSO           |
| Spectrometer Frequency | 500.36         |
| Pulse Sequence         | zg30           |
| Number of Scans        | 16             |
| Temperature            | 299.8          |
| Nucleus                | <sup>1</sup> H |



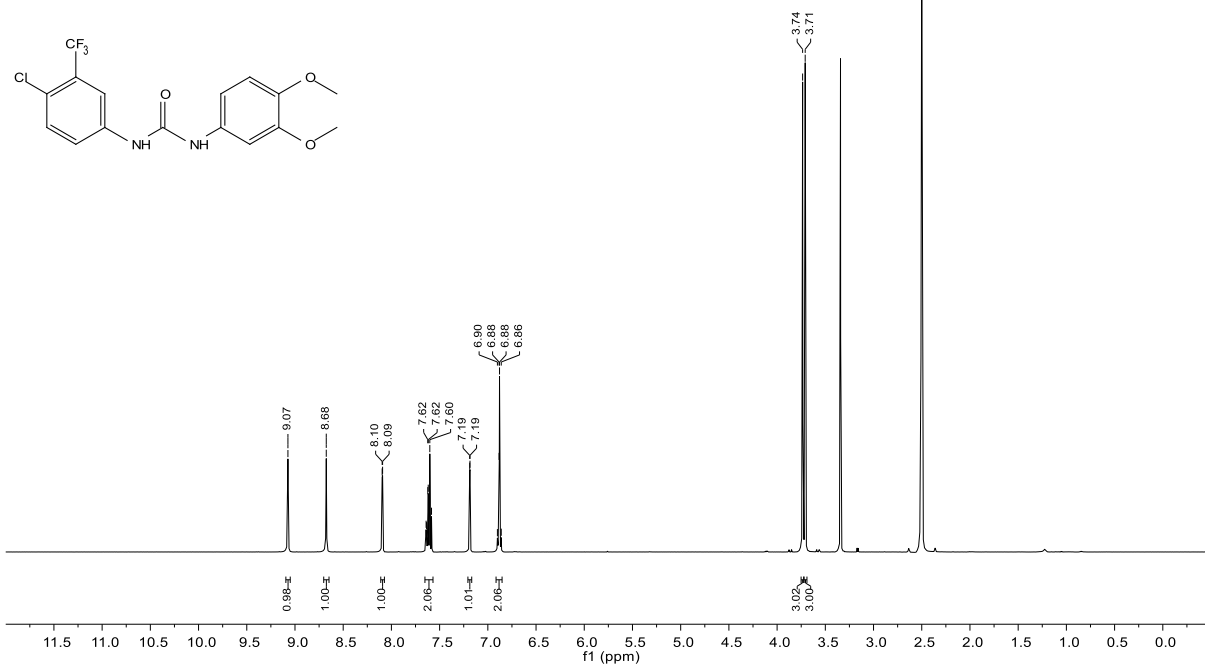
## 3.36

| Parameter              | Value           |
|------------------------|-----------------|
| Solvent                | DMSO            |
| Spectrometer Frequency | 125.82          |
| Pulse Sequence         | zgpg30          |
| Number of Scans        | 256             |
| Temperature            | 299.9           |
| Nucleus                | <sup>13</sup> C |



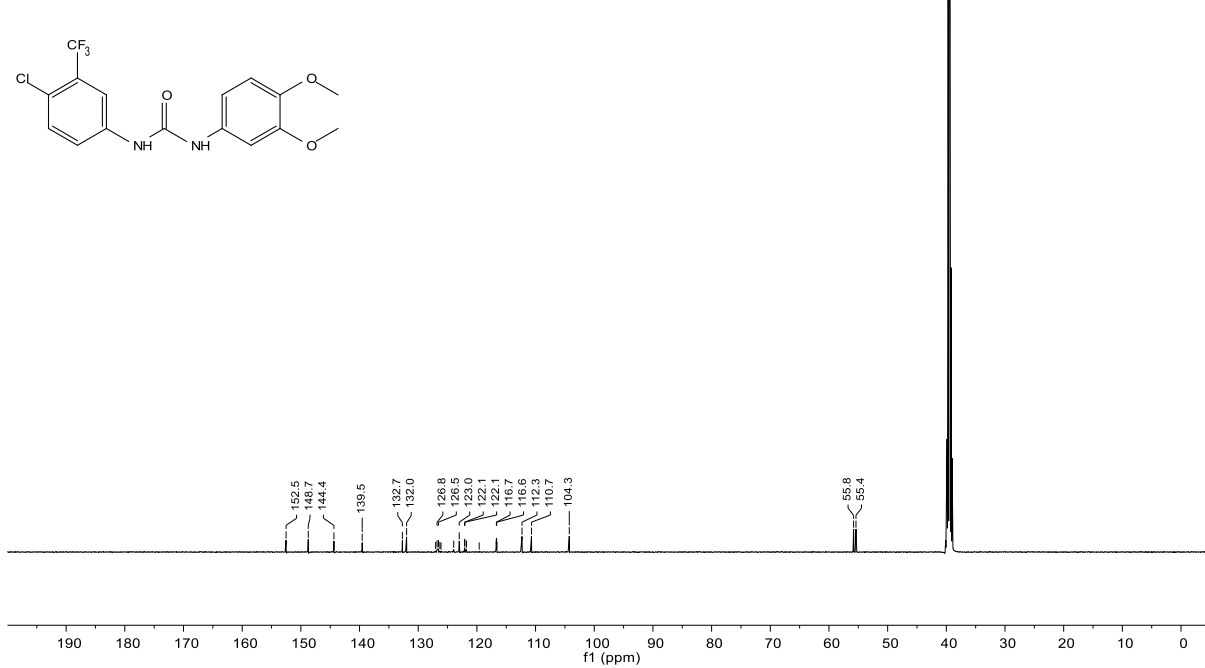
3.37

| Parameter              | Value          |
|------------------------|----------------|
| Solvent                | DMSO           |
| Spectrometer Frequency | 500.36         |
| Pulse Sequence         | zg30           |
| Number of Scans        | 16             |
| Temperature            | 300.0          |
| Nucleus                | <sup>1</sup> H |



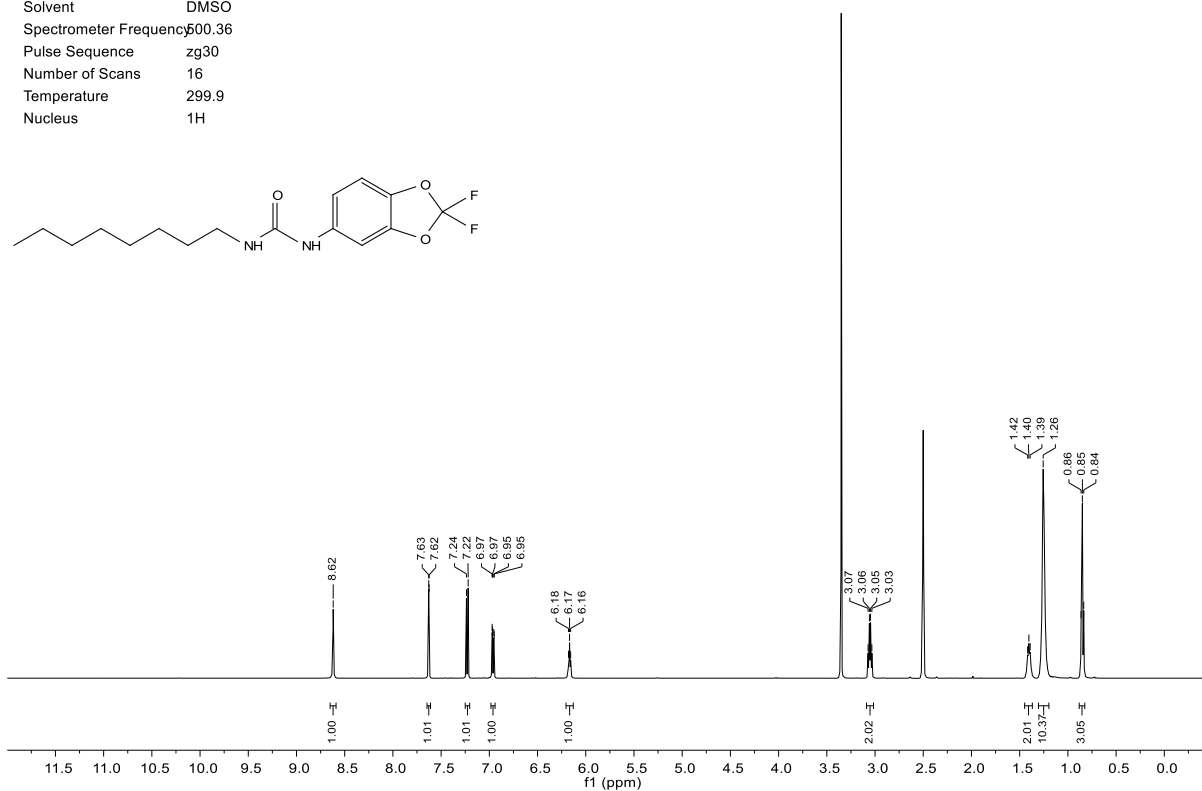
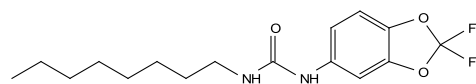
3.37

| Parameter              | Value           |
|------------------------|-----------------|
| Solvent                | DMSO            |
| Spectrometer Frequency | 125.82          |
| Pulse Sequence         | zgpg30          |
| Number of Scans        | 512             |
| Temperature            | 300.0           |
| Nucleus                | <sup>13</sup> C |



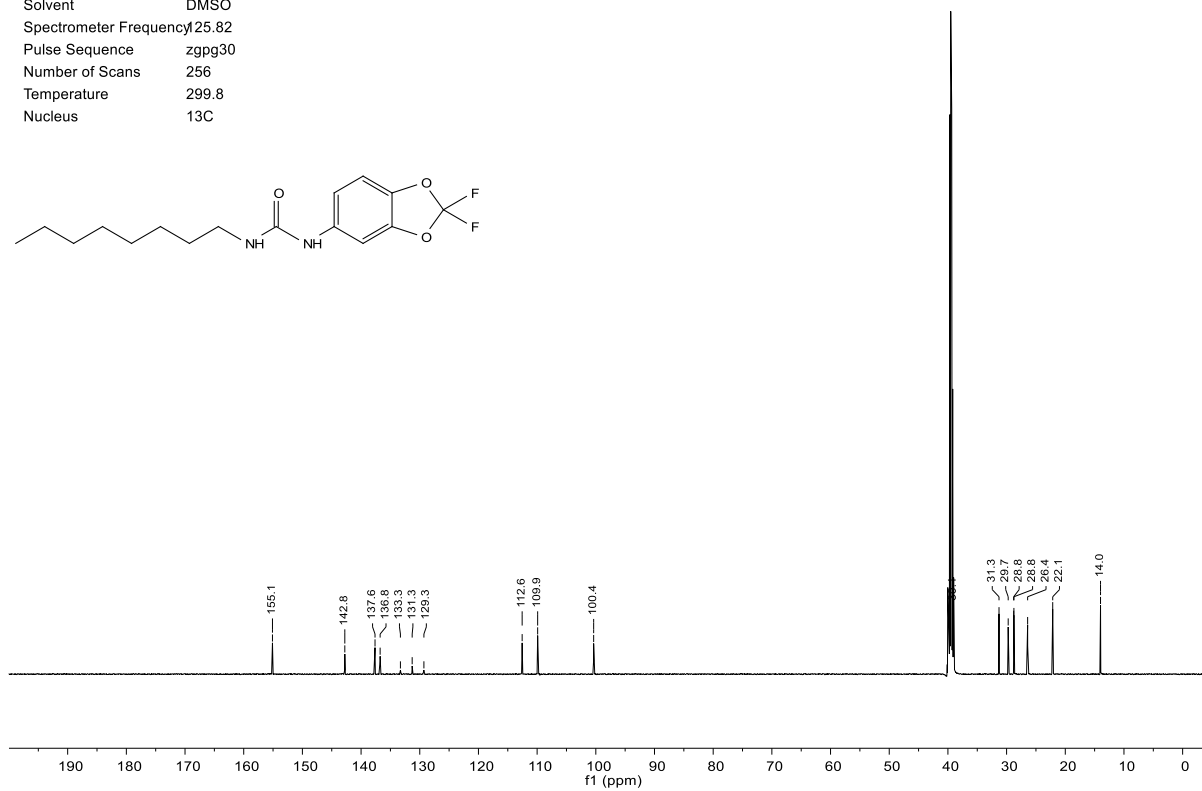
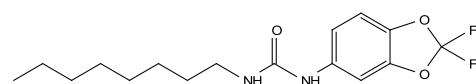
3.38

| Parameter              | Value          |
|------------------------|----------------|
| Solvent                | DMSO           |
| Spectrometer Frequency | 500.36         |
| Pulse Sequence         | zg30           |
| Number of Scans        | 16             |
| Temperature            | 299.9          |
| Nucleus                | <sup>1</sup> H |



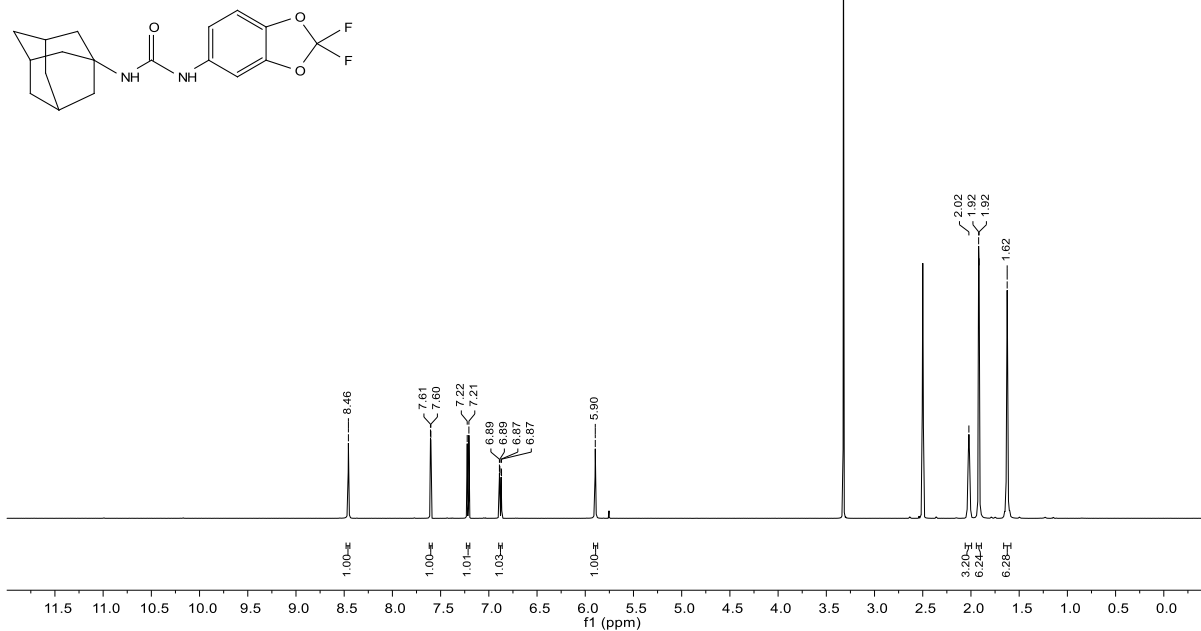
3.38

| Parameter              | Value           |
|------------------------|-----------------|
| Solvent                | DMSO            |
| Spectrometer Frequency | 125.82          |
| Pulse Sequence         | zgpg30          |
| Number of Scans        | 256             |
| Temperature            | 299.8           |
| Nucleus                | <sup>13</sup> C |



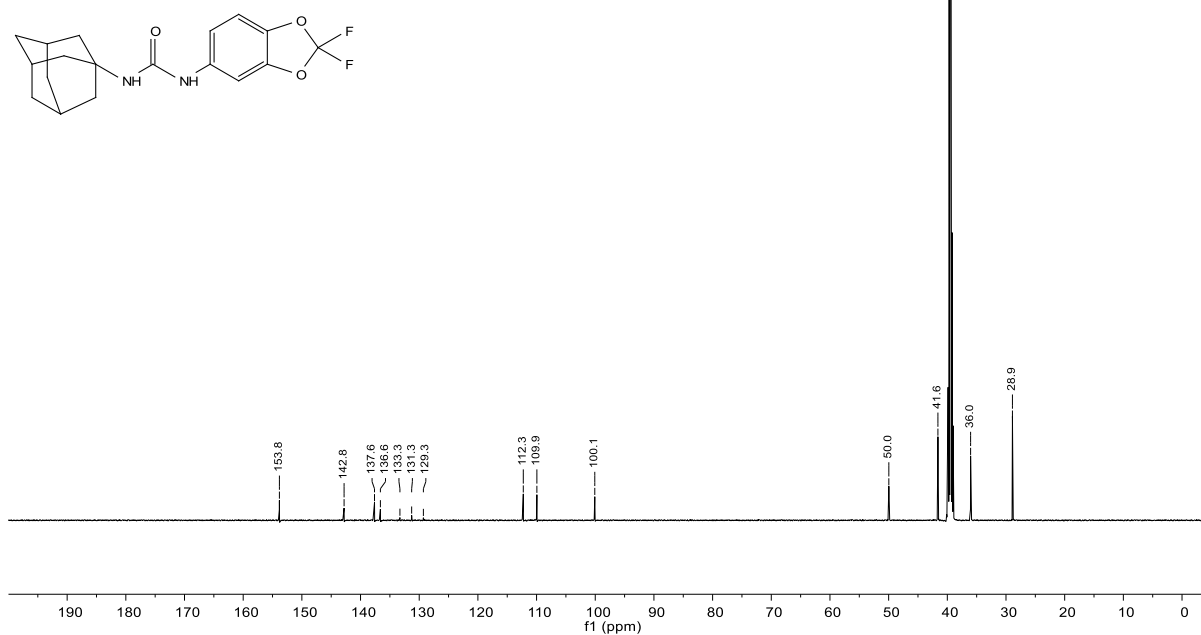
## 3.39

| Parameter              | Value        |
|------------------------|--------------|
| Solvent                | DMSO         |
| Spectrometer Frequency | 500.13       |
| Pulse Sequence         | zg30         |
| Number of Scans        | 16           |
| Temperature            | 298.0        |
| Nucleus                | $^1\text{H}$ |



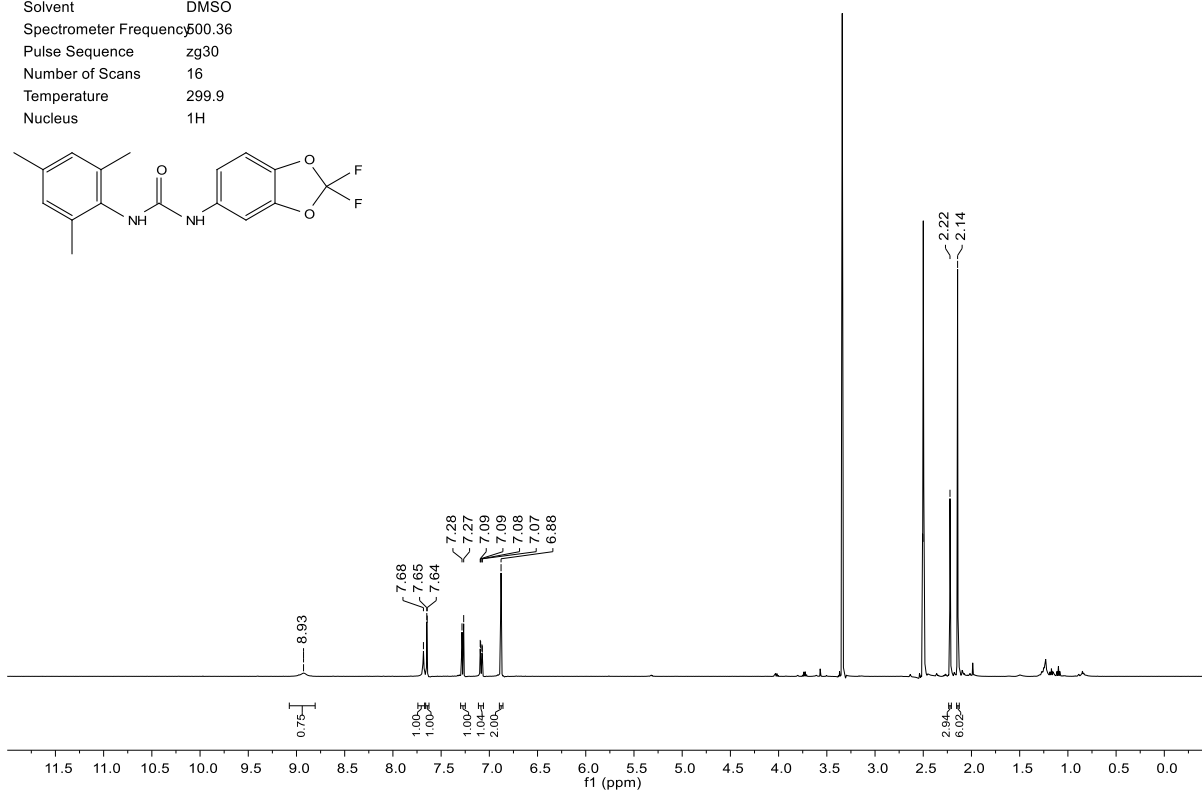
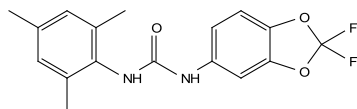
## 3.39

| Parameter              | Value           |
|------------------------|-----------------|
| Solvent                | DMSO            |
| Spectrometer Frequency | 125.82          |
| Pulse Sequence         | zgpg30          |
| Number of Scans        | 256             |
| Temperature            | 299.8           |
| Nucleus                | $^{13}\text{C}$ |



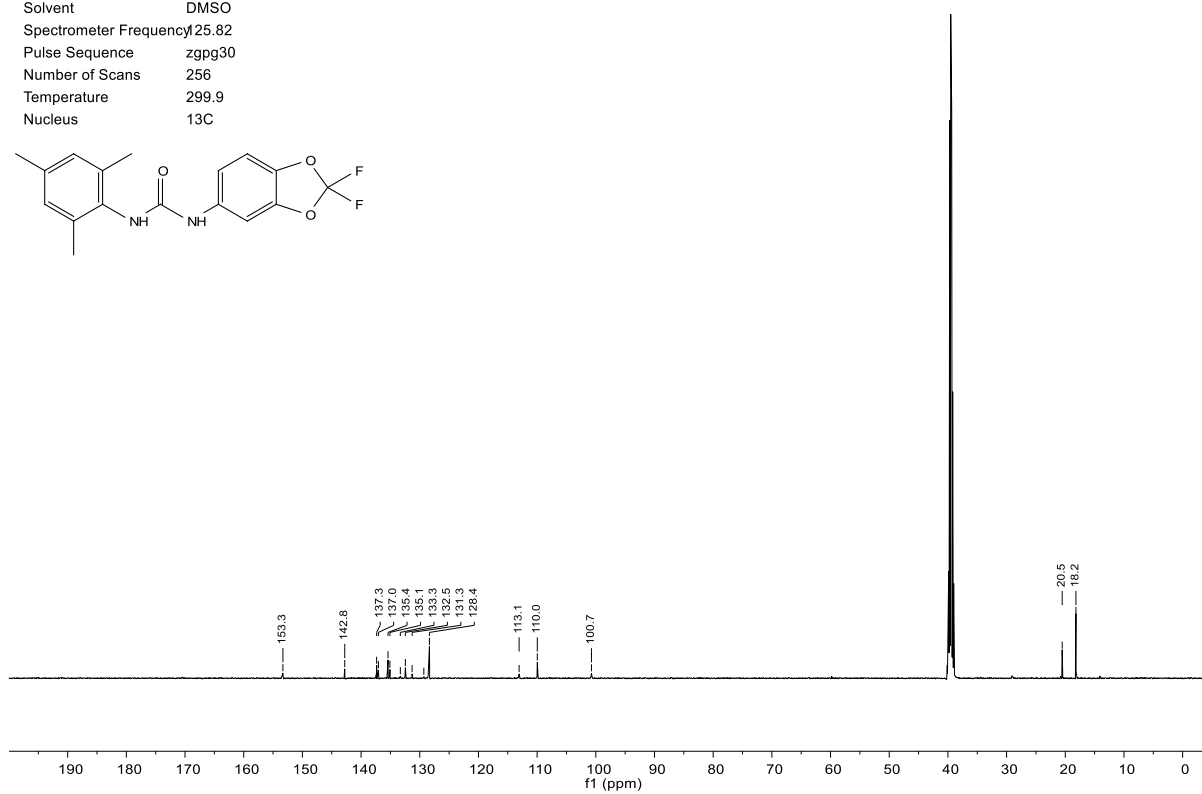
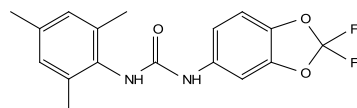
## 3.40

| Parameter              | Value          |
|------------------------|----------------|
| Solvent                | DMSO           |
| Spectrometer Frequency | 500.36         |
| Pulse Sequence         | zg30           |
| Number of Scans        | 16             |
| Temperature            | 299.9          |
| Nucleus                | <sup>1</sup> H |



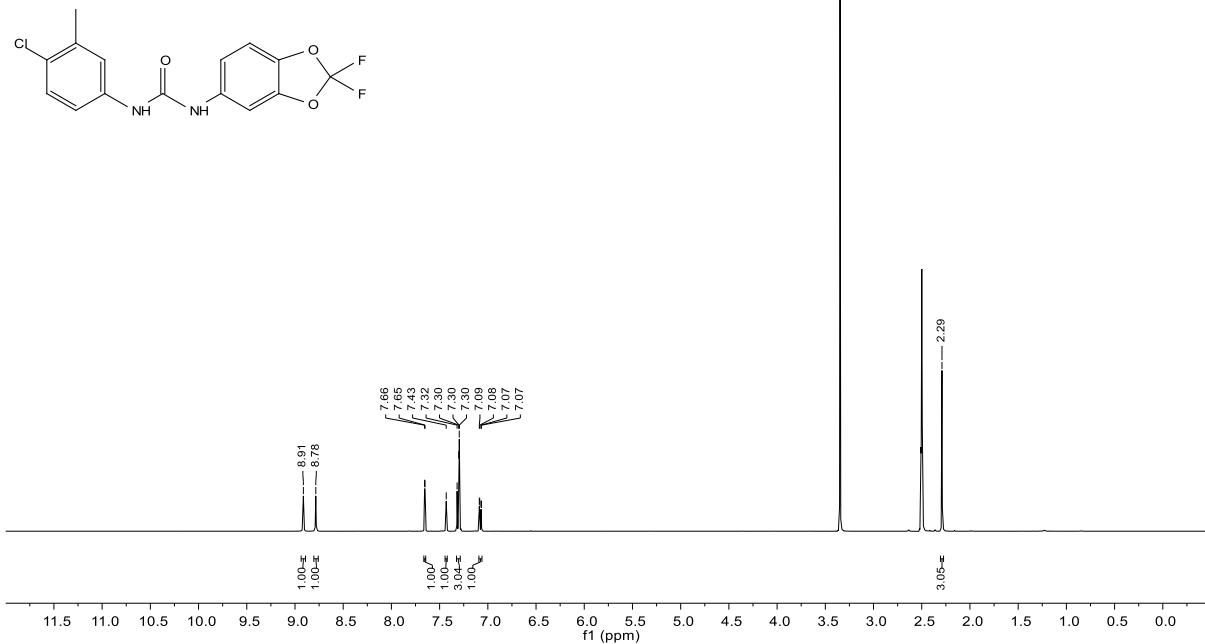
## 3.40

| Parameter              | Value           |
|------------------------|-----------------|
| Solvent                | DMSO            |
| Spectrometer Frequency | 125.82          |
| Pulse Sequence         | zgpg30          |
| Number of Scans        | 256             |
| Temperature            | 299.9           |
| Nucleus                | <sup>13</sup> C |



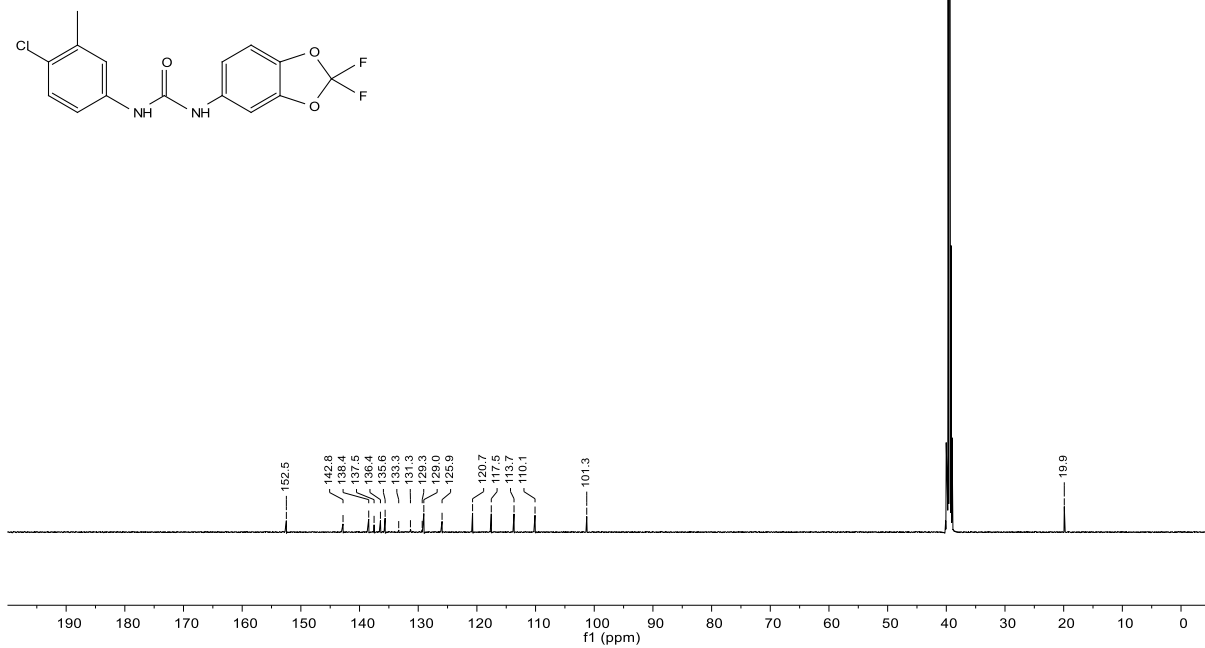
3.41

| Parameter              | Value          |
|------------------------|----------------|
| Solvent                | DMSO           |
| Spectrometer Frequency | 500.36         |
| Pulse Sequence         | zg30           |
| Number of Scans        | 16             |
| Temperature            | 299.9          |
| Nucleus                | <sup>1</sup> H |



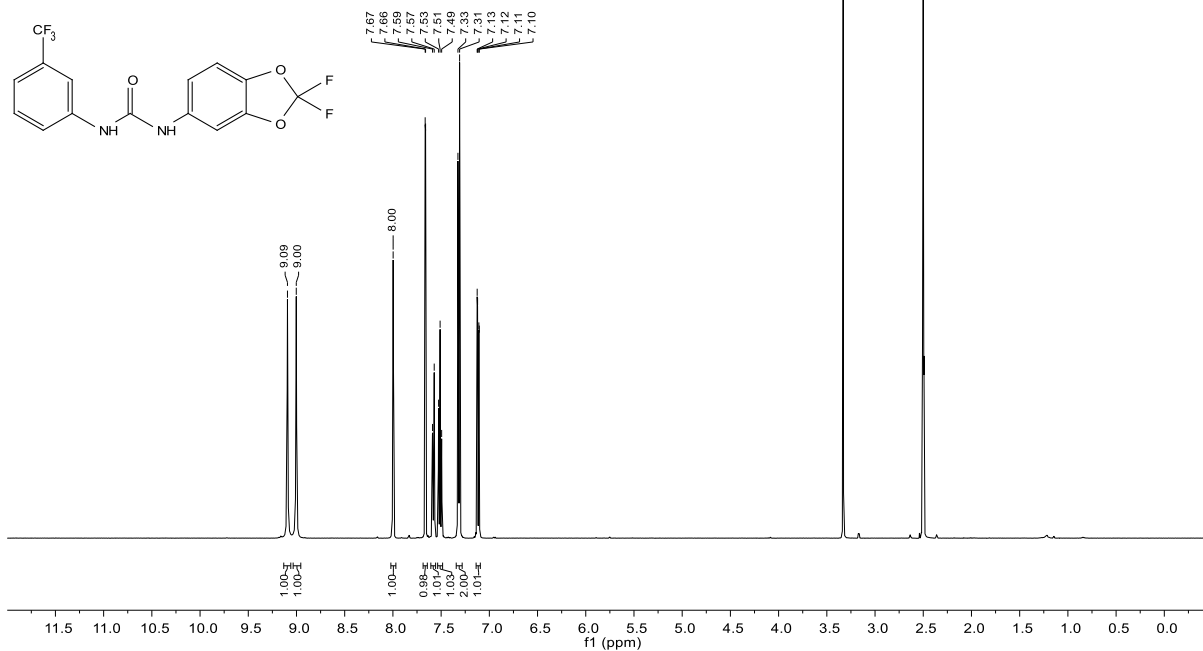
3.41

| Parameter              | Value           |
|------------------------|-----------------|
| Solvent                | DMSO            |
| Spectrometer Frequency | 125.82          |
| Pulse Sequence         | zgpg30          |
| Number of Scans        | 256             |
| Temperature            | 299.9           |
| Nucleus                | <sup>13</sup> C |



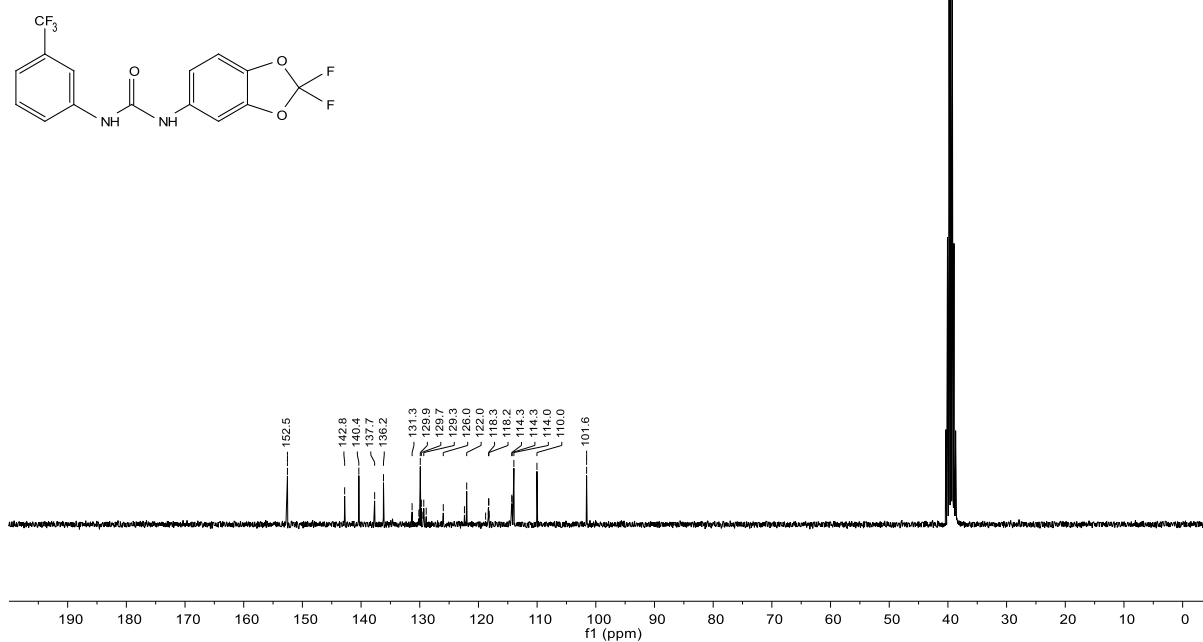
3.42

| Parameter              | Value        |
|------------------------|--------------|
| Solvent                | DMSO         |
| Spectrometer Frequency | 500.13       |
| Pulse Sequence         | zg30         |
| Number of Scans        | 16           |
| Temperature            | 298.0        |
| Nucleus                | $^1\text{H}$ |



3.42

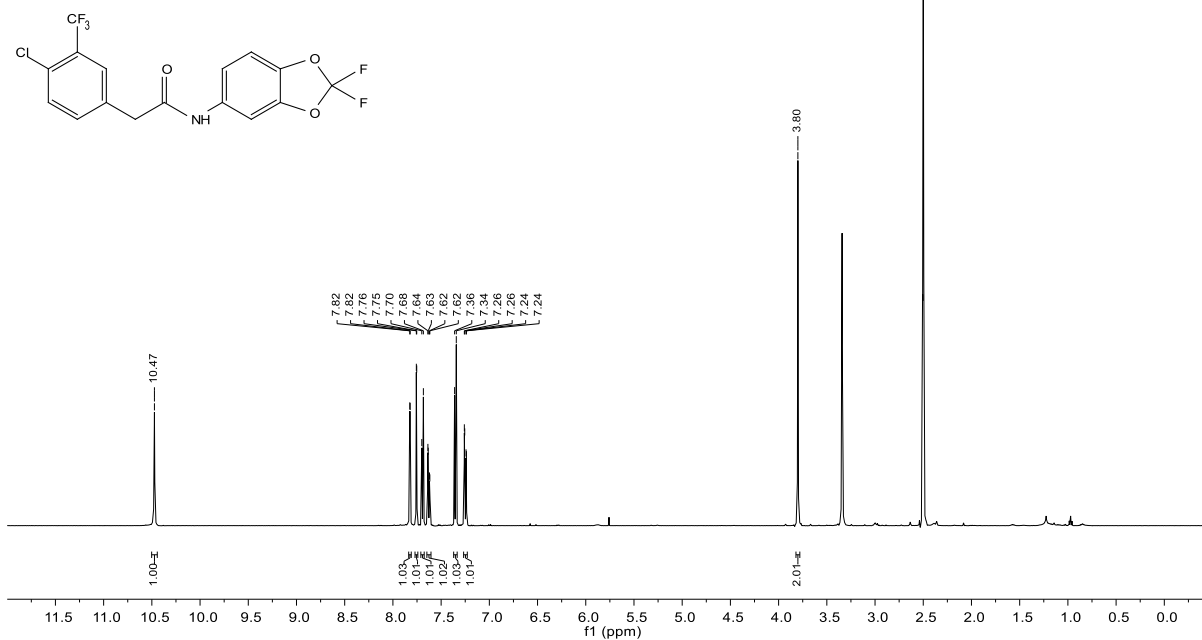
| Parameter              | Value           |
|------------------------|-----------------|
| Solvent                | DMSO            |
| Spectrometer Frequency | 75.47           |
| Pulse Sequence         | zgpg30          |
| Number of Scans        | 1024            |
| Temperature            | 298.0           |
| Nucleus                | $^{13}\text{C}$ |





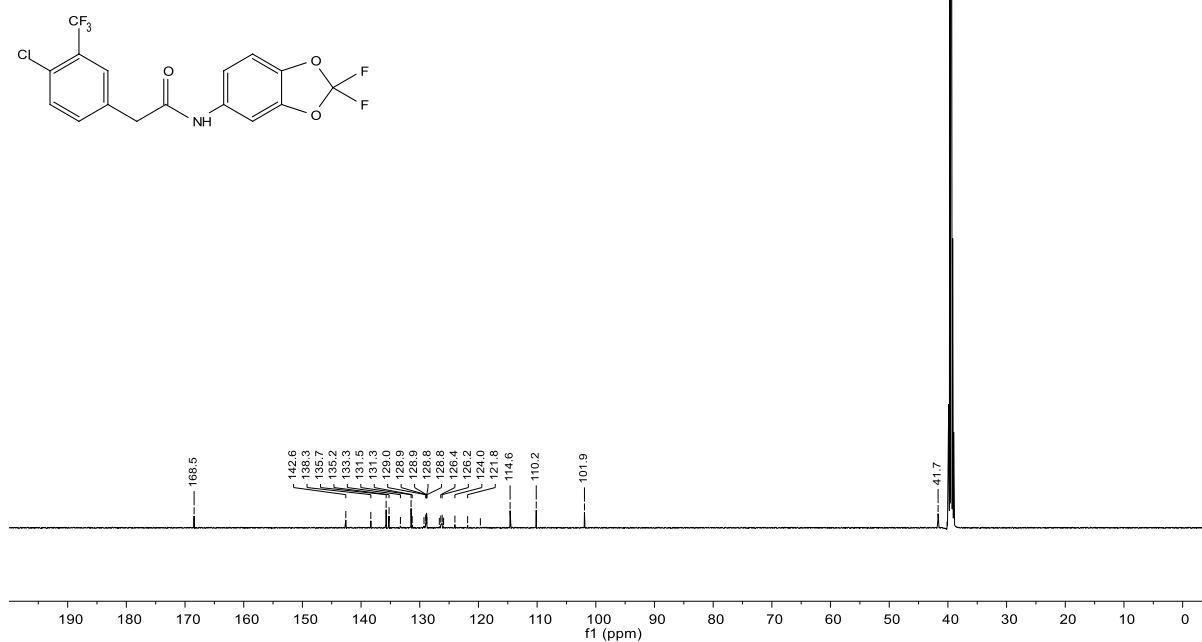
3.44

| Parameter              | Value          |
|------------------------|----------------|
| Solvent                | DMSO           |
| Spectrometer Frequency | 500.36         |
| Pulse Sequence         | zg30           |
| Number of Scans        | 16             |
| Temperature            | 299.9          |
| Nucleus                | <sup>1</sup> H |



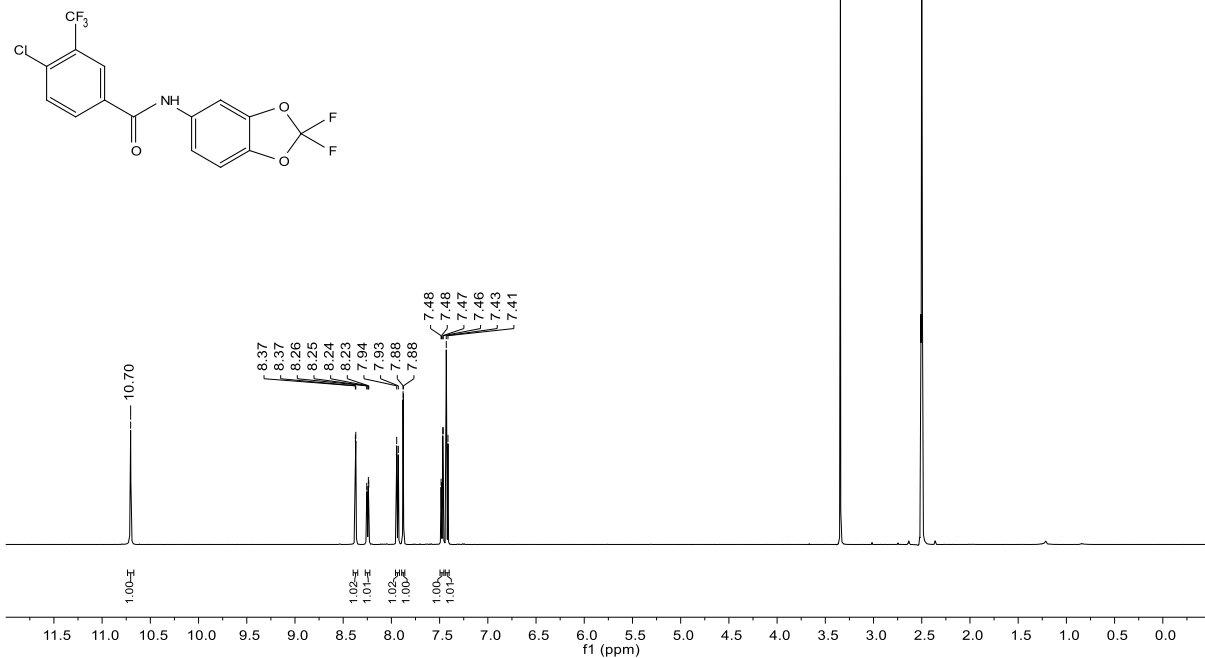
3.44

| Parameter              | Value           |
|------------------------|-----------------|
| Solvent                | DMSO            |
| Spectrometer Frequency | 125.82          |
| Pulse Sequence         | zgpg30          |
| Number of Scans        | 256             |
| Temperature            | 299.9           |
| Nucleus                | <sup>13</sup> C |



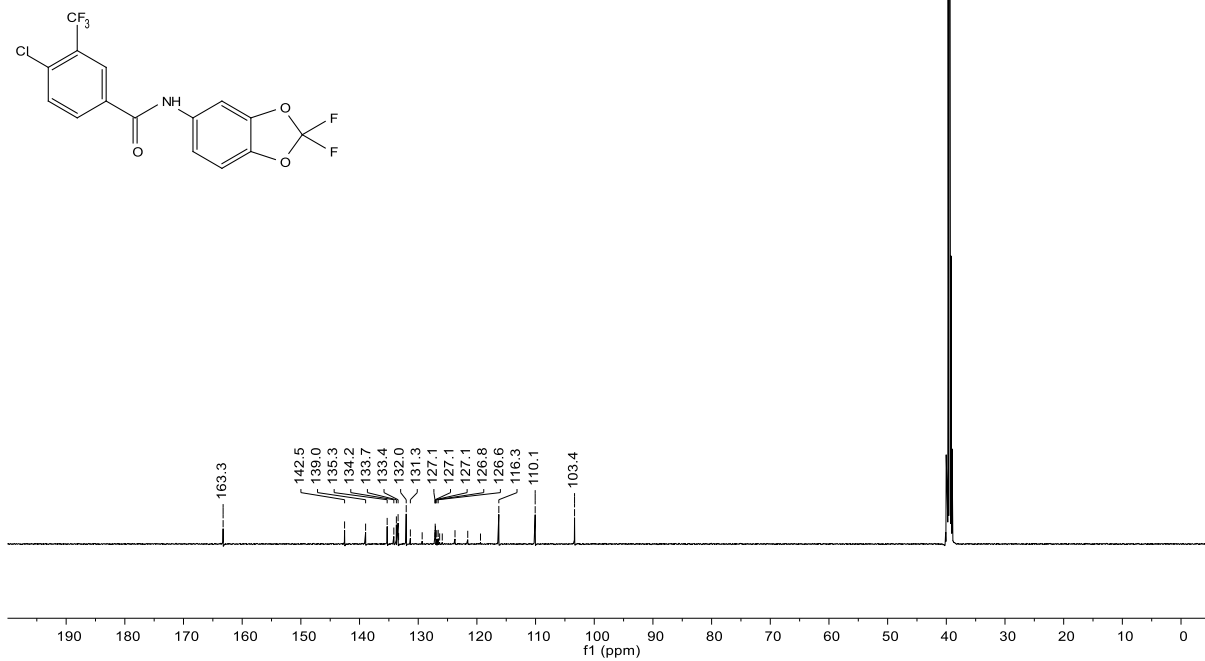
3.45

| Parameter              | Value          |
|------------------------|----------------|
| Solvent                | DMSO           |
| Spectrometer Frequency | 500.36         |
| Pulse Sequence         | zg30           |
| Number of Scans        | 16             |
| Temperature            | 299.9          |
| Nucleus                | <sup>1</sup> H |



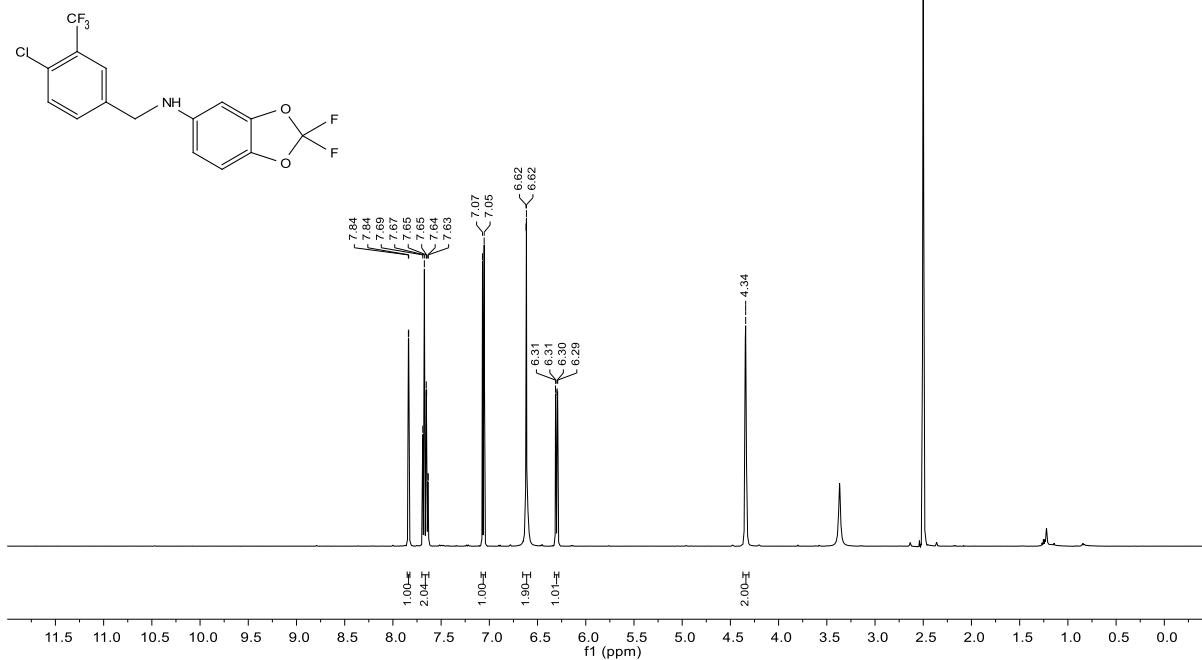
3.45

| Parameter              | Value           |
|------------------------|-----------------|
| Solvent                | DMSO            |
| Spectrometer Frequency | 125.82          |
| Pulse Sequence         | zgpg30          |
| Number of Scans        | 256             |
| Temperature            | 299.9           |
| Nucleus                | <sup>13</sup> C |



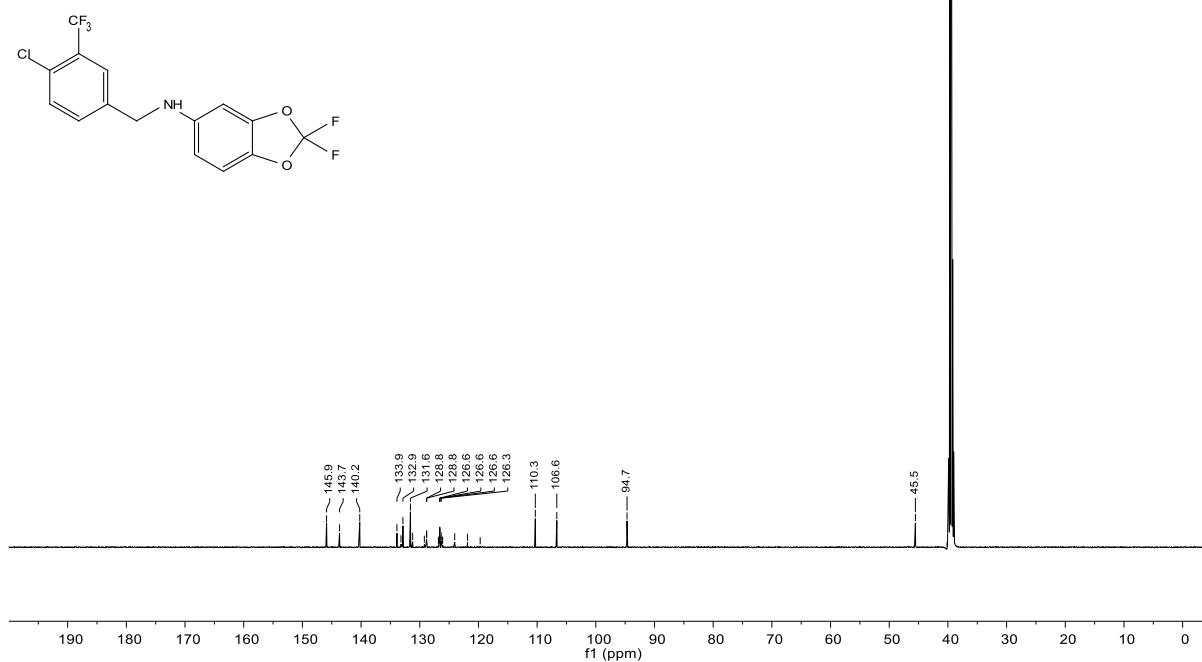
3.46

| Parameter              | Value          |
|------------------------|----------------|
| Solvent                | DMSO           |
| Spectrometer Frequency | 500.36         |
| Pulse Sequence         | zg30           |
| Number of Scans        | 16             |
| Temperature            | 299.9          |
| Nucleus                | <sup>1</sup> H |



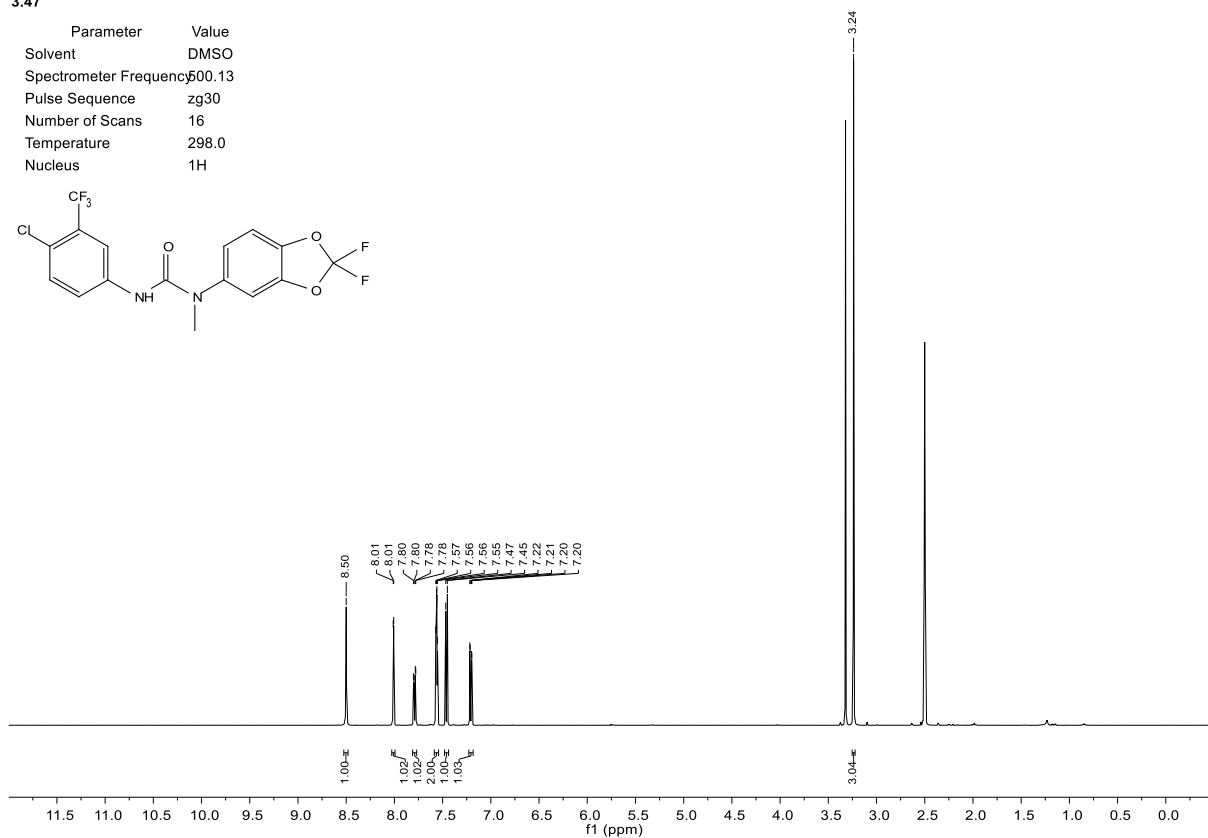
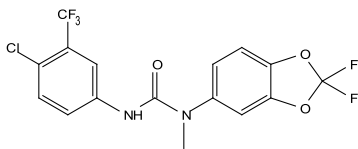
3.46

| Parameter              | Value           |
|------------------------|-----------------|
| Solvent                | DMSO            |
| Spectrometer Frequency | 125.82          |
| Pulse Sequence         | zgpg30          |
| Number of Scans        | 256             |
| Temperature            | 299.9           |
| Nucleus                | <sup>13</sup> C |



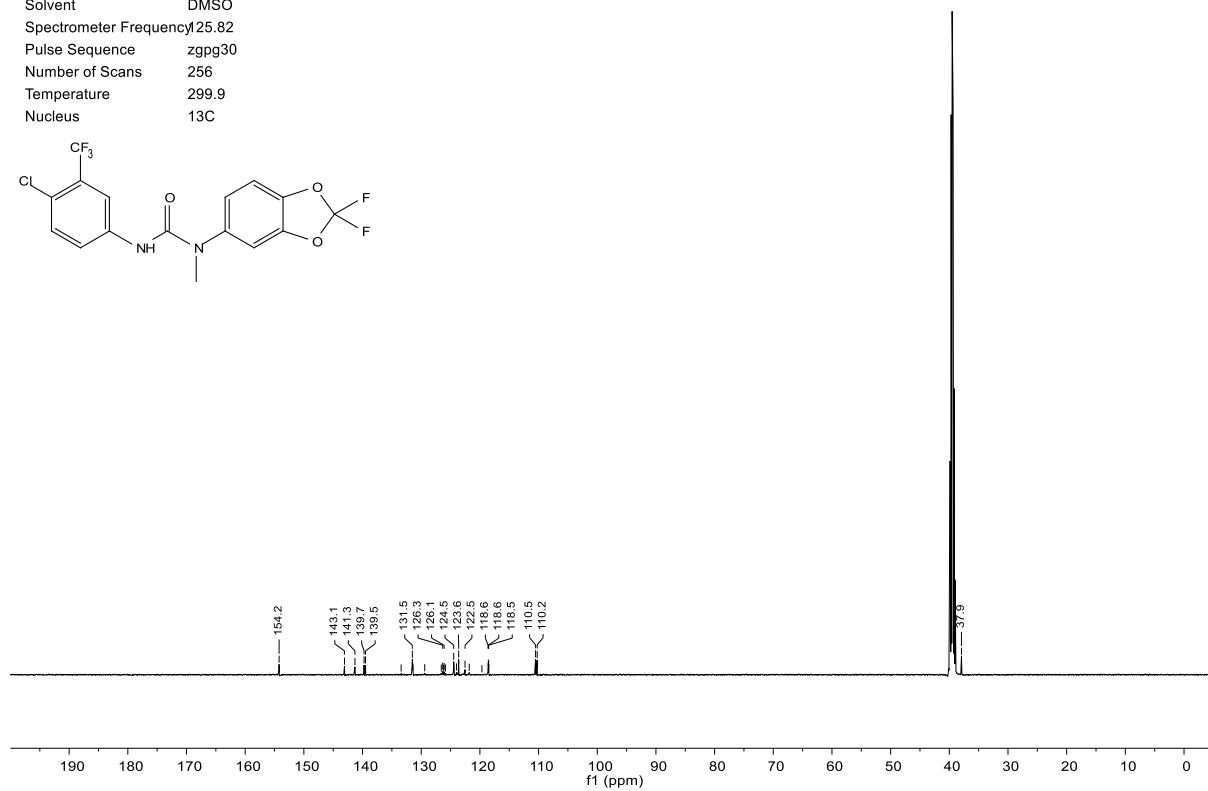
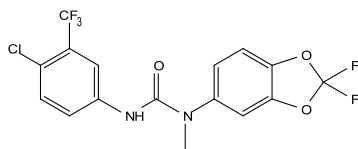
3.47

| Parameter              | Value          |
|------------------------|----------------|
| Solvent                | DMSO           |
| Spectrometer Frequency | 500.13         |
| Pulse Sequence         | zg30           |
| Number of Scans        | 16             |
| Temperature            | 298.0          |
| Nucleus                | <sup>1</sup> H |



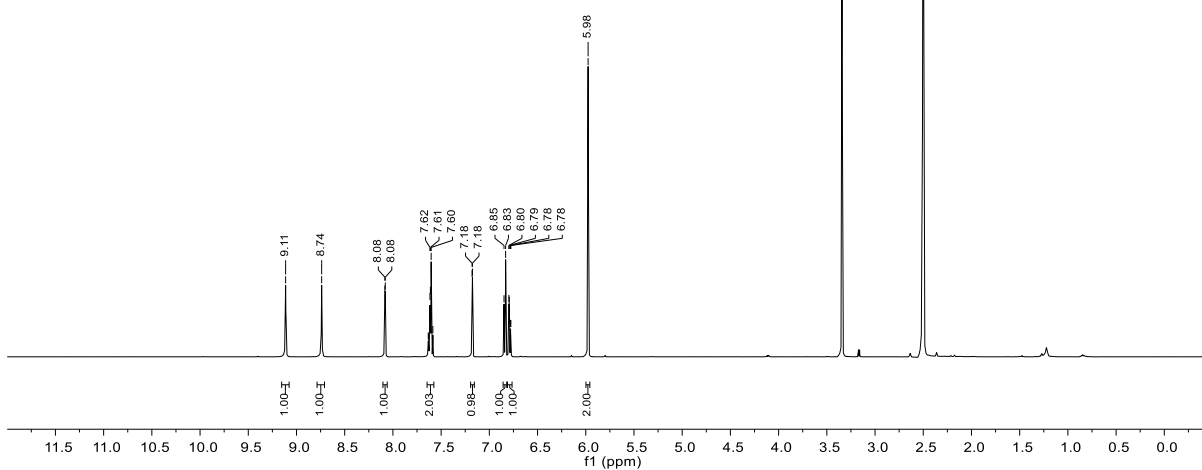
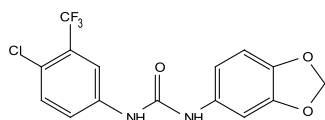
3.47

| Parameter              | Value           |
|------------------------|-----------------|
| Solvent                | DMSO            |
| Spectrometer Frequency | 125.82          |
| Pulse Sequence         | zgpg30          |
| Number of Scans        | 256             |
| Temperature            | 299.9           |
| Nucleus                | <sup>13</sup> C |



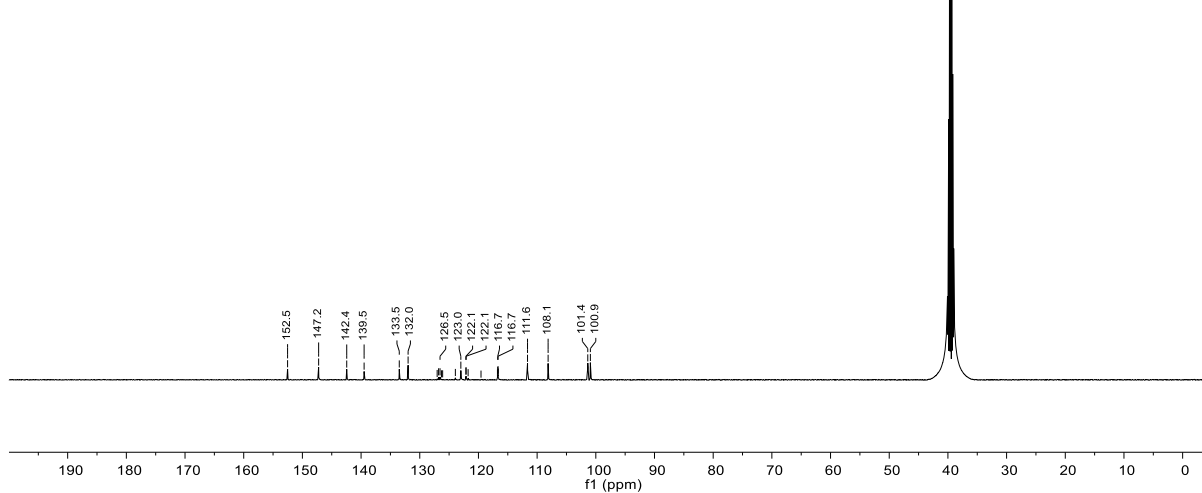
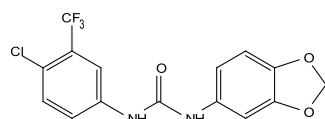
3.48

| Parameter              | Value          |
|------------------------|----------------|
| Solvent                | DMSO           |
| Spectrometer Frequency | 500.36         |
| Pulse Sequence         | zg30           |
| Number of Scans        | 16             |
| Temperature            | 300.0          |
| Nucleus                | <sup>1</sup> H |



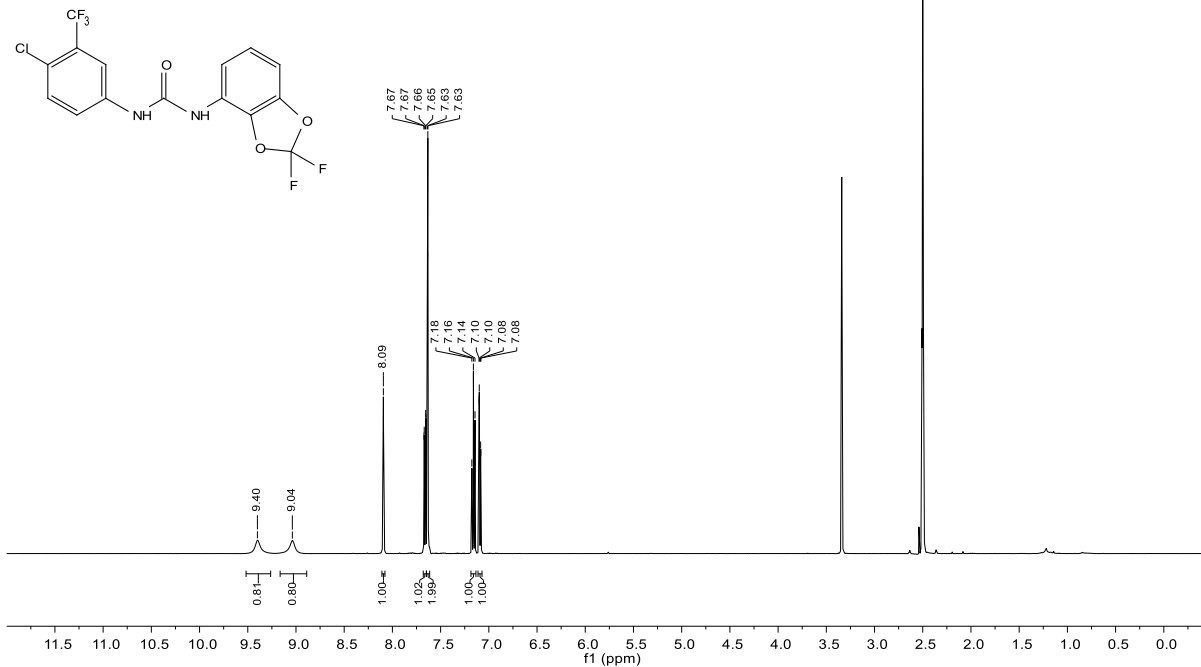
3.48

| Parameter              | Value           |
|------------------------|-----------------|
| Solvent                | DMSO            |
| Spectrometer Frequency | 125.82          |
| Pulse Sequence         | zgpg30          |
| Number of Scans        | 512             |
| Temperature            | 300.0           |
| Nucleus                | <sup>13</sup> C |



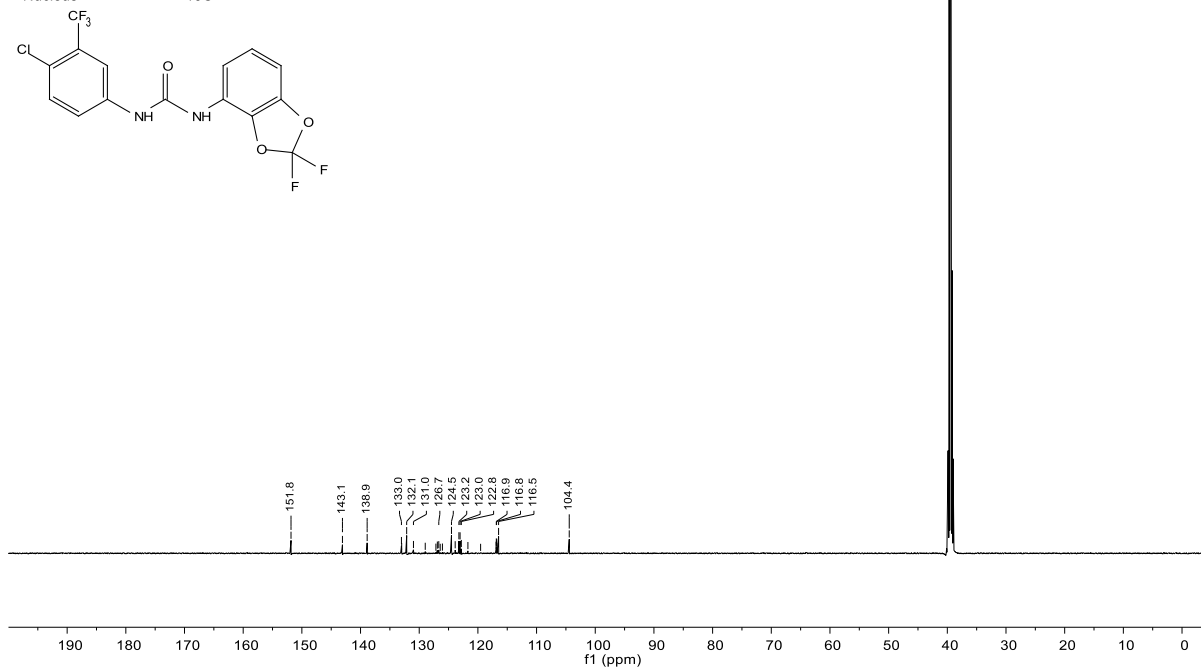
## 3.49

| Parameter              | Value          |
|------------------------|----------------|
| Solvent                | DMSO           |
| Spectrometer Frequency | 500.36         |
| Pulse Sequence         | zg30           |
| Number of Scans        | 16             |
| Temperature            | 299.9          |
| Nucleus                | <sup>1</sup> H |



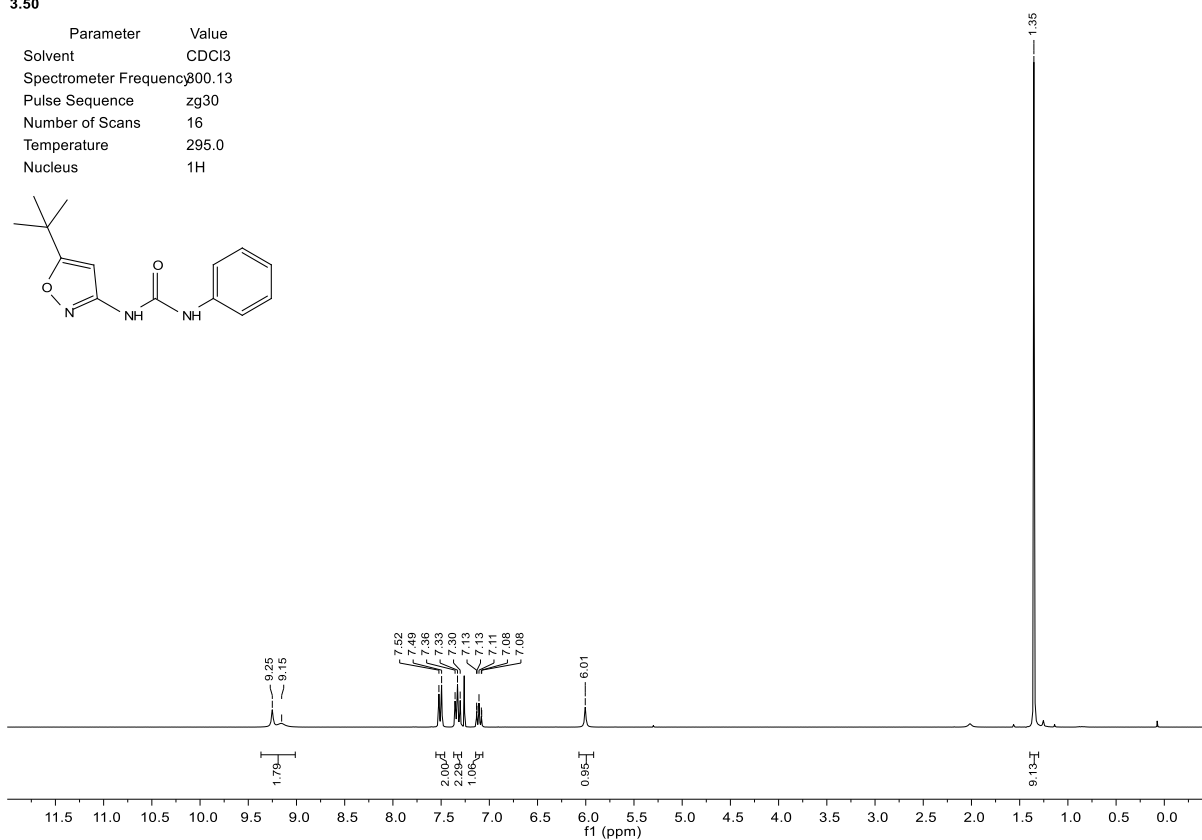
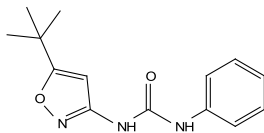
## 3.49

| Parameter              | Value           |
|------------------------|-----------------|
| Solvent                | DMSO            |
| Spectrometer Frequency | 125.82          |
| Pulse Sequence         | zgpg30          |
| Number of Scans        | 256             |
| Temperature            | 299.9           |
| Nucleus                | <sup>13</sup> C |



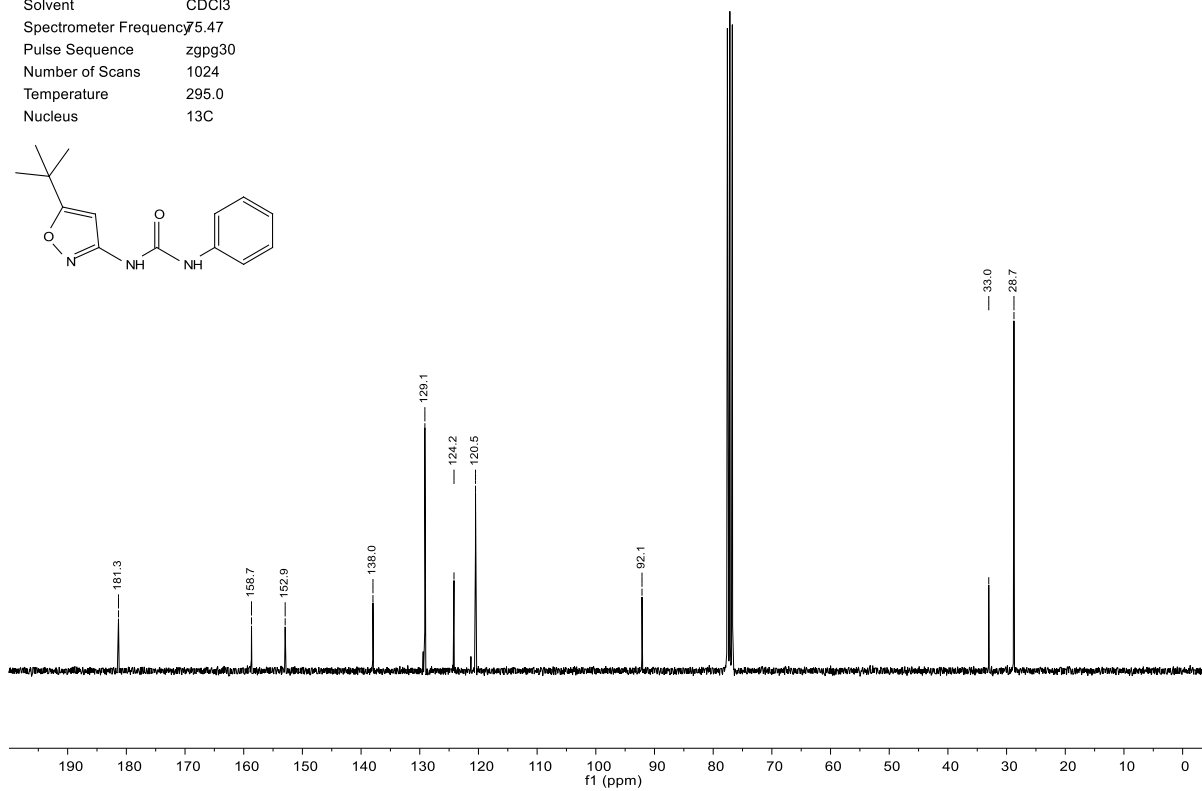
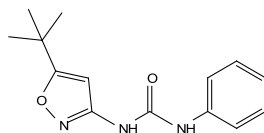
3.50

| Parameter              | Value             |
|------------------------|-------------------|
| Solvent                | CDCl <sub>3</sub> |
| Spectrometer Frequency | 800.13            |
| Pulse Sequence         | zg30              |
| Number of Scans        | 16                |
| Temperature            | 295.0             |
| Nucleus                | <sup>1</sup> H    |



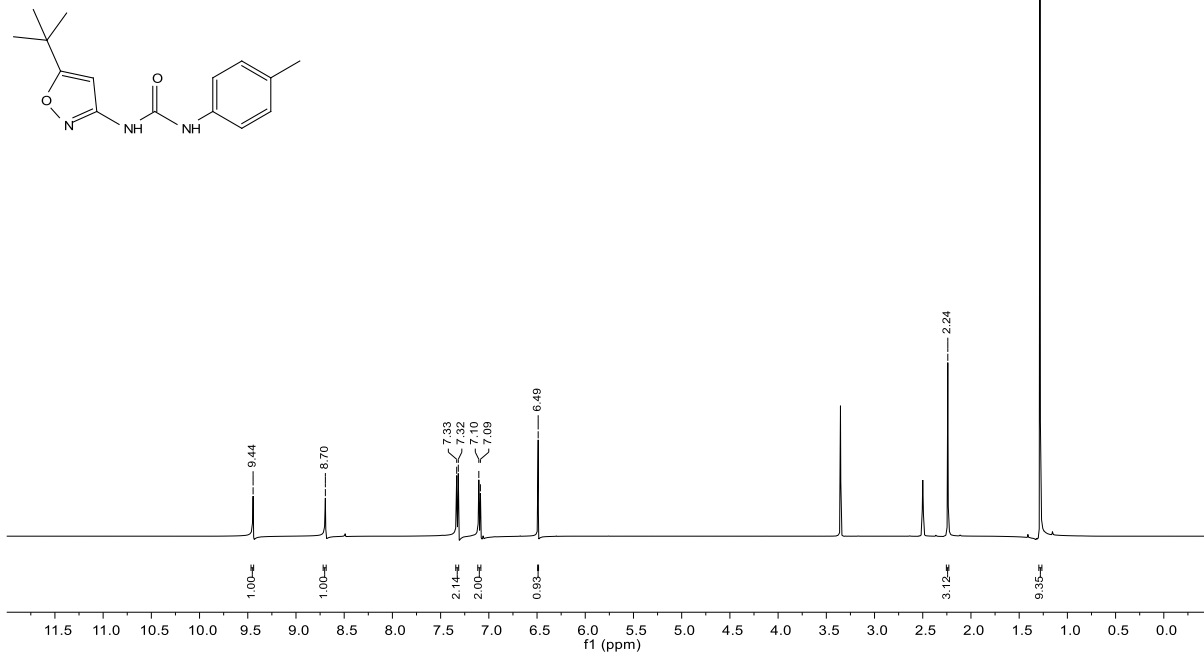
3.50

| Parameter              | Value             |
|------------------------|-------------------|
| Solvent                | CDCl <sub>3</sub> |
| Spectrometer Frequency | 75.47             |
| Pulse Sequence         | zpgg30            |
| Number of Scans        | 1024              |
| Temperature            | 295.0             |
| Nucleus                | <sup>13</sup> C   |



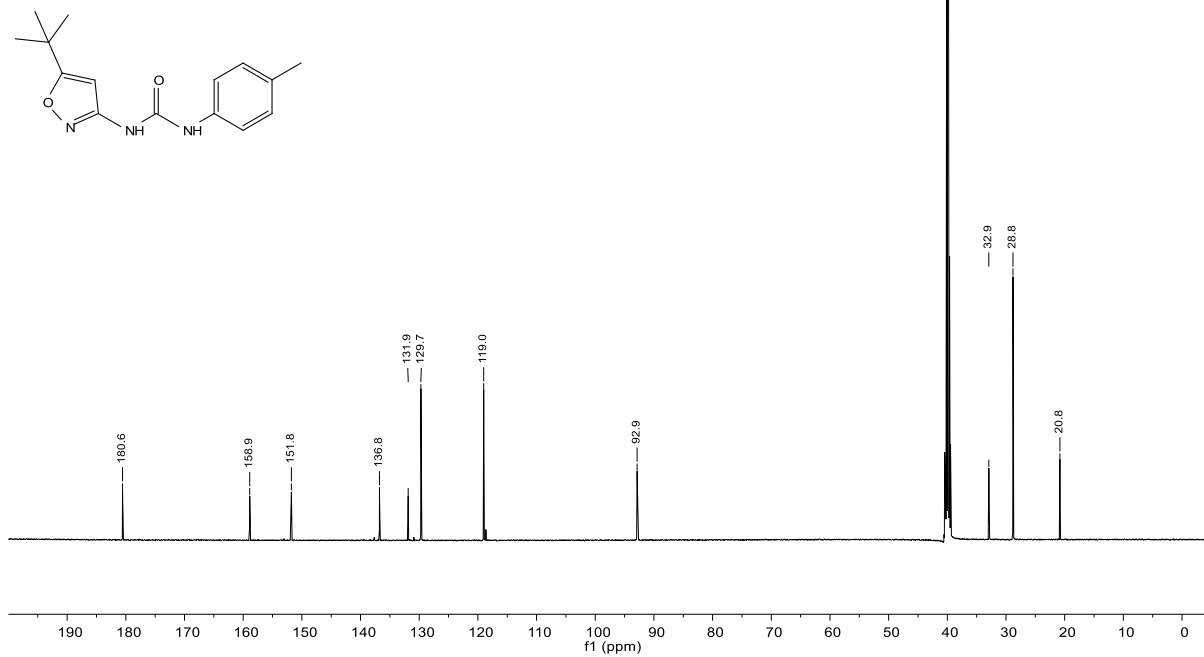
3.51

| Parameter              | Value        |
|------------------------|--------------|
| Solvent                | DMSO         |
| Spectrometer Frequency | 500.36       |
| Pulse Sequence         | zg30         |
| Number of Scans        | 16           |
| Temperature            | 299.8        |
| Nucleus                | $^1\text{H}$ |



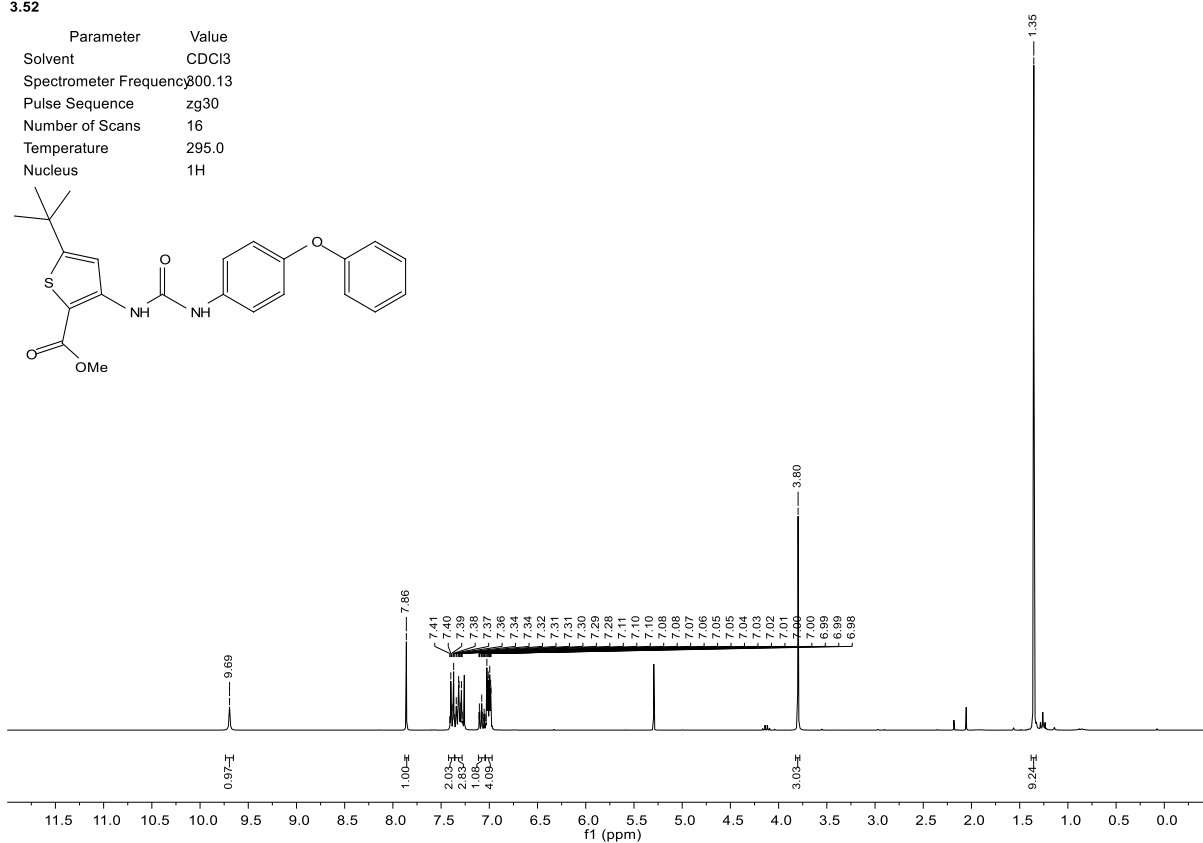
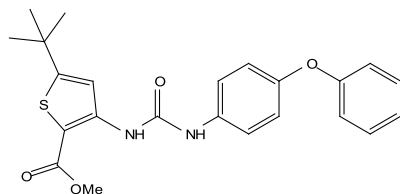
3.51

| Parameter              | Value           |
|------------------------|-----------------|
| Solvent                | DMSO            |
| Spectrometer Frequency | 125.82          |
| Pulse Sequence         | zgpg30          |
| Number of Scans        | 256             |
| Temperature            | 299.9           |
| Nucleus                | $^{13}\text{C}$ |



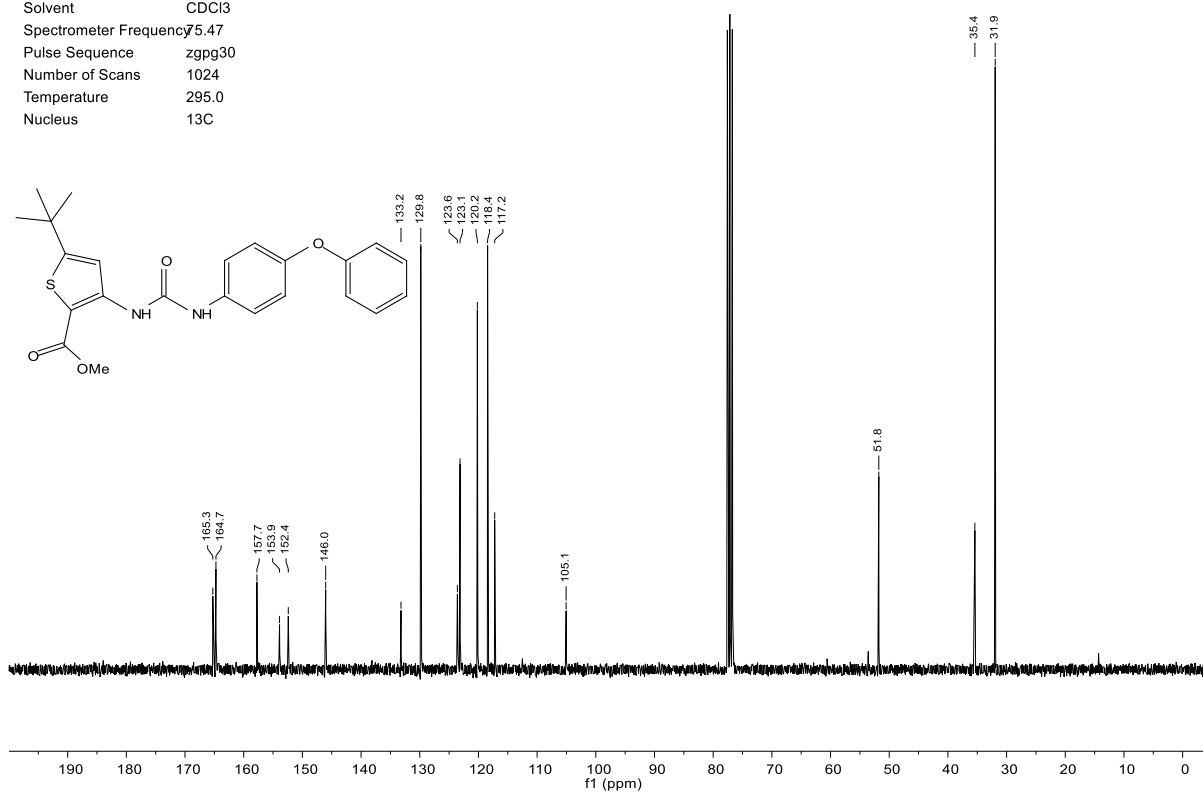
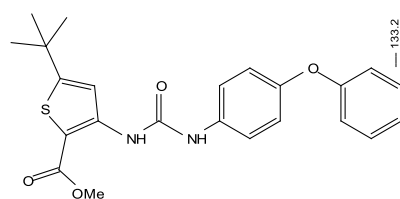
3.52

| Parameter              | Value             |
|------------------------|-------------------|
| Solvent                | CDCl <sub>3</sub> |
| Spectrometer Frequency | 800.13            |
| Pulse Sequence         | zg30              |
| Number of Scans        | 16                |
| Temperature            | 295.0             |
| Nucleus                | <sup>1</sup> H    |



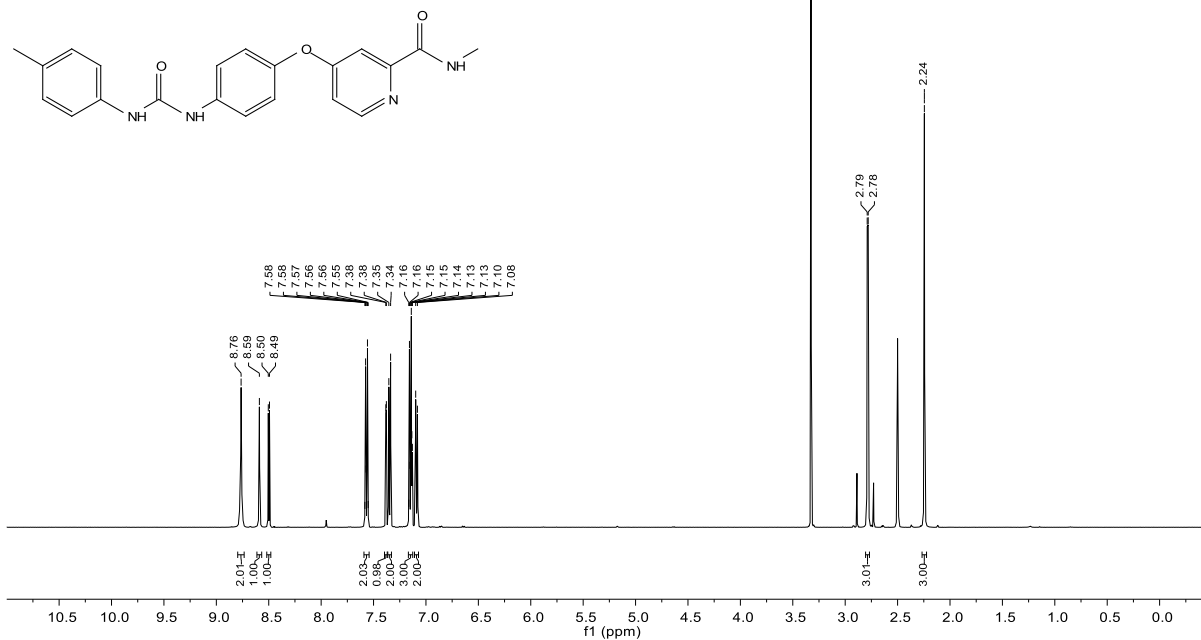
3.52

| Parameter              | Value             |
|------------------------|-------------------|
| Solvent                | CDCl <sub>3</sub> |
| Spectrometer Frequency | 75.47             |
| Pulse Sequence         | zpgg30            |
| Number of Scans        | 1024              |
| Temperature            | 295.0             |
| Nucleus                | <sup>13</sup> C   |



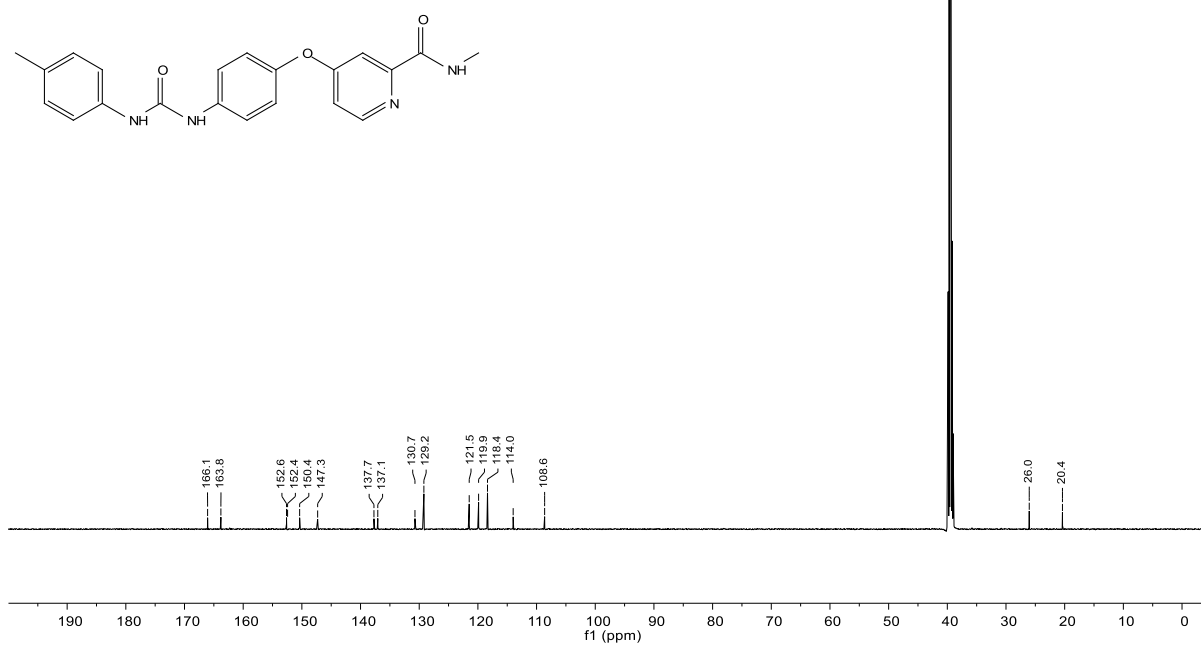
## 3.53

| Parameter              | Value          |
|------------------------|----------------|
| Solvent                | DMSO           |
| Spectrometer Frequency | 500.13         |
| Pulse Sequence         | zg30           |
| Number of Scans        | 16             |
| Temperature            | 298.0          |
| Nucleus                | <sup>1</sup> H |



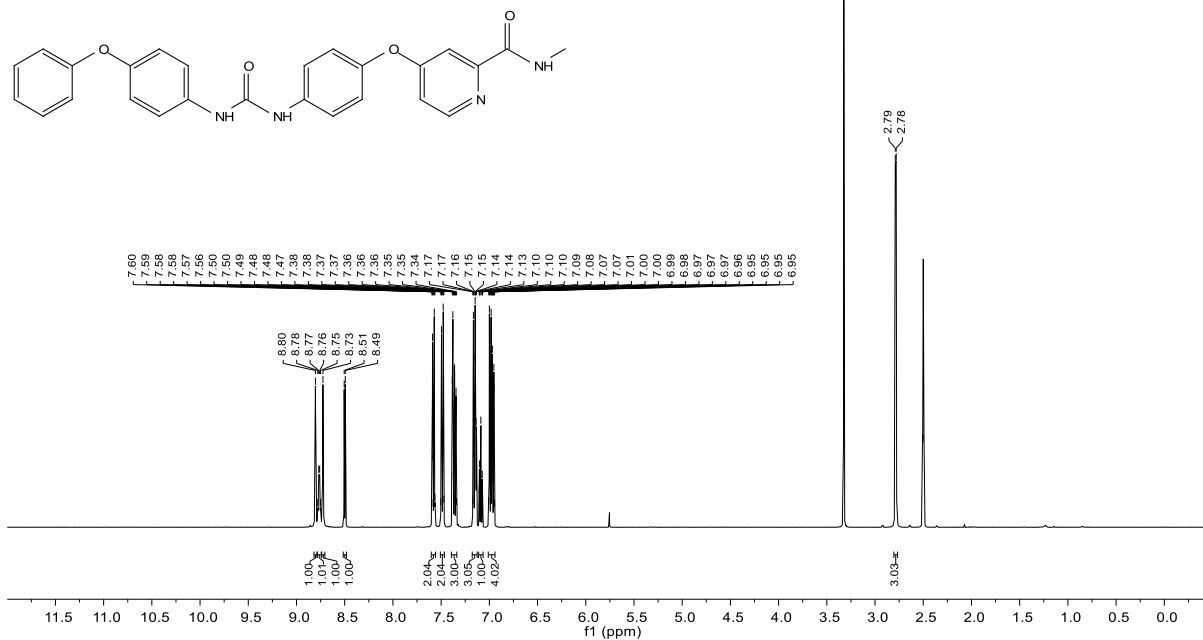
## 3.53

| Parameter              | Value           |
|------------------------|-----------------|
| Solvent                | DMSO            |
| Spectrometer Frequency | 125.82          |
| Pulse Sequence         | zgpg30          |
| Number of Scans        | 256             |
| Temperature            | 300.0           |
| Nucleus                | <sup>13</sup> C |



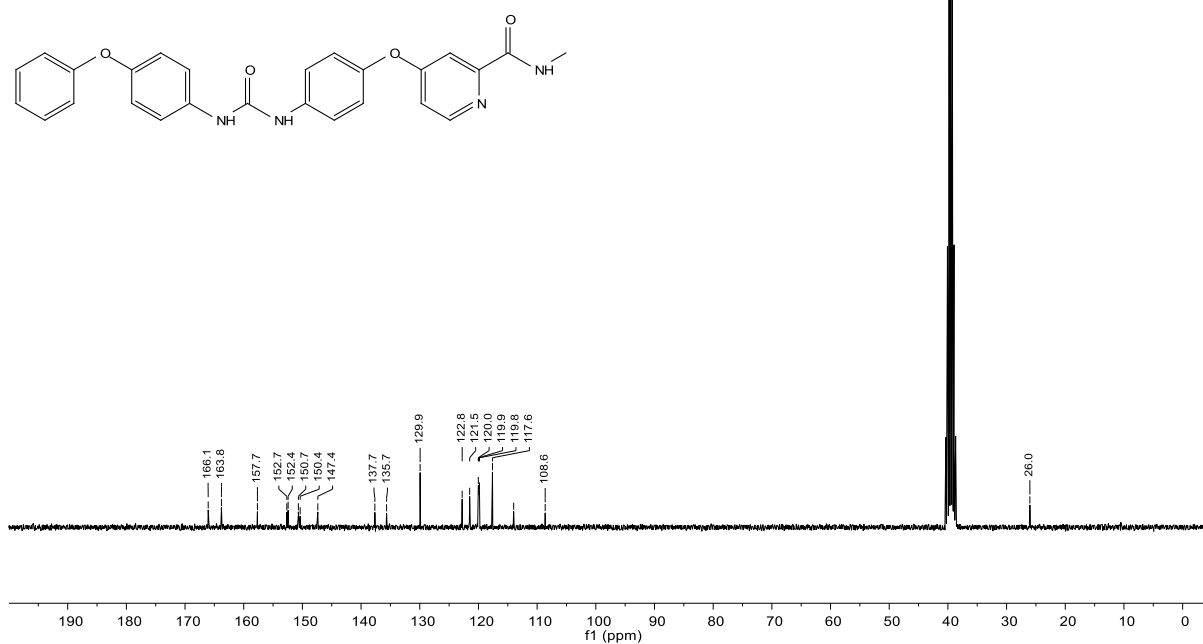
3.54

| Parameter              | Value          |
|------------------------|----------------|
| Solvent                | DMSO           |
| Spectrometer Frequency | 500.13         |
| Pulse Sequence         | zg30           |
| Number of Scans        | 16             |
| Temperature            | 298.0          |
| Nucleus                | <sup>1</sup> H |



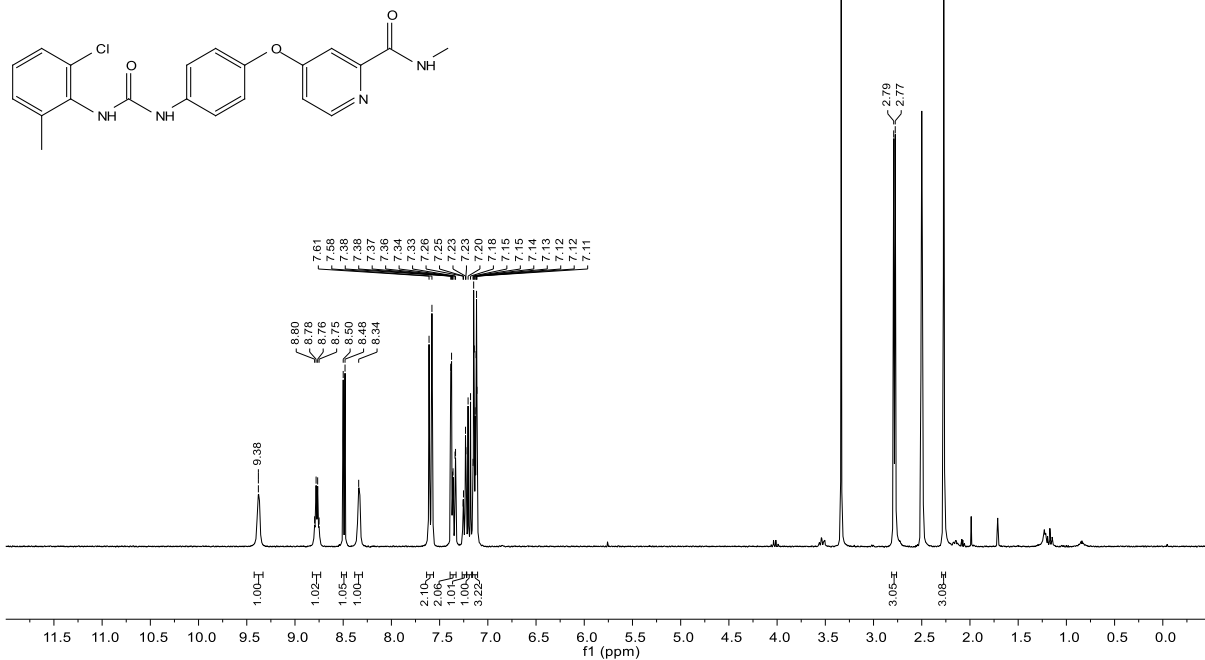
3.54

| Parameter              | Value           |
|------------------------|-----------------|
| Solvent                | DMSO            |
| Spectrometer Frequency | 75.47           |
| Pulse Sequence         | zgpg30          |
| Number of Scans        | 1024            |
| Temperature            | 295.0           |
| Nucleus                | <sup>13</sup> C |



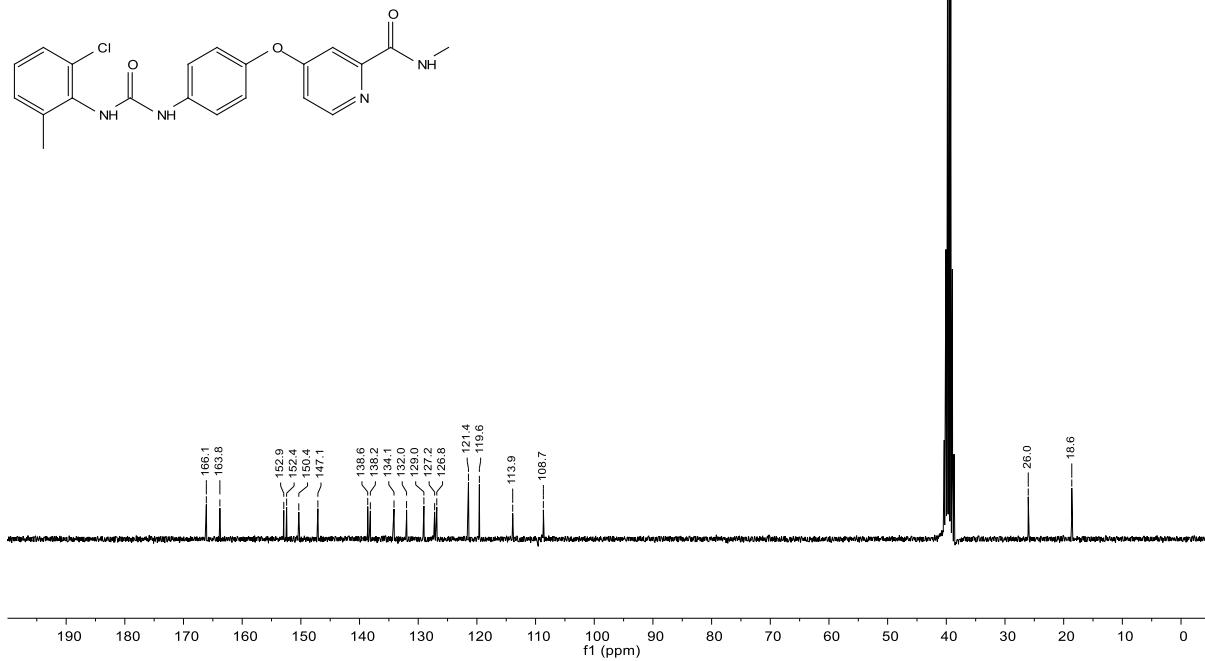
3.55

| Parameter              | Value          |
|------------------------|----------------|
| Solvent                | DMSO           |
| Spectrometer Frequency | 800.13         |
| Pulse Sequence         | zg30           |
| Number of Scans        | 16             |
| Temperature            | 295.0          |
| Nucleus                | <sup>1</sup> H |



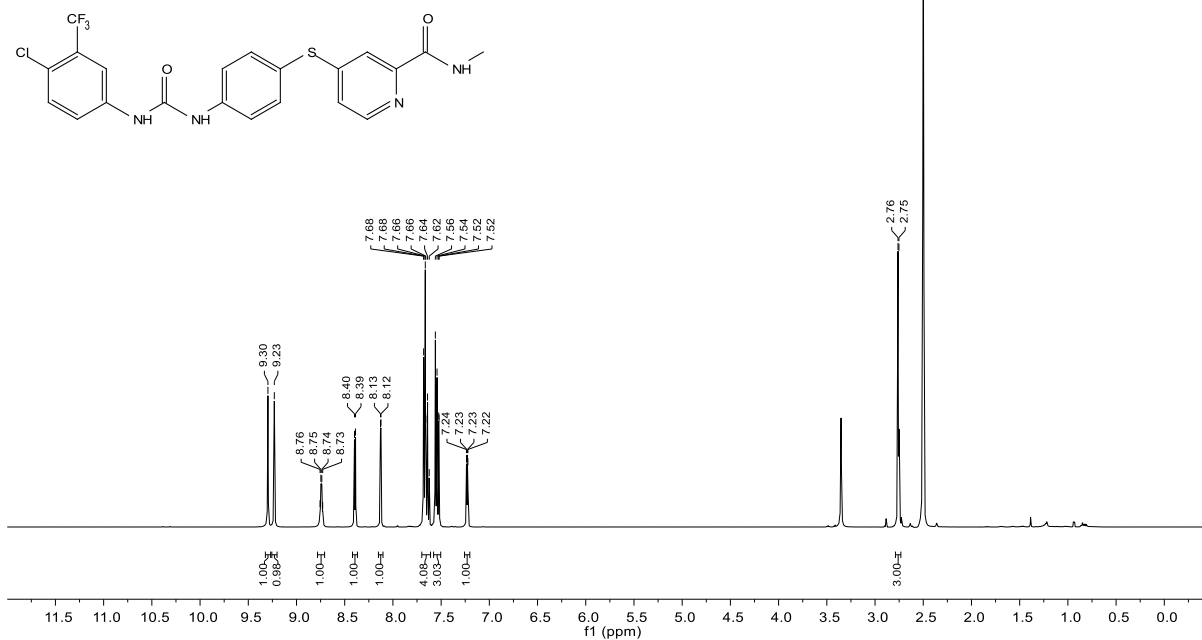
3.55

| Parameter              | Value           |
|------------------------|-----------------|
| Solvent                | DMSO            |
| Spectrometer Frequency | 75.47           |
| Pulse Sequence         | zgpg30          |
| Number of Scans        | 1024            |
| Temperature            | 295.0           |
| Nucleus                | <sup>13</sup> C |



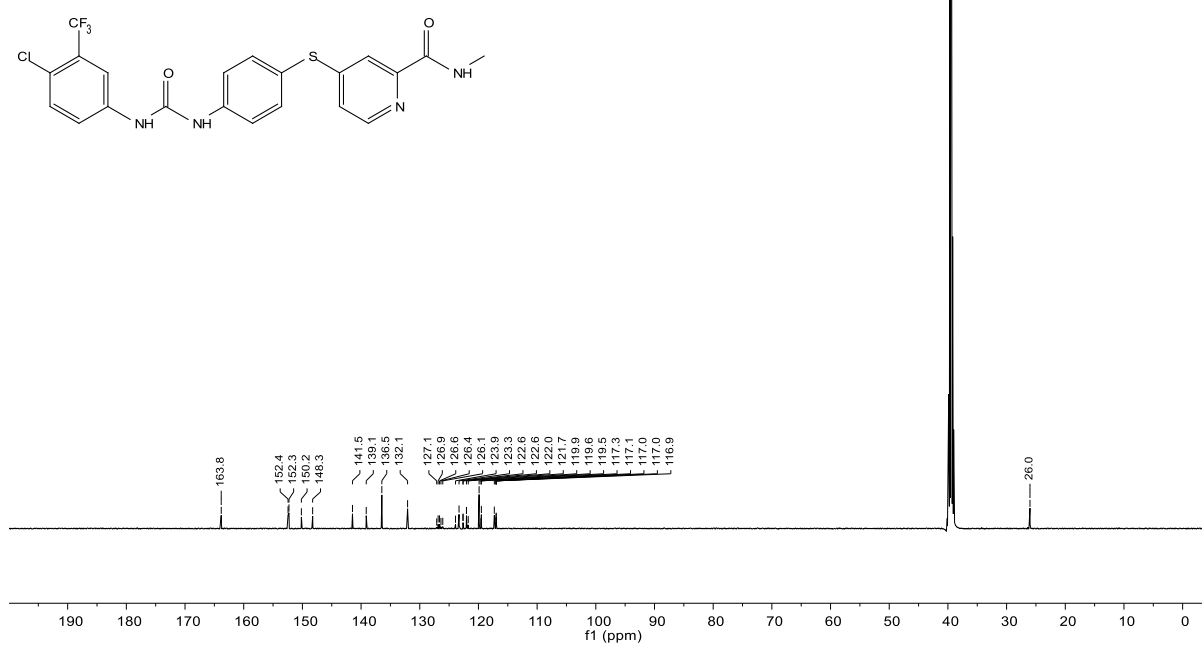
3.56

| Parameter              | Value          |
|------------------------|----------------|
| Solvent                | DMSO           |
| Spectrometer Frequency | 500.36         |
| Pulse Sequence         | zg30           |
| Number of Scans        | 16             |
| Temperature            | 299.9          |
| Nucleus                | <sup>1</sup> H |



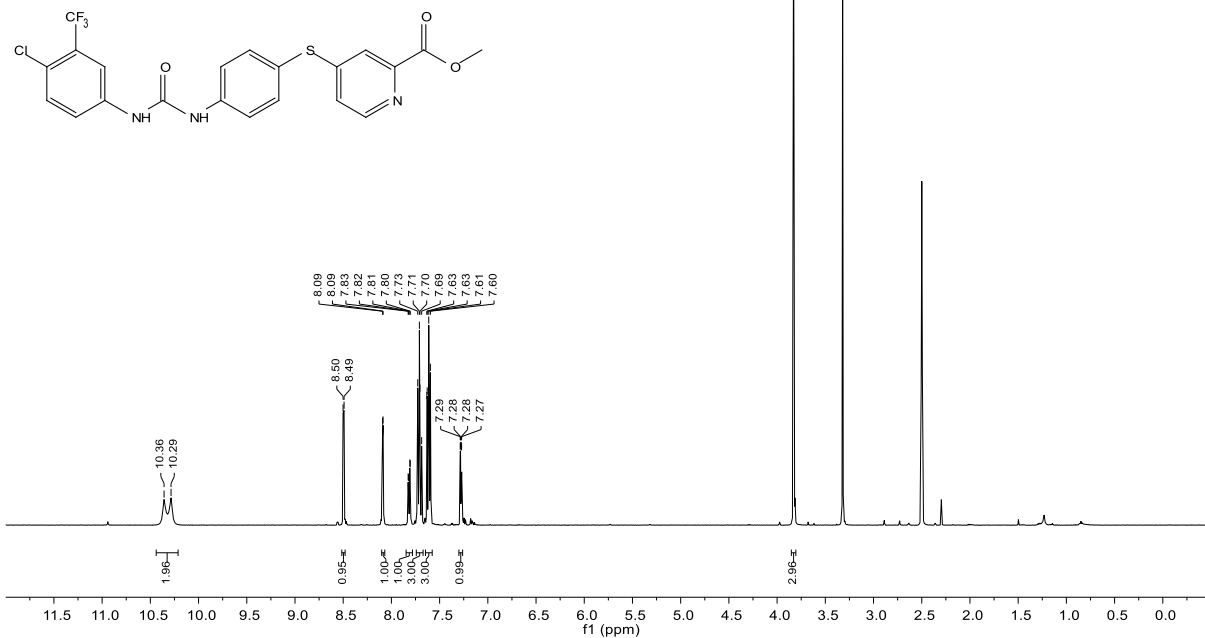
3.56

| Parameter              | Value           |
|------------------------|-----------------|
| Solvent                | DMSO            |
| Spectrometer Frequency | 125.82          |
| Pulse Sequence         | zgpg30          |
| Number of Scans        | 256             |
| Temperature            | 299.9           |
| Nucleus                | <sup>13</sup> C |



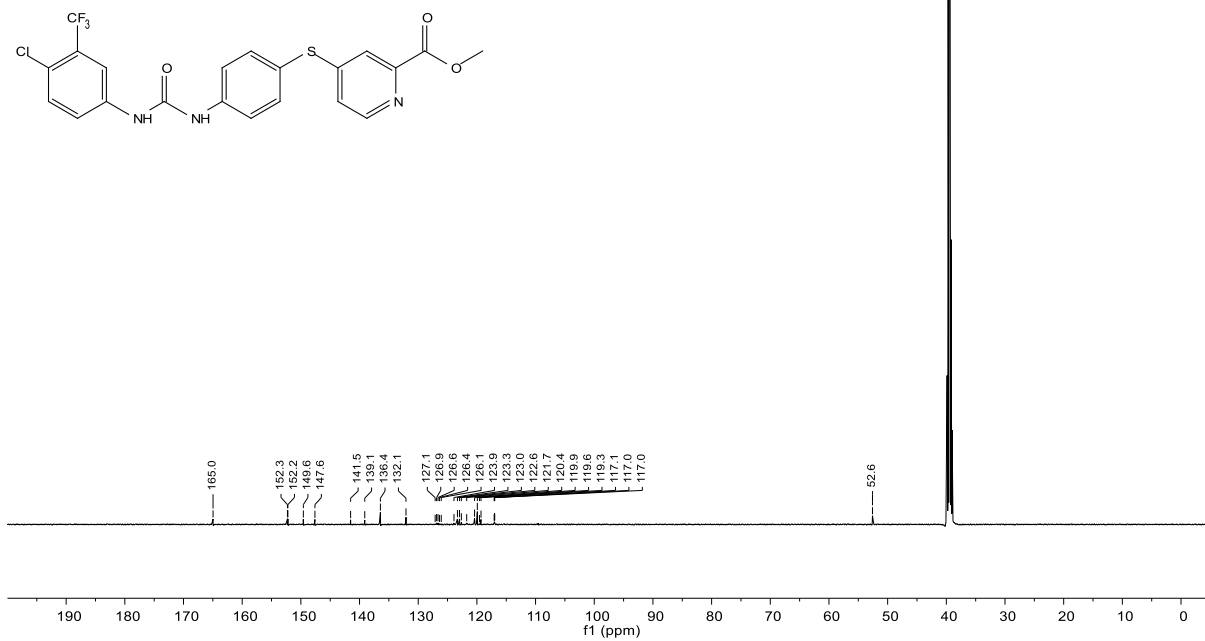
3.57

| Parameter              | Value          |
|------------------------|----------------|
| Solvent                | DMSO           |
| Spectrometer Frequency | 500.13         |
| Pulse Sequence         | zg30           |
| Number of Scans        | 16             |
| Temperature            | 298.0          |
| Nucleus                | <sup>1</sup> H |



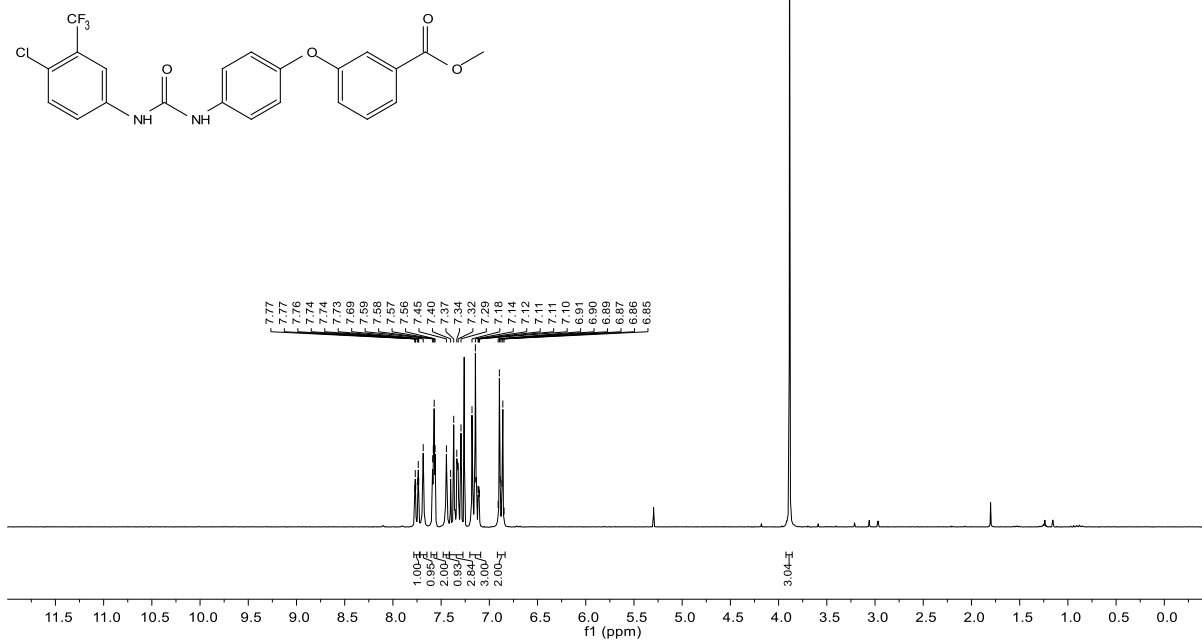
3.57

| Parameter              | Value           |
|------------------------|-----------------|
| Solvent                | DMSO            |
| Spectrometer Frequency | 125.82          |
| Pulse Sequence         | zgpg30          |
| Number of Scans        | 256             |
| Temperature            | 300.0           |
| Nucleus                | <sup>13</sup> C |



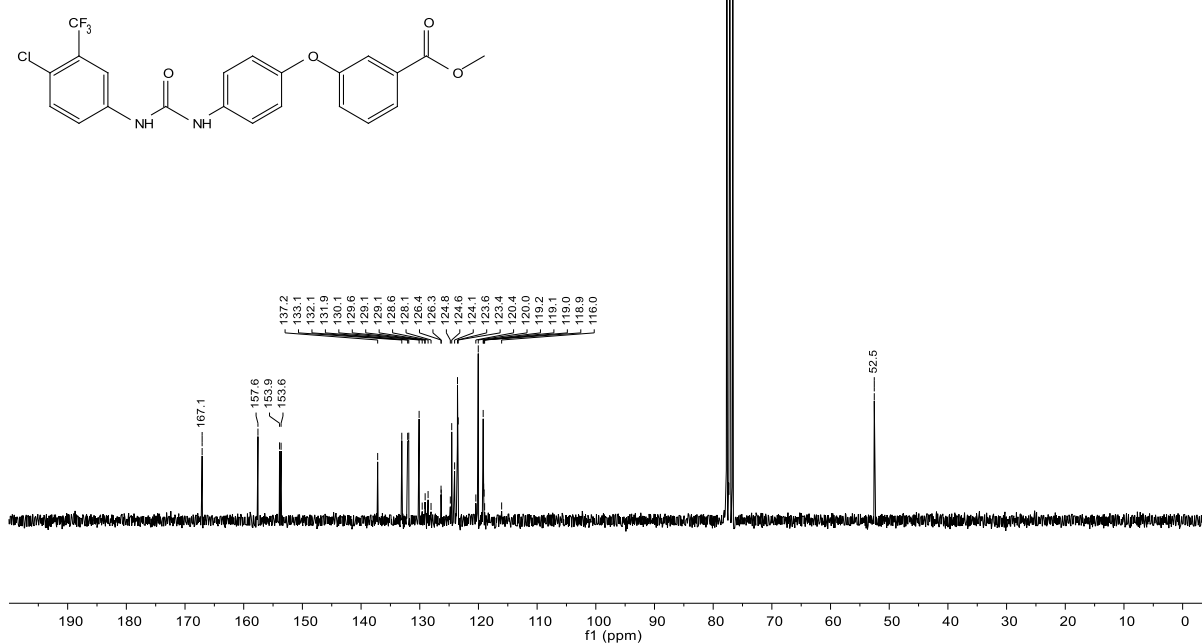
3.58

| Parameter              | Value             |
|------------------------|-------------------|
| Solvent                | CDCl <sub>3</sub> |
| Spectrometer Frequency | 250.13            |
| Pulse Sequence         | zg30              |
| Number of Scans        | 16                |
| Temperature            | 300.0             |
| Nucleus                | <sup>1</sup> H    |



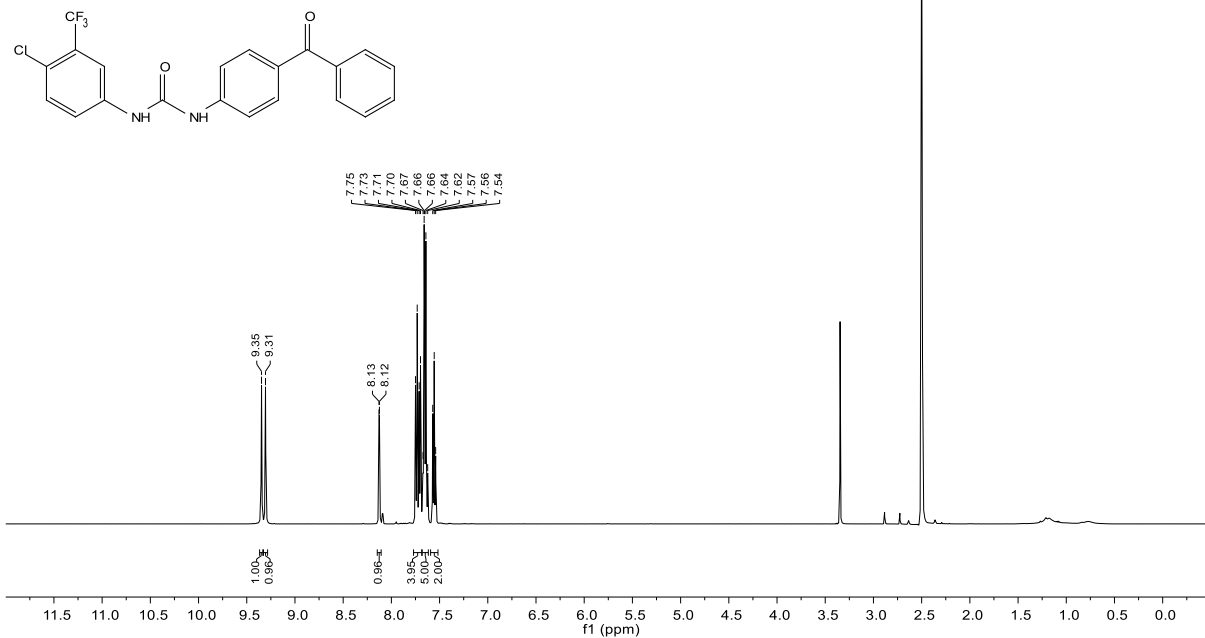
3.58

| Parameter              | Value             |
|------------------------|-------------------|
| Solvent                | CDCl <sub>3</sub> |
| Spectrometer Frequency | 62.90             |
| Pulse Sequence         | zpgg30            |
| Number of Scans        | 1024              |
| Temperature            | 300.0             |
| Nucleus                | <sup>13</sup> C   |



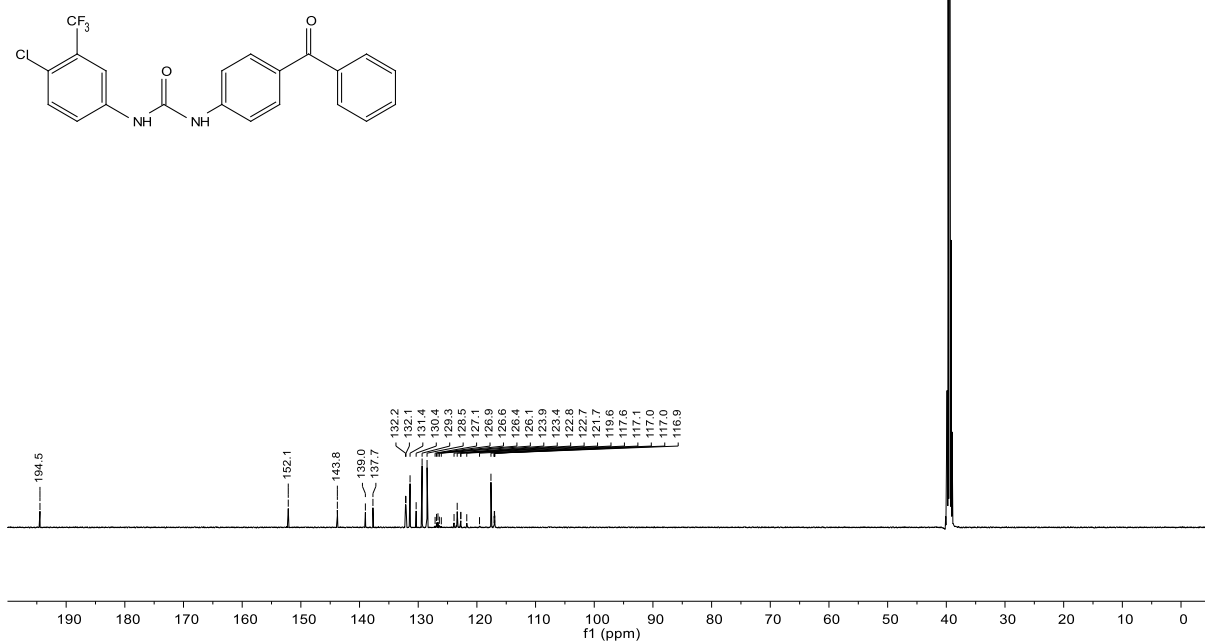
3.59

| Parameter              | Value          |
|------------------------|----------------|
| Solvent                | DMSO           |
| Spectrometer Frequency | 500.36         |
| Pulse Sequence         | zg30           |
| Number of Scans        | 16             |
| Temperature            | 299.9          |
| Nucleus                | <sup>1</sup> H |



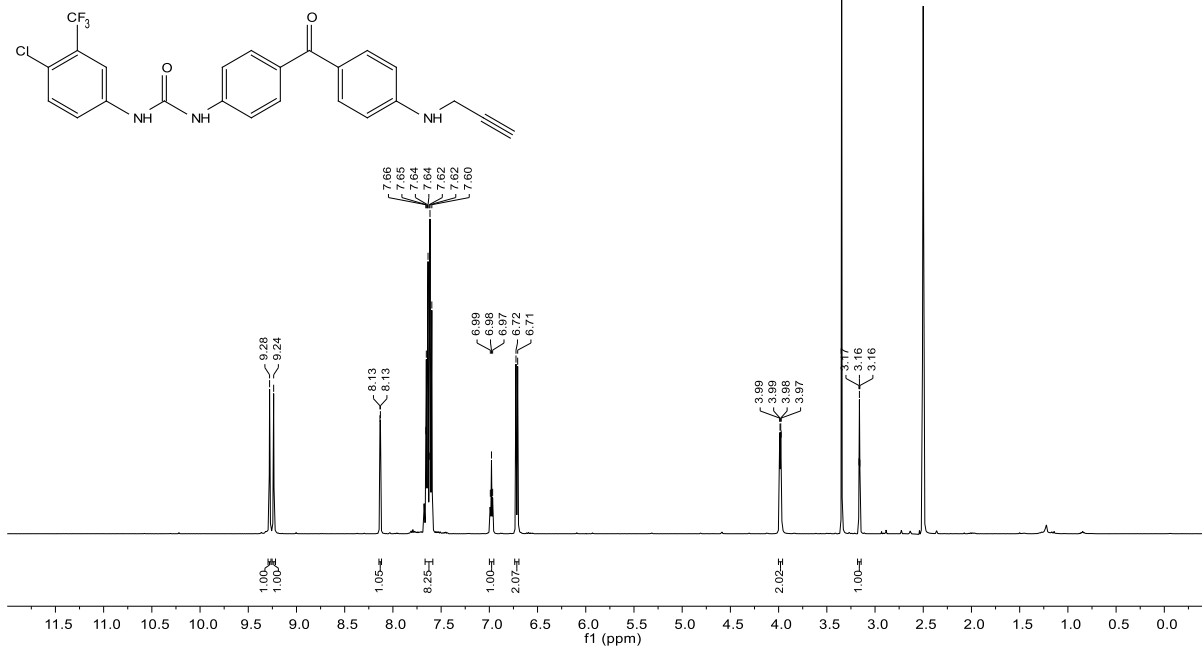
3.59

| Parameter              | Value           |
|------------------------|-----------------|
| Solvent                | DMSO            |
| Spectrometer Frequency | 125.82          |
| Pulse Sequence         | zgpg30          |
| Number of Scans        | 256             |
| Temperature            | 299.8           |
| Nucleus                | <sup>13</sup> C |



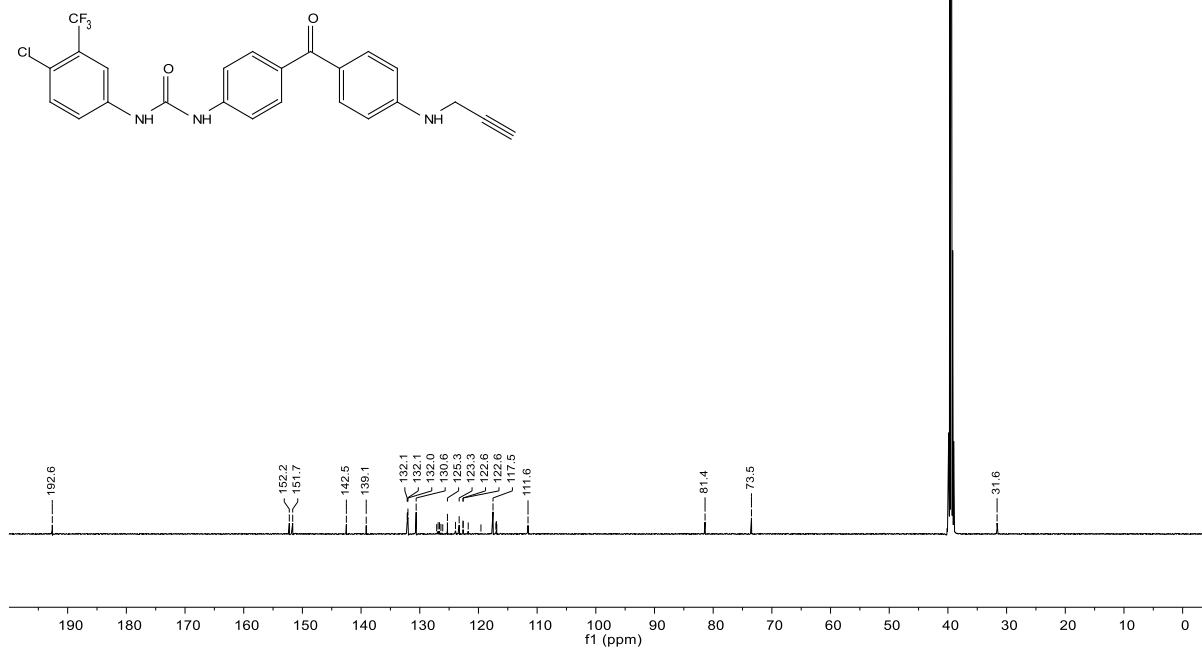
3.60

| Parameter              | Value          |
|------------------------|----------------|
| Solvent                | DMSO           |
| Spectrometer Frequency | 500.36         |
| Pulse Sequence         | zg30           |
| Number of Scans        | 16             |
| Temperature            | 299.9          |
| Nucleus                | <sup>1</sup> H |



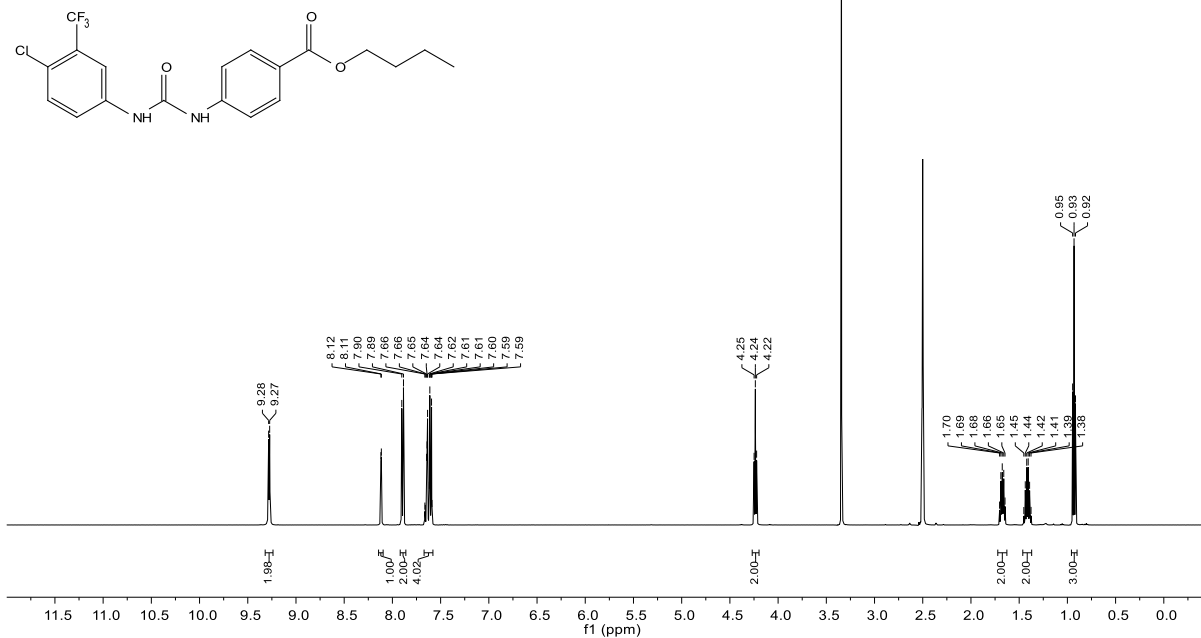
3.60

| Parameter              | Value           |
|------------------------|-----------------|
| Solvent                | DMSO            |
| Spectrometer Frequency | 125.82          |
| Pulse Sequence         | zgpg30          |
| Number of Scans        | 256             |
| Temperature            | 299.8           |
| Nucleus                | <sup>13</sup> C |



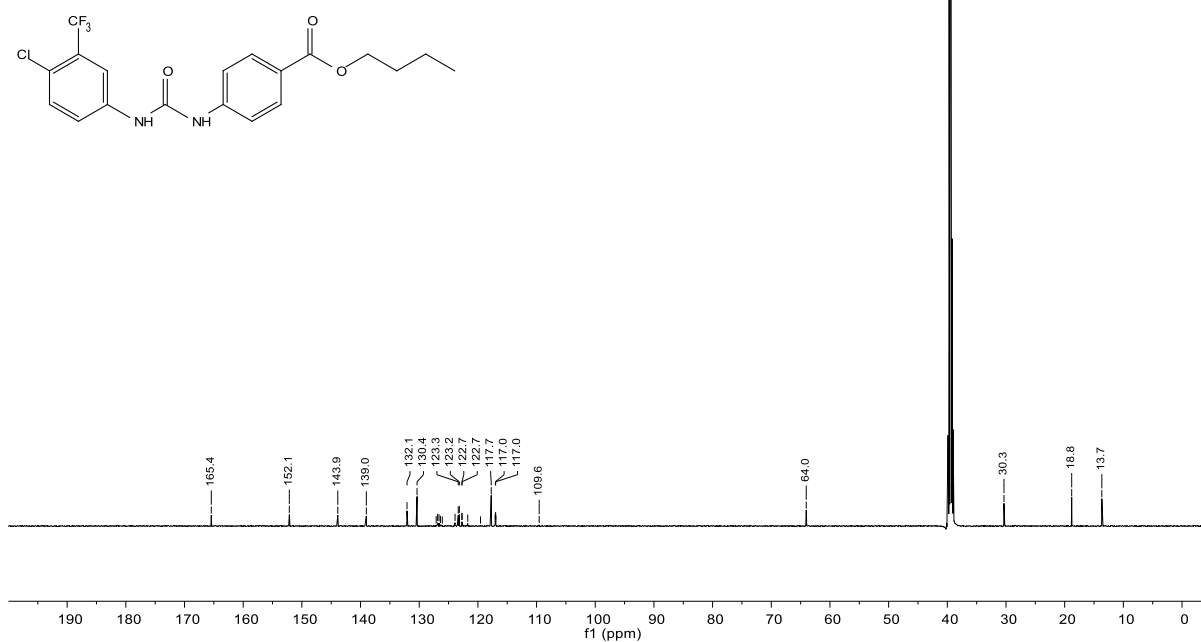
## 3.61

| Parameter              | Value        |
|------------------------|--------------|
| Solvent                | DMSO         |
| Spectrometer Frequency | 500.36       |
| Pulse Sequence         | zg30         |
| Number of Scans        | 16           |
| Temperature            | 299.9        |
| Nucleus                | $^1\text{H}$ |



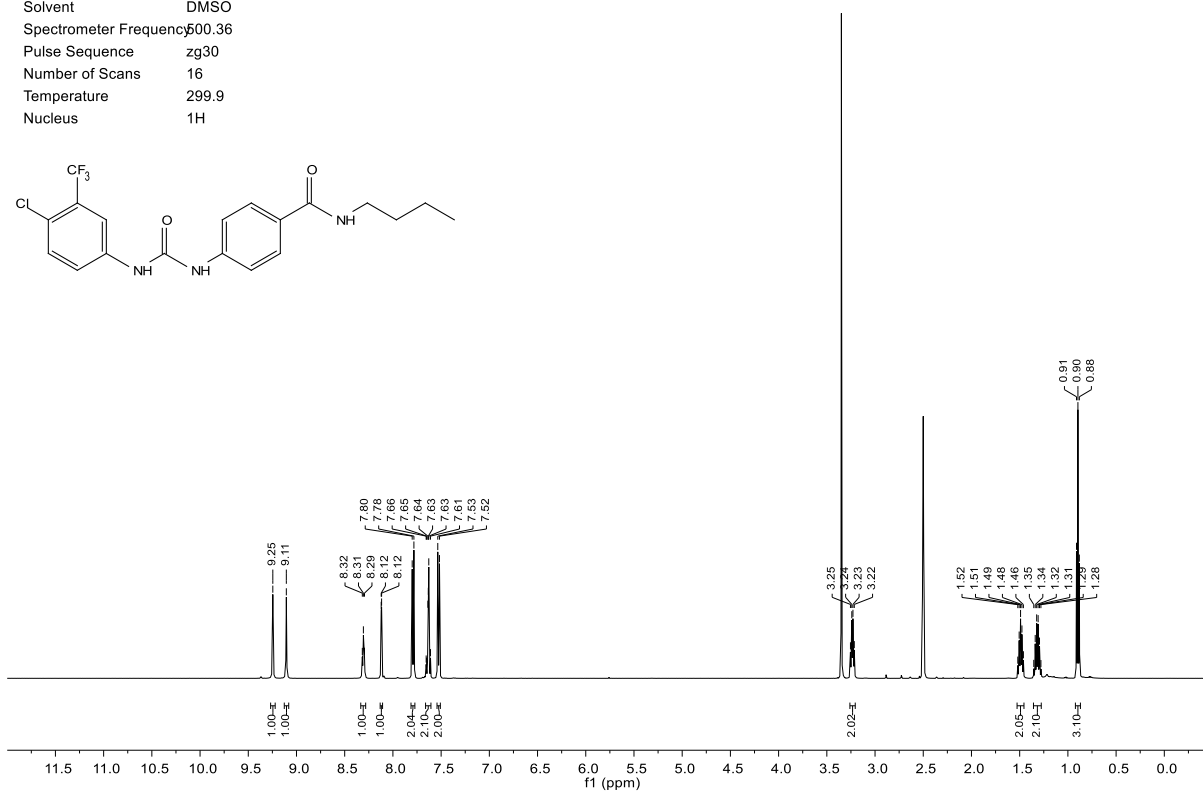
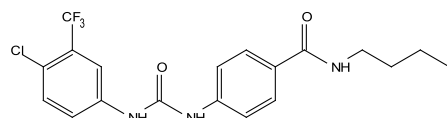
## 3.61

| Parameter              | Value           |
|------------------------|-----------------|
| Solvent                | DMSO            |
| Spectrometer Frequency | 125.82          |
| Pulse Sequence         | zgpg30          |
| Number of Scans        | 256             |
| Temperature            | 299.9           |
| Nucleus                | $^{13}\text{C}$ |



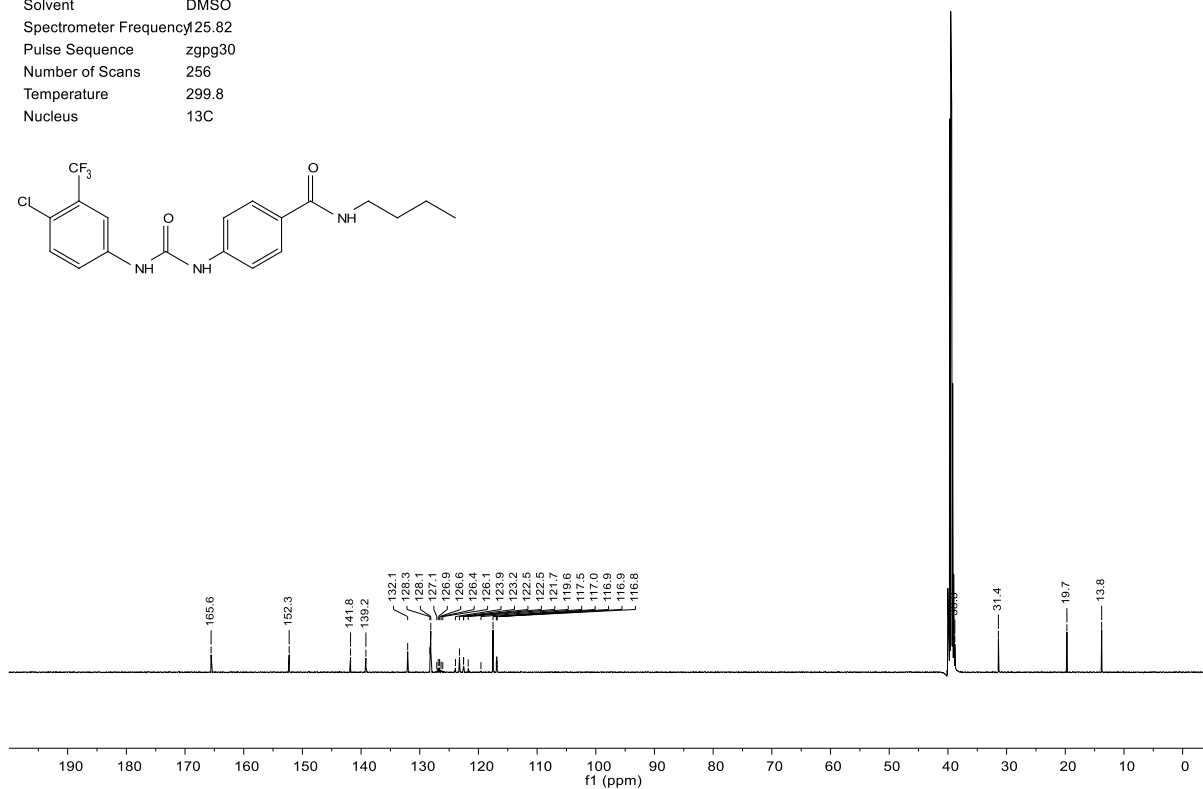
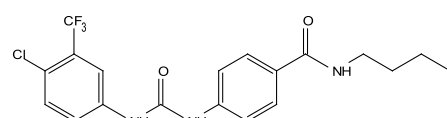
3.62

| Parameter              | Value          |
|------------------------|----------------|
| Solvent                | DMSO           |
| Spectrometer Frequency | 500.36         |
| Pulse Sequence         | zg30           |
| Number of Scans        | 16             |
| Temperature            | 299.9          |
| Nucleus                | <sup>1</sup> H |



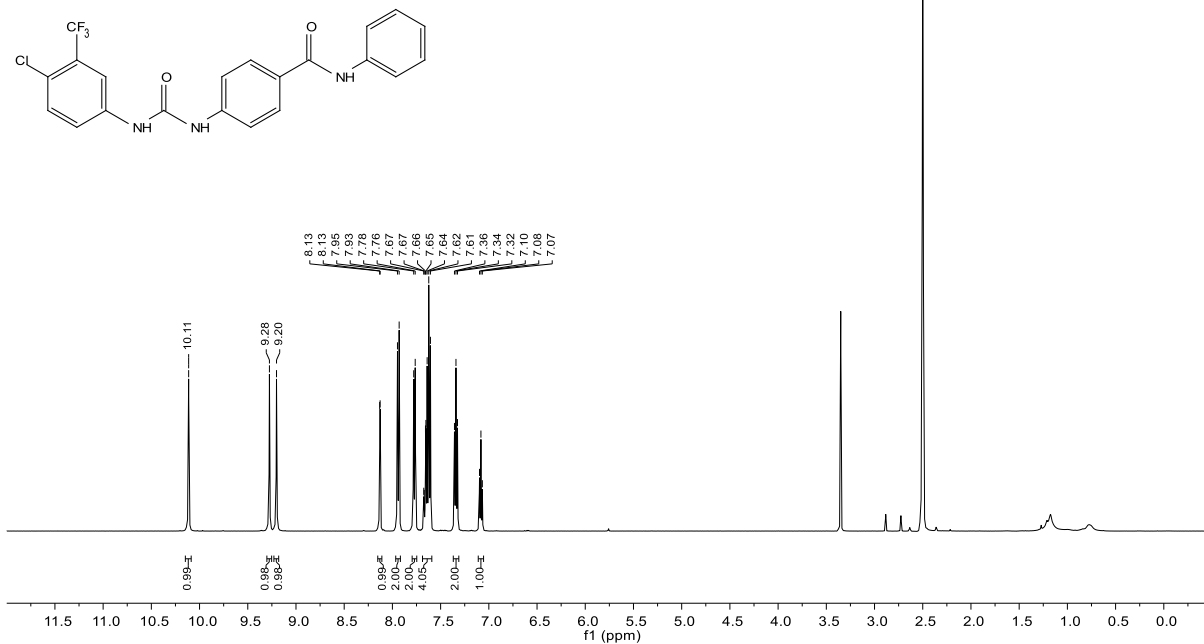
3.62

| Parameter              | Value           |
|------------------------|-----------------|
| Solvent                | DMSO            |
| Spectrometer Frequency | 125.82          |
| Pulse Sequence         | zgpg30          |
| Number of Scans        | 256             |
| Temperature            | 299.8           |
| Nucleus                | <sup>13</sup> C |



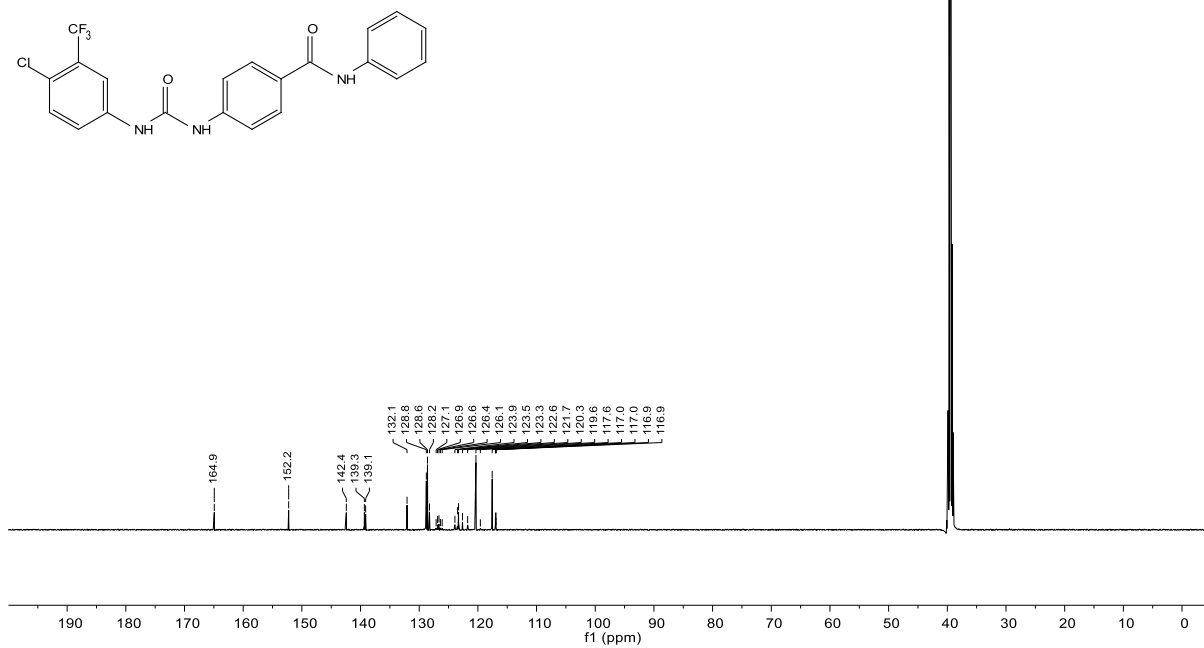
## 3.63

| Parameter              | Value        |
|------------------------|--------------|
| Solvent                | DMSO         |
| Spectrometer Frequency | 500.36       |
| Pulse Sequence         | zg30         |
| Number of Scans        | 16           |
| Temperature            | 299.9        |
| Nucleus                | $^1\text{H}$ |



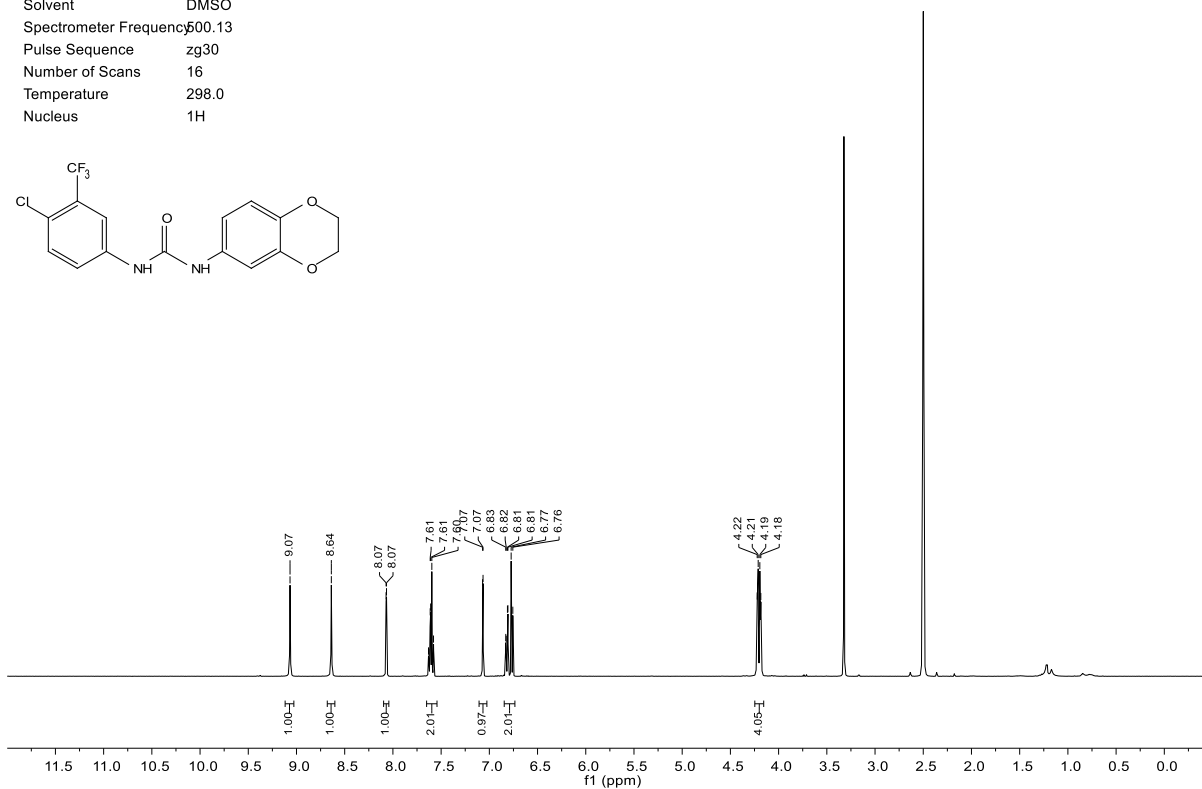
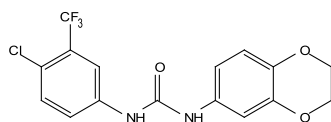
## 3.63

| Parameter              | Value           |
|------------------------|-----------------|
| Solvent                | DMSO            |
| Spectrometer Frequency | 125.82          |
| Pulse Sequence         | zgpg30          |
| Number of Scans        | 256             |
| Temperature            | 299.8           |
| Nucleus                | $^{13}\text{C}$ |



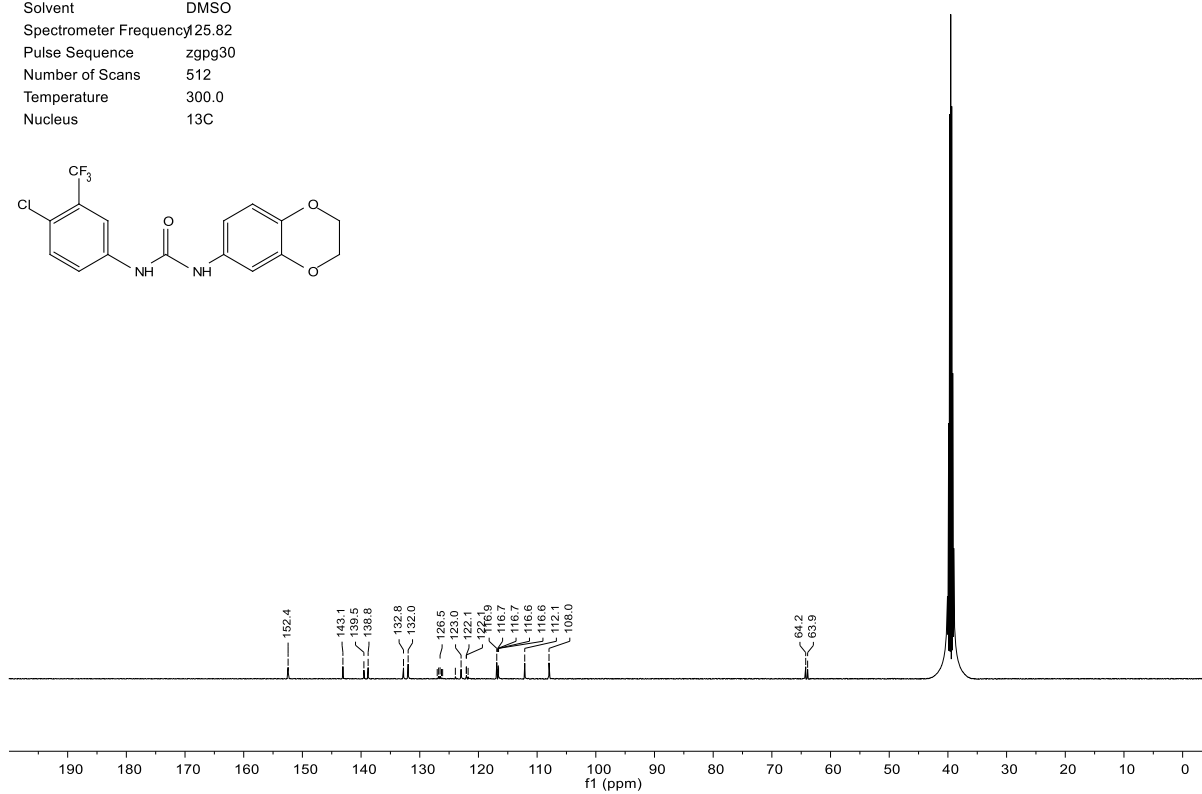
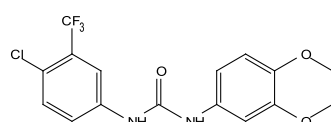
3.64

| Parameter              | Value          |
|------------------------|----------------|
| Solvent                | DMSO           |
| Spectrometer Frequency | 500.13         |
| Pulse Sequence         | zg30           |
| Number of Scans        | 16             |
| Temperature            | 298.0          |
| Nucleus                | <sup>1</sup> H |



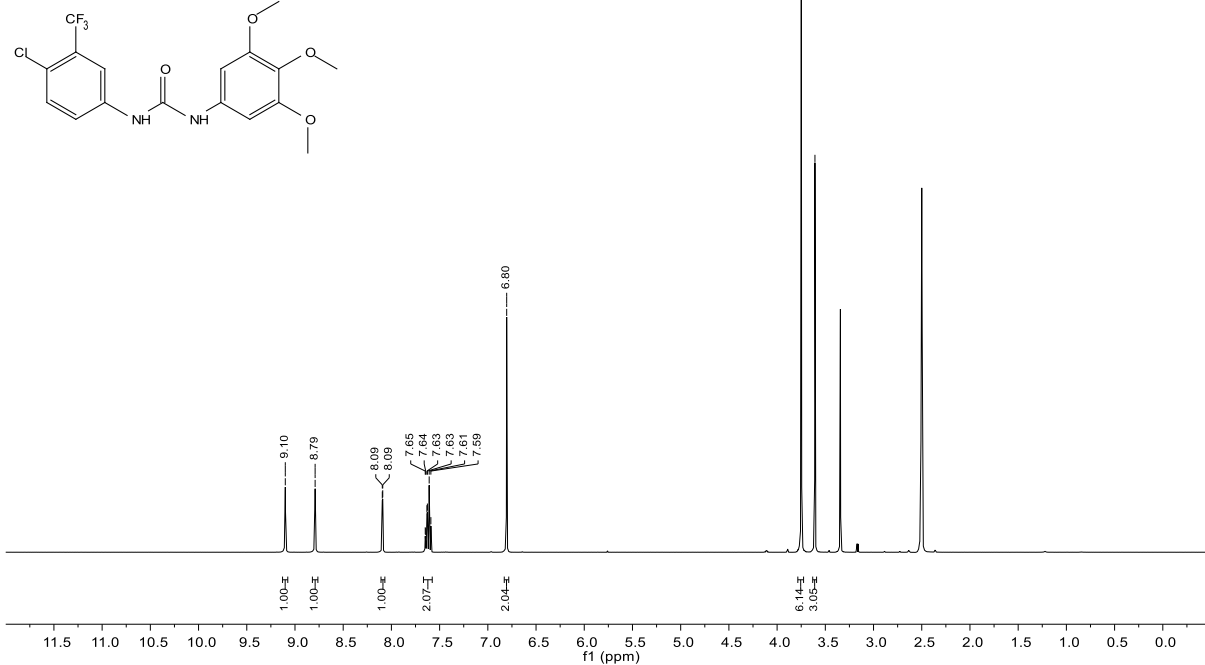
3.64

| Parameter              | Value           |
|------------------------|-----------------|
| Solvent                | DMSO            |
| Spectrometer Frequency | 125.82          |
| Pulse Sequence         | zgpg30          |
| Number of Scans        | 512             |
| Temperature            | 300.0           |
| Nucleus                | <sup>13</sup> C |



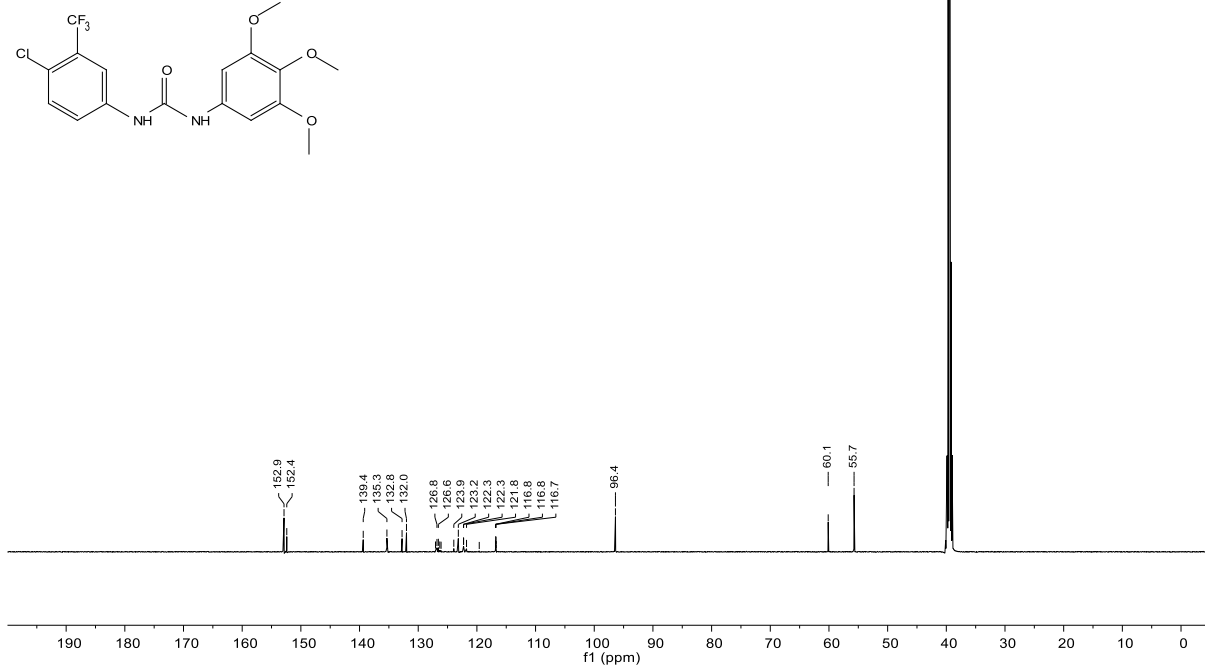
3.65

| Parameter              | Value          |
|------------------------|----------------|
| Solvent                | DMSO           |
| Spectrometer Frequency | 500.36         |
| Pulse Sequence         | zg30           |
| Number of Scans        | 16             |
| Temperature            | 300.0          |
| Nucleus                | <sup>1</sup> H |



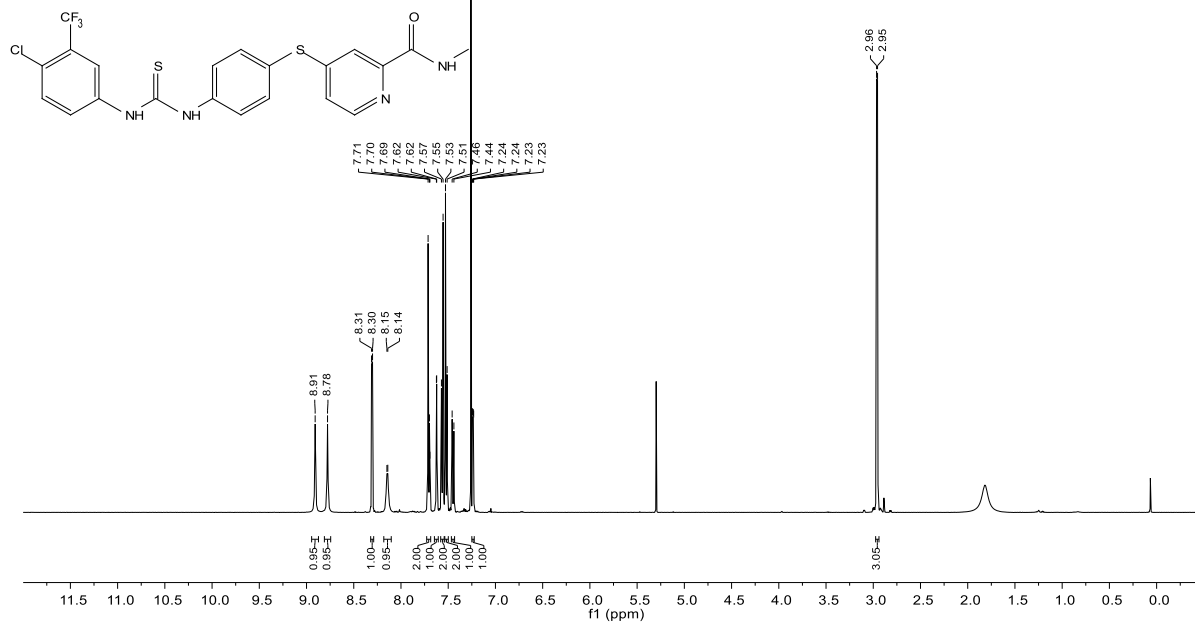
3.65

| Parameter              | Value           |
|------------------------|-----------------|
| Solvent                | DMSO            |
| Spectrometer Frequency | 125.82          |
| Pulse Sequence         | zgpg30          |
| Number of Scans        | 512             |
| Temperature            | 300.0           |
| Nucleus                | <sup>13</sup> C |



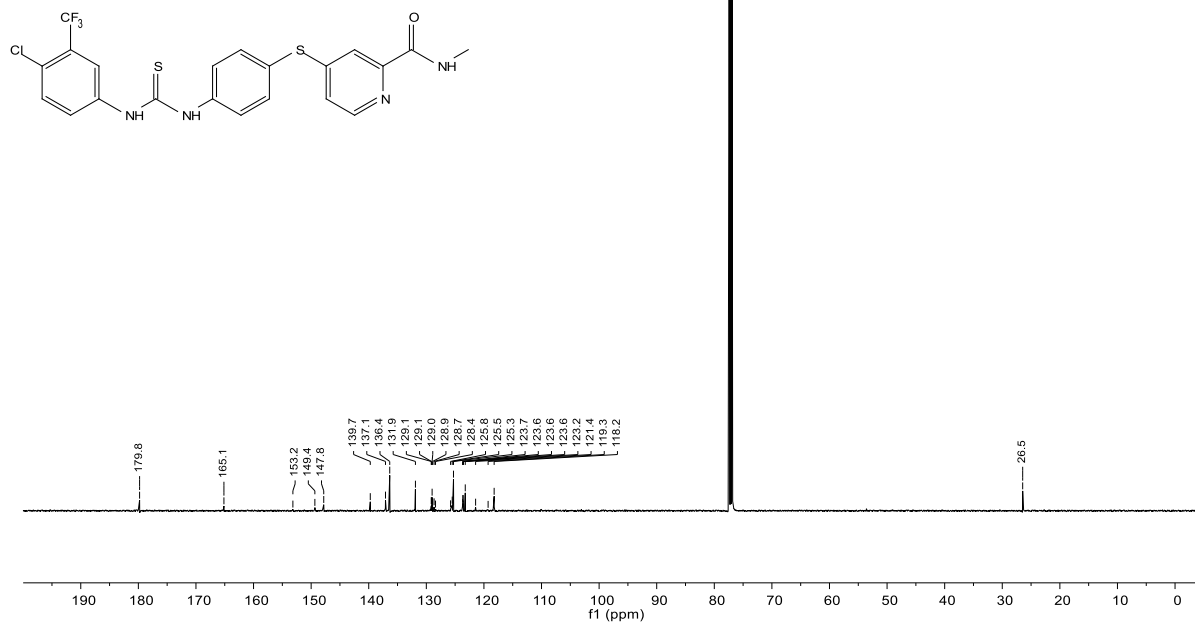
3.66

| Parameter              | Value             |
|------------------------|-------------------|
| Solvent                | CDCl <sub>3</sub> |
| Spectrometer Frequency | 500.36            |
| Pulse Sequence         | zg30              |
| Number of Scans        | 16                |
| Temperature            | 300.0             |
| Nucleus                | <sup>1</sup> H    |



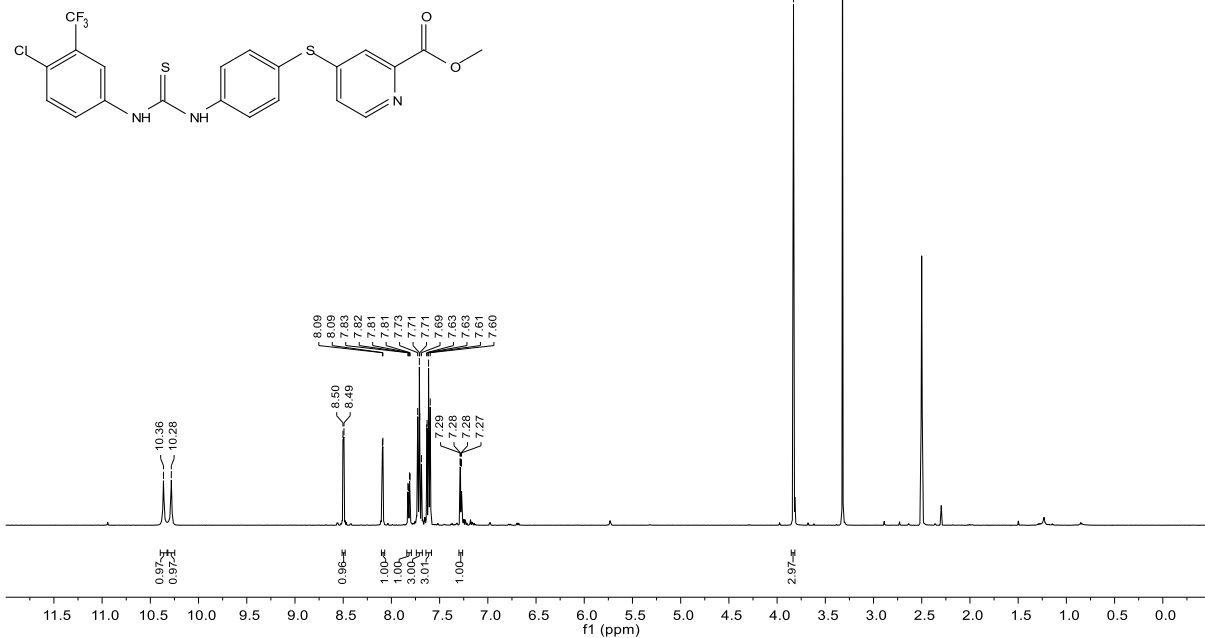
3.66

| Parameter              | Value             |
|------------------------|-------------------|
| Solvent                | CDCl <sub>3</sub> |
| Spectrometer Frequency | 125.82            |
| Pulse Sequence         | zgpg30            |
| Number of Scans        | 256               |
| Temperature            | 300.0             |
| Nucleus                | <sup>13</sup> C   |



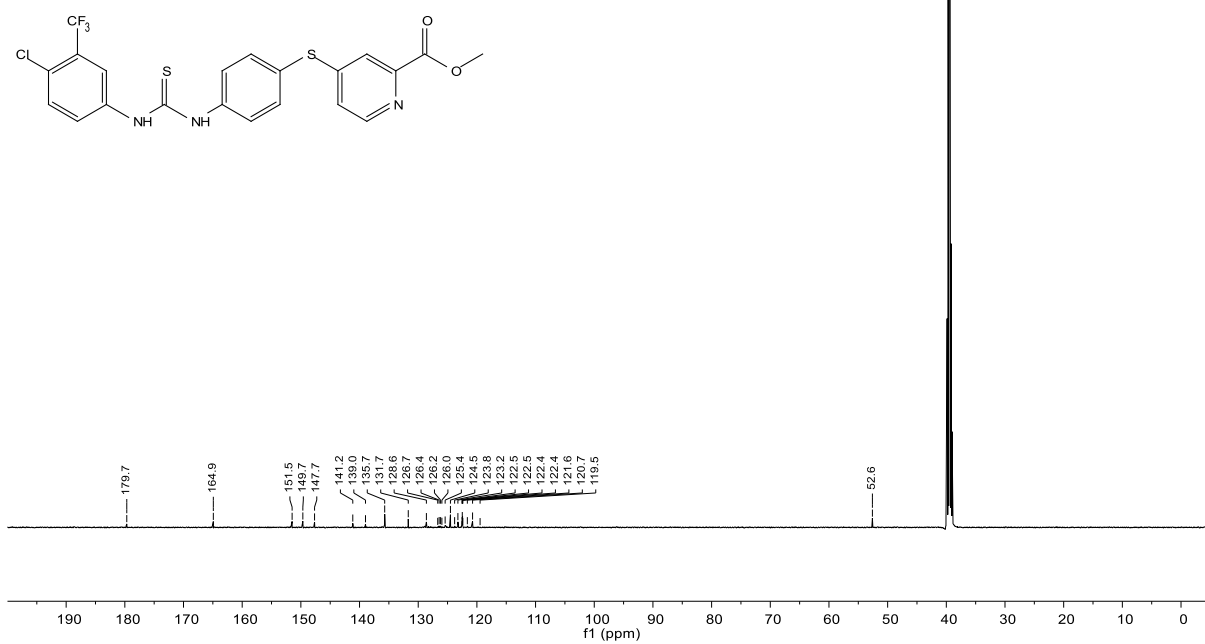
3.67

| Parameter              | Value          |
|------------------------|----------------|
| Solvent                | DMSO           |
| Spectrometer Frequency | 500.13         |
| Pulse Sequence         | zg30           |
| Number of Scans        | 16             |
| Temperature            | 298.0          |
| Nucleus                | <sup>1</sup> H |



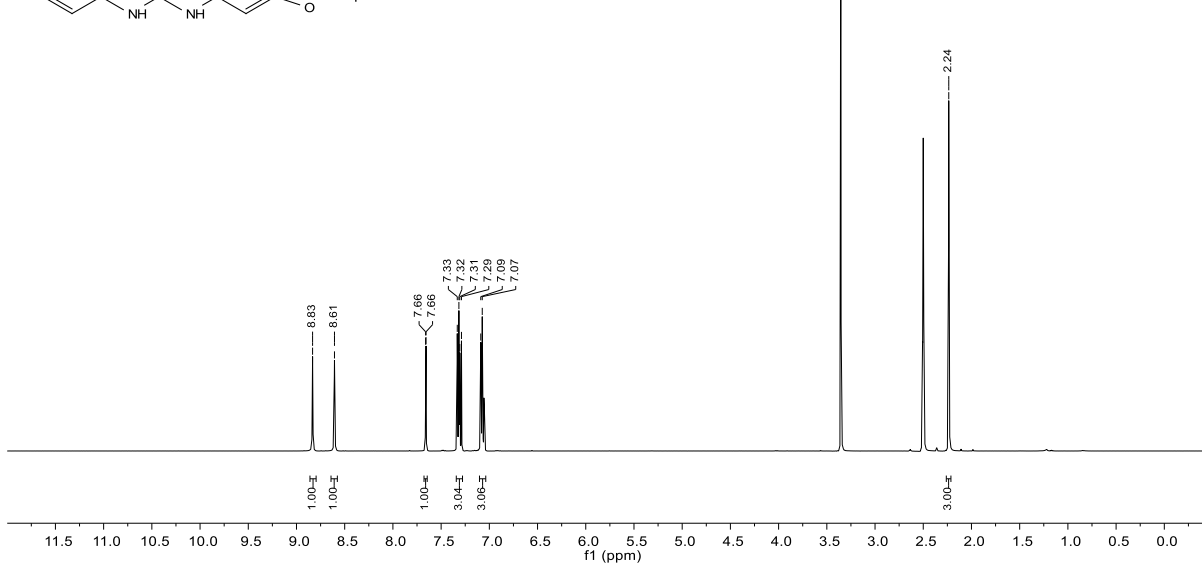
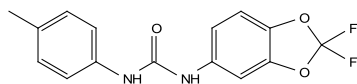
3.67

| Parameter              | Value           |
|------------------------|-----------------|
| Solvent                | DMSO            |
| Spectrometer Frequency | 125.82          |
| Pulse Sequence         | zgpg30          |
| Number of Scans        | 256             |
| Temperature            | 300.0           |
| Nucleus                | <sup>13</sup> C |



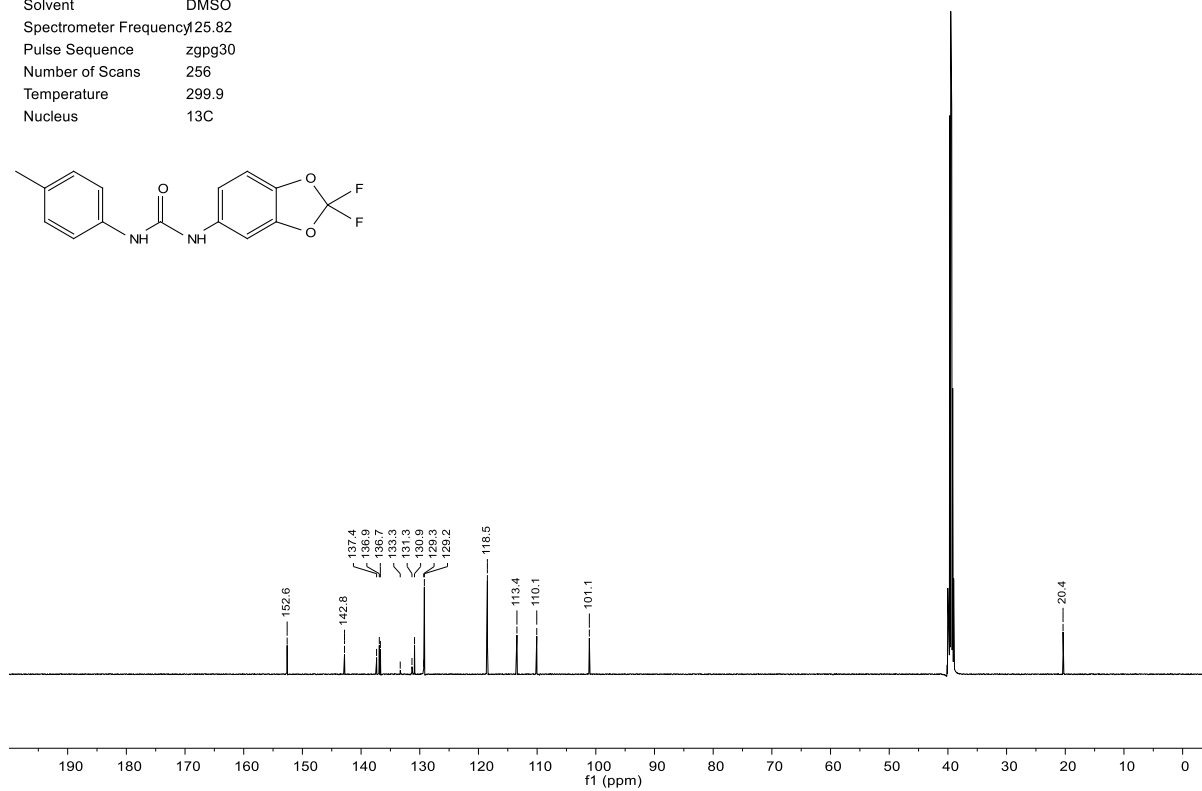
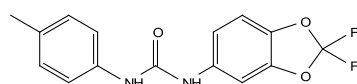
3.68

| Parameter              | Value        |
|------------------------|--------------|
| Solvent                | DMSO         |
| Spectrometer Frequency | 500.36       |
| Pulse Sequence         | zg30         |
| Number of Scans        | 16           |
| Temperature            | 299.9        |
| Nucleus                | $^1\text{H}$ |



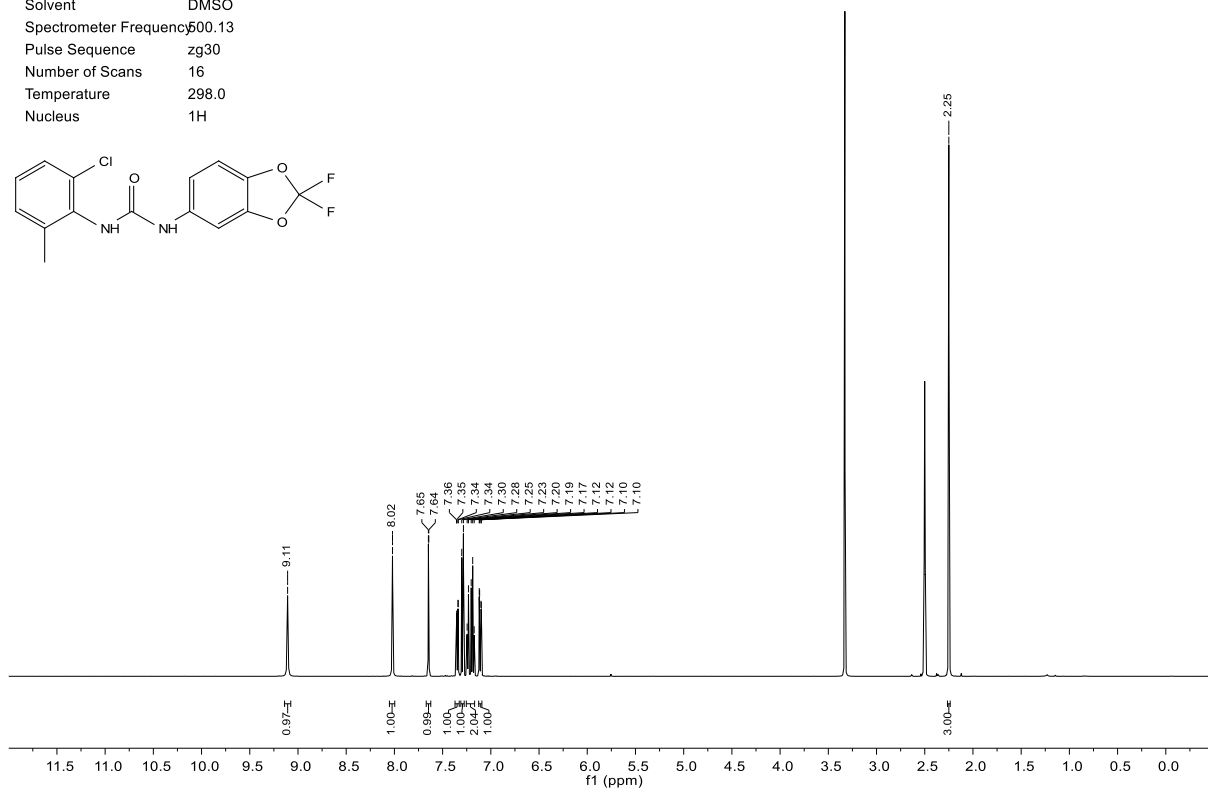
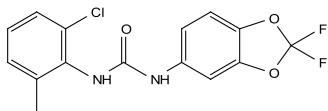
3.68

| Parameter              | Value           |
|------------------------|-----------------|
| Solvent                | DMSO            |
| Spectrometer Frequency | 125.82          |
| Pulse Sequence         | zgpg30          |
| Number of Scans        | 256             |
| Temperature            | 299.9           |
| Nucleus                | $^{13}\text{C}$ |



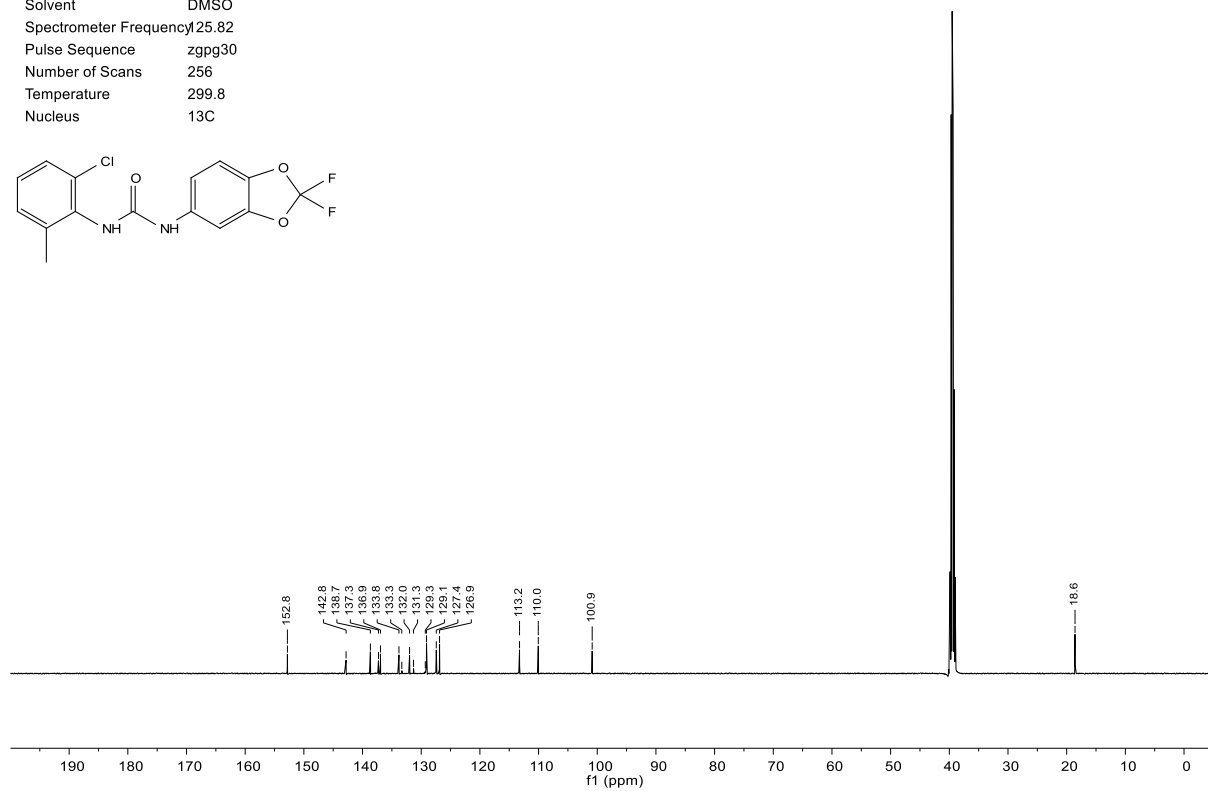
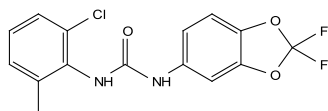
3.69

| Parameter              | Value          |
|------------------------|----------------|
| Solvent                | DMSO           |
| Spectrometer Frequency | 500.13         |
| Pulse Sequence         | zg30           |
| Number of Scans        | 16             |
| Temperature            | 298.0          |
| Nucleus                | <sup>1</sup> H |



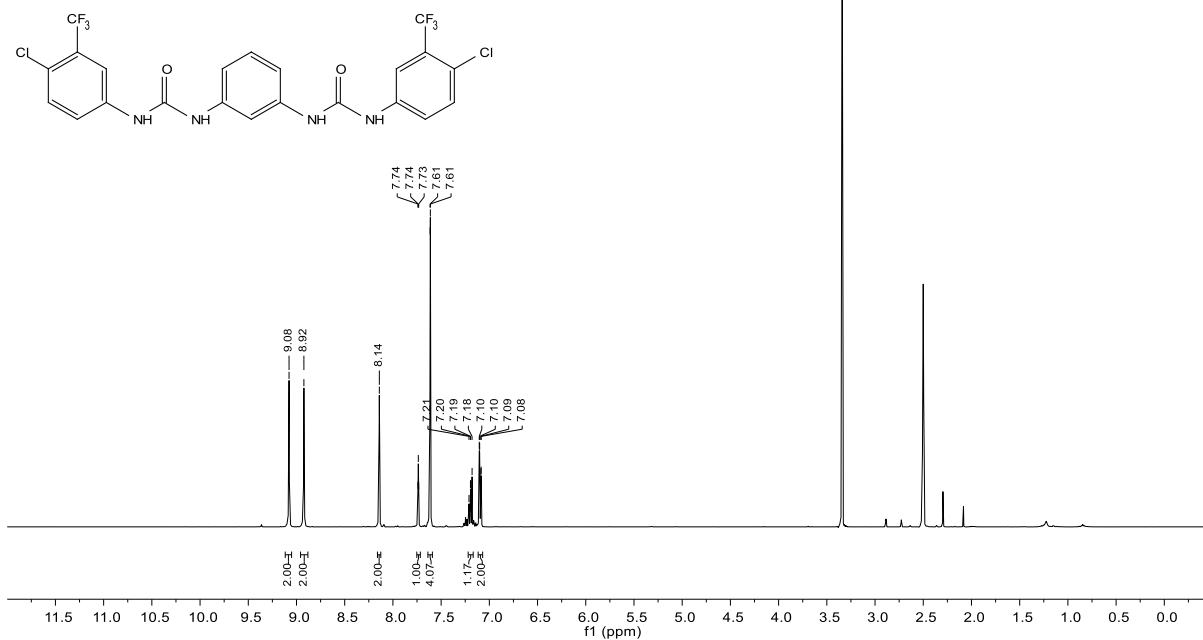
3.69

| Parameter              | Value           |
|------------------------|-----------------|
| Solvent                | DMSO            |
| Spectrometer Frequency | 125.82          |
| Pulse Sequence         | zgpg30          |
| Number of Scans        | 256             |
| Temperature            | 299.8           |
| Nucleus                | <sup>13</sup> C |



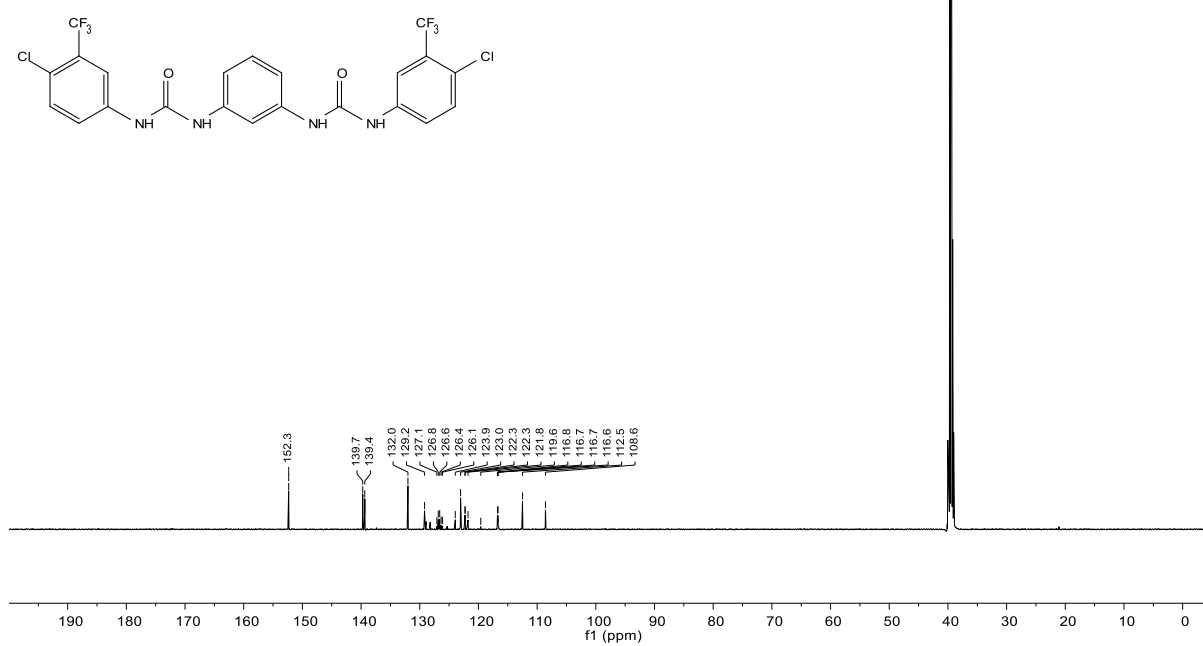
## 3.70

| Parameter              | Value        |
|------------------------|--------------|
| Solvent                | DMSO         |
| Spectrometer Frequency | 500.36       |
| Pulse Sequence         | zg30         |
| Number of Scans        | 16           |
| Temperature            | 300.0        |
| Nucleus                | $^1\text{H}$ |



## 3.70

| Parameter              | Value           |
|------------------------|-----------------|
| Solvent                | DMSO            |
| Spectrometer Frequency | 125.82          |
| Pulse Sequence         | zgpg30          |
| Number of Scans        | 256             |
| Temperature            | 299.9           |
| Nucleus                | $^{13}\text{C}$ |



## 8. CURRICULUM VITAE

### Philipp Kleiner

Date of birth                      June 21, 1986  
*Nürnberg, Germany*

#### Education

- 05.2013 – 02.2018              Ph.D. Chemistry  
*Technische Universität München, Germany*
- Ph.D. thesis under the supervision of Prof. Dr. Stephan A. Sieber, Chair of Organic Chemistry II, *Technische Universität München, Germany*
- “Insights into photocrosslinker-associated off-target protein binding and discovery of a small molecule antibiotic active against multidrug-resistant Gram-positive pathogens”*
- 08.2012 – 04.2013              M.Sc. Chemistry  
*Technische Universität München, Germany*
- M.Sc. thesis under the supervision of Prof. Dr. Stephan A. Sieber, Chair of Organic Chemistry II, *Technische Universität München, Germany*
- “Synthesis and biological activity investigations of natural products containing tetramic and tetronic acid moieties“*
- 10.2011 – 07.2012              M.Sc. Studies Chemistry  
*University of Bristol, United Kingdom*
- 10.2010 – 09.2011              M.Sc. Studies Chemistry  
*Technische Universität München, Germany*
- 09.2007 – 09.2010              B.Sc. Chemistry  
*Technische Universität München, Germany*
- B.Sc. thesis under the supervision of Prof. Dr. Bernhard Rieger, WACKER-Chair of Macromolecular Chemistry, *Technische Universität München, Germany*
- “Influence of temperature and pressure upon the polymerization behaviour of an activated nickel  $\alpha$ -diimine complex“*